A TALE OF TWO CONTINENTS: REFINING THE TEPHROSTRATIGRAPHIES FOR TWO HIGHLY VOLCANICALLY ACTIVE CENTRES; CAMPI FLEGREI, ITALY AND LAKE SUIGETSU, CENTRAL JAPAN

SOPHIE OLIVIA VINEBERG

St Anne's College
Research Laboratory for Archaeology and the History of Art (RLAHA)
University of Oxford



This thesis is submitted to the University of Oxford for the degree
Doctor of Philosophy in Archaeological Science
Michaelmas Term 2024

Supervised by Prof. Victoria Smith (University of Oxford) and Dr Paul Albert (Swansea University)

A tale of two continents: refining the tephrostratigraphies for two volcanic regions; Campania, Italy and Lake Suigetsu, central Japan

Sophie Vineberg, St Anne's College
Submitted to the University of Oxford for the degree Doctor of Philosophy in Archaeological Science
Michaelmas Term 2024

Abstract
This thesis refines the tephrostratigraphies for the very productive volcanic regions in both Italy and Japan. Tephra is routinely used in the dating and correlation of Late Quaternary paleoenvironmental and archaeological records. The ability to characterise tephra using both their visual (i.e. grain size, colour, morphology) as well as their geochemical (major and trace element glass compositions) properties underpins the capability to identify the eruption source and distinguish successive deposits from the same volcano. Whilst near-vent (proximal) eruption sequences are fundamental to the reconstruction of past volcanic histories by providing stratigraphic, chronological and geochemical constraints, they are often destroyed and/or buried by voluminous eruption deposits from large volcanic eruptions. Distal sedimentary archives (e.g. lacustrine and marine cores) overcome such preservation and accessibility issues. The isolation of non-visible (<125 μm) tephra deposits (cryptotephra) in more distally located sites have the potential to provide accessible, tephra records that have not been subjected to the same preservation issues as at proximal locations. Thus, integration of the proximal-distal records is fundamental in refining tephrochronological frameworks of volcanic systems which are required to accurately reconstruct eruption histories and assess associated hazards. By conducting detailed stratigraphic and geochemical (majors and trace elements) investigations, this research advances our knowledge of the timing, frequency, and magnitude of explosive eruptions in both the Campanian and Japanese volcanic regions over the past 200,000 years. This thesis demonstrates the merit of integrating the proximal-distal records for understanding of the timing and ash dispersals of pre-historic eruptions.

The Campanian Volcanic Zone (CVZ) comprises multiple active volcanoes and includes the highly productive Campi Flegrei and Ischia caldera systems. These caldera volcanoes have produced probably the largest eruptions in Europe in the past 200 ka, such as the Monte Epomeo Green Tuff (MEGT; Ischia) at ca. 56 ka and the Campanian Ignimbrite (CI; Campi Flegrei) at ca. 40 ka, which form widespread isochrons across the Mediterranean region. The CI eruption was the largest in Europe for the last 200 kyr and as such sequences located in medial and proximal locations are often buried underneath large tephra deposits and thus many of the pre-CI deposits have not been physically or geochemically studied in great detail. This chapter presents a detailed tephrostratigraphy for pre-CI eruption activity using the units preserved within a sequence at the coastal Acquamorta outcrop, on the western side of the CI caldera rim. Both the MEGT and CI units are present in the section, and they bracket twelve eruption units that were logged and sampled. Major and trace element glass chemistry analysis distinguishes three eruptions from Ischia and nine from Campi Flegrei, constraining the tempo of volcanic activity between two major caldera-forming eruptions. This study highlights that Campi Flegrei experienced at least nine eruptions within 16 ka leading up to the CI eruption, suggesting continuous magmatic activity before the catastrophic event. Furthermore, many of the Ischia and Campi Flegrei tephras preserved at Acquamorta indicate that successive eruptions from each volcano are broadly compositionally homogenous, with small compositional shifts over time observed in those from Campi Flegrei. The results highlight the need for further detailed chrono-stratigraphic and geochemical data from tephra deposits located across the CI caldera to generate more complete eruption histories and magmatic systems for the CVZ volcanoes to ensure proximal-distal correlations are robust

The Lake Suigetsu sedimentary record (central Honshu, Japan) provides a key tephro-stratotype of explosive volcanism for Japan spanning the last 200 ka. Whilst the whole sedimentary sequence has been investigated for the presence of visible tephras, only sediments within the last 50 kyr have been studied for their preservation of cryptotephra deposits. The Lake Suigetsu sediments between 120 and 50 ka (20 m of sediment) were examined for the preservation of cryptotephra deposits to further refine the Late Quaternary tephrostratigraphic framework for the East Asian/Pacific region. The high-resolution sediments of Lake Suigetsu offer unprecedented insight into the timing, frequency and dispersal of ash-fall events dispersed over this now heavily populated region of East Asia. Forty-one further crypto-/tephra horizons are identified during this interval interspersed between visible tephra layers associated with large-magnitude eruptions and regional event markers (e.g., Aso-4, K-Tz, Ata). The newly identified deposits are geochemically analysed (major and trace elements) and the chemical fingerprints are used to trace these deposits to subduction related volcanoes located along the three main Japanese islands (Kyushu, Honshu and Hokkaido), and nearby intraplate volcanoes. This cryptotephra investigation, and the acquisition of new geochemical data for several widespread tephra layers, revealed distal ash-fall from two notable large magnitude (≥M6.0) eruptions, the Plinian Sambe Kisuki (SK) eruption and the caldera-forming Toya eruption, both of which are important widespread tephrostratigraphic markers suitable for linking regional terrestrial and marine sequences in MIS5d and MIS5c, respectively. The presence of the Toya caldera-forming eruption is the largest eruption from Hokkaido to be reported in Lake Suigetsu and significantly expands the geographical limits of ash-fall for this event events and can thus be used over wide areas to synchronise records. Although some widespread tephrostratigraphic markers were correlated (e.g. SK, Toya) numerous eruption deposits which have not yet been correlated to specific eruption events due to limited glass geochemistry for eruption deposits, incomplete eruption stratigraphies and similar melt compositions erupted from a volcano over long periods of time.

The Aso caldera in central Kyushu, SW Japan, is one of the largest and most active volcanoes in the world. Volcanic activity recorded from the Aso system is characterised by four caldera-forming eruptions (Aso-1 to -4) and inter-caldera activity from multiple central cones. Twenty volcanic deposits (four visible tephras and sixteen cryptotephras) have previously been identified in the Lake Suigetsu sediments spanning 120 – 30 ka and have been geochemically characterised and correlated to Aso as their volcanic source. However only four of these have been correlated to their proximal counterpart (i.e. Aso-Kpfa, ACP4, Aso-4 and Aso-ABCD) due to the lack of geochemical characterisation of many proximal units. In this chapter, further geochemical characterisation (majors and traces) of the >30 ka silicic Aso tephras from well-established sequences are presented and key diagnostic features identified to further aid integration of sequences. Through detailed glass chemistry analysis, a further seven of the Aso tephras preserved in Lake Suigetsu have been correlated with their proximal counterpart. Significantly, the identification of these tephra deposits in Lake Suigetsu provides better ages for many of these eruptions, and constrains repose periods between eruptions e.g. 400 years between the two phases of ACP4 activity and 4.8 ka between the Aso-4X and Aso-4 caldera eruptions. This investigation reveals that there are seven eruption deposits in the Lake Suigetsu record that are not yet observed in the exposed near-vent sequences, suggesting potential eruption under-recording. In the exposures studied, some deposits may have been removed or buried by subsequent large eruptions for instance the Aso-4 caldera-forming eruption.

Acknowledgements

Completing a PhD is often described as a journey. In my case, it felt more like an endurance test set against the backdrop of a global circus. This thesis was written during truly wild times: Brexit, a global pandemic, a rapid-fire succession of four Prime Ministers and the bold decision to buy a flat (complete with 1980s decor) just months before submission. Admittedly, it took longer than planned - but it's finally done. For that, I owe a lot of gratitude. They say it takes a village to raise a child, and a small nation-state to complete a PhD.

First and foremost, I extend my deepest gratitude to Prof. Victoria Smith (University of Oxford) and Dr Paul Albert (Swansea University) for their invaluable supervision. Vic, your technical expertise, insightful (and impressively thorough) feedback has been instrumental in elevating this research. Paul, your meticulous attention to geochemical detail has significantly enhanced my understanding and improved the overall quality of this work. Your moral support, particularly during the inevitable final-stage struggles of thesis writing, has been greatly appreciated. I must also sincerely thank Dr Danielle McLean (University of Oxford) for being an exceptional unofficial supervisor. Your continual guidance, enthusiasm and shared love for chai lattes have made the Oxford Tephra Lab an enjoyable and supportive environment, even in the most chaotic of times.

To all my collaborators, I am truly grateful for your contributions, without which this thesis would not have been possible. I also extend my appreciation to the technical staff and researchers at the University of Oxford, Swansea University and Royal Holloway, University of London, for their invaluable support.

I am deeply grateful to NERC, the Oxford Doctoral Training Programme (DTP), and St Anne's College for funding this project and enabling the research opportunities it provided. I also extend my thanks to the administrative teams at the School of Archaeology and the DTP for their assistance throughout my doctoral journey.

My sincere thanks go to Profs. Christopher Bronk Ramsey and David Pyle (University of Oxford) for their invaluable feedback and constructive suggestions, which have helped refine my ideas and strengthen this research. I also wish to thank Profs. Christine Lane (University of Cambridge) and Simon Blockley (Royal Holloway, University of London) for encouraging me to pursue a doctorate and for their continued support and advice beyond my studies at Cambridge and Royal Holloway. A special thanks to Mr. Mike Downie (RGS Newcastle) for believing in me all those years ago and for maintaining an interest in my journey – from a U to a PhD.

I also wish to thank Prof. David Pyle (University of Oxford) and Dr Will Hutchison (University of St. Andrews) for examining my viva and making it not just quick and painless, but surprisingly pleasant. Your insightful feedback and constructive discussion were invaluable in shaping this thesis into its final, polished form.

Finally, I would like to express my deepest gratitude to my family and friends. To my long-suffering parents, watching NUFC week-in, week-out with you has instilled in me the importance of resilience and perseverance from a young age. Most of all, thank you for your unwavering (financial) support. To Sarah and Seb, your lifelong ability to create chaos has, in its own way, prepared me for the rollercoaster of a PhD. Thank you for always keeping me grounded with frequent reminders of my signature 'Sophieisms'. Ali, Dan, Beth and Imogen, thank you for being there with a bottle of something, whether for venting or celebrating. And finally, to my partner, Hamish, thank you for your endless patience, encouragement and remarkable ability to endure my academic rants and questionable work-life balance.

And to academia - it's not me, it's you.

Table of Contents

Abstract ***i***
Acknowledgements ***iii***
Table of Contents ***iv***
List of Figures ***viii***
List of Tables ***xii***

Chapter 1: Introduction

Overview **1**
1. Volcanic hazards **1**
1.2. Methods to reconstruct volcanic histories **2**
3. Tephrostratigraphic frameworks **11**
4. Study sites and previous regional tephra studies **12**
1.4.1. Campania, Italy **13**
1.4.2. Japan **19**
5. Project aim and objectives **28**
6. Thesis guide **28**

Chapter 2: Materials and Methods

Overview **30**
2.1. Cryptotephra extraction and laboratory preparation **30**
2.2. Visual analysis of shards **33**
2.2. Compositional analysis **34**

Chapter 3: Study sites

Overview **39**
3.1. Context **39**
3.2. Proximal site: Acquamorta, Campania, Italy **40**
3.3. Proximal Japanese sampling sites **42**
3.3.1. Aso **44**
3.3.2. Kirishima **52**
3.3.3. Sambe **54**
3.4. Distal: Lake Suigetsu **55**
3.4.1. Geological and hydrological setting **55**
3.4.2. Coring campaigns **57**

Chapter 4: Insights into the explosive eruption history of the Campanian volcanoes prior to the Campanian Ignimbrite eruption

Author list and Highlights **61**
Abstract **61**
4.1. Introduction **62**
4.2. Campanian volcanic centres and eruptions prior to the Campanian Ignimbrite **67**
4.2.1. Campi Flegrei **67**
4.2.1.1. Compositions of pre-CI Campi Flegrei tephra **68**
4.2.1.2. Distal records of Campi Flegrei tephra (Pre-CI) **68**
4.2.2. Ischia **69**

4.2.2.1. Compositions of pre-CI Ischia tephra 70
4.2.2.2 Distal pre-CI Ischia tephra 70
4.2.3 Procida 71
4.3. Study Site 72
4.4. Methods 73
4.4.1. Eruption stratigraphy 73
4.4.2. Glass chemistry 73
4.5. Results 74
4.5.1. Pre-CI eruption stratigraphy 74
4.5.2. Glass geochemistry 77
4.6. Discussion 81
4.6.1. Composition and source of the Acquamorta tephra units 81
4.6.2. Ischia tephra 81
4.6.3. Campi Flegrei tephra 83
4.6.3.1 Group B 87
4.6.3.2 Group C 88
4.6.3.3 Group D 89
4.6.4. Eruption history 91
4.6.4.1. Ischia 92
4.6.4.2. Campi Flegrei 93
4.6.5. Magmatic system 94
4.7. Conclusion 96

Chapter 5: A detailed record of large explosive eruptions from Japan between ~120 and 50 ka preserved at Lake Suigetsu

Author list and Highlights 98
Abstract 98
5.1. Introduction 99
5.2. Study Site 102
5.3. Eruption histories of volcanoes in and around Japan between ~120 and 50 ka 102
5.3.1. The Central Volcanic Region (CVR) associated with the Ryuku-Kyushu Arc 105
5.3.2. The Southern Volcanic Region (SVR) associated with the Ryuku-Kyushu Arc 106
5.3.3. SW Japan Arc (SWJA) 107
5.3.4. Izu Bonin Arc 108
5.3.5. Norikura Volcanic Zone (NVZ) 109
5.3.6. NE Japan Arc (NEJA) 109
5.3.7. Kurile Arc 110
5.3.8. Intra-plate 110
5.4. Materials and methods 111
5.4.1. Cryptotephra extraction techniques 111
5.4.2. Reference tephra samples 112
5.4.3. Glass compositions 112
5.4.4. The Lake Suigetsu core and its chronology 114
5.5. Results 115
5.5.1. Tephrostratigraphy 115
5.5.2. Glass geochemical compositions 118
5.6. Discussion 127
5.6.1. Provenance of the SG14 tephra layers erupted ~120 - 127

50 ka
5.6.1.1 Kyushu (SVR and CVR) **128**
5.6.1.2. Honshu (SWJA, Izu-Bonin Arc and NVZ) **134**
5.6.1.3. Honshu/Hokkaido (NEJA and Kurile Arc) **140**
5.6.1.4. Intraplate **142**
5.6.1.5. Tephra that cannot be attributed to a source **143**
5.6.2. Identifying volcanic sources and eruptions of the Lake Suigetsu tephra **144**
5.6.2.1. Limited glass geochemistry for eruption deposits **144**
5.6.2.2. Incomplete eruption stratigraphies **145**
5.6.2.3. Similar melt compositions erupted from a volcano over long periods of time **145**
5.6.3. Tephra dispersal **146**
5.6.4. Widespread markers for tephra correlation **149**
5.7. Conclusion **149**

Chapter 6: Revealing the timing and dispersal of large explosive eruptions at Aso volcano (Japan) by integrating proximal and distal tephra records following the Aso-3 eruption

Author list and Highlights **151**
Abstract **152**
6.1. Introduction **152**
6.2. 30 to ~130 ka Aso eruption history **156**
6.2.1. Post-Aso-4 **157**
6.2.2. Pre-Aso-4 **162**
6.3. Methods **169**
6.3.1. Proximal tephra units **169**
6.3.2. Distal Lake Suigetsu crypto-/tephra deposits **169**
6.3.3. Geochemical composition of proximal tephras **170**
6.4. Results **171**
6.4.1. Post-Aso-4 **178**
6.4.2. Aso-4 and Aso-4X **181**
6.4.3. Stage 5 (Aso-Y) **183**
6.4.4. Stage 4 (Aso-ABCD, Aso-EF, Aso-G, Aso-HI, Aso-JKL, Aso-M) **183**
6.4.5. Stage 3 (Aso-N/Z-2, Aso-Z6) **185**
6.5. Discussion **186**
6.5.1. Correlations **186**
6.5.1.1. Post-Aso-4 **188**
6.5.1.2. Pre-Aso-4 **191**
6.6. Implications **197**
6.6.1. Frequency, tempo and dispersal **197**
6.6.2. Constrained eruption chronology **199**
6.6.3. Geochemical compositions **199**
6.7. Conclusions **200**

Chapter 7: General Discussion and Conclusions

Overview **202**
7.1. Objective 1: Augment the tephrostratigraphic records of Campania (Italy) and Lake Suigetsu (Japan). **202**

7.2. Objective 2: Provide detailed geochemical characterisation of the volcanic glasses. Use their major and trace element compositions to determine their source regions, volcanoes and specific eruptions. 207
7.2. Objective 3: Identify key isochrons to aid the integration and synchronisation of proximal and distal records. 210

Consolidated list of references 217

Supplementary Material
Appendix A: Supplementary Material for Article 1 243
Appendix B: Supplementary Material for Article 2 268
Appendix C: Supplementary Material for Article 3 334

List of Figures

Chapter 1: Introduction

Figure 1.1: Distal tephra dispersal and deposition in a Quaternary landscape downwind of a volcano. **7**

Figure 1.2: Criteria used to decipher primary ash-fall events within the Lake Suigetsu sedimentary sequence. **10**

Figure 1.3: The RESET ('Response of Humans to Abrupt Environmental Transitions') tephra lattice. **12**

Figure 1.4: Locations of Campanian volcanoes and the Acquamorta outcrop. **14**

Figure 1.5: Major and trace element glass compositions of large magnitude Campanian sources over the last 40 ka and useful elements for discriminating various volcanic centres. **16**

Figure 1.6: Eruption history of Campi Flegrei. **18**

Figure 1.7: Locations of Lake Suigetsu and major Quaternary volcanic centres from across East Asia and the dispersal of large magnitude eruptions over the last 200 ka. **20**

Figure 1.8: Major and trace element glass compositions of large magnitude Campanian sources over the last 150 ka and useful elements for discriminating various volcanic centres. **24**

Figure 1.9: Current tephrostratigraphic record of Lake Suigetsu spanning the last 160 ka. **26**

Chapter 2: Methods and Materials

Figure 2.1 Sampling strategy employed for the SG14 master core for the 120 – 50 ka section. **31**

Figure 2.2: Cryptotephra extraction protocol. **32**

Figure 2.3: Representation/classification guide of the glass-shard morphologies, microphenocryst and vesicle content, identified during investigation of the SG14 core. **34**

Figure 2.4: The preparation and procedure for mounting both visible tephra and cryptotephra samples for geochemical analyses. **35**

Figure 2.5: SEM image showing laser ablation pits on vesicular tephra. **38**

Chapter 3: Study Sites

Figure 3.1: Photos of the Acquamorta tephra units. **41**

Figure 3.2. Locations of Lake Suigetsu and proximal outcrops sampled in this study and major Quaternary volcanic centres and arcs from across East Asia. **43**

Figure 3.3: Representative photos of the post-Aso-4 tephra units. **45**
Figure 3.4: Representative photos of the pre-Aso-4 tephra units. **46**

Figure 3.5: Photos of the Kirishima tephra units. **53**

Figure 3.6: Photos of the Sambe tephra units. **55**

Figure 3.7: Proximity of Lake Suigetsu to Lake Biwa and major Japanese cities and coring positions of the SG93, SG06 and SG14 campaigns **56**
Figure 3.8: Photographic record of the litho-stratigraphy of the SG06 core. **58**

Figure 3.9: Stratigraphic alignment of parallel sediment cores 'SG06' and 'SG12'. **60**

Chapter 4: Insights into the explosive eruption history of the Campanian volcanoes prior to the Campanian Ignimbrite eruption

Figure 4.1: Schematic of the known pre-40 ka eruptions of the CVZ volcanoes. **63**

Figure 4.2: Maps showing the locations of proximally and distally located sedimentary sequences across the Mediterranean which contain pre-40 ka tephra units. **65**

Figure 4.3: Photos and stratigraphic log of the Acquamorta outcrop. **76**

Figure 4.4: Relative stratigraphic order and the major and trace element compositions of the tephra units at Acquamorta. **79**

Figure 4.5: Glass compositions of the Ischia tephras preserved at Acquamorta. **82**

Figure 4.6: Glass compositions of the Campi Flegrei tephras preserved at Acquamorta. **84**

Figure 4.7: Compositional groups of the Campi Flegrei tephras preserved at Acquamorta. **86**

Figure 4.8: Glass compositions of the Group D tephras. **90**

Chapter 5: A detailed record of large explosive eruptions from Japan between ~120 and 50 ka preserved at Lake Suigetsu

Figure 5.1: Quaternary Japanese volcanoes and the ash dispersal boundaries for various widespread tephra layers and the proximity of Lake Suigetsu to Lake Biwa and major Japanese cities and positions of all three coring campaigns. **101**

Figure 5.2: Relative stratigraphic order of known eruptions (~130 – 50 ka), based largely on the proximal stratigraphies, in and around Japan. **104**

Figure 5.3: Sedimentary records that contain identified and correlated tephras in the ~120 – 50 ka interval. **106**

Figure 5.4: Glass shard concentrations in the sediments spanning ~120 – 50 ka of the Lake Suigetsu (SG14) core. **117**

Figure 5.5: Major element glass compositions of the crypto-/tephras preserved in the SG14 sediments spanning ~120 – 50 ka. **124**

Figure 5.6: Trace element glass compositions of the crypto-/tephras preserved in the SG14 sediments spanning ~120 - 50 ka. **126**

Figure 5.7: Major and trace element compositions of the SG14 cryptotephras (~120 – 50 ka) derived from the SVR in comparison for major eruptive SVR centres. **129**

Figure 5.8: Major and trace element compositions of the SG14 crypto-/tephras (~120 – 50 ka) from the CVR. **133**

Figure 5.9: Major and trace element compositions of the SG14 cryptotephras (~120 – 50 ka) from the SWJA. **135**

Figure 5.10: Major and trace element compositions of the SG14 cryptotephras (~120– 50 ka) erupted from the Izu-Bonin Arc. **137**

Figure 5.11: Major and trace element compositions of the SG14 cryptotephras (~120 – 50 ka) from the NVZ. **134**

Figure 5.12: Major and trace element compositions of the SG14 cryptotephra deposits (~120 – 50 ka) from the NEJA, Kurile Arc and Intraplate volcanoes. **141**

Figure 5.13: Major and trace element compositions of the SG14 cryptotephra deposits (~120 – 50 ka) from unknown volcanic arcs and centres. **143**

Figure 5.14: Summary of the augmented Lake Suigetsu (SG14) tephrostratigraphy (visible and cryptotephra deposits) spanning ~120 – 50 ka plotted against the MIS positions. **147**

Chapter 6: Revealing the timing and dispersal of large explosive eruptions at Aso volcano (Japan) by integrating proximal and distal tephra records following the Aso-3 eruption

Figure 6.1: The locations of the Aso caldera, Lake Suigetsu (and coring campaigns) and proximal sampling sites. **154**

Figure 6.2: Post-Aso-4 stratigraphic relations of silicic Aso tephras. **160**

Figure 6.3: Stratigraphic relationships of the Aso units logged between Aso-3 and Aso-4. **165**

Figure 6.4: Major and trace element glass compositions of the Aso tephra units preserved in proximal outcrops around the Aso caldera and in the Lake Suigetsu sedimentary archive. **177**

Figure 6.5: Major and trace element geochemical variability of volcanic glasses from large magnitude silicic eruptions between the Aso-4 and AT tephra layers. **179**

Figure 6.6: Major and trace element geochemical variability of volcanic glasses from large magnitude silicic eruptions between the Aso-3 and Aso-4 tephra layers. **182**

Figure 6.7: Major and trace element glass compositions of the Aso crypto-/tephra deposits preserved between the Aso-4 and AT tephra layers in the Lake Suigetsu sequence compared to reference chemical datasets produced for chrono-stratigraphically relevant eruption units. **189**

Figure 6.8: Major and trace element glass compositions of the Aso crypto-/tephra deposits preserved between the Aso-3 and Aso-4 tephra layers in the Lake Suigetsu sequence compared to reference chemical datasets produced for chrono-stratigraphically relevant eruption units. **193**

Figure 6.9: major and trace elements useful for recognising variations in the volcanic glasses erupted from twenty-seven tephra units preserved between the Aso-3 and AT tephras in outcrops around the caldera which have been geochemically analysed. The relative stratigraphic order of the proximally analysed units and summary of the augmented Lake Suigetsu (SG14) Aso tephrostratigraphy interbedded with other key widespread marker layers spanning 120 – 30 ka. **196**

Chapter 7: General Discussion and Conclusions

Figure 7.1: Summary of the Lake Suigetsu tephrostratigraphy and tephra research presented in this thesis. **205**

Figure 7.2: Tephrostratigraphic framework for Japan constructed for the past 100 ka. **213**

Figure 7.3: Locations of key Japanese sedimentary archives. **214**

List of Tables

Chapter 1: Introduction

Table 1.1 Widespread Japanese tephras from the last 250 ka. **22**

Chapter 3: Study Sites

Table 3.1: Widespread tephra samples analysed in this thesis. **44**

Chapter 4: Insights into the explosive eruption history of the Campanian volcanoes prior to the Campanian Ignimbrite eruption

Table 4.1: EMP and LA-ICP-MS of representative analysis shards from the deposits preserved between the MEGT and CI identified at Acquamorta. **78**

Chapter 5: A detailed record of large explosive eruptions from Japan between ~120 and 50 ka preserved at Lake Suigetsu

Table 5.1: Key East Asian eruption deposits reported in proximal and medial locations in the ~120 – 50 ka timeframe that are most likely to be preserved in the Lake Suigetsu sediments. **103**

Table 5.2: Summary of the tephra layers (visible and cryptotephra) within the ~120 – 50 ka sediments of Lake Suigetsu. **116**

Table 5.3: Average EMP and LA-ICP-MS element chemistry of the ~120 – 50 ka Lake Suigetsu crypto-/tephras. **119**

Table 5.4: Average EMP element glass compositions of proximal tephra deposits analysed as part of this study to compare to the ~120 – 50 ka Lake Suigetsu crypto-/tephras. **128**

Chapter 6: Revealing the timing and dispersal of large explosive eruptions at Aso volcano (Japan) by integrating proximal and distal tephra records following the Aso-3 eruption

Table 6.1: Explosive eruptions defined from exposures around Aso volcano between Aso-3 and the AT (Aira). **157**

Table 6.2: Average EMP and LA-ICP-MS element glass compositions of the of the proximal Aso units sampled between Aso-3 and the AT marker beds. **172**

Table 6.3: Summary of the Aso derived crypto-/tephra layers identified in the sediments of the Lake Suigetsu between 30–120 ka. **187**

Chapter 1: Introduction

This chapter introduces the need for refining the tephrostratigraphic records for volcanically active centres in densely populated regions and outlines the principles of tephrochronology. It is beyond the scope of this thesis to consider tephrochronology in its entirety, readers wishing to read further into the subject should refer to comprehensive reviews provided by Lane et al. (2017), Davies (2015), Lowe (2011) and Alloway et al. (2007). This chapter also introduces the study sites, which are located in Italy and Japan, and outlines previous work conducted in these regions as well as the motivation for this study alongside the research aim and objectives which will be addressed in the remainder of this thesis.

1.1 Volcanic hazards

Volcanic eruptions have had a fundamental influence on the Earth's evolution throughout its 4.54 Gyr history through their influence on landscape evolution and development of the atmosphere. The effects associated with volcanic eruptions (such as ash-fall, release of toxic gases and destructive lahars) pose significant risks to both the surrounding environments and the human populations existing within. Large explosive eruptions with a Volcanic Explosivity Index [VEI] (Newhall and Self, 1982) or Magnitude [M] (Pyle, 1995, 2000) ≥4 can affect the global climate ("volcano-climate impacts") through the injection of gases, aerosols and ash into the stratosphere (Aubry et al., 2022). Conversely, processes by which climate change affects volcanic processes ("climate-volcano impacts") through processes such as deglaciation (Hall, 1982; Rampino et al., 1979) or sea-level change (Matthews, 1968; Walcott, 1972) have also been hypothesised. However, the mechanisms for climate-volcano impacts require much further investigation (see Aubry et al 2022). Given the current rate and scale of anthropogenically driven climatic change (see IPCC, 2021), improving understanding of these complex interactions between climate and explosive volcanism have operated over long timescales (i.e. millennia) is fundamental to understanding the risk posed by future volcanism and thus improving the preparedness of populations for such event.

Understanding the level of volcanic risk is essential for populations living nearby highly active volcanic centres which can also result in major societal and economic disruption. Globally, over twenty-nine million people live within 10 km of active volcanoes, and approximately eight-hundred million people live within 100 km (Brown et al., 2014). Furthermore, many major urban areas are located near active volcanic centres which are capable of explosive volcanism, including Naples, Italy and the capital cities of Mexico, Japan and the Philippines which all have candidates to produce VEI 7 (caldera-forming) eruptions in future millennia (see Newhall et al., 2018). Given the proximities of large numbers of people globally and major cities located near volcanoes and the possibility of

caldera-generating eruptions signifies the need to perceive the risk these centres pose. Thus, understanding how these systems operate pre-, syn- and post-eruption is provides critical information fundamental to generating accurate hazard assessments. The instrumental record (since ca. 1815), including the recent advances in spatial and temporal coverage and resolution of spaceborne observations, has advanced our understanding of volcanic eruptions and the dispersal of volcanic ash and aerosols (e.g. Wilkins et al., 2016). However, the low recurrence rate of large explosive eruptions (e.g. 50 – 100 years for VEI 6; Newhall et al., 2018) means only a limited number have occurred during the instrumental period (e.g. 1815 Tambora, 1991 Mt Pinatubo). Furthermore, a statistical reanalysis of the Large Magnitude Explosive Volcanic Eruptions (LaMEVE) database (Crosweller et al., 2012) suggest that even less explosive events (VEI ≥4) are significantly under-recorded when considering time periods of hundreds-of-thousands of years (see Kiyosugi et al., 2015). The limited number and styles of eruptions and climatic variability over the last few centuries have constrained our ability to fully understand the range of eruption behaviours and their impacts on climate. By studying the stratigraphic records generated by successive eruptions over longer timescales (i.e. 10s – 100s kyr) allows us to gain a more comprehensive view of how systems which are capable of producing explosive volcanism have operated in the past (i.e. magma generation, ash dispersal, recurrence intervals) and thus better inform how they are likely to do so in the future (essential for the generation of accurate hazard assessments for nearby populations) and help addresses scientific hypotheses such as the role of climate on volcanic activity and vice versa.

1.2. Methods to reconstruct volcanic histories

Tephra, from the Greek word τέφρα meaning ‘ashes’, is defined as all the explosively-erupted, unconsolidated pyroclastic (fragmental) products of a volcanic eruption and thus encompasses all volcanological grain sizes: ash (<2 mm), lapilli (2 – 64 mm) and larger clasts and boulders (> 64 mm) (Lowe, 2011; Thorarinsson, 1944). Explosive volcanism (sub-Plinian/Plinian eruptions) is responsible for the widespread dispersal of volcanic ash (referred to as tephra throughout the remainder of this thesis), predominantly composed of volcanic glass, into medially (10 – 50 km) and distally (>50 km) located regions.

The ability to accurately identify the primary ash-fall within the region underpins the accurate reconstruction of eruption histories. Tephra generation and deposition are relatively instantaneous in geological time, and the resulting ash beds (tephra layers) preserved within sedimentary sequences (e.g. peat, ice and lake and marine sediments) represent these short-lived events. These tephras often stand out as distinctive horizons within sedimentary

sequences due to their colour and grain-size. The colour of a tephra is linked to the eruption type, geochemistry of the tephra and volcanic system it results from. For example, basaltic tephra has lower silica content (45 – 51 wt.% SiO_2) and results in a black or dark grey coloured tephra, (e.g. Hekla DH tephra, Iceland; Gudmundsdóttir et al., 2011) whilst tephras that are pale or whiter in colour reflect a higher silica content (>70 wt.% SiO_2) (e.g. Minoan eruption, Santorini; Druitt et al., 2007). Similarly, the grading (variation in particle size within a deposit) and sorting (uniformity of particle sizes) of tephra units are indicative of the energy of the eruption, distance from the vent, and the transport processes (see: Bonadonna and Houghton, 2005; Sparks 1992). Thus, the physical properties of tephra layers can provide valuable insights into past volcanic eruptions and the environmental conditions at the time of deposition.

The instantaneous deposition and incorporation into sedimentary sequences over vast geographical areas mean tephra layers can be an incredibly useful isochronous markers to correlate records (tephrostratigraphy) (Lowe et al., 2008; Pyle et al., 2006; Machida and Arai, 2003). Tephrostratigraphy, like any stratigraphy, is underpinned by the Law of Superposition, which applies to any study that connects or correlates deposits in one place to those at another. Correlating records on visual and morphological properties alone is often not reliable, and certainly cannot be done over large distances as the characteristics (e.g., grain-size and thickness) change considerably (Pyle, 1989). For instance, tephra grain size reduces as distance increases from the volcanic vent and away from the axis of fallout, as larger grains are unable to be transported the same distance as smaller grains (Pyle, 1989). The characterisation of tephras, both visually by physical properties (i.e. mineralogical examination by optical microscopy) and through laboratory analyses (e.g. geochemical analysis of glass shards or loose mineral grains) is fundamental to the accurate identification, and thus correlation, of tephra layers.

Tephra studies rely on the geochemical characterisation of the glass shards within the tephra deposits to decipher their compositional geochemical “fingerprint”. The major and trace element composition of volcanic glass shards are determined by the source magma composition, the degree of partial melting, fractional crystallisation, magma mixing, crustal assimilation, degassing and the eruptive processes that influence cooling and quenching (Sparks, 2003). Thus, the geochemical composition of glass shards (a component of tephra where magma rapidly fragments) erupted reflects the structure and composition of the magma from which it formed and thus it is possible to identify the volcanic source and provide detailed geochemical characteristics for individual tephra layers. By analysing the elemental compositions of volcanic glass shards and establish distinguishing geochemical

features of specific tephra layers, it has been possible to correlate sites across vast geographical areas (Matsu'ura et al., 2011; Smith et al., 2011a). Ultimately, the ability to geochemically characterise tephra deposits have meant the utilisation of tephra layers has become a powerful correlation tool in Quaternary research (Lowe 2011; Alloway et al., 2007; Shane 2000).

A variety of analytical techniques are employed to geochemically characterise tephras. Bulk rock analysis (typically analysed using techniques like X-ray fluorescence (XRF)) was relied upon by early tephra studies (e.g., Lowe, 1988; Thorarinsson 1944). Bulk rock analysis involves examining the whole-rock composition of tephra deposits (provide an average composition for the clasts) rather than focusing on individual glasses/minerals.This analytical technique is problematic for compositionally bi-modal (heterogenous) tephra deposits as the average composition will not be representative of the magma compositions at the time of the eruption (Balascio et al., 2015; Francus et al., 2009). Heterogeneity within a deposit may arise due to variable proportion of phenocrysts and lithic material within juvenile (i.e. magmatic) component of the tephra (Ukstins and Peate et al., 2008). Thus, the identification of compositional heterogeneity is essential to ensure robust correlations between sedimentary sequences, particularly where this is diagnostic of a specific eruption (e.g. Alloway et al., 2017; Abbott et al., 2016; Pearce et al., 2014; Westgate et al., 2013; Tomlinson et al., 2012; Shane et al., 2008). For example, the whole rock analyses of the Upper and Lower Pumice eruptions of Nisyros, Greece, mask the compositional variation between the two eruptions (see Tomlinson et al., 2012). Consequently, single grain analytical techniques are favoured as they allow individual volcanic glass shards to be analysed, which can have distinct chemical compositions within the same tephra layer (e.g. Smith et al., 2013; Tomlinson et al., 2012; Shane et al., 2000, 2008; Hunt and Hill, 2001). Two single-grain analytical techniques are now commonly employed:

i) Electron Microprobe Analysis (EMPA) to determine the major and minor element compositions (elements with abundances that are typically >0.1 wt.%).
ii) Laser Ablation Inductively Coupled Plasma-Mass Spectrometry (LA-ICP-MS) for trace element compositions.

EMPA is routinely used to determine the major-element composition of individual glass shards and is the key technique for quantifying the major and minor element compositions of tephras (Turney et al., 2004; Hunt and Hill, 1993). This analysis is typically undertaken using Wavelength Dispersive Spectroscopy-Electron Microprobe Analysis (WDS-EMPA), but it can also be undertaken using Electron Dispersive Spectroscopy-Scanning Electron Microscopy (EDS-SEM). The accuracy of WDS-EMPA can reach ±1 % (relative) for major elemental

analysis and detection limits down to tens of parts per million (by weight) can be obtained, which is considerably better than analysis via EDS-SEM (Goldstein et al., 2017). The higher degree of precision and accuracy afforded by WDS-EMPA allows for detailed geochemical fingerprinting of tephra layers, crucial for tephrochronology and correlation (Lowe, 2011; Hunt and Hill 1996; Westgate and Gorton 1981). Thus, EMPA is the most employed technique to quantitatively analyse the major element composition of tephra deposits (e.g. Hopkins et al., 2021; Albert et al., 2019b; Tomlinson et al., 2014, 2015; Pyne-O'Donnell, 2012).

While EMPA is the widely accepted and routine technique for fingerprinting determining the elemental composition of tephras, there are several challenges and limitations associated with this approach. A significant issue with using major element glass geochemistry is the challenge of inter- and intra-laboratory comparisons. Differences in operating setups can often affect the accuracy of results and thus, make it difficult to compare data as compositional differences between glass shards from individual eruptions are often only subtly different (e.g. Kuehn et al., 2009; Larsen and Eriksson, 2008; Westgate et al., 2008). Variations in calibration procedures, instrument settings and analytical protocols can lead to discrepancies in the reported compositions of volcanic glass and minerals, thus potentially affecting tephra correlations (Kuehn et al., 2011). The International Focus Group on Tephrochronology and Volcanism (INTAV) of the International Union for Quaternary Research (INQUA) has been integral in standardising and refining sample collection, geochemical analysis and data reporting to ensure consistency and reliability across tephra laboratories (see Kuehn et al., 2011). Moreover, even if the analytical conditions outlined by INTAV are adhered to, the precision of EMPA is not always sufficient to differentiate deposits on the basis of major-element compositions. Successive tephras from the same volcanic source and from closely spaced systems can erupt glasses have similar chemical signatures which cannot be distinguished using EMPA alone (e.g. Jensen et al., 2014; Pearce et al., 2004).

Magmatic processes produce a wider variability in trace elements than major elements and thus provides additional information on petrogenesis. Trace element composition is more strongly controlled by subtle variations in source composition and by magmatic processes (Lowe et al., 2017). This has been exploited by Laser Ablation Inductively Coupled Plasma-Mass Spectrometry (LA-ICP-MS) to enable discrimination between glasses which exhibit similar major-element geochemical compositions (e.g. Pearce et al., 2014, 2007; Westgate et al., 2013; Tomlinson et al., 2010; Allan et al., 2008). The application of grain-specific trace element analyses is increasingly employed in tephra studies to assess its

potential as a tool to geochemically distinguish tephras and robustly test proximal-distal correlations (Tomlinson et al., 2010, 2012; Kuehn et al., 2011; Smith et al., 2011a; Pearce et al., 2004, 2007)

Once the stratigraphic, physical and geochemical properties of a tephra are determined, the next challenge is to establish the age of the volcanic deposit. Where an age can be assigned to a tephra horizon, this offers a powerful dating tool in establishing a precise chronological framework for geological, climatic, and archaeological events and understanding of the timing and impact of volcanic eruptions. An age for tephra layer can be obtained (tephrochronology) through a variety of methods. Commonly employed radiometric techniques include the radiocarbon (^{14}C) dating of associated organic macrofossils (e.g., Plunkett et al., 2016), zircon double dating (i.e. the combined use of U-Pb geochronology and (U-Th)/He thermochronology to determine both crystallisation and cooling histories; e.g., León et al., 2021; Danišík et al., 2017, 2020) and by $^{40}Ar/^{39}Ar$ (e.g., Mark et al., 2014). However, such techniques rely on the abundance of minerals within the deposits that are suitable for such dating techniques (i.e. K-rich mineral phases such as sanidine and orthoclase in the case of $^{40}Ar/^{39}Ar$ dating, and organic material for radiocarbon dating), which are not always readily available in sedimentary archives. Nevertheless, $^{40}Ar/^{39}Ar$ dating has been successfully applied to products of highly potassic explosive eruptions such as those from Ulleungdo, South Korea (e.g. Smith et al., 2011a) and Campania (e.g. Monaco et al., 2022; Deino et al., 2004; De Vivo et al., 2004). Precise ages for eruptions have been afforded by indirect dating methods for sedimentary archives that have detailed age models (e.g., OxCal Bayesian age-models; Bronk Ramsey, 2008, 2015; Lane et al., 2011), and/or are underpinned by incremental chronologies (e.g., annually laminated varves (Lane et al., 2015; Tomlinson et al., 2015; Wutke et al., 2015; Smith et al., 2013; Blockley et al., 2007; Wulf et al., 2004) or annual layer counting in ice cores (Davies et al., 2007)). The age of the tephra can then be transferred to any sequence that contains the same volcanic deposits and in this way, tephrochronology is an age-equivalent dating method.

Whilst there is no temporal limit to the application of tephrochronology, it is limited and ruled by the magnitude and frequency of the eruptions and nearby volcanic centres. The style and the strength and direction of prevailing winds at the time of the eruption have been known to restrict the spatial extent of tephra following a volcanic eruption (e.g. Carey and Sparks, 1986). Near-vent (proximal; <10 km) tephra records are often incomplete due to factors related to the dynamic and hazardous environments close to volcanoes syn- and post-eruption. For instance, the area near the volcanic vent is subject to intense erosional forces (e.g. heavy rainfall, lahars and pyroclastic-flows) and tectonic activity, which can

rapidly erode and rework freshly deposited tephra, as well as burial by subsequent eruptions which can disturb or completely remove earlier tephra deposits, leading to gaps or disturbances in the stratigraphic record (e.g. unconformities). These factors make near-vent tephra records incomplete and has resulted in a fragmented understanding of their eruption histories.

Methodological developments have enabled the isolation of non-visible (<125 μm) tephra deposits (cryptotephra; from the Greek word *kryptein* meaning 'to hide') with glass shard concentrations that do not form a clear macroscopic layer. Distally located sites have the potential to provide accessible, tephra records that have not been subjected to the same preservation issues as at proximal locations. The smaller size of cryptotephra enables them to be transported over great distances, thus expanding the application of (crypto)tephrochronology to increasingly distal located sedimentary archives (see Fig. 1.1).

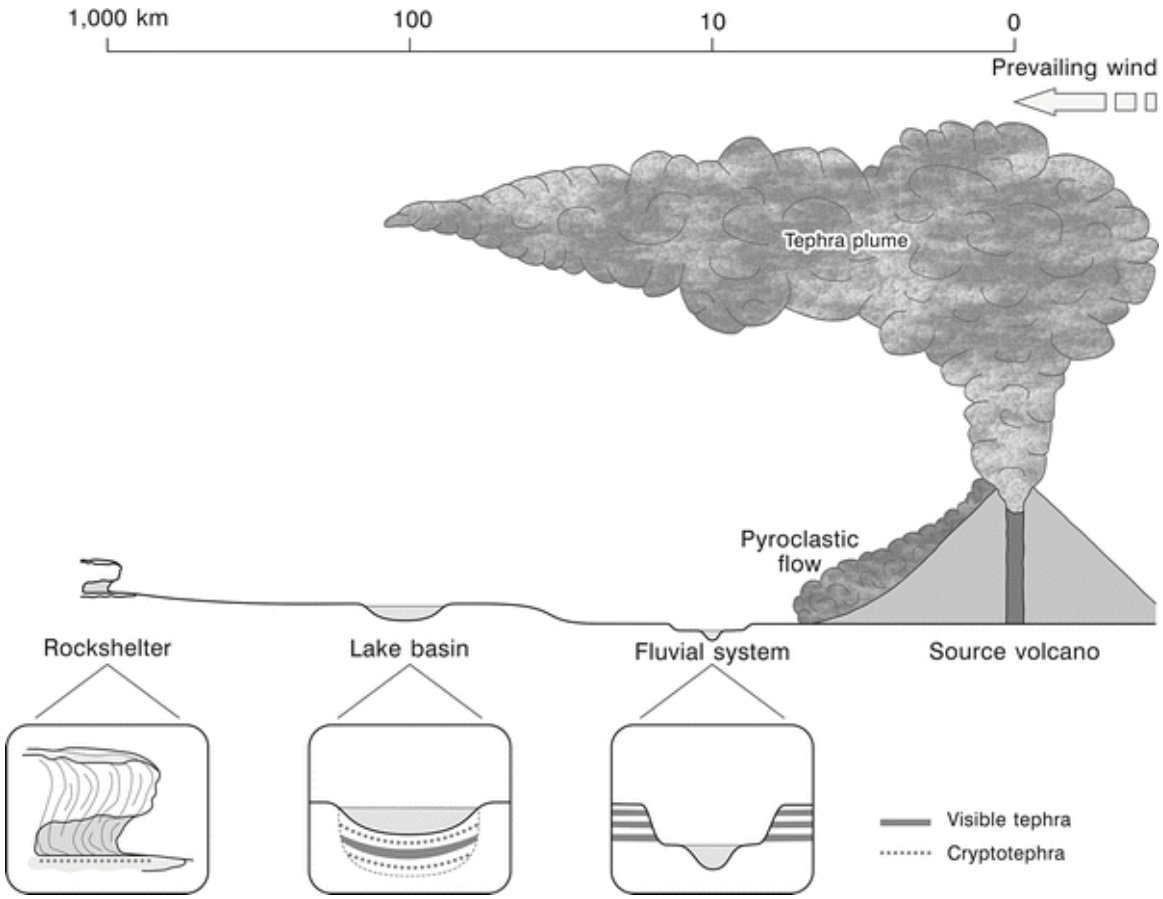


Figure 1.1: A schematic illustration of distal tephra dispersal and deposition in a Quaternary landscape downwind of a volcanic centre where three major explosive eruptions have taken place. Taken from Lane and Woodward (2017).

The ability to accurately identify and precisely locate volcanic glass shards within a sedimentary sequence is fundamental to cryptotephra studies. Methodologies for detecting cryptotephra deposits, of which there are several, can be sub-divided into destructive and non-destructive techniques. Conventional laboratory methods for detecting cryptotephra glass shards, whereby the shards are extracted from the host sediments, are often destructive. Early studies removed organic material by ashing or by acid digestion of the sediments (van den Bogaard and Schmincke, 2002; Dugmore et al., 1992). Whilst ashing and chemical digestion afford high shard retrieval rates, the high temperatures required and chemicals involved in these treatments can compromise the geochemical composition of the shards (see Blockley et al., 2005) leading to potential problems characterising the shards based on geochemical correlations. Utilising heavy-liquid density-separation, involving several stages of heavy liquids (e.g. sodium polytungstate, SPT; Blockley et al., 2005), has proven to be an effective, and crucially, less-destructive way to extract the volcanic glass shards from the lighter (typically organic) and denser (minerogenic) components of the sediment matrix (e.g. Blockley et al., 2005; Turney 1998). Density-separation has become the standard extraction technique in cryptotephra studies as it allows for the primary positioning of the cryptotephra peak (i.e. the eruption event) to be identified and no physical or chemical alteration to the glass shards (see: Davies et al., 2007; Blockley et al., 2005; Turney et al., 2004; Hall and Pilcher, 2002; Turney, 1998).

Unlike methods for extracting, quantifying and chemical characterisation of cryptotephras, the sampling resolution and the methods by which horizons are prioritised for geochemical analyses have not undergone progressive refinements to procedures. The most common technique to locate a horizon of cryptotephra is to scan the sedimentary sequence at low-resolution (i.e. 5 – 10 cm), to approximate the peak shard concentration, before a refinement at a higher resolution (typically 1 cm) to more precisely locate the position of the isochron (e.g. Albert et al., 2024; McGuire et al., 2022; McLean et al., 2018; van der Bilt et al 2017; Lane et al., 2014). As such, the sampling resolutions and the resultant segment favoured for geochemical analysis remain ad hoc and subjective.
In an attempt to overcome this issue, a contiguous sampling strategy for entire sedimentary sequences has recently been advocated for (see Timms et al., 2018). Such high-resolution sampling (1 cm or higher) of sedimentary records located across Scotland have provided a more coherent and complex narrative to the history of volcanic events deposited during the last glacial-interglacial transition (e.g. Timms et al., 2017; Matthews et al., 2011; MacLeod, 2008). However, for longer records (spanning over 100 kyr) in volcanically active centres where background shard concentrations are considerably higher than those in Scotland (e.g. Albert et al., 2024; Martin-Jones et al., 2024; McGuire et al., 2022; Chen et al., 2019;

McLean et al., 2018; Wulf et al., 2018), this sampling strategy will be incredibly time- and resource-consuming.

Given the lower shard retrieval rates by stepped density extraction method compared with other destructive method (i.e. ashing and acid digestion) and the destruction of significant amounts of core material, studies which employ this standard extraction procedure typically target sections of long sequences to identify potential cryptotephra horizons (e.g. Albert et al., 2024; van der Bilt et al., 2017; Blockley et al., 2015). Thus, a major focus of current efforts is on increasing the speed at which entire sequences can be analysed without compromising the geochemical composition of the volcanic glass shards. Non-destructive techniques such as micro X-ray fluorescence (μXRF) facilitate continuous scanning of sediment cores, allowing whole sedimentary sequences to be scanned and are thus much less time and resource consuming. μXRF has been effective in identifying thick, visible ash layers preserved in marine and lacustrine records (e.g. McCanta et al., 2015; Kylander et al., 2011; Lim et al., 2008). However, μXRF routinely under-reports (typically only 10% of cryptotephras) when compared with conventional laboratory extraction methods (e.g. McLean et al., 2022; Gehrels et al., 2008). McLean et al. (2022) revealed for the cryptotephras μXRF detected it was possible to refine their stratigraphic position from 1 cm to >1 mm, improving the precision of the positions and thus modelled ages of isochrons and can help discriminate remobilisation (e.g. reworking; see below) events. As yet, μXRF core scanning should not be used as an independent method for detecting cryptotephra deposits but can provide a powerful tool when used in conjunction with traditional density extraction techniques (McLean et al., 2022).

Reworking of glass shards from their primary deposition to another stratigraphic position within the sedimentary sequence (vertical dissemination) can complicate stratigraphic interpretations as it can create an "apparent" tephra layer that isn't contemporaneous with surrounding sediments. This reworking may result from post-depositional processes bioturbation, sedimentary processes (e.g. freeze-thaw cycles) or groundwater movement, all of which can transport shards within the sediment column (e.g. Pyne-O'Donnell et al., 2012; Beierle and Bond, 2002). Careful stratigraphic and sedimentological analysis (along with examining shard morphology and geochemical analysis) can help identify primary versus reworked cryptotephra deposits within a sedimentary sequence (e.g. McLean et al., 2018). The identification of a sharp discrete peak in shard concentration profiles is indicative of a rapid input, reflecting the exact timing of the volcanic eruption and the position of the isochron. In contrast, a more diffuse peak or multiple peaks closely spaced together are both indicators of vertical dissemination of shards

(see Davies, 2015). Peaks in shard concentrations can result from high-energy events (e.g. flood events and earthquakes) and will typically incorporate volcanic glasses from several older eruptions, meaning the shards will often consist of several morphologies, sizes and geochemical affinities (Fig. 1.2). This highlights the due diligence that must be undertaken when identifying discrete cryptotephra isochrons within sedimentary sequences including a comprehensive understanding of local catchment conditions alongside the relative timing of the inputs when working with lacustrine sequences (Davies, 2015). Ultimately, peaks in volcanic glass concentrations are considered to be a primary tephra if the shards possessed a consistent morphology, size and geochemical affinity that was different from the known background compositions (Fig.1.2; McLean et al., 2018).

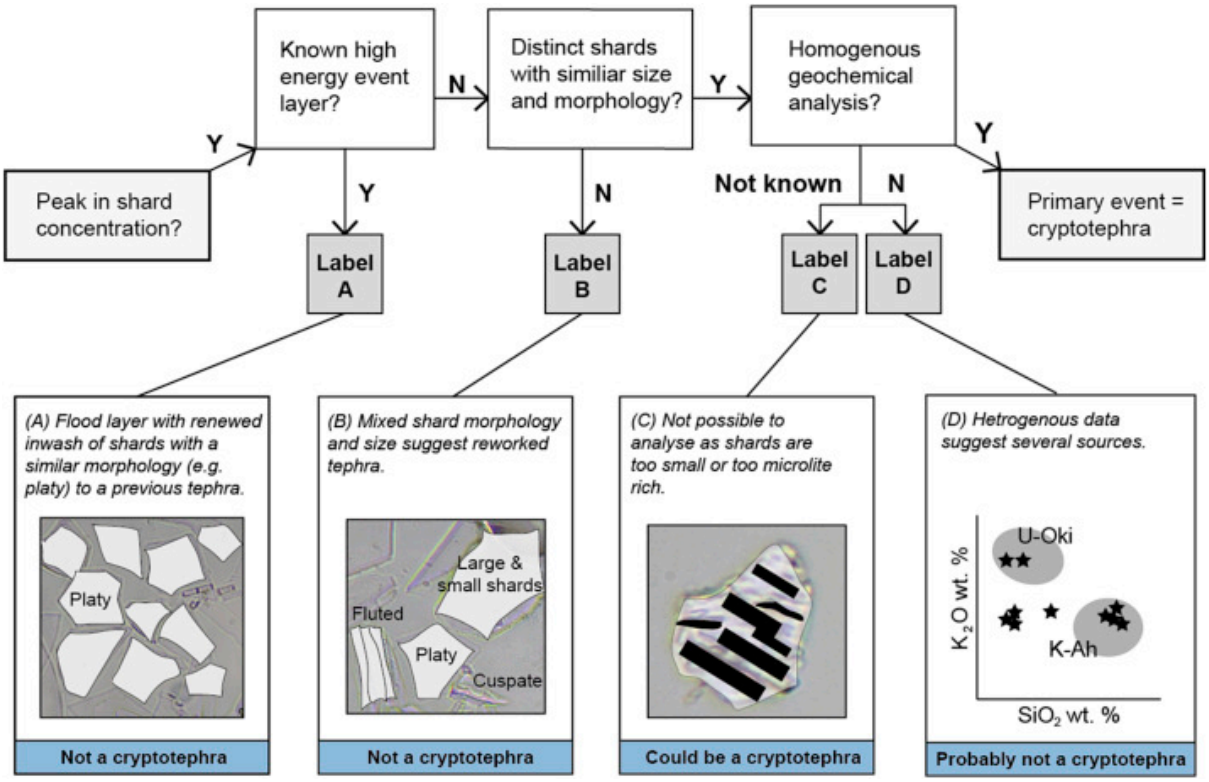


Figure 1.2: Criteria used to decipher primary ash-fall events within the Lake Suigetsu sedimentary sequence (Y = yes, N = no). Peaks in glass concentration that fail these criteria and unlikely to reflect a primary event. Taken from McLean et al. (2018).

Studying more distally located sedimentary sequences (such as marine, lacustrine and ice cores) can reveal previously unknown eruptions, especially those from volcanoes that are not well-studied or have inaccessible proximal deposits. For example, Campi Flegrei, Campania Italy, has been volcanically active for 200 ka but details for eruptions are only well constrained for the last 15 kyr (e.g. Smith et al., 2011a). This has limited understanding of eruptive history of Europe's most active volcano. The high-resolution Lago Grande di Monticchio sequence spans 135 kyr, situated 125 km east of Campania, has

revealed more information regarding the magnitude and tempo of past volcanism (e.g. Tomlinson et al., 2014; Wulf et al., 2004, 2012) as well as establishing direct correlations with other records on the basis of tephrostratigraphy (e.g. Di Roberto et al., 2018; Sulpizio et al., 2010). However, the potential for tephras to become emplaced in sedimentary archives is influenced by the rate of sedimentation as well as taphonomic processes (Davies, 2015; Pyne-O'Donnell et al., 2008). Furthermore, the full compositional range of an eruption may not always be identified in distally located tephras. This is primarily due to melts of different eruptions often not being erupted simultaneously, which may coincide with changes in wind direction and thus dispersal patterns (e.g. Schmincke et al., 1999). The paucity in the characterisation of proximal tephras can lead to issue in identifying potential correlatives between archives, especially for those distally located (e.g. Larsen and Eiríksson, 2008).

1.3. Tephrostratigraphic frameworks

Identifying co-located isochrons within archives across a geographic region allows the integration of independent tephrostratigraphic records to form a network of sites that are bound by co-located markers, known as tephrostratigraphic frameworks (also referred to as lattices). The most detailed and well-known of these being the event stratigraphy for the North Atlantic generated by the International Working Group INTIMATE (INTegration of Ice-core, Marine and TErrestrial records; Blockley et al., 2012, 2014; Lowe et al., 2008). As part of further crypto-/tephra investigation of sedimentary sequences across Europe as part of the RESET ('Response of Human to Abrupt Environmental Transitions') project has enabled the tephrostratigraphic framework to integrate and synchronise chronologies of significant archaeological and environmental sites at the regional scale (see Fig. 1.3). The continual expansion of both tephra and cryptotephra studies (both in number and of their reach into new geographical regions; see Lane et al., 2017) has led to the development of further regional tephrostratigraphic frameworks (e.g. Abbott et al., 2018; Fontijn et al., 2016; Mackay et al., 2016; Nakamura, 2016; Bourne et al., 2015; Lowe et al., 2015; Blockley et al., 2014; Davies et al., 2014). By identifying co-located isochrons within archives across a region, these frameworks are able to:

i) Incorporate new and lower magnitude events;
ii) Help resolve the stratigraphic positioning of eruptions closely spaced in time;
iii) Constrain chronologies;
iv) Improve understanding of the number, style and frequency of eruptions;
v) Establish which eruptions have a diagnostic geochemical signature and geochemical databases can be furnished with data;
vi) Extend the known geographical footprint of ash fallout from individual eruptions.

Tephrostratigraphic frameworks are typically underpinned by key reference sites (refreered to as tephrostratotypes) which offer both tephrostratigraphic sequences and a precise chronology of eruptive events (e.g. the Greenland ice cores; Cook et al., 2022; Bourne et al., 2015; Abbott et al., 2012). For example, the discovery of the B-Tm tephra in the Lake Suigetsu record, Japan has created a direct tie-point between this mid-latitude paleoclimate archive and the Greenland ice cores, as well as other key paleoenvironmental archives in Japan and China (see McLean et al., 2016).

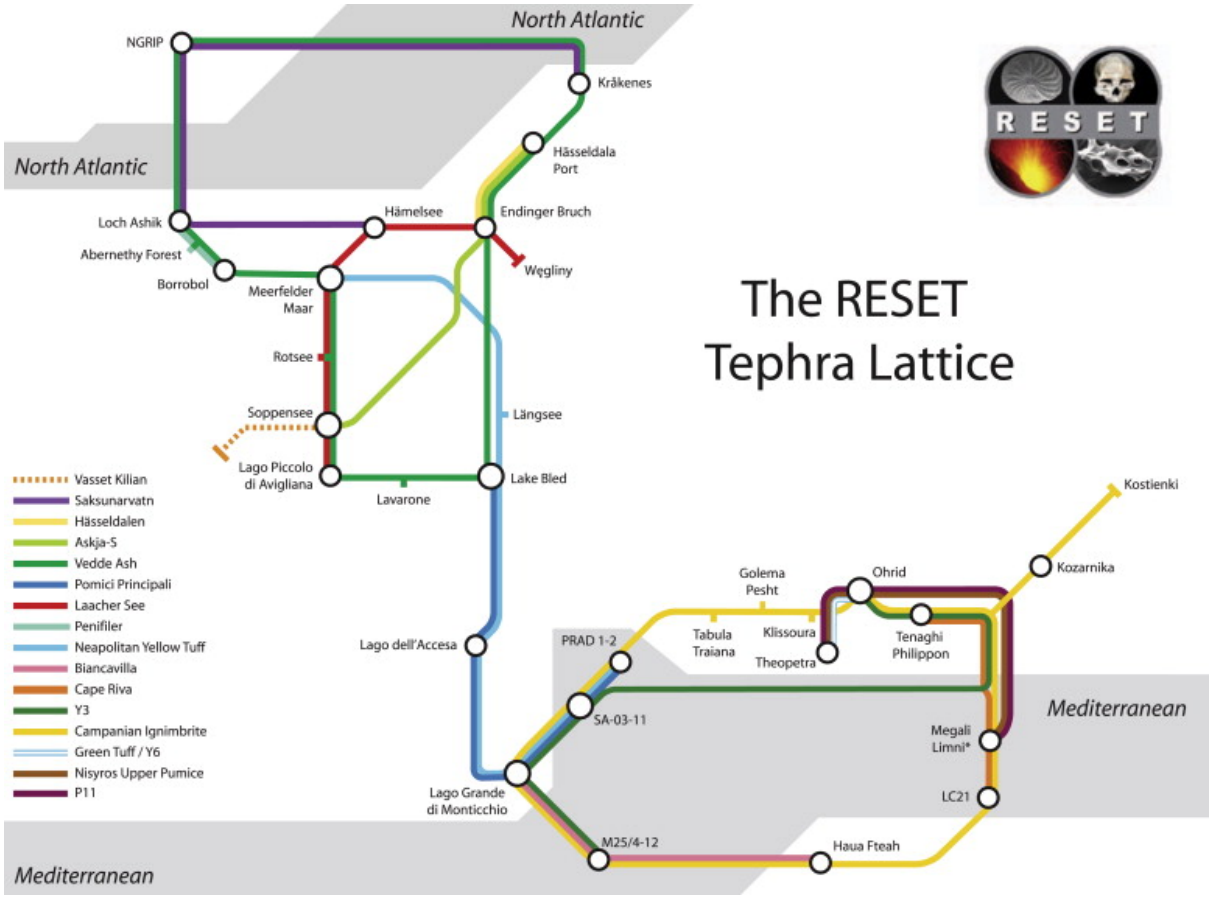


Figure 1.3: A schematic representation of the RESET ('Response of Humans to Abrupt Environmental Transitions') tephrostratgraphic framework, also known as a lattice, which shows the sedimentary archives in Europe and the Mediterranean that can be precisely correlated using co-located isochrons. Taken from Lowe et al. (2015).

1.4. Study sites and previous regional tephra studies

This section outlines the context and background for the research presented in this thesis before presenting the study sites selected to address the research gaps outlined that

are relevant to Chapters 4 – 6. The Campanian section below (Section 1.4.1.) relates to Chapter 4 whilst the Japanese section (Section 1.4.2) relates to Chapters 5 and 6.

1.4.1. Campania, Italy (relevant to Chapter 4)

The densely populated city of Naples, the regional capital of Campania, is the third-largest city of Italy and is a prime example of a high-risk volcanic area. The city itself is located between two active volcanoes (Campi Flegrei and Somma-Vesuvius) and is close to a third active volcano (the island of Ischia), as well as the monogenetic Procida volcano (see Fig. 1.4). Campi Flegrei, Ischia, Procida, and Vesuvius are all part of the Campanian Volcanic Zone (CVZ) in southern Italy and are influenced by the subduction of the African plate beneath the Eurasian plate. Campi Flegrei is the most productive volcano in central Europe, including enormous caldera-forming events: Campanian Ignimbrite (CI), 39.85 ± 0.14 ka, $^{40}Ar/^{39}Ar$ (Giaccio et al. (2017), Masseria del Monte Tuff (MdMT) at 29.3 ± 0.7 ka $^{40}Ar/^{39}Ar$ (Albert et al., 2019b) and the Neapolitan Yellow Tuff (NYT) at 14.90 ± 0.4 ka, $^{40}Ar/^{39}Ar$ (Deino et al., 2004). The island of Ischia is the most westerly of the CVZ volcanoes and is thought to represent the remnants of a larger volcano (Orsi et al., 2004), and at least one caldera collapse is attributed to the Monte Epomeo Green Tuff (MEGT) eruption at 56 ka (Brown et al., 2007; Buchner et al., 1996; Civetta et al., 1991; Orsi et al., 1991). Together with surrounding towns and villages, the city of Naples has been growing between these volcanoes (Orsi et al. 2003). Thus, it is imperative that detailed tephrostratigraphic records are compiled to gain a holistic understanding of the potential volcanic risk to the highly populated region of Campania.

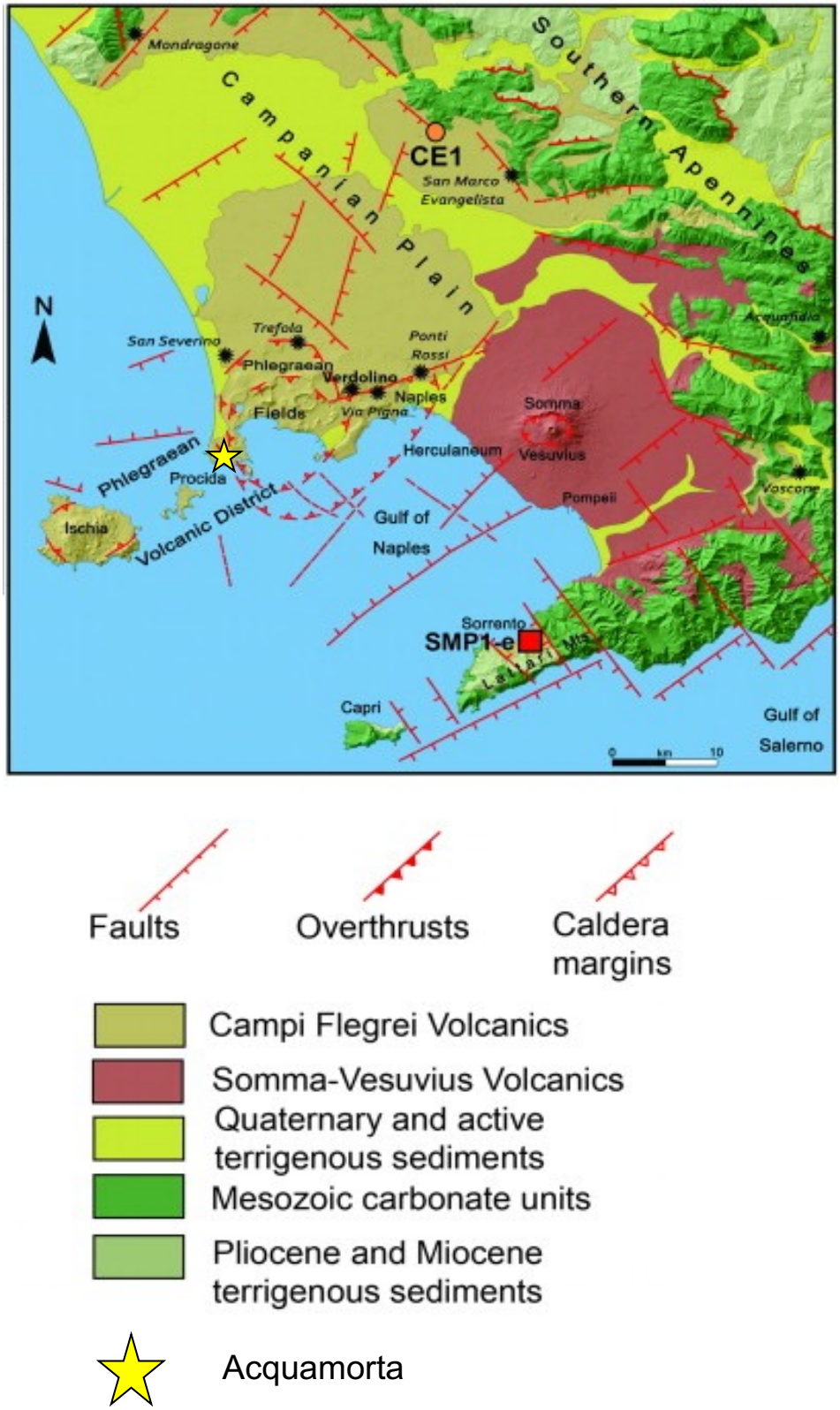


Figure 1.4: The volcanoes in the Campanian volcanic zone, Campi Flegrei, Somma-Vesuvius and Ischia, and the location of the Acquamorta site in relation to the caldera walls of Campi Flegrei. Adapted from Tomlinson et al. (2012).

Distinguishing the volcanic deposits of the different CVZ volcanoes using glass chemistry has proved challenging owing to their similar geochemical compositions (see Tomlinson et al., 2015). Furthermore, successive eruptions from the same volcanic centre are often incredibly similar in composition (e.g. Smith et al., 2011a; Pabst et al., 2008) which may result in erroneous correlations between sequences and further heightens difficulties in generating detailed tephrostratigraphies of the CVZ. Whilst differentiating CVZ sources can be challenging due to geochemical similarities, SiO_2 vs. CaO, CaO vs. Na_2O/K_2O and CaO vs. MgO plots and CaO/FeO_t and Cl elements are useful for discriminating individual CVZ centres (Fig.1.5; Tomlinson et al., 2015). The large (VEI/M 6) eruptions of the CI (e.g. Giaccio et al., 2017; Smith et al., 2016; Tomlinson et al., 2012) and MdMT (Albert et al., 2019b) from Campi Flegrei, and the Schiappone and MEGT from Ischia (Tomlinson et al., 2014) tend to tap multiple, relatively homogeneous magma batches. Compositional shifts are seen at Campi Flegrei following the CI eruption (Tomlinson et al., 2012; Di Renzo et al., 2011; Arienzo et al., 2009; Pabst et al., 2008; D'Antonio et al., 2007; Pappalardo et al., 1999), and at Ischia following the eruption of the MEGT (Tomlinson et al., 2014; Brown et al., 2008; Civetta et al., 1991).

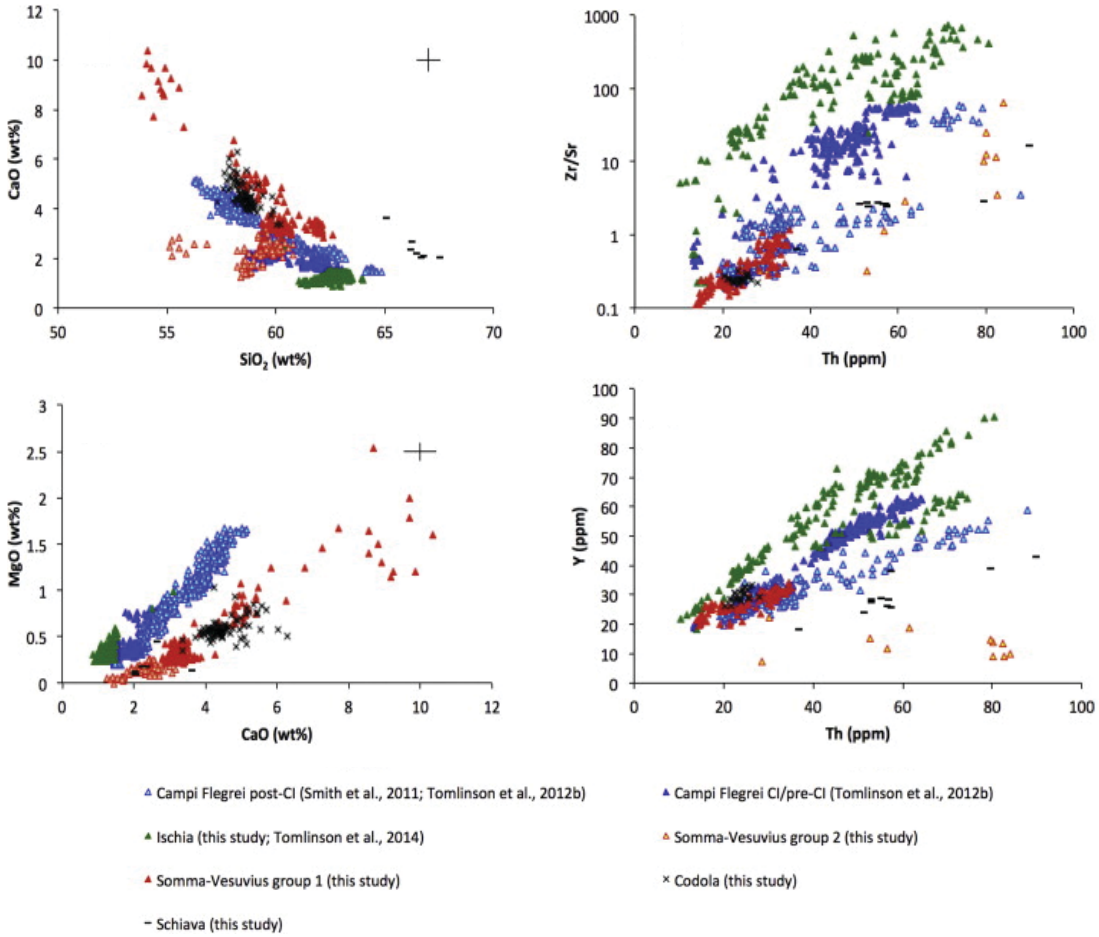


Figure 1.5: Major (SiO_2, CaO, MgO) and trace (Zr/Sr, Y, Th) element glass compositions of large magnitude CVR eruptions obtained (last 40 ka) from near source (proximal) deposits (from Tomlinson et al., 2015). Error bars on plots represent repeat analysis of MPI- DING StHs6/80-G. Figure adapted from Tomlinson et al., 2015.

The high frequency of explosive volcanic activity in the CVZ during the Late Quaternary has made tephra layers particularly powerful chronological and correlation tools across the Mediterranean region (e.g. Giaccio et al., 2008; Wagner et al., 2008; Pyle et al., 2006; Wulf et al., 2004; Fedele at al., 2003; Schmidt et al., 2002). As mentioned, the CI eruption at 39 ka (the Y5 layer in marine cores; Ton-That et al., 2001; Thunell et al., 1979) is the largest eruption in Europe for the last 200 kyr and has been traced over an area of about 5,000,000 km^2, comprising of the whole central and eastern Mediterranean basin (Giaccio et al., 2008; Pyle et al., 2006) and has been identified in sediment cores thousands of kilometres away in northern Africa (Smith et al., 2016; Costa et al., 2012; Lowe et al., 2012; Fedele et al., 2003) and Russia (Pyle et al., 2006 and references therein). As such, the CI has become a powerful tool for assessing the age and environmental context of archaeological sites in south-east Europe (e.g., Lowe et al., 2012; Giaccio et al., 2008; Pyle et al., 2006; Fedele et al., 2003). Similarly, the NYT at 15 ka is a useful isochron across the Mediterranean and found over a vast geographical area and found in both marine (e.g.

Calanchi et al., 1998; Paterne et al., 1988) and terrestrial archives (e.g. Lane et al., 2015; Morley and Woodward, 2011). In addition, volcanic ash of some post-15 ka eruptions are found as visible layers in many paleoclimate archives e.g., Lago Grande di Monticchio (LGdM), Italy (Wulf et al., 2008), Lake Bled, Slovenia (Lane et al., 2011), and the Adriatic Sea (Albert et al., 2012; Bourne et al., 2010; Siani et al., 2004). The ability to integrate archaeological and paleoenvironmental archives which are distributed over large geographic areas, using key isochrons originating from the Campi Flegrei volcano highlights the potential for tephrochronology in this region.

Whist many stratigraphical, volcanological and petrological studies have been undertaken on these two most powerful Phlegraean eruptions (CI and NYT) and those post-dating them (e.g. Smith et al., 2011a), research into pre-40 ka sections is more limited as sequences located in medial and proximal locations are often buried underneath large tephra deposits (Fig. 1.6). Nevertheless, distal and proximal records allude to explosive activity pre-dating the CI eruption (see Fig. 1.6); albeit an incomplete eruptive history record. Detailed stratigraphic logging of exposures around the Campi Flegrei calderas by Orsi et al. (1996) revealed complex eruption sequences. Tentative correlations have been made between proximal and medial sequences based primarily on physical description (Orsi et al., 1996) and limited whole rock geochemical data (Pappalardo et al., 1999). The lack of glass geochemical data for all the units prevents robust correlations to volcanic sources as well as between archives and thus, limits understanding regarding the magnitude, tempo and dispersal of past volcanic eruptions in the CVZ.

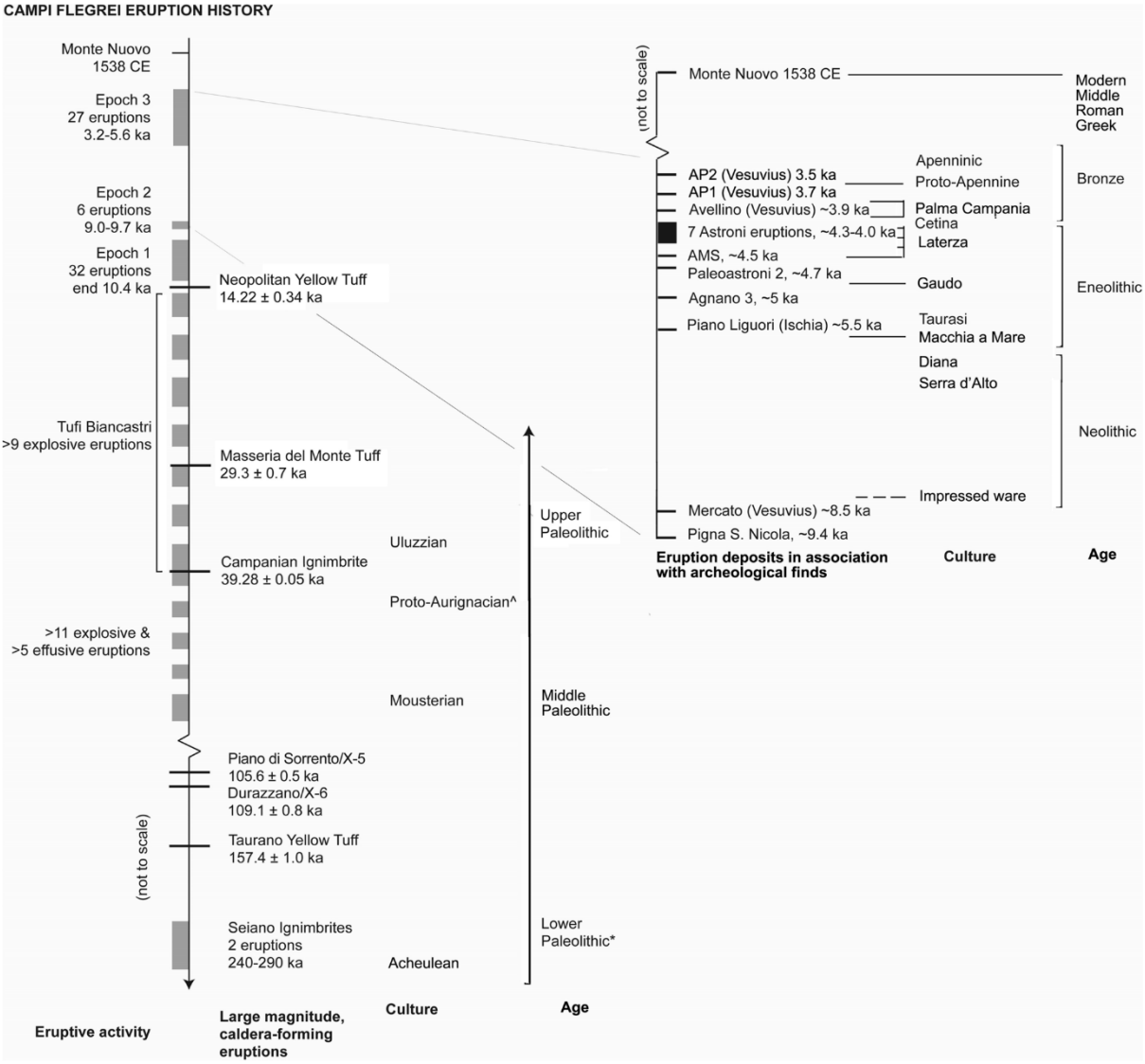


Figure 1.6: The eruption history of Campi Flegrei and the cultural occupations (last 10 ka; right) in and around the Campanian region. Taken from Costa et al. (2022)

More distally located sedimentary sequences have provided further insights into the CVZ volcanoes prior to caldera-generating eruptions. The occurrence of varves within the Lago Grande Monticchio (LGdM) sediments, situated 125 km east of Campi Flegrei, gives tight chronological control of the record (spanning the past 135 ka) and thus has been the focus of intense studies or paleoclimatic reconstruction (e.g. Watts, 1985; Watts et al., 1996). Critically, the tephrochronological investigations of this archive have shown that the LGdM cores are a valuable record of explosive volcanism in Italy (see: Wutke et al., 2015; Wulf et al., 2012, 2004). The recent identification of another Campi Flegrei caldera-forming eruption (Y3) at ca. 30 ka BP in the LGdM sediments (Albert et al., 2019b) has further highlighted the role of distal stratigraphy in constraining the tempo of past volcanic activity in highly productive regions. Furthermore, unreported tephra deposits have been identified within the LGdM archive which have been correlated with volcanoes across the CVZ,

including numerous Campi Flegrei eruptions pre-dating the 40 ka CI eruption (Wutke et al., 2015; Wulf et al., 2004, 2012). Other lacustrine records allude to CVZ activity in the lead up to the CI: Fucino, 130 km north of Campi Flegrei, contains one tephra layer preserved between the MEGT and CI (Giaccio et al., 2017), whilst the Tenaghi Philippon sequence on mainland Greece, 675 km east of Campi Flegrei, contains six cryptotephra deposits preserved within the 1.25 m sediments beneath the CI (Wulf et al., 2018). However, correlations for these eruptions have been limited by the lack of grain-specific glass analyses of proximal tephras which are fundamental for robust proximal-distal correlations. Smith et al. (2011) have demonstrated the capacity for improved geochemical databases for younger sections (<15 kyr) through detailed characterisation of proximally located tephra units. Thus, detailed stratigraphic and geochemical characterisations for older sections (pre-40 ka) of proximal outcrops across Campania are required for the full potential for tephra layers to be realised in this region.

1.4.2. Japan (Chapters 5 and 6)

The East Asia/Pacific region is home to over 30% of the global population (Ha et al., 2012; Cook et al., 2010) and the location of a high concentration of volcanoes (Fig. 1.7). Across the islands of Japan, there are over 130 volcanic centres which are known to have been active during the Late Quaternary (Crosweller et al., 2012; Machida and Arai, 2003); some of which have produced several of the largest magnitude volcanic eruptions over the last 200 kyr (Newhall et al., 2018). Several nuclear power stations operate in central Honshu Island, and they are near volcanoes that have been highly active throughout the Quaternary (see Fig. 1.7), including the Aira caldera and Sakurajima (southern Kyushu), Aso (northern Kyushu), Daisen and Sambe (southwest Honshu) (e.g. Albert et al., 2019a; Machida and Arai 2003; Machida et al., 1999). The tsunami associated with the 2011 Tohoku earthquake highlighted the sensitivity of such infrastructure works in Japan to natural hazards. Understanding of the potential risks from volcanoes which have been documented to erupt explosively is a key component for accurate hazard assessments. The combination of numerous volcanoes which have produced explosive eruptions, combined with densely populated areas with associated infrastructures (i.e. airports, nuclear power plants) highlights the need to accurately understand past eruptive histories in the east Asia/Pacific region. However, the burial, destruction, and erosion of proximally located eruption deposits by subsequent eruptions has resulted in an incomplete geological record and thus a fragmented understanding of eruption histories. Distally located sedimentary archives offer a valuable resource that could be used to improve the accuracy of natural hazard assessments for the East Asia/Pacific region.

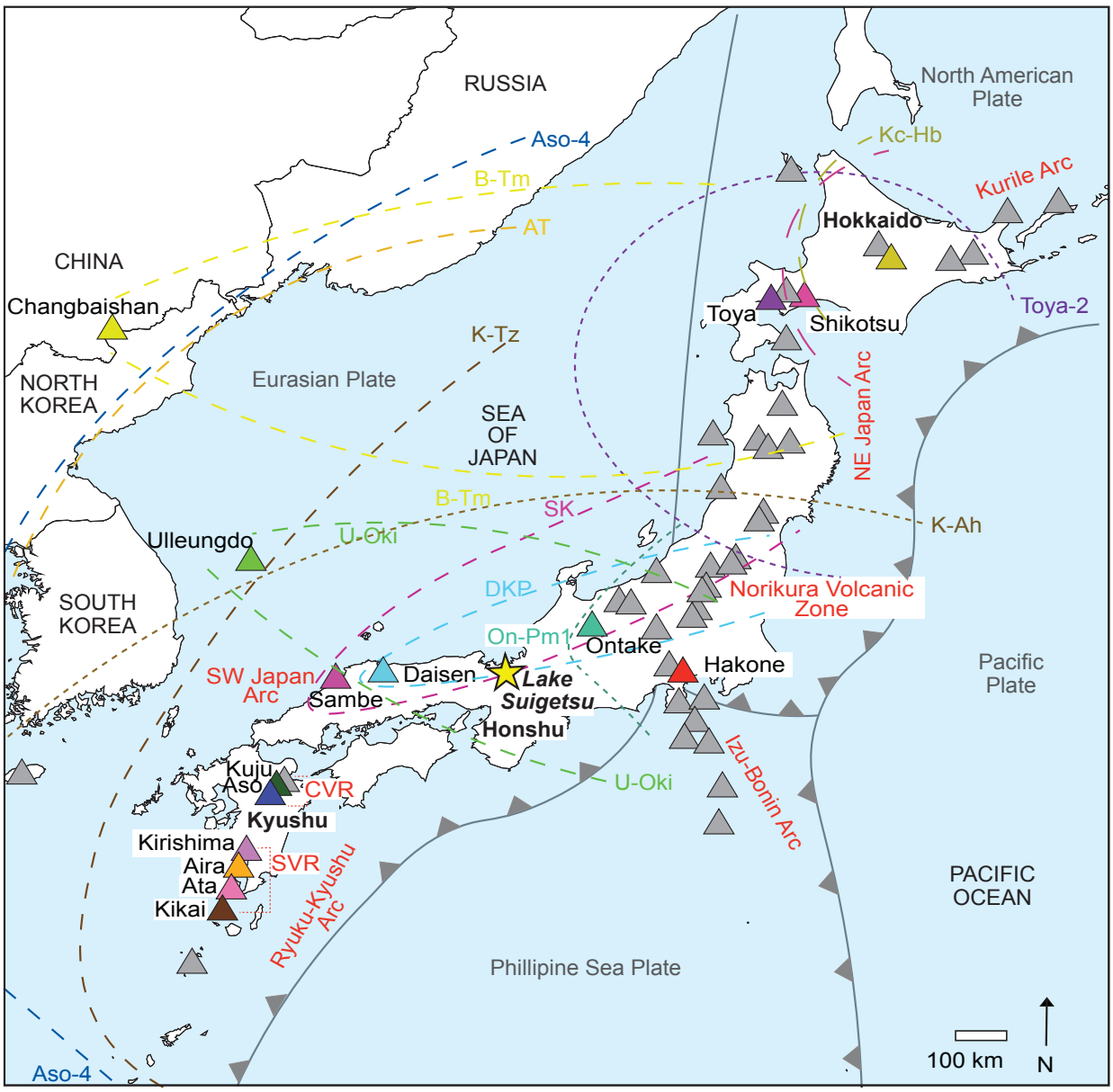


Figure 1.7: Volcanoes (grey triangles) that have been active in and around Japan in the Quaternary and the volcanic arcs. The volcanoes that are mentioned in the text and likely sources of the tephra in Lake Suigetsu in this period are labelled and coloured. The dashed lines denote the ash dispersal boundaries for various widespread tephra layers (as labelled), which are from (Machida, 2002). The location of Lake Suigetsu is shown by a yellow star.

More than 40 years of tephra studies have been undertaken in and around Japan with Machida and Arai (1983) establishing the foundation of tephrochronology in Japan. Widespread tephra isochrons are routinely identified within Late Quaternary sedimentary sequences across the islands of Japan (e.g. Matsu'ura and Komatsubara, 2024; Albert et al., 2019a; Lim et al., 2013; Smith et al., 2013; Machida and Arai, 2003). Active and buried calderas on Kyushu Island have been the focus of some of the largest known eruptions in the Quaternary (Table 1.1; Machida, 1999). Most notably, the Aira-Tanzawa (AT; 30 ka) eruption (the VEI 7 eruption of Aira caldera, Kyushu Island) ejected vast quantities of bulk

tephra in the realm of 463 km^3 (Machida, 1999). Owing to the huge volume of tephra produced by the AT eruption, ash deposits have been dispersed over the Japanese islands, the Sea of Japan and the Pacific Ocean (Ikehara et al., 2013; Katoh et al., 2007; Machida and Arai, 2003 and references therein). Aso (Kyushu Island) is one of the largest active volcanoes in the world. The caldera is believed to be formed by a series of VEI 6 – 7 eruptions: Aso-1 (ca. 270 ka), Aso-2 (ca. 140 ka), Aso-3 (ca. 112 – 134 ka) and Aso-4 (ca. 86 ka) (Table 1.1; Albert et al., 2019a; Machida and Arai, 2003). Volcanic ash from each of these discrete caldera-forming events have been dispersed across vast regions of East Asia (e.g. Chen et al., 2019; Derkachev et al., 2019; Lim et al., 2013; Smith et al., 2013; Machida and Arai, 2003). Whilst many tephra isochrons identified across the islands and oceans around Japan originate from Japanese volcanoes, tephras originating from other volcanic sources (e.g. North Korea/China and South Korea) have also been identified in and around Japan. Tephra erupted from intraplate volcanoes Ulleungdo (South Korea) and Changbaishan (North Korea/China border) were also dispersed across the Sea of Japan (Lim et al., 2013; Ikehara et al., 2004; Arai et al., 1981) and to the coastal regions of Japan (e.g., McLean et al., 2016, 2018; Chen et al., 2019; Smith et al., 2013; Nagahashi et al., 2004).

Table 1.1: A list of Quaternary widespread tephra layers in and around Japan through the last 250 ka. Adapted from Machida (1999).

Volcano–tephra (symbol)	Age (in ka) (see Machida 1999[a])	Marine isotope stage (MIS)	Eruption sequence[b]	Eruption bulk volume (km^3)	Petrographic properties		References
					Volcanic glass[c]	Phenocryst[d]	
Baegdusan–Tm	1–1.1	1	p, i, c	50	pm, bw	af, (am, cpx)	Machida et al. (1990)
(B-Tm)	A, C				1.511–1.522	af 1.521–1.525	
Kikai–Ah	6.3	1	p, i, c	>150	bw, pm	opx, cpx	Machida and Arai (1978)
(K-Ah)	C				1.508–1.516	opx 1.708–1.713	
Ulreung–Oki	9.3	1/2	p, i	>10	pm	bi, am, cpx	Machida and Arai (1983)
(U-Oki)	C				1.518–1.524	af 1.522–1.524	Machida et al. (1984)
						ho 1.726–1.740	
Towada–H	12–13	2	p, i	50	pm	opx, cpx, ho	Hayakawa (1985)
(To-H)	C				1.502–1.509	opx 1.705–1.708	Arai et al. (1986)
						ho 1.669–1.673	
Aira–Tn	24–25	2/3	p, i, c	>450	bw, pm	opx, cpx, (ho, qt)	Machida and Arai (1976)
(AT)	C				1.498–1.501	opx 1.728–1.734	
Kutcharo–Shoro	30–35	3	pp, i	100	pm, bw	opx, cpx	Arai et al. (1986)
(Kc-Sr)	C, ST				1.502–1.505	opx 1.707–1.710	
Shikotsu-1	40	3	p, i	200	pm, bw	opx, ho, (cpx); qt	Katsui (1963)
(Spfa-1, Spfl)	C				1.500–1.505	opx 1.729–1.735	Arai et al. (1986)
						ho 1.688–1.691	
					Volcanic glassc	Phenocrystd	
Daisen–Kurayoshi	43–55	3	p, (i)	>20	pm	ho, opx, (bi)	Machida and Arai (1979)
(DKP)	U, ST				1.508–1.514	opx 1.702–1.708	
						ho 1.673–1.680	
Aso-4	84–89	5a/5b	i, c	>600	bw, pm	ho, opx, cpx	Machida et al. (1985)
(Aso-4)	KA, MIS				1.506–1.510	opx 1.699–1.701	Ono et al. (1977)
						ho 1.685–1.691	
Kikai–Tz	77–101	5c/5b	pp, i, c	>150	bw, pm	opx, cpx; qt	Machida and Arai (1992)
(K-Tz)	TL				1.494–1.500	opx 1.705–1.709	
Ontake-1	95	5c	p	50	pm, (bw)	ho, bi, (opx)	Kobayashi et al. (1968)
(On-Pml)	FT, MIS				1.500–1.503	opx 1.706–1.711	Machida and Arai (1992)
						ho 1.681–1.690	
Ata	95–110	5c	pp, p, i, c	>300	bw, pm	opx, cpx, (ho)	Machida and Arai (1992)
(Ata)	MIS				1.508–1.512	opx 1.704–1.708	
Sambe–Kisuki	95–100	5c	p	20	pm	bi; qt	Toyokura et al. (1991)
(SK)	ST				1.494–1.498		
Toya	103–123	5c/5d	p	>150	pm, bw	(opx, cpx, ho; qt)	Machida et al. (1987)
(Toya)	TL				1.494–1.498	opx 1.711–1.761	
						ho 1.674–1.684	
Aso-3	110–123	5d	p, i, c	>150	pm, bw	opx, cpx	Machida and Arai (1994)
(Aso-3)	TL, KA				1.514–1.519	opx 1.702–1.705	
Kutcharo–Hb	100–130	5d/5e	pp, p, i, c	≫150	bw, pm	opx, cpx	Machida et al. (1987)
(Kc-Hb)	FT, ST				1.502–1.506	opx 1.705–1.710	Okumura (1988)
Ata–Toihama	200–250	7/8	p, i, c	≫150	bw, pm	ho, opx, bi; qt	Machida and Arai (1992)
(Ata-Th)	MIS				1.498–1.500	opx 1.714–1.718	
						ho 1.670–1.674	
Hakkoda-2	ca. 250	?	i	>50	pm	opx, (cpx); qt	Machida and Arai (1992)
(Hkd-2)	KA, TL				1.501–1.503	1.713–1.718	
Aso-1	255		p, i, c	≫50	pm, bw	opx, cpx	Shirai et al. (1997)
(Aso-1)	MIS				1.518–1.521	opx 1.703–1.713	
Kakuto	ca. 340	9	i, c	>100	bw, pm	opx, cpx, (ho)	Machida and Arai (1992)

Footnote: [a] Dating method: A, archeology; C, radiocarbon; U, uranium series; MIS, marine isotope stratigraphy; ST, stratigraphy; KA, K-Ar; TL, thermoluminescence; FT, fission track.
[b] Eruption sequence:arranged in chronological order from older to younger. pp, phreato-plinian; c, co-ignimbrite ash; i, ignimbrite; p, plinian.
[c] Volcanic glass: pm, pumiceous type; bw, bubble-walled type.
[d] Phenocryst: af, alkali feldspar; am, amphibole; ho, hornblende; cpx, clino-pyroxene; opx, orthopyroxene; qt, quartz; bi, biotite; numerals are refractive indices.

Owing to the dispersal of ash over Japan and its marine basins, tephra deposits are frequently identified in sedimentary archives in and around Japan. Thus, tephras are routinely used to understand more about the magnitude, tempo and dispersal of past volcanic eruptions in East Asia. Many scientific drilling campaigns (e.g. International Ocean Drilling Program [IODP]) have extracted sediment cores from the Sea of Japan/East Sea (Ikehara et al., 2004; Park et al., 2003; Machida and Arai, 1983; 1999). These archives provide a detailed sequence of the high-magnitude silicic eruptions derived from the

Japanese Islands and the Korean Peninsula (e.g., Kutterolf et al., 2018; Sagawa et al., 2018; Schindlbeck et al., 2018; Mahony et al., 2016; Ikehara, 2015; Furuta et al., 1986; Machida and Arai, 1983; Arai et al., 1981). Lacustrine sediments formed in low-energy environments provide detailed records of past eruption events and can form key regional tephro-stratotypes as their higher sedimentation rates often resolve thinner and finer ashes that may not be preserved in the marine realm. There are numerous high-resolution lacustrine sedimentary sequences that have been obtained from Japan that have tephra studies, including Lake Suigetsu (Albert et al., 2019a, 2024; McLean et al., 2016, 2018, 2020a; Smith et al., 2011b, 2013), Lake Biwa (Nagahashi et al., 2004), Ichi-no-Megata (Okuno et al., 2011), Lake Kushu (Chen et al., 2019) and Lake Nojiri (Kumon et al., 2003), and these provide some of the most robust and stratigraphically constrained evidence of Japanese and Korean eruptions. These distal archives have proven increasingly important for building more detailed inventories of ash-fall events and provide insight to the lower magnitude and/or local eruption events.

Glass compositional datasets (major elements) for most widespread ash layers in East Asia are now well established (e.g., Albert et al., 2019a; Nakamura, 2016; Kimura et al., 2015; Nagahashi et al., 2013; Smith et al., 2013; Aoki and Machida, 2006; Furukawa and Nanayama. 2006; Machida and Arai, 2003) and can be used to robustly provenance crypto-/tephra preserved in distal sequences (Albert et al., 2019a, 2024; McLean et al., 2018). The K_2O content offers a first order major element to discriminate the eruption deposits from volcanic arcs and centres (Fig.1.8). The Aso caldera produces volcanic glasses ranging from trachy-dacite to rhyolite and has the highest known K_2O for Japan (3 – 6 wt.%) and thus characterised by a distinctive K_2O enrichment trend (Fig. 1.8). However, many other regions show overlap and difficult to identify specific volcanic source (Fig. 1.8; Albert et al., 2019a). Trace element compositions are essential for differentiating Japanese volcanic sources due to their subduction genesis and using the Y, Rb, Zr, Nb and Th contents can be distinguished (Fig.1.8; Albert et al., 2019a). Intraplate volcanoes, such as Changbaishan and Ulleungdo, produce alkaline tephra that is geochemically distinct from Japanese arc volcanoes notably lacking Nb and Ta depletions and showing more enriched Zr compositions. These characteristics make their glasses easily distinguishable from those of Japanese arc volcanoes (Albert et al., 2019a; Kimura et al., 2015; Machida and Arai, 2003), and their distal deposits can be easily discriminated from other intra-plate sources in the back-arc (e.g., Doki and Jeju volcanoes; Brenna et al., 2014).

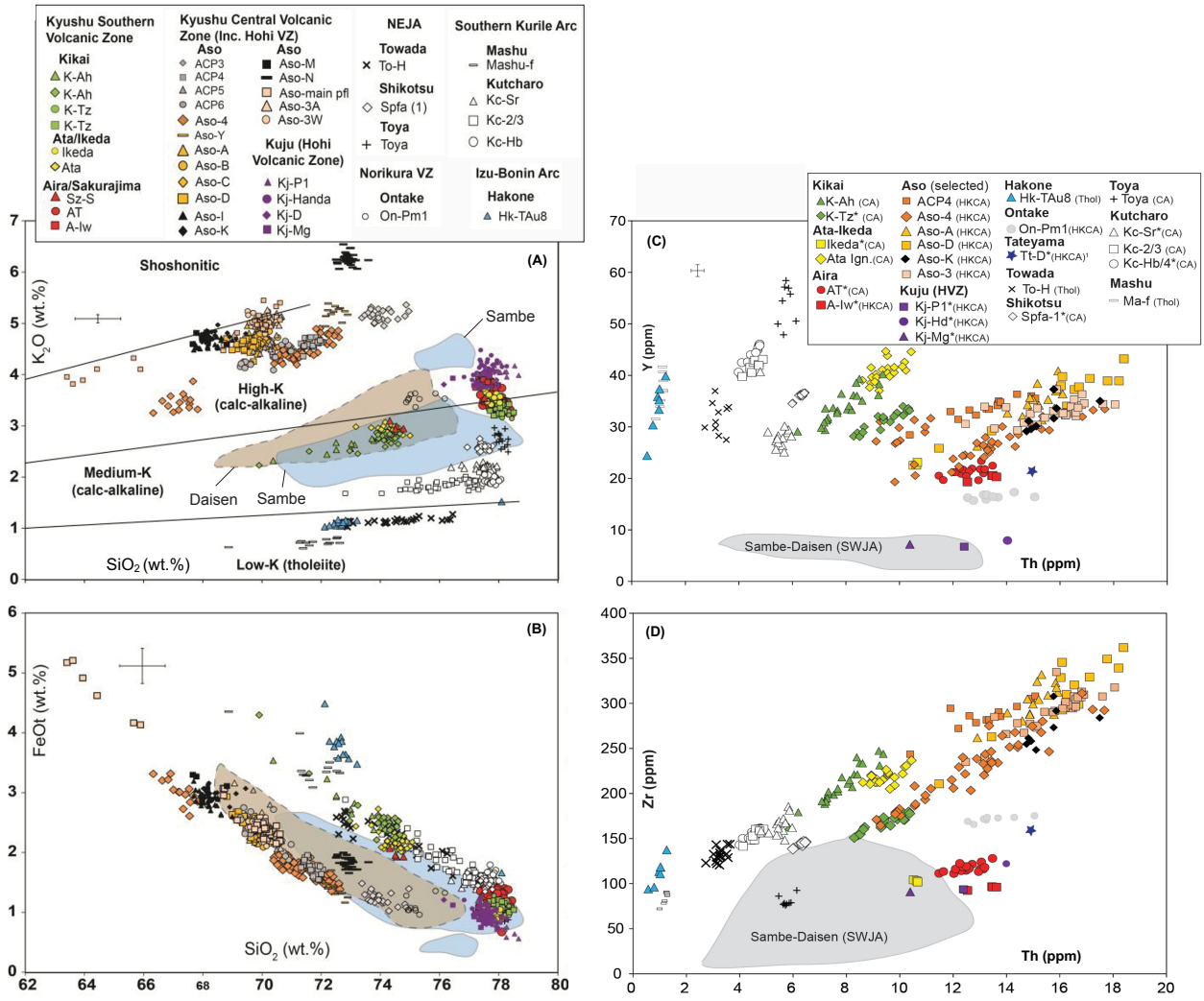


Figure 1.8: Major (SiO_2, K_2O and FeO_t) and trace (Th, Y, Zr) element glass compositions of large magnitude Japanese eruptions obtained (last 150 ka) from near source (proximal) deposits (from Albert et al., 2019a). Glasses are plotted on the whole rock classification scheme of Peccerillo and Taylor (1976) and range from Low-K (Tholeiitic) to High-K (Calc-alkaline)/Shoshonitic affinities. Error bars on plots represent repeat analysis of MPI-DING StHs6/80-G. Figure adapted from Albert et al. (2019a).

The Lake Suigetsu sedimentary archive provides a key stratotype of explosive volcanism in east Asia spanning the last ~200 kyr. Throughout the coring campaigns, numerous tephra deposits have been described and characterised. A comprehensive study of the thirty visible tephras preserved in the SG06 core was compiled by Smith et al. (2013) who described and geochemically characterised (major elements) for each of the units identified (Fig. 1.9). Data from proximal deposits and analysis of Lake Suigetsu tephras significantly extended the glass compositions and meant tephra layers from multiple widespread eruptions were confirmed in the Lake Suigetsu sequence including the K-Ah, U-Oki, AT, Aso-4, K-Tz, Aso-ABCD and Ata tephras (Fig. 1.9; Smith et al., 2013). However, many of the Lake Suigetsu visible tephra horizons could not be correlated to known

eruptions, and highlighted that a detailed glass chemistry database of eruptions and volcanoes across Japan was required to identify the origin of the layers in Lake Suigetsu. Lake Suigetsu is ideally situated 150 km from the nearest caldera (Ontake) so is not inundated with locally sourced volcanic glass, which can hinder the identification of low-concentration cryptotephra. Cryptotephra investigations undertaken through the Lake Suigetsu sediments have been completed for the Holocene and Late Pleistocene (0 – 20 ka and 30 – 50 ka; Fig. 1.9), and these studies reveal volcanic deposits from an additional eight volcanic centres to the ten volcanic centres identified from the visible tephras and indicate that there are four times as many cryptotephra preserved relative to visible tephras (e.g. Albert et al., 2024; McLean et al., 2018, 2020a).

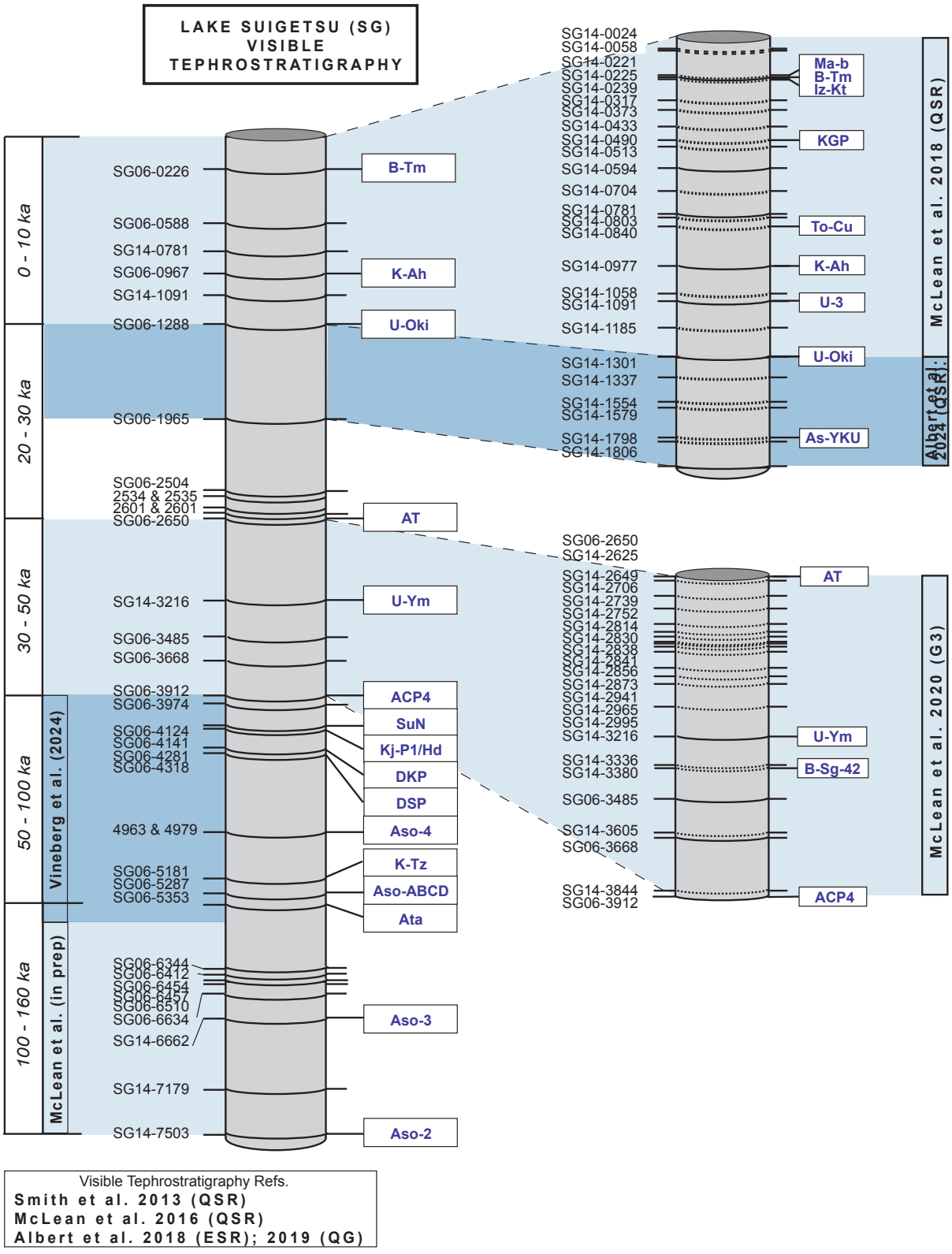


Figure 1.9: Current tephrostratigraphy of Lake Suigetsu (SG06 and SG14), including both visible tephra (solid lines) and non-visible cryptotephra (dashed lines) deposits, spanning the last 160 ka. The 120 – 50 ka section used in this study is highlighted as Vineberg et al. (2024).

In total, seventy-six visible tephra and cryptotephra deposits have been identified and geochemically characterised in the Lake Suigetsu sediments so far (Albert et al., 2018, 2019a, 2024; McLean et al., 2016, 2018, 2020a; Smith et al., 2013). Whilst many of the crypto-/tephra layers have been correlated to arc volcanoes located on Honshu and Kyushu (Smith et al., 2013; Albert et al., 2019a), several layers are from centres located >1000 km away from Hokkaido and the intraplate volcanoes (Ulleungdo; South Korea and Changbaishan; North Korea) from outside Japan (Albert et al., 2018, 2019a; McLean et al. 2016, 2018, 2020a; Smith et al., 2011b). Lake Suigetsu has been an integral archive for linking Holocene sequences regionally and even at the hemispheric scale with the Greenland ice cores (see McLean et al., 2016) as well as providing significant constraints on the tempo and dispersal of past eruptions including lower magnitude events which have been missing from proximal record that has significantly improved the understanding and order of eruptions events in East Asia.

Extending cryptotephra studies into deeper time advances understanding of long-term volcanic activity, environmental changes, and earth system dynamics. Whilst the Lake Suigetsu sedimentary sequence spanning ~200 kyr has been investigated for the presence of visible tephra layers (see: Albert et al., 2019; Smith et al., 2011, 2013), only the sediments in last 50 kyr have been studied for the preservation of cryptotephra deposits (see: Albert et al., 2024; McLean et al., 2018, 2020a, 2020b). Furthermore, despite the well constrained chronology for the last 60 ka of the Lake Suigetsu sedimentary sequence (Bronk Ramsey et al., 2012, 2020; Staff et al., 2011), a robust chronology is lacking for older sections. By conducting cryptotephra investigations into deeper sections (ie pre-50 ka), has the potential to improve the chronology and synchronisation of archives through the identification of key widespread markers in this timeframe (see Table 1.1) as well as to provide insights into eruption frequency, magnitude, and geochemical evolution of volcanic systems through glacial-interglacial cycles.

1.5. Project aim and objectives

This project aims to refine the tephrostratigraphies for the very productive volcanic regions in both Italy and Japan through the integration of proximal and distal records. To achieve this aim, the following research objectives:

- **Objective 1:** Augment the tephrostratigraphic records of Campania (Italy) and Lake Suigetsu (Japan).
- **Objective 2:** Provide detailed geochemical characterisation of the volcanic glasses. Use their major and trace element compositions to determine their source regions, volcanoes and specific eruptions.
- **Objective 3:** Identify key isochrons to aid the integration and synchronisation of proximal and distal records.

1.6. Thesis guide

The central data chapters of this thesis (Chapters 4 – 6) are written in the format of journal articles, two of these are published and the other will be submitted to a journal soon. The thesis is structured as follows:

Chapter 1: Introduction

This chapter outlines the key literature relating to the subject area of this thesis, focusing on tephra science and providing background information on the study areas - Campania, Italy and Japan.

Chapter 2: Materials and Methods

This chapter outlines all the materials and methods employed in this thesis. Further details of the specific methods used are detailed within each data chapter (Chapters 4 – 6).

Chapter 3: Study sites

This chapter introduces the proximal distal study sites investigated for this thesis. This chapter provides details about specific Campanian and Japanese outcrops and the tephras sampled from these locations as well as the location and coring history of Lake Suigetsu.

Chapter 4: Insights into the explosive eruption history of the Campanian volcanoes prior to the Campanian Ignimbrite eruption

This article presents a detailed tephrostratigraphy of the twelve units preserved beneath the caldera-forming Campanian Ignimbrite at a proximal coastal outcrop. Geochemical characterisation of these units reveal compositional variations in tephra deposits from Campi Flegrei, indicating volcanic activity without significant repose periods before the CI eruption. This article was published in 2023 in *Journal of Volcanology*. https://doi.org/10.1016/j.jvolgeores.2023.107915

Chapter 5: A detailed record of large explosive eruptions in East Asia between ~120 and 50 ka preserved in the sediments of Lake Suigetsu, Japan

This article presents the results of a detailed cryptotephra investigation of the Lake Suigetsu sediments spanning 50 – 120 ka. The Lake Suigetsu tephrostratigraphy for this interval was extended from nine visible units (Smith et al., 2013) to fifty ash layers identified using cryptotephra extraction techniques. This study integrates the tephrostratigraphies from all eight Japanese volcanic arcs with those of the from intraplate sources located west of Japan. These findings further establish Lake Suigetsu as the single most comprehensive record of East Asian volcanism and identifies a number of isochrons which may be useful for future studies to correlate with. This article was published in 2024 in *Quaternary Science Reviews*. https://doi.org/10.1016/j.quascirev.2024.109021

Chapter 6: Integrating proximal-distal records of explosive volcanism from Aso caldera (Japan) prior to 30 ka

This article integrates the proximal and distal records of Aso activity. Detailed geochemical characterisation of Aso units preserved in near-vent sequence was carried out to improve the reference dataset for one of Japan's most active volcanoes. This study integrates Aso deposits preserved in proximal outcrops with those previously identified within the distally located Lake Suigetsu record to refine the understanding of the Aso system's eruption frequency, chronology, and geochemical signatures. These findings underscore the importance of integrating proximal and distal records to enhance the understanding of the timing and ash dispersal patterns of prehistoric eruptions.

Chapter 7: General Discussion and Conclusions

This chapter brings together a discussion of the overarching aim of this research project and the insights that can be established from building very detailed dossiers of eruption events. Directions for future research are also outlined in this chapter.

Chapter 2: Methods and Materials

This chapter introduces the materials and methodologies utilised in this thesis for both tephra and cryptotephra identification and characterisation. Specific materials and methods are also presented in each of the results chapters (Chapters 4 – 6).

2.1. Cryptotephra extraction and laboratory preparation

To identify cryptotephra deposits preserved in the sediments spanning 120 – 50 ka, the master SG14 core was continuously and contiguously sub-sampled at ca. 5 cm (low) resolution from 38.83 to 59.79 m composite depth (CD). Positions of elevated shard concentrations in the low-resolution samples were resampled at 1 cm (high) resolution, which were used to refine the stratigraphic position of the cryptotephra peak (Fig. 2.1). All samples and blanks, to test for any laboratory contamination, were wet sieved and the >25 μm fraction were processed using the heavy liquid floatation method outlined by Blockley et al (2005) (Fig. 2.2). This stepped floatation method is shown to reliably concentrate the glass shards in the Lake Suigetsu sediments so that cryptotephra peaks can be resolved (Albert et al., 2024; McLean et al., 2018, 2020a, 2022).

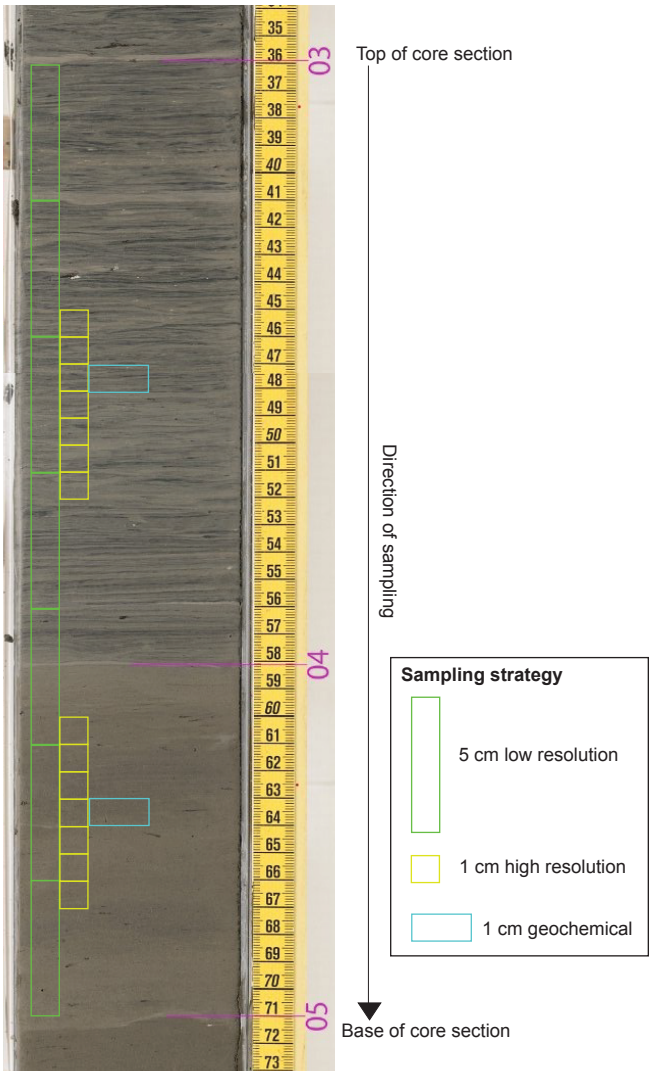


Figure 2.1: Schematic diagram showing the three stepped sampling strategy employed for the SG-14 master core for the 50 – 120 ka. Continuous and contiguous sampling was undertaken. 1 cm samples were taken either side of the 5 cm target to accurately position the isochron.

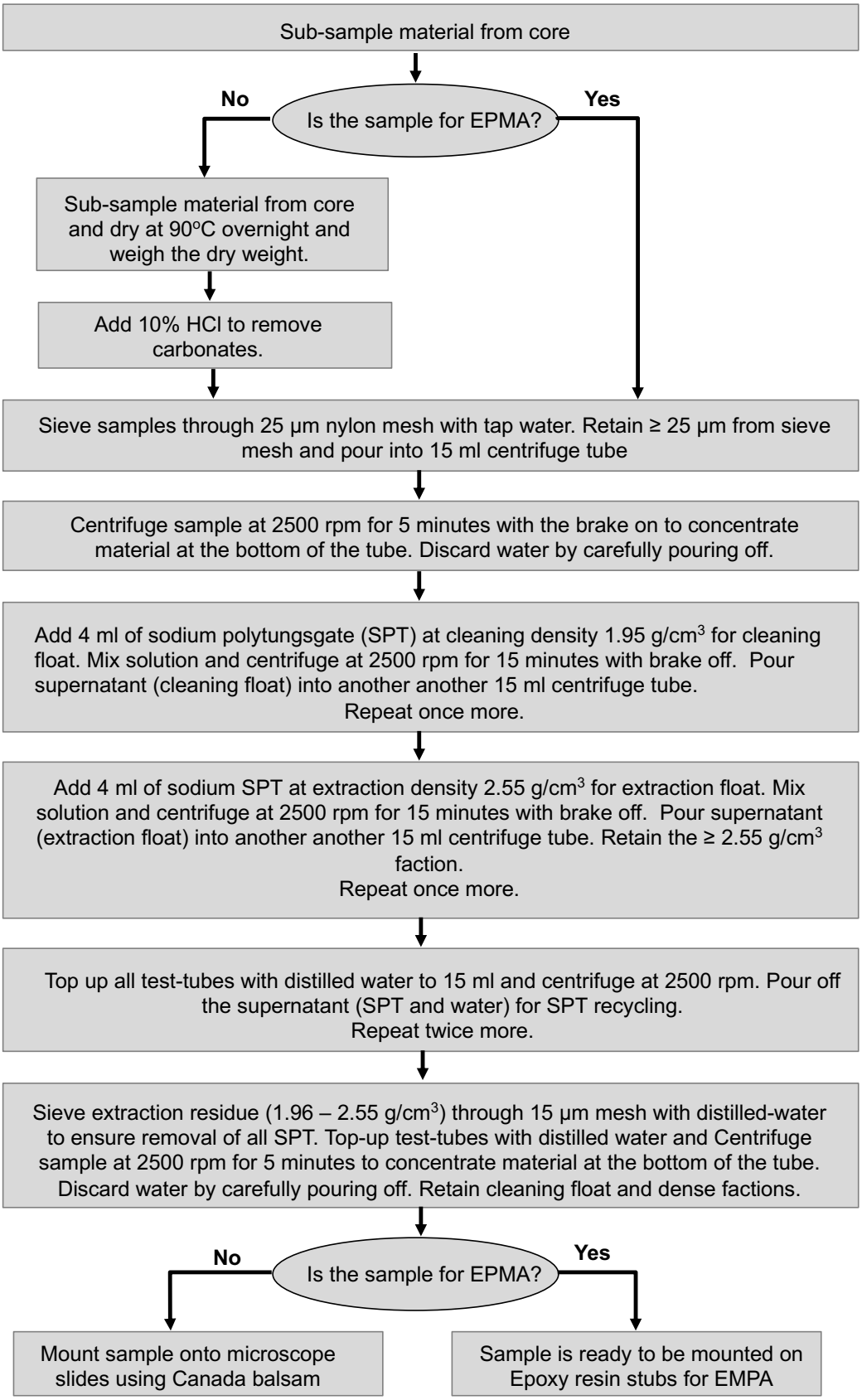


Figure 2.2: Cryptotephra extraction protocol. Modified from Blockley et al. (2005).

Samples taken above visible tephra layers (e.g. following the 2.8 cm thick K-Tz tephra) have high shard concentrations due to mobilisation of the shards within the catchment (referred to as background). These samples were processed as outlined above and then spiked with a known quantity of *Lycopodium* pollen spores after the sample has been sieved and floated. Each *Lycopodium* tablet has a particular spore count (i.e. 9666 spores per tablet). The tephra and *Lycopodium* solution was mounted on microscopic slides, and both were counted, and the concentration of glass shards was estimated using the following equation (Payne and Gehrels, 2010):

$$C = l \times \left(\frac{a}{bd}\right)$$

Where *a* is the number of glass shards counted, *b* is the number of *Lycopodium* spore counted, *d* is the sample dry weight and *l* is the number of *Lycopodium* spores in each tablet according to the manufacturer estimate determined using an electronic particle counter. The resulting counts are expressed as shards/gram using weights of the dry samples that were taken before sample processing, but were capped at 20,000 s/g as the accuracy of counting spiked samples is undetermined.

2.2. Visual analysis of shards

Fundamentally, the effective use of cryptotephra horizons as isochronous markers requires their precise and accurate location within a sedimentary sequence. To better understand the extracted tephra samples and their componentry, they were studied using binocular microscopy to assess the various constituents by quantitative and qualitative means. The abundance of glass shards was classified using semi-quantitative techniques using a light microscope to quantify the number of shards per gram of dried sediment (shards/gram). Shard concentration profiles were plotted by the shard concentrations (shards/gram) against their composite core depth to identify the location of the peaks in glass shard concentrations that define the cryptotephra deposits. The identification of a sharp discrete peak in shard profiles is indicative of a rapid input, reflecting the exact timing of the volcanic eruption (see Davies et al., 2015). In the Lake Suigetsu sequence, peaks in shard concentrations were ultimately evaluated using a set of criteria outlined in Fig. 1.2 that considers the potential for reworked cryptotephra deposits within the sequence. One of these methods was to record the morphological features of the shards, as in Fig. 2.3. Where background shard concentrations were high, particularly in the sediments above visible tephra layers, differences in the morphological features and colour of the shards were also

used to help identify the stratigraphic position of new primary ash-falls. The following characteristics of the glass shards were also recorded (Fig. 2.3):

(i) Colour (e.g., clear or brown)
(ii) Size (length of the longest axis of shards in the fraction extracted)
(iii) Morphology (e.g., pumice, blocky, platy, cuspate or fluted)
(iv) Vesicle size (small/microvesicular or large), shape (elongated or rounded) and density (rich or poor)
(v) Microlite density (rich or poor)

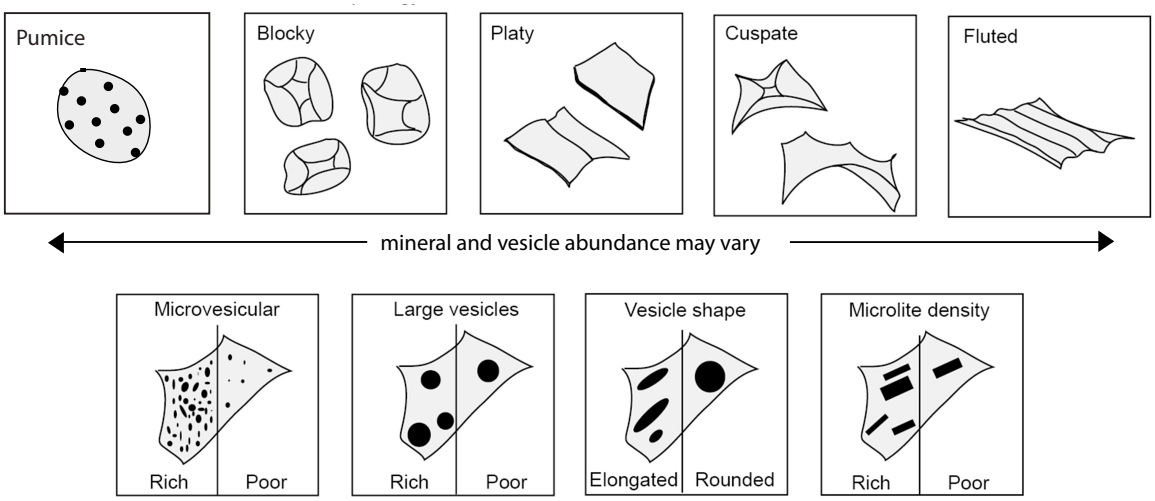


Figure 2.3: A schematic representation/classification guide of the glass-shard morphologies, and the microphenocryst and vesicle content. Modified from McLean et al. (2018).

2.3. Compositional analysis

After sieving/extracting the tephra and cryptotephra samples, glass shards were prepared for geochemical characterisation; their procedure dependent on the whether it was a visible tephra or cryptotephra (Fig. 2.4). In summary, the samples were mounted onto stubs Struers SpeciFix 20 or in holes drilled in EpoFix 20 Epoxy resin stubs, which were covered or backfilled, respectively, to seal the shards. The glass shards in the block were sectioned to expose the fresh surfaces using progressively finer Silicon Carbide grinding papers (P1200, P2500, and P4000; Fig. 2.4). The resin stub was then machine-polished using increasingly finer grades of diamond suspensions (3 and 1 μm; Fig. 2.4). To avoid contaminating the grinding and polishing pads, the stubs was cleaned in a beaker filled with distilled water placed in an ultrasonic bath for several minutes between each sectioning polishing stage. All stubs mounted with cryptotephra were photographed to create maps of the shards at the surface of the stub to aid EMPA efficiency and to label the individual shards analysed for future LA-ICP-MS. The stubs were finally placed in a beaker filled with

Petroleum Ether which was placed in an ultrasonic bath for five minutes in order to thoroughly clean them; they were dried with lint-free tissue. Stubs were then carbon-coated for EMPA to create a conductive surface that prevents the accumulation of charge on the sample during analysis, which would otherwise interfere with the accuracy of the electron beam and the resulting elemental data (see Innes et al., 2024; Iverson et al., 2017).

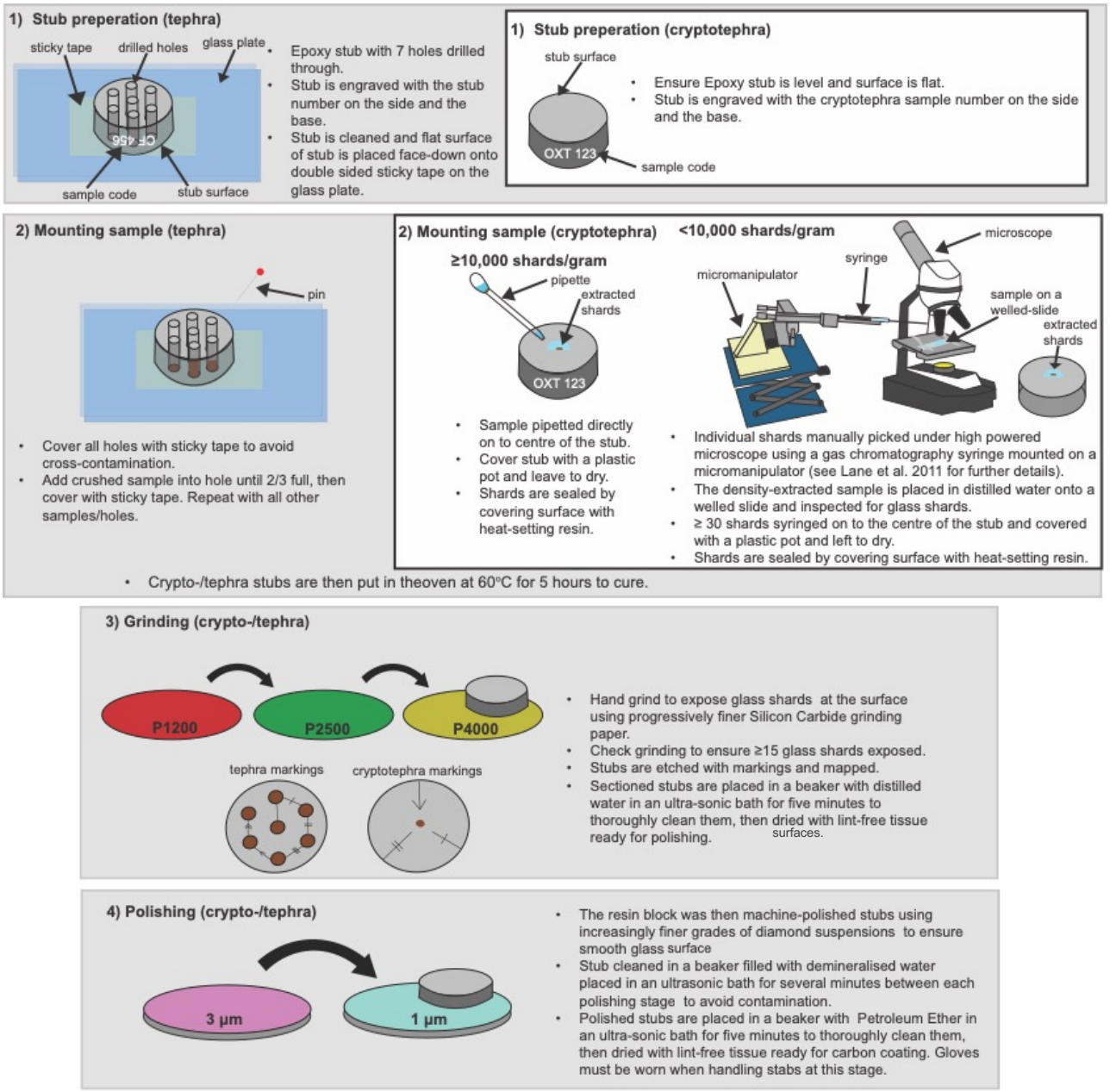


Figure 2.4: Preparation and procedure for mounting both visible tephra and cryptotephra glass shards in Struers resin for EMPA (modified from Lowe, 2011 and Lane et al., 2011).

All crypto-/tephra deposits (whether proximal or distal) were geochemically analysed via EMPA and most (where possible; see below) were also analysed using LA-ICP-MS. This section briefly describes the theory behind wavelength dispersive electron microprobe

analysis (WDS-EMPA) and LA-ICP-MS and the conditions used during analysis. In this thesis, the major and trace element compositions of glass-shards was obtained using the same methods throughout. All major and trace element data, and secondary standards, are reported in Appendices A – C.

Major and minor element chemistry of the glass-shards from both proximal and distal crypto-/tephra deposits were analysed at the Research Laboratory for Archaeology and the History of Art, University of Oxford, using a wavelength-dispersive (WDS) JEOL JXA-8200 EMP equipped with five spectrometers. WDS-EMP works by directing a focussed beam of electrons at the glass surface, causing the emission of X-rays which are subsequently diffracted by an analyser crystal within the spectrometers to the detector. The position of the analyser crystal is moved within the spectrometer to change the crystal angle that allows particular X-rays of particular elements to be selected (based on wavelength). The number of counts are collected by the detector which, when calibrated, provide quantitative information on the elemental concentrations within a sample.

An accelerating voltage of 15 kV, current of 6 nA and a defocussed 10 μm beam diameter were used to analyse all shards. Thirty shards were analysed for each sample where possible. To minimise the effect of Sodium (Na) migration, Na was analysed first on the spectrometer. Counts on the elemental peaks were collected for 60 s (P), 50 s (Cl), 40 s (Mn), 30 s (Si, Ca, K, Al, Ti, Fe, Mg), and 12 s (Na), and for half of the total peak time on each of the background positions on either side of the peak. Prior to analysis, the EMPA was calibrated for each element using a suite of primary mineral standards. To verify the calibration, the following Max Planck Institute reference glasses (MPI-DING) were used as secondary standards: StHs6-80/G, ATHO-G, and GOR132-G (Jochum et al., 2006). These were analysed at the beginning, during and at the end of all sample runs. The averaged values of these lie within two standard deviations of the preferred values (see Jochum et al., 2006). Analyses with analytical totals <94% were discarded as they are not thought to be representative of the true melt composition. Microphenocrysts, vesicles and resin were avoided during analyses. All analyses presented have been normalised to 100% for comparative purposes and to reduce the effect of the secondary rehydration of the glass (Shane et al., 2008). Bi-variate oxide plots are routinely used to distinguish individual tephras (Lowe et al., 2008) as visual presentation of geochemical data areusually sufficient to identify the elemental range, clustering of data and outliers (Mackay et al., 2016; Kuehn et al., 2009). Statistical tools are often viewed as a complementary to the visual data-presentation techniques and not a staple requirement (Lowe et al., 2017). Error bars on plots

in Chapters 4 – 6 show 2 times the standard deviation of replicate analyses of MPI-DING StHs6/80-G.

Analyses of both distal and proximal crypto-/tephra deposits were performed using an Agilent 8900 triple quadrupole LA-ICP-MS (laser ablation inductively coupled plasma mass spectrometry; ICP-QQQ) coupled to a Resonetics 193 nm ArF excimer laser-ablation device in the Department of Earth Sciences, Royal Holloway, University of London. This technique involves focusing a laser onto an area of a tephra sample, typically just a few microns in diameter (Fig. 2.5), vaporising part of the sample. The vaporised material is then transported by a carrier gas into the inductively coupled plasma, where it is ionised and analysed by a mass spectrometer (Tomlinson et al., 2010).

The full analytical procedures and operating conditions are outlined in Tomlinson et al. (2010). A range of crater sizes were used (20, 25 and 34 μm) owing to variability in the sample's vesicularity of pumices/scoria and shard sizes (distal tephras often require smaller laser spots) which determine the size of glass surfaces available for analysis (Fig. 2.5). The laser energy density on the target was 3.0 Jcm^{-2}, the repetition rate was 5 Hz. The ablation time used was 40 s, preceded and succeeded by 20 s of counting of the gas blank. This blank signal and ablation through the glass into the resin mounts do not contribute to the background signal, were then subtracted from the sample signal to correct for gas-generated interferences (Tomlinson et al., 2010). Typically, blocks of eight glass shards and at least one MPI-DING reference glass were bracketed by the NIST612 glass adopted as the calibration standard. The MPI-DING reference glasses were used to monitor analytical accuracy (Jochum et al., 2006). The internal standard applied was ^{29}Si (as determined by WDS-EMPA). Low abundance isotopes of Si and Ca, whose concentrations are determined previously by EMPA, are commonly used as internal standards for LA-ICP-MS (Tomlinson et al., 2010). Geochemically distinct reference glasses were used to cover the geochemical spectrum often observed within tephra deposits; evolved felsic [ATHO-G (rhyolite)] through to intermediate [StHs6-80/G (andesite)]. Accuracies of LA-ICP-MS analyses were monitored using the ATHO-G and StHs6/80-G MPI-DING glasses and accuracies were typically ≤ 6%. Relative standard deviations (% RSD) of LA-ICP-MS analyses are 5 – 10% for Rb, SR, Y, Zr, Nb, Ba, La, Ce, Pr, Nd, Th, ; 10 – 20% RSD for mid to heavy rare Earth elements (Sm-Yb), Ta, Pb; and 20 – 30% RSD for GD and Lu. RSD increases with smaller spot sized (20, and 25 μm). Secondary standard analyses ran alongside individual tephras are reported in Appendices A – C.

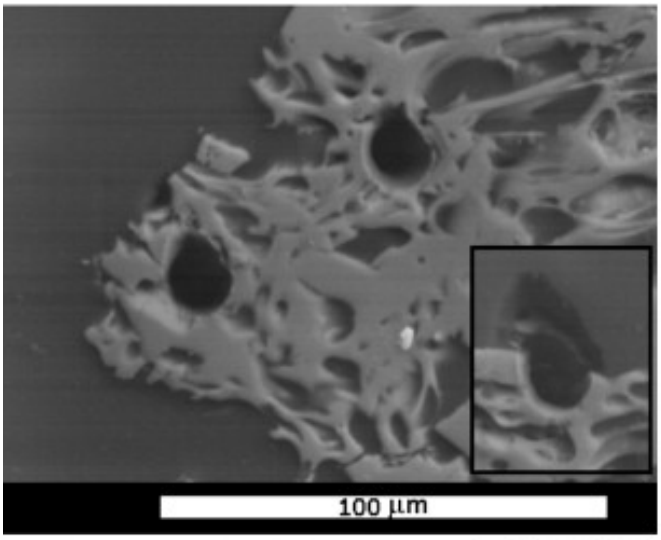


Fig. 2.5: Back scatter electron images showing sharp and round laser ablation pits in tephra sample, the inset shows ablation at the edge of the glass sample, the ablation pit is round in the sample but ablation is less controlled in the resin. Taken from Tomlinson et al. (2010).

The raw data from the mass spectrometer show counts (signals) for each element need to be converted into actual concentrations (e.g. parts per million, ppm). LA-ICP-MS data reduction was performed manually using a Microsoft Excel macro that allows for the removal of signal compromised by the occurrence of microcrysts. The first stage of data reduction involves subtracting the mean background signal from the sample signal for each element. The elemental concentrations are calculated using the formula outlined by Longerich et al. (1996):

$$C_{IS}^{sample} \times \frac{I_i^{sample}}{I_{IS}^{sample}} \times \frac{C_i^{ref}}{C_{IS}^{ref}} \times \frac{I_{IS}^{ref}}{I_i^{ref}}$$

Where C is the concertation, I is intensity, IS is the internal standard (here ^{29}Si), ref is the external calibration standard (here NIST612) and I is the isotope. The full details of time slice data reduction methods are described in Tomlinson et al. (2010).

As well as bi-variate plots, primitive mantle-normalised plots are a powerful tool in geochemistry for deciphering the history and processes involved in the formation of volcanic and mantle-derived rocks. The shape of the curve provides a "geochemical fingerprint" that can be used to compare different rocks or to infer the conditions under which the rock formed. For example, elements like Large Ion Lithophile Elements (LILEs) enriched via crustal contamination, and High Field Strength Elements (HFSEs) are depleted through subduction zone processes (Pearce and Peate, 1995). The error bars typically smaller than the symbols on plots, but error bars shown and represent 2 times the standard deviation of replicate analyses of MPI-DING StHs6/80-G

Chapter 3: Study sites

This chapter introduced both the proximal and distal study sites targeted for this thesis. This chapter provides detailed descriptions of the tephra units which were sampled for geochemical characterisation from sites located across Kyushu and Honshu in Japan (Chapters 5 and 6) and at Acquamorta in Italy (Chapter 4). This chapter also presents the distally located Lake Suigetsu sedimentary archive which is of relevance to Chapters 5 and 6.

3.1. Context

Near-source tephra samples were collected from sites in both Italy and Japan as part of this thesis to provide geochemical data for these units, most of which have not been analysed before. An outcrop located on the Campi Flegrei caldera wall was sampled and the tephras were chemically analysed to determine the provenance of the units preserved at this site (Chapter 4). Known and published eruption stratigraphies were targeted at various outcrops across Japan to provide reference geochemical data for many widely reported layers, which have not previously been analysed, to aid further correlations with distally located records (Chapters 5 and 6). During all sampling trips in Italy and Japan, we were accompanied by collaborators who have worked on the tephra stratigraphies in detail as part of their work. All sections had been logged, and we sampled from these logged sites. At each of these outcrops, the characteristics of the relevant tephra units were documented including layer thickness, and qualitative grain size, sorting, and mineral content as well as any evidence for time (e.g. unconformities and soils) and any depositional structures (e.g. layering, grading and cross-bedding). Representative samples of these units were collected vertically through proximal sequences (typically scoria, pumice-lapilli and ash) where the stratigraphy is well-defined. Details of the reference deposits analysed as part of this study are outlined in sections 3.2. (Italy; Chapter 4) and 3.3. (Japan; Chapters 5 and 6). In the laboratory, bulk representative samples comprising of pumice clasts and ash were crushed and wet sieved through a than 25 μm nylon mesh. Samples were dried in an oven at 60^{o}C overnight and then crushed to allow for single grain geochemical analyses to be undertaken to provide the representative composition of the melt (see Chapter 2).

Lake Suigetsu sediment cores were investigated for the presence of cryptotephra deposits preserved in deeper time (i.e. pre-50 ka). Section 3.4. presents the hydrological and geological setting of the lake and the history of past coring campaigns.

3.2. Proximal Site: Acquamorta, Campania, Italy (Chapter 4)

The Acquamorta outcrop (40°47′39.8″ 014° 02′ 37.2″), is located on the west side of the CI caldera ring fault (Fig. 1.4) and has previously been described, although not in great detail and without geochemical analyses (see: Orsi et al.,1996; Perrotta et al.,1994; Rosi et al., 1988). The distinctive units that can be seen in the section are the CI from Campi Flegrei and the MEGT unit from Ischia which has been geochemically characterised at this Acquamorta site (see Tomlinson et al., 2014). The units between the MEGT and the CI were accessible to describe and sample for this thesis. Distinct eruption units, separated by paleosols and had sharp basal contacts, were given a number and AQ prefix. Samples for geochemical analysis were given a number and CF prefix. All units observed between the MEGT and CI were logged in detail (see below) and sampled for geochemical analysis (Chapter 4).

The AQ-2 tephra (CF268) Is the lowermost unit sampled at Acquamorta and directly overlays the MEGT unit (Fig 3.1D,E) and is 60 cm thick and comprised of pods (7 cm high by 15 cm long) of clast supported fine-medium sized lapilli (CF268). Directly above is the 80 – 90 cm thick AQ-3 unit which is a massive, white-grey, moderately-sorted fine ash unit with some small pumices (CF269; Fig. 3.1C). At 10 – 15 cm from the base of AQ-3 there is a band of flow aligned, angular pumices which is 5 cm in thickness. Overlying is the AQ-4 unit which measures as 57 cm in thickness of alternating ash and pumice layers where pumices are 0.5 – 3.0 cm in size with some dark black/grey lithics (10% in total) and are mildly vesicular with crystals of sanidine and some pyroxene (Fig. 3.1C). At the base of AQ-4 unit there is a 32 cm thick white sub-unit composed of fine ash which is followed by a package of sub-units composed of alternating pumice and ash layers CF270). At the top of the AQ-4 unit, there is a 25 cm thick clast supported angular pumice-lapilli sub-unit (CF271), capped by a distinct clearly well-developed soil (Fig. 3.1C). Above the well-developed soil lies the 1 m thick AQ-5 unit (Fig. 3.1C). At the base of AQ-5 there is a brown-grey ash-sized reworked material with angular clasts of white pumices (0.2 – 2.0 cm) which are not evenly dispersed throughout. This brown layer is followed by 10 cm thick, laterally discontinuous zone with angular pumices (CF272). The following AQ-6 unit is 20 cm thick undulating layer of white-grey coarse ash (CF274) with some banding (weathering) observed. Above the AQ-6 unit there is an overlaying 17 – 20 cm thick dark brown soil (with occasional white-grey pumice) upon which the 40 cm thick AQ-7 unit which is composed of a coarse lapilli pumice layer followed by grey ash with brown beds (CF275), is found (Fig. 3.1B). The following 40 cm thick AQ-8 unit is a poorly-sorted fine- to coarse- grey ash (CF276). The large (90 cm thick) AQ-9 unit is comprised of poorly-sorted, yellow ash with some pumice laminations and

accretionary lapilli (Fig. 3.1B). At the top of AQ-9 there is a well-sorted clast supported unit with 1 – 4 cm pumices (CF278A) followed by a 9 – 12 cm thick laminated, poorly-sorted ash unt (CF278B). The 15 cm thick AQ-11 unit is a lateral zone of pods of ash with 1 mm pumice-lapilli (CF280). The AQ-12 unit lies upon a 3 cm thick brown paleosol with a sharp but undulatory contact and is 5 – 9 cm in thickness and composed of fine yellow disturbed ash layer with a 1 cm thick coarser white pumice-lapilli (CF281) with some obsidian lithics (Fig. 3.1A). At 5 cm below the CI is the AQ-13 unit (Fig. 3.1A) which is a 15 cm thick disturbed laterally continuous white ash (CF282).

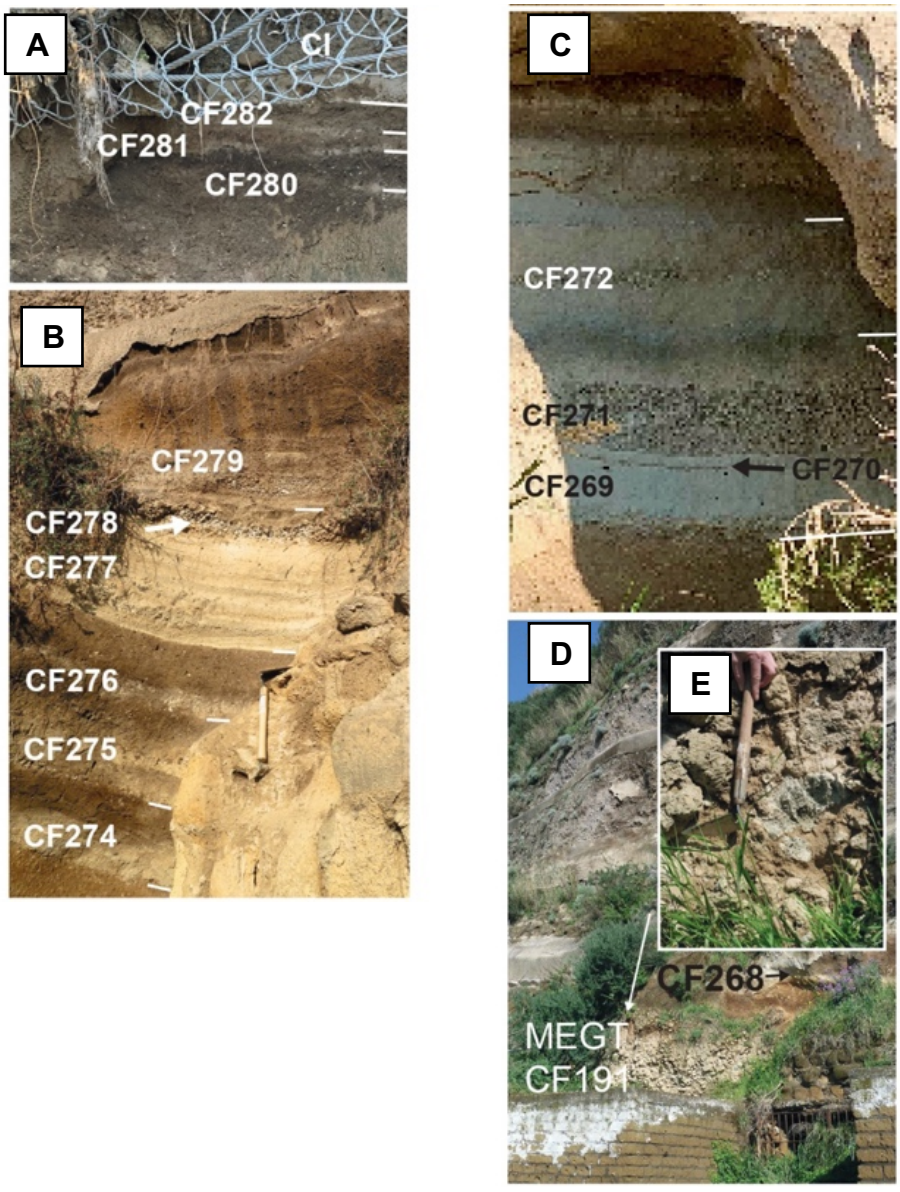


Fig. 3.1: Photographs of the tephra sequence preserved bwteen the MET and CI marker beds at Acquamorta. Adapted from Vineberg et al. (2023).

3.3. Proximal Japanese sampling sites (Chapters 5 and 6)

Tephra samples were obtained from ten terrestrial sites and one marine core located across Kyushu and southwest Honshu (Fig. 3.2) to provide reference datasets for many widespread Japanese tephras which have not previously been geochemically characterised in great detail (Table 3.1; Chapters 5 and 6). Below the outcrops located near Aso, Kirishima and Sambe volcanoes which were sampled for this thesis are described in Sections 3.3.1. – 3.3.3.

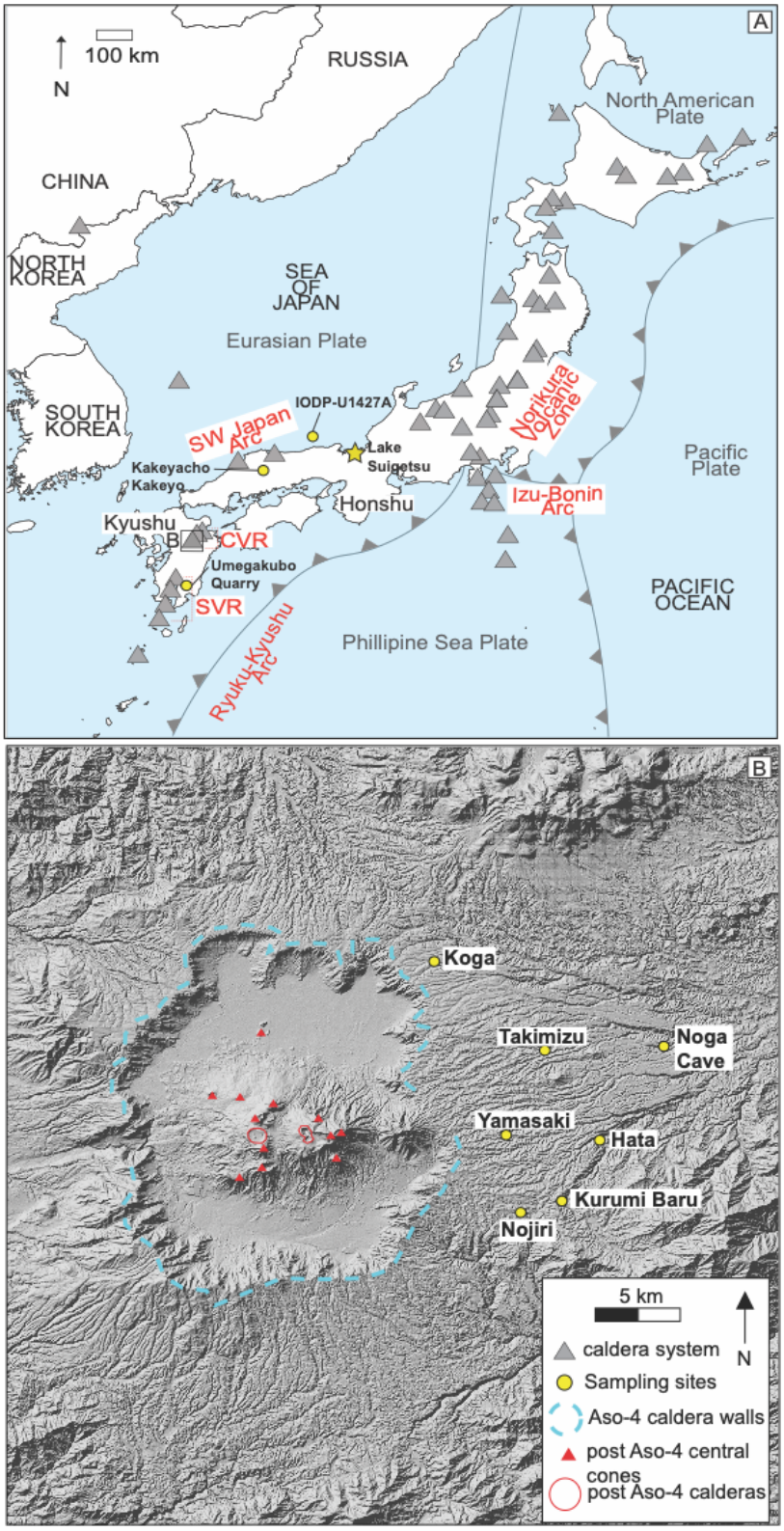


Figure 3.2. (A) Volcanoes (grey triangles) that have been active in and around Japan in the Quaternary. The red labels are the volcanic arcs: SVR = Southern Volcanic Region; CVR = Central Volcanic Region; SWJA = South West Japan Arc; NVZ = Norikura Volcanic Zone; NEJA = North East Japan Arc. The position of Lake Suigetsu is shown by a yellow star. (B) Locations of stratigraphic sections discussed in this thesis (yellow circles). Blue dashed line denotes the Aso-4 caldera walls. Red triangles show peaks of the post Aso-4 central cones and the red dashed lines denote caldera walls.

Table 3.1: Widespread tephra samples analysed in this thesis. See Fig. 3.2 for site location on map. See text for the grid reference of each site.

Volcano	Eruption	Tephra	Magnitude	Volume (km^3)	Dispersal	Sampled	Age cal yrs BP or Ka	Sample location	Sample Ref.	Proximity to source
Kyushu Central Volcanic Region (CVR)										
Aso Caldera	Ash above Aso-KPfa	Ash above Aso-KPfa	-	-	-	Ash	>AT; <Aso-KPfa	Takimizu	FLF57	proximal
	Aso-KPfa	Aso-KPfa	-	2.21	E and S	Pumice	30,164 ± 217[a]	Takimizu	FLF56	proximal
	ACP-3	ACP-3	-	0.07	ENE	Pumice	>Aso-Kpfa;<ACP4	Takimizu	FLF58	proximal
								Takimizu	FLF60	proximal
								Takimizu	FLF61	proximal
								Takimizu	FLF62	proximal
	ACP-4	ACP-4	4.6	0.43	E	Pumice	49,974 ± 33[a]	Takimizu	FLF63	proximal
								Koga	FLF189	proximal
								Koga	FLF190	proximal
								Koga	FLF191	proximal
	ACP-6	ACP-6	4.3	0.21	E	Pumice	~60[b]	Koga	FLF186	proximal
	YmP5	YmP5	-	-	ESE - ENE	Pumice	>ACP6; <YmP6	Yamasaki	A9746 P-B4	proximal
	YmP6	YmP6	-	-	ESE - ENE	Pumice	>YmP5; <YmP7	Yamasaki	A9746 P-B5/4	proximal
	YmP7	YmP7	-	-	ESE - ENE	Pumice	>YmP6; <YmP8	Yamasaki	A9746 P-B5	proximal
	YmP8	YmP8	-	-	ESE - ENE	Pumice	>YmP7; <NjP	Yamasaki	A9746 P-B6	proximal
	NjP	NjP	-	-	SE	Pumice	84[b]	Nojiri	FLF52	proximal
								Kurumi Baru	FLF194	proximal
	Aso-4X	Aso-4X	-	-	-	Pumice	>Aso-4; <Aso-Y	Kurumi Baru	FLF195	proximal
								Kurumi Baru	FLF196	proximal
	Aso-Y	Aso-Y	4.0	-	ENE	Pumice	91.4[c]	Noga Cave	FLF65	proximal
						Ash		Kurumi Baru	FLF248	proximal
		Aso-A				-		-	-	-
	Aso-ABCD	Aso-B	5.0	8.10	ENE	-	97.9 ± 6.0[a]	-	-	-
		Aso-C				-		-	-	-
		Aso-D				Pumice		Hata	FLF236	proximal
						Lapilli		Noga Cave	FLF74	proximal
		Aso-E				Pumice (lower)		Hata	FLF232	proximal
	Aso-EF		-	1.70	-	Ash (middle)	99.2[c]	Hata	FLF233	proximal
						Ash (upper)		Hata	FLF234	proximal
		Aso-F				Pumice		Noga Cave	FLF73	proximal
						Pumice		Hata	FLF230	proximal
	Aso-G	Aso-G	-	0.40	-	Pumice	100.5[c]	Hata	FLF229	proximal
						Pumice (base)		Katayama	FLF208	proximal
		Aso-H				Pumice (lower)		Katayama	FLF213	proximal
	Aso-HI		5.0	5.00	ENE	Pumice (upper)	102.6[c]	Katayama	FLF217	proximal
						Ash (top)		Katayama	FLF219	proximal
		Aso-I				Pumice (base)		Katayama	FLF206	proximal
						Pumice (top)		Katayama	FLF207	proximal
		Aso-J				Pumice (base)		Katayama	FLF202	proximal
						Pumice (middle)		Katayama	FLF203	proximal
	Aso-JKL	Aso-K	5.0	2.10	ENE	Pumice (lower)	103.3[c]	Katayama	FLF200	proximal
						Pumice (upper)		Katayama	FLF201	proximal
		Aso-L				Pumice		Katayama	FLF197	proximal
						Pumice		Katayama	FLF247	proximal
	Aso-M	Aso-M	5.0	2.50	ENE	Pumice	104.7[c]	Noga Cave	FLF72	proximal
	Aso-N/Z2	Aso-N/Z3	-	-	-	Ash (lower)	>AsoM; <Aso-Z6	Noga Cave	FLF67	proximal
						Ash (upper)		Noga Cave	FLF69	proximal
	Aso-Z6	Aso-Z6	-	0.40 (total)	-	Pumice	108.4 - 105.0[c]	Katayama	FLF227	proximal
Kyushu Southern Volcanic Region (SVR)										
Kirishima	Awaokoshi	Kr-Aw	-	-	ENE	Scoria	<Kr-Aw	Umegakubo Quarry	FLF181	proximal
						Pumice		Umegakubo Quarry	FLF176	proximal
	Iwaokoshi	Kr-Iw	-	-	ENE	Pumice	40-45[d]	Umegakubo Quarry	FLF177	proximal
						Scoria		Umegakubo Quarry	FLF178	proximal
South-West Japan Arc (SWJA)										
Sambe	Kisuki	SK	6.3	20	NE	Pumice	~100[d,e]	IODP-U1427A	FLF04	medial
						Pumice		Kakeyacho Kakeyo	FLF133	proximal

3.3.1. Aso (Chapter 6)

Eight outcrops to the east and north-east of the Aso-4 caldera wall, for which there are published logs for post-Aso-4 (Fig. 3.3; Miyabuchi, 2011, 2009) and pre-Aso-4 (Fig. 3.4; Hoshizumi et al. 2022) sections were sampled during field campaigns in 2022 and 2023 (Fig. 3.2). Samples for geochemical analysis were given a number and FLF or A9746 prefix.

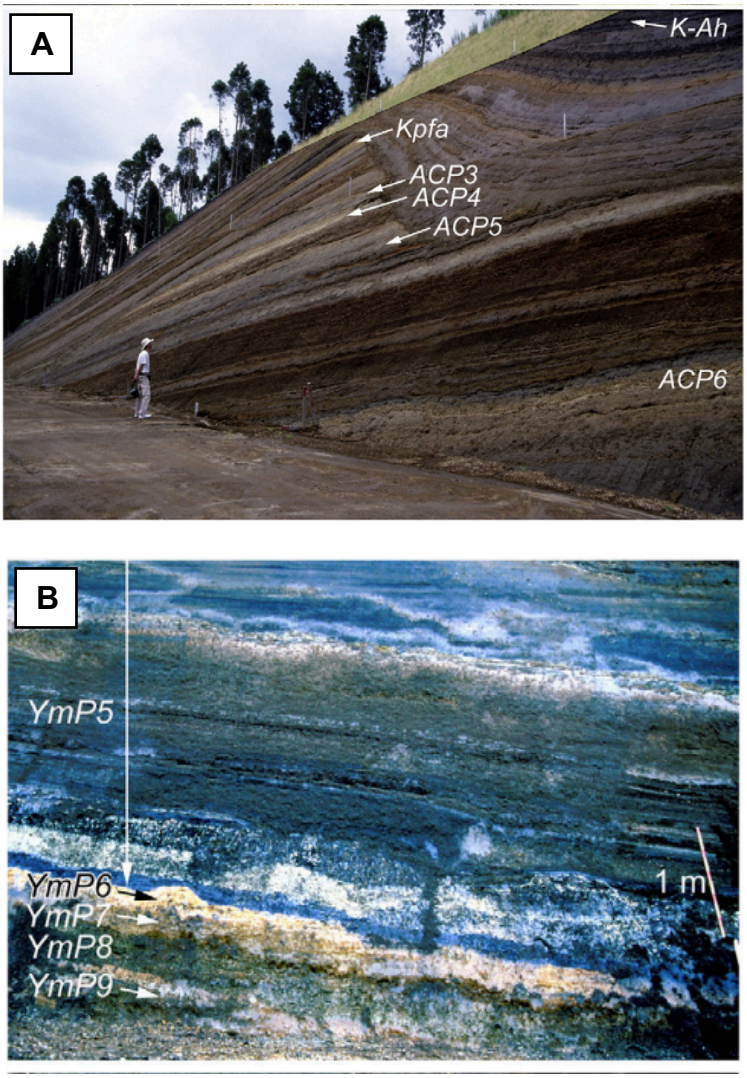


Figure 3.3: Photographs of representative tephra sequences above the Aso-4 pyroclastic-flow deposit. Taken from Miyabuchi (2009)

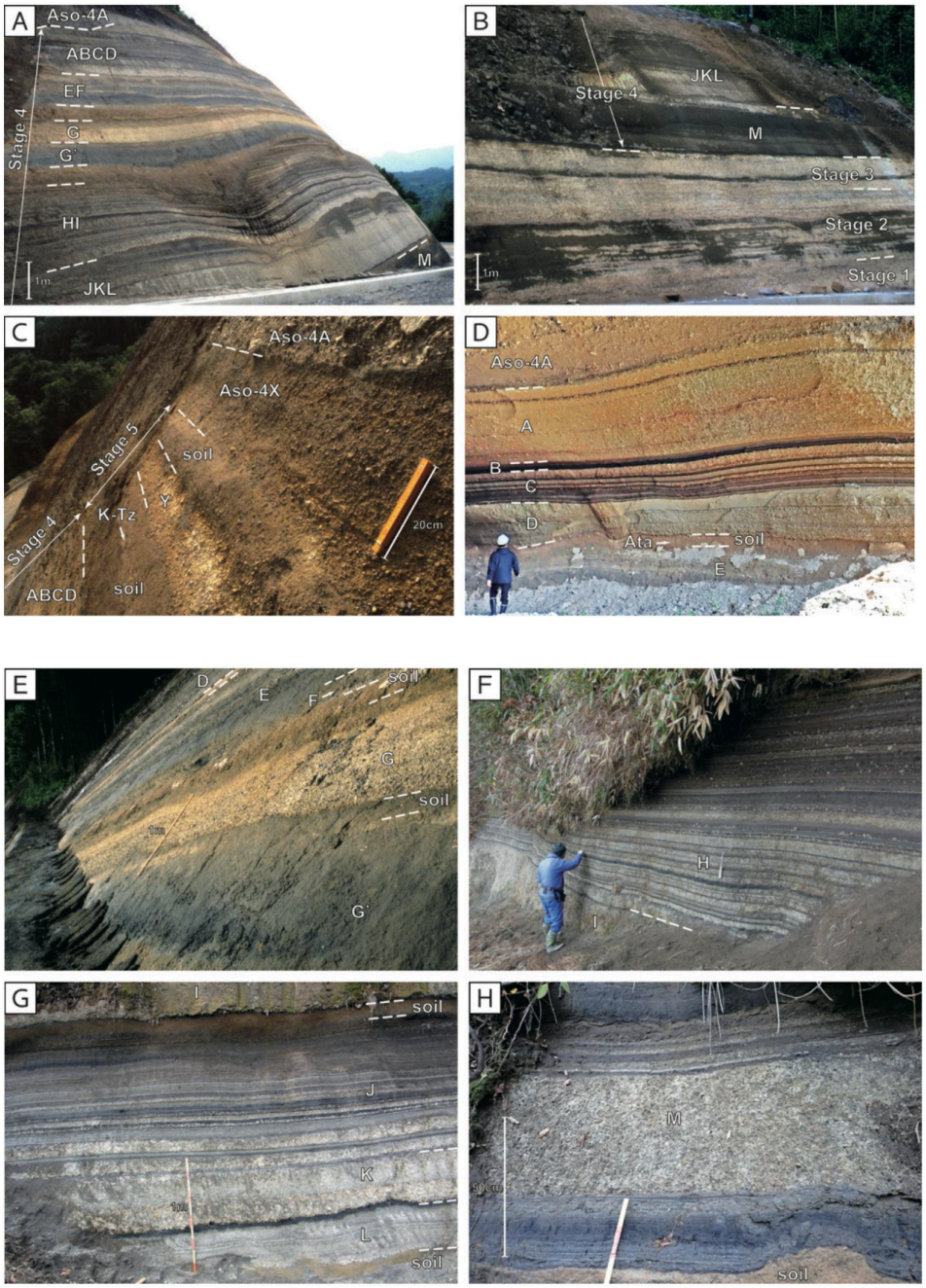


Figure 3.4: Photographs of representative tephra sequences beneath the Aso-4 pyroclastic-flow deposit. Taken from Hoshizumi et al. (2022).

Hata

The Hata sequence is located 8 km to the east of the caldera wall (35.10219 N, 131.31419 E; Fig. 3.2B). The site was logged by Hoshizumi et al., (2022) and revealed several pyroclastic deposits preserved beneath the Aso-4 tephra. Three tephra units were sampled from this outcrop: Aso-D, Aso-EF and Aso-G (Table 3.1).

The Aso-G tephra was first recognised by Hoshizumi et al. (2022) at a proximal outcrop at Hinatame (11 km to the east of the caldera wall), but it was noted as missing from sequences further northeast. At Hata, the Aso-G tephra is 96 cm in thickness. At the base there is 60 cm well-sorted, clast supported, pumice-lapilli fallout followed by 36 cm of ash and lapilli which is poorly-sorted with more frequent pumices at the top (FLF229). Overlying Aso-G, the Aso-EF tephra (measuring 1.05 m thick) was identified. The Aso-E unit is 87 cm thick and at the base there is an oxidised red layer then 7 cm of well-sorted pumice-lapilli (FLF232), followed by 80 cm of alternating ash lapilli with scattered pumice in some ash beds (FLF233/234). Directly overlying is the Aso-F unit, which is an 18 cm thick unit of reversely graded, well-sorted, pumice-lapilli which is clast supported with a diffuse wavy top (FLF230). The Aso-D tephra (lowermost sub-unit of Aso-ABCD) was identified on top of Ata bearing sediments (unconformity). The basal fall of Aso-D was sampled (FLF236) for this thesis.

Katayama

At Katayama, Takamori Town, Kumamoto Prefecture, 7 km southeast of the Aso caldera (32.84887 N, 131.24961 E; Fig. 3.2B), three tephra units preserved beneath Aso-4 (Aso-HI, Aso-JKL and Aso-Z6; Table 2.1) were logged and sampled.

Towards the base of the exposed sequence at Katayama, the Aso-Z6 tephra is preserved as a 27 cm thick unit comprised of alternating pumice and ash layers. At base of the tephra there is a 7 cm thick well-sorted white pumice-lapilli layer (FLF227), which is covered by a 20 cm thick black to blue-grey volcanic ash layer with 2 mm diameter grain size.

Further up the Katayama sequence, the Aso-JKL unit was identified. Hoshizumi et al (2022) refined the Aso-KL tephra layer of Ono and Watanabe (1983) to include the previously unreported Aso-J unit. At Katayama, the Aso-JKL tephra is found directly above a thick soil separating it from the underlying Aso-M unit (Fig. 3.4A). The total thickness of the Aso-J sub-unit is 1.71 m of moderately to well-sorted alternating pumice-lapilli (2 cm maximum) and white and dark ash layers. The lowermost Aso-L unit is 38 cm thick and three sub-samples were taken from this tephra. At the base, above a soil, there is 28 cm of alternating layers of pumice-lapilli and ash that is moderately-sorted. A coarse pumice-lapilli layer was sampled (FLF197) as well as a 4 cm thick dark ash bed (FLF198) and a 6 cm thick white/light ash bed (FLF199). Directly above this unit is the Aso-K unit, with no evidence for soil development or an unconformitiy. At the base of the Aso-K unit there is thick white coarse pumice-lapilli fall layer (3.5 cm maximum) that well-sorted with some lithics (1.4 cm

maximum), which is overlain by a 52 cm thick pumice section (FLF200). Above which is the Aso-K upper pumice, measuring 34 cm thick of reversely graded, well-sorted pumice-lapilli (2.5 cm maximum) and is lithic poor (FLF201). Above is the Aso-J unit. The upper 68 cm of the Aso-J unit is only alternating ash beds no pumice-lapilli. Both pumices from the base (FLF202) and middle (FLF203) of the Aso-J unit were sampled for geochemical analysis.

The Aso-HI eruptive succession is the second largest pre-Aso-4 caldera eruption, and measures at 6.07 m in thickness at Katayama, where the Aso-I unit is defined as a 1.0 m thick pumice layer, overlain by Aso-H a 5.1 m thick package of alternating layers of pumice and ash beds, containing obsidian fragments (Fig. 3.4F). The total thickness of the lower Aso-I unit is 1.0 m and the base (32 cm thick) is reversely graded with coarser pumices at the base which are clast supported and well-sorted (FLF206). The top of Aso-I does not show clear grading and more moderately-sorted than the lower sections of Aso-I but still clast-supported fine lapilli; the upper pumices (maximum 2.8 cm) from this sub-unit were sampled (FLF207). Directly above lies the Aso-H unit. Owing to the thickness of the Aso-H unit, at Katayama, for chemical characterisation, it was sub-divided into four sub-units labelled Aso-H1-4 (in ascending order) where the lowermost sub-units (Aso-H1–3) are all pumice layers, whilst the uppermost sub-unit (Aso-H4) is an ash layer. Aso-H1 (base) is a 1.2 m thick sub-unit comprised of alternating ash and pumice-lapilli layers, which are moderately to well-sorted and clast supported. The ash beds are comprised of coarse ash which are either grey or black/brown in colour, and some beds are reversely graded. The uppermost pumice-lapilli bed from the H1 sub-unit was sampled for geochemical analysis (FLF208). The next sub-unit is Aso-H2 (lower), which is a 1.5 m total thickness and starts with 7.5 cm bed of finely bedded grey-brown ash, followed by 10 cm of well-sorted pumice-lapilli, maximum pumice clast sizes of 2.3 cm. The darkest fine lapilli to coarse ash layer towards the base of the sub-unit which is 5 cm thick was sampled for analysis (FLF212), as well as the thickest pumice bed found towards the middle of the sub-unit (FLF213) which had maximum pumice clasts of 3.5 cm and lots of obsidian (largest 0.6 cm) making up dark beds. The overlaying Aso H3 (upper) sub-unit which measures 1.12 m total thickness and is composed of moderately-sorted pumice-lapilli layers alternating with ash beds and obsidian clasts (maximum 2.6 cm). Within upper alternating beds some very large pumice clasts up to 6 cm. A middle pumice layer was sampled for geochemical analysis (FLF217). The uppermost Aso-H4 (top) sub-unit recorded by Hoshizumi et al., (2022) is 1.3 m thick. However, upon our field campaign in 2023 it was eroded and thus we were unable to see the full thickness of this sub-unit, but we were able to establish ourselves within the sequence by the presence of an ashy white bed. Aso-H4 is made up of alternating lapilli at and ash layers, a middle pumice layer (13 cm thick) was sampled for geochemical analysis (FLF219).

Koga

The Koga sequence is located 3 km to the east of the Aso-4 caldera wall (32.98676 N, 131.16254 E; Fig. 3.2B). The site was logged by Miyabuchi (2009) and several pyroclastic deposits preserved above the Aso-4 tephra were noted. Two tephra units (ACP4 and ACP6; Table 2.1) were logged and sampled from this outcrop.

Aso central cone pumice 6 (ACP6) is one of the key beds among the post-caldera tephras (Takada, 1989). The ACP6 tephra is composed mainly of poorly-sorted pumice and ash beds (Fig. 3.3A). A 9 cm thick clast supported, well-sorted pumice unit (maximum 1 cm) was sampled for geochemical analysis (FLF186).

Further up the sequence at Katayama, the Aso central cone pumice 4 (ACP4; Takada, 1989), one of the largest pumice-fall deposits from the post-caldera central cones, was logged and sampled (Fig. 3.3A). The lowermost fall unit is thickest and composed of fine, pale yellow, well-vesiculated pumice-lapilli (0.6 cm mode) and includes abundant obsidian clasts (FLF190). The lower to middle units contain scattered banded pumice. The uppermost unit is 17 cm thick and includes coarser poorly vesiculated pumice-lapilli clasts (FLF191).

Kurumi Baru

At the Kurumi Baru site, located 9 km east of the Aso-4 caldera wall (32.83909 N, 131.24609 E; Fig. 3.2B). The site was logged by Hoshizumi et al (2022) and revealed several pyroclastic deposits preserved beneath the Aso-4 tephra. Both the Aso-Y and overlying Aso-4X tephras (Table 3.1; Fig. 3.4C) were sampled for geochemical analysis.

The Aso-Y tephra is a white pumice fall layer consisting of a single fall unit and is mainly composed of pumice with a maximum diameter of 1 cm (FLF248). The Aso-Y tephra contains plagioclase, biotite, hornblende and traces of clinopyroxene and orthopyroxene. Above the Aso-Y tephra lies the Aso-4X unit, however between these tephras there is an unconformity. The Aso-4X unit observed at Kurumi Baru has a total thickness of 1.3 m. It is directly overlain by Aso-4 pyroclastic-flow deposits and considered to be the basal Plinian fall of the Aso-4 pyroclastic-flow eruption (Fig. 3.4C; Hoshizumi et al., 2022). The lower unit is coarsely graded with pumice clasts up to 3.5 cm and maximum 1 cm lithics (FLF194). The upper unit is 57 cm in thickness and comprised of alternating units where grain size and lithic content varies (FLF196). Throughout the Aso-4X unit there are biotite and hornblende phenocrysts.

Noga Cave

Noga Cave is located 13 km to the east of the Aso-4 caldera wall (32.94062 N, 131.31076 E; Fig. 2.2B) and has been logged by Hoshizumi et al (2022) (Fig. 3.4). Five tephra units (Aso-Y, Aso-EF, Aso-L, Aso-M and Aso-N/Z2) were logged and sampled from this outcrop.

The Aso-N/Z2 tephra at Noga Cave is 19 cm thick and comprised of pumice-lapilli that is well-sorted and has normal to reverse grading. At the base, there is 9 cm of normally graded lapilli (3 cm maximum), then the unit coarsens upwards (reversely graded), with a darker lithic-rich layer at the transition from normal to reverse grading (FLF67). The lower pumice unit was analysed by Albert et al., (2019b). Above there is a 10 cm thick fine ash deposit with sporadic pumices (FLF69) that is capped by a lithic rich fine black ash. Above Aso-N/Z2 is the Aso-M tephra, which has previously been geochemically analysed (see Albert et al., 2019b). The Aso-M tephra is 9 cm thick, and comprised of well-sorted pumice-lapilli (1.5 cm maximum) with no clear grading and is lithic poor (FLF72) then overlain by a mafic ash layer. Above the Aso-M tephra is a thin soil layer upon which the Aso-L unit lies (Fig. 3.4B). At the base of the Aso-L unit at Noga Cave there is 5 cm of pumice-lapilli (FLF247) topped with dark grey ash.

Further up the sequence at Noga Cave, the Aso-EF unit is observed. Above the soil overlaying the Aso-ABCD tephra lies the Aso-EF tephra. The Aso-F tephra is a 1.34 m thick unit of largely comprised of ash layers. At the base there is 8 cm of normally graded pumice-lapilli (1 cm maximum), which was sampled for geochemistry (FLF73), and capped by 60 cm of laminated ash, and 6 cm of diffuse weathered pumice. At the top of Aso-F there is 60 cm of ash, with some diffuse pumice. Directly above lies the Aso-E unit which is a 36 cm package of alternating pumice and ash deposits. At the base of Aso-E there is 5 cm of sorted, normally graded basal pumice (2.5 cm maximum), which is followed by a 22 cm series of alternating fine pumice-lapilli and ash layers with thin bedding visible in places, and is capped by 9 cm of ashy sediments which contains biotite. A coarse pumice-lapilli from the middle of Aso-E was sampled for geochemical analysis (FLF74). Except for the pumice layer at the base of the Aso-F unit, all layers contain plagioclase orthopyroxene, and clinopyroxene phenocrysts (1 mm) but no hornblende.

The Aso-Y tephra preserved at Noga Cave is 8 – 13 cm thick and comprised of moderately to well-sorted pumice-lapilli (1.6 cm maximum), with lenses of coarser pumice along the section and is lithic rich, and some large free crystals, biotite and hornblende (FLF65).

Nojiri

Nojiri is located 5 km east of the Aso caldera rim (32.82325 N, 131.22318 E; Fig 3.2B). The Nojiri pumice (NjP; Table 3.1) is the first moderate-large eruption post-Aso-4 and it consists of weathered pumice clasts (Miyabuchi, 2009). It is related to one of the largest eruption events to have occurred at the post-Aso central pumice cones. At Nojiri, the NjP reaches a maximum thickness of 1.30 m and is divided into lower and upper parts by an olive-brown 10-cm-thick silty ash. The lower part (77 cm thick) is composed of light pale/yellow weathered pumice clasts (average 4 cm) with small amounts of lithic and dark coloured pumice (FLF52). The upper part is 45 cm thick and contains pale-yellow weathered pumice (average 2.5 cm) with small amounts of black lithic and obsidian clasts. The pumice clasts in the lower part include hornblende phenocrysts; in contrast, those in the upper part contain hornblende and biotite phenocrysts in addition to plagioclase, orthopyroxene and clinopyroxene which are present throughout. However, the NjP is highly weathered, hindering the ability to obtain geochemical data for this tephra.

Takimizu

Takimizu is located 7 km east of the Aso caldera rim (32.93166 N, 131.24803 E; Fig. 3.2B) and two tephras (ACP3 and Aso-Kpfa; Table 2.1) were sampled from this site. The Kusasenrigahama pumice (Aso-Kpfa; Watanabe et al., 1982) is one of the most distinctive fallout deposits, which can be easily recognised around Aso caldera. The Aso-Kpfa is divided into six fall units of alternating pumice-lapilli and ash layers and is underlain by a thick black humic soil. At the base, there is 35 cm of well-sorted pumices, capped by 1 cm of ash, followed by 3.5 cm pumice-lapilli, and then a thin 0.5 cm layer of ash with a final 16 cm of pumice-lapilli at the top (FLF56). Above the Aso-Kpfa is a moderately-sorted fine ash layer with the presence of pumice-lapilli which was also sampled (FLF57).

The ACP3 at Takimizu is a diffuse 12 cm thick unit composed of poor to moderately-sorted pumice layer with ash between the pumices (FLF58). The pumices (4 cm maximum) are white with black shiny crystals (biotite). Above lies the ACP4 tephra, which is composed of a series pumice-lapilli fall layers. At the base there is 5 cm of well-sorted, fine pumice-lapilli (2.5 cm maximum) which grades into coarser moderately to well-sorted 35 cm pumice-lapilli (FLF61). The tephra then grades sharply into 5 cm finer, well-sorted pumice-lapilli (typical 0.3 cm clasts) (FLF62) and coarse ash, which is darker in appearance (lithics) followed by a further 5 cm of coarser pumice-lapilli (FLF63), typically 0.5 cm. There are diffuse pumices (1 cm maximum) in the 5 cm of tephric soil above, which may have been bioturbated.

Yamasaki

Thirteen eruption units have been identified in a 15 m thick sequence at Yamasaki termed the Yamaski Pumices (YmP) 13 to 1 (YmP13 – YmP1; Table 3.1) in ascending order (Fig. 3.3B ; Miyabuchi et al., 2003). These deposits are frequently subdivided by thin soil beds. Despite the number of YmP tephras logged in proximal sequences, none of the units have been geochemically characterised. Four of these pumice units (YmP5 – YmP8) were sampled for this thesis (see Table 3.1). All four of these units (YmP8 – YmP5; Fig 3.3B) contain plagioclase, clinopyroxene, orthopyroxene and magnetite phenocrysts. The YmP5 is the thickest, and measures 2.3 – 2.5 m thick and is comprised of a lower pumice bed (A9746 P-B4) and thin ash layers, overlain by scoria-fall. The YmP5 unit has an unconformity at the top and is believed to have erupted over a relatively short period and is the key marker bed of the YmP tephras (Mitabuchi et al., 2003; Miyabuchi, 2009). The underlying YmP6 (A9746 P-B5/4), YmP7 (A9746 P-B5), and YmP8 (A9746 P-B6) were also sampled for geochemistry.

3.3.2. Kirishima (Chapter 5)

Kirishima Iwaokoshi (Kr-Iw) and Awaokoshi (Kr-Aw) tephra samples were collected for geochemical characterisation from an abandoned Quarry site in Umegakubo, Takahara Town (31.96448 N, 130.95711 E) 18 km north-east of the Kirishima complex. This B-1 sequence was previously reported by Nagoka et al. (2010). On visiting the B-1 section reported by Nagoka et al. (2010) the lowermost Kakuto (KKT) and Umegakubo tephra units were no longer exposed. The Aira – Iwato (A-Iw) white pumice-lapilli fall deposit was identified at the base the stratigraphy (Fig. 3.4; Table 3.1). It is overlain by two prominent tephra units in the volcanic stratigraphy of the Kirishima volcanic complex, the Iwaokoshi (Kr-Iw) tephra from the Onaminoike volcano, and Awaokoshi tephra (Kr-Aw) from the Hinamori volcano (Nagoka et al., 2010).

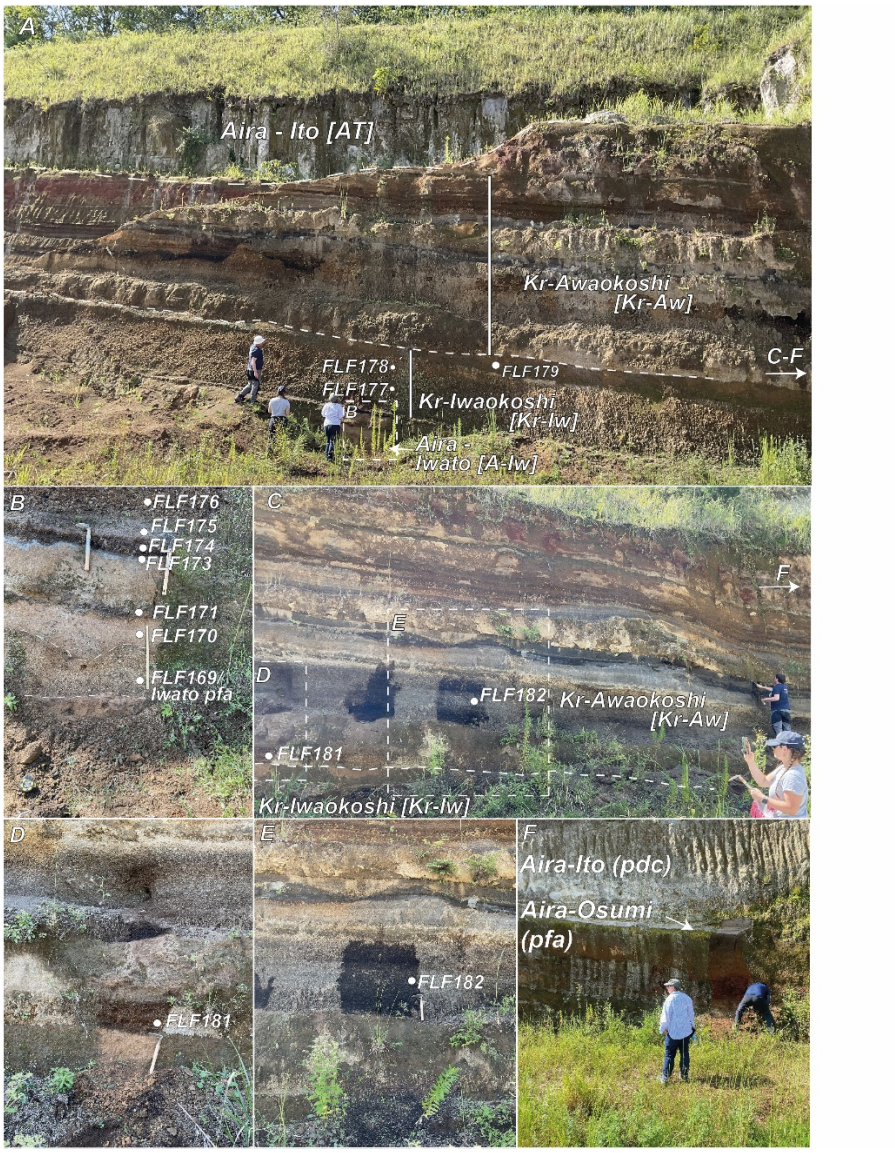


Figure 3.5: Umegakubo Quarry, Takahara Town where reference samples of the Kirishima Iwaokoshi (Kr-Iw) and Awaokoshi (Kr-Aw) tephra units were collected north-east of the Kirishima volcanic complex, and stratigraphically position between the Aira-Iwato and Aira-Ito tephra deposits. Marked are the positions of samples (FLF) collected for geochemical fingerprinting and comparison with the Lake Suigetsu tephra layers. Taken from Vineberg et al. (2024)

The Kr-Iw tephra sequence begins with a thin grey medium to coarse ash (1 cm), and capped by 9 cm of moderately-sorted, fine pumice and scoria lapilli (FLF175), where maximum clasts sizes are 0.9 cm. This is then overlain by 1.39 m thick bed of moderately to well-sorted, clast supported pumice-lapilli, which displays reverse to normal grading (Fig. 3.5). Samples were collected from the finer pumice-lapilli base (FLF176), the coarsest pumice-lapilli (FLF177), at the base of the normal graded portion (~30 cm), and where maximum pumice-lapilli clasts reach 6.5 cm and lithics are up to 3 cm. The uppermost 20 cm of pumice-lapilli were also sampled (FLF178) (Fig. 3.5). The pumices were generally crystal poor (orthopyroxene and clinopyroxene), and showed evidence of mingling / banding, with

lighter and darker glasses. The Kr-lw pumice fall was capped by 44 cm of predominantly, poorly-sorted ash and pumice/scoria lapilli, along with laterally discontinuous layers/pods of clast supported, moderately-sorted pumice and scoria lapilli.

The Kr-Aw tephra from Hinamori volcano was observed above the Kr-lw unit and is comprised of 30 cm of well-sorted, clast-supported, alternating fine- to coarse-grained scoria/pumice-lapilli fall (FLF181), and maximum scoria clasts are 3 cm. This is overlain by a poorly-sorted ash unit, containing pumice, scoria and lithics (77 cm thick). This unit is capped by 67 cm of normally graded, well-sorted, clast supported scoria fall (FLF182), representing the single thickest fall deposit of the Kr-Aw eruptive sequence, above this are multiple thinner alternations of coarse- and fine-grained scoria lapilli beds, with the total thickness of the Kr-Aw tephra being ~6 m. Some of the poorly-sorted units within the Kr-Aw tephra sequence, may represent remobilised volcanic material, and be indicative of eruptive hiatuses, meaning the 'Kr-Aw tephra' could represent multiple eruptions.

3.3.3. Sambe (Chapter 5)

The Sambe Kisuki (SK) was sampled for geochemical characterisation and dating ($^{40}Ar/^{39}Ar$; Zircon Double Dating; ZDD) at Kakeyacho Kakeya, Unnan, Honshu (35.21120 N, 132.81508 E) 25 km north-east of Sambe volcano. The SK tephra rests on a paleosol and comprises of a 2 m thick, well-sorted, clast supported, pumice-lapilli unit, with reverse to normal grading through the unit (Fig. 3.6A,B). The maximum pumices within this pumice fall deposit were 3 cm, and it was at this coarsest level that the samples were taken for analysis (FLF132/133). The pumices are heavily weathered (Fig. 3.6B); however some fresh glass matrix was observed within some pumices, which also contained abundant biotite. Above the SK tephra was a 1 mthick paleosol, and upon this soil is another 30 cm thick, normally graded, well-sorted, clast supported white pumice-lapilli, which alternated with thinner ash beds. This unit is considered to also derive from Sambe volcano, and based on stratigraphic position is most likely the Sambe SuN tephra. We also carried out further detailed chemical analyses of a well-sorted SK tephra deposit preserved in the IODP Sea of Japan marine core, U1427A (Fig. 3.6C), which offers an additional sample for the SK tephra deposit. Sagawa et al. (2018) identified the SK tephra in this marine core based on its major element glass chemistry, here we supplement this with additional trace element (LA-ICP-MS) characterisation of the distal tephra unit.



Figure 3.6: (A) Sambe Kisuki (SK) at a Kakeyacho Kakeya, Unnan, Honshu (B) shows the heavily weathered clast- supported pumice-lapilli clasts; (C) the well-sorted SK tephra preserved in IODP U1427 and reported by Sagawa et al. (2018). Taken from Vineberg et al. (2024).

3.4. Distal tephra record: Lake Suigetsu (Chapter 5)

The Lake Suigetsu sedimentary sequence was analysed for cryptotephra preservation between 120 and 50 ka. The geological and hydrological conditions of the Lake Suigetsu catchment and subsequent coring campaignsof the lake are outlined below.

3.4.1. Geological and hydrological setting

Lake Suigetsu, Honshu Island, Japan (35°35′0″N, 135°53′0″E) is located within a small tectonic basin situated on the western side of the Mikata fault line (Fig. 3.7C). It is the largest of the of the 'Mikata Five Lakes' covering an area of 4.3 km^2 (a perimeter of ~10 km and diameter of ~2 km) and has a water depth of ~34 m (Kitagawa and van der Plicht, 1998).

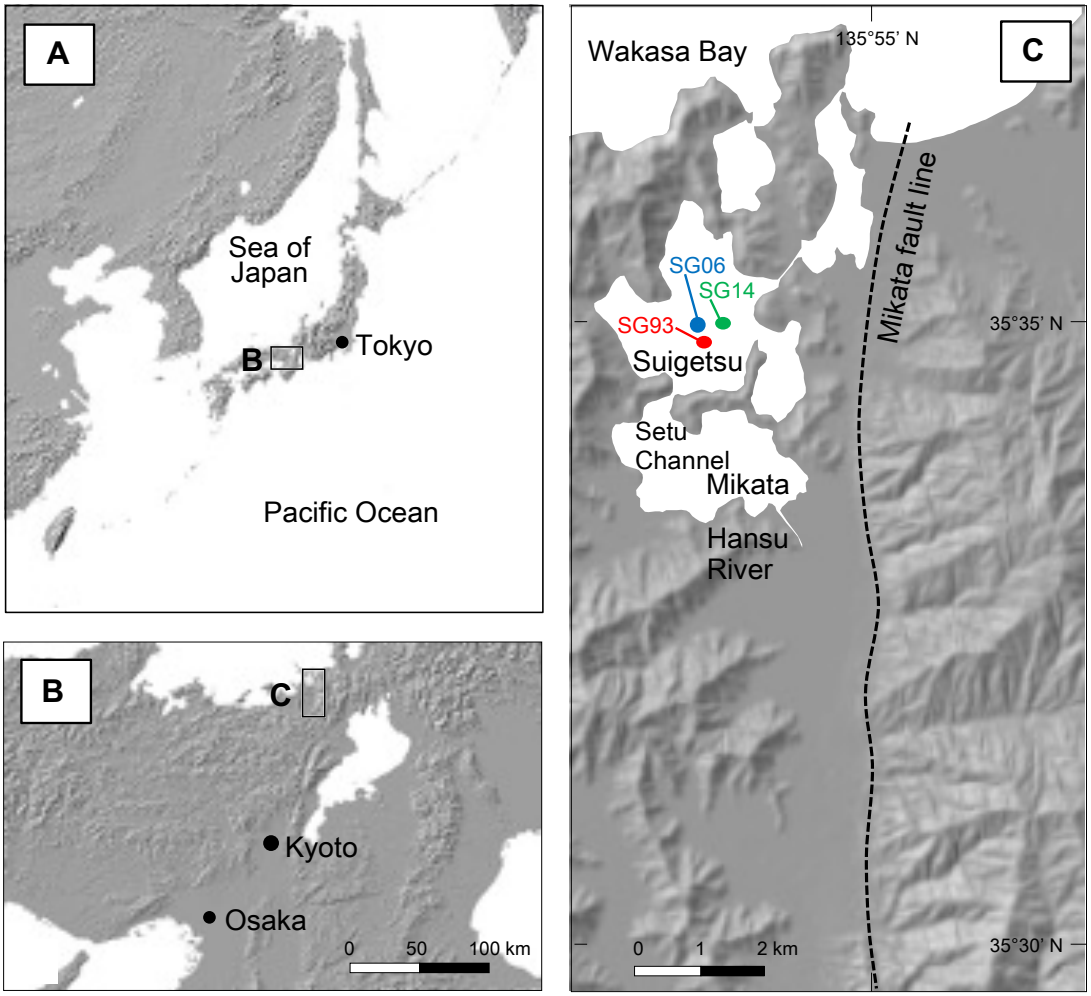


Figure. 3.7: (A) Map of Japan (B) Proximity of Lake Suigetsu to major Japanese cities. (C) Location of Lake Suigetsu as part of the five Mikata Lakes, adjacent to Wakasa Bay. The positions of all three coring campaigns are marked. Modified from Nakagawa et al. (2005).

The lake has a small catchment area, is currently vegetated by vegetated by temperate broadleaf and mixed forest and is surrounded by a ring of Paleozoic hills (maximum elevation 400m) (Nakagawa et al., 2005; Kitagawa et al., 1995; Yasuda, 1982). The main tributary is the Hasu River that enters on the southeast edge of Lake Mikata, which flows through the narrow Seto Channel (~2 m in depth) into Lake Suigetsu (Fig. 3.7C). The coarse sediment is deposited in Lake Mikata before the water reaches Lake Suigetsu (Nakagwa et al., 2005). The deep-water column (34 m) and low-energy environment hinder the mixing of sediments. This unique hydrological configuration and geomorphic protection means that sedimentary regime is highly stable and dominated by fine-grained continuous deposition of fine-grained clastic sediments (Nakagawa et al., 2021).

3.4.2. Coring campaigns

Lake Suigetsu has been cored multiple times over the last three decades. The coring campaign in 1993 ('SG93') retrieved a single 72.4 m piston core from the basal sediments and revealed a significant proportion of the sequence was annually laminated (varved; Nakagawa et al., 2003; Kitagawa and van der Plicht, 1998; Kitagawa et al., 1995). Varve counting permitted a high-precision independent chronology for the SG93 core and was combined with over 250 accelerator mass spectrometer (AMS) radiocarbon (^{14}C) ages from terrestrial plant macrofossils generating a terrestrially-based atmospheric radiocarbon calibration dataset from 45,000 cal. yr BP to present (Kitagawa and van der Plicht, 1998). However, the extended tree-ring based datasets (Reimer et al., 2014) indicated that the SG93 chronology was too young. Missing varves were possible since a single borehole with no overlapping sections was recovered, and there could be gaps of unknown durations between successive segments (Nakagawa 2012; Kitagawa and van der Plicht, 2000). This was confirmed by a statistical re-analysis by Staff et al. (2010).

The lake was redrilled in 2006 (~250 m north from the SG93 borehole; Fig 3.7C) as part of the 'Lake Suigetsu Varved Sediment Project'. The aim of this campaign was to obtain a complete 'master' sedimentary sequence to provide sediment for: a high-resolution paleoenvironmental reconstruction for the East Asian monsoon across the last glacial-interglacial cycle; and to establish a purely terrestrial radiocarbon calibration dataset for the complete radiocarbon dating range (last ca. 60 kyr). A complete 'master' core was obtained, that reached the base of the sedimentary profile (73.2 m), by recovering overlapping cores from four parallel boreholes (A, B, C and D; Fig. 3.8) situated ~20 m apart (Nakagawa et al., 2012). Each core segment was ~1 m in length, however the piston extraction meant that the top 5 cm of each 1 m core section may be disturbed, and thus not included as part of the master sequence (Nakagawa, 2012). Numerous geochronological methods were applied to the core to create a precise chronology for the last 50 kyr. Varve counting revealed it is the longest continuously varved record from the Quaternary (Schlolaut et al., 2012, 2018), tephrochronology revealed key radiometrically dated tephra layers (Smith et al., 2011b; Smith et al., 2013) and optical stimulated luminescence (OSL) has provided independent age estimates that support and extend beyond radiocarbon chronologies (Staff et al., 2024, 2013). Notably, the 182 ^{14}C determinations from terrestrial plant macrofossils enabled a comparison to the tree-ring derived calibration. The combination of varve counts and radiocarbon determinations allow the calibration curve to be extended beyond the dendrochronological 12,550 cal. BP limit. (Staff et al., 2011).

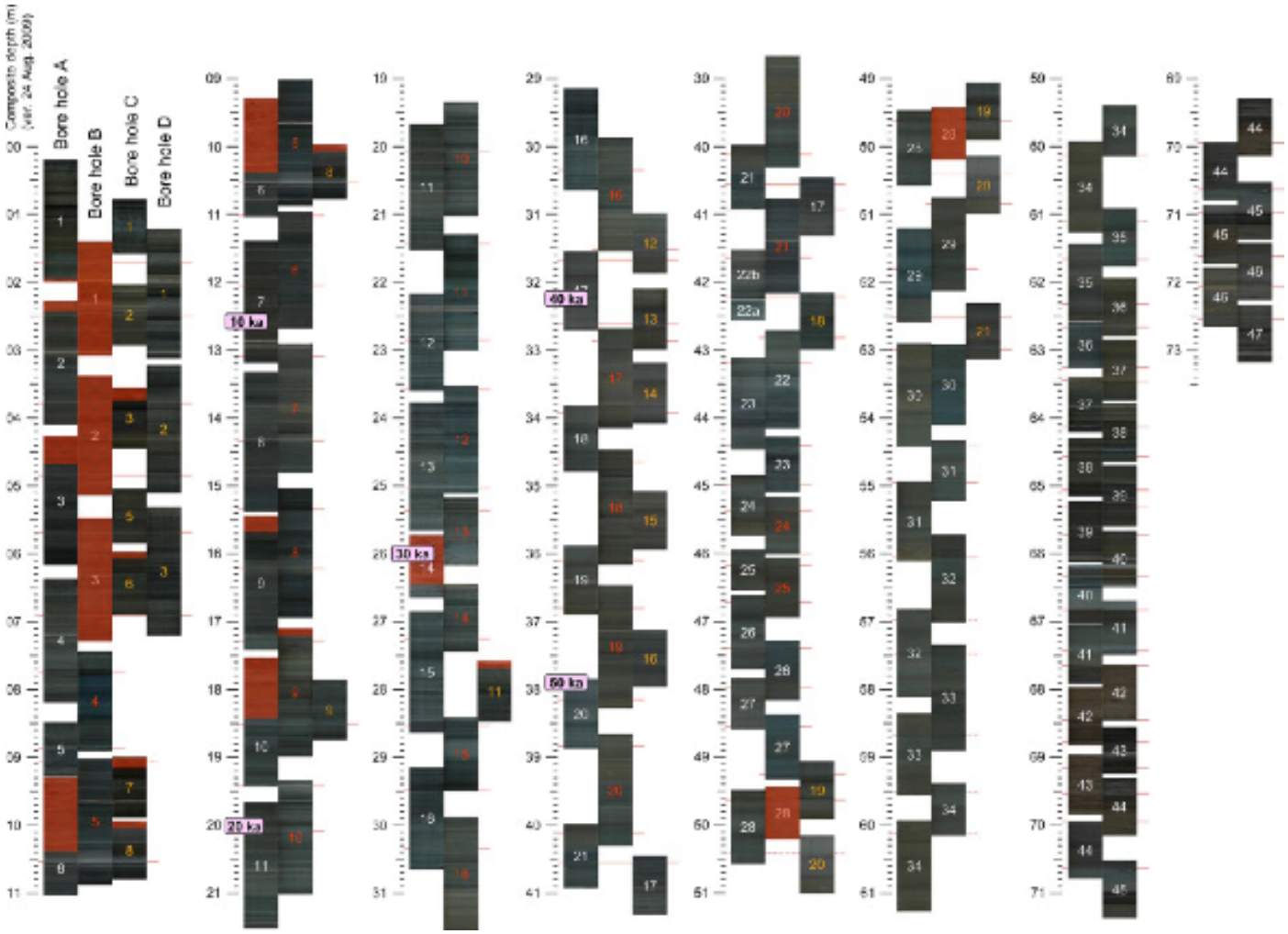


Figure 3.8: Photographic record of the litho-stratigraphy of the SG06 core. Colours of core numbers that are in red = magnetically oriented using *in-situ* sensor; orange = Geographically oriented using marks on rods; white = no orientation. Red shades on core images = disturbed sediments. Taken from Nakagawa 2012.

Improved techniques of varve counting (using thin-section microscopy and ultra-high x-ray fluorescence (XRF)) allowed the precise comparison and alignment of the SG06 against the SG93 profile and allow the integration of both radiocarbon datasets (Bronk Ramsey et al., 2012). As a result, 808 radiocarbon dates from terrestrial macrofossils form the Lake Suigetsu dataset, and the varve counts extend the terrestrial radiocarbon calibration curve to 52,800 cal. yr BP (Bronk Ramsey et al., 2012; Staff et al., 2011). Thus, Lake Suigetsu is used as a key record for the IntCal dataset (Ramsey et al., 2012, 2023) and used to calibrate radiocarbon measurements (e.g. IntCal20; Reimer et al., 2020). The impressive chronology has not only aided understanding for the tempo of volcanism in the region, but also the rates and dynamics past environmental change (e.g. Rex et al., 2022; Nakagawa et al., 2021; Schlolaut et al., 2014; Tyler et al., 2010).

The SG12 coring campaign at Lake Suigetsu, conducted in 2012, focussed on collecting additional sediments cores to fill any stratigraphic gaps in the SG06 record. In 2014 a subsequent coring campaign was undertaken (~320 m east of the SG06 boreholes; Fig. 2.7C) to obtain another continuous sequence (named SG14) for further material for scientific analysis and for thin sections for display at a purpose-built museum (Fukui Varve Museum, Fukui Prefecture). The SG14 master sequence comprises core sections from four overlapping boreholes (E, F, G and H), that extends to a thick gravel at ~98 m (~25 m deeper than SG06). The core was logged and key event layers were chosen as reference points to tie the sequence both between boreholes and with the SG06 master sequence (as in Fig 3.9). Marker horizons are typically visible volcanic ash layers or clay rich laminations which would remain visible under oxidation and clearly present in all sections. The SG14 sequence (correlation model 30 May ’17) has been precisely tied to the SG06 composite core (correlation model 08 May ’16) using 361 marker layers. These correlations allow the high-precision SG06 chronology (Bronk Ramsey et al., 2012) to be transferred to the SG14 core.

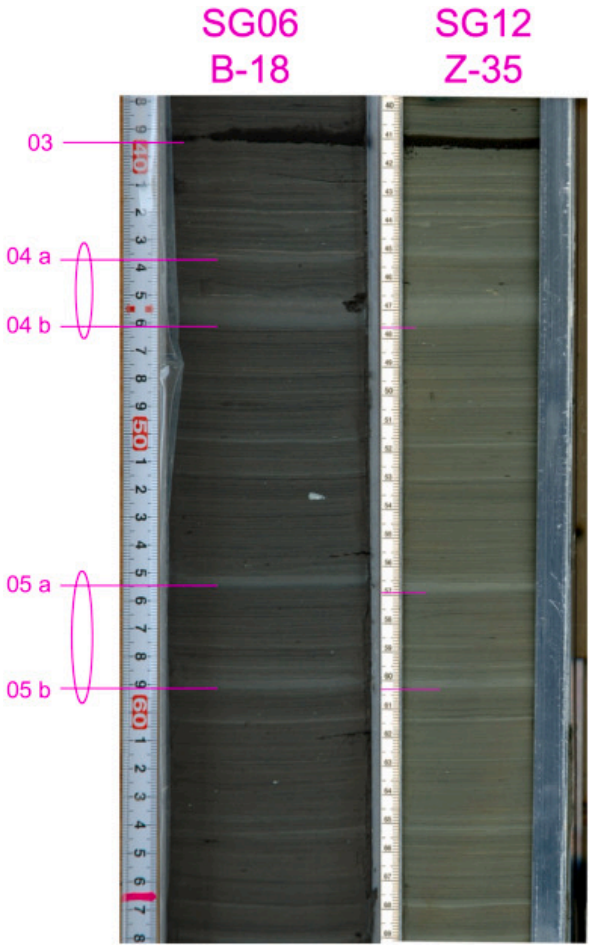


Figure 3.9: Stratigraphic alignment of parallel sediment cores ‘SG06’ and ‘SG12’ enabled via the regular, visibly distinctive macroscopic event layers (Nakagawa et al., 2012). Example shown is between SG06 core section B-18 and SG12 core section Z-35. Taken from Staff et al., 2024.

Chapter 4: Insights into the explosive eruption history of the Campanian volcanoes prior to the Campanian Ignimbrite eruption

Sophie O. Vineberg[a*], Roberto Isaia[bc], Paul G. Albert[d], Richard J. Brown[e], Victoria C. Smith[a]

[a] *Research Laboratory for Archaeology and the History of Art, University of Oxford, UK*
[b] *Osservatorio Vesuviano, INGV, Italy*
[c] *IGAG CNR, Rome, Italy*
[d] *Department of Geography, Swansea University, UK*
[e] *Department of Earth Sciences, University of Durham, UK*

Highlights:

- Ischia and Campi Flegrei were very active between caldera-forming eruptions: twelve units identified between 56 ka and 40 ka.
- Ischia tephras have similar glass compositions having implications for using them and the Schiappone tephra as marker layers.
- The compositions of the nine Campi Flegrei tephras can be categorised into three glass chemistry groups.
- Glass compositions become more evolved over time, extending toward a composition that is also present in the CI deposits.

Abstract:

The Campanian Volcanic Zone (CVZ) comprises multiple active volcanoes and includes the highly productive Campi Flegrei and Ischia caldera systems. These caldera volcanoes have produced probably the largest eruptions in Europe in the past 200 kyr, such as the Monte Epomeo Green Tuff (MEGT; Ischia) at ca. 56 ka and the Campanian Ignimbrite (CI; Campi Flegrei) at ca. 40 ka, which form widespread isochrons across the Mediterranean region. These closely-spaced volcanic centres erupt phonolitic to trachytic glass compositions that are similar, and thus it can be challenging to correlate tephra deposits to specific volcanic sources. Here we present a detailed tephrostratigraphy for pre-CI eruption activity using the units preserved within a sequence at the coastal Acquamorta outcrop, on the western side of the CI caldera rim. Both the MEGT and CI units are present in the section, and they bracket twelve eruption units that were logged and sampled. New major and trace element glass chemistry data have been acquired for these Acquamorta tephra deposits. Three eruption deposits from Ischia and nine from Campi Flegrei are identified, which helps constrain the tempo of volcanic activity of these centres between the large caldera-forming eruptions. The three Ischia tephra deposits between the MEGT and the CI are indistinguishable based on both major and trace element glass chemistry and cannot be correlated to a specific or

known eruption in this interval, such as the Schiappone tephra. The compositional variations between the Campi Flegrei eruptions reveal temporal shifts in the composition of the tephra deposits that reflect changes in the magmatic system prior to the CI eruption. These deposits indicate that there were at least nine eruptions at Campi Flegrei within 16 kyr of the enormous CI eruption, and suggest that there was no significant period of repose before the caldera-generating eruption.

Key words: Tephrostratigraphy, Campi Flegrei, Ischia, Volcanism, Volcanic glass chemistry, Eruption records, Magmatic systems

4.1. Introduction

Records of past volcanism reveal the magnitude, frequency, tephra dispersal and how magma systems have evolved over time. Near-vent (proximal) eruption sequences are fundamental to the reconstruction of past volcanic histories by providing stratigraphic, chronological and geochemical constraints. However, proximal outcrops near volcanoes, especially caldera systems that have produced large explosive eruptions (i.e. those with volcanic explosivity index (VEI) ≥6; Newhall and Self, 1982) are often destroyed and/or buried by voluminous eruption deposits. As a result, only fragmentary eruption records are typically preserved or accessible at sites around the vent (Fig. 4.1.). Distal sedimentary archives (e.g. lacustrine, marine cores) overcome such preservation and accessibility issues and often contain more tephra deposits associated with small- and medium-sized eruptions than their proximal counterparts (e.g. Giaccio et al., 2017; Wutke et al., 2015; Bourne et al., 2010; Wulf et al., 2004, 2008). The absence of such deposits in the proximal record hampers precise correlations in medial and distal areas as data on the number, frequency and full geochemical range of eruptions are poorly constrained. This impacts both the reconstruction of the volcanic history and the tephrochronological framework of the mid-distal proxy record.

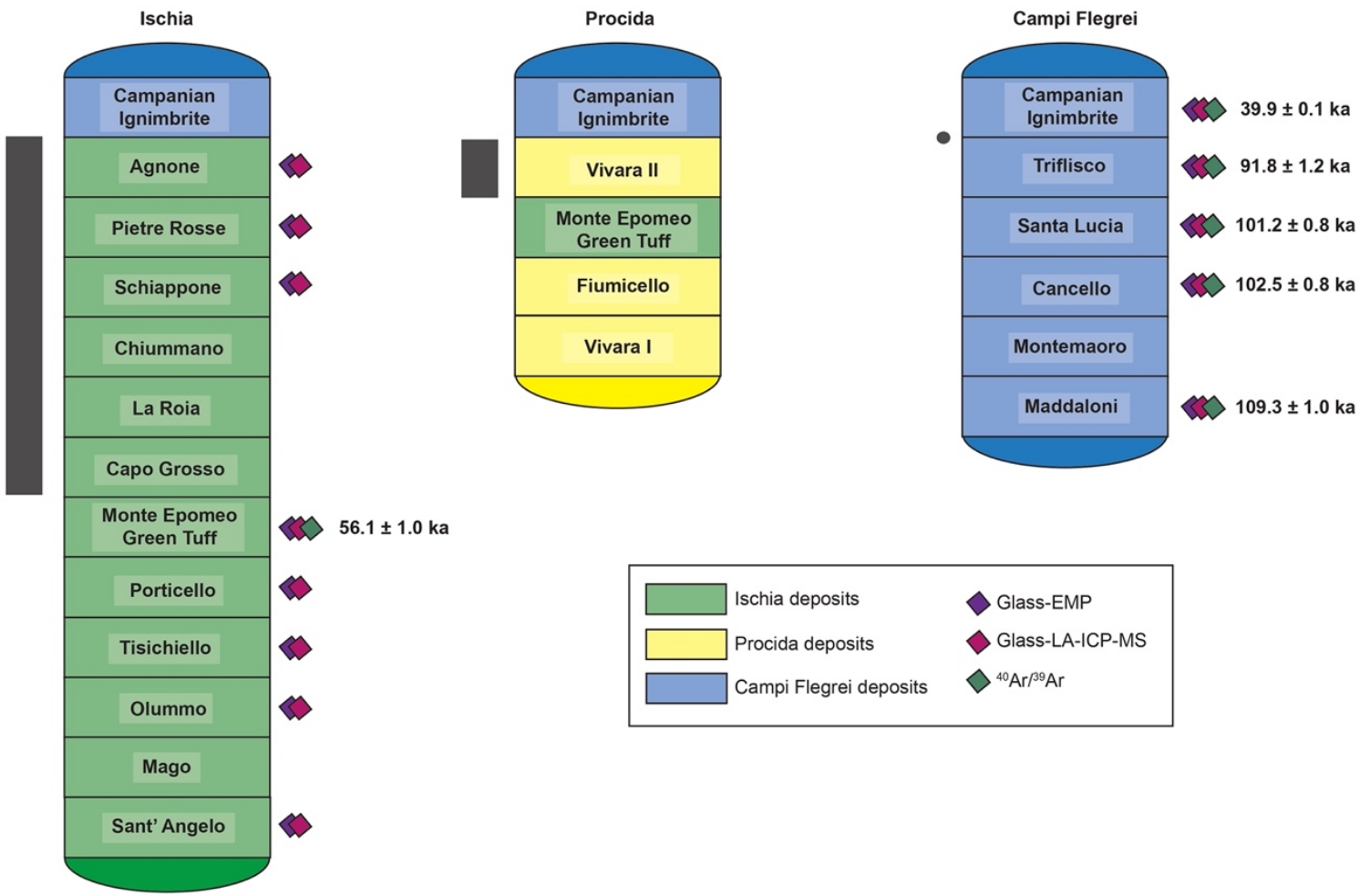


Figure 4.1: The known pre-CI eruptions from the CVZ volcanoes: Ischia (Brown et al., 2008; Civetta et al., 1991); Procida (De Astis et al., 2004) and Campi Flegrei (Monaco et al., 2022). We note that these are not complete stratigraphies and the timescales may vary between units. Units that have major element glass data (Tomlinson et al., 2012, 2014 Monaco et al., 2022), trace element glass data (Monaco et al., 2022; Tomlinson et al., 2012, 2014) and $^{40}Ar/^{39}Ar$ ages (Monaco et al., 2022; Giaccio et al., 2017) are marked. Grey bars and dot denote the stratigraphic position of the Acquamorta sequence that is the focus of this study.

The Campanian Volcanic Zone (CVZ) consists of four volcanoes: Campi Flegrei (Phlegraean Fields), Ischia, Procida and Somma-Vesuvius (Fig. 4.2A), which have experienced explosive activity throughout the Late Pleistocene. Both Ischia and Campi Flegrei have produced caldera-forming eruptions in the last 100 kyr, with at least three large magnitude eruptions from the Campi Flegrei volcano: the Campanian Ignimbrite (CI, 39.9 ± 0.1 ka; Giaccio et al., 2017), the largest eruption in Europe for the past 200 kyr; the Masseria del Monte Tuff (MdMT, 29.3 ± 0.7 ka; Albert et al., 2019b), that corresponds to the widespread Y-3 marker layer (e.g. Keller et al., 1978); and the Neapolitan Yellow Tuff (NYT, 14.2 ± 0.2 ka; Bronk Ramsey et al., 2015). Ischia produced the caldera-forming Monte Epomeo Green Tuff (MEGT; Brown et al., 2008) at 56.1 ± 1.0 ka (Giaccio et al., 2017). These four tephra units form key chronostratigraphic markers and have aided in the synchronisation and chronology of Late Pleistocene sedimentary sequences across the central Mediterranean region (e.g. Giaccio et al., 2017; Albert et al., 2015; Bourne et al., 2010; Wulf et al., 2004, 2012, 2018; Fedele et al., 2003; Schmidt et al., 2002). These marker units are prominent around the calderas, but tephra deposits from eruptions preceding these events are not well exposed in proximal regions. Thus, the eruption history within the CVZ is not well constrained for the periods leading up to these voluminous eruptions.

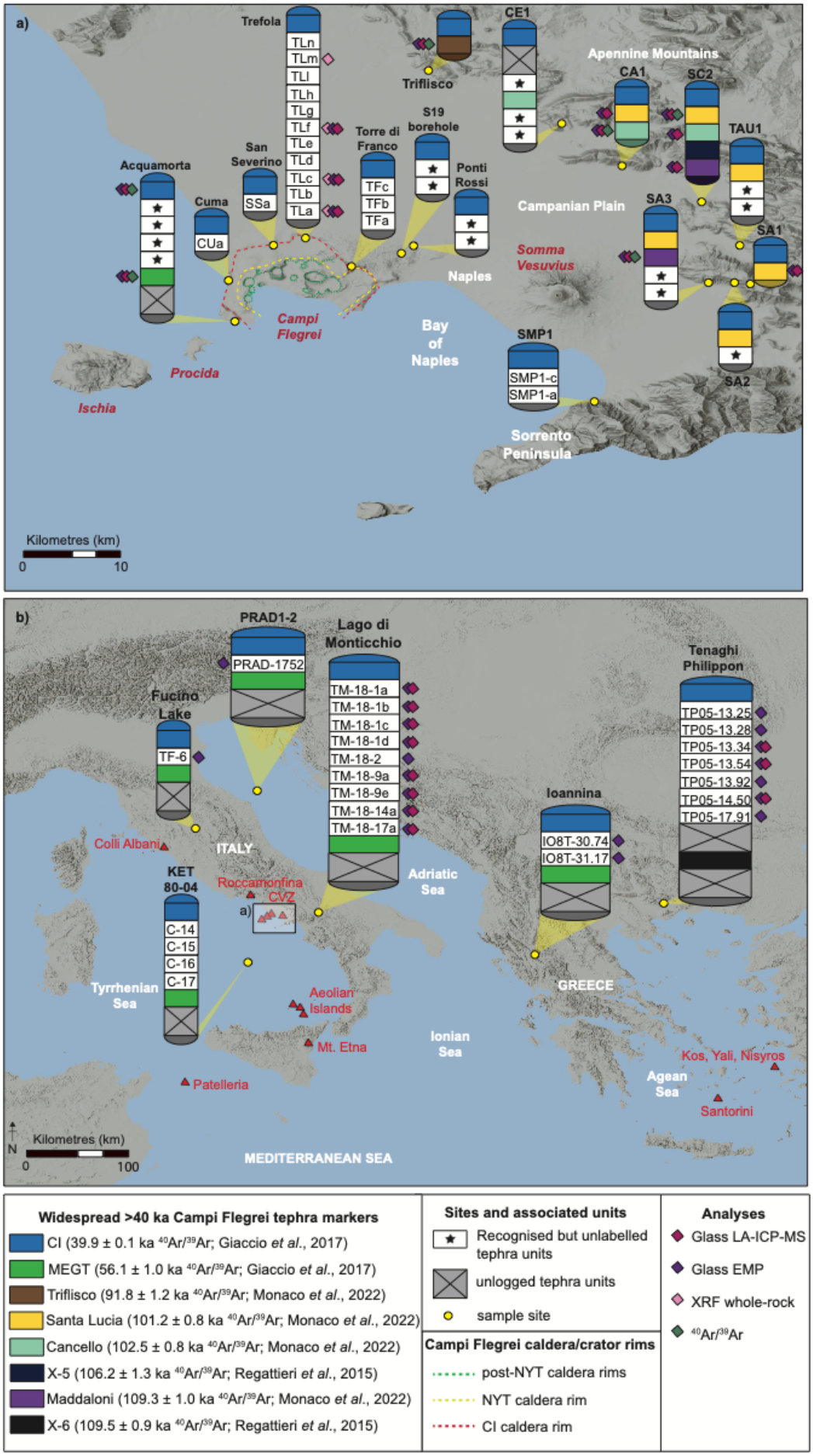

a)
Trefola
TLn
TLm
TLl
TLh
TLg
TLf
TLe
TLd
TLc
TLb
TLa
Triflisco
CE1
Apennine Mountains
CA1
SC2
TAU1
S19 borehole
Torre di Franco
TFc
TFb
TFa
San Severino
SSa
Ponti Rossi
Acquamorta
Cuma
CUa
Campanian Plain
SA3
SA1
SA2
Somma Vesuvius
Naples
Campi Flegrei
Bay of Naples
SMP1
SMP1-c
SMP1-a
Procida
Ischia
Sorrento Peninsula
Kilometres (km)
0
10
b)
PRAD1-2
PRAD-1752
Lago di Monticchio
TM-18-1a
TM-18-1b
TM-18-1c
TM-18-1d
TM-18-2
TM-18-9a
TM-18-9e
TM-18-14a
TM-18-17a
Tenaghi Philippon
TP05-13.25
TP05-13.28
TP05-13.34
TP05-13.54
TP05-13.92
TP05-14.50
TP05-17.91
Fucino Lake
TF-6
Ioannina
IO8T-30.74
IO8T-31.17
Colli Albani
ITALY
KET 80-04
C-14
C-15
C-16
C-17
Roccamonfina
CVZ
a)
Adriatic Sea
Tyrrhenian Sea
Aeolian Islands
Mt. Etna
Patelleria
Ionian Sea
GREECE
Kos, Yali, Nisyros
Agean Sea
Santorini
N
Kilometres (km)
0
100
MEDITERRANEAN SEA
Widespread >40 ka Campi Flegrei tephra markers
CI (39.9 ± 0.1 ka 40Ar/39Ar; Giaccio et al., 2017)
MEGT (56.1 ± 1.0 ka 40Ar/39Ar; Giaccio et al., 2017)
Triflisco (91.8 ± 1.2 ka 40Ar/39Ar; Monaco et al., 2022)
Santa Lucia (101.2 ± 0.8 ka 40Ar/39Ar; Monaco et al., 2022)
Cancello (102.5 ± 0.8 ka 40Ar/39Ar; Monaco et al., 2022)
X-5 (106.2 ± 1.3 ka 40Ar/39Ar; Regattieri et al., 2015)
Maddaloni (109.3 ± 1.0 ka 40Ar/39Ar; Monaco et al., 2022)
X-6 (109.5 ± 0.9 ka 40Ar/39Ar; Regattieri et al., 2015)
Sites and associated units
Recognised but unlabelled tephra units
unlogged tephra units
sample site
Campi Flegrei caldera/crator rims
post-NYT caldera rims
NYT caldera rim
CI caldera rim
Analyses
Glass LA-ICP-MS
Glass EMP
XRF whole-rock
40Ar/39Ar

Figure 4.2: (A) Map showing the location of the Campanian Volcanic Zone (CVZ) and the Quaternary volcanic centres Ischia, Procida and Campi Flegrei. Map of the Campi Flegrei caldera and its major structures, modified from Vitale and Isaia (2014). The locations where proximal records with units that have been logged and characterised between the MEGT and CI across the Campanian Plain: Acquamorta (Tomlinson et al., 2014; De Astis et al., 2004; Orsi et al., 1996; ; Perrotta and Scarpati, 1994; Rosi et al., 1988); Cuma (Orsi et al., 1996); San Severino (Orsi et al., 1996); Trefola (Tomlinson et al., 2012; Orsi et al., 1996); Torre di Franco (Orsi et al., 1996); Ponti Rossi (Orsi et al., 1996); S19 borehole (Albert et al., 2019b; Isaia et al., 2018;); CE1 = Cervino (Di Vito *et al.* 2008); SIMP-1 (Di Vito *et al.,* 2008). Also shown are sites from the foothills of the Apennine Mountains where older (>56 ka) Campi Flegrei deposits have been identified and characterised (Monaco *et al.,* 2022; Di Vito *et al.,* 2008). Units beneath the CI that have been observed but are not labelled or correlated to others elsewhere are shown by white boxes with stars. (B) Location of the distal records that have tephra units, with Campanian glass compositions, beneath the CI and above the X-6; Fucino (Giaccio *et al.,* 2017); Monticchio (Tomlinson et al., 2015; Wutke et al., 2015; Wulf et al., 2004); Ioannina (McGuire et al., 2022); KET80-04 (Paterne et al., 1988); PRAD1-2 (Bourne et al., 2010).

Deposits from CVZ eruptions preceding the CI eruption are present in both proximal and distal tephra sequences. However, the number of eruptions and their timing is poorly constrained. Deposits separated by paleosols under the CI occur along the caldera wall faults (e.g. Di Vito et al*.,* 2008; De Vivo et al., 2001; Pappalardo et al., 1999; Orsi et al., 1996; Rosi et al., 1987). Research on tephra sequences across the Campanian Plain reveal numerous tephra deposits including two key Late Quaternary (Marine Isotope Stage; MIS 5e) central Mediterranean tephrostratigraphic markers (the X-5 and X-6 tephras), however there is a paucity of deposits between 90 and 40 ka (see: Monaco et al., 2022; Donato et al., 2016; Giaccio et al., 2012). Furthermore, the sediment core from Lago di Monticchio (LGdM; Fig. 4.2B) is a valuable record of explosive volcanism in Italy, with at least nine tephra deposits between the MEGT and CI which are attributed to pre-CI Campi Flegrei and Ischia events based on geochemical evidence (see: Wutke et al., 2015; Wulf et al., 2004, 2008). The lack of geochemical data for the pre-CI units in proximal sectors prevents correlations of distal tephras to proximal pre-CI deposits. As such, many pre-CI distal tephra deposits have not yet been ascribed to a particular proximal equivalent (e.g. Giaccio et al., 2017; Wulf et al., 2012; Munno and Petrosino, 2007). Such uncertainties surrounding the origins and incompleteness of geochemical characterisation of these pre-CI units inhibits their use for any volcanological purposes and limit their tephrochronological potential.

Here we address this knowledge gap by focussing on a sequence located on the western side of the CI caldera wall that is exposed between the MEGT and CI. In this research we present stratigraphic descriptions of the deposits and their glass chemistry and then use this geochemical data to assess tephra correlations across the southern Mediterranean.

4.2. Campanian volcanic centres and eruptions prior to the Campanian Ignimbrite

All CVZ volcanoes have been active over the past 100 kyr, dispersing tephra across the Mediterranean and beyond (e.g. Smith et al., 2016; Tomlinson et al., 2014; Bourne et al., 2010; Brown et al., 2008; Orsi et al., 1996). The CVZ volcanoes produce similar glass compositions but the specific volcanic source can be identified. Useful elements, ratios (e.g. CaO, Na_2O, Na_2O/K_2O, Nb, Th, Zr/Sr) and bivariate plots (e.g. CaO vs SiO_2, MgO vs CaO, Na_2O/K_2O vs CaO, Y vs Th, Zr/Sr vs Th) that help differentiate the volcanic source for trachytic to phonolitic tephra from the CVZ volcanoes are outlined in Giaccio et al. (2017) and Tomlinson et al. (2015). Whilst the Somma-Vesuvius volcano is part of the CVZ, there are no explosive deposits recorded prior to the Pomici di Base eruption at 22.1 ± 0.4 ka (Bronk Ramsey et al., 2015; Cioni et al., 1999) and thus we do not consider it as a potential source for these tephra deposits presented in this study.

4.2.1. Campi Flegrei

Campi Flegrei is the largest volcano in the CVZ, and it hosts a 13 km wide nested caldera which encompasses the outskirts of the city of Naples and extends beneath the Gulf of Pozzuoli (see Fig. 4.2A). The earliest eruptions ascribed to this volcanic system include the three Seiano Ignimbrites (290 – 240 ka), the Taurano Yellow Tuff (~157 ka) and the Durazzano Ignimbrite (~116 ka; Rolandi et al., 2003; De Vivo et al., 2001). Medial outcrops on the Campanian Plain (Di Vito et al., 2008) and Sorrento Peninsula (Rolandi et al., 2003; De Vivo et al., 2001) record tephra deposits from at least seven eruptions which, based on stratigraphic and geochemical data, have been linked to Campi Flegrei and were erupted between 290 and 110 ka (Fig. 4.2A). Four of these units (Triflisco, Santa Lucia, Cancello, and Maddaloni) are preserved within the foothills of the Apennine Mountains, 60 km east of Campi Flegrei (Fig. 4.2A), were erupted 110 – 90 ka (Fig. 4.1; Monaco et al., 2022). The nested caldera was generated and modified during the CI, MdMT and the NYT eruptions at 40 ka, 29 ka and 14 ka, respectively. There have been >70 eruptions within the caldera since the NYT (e.g. Smith et al., 2011a; Isaia et al., 2009; Orsi et al., 2004; Di Vito et al., 1999). Details on the activity in the 25 kyr period between the CI and NYT eruptions is limited with only a few sections logged (Albert et al., 2019b; Orsi et al., 2004).

Some proximal sections reveal tephra deposits below the CI eruption. Eleven separate units are seen beneath the CI at Trefola, three at Torre di Franco and one at both Cuma and San Severino (see Fig. 4.2A). Many of the pre-CI units have not been

characterised with some whole-rock data on a selection of units (Giaccio et al., 2017; Pabst et al., 2008; Pappalardo et al., 1999), and limited glass data (Tomlinson et al., 2012).

4.2.1.1. Compositions of pre-CI Campi Flegrei tephra

The chemical composition of the older pre-CI Campi Flegrei glasses range from high-K phonolites to trachytes. They are moderately to highly evolved and characterised by their low SiO_2 and high CaO, FeO_t and Al_2O_3 concentrations relative to the CI and show decreasing CaO, FeO_t and Al_2O_3 with increasing SiO_2 (see: Giaccio et al., 2017; Tomlinson et al., 2012). Many of the successive tephra units have overlapping major and trace element glass compositions, which means it is difficult to differentiate the deposits (Tomlinson et al., 2012, 2015; Wutke et al., 2015). Proximal pre-CI Campi Flegrei deposits are studied in the most detail at Trefola, with XRF whole-rock data of only a selected number of tephra units from the sequence (see Fig. 4.2A). Three compositional clusters have been identified for these pre-CI Campi Flegrei deposits based on the available XRF and isotope data for selected deposits (see: Pabst et al., 2008; Pappalardo et al., 1999). The TLa and TLc units are defined as Pre-CI Group 1; TLf, to Tli units defined as Pre-CI Group 2; and the TLm unit defined as Pre-CI Group 3 (Pabst et al., 2008). Glass from the TLa, TLc, and TLf units have been analysed and they show that incompatible element enrichment in these units decreases with time (TLa>TLc>TLf; Tomlinson et al., 2012), and their glass compositions are different to those documented after the large CI and NYT eruptions (e.g. Forni et al., 2018; Di Renzo et al., 2011; Smith et al., 2011a; Pappalardo et al., 1999).

4.2.1.2. Distal records of Campi Flegrei tephra (Pre-CI)

Sedimentary records across the central Mediterranean reveal at least fourteen Campi Flegrei derived distal eruption deposits between ~65 ka and the CI. The varved (annually laminated) LGdM sediment record, 90 km east of the CVZ, contains numerous tephra and cryptotephra deposits (termed the TM-18 tephras; Fig 4.2B) between the MEGT (TM-19) and the CI (TM-18), making it a key record of past volcanism in the CVZ (Wutke et al., 2015; Wulf et al., 2004; 2018;). Four tephras (TM-18-1a-d) were deposited within 600 varve years of the CI at LGdM, and they show a very strong geochemical affinity with Campi Flegrei products and the glass compositions of the CI (see Wutke et al., 2015). Of these tephras, Wulf et al. (2018) identify the compositionally distinct, 1 cm thick, grey-brown TM-18-1d tephra as the most useful marker, as glass compositions show decreased SiO_2 compared to

the other (TM-18-1a-c) deposits and display more enriched incompatible element contents (53-89 ppm Th; 21-33 ppm U; 131-198 ppm Nb; 681-1072 ppm Zr).

The lacustrine record of Fucino, 130 km north of Campi Flegrei, contains one tephra layer preserved between the MEGT and CI (TF-6; Fig. 4.2B), which is tentatively correlated to the TLc unit at Trefola based on stratigraphic, chronological and geochemical data (Giaccio et al., 2017). The Tenaghi Philippon sequence on mainland Greece, 675 km east of Campi Flegrei, contains six cryptotephra deposits preserved within the 1.25 m sediments beneath the CI, corresponding to 40.1 – 46.7 kyr cal. BP (Wulf et al., 2018). Here the LGdM TM-18-1d has been tentatively identified as a cryptotephra (TP05-13.34; Wulf *et al.*, 2018). The remaining five cryptotephra deposits (TP05-13.25, TP05-13.28, TP05-13.54, TP05-13.92 and TP05-14.50) at Tenaghi Philippon (Fig. 3.2B), and pre-CI two cryptotephra deposits (IO8T-30.74 and IO8T-31.17) identified between 0.6 – 1m below the CI at Ioannina (Greece), located 450 km east of Campi Flegrei (Fig. 3.2B), show geochemical similarities with the LGdM TM-18-1a-c tephras and the CI (see: McGuire et al., 2022; Wulf et al., 2018). All seven of these cryptotephra deposits were interpreted to reflect down core remobilisation of CI glasses due to their overlapping geochemical data with the CI, despite both sites showing discrete peaks in shard concentration relative to background concentrations almost 2 m below the CI tephra. Further work on the proximal sections can reveal whether the similar chemistries of successive units at these distal sites reflects reworking or different eruptions of compositionally similar magmas.

4.2.2. Ischia

Ischia is the most westerly of the CVZ volcanoes, located on the same NE-SW trending fault system as the Campi Flegrei volcano (Fig. 4.2A), and is thought to represent the remnants of a larger volcano (Orsi et al., 2004; Santacroce et al., 2003). The eruption history of Ischia is documented back to ~150 ka (Poli et al., 1987) and has been active into historical times with the latest eruption in 1302 CE. Volcanic activity has been divided into five phases: >150 – 75 ka; 75 – 55 ka; 55 – 33 ka; 28 – 12 ka; 12 ka – 1302 CE (Brown et al., 2008; Poli et al., 1987). The 55 – 33 ka phase of activity is characterised by several explosive events including the MEGT (Poli et al., 1987) that occurred at ~56 ka and resulted in caldera collapse across all or part of the island (Brown et al., 2008; Buchner, 1996; Civetta et al., 1991; Orsi et al., 1991; Vezzoli 1988). The widespread Y-7 tephra marker, traced as far as the Ionian Sea, has been correlated with the MEGT eruption (Tomlinson et al., 2014), but this has been disputed based on mineral compositions (D'Antonio et al., 2021). The

proximal outcrops on the island of Ischia preserve the deposits of at least six explosive eruptions between the MEGT and CI, while a further five units have been identified below the MEGT (Fig. 4.1).

3.2.2.1. Compositions of pre-CI Ischia tephra

Glass compositions of tephra from Ischia are phono-trachytic in composition and show minor overlap with Pre-CI Campi Flegrei/CI tephra deposits (see Tomlinson et al., 2014). Pre-MEGT tephra deposits are characterised by low CaO, and high SiO_2 and Na_2O relative to the MEGT, with a trend of decreasing Na_2O and FeO_t with increasing K_2O (Tomlinson et al., 2014, 2015). The studied Ischia glasses have a wide range of incompatible trace element concentrations, and extend to highly enriched concentrations (e.g. Zr ranging from 160 to 1110 ppm; Tomlinson et al., 2014) that are characterised by high Zr/Sr ratios (up to 670; Tomlinson et al., 2015). There is a significant change in the composition of Ischia tephras prior to and following the caldera-forming MEGT eruption (Tomlinson et al*.,* 2015). Relative to pre-MEGT and MEGT glasses, post-MEGT deposits are displaced to lower MgO, FeO_t, TiO_2 and incompatible element contents (Tomlinson et al., 2014). Nevertheless, despite the Ischia eruption stratigraphy being better resolved than that for Campi Flegrei, glass geochemical data arestill lacking for several post-MEGT tephra units (e.g. the Chiammano, La Roia and Capo Grosso tephras; Fig. 4.1.).

4.2.2.2. Distal pre-CI Ischia tephra

Medial to distal records from across Italy preserve at least eleven tephra deposits from Ischia between the CI and MEGT in both marine and terrestrial sequences. Five pre-CI Ischia tephra deposits have been identified in marine cores (Fig. 4.2B), one being a cryptotephra deposit from the Adriatic Sea (PRAD-1752; Bourne et al., 2010) and four visible tephra deposits the Tyrrhenian Sea (C-14, C-15, C-16 and C-17; Paterne et al., 1986, 1988). The SMP1-a fallout deposit preserved beneath the CI on the Sorrento Peninsula (Fig. 4.2A) has been correlated to Ischia based on XRF data (Di Vito et al., 2008). Furthermore, the tephra deposit in the Adriatic Sea (PRAD-1752) and SMP1-a tephra have been correlated with the LGdM TM-18-1 tephra (Wutke et al., 2015). However, neither the specific stratigraphic position within the LGdM sequence nor geochemical data has been published for the TM-18-1 tephra and therefore, it is not discussed further in this study.

A further thirteen Ischia tephra deposits are reported between 104 and 40 ka in the LGdM record (Tomlinson et al., 2014), including the distal equivalent of the MEGT (TM-19; Wulf et al., 2004). Five of these LGdM deposits are preserved between the MEGT and CI (TM-18-2, TM-18-9a, TM-18-9e, TM-18-14a and TM-18-17a; Tomlinson et al., 2014), and of these markers, Wulf et al. (2018) identify the TM-18-14a and TM-18-9e tephras as the most useful marker horizons due to their distinctive geochemical compositions relative to the other Ischia deposits in the sequence. Two of these LGdM tephra deposits have been correlated to the Schiappone (TM-18-17a) and the Pietre Rosse (TM-18-14a) eruption units (Tomlinson et al., 2014). The LGdM TM-18-17a glasses are compositionally variable (61.7 – 62.8 wt.% SiO_2, 13 – 24 ppm Th and 204 – 360 ppm Zr) and show a complete overlap with the proximal Schiappone tephra with the dominant population of the glass compositions lying within the least evolved member (Tomlinson et al., 2014). Furthermore, the whole rock chemical data presented by Paterne et al. (1986, 1988) for the C-16 tephra preserved in multiple cores from the Tyrrhenian Sea show highly variable glass compositions and some that overlap with the most evolved Schiappone glasses (Tomlinson et al., 2014). Whilst the marine C-17 Ischia tephra also displays geochemical similarities with the TM-18-17a glasses, the whole rock data for the C-17 deposit extends to higher (~1) K_2O/Na_2O and lower (0.67 – 0.91 wt.%) CaO values (Tomlinson et al., 2014). Therefore, the TM-18-17a and C-16 tephra marine deposits are believed to be distal correlatives of the Schiappone tephra (Tomlinson et al., 2014). A re-assessment of the glass chemistry of the Tyrrhenian Sea Ischia layers is required to verify correlations.

The three remaining Ischia deposits between the MEGT and CI in the LGdM core have not been correlated to specific eruptions. Whilst the LGdM TM-18-9e tephra shares geochemical similarities with the proximal Agnone deposit, the CaO is much lower (up to 30% lower; Tomlinson et al., 2014). Although the post-MEGT LGdM TM-18-9a tephra is a moderately evolved (335 – 454 ppm Zr; 22 – 32 ppm Th), it is compositionally between the Agnone and Pietre Rosse deposits and does not correlate with any known proximal eruption unit (Tomlinson et al., 2014). The youngest pre-CI LGdM Ischia tephra (TM-18-2) has tentatively been correlated to the C-14 Tyrrhenian Sea tephra based on whole rock XRF compositions (Wutke et al., 2015).

4.2.3 Procida

The Island of Procida sits between Ischia Island and Campi Flegrei in the Gulf of Pozzuoli, (Fig. 4.2A). It is comprised of overlapping, eroded edifices of five monogenic

explosive eruptions: Vivara, Terra Murata, Pozzo Vechio, Fiumicello and Solchaiario (Rosi et al., 1988). Procida has been active from ~80 ka until the Solchario eruption (De Astis et al., 2004), which, based on ^{14}C ages from paleosols below and above the unit, has an eruption age of 23,005-24,201 cal yrs BP (19,620 ± 270 yrs BP; Alessio *et al.,* 1976). Little geochemical or chronological data areavailable for units preceding the Solchario eruption.

The interbedding of pyroclastic deposits on Procida with those from Campi Flegrei and Ischia has provided stratigraphic and chronological constraints on some of the eruptions (Fig. 4.1). Two units, Vivara I and the younger Fiumicello, occur below the MEGT indicating that they erupted pre-56 ka; and the Vivara II deposit sits between the MEGT and the CI (Fig. 4.1: De Astis et al., 2004). No Procida tephra deposits between the MEGT and CI have been identified in distal settings. Whole rock data for the pre-CI Fiumicello and post-CI Solchiaro eruptions indicates both are trachybasaltic (Scandone et al., 1991; Rosi et al., 1988).

4.3. Study Site

This study aims to improve the pre-CI (<40 ka) eruption history by reconstructing a detailed proximal tephrostratigraphy for pre-CI eruption activity through visual description and geochemical characterisation. We utilise a coastal outcrop at Acquamorta, also referred to as Monte di Procida (see: Perrotta et al., 2010; Orsi et al., 1996; Rosi et al., 1988), on the west side of the CI caldera ring fault (40° 47'39.8" 014° 02' 37.2"; Fig 4.2A), 14 km from Ischia and 5 km from Procida.

Numerous pyroclastic deposits beneath the CI were previously noted at Acquamorta and nearby Torregaveta (e.g. Orsi et al., 1996; Rosi et al., 1988) and thought to be from multiple volcanic sources (Campi Flegrei, Procida and Ischia). However, the number of units extending from the base of the sequence up to the CI differs between publications; Rosi et al. (1988) observed six units, Orsi et al., (1996) identified five units, and Perrotta and Scarpati (1994) noted four units. None of these previous studies presented details of the units or any compositional analyses. A >0.5 m thick green-grey coarse pyroclastic density current (PDC) deposit, the base of which is not exposed, outcrops at Acquamorta. This has been correlated to the MEGT eruption using glass chemistry (see Tomlinson et al., 2014). The Fiumicello tephra from Procida, a 1.3 m thick distinctively grey bedded unit, outcrops below the MEGT (Perrotta et al., 2010; De Astis et al., 2004; Rosi et al., 1988) and to the left (north) of the section that we sampled. These pre-MEGT units are behind concrete or metal

netting and higher up in the section. These units dip below the beach at the section that we sampled so that only the units between the MEGT and the CI are accessible; consequently, this study focusses on these eruption deposits.

4.4. Methods

4.4.1. Eruption stratigraphy

The Acquamorta outcrop was logged and sampled during field campaigns in 2013, 2014 and 2021. Representative samples were collected for geochemical characterisation. Paleosols have allowed numerous eruption units to be defined, which have been given a number and AQ prefix. Samples for geochemical analysis were given a number and CF prefix.

4.4.2. Glass chemistry

In the laboratory, bulk representative samples comprising of pumice clasts and ash were crushed and wet sieved to remove the fraction <80 μm. Samples were dried in an oven at ~60^{o}C and mounted in epoxy for analysis.

Major element glass compositions of the samples were analysed using a JEOL-8600 and a JEOL JXA-8200 wavelength dispersive electron microprobe (WDS-EMP) equipped with 5 spectrometers located in the Research laboratory for Archaeology and the History of Art (RLAHA), University of Oxford, U.K. To minimise alkali-loss in the glass, an accelerating voltage of 15 kV, a 6 nA beam current and a beam diameter of 10 μm were used. Peak counting times were 12 s for Na, and other major elements collected for 30 s except for Mn, Cl and P which were collected for 50 s. Background counts were collected for the same total amount of time as those on peak, with half the time either side of the peak. The instrument was calibrated with mineral standards and the calibration was checked with the MPI-DING references glasses including the evolved felsic [ATHO-G (rhyolite)], through intermediate [StHs6/80-G (andesite)] to mafic [GOR128-G (Komatiite)] glasses (Jochum et al., 2006). Due to variable secondary hydration of glasses (e.g. Shane et al., 2008), all the analyses presented in the text, tables and graphs have been normalised to 100% for comparative purposes. Analyses with analytical totals <94% were discarded as they are not thought to be representative of the melt composition. Error bars on plots represent reproducibility, calculated as 2 standard deviations of replicate analyses of MPI-DING StHs6/80-G glasses.

The trace element compositions of individual glass shards in selected tephra units were determined using an Agilent 8900 triple quadrupole LA-ICP-MS (laser ablation inductively coupled plasma mass spectrometry; ICP-QQQ) coupled to a Resonetics 193 nm ArF excimer laser-ablation device in the Department of Earth Sciences, Royal Holloway, University of London. The full analytical procedures adopted for volcanic glass analysis follow those outlined in Tomlinson et al. (2010). A range of crater sizes were used (20, 25 and 34 μm) owing to variability in the sample's vesicularity and thus the size of glass surfaces available for analysis (see Appendix A). The laser energy density on the target was 3.0 Jcm^{-2}, the repetition rate was 5 Hz. The analyses comprised a count time of 40 s on the sample, and 40 s on the gas blank to allow the subtraction of the background signal. Typically, blocks of eight glass shards and one MPI-DING reference glass were bracketed by the NIST612 glass adopted as the calibration standard. The internal standard applied was ^{29}Si (determined by EMP-WDS analysis). In addition, MPI-DING reference glasses were used to monitor analytical accuracy (Jochum et al., 2006). LA-ICP-MS data reduction was performed in Microsoft Excel, as described in Tomlinson et al. (2010). Accuracies of LA-ICP-MS analyses were monitored using MPI-DING reference glasses, ATHO-G and StHs6/80-G, and accuracies were typically ≤ 6% for the majority of elements measured. For consistency with EMP error reporting, error bars on plots show 2 times the standard deviation of replicate analyses of MPI-DING StHs6/80-G. All major and trace element data are available in Appendix A.

4.5. Results

4.5.1. Pre-CI eruption stratigraphy

Twelve units separated by paleosols were identified in a 6 m succession between the MEGT and the CI at Acquamorta (Fig. 4.3A). The units vary in thickness, grain size and colour, and each had a sharp basal contact (Fig. 4.3B-F). Many of the tephra deposits in this record at Acquamorta are relatively thin despite their proximity to the different sources region, suggesting that it was not on the main dispersal axis for the eruptions or that deposits are not well preserved. The prevailing winds are to the east, with very few eruption deposits preserved on the western side of the caldera; even the Plinian phase of the CI eruption is not preserved at Acquamorta. Clasts vary in colour (white-grey to brown-black), vesicularity and crystal content even within a single eruption deposit. Glass shard morphologies show little variation between the units with a range in vesicularity and microlite abundance across the units. Backscattered electron images reveal clasts of some units (for instance AQ-8) are poorly vesiculated with small (<25 μm) round vesicles. While the AQ-12

unit has large glass shards with highly abundant large vesicles (>200 μm) making it distinct from any other unit analysed in this study (see Appendix A).

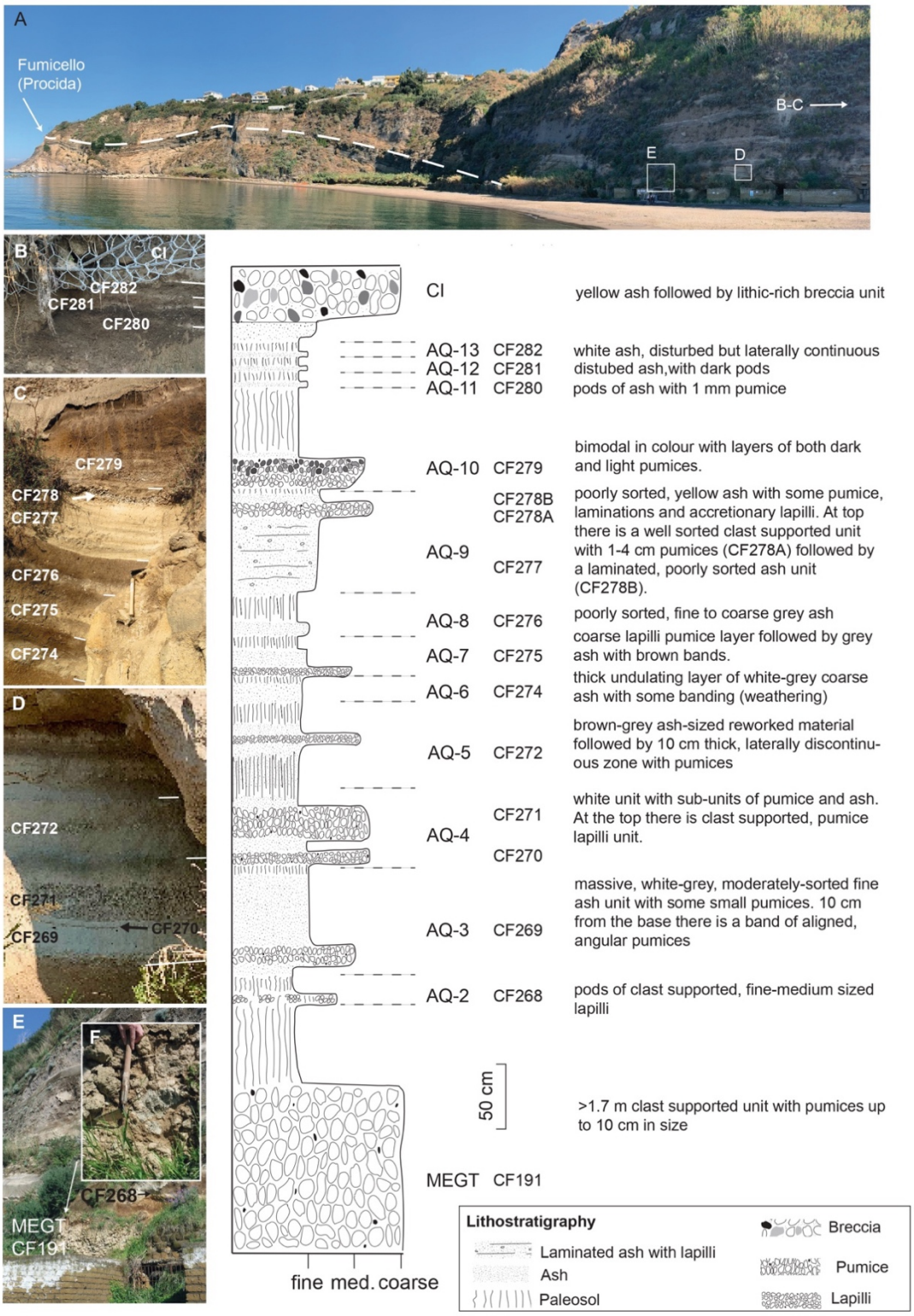


Figure 4.3: A) The Acquamorta outcrop and the positions of the four sampling sections (B-F) indicated by white boxes. Numerous tephra units are observed in this outcrop, including the Fiumicello (dashed white line) from Procida. The tephra units observed in sections B and C are located on the southern side of the exposure below the CI. B-F) Annotated photos of the units (AQ-2 – AQ-13) and geochemical samples (CF-prefixes) from the sampled sections along the exposure. The composite tephrostratigraphy for the Acquamorta outcrop between the MEGT and CI showing the units (AQ-prefix) and geochemical samples (CF-prefix) as well as the unit descriptions.

4.5.2. Glass geochemistry

Sixteen samples from the twelve tephra units were geochemically analysed. Representative major and trace element analyses are reported in Table 4.1. All twelve units are alkalic and straddle the phonolite-trachyte boundary (Fig. 4.4A). There is a wide compositional range in the major element compositions of the units spanning the entire investigated sequence, with, 58.83 – 63.23 wt.% SiO_2, 6.10 – 8.73 wt.% K_2O, 5.33 – 7.83 wt.% Na_2O, 1.23 – 2.23 wt.% CaO, 1.79 – 3.60 wt.% FeO_t (*n* = *453*). Trace element compositions display a range of concentrations: 2.8 – 77.6 ppm Sr, 345 – 1001 ppm Zr, 53.5 – 185 ppm Nb, 32.1 – 77.3 ppm Y, 51.1 – 116 ppm Nd, and 24.6 – 79.4 ppm Th (*n* =*121*). There is little heterogeneity within individual units (i.e. similar to analytical uncertainty). Unit AQ-6 shows the greatest degree of variability in major elements (Fig. 4.4A-D), and units AQ-6 and AQ-13 show the greatest variability in trace element concentrations (Fig. 4.4E-F). On the basis of the major glass element data, it is possible to recognise four compositional groups (see Fig. 4.4A-F). These groups also have different trace element compositions. Here we highlight the key compositional features that allow the discrimination of these groups, and thus the diagnostic chemistry that can be used to aid correlations.

Table 4.1: EMP and LA-ICP-MS of representative analysis shards from the deposits preserved between the MEGT and CI identified in this study. It should be noted that n is the size of the population from which the representative analysis was selected. All EMP data has been normalised to 100%.

Tephra unit	**AQ-13**	**AQ-12**	**AQ-11**	**AQ-10**	**AQ-9**	**AQ-9**	**AQ-9**	**AQ-8**	**AQ-7**	**AQ-6**	**AQ-5**	**AQ-4**	**AQ-4**	**AQ-4**	**AQ-3**	**AQ-2**
Sample	CF282	CF281	CF280	CF279	CF278A	CF278B	CF277	CF276	CF275	CF274	CF272	CF271	CF192	CF270	CF269	CF268
Compositional Group	Group D	Group D	Group A	Group C	Group C	Group C	Group C	Group A	Group C	Group C	Group A	Group C	Group C	Group C	Group B	Group B
(wt.%)	Avg.	Avg.	Avg.	Avg.	Avg.	Avg.	Avg.	Avg.	Avg.	Avg.	Avg.	Avg.	Avg.	Avg.	Avg.	Avg.
SiO_2	60.71	61.22	62.53	59.91	59.98	59.65	59.7	62.52	59.92	60.02	62.65	60.29	59.68	60.26	59.76	59.31
TiO_2	0.42	0.43	0.48	0.46	0.46	0.41	0.41	0.45	0.42	0.47	0.47	0.4	0.5	0.44	0.42	0.41
Al_2O_3	18.92	18.8	18.61	19.13	19.08	19.27	18.93	18.78	18.97	18.92	18.44	18.68	18.88	18.9	19.2	19.22
$FeOt_t$	2.91	2.98	2.38	3.22	3.12	3.06	3.3	2.3	3.15	3.18	2.51	2.94	3.14	3.18	3.34	3.34
MnO	0.23	0.23	0.18	0.33	0.29	0.31	0.26	0.15	0.34	0.2	0.17	0.3	0.22	0.22	0.17	0.2
MgO	0.32	0.31	0.34	0.2	0.29	0.24	0.25	0.26	0.25	0.27	0.32	0.32	0.35	0.27	0.31	0.39
CaO	1.73	1.74	1.47	1.65	1.74	1.7	1.69	1.35	1.72	1.79	1.35	1.81	1.83	1.75	2	2.12
Na_2O	6.35	6.23	6.26	7.46	7.18	7.31	7.6	6.26	7.08	6.92	6.31	6.85	6.98	6.52	5.58	6.12
K_2O	7.61	7.3	7.21	6.64	6.7	6.87	6.67	7.16	7.04	7.12	7.03	7.38	7.32	7.35	8.17	7.85
P_2O_5	0.03	0.05	0.02	0.05	0	0.05	0/06	0.09	0.02	0.06	0.07	0	0.06	0	0.06	0.04
Cl	0.77	0.71	0.52	0.96	1.15	1.14	1.14	0.69	1.08	1.05	0.67	0.95	1.02	1.09	0.98	0.99
Analytical total	95.87	96.54	95.27	95.08	96.7	97.84	96.41	96.92	97.02	97.25	96.67	97.63	94.92	98.68	95.99	94.13
(n)	*17*	*21*	*18*	*15*	*33*	*24*	*8*	*30*	*21*	*31*	*23*	*41*	*4*	*26*	*46*	*39*
(ppm)	Avg.	-	Avg.	-	Avg.	Avg.	-	Avg.	-	Avg.	Avg.	Avg.	Avg.	-	Avg.	Avg.
Rb	465	-	361	-	583	587	-	356	-	472	353	462	469	-	407	418
Sr	18.6	-	24.8	-	5.28	3.96	-	32.3	-	13.7	21.9	6.49	6.67	-	38.5	26.5
Y	54.4	-	40.2	-	72.2	77.3	-	41.1	-	61.6	43.2	57.1	50.5	-	45.6	48.1
Zr	665	-	414	-	929	987	-	411	-	755	446	697	617	-	535	578
Nb	120	-	66.5	-	177	178	-	66.9	-	142	72.3	131	121	-	102	111
Ba	11.8	-	14.7	-	1.83	1.46	-	29.6	-	11.3	15	8.01	3.67	-	12	7.7
La	127	-	85.6	-	170	179	-	88	-	143	89.8	135	119	-	109	116
Ce	243	-	166	-	330	342	-	170	-	273	178	259	231	-	207	223
Pr	24.3	-	17.7	-	32	34	-	18	-	27.1	18.5	25.9	22.8	-	20.9	22.2
Nd	84.6	-	64.7	-	108	116	-	66	-	95.5	65.2	88	77.7	-	72.7	77.7
Sm	14.6	-	11.8	-	18.4	19.5	-	12	-	16.5	12	15.6	13.6	-	12.8	13
Eu	1.35	-	1.46	-	1.21	1.29	-	1.37	-	1.35	1.37	1.41	1.17	-	1.75	1.67
Gd	10.7	-	9.33	-	15.2	16.2	-	8.98	-	12.2	9.44	12.8	``.0	-	10	10.5
Dy	9.8	-	7.39	-	13	14.1	-	7.78	-	10.9	8.13	10.5	9.53	-	8.26	8.92
Er	5.56	-	3.95	-	7.65	8.28	-	4.12	-	6.3	4.45	5.76	4.89	-	4.45	4.83
Yb	5.59	-	4.03	-	7.79	8.45	-	4.24	-	6.78	4.56	5.73	4.82	-	4.64	5.03
Lu	0.81	-	0.62	-	1.15	1.19	-	0.62	-	0.93	0.67	0.84	0.74	-	0.68	0.74
Hf	14.3	-	9.44	-	19.5	20.7	-	9.2	-	16.6	10.4	14.5	13	-	11.4	12.5
Ta	5.68	-	3.39	-	8.22	8.62	-	3.47	-	6.78	3.72	6.11	5.45	-	4.8	5.25
Pb	64.8	-	50.3	-	86.3	75.6	-	45.2	-	71.2	49.3	67.8	77.7	-	62.3	62
Th	51.8	-	29.5	-	73	79.4	-	29.3	-	62.1	31.1	54.4	47.9	-	42.4	46.2
U	18.6	-	9.04	-	27.4	28.6	-	9.27	-	21.7	10	19.5	18	-	14.7	16.8
(n)	*11*	-	*5*	-	*6*	*9*	-	*16*	-	*9*	*11*	*7*	*12*	-	*13*	*13*

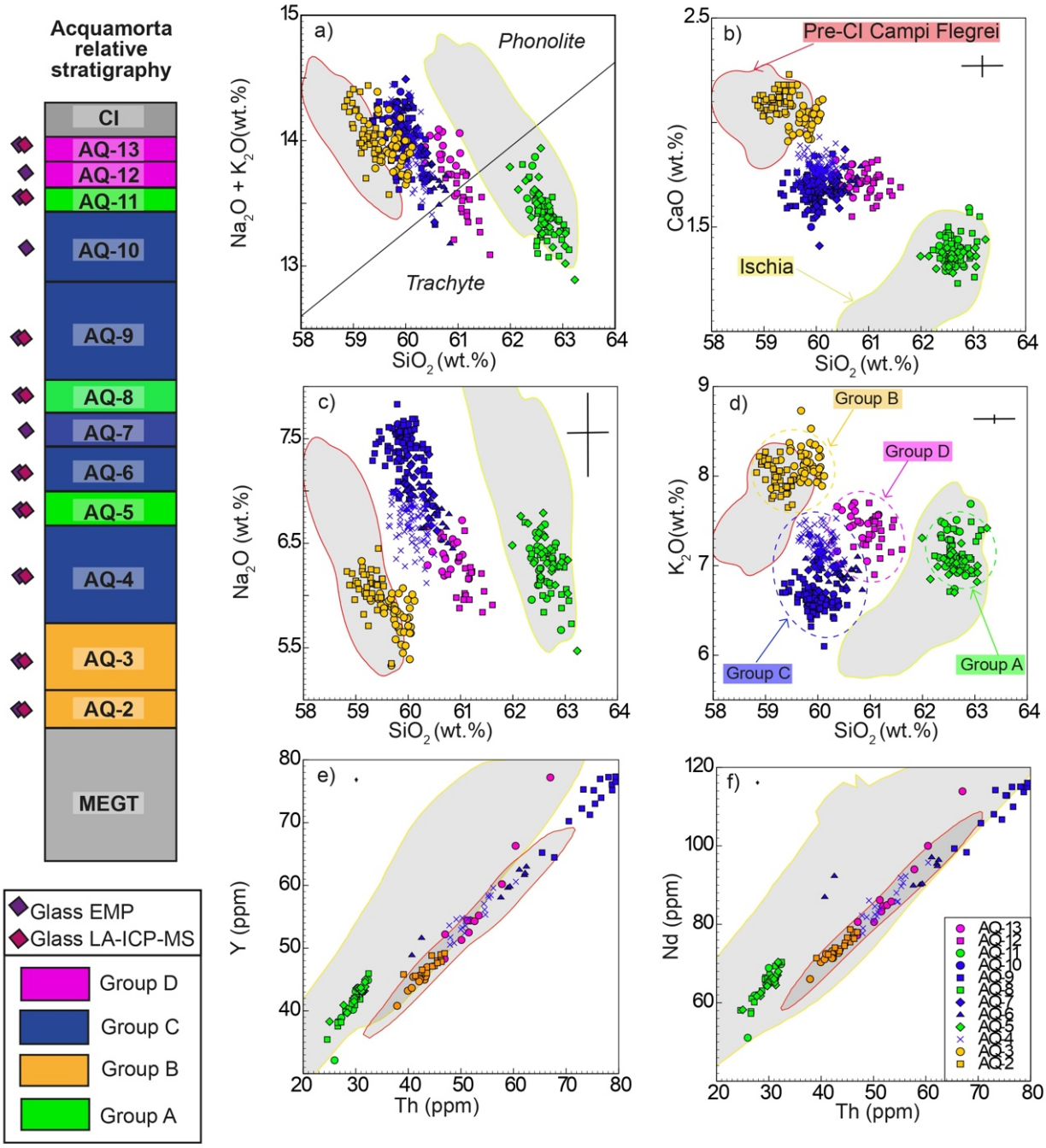


Figure 4.4: The relative stratigraphic order and the glass composition of the twelve tephra units at Acquamorta. Please see figure one to see how the Acquamorta stratigraphy fits into the eruption stratigraphies of the CVZ. Colours correspond to the compositional group defined using major (EMP) and trace element (LA-ICP-MS) glass compositions. A-D) Major and E,F) Trace element compositions. The limited (3 units) published Pre-CI Campi Flegrei (grey shaded area with red outline) and Ischia (grey shaded area with light green outline) glass compositions are shown as fields (Tomlinson et al., 2012, 2014, 2015). These new Group C and D have glass compositions that are consistent with Campi Flegrei and expand the database of pre-CI glass compositions. The groups are indicated by dashed ellipses in Fig.4d. Errors are 2 s.d. calculated using replicate analyses of MPI-DING StHs6/80 glass.

Group A includes the following three units: AQ-5, AQ-8 and AQ-11 and is dominated by glass populations which firmly fall within the trachytic compositional field (Fig. 4.4A). This group of glasses (*n = 71*) are tightly clustered and are characterised by the highest SiO_2 (62.65 ± 0.47 wt.%) and lowest Al_2O_3, (18.65 ± 0.34 wt.%), CaO (1.38 ± 0.14 wt.%) and FeO_t (2.34 ± 0.29 wt.%) contents. The Group A glasses plot separately from all other units analysed at Acquamorta and are most easily separated using SiO_2 vs. Na_2O and SiO_2 vs. K_2O plots (Fig. 4.4C,D). In terms of trace element contents (*n = 41*), the Group A tephra units possess the lowest Th (29.5 ± 4.0 ppm), Nb (69.3 ± 9.2 ppm), Nd (64.5 ± 8.0 ppm) and Zr (426 ± 55.7 ppm) and higher Zr/Th (14.4 ± 0.8) and Y/Th (1.40 ± 0.1) relative to the other three compositional groups identified at Acquamorta (Table 4.1). Group A is easily separated using Th vs. Y and Th vs. Nd from the three other groups (Fig. 4.4E,F).

In contrast, Groups B, C and D are dominated by phonolitic glass components and show varying degrees of overlap in both major and trace element data (Fig. 4.4). Nonetheless, they can be separated on using specific major elements, particularly unit-to-unit variations in K_2O and Na_2O content (Fig. 4.4C-D).

Glasses from AQ-2 and AQ-3, directly above the MEGT (Fig. 4.3), form Group B, and display only minor overlap in both major and trace elements (Fig. 4.4). These glasses (*n = 85*) are characterised by higher CaO (2.06 ± 0.13 wt.%) and K_2O (8.07 ± 0.37 wt.%) and lower SiO_2 (59.52 ± 0.69 wt.%) and Na_2O (5.94 ± 0.45 wt.%) contents relative to units in Groups C and D, and as such are easily distinguished using SiO_2 vs. CaO, SiO_2 vs. Na_2O and SiO_2 vs. K_2O plots (Fig 4.4B-D). Whilst trace element contents (*n = 26*) are lower in Th (43.1 ± 4.6 ppm), Nd (73.7 ± 5.6 ppm), Y (46.1 ± 3.7 ppm) and Zr (552 ± 50.4 ppm), they show a slight overlap with both Group C and D, yet they are most easily distinguished by their lower Zr/Sr ratio (17.4 ± 7.02).

The five units, AQ-4, AQ-6, AQ-7, AQ-9 and AQ-10, have similar compositions and form Group C and exhibits the greatest geochemical variability in both major and trace element concentrations compared with any of the pre-CI compositional groups identified at Acquamorta (Fig. 4.4). This group of glasses (*n = 203*) is more evolved than the underlying Group B glasses (See Fig 4.4B-D) with higher SiO_2 (60.06 ± 0.56 wt.%) and Na_2O (7.03 ± 0.75 wt.%) and lower K_2O (6.93 ± 0.60 wt.%). The trace element contents of the Group C tephras (*n = 43*) are characterised by higher Zr (771 ± 280.0 ppm), Nb (145 ± 50.1 ppm), Nd (95.7 ± 24.3 ppm), Th (70.0 ± 22.9 ppm), and significantly higher Zr/Sr ratios (116 ± 161.0), relative to those of both Groups B and D (Fig. 4.4E,F).

The two units directly beneath the CI (AQ-12 and AQ-13) form the Group D compositional group and straddle the phonolite-trachyte boundary (Fig. 4.4A). Group D glasses (*n = 38*) show some overlap with the Group C glasses in terms of major element composition, however the Group D units are more evolved having slightly higher SiO_2 (60.95 ± 0.58 wt. %) and K_2O (7.40 ± 0.39 wt.%), and lower FeO_t (2.96 ± 0.23 wt.%) and Na_2O (6.28 ± 0.46 wt.%) contents and are most easily distinguished from the geochemically similar Group C deposits using SiO_2 vs. K_2O plots (Fig. 4.4D). Levels of incompatible trace element enrichment in the Group D glasses (Th = 53.6 ± 11.4 ppm, Nd = 88 ± 21.0 ppm and Y = 57 ± 16.2 ppm) are restricted to those consistent with the least evolved Group C deposits (e.g. AQ-4), this considerable overlap means Groups C and D glasses cannot be reliably distinguished using trace element analysis alone (Fig. 4.4E,F).

4.6. Discussion

4.6.1. Composition and source of the Acquamorta tephra units

All samples analysed in this study can be correlated to either Campi Flegrei or Ischia based on glass composition (comparing to the data of Tomlinson et al., 2012, 2014). These Acquamorta analyses have also been compared to those of distal tephra layers with CVZ glass compositions (McGuire et al., 2022; Giaccio et al., 2017; Wutke et al., 2015; Bourne et al., 2010; Wulf et al., 2004, 2008, 2012, 2018). These new geochemical data indicate that successive eruptions often share similar glass compositions (Fig. 4.4).

4.6.2. Ischia tephra

The Group A tephra deposits preserved between the MEGT and CI at Acquamorta fall within the glass compositional field for Ischia deposits (Fig. 4.4) and are consistent with published compositions for post-MEGT eruptions (Tomlinson et al., 2014). They have high SiO_2 (62.65 ± 0.47 wt.%) and low CaO (1.38 ± 0.13 wt.%), along with increasing K_2O and CaO and decreasing Na_2O and FeO_t with increasing SiO_2 (Fig. 4.5A,C,D). These Acquamorta Ischia units are relatively similar in thickness, do not have any particularly unique visual characteristics, and are indistinguishable using both major and trace element data (Figs. 4.4, 4.5); thus, they cannot be correlated to other units in and around the calderas.

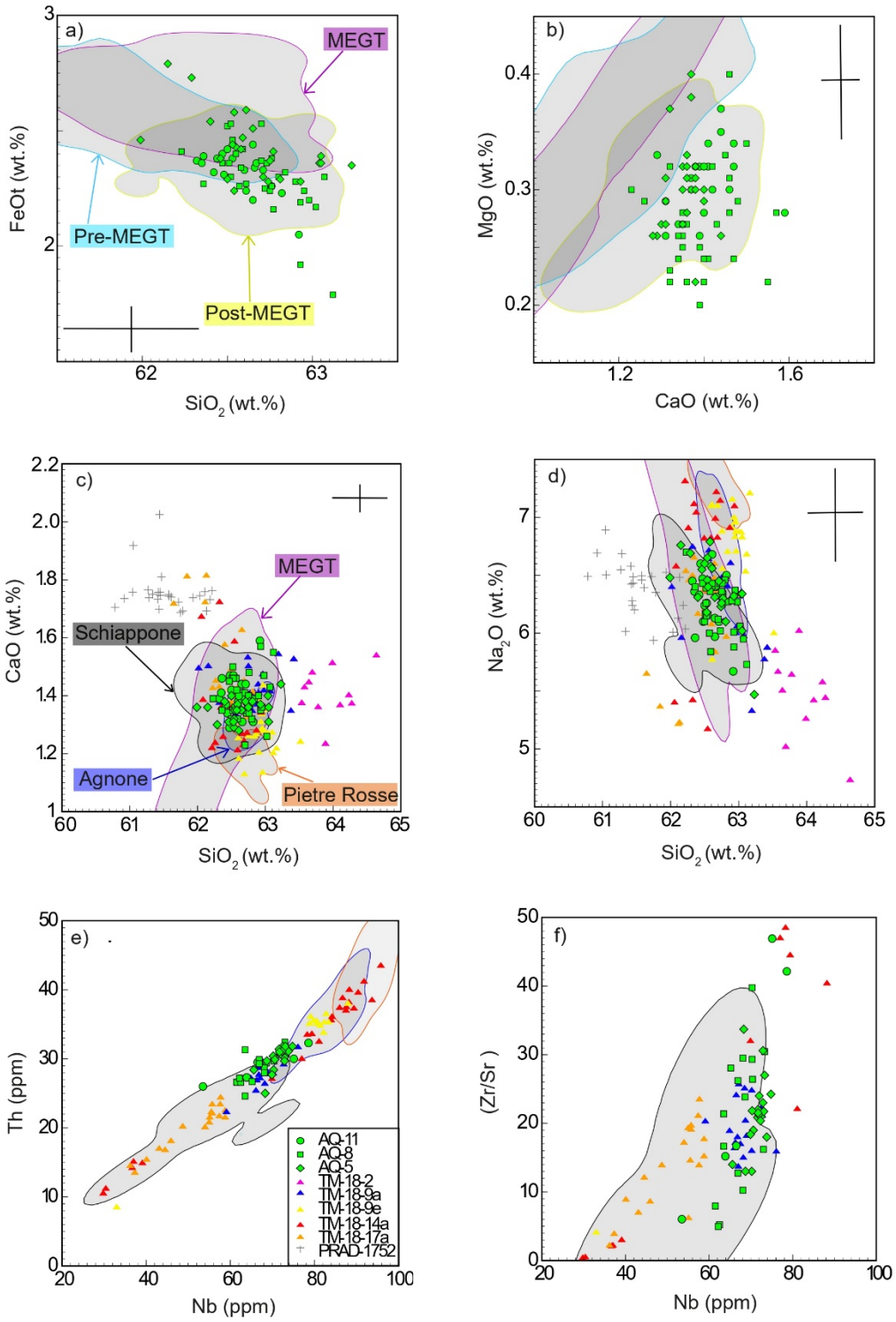


Figure 4.5: A,B) Glass composition of the Acquamorta Ischia layers compared to proximal glass chemistry data for pre-MEGT, MEGT and post-MEGT Ischia deposits (data from Tomlinson et al., 2014). As expected, the composition of the Acquamorta units overlap with post-MEGT deposits. C-F) Major (C,D) and trace element (E,F) plots of Post-MEGT Ischia units identified at Acquamorta plotted with data from the MEGT and post-MEGT Ischia eruption units (plotted as fields; Tomlinson et al., 2014), and distal tephras from LGdM (Wutke et al., 2015; Tomlinson et al., 2014;) and the PRAD1-2 core (Bourne et al., 2010). Errors are 2 s.d. calculated using replicate analyses of MPI-DING StHs6/80 glass.

While the three Ischia units at Acquamorta fall within the broad range in glass compositions characteristic of the Schiappone tephra, their tight overlapping compositional clusters make it difficult to correlate any Acquamorta unit to this particular eruption (Fig. 4.5C-F). The TM-18-17a tephra in the LGdM sequence and the C-16 tephra from the Tyrrhenian Sea have previously been correlated to the Schiappone eruption based on complete geochemical overlap, but with the dominant population lying within the least evolved member of the Schiappone tephra (Tomlinson et al., 2014). Furthermore, the PRAD-1752 cryptotephra from the Adriatic Sea has also been proposed as a correlative to the Schiappone tephra (see: Tomlinson et al., 2014; Bourne et al., 2010), but the compositions are inconsistent and, based on our acquisition of new glass chemistry, PRAD-1752 must correlate to a different unit not preserved at Acquamorta (Fig. 4.5C,D). Although the Acquamorta Ischia tephras show a good overlap in major element data with both the Schiappone tephra and the equivalent TM-18-17a tephra (Fig. 4.5C,D), trace element data reveal all three deposits have a closer geochemical affinity with the younger TM-18-9a Ischia unit preserved in the LGdM that has a varve age of 41,420 yrs BP (Fig. 4.5E,F), and which has not yet been correlated to a proximal deposit on Ischia.

The three Acquamorta proximal units and the TM-18-9a tephra show overlap with the Schiappone tephra but extend to higher Th (~9 ppm) and Nb (~1 ppm) relative to the Schiappone LGdM equivalent (TM-18-17a). The very similar compositions of these units at Acquamorta highlights that correlations to particular Ischia units both proximally and distally are challenging. Furthermore, it is not known whether these are associated with known Ischia eruptions for which there is no glass chemistry (i.e. Capo Grosso, La Roia, Chiummano; Fig. 4.1) or other eruptions that are not observed elsewhere. The Ischia units identified within this study re-affirm that Ischia produced multiple chemically indistinct eruptions in the 16 kyr following the large MEGT eruption, and show that the magmatic system and processes prior to the eruptions were similar prior to each of these events.

4.6.3 Campi Flegrei tephra

The major and trace element glass compositions of tephras in Groups B, C and D are consistent with eruptions from Campi Flegrei (Fig. 4.4). These pre-CI Campi Flegrei groups are most clearly separated from the Ischia deposits (Group A) using SiO_2 vs. CaO, SiO_2 vs. Na_2O and Th vs. Y (Fig. 4.4B,C,E). These glasses display slightly decreasing FeO_t with increasing SiO_2 (Fig. 4.6B) and are moderately to highly evolved with Zr/Sr ratios ranging from 9.96 to 355 ppm, which is compatible with major and trace element data of

other analysed pre-CI units (Tomlinson et al., 2012). The trace element data obtained for these pre-CI units does not help further distinguish the three pre-CI Campi Flegrei compositional groups, as many of the units overlap (Fig 4.4F-H), however some units possess distinct characteristics that may aid future individual tephra correlations.

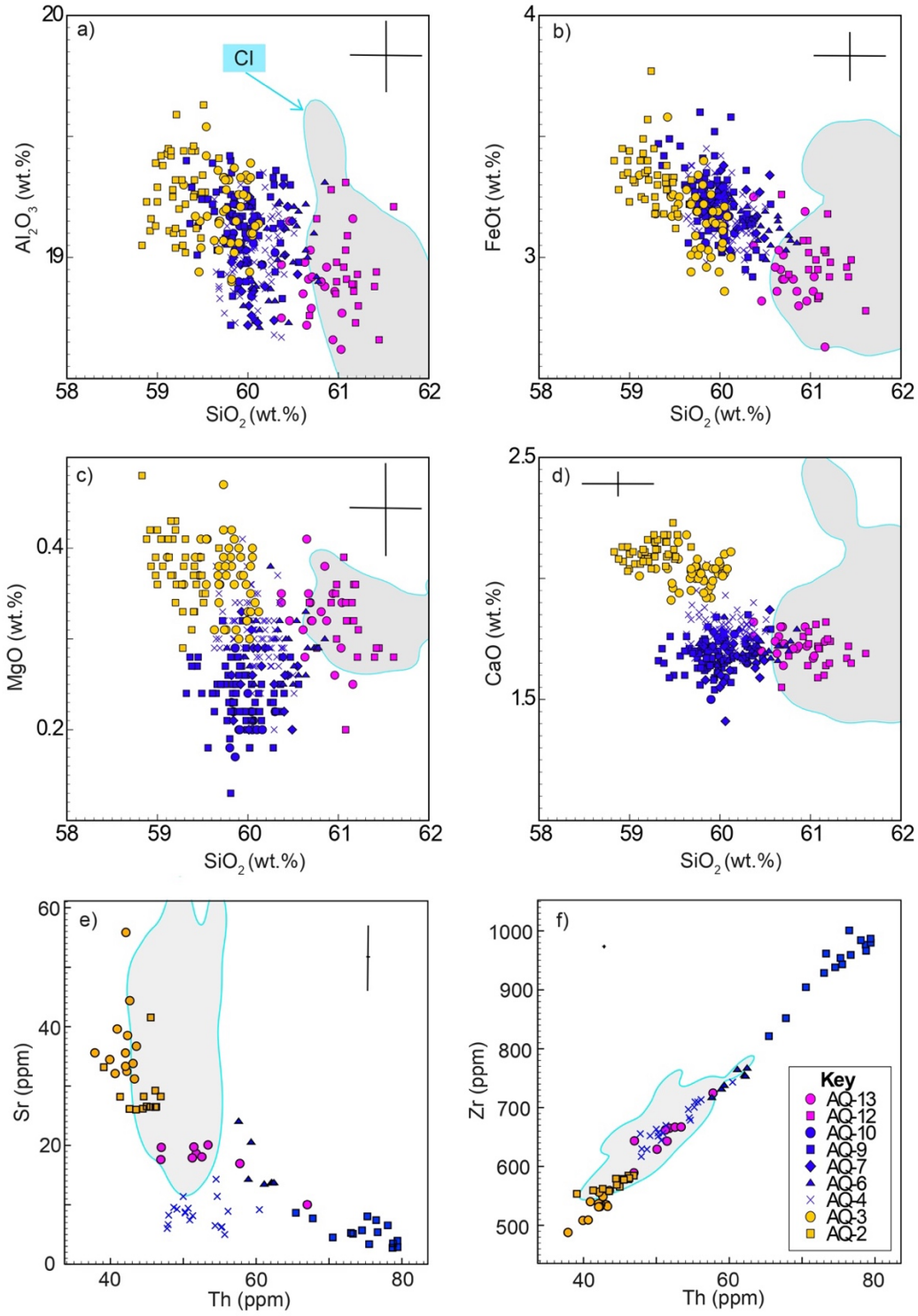


Figure 4.6: Major A-D) and trace E,F) element compositions of all nine pre-CI Campi Flegrei tephra units from the three compositional groups sampled at Acquamorta plotted alongside the compositional field of the CI (grey shaded area with blue outline; data from Tomlinson et al., 2012). Errors are 2 s.d. calculated using replicate analyses of MPI-DING StHs6/80 glass.

The major element data for the nine pre-CI Campi Flegrei deposits reveal that the pre-CI deposits span a wider compositional range than previously reported for proximal pre-CI deposits (Fig. 4.6A-D). The youngest group, Group D, has compositions that extend into the CI compositional field for the initial Plinian phase (Fig. 4.6).

It has previously been noted, using XRF whole rock data, that the pre-CI Campi Flegrei deposits have a more restricted compositional range than the CI (Pabst et al., 2008). Three pre-CI compositional groups were proposed by Pabst et al. (2008) based on whole rock and isotope data obtained from units at Trefola (Pappalardo et al., 1999). Glass compositions of a selection of these units analysed by Tomlinson et al. (2012) correspond to Pabst's Pre-CI Group 1 (TLc) and Pre-CI Group 2 (TLf). There is no glass chemistry for Pabst's Pre-CI Group 3. The Campi Flegrei chemical groups at Acquamorta do not clearly map onto those of Pabst et al. (2008), but both datasets show changes over time (Fig. 4.7A-C). The shifts in major and trace element glass compositions that denote the three Campi Flegrei compositional groups represent changes in the magmatic system (Fig. 4.6).

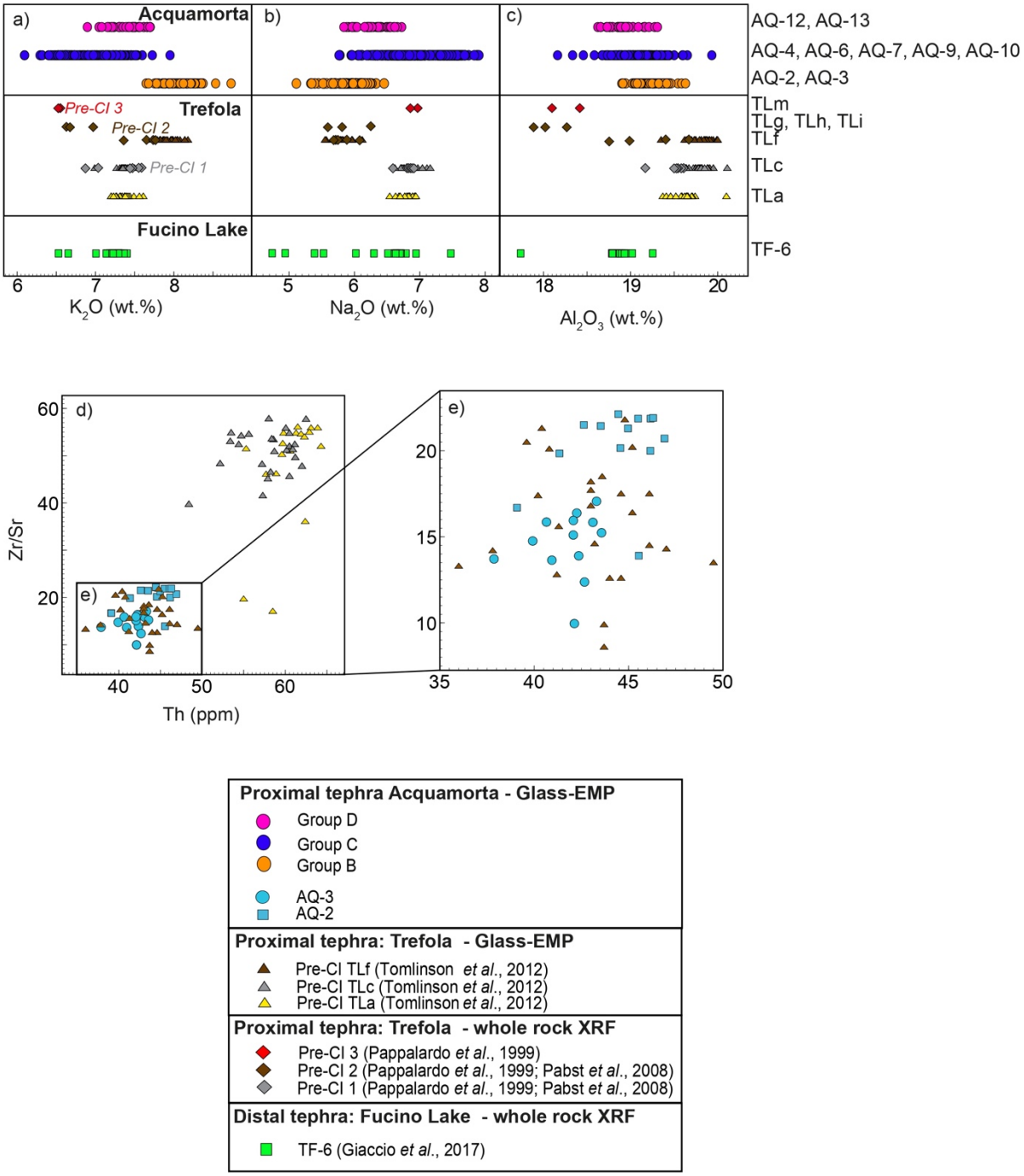


Figure 4.7: A-C) Major element plots of the three pre-CI Campi Flegrei compositional groups from Acquamorta alongside the units from Fucino Lake (distal) and Trefola (proximal), including three pre-CI compositional groups defined by Pabst et al., 2008. D,E) Trace element plots of the Group B units from Acquamorta (AQ-2 and AQ-3) with three units from Trefola (TLa, FLc and TLf). Data from: (1) XRF whole-rock (Pabst et al., 2009; Pappalardo et al., 1999) and (2) data from glass shards (Giaccio et al., 2017; Tomlinson et al., 2012)

Whilst the geochemical data has enabled us to discern three compositional groups between 56 and 40 ka, the eruption units within these groups share similar major and trace element compositions (Fig. 4.6). Thus, we cannot correlate individual tephra units from Acquamorta to layers in other distal or proximal records. Here we discuss the visual descriptions and detailed geochemical data of these compositional groups and discrete units, where useful, to aid future correlations.

4.6.3.1 Group B

Group B is comprised of the two lowermost tephra units: the 0.25 m thick unit of pods of clast supported pumice-lapilli (AQ-2) and the 0.90 m thick deposit comprising of white/grey massive ash with a basal band of clast-supported angular pumices (AQ-3), which are separated by a well-developed paleosol (Fig. 4.3). They present the least evolved glass compositions of the pre-CI units analysed in this study and are characterised by elevated K_2O and CaO contents relative to the other Campi Flegrei units analysed (Figs. 4.4D, 4.6D). Indeed, the alkali ratio of the glasses are elevated relative to the other Pre-CI CF glasses analysed at Acquamorta ($K_2O/Na_2O = 1.36 \pm 0.15$). This, combined with elevated Ba and Sr contents, relative to the dominant populations of the other groups, probably indicates a lesser degree of K-feldspar fractionation.

The chrono-stratigraphically separated Group B units share partially overlapping major and trace element chemical compositions (Fig. 4.4). The glasses from the AQ-3 unit, despite slightly higher SiO_2, are less enriched than AQ-2 glasses (Fig. 4.4B,C). The AQ-2 unit is dominated by glasses with lower SiO_2 and higher CaO contents relative to the overlaying AQ-3 unit and thus can be separated using the SiO_2 vs. CaO plot (Fig. 4.6D). The levels of incompatible trace element enrichment differ too. Whilst levels of incompatible trace element enrichment are greater in the AQ-2 glasses, which is illustrated by Nb, Zr and Th contents, they also extend to slightly lower Sr, Ba and Eu contents than those of the AQ-3 glasses, indicative of greater K-feldspar fractionation (Fig. 4.6E,F; Table 4.1).

The geochemical characteristics of the two Acquamorta Group B tephras are similar to the TLf unit at Trefola (Fig. 4.7), but the Al_2O_3 contents of TLf are higher suggesting that they are different eruption deposits. The trace element contents of TLf are heterogenous, encompassing the full compositional range observed in both AQ-2 and AQ-3 (Fig. 4.7D,E). The TLf unit has been regarded as a useful Pre-CI Campi Flegrei marker layer because of its geochemical characteristics and because it is thought to be associated with a large

eruption as the deposits at Trefola are ~13 m thick (Orsi *et al.,* 1996; Pappalardo *et al.,* 1999; Pabst *et al.*, 2008; Tomlinson *et al.*, 2012). Our data indicate that there are at least three eruptions with the similar TLf geochemistry so correlations to TLf need to be based on more than just the chemical similarity.

4.6.3.2 Group C

The five units in Group C (AQ-4, AQ-6, AQ-7, AQ-9 and AQ-10) make up 3.50 m of the 6 m-thick exposure (Fig. 4.3). Group C glasses are more geochemically evolved than the underlying Group B glasses (Fig. 4.4A-E) and display the greatest compositional diversity of the three pre-CI Campi Flegrei groups (Fig. 4.7A-C). Group C deposits are characterised by lower MgO content, relative to the other two Campi Flegrei groups (Fig. 4.6C), and possess the highest Na_2O contents of all deposits at Acquamorta giving total alkalis values of 13.69 ± 0.46 wt.% and K_2O/Na_2O ratios of 0.99 ± 0.18. Individual units within Group C are largely indistinguishable on major element chemistry. However, the two uppermost units; AQ-9 (0.75 m thick of poorly-sorted yellow ash with some laminations and accretionary lapilli) and AQ-10 (0.75 m of thick well-sorted pumices) are two of the thickest units in the sequence (see Fig. 4.3) and display the greatest geochemical heterogeneity of any of the Acquamorta units (Fig. 4.4). Both AQ-9 and AQ-10 units plot distinctly within Group C with lower K_2O and higher Na_2O contents than the other units in this group and can easily be separated from other units which comprise the Group C glasses using SiO_2 vs. K_2O and SiO_2 vs. Na_2O plots (Fig. 4.4C,D). Furthermore, the AQ-9 unit has a very distinctive trace element composition representing the most enriched glasses (>70 ppm Th) at Acquamorta (Fig. 4.4E,F). We therefore tentatively suggest that the AQ-9 and AQ-10 units could represent a sub-group within the Group C glasses. Additionally, using the dominant population of the AQ-6 glasses, the unit can largely be distinguished from other Group C units (AQ-4 and AQ-9) at a trace element level (Fig. 4.4E,F). Whilst we have been unable to correlate any of the Group C glass with proximal or distal pre-CI deposits, we propose the geochemical features of these units may aid future correlations.

The Acquamorta pre-CI Group C tephras show some geochemical similarities with the deposits from Trefola but have lower Al_2O_3 and K_2O, and elevated Na_2O contents (Fig 4.7A-C). The 2 cm thick TF-6 tephra in the Fucino record (130 km north of Campi Flegrei; Fig. 4.2B) has been correlated to TLc (Giaccio et al., 2017). However, the TF-6 unit has much lower Al_2O_3 content (~1.25 wt%) than the TLc tephra unit (Fig. 4.7C) and is more similar to Acquamorta Group C glasses. The TF-6 unit is compositionally identical to the AQ-

4 unit, which has distinctive Na_2O contents relative to the rest of the Group C glasses (Fig. 4.7B). We argue that the TF-6 unit is not the distal equivalent of the TLc but instead most likely correlates to AQ-4. As there is no published trace element data the TF-6 unit we are unable to verify the correlation. While major element concentrations in AQ-4 are fairly homogenous, this >0.5 m thick unit has a somewhat bimodal trace element signature (e.g. two Th populations at 50.1 and 55.0 ppm; Figs. 4.4E,F, 4.6E,F), which could prove useful for future correlation purposes.

4.6.3.3 Group D

The two eruption units identified directly below the CI (AQ-12 and AQ-13) at Acquamorta are compositionally distinct relative to other pre-CI groups with a Campi Flegrei chemistry. Both units are 2 cm thick fine ash deposits and are separated by a well-developed paleosol (Fig. 4.3). Group D glasses have higher SiO_2 (60.95 ± 0.58 wt.%) and K_2O (7.40 ± 0.39 wt.%) and slightly lower Na_2O (6.28 ± 0.465 wt.%) than the underlying pre-CI Group C Campi Flegrei deposits (Table 4.1; Fig. 4.4C,D). The only tephra deposit from the Group D glasses with trace element data (AQ-13) displays significant heterogeneity and consequently overlaps with many of the pre-CI tephras from both Group B and Group C (Fig. 4.4E,F). However, on the Nb vs. Th plot it is clear that at overlapping Th content the dominant population of AQ-13 (ca. 53 ppm Th) contains lower levels of Nb enrichment relative to the other pre-CI tephra units (e.g. AQ-4), and is instead more consistent with the overlying CI deposits. Both the AQ-12 and AQ-13 units identified at Acquamorta are the only units at the site to overlap with the CI in both major and trace elements (Fig. 4.6) and therefore justifies their classification as a separate compositional group (Group D).

These Group D glasses are compositionally similar to the initial fallout phase of the CI eruption (Fig. 4.8). Major and trace element data show considerable overlap of the Group D glasses with the four distal LGdM TM-18-1a-d visible tephra units (Fig. 4.8) erupted c. 600 years before the CI whose geochemical affinity with the CI deposit has previously been reported (see Wutke et al., 2015). The TM-18-1d tephra deposit is geochemically distinct relative to the three younger TM-18-1a-c tephra deposits (see Wutke et al., 2015). The AQ-12 and AQ-13 tephra units (which comprise the Group D glasses) display a greater geochemical similarity with the TM-18-1a-c tephra deposits (Fig. 4.8C-F). Due to the inability to geochemically distinguish the two units from the Group D compositional group or the three TM-18-1a-c tephras, we are unable to more precisely resolve this proximal-distal correlation.

Whilst we cannot provide a unit-to-unit correlation, we suggest a geochemical package-to-package correlation between the Group D and TM-18-1a-c units.

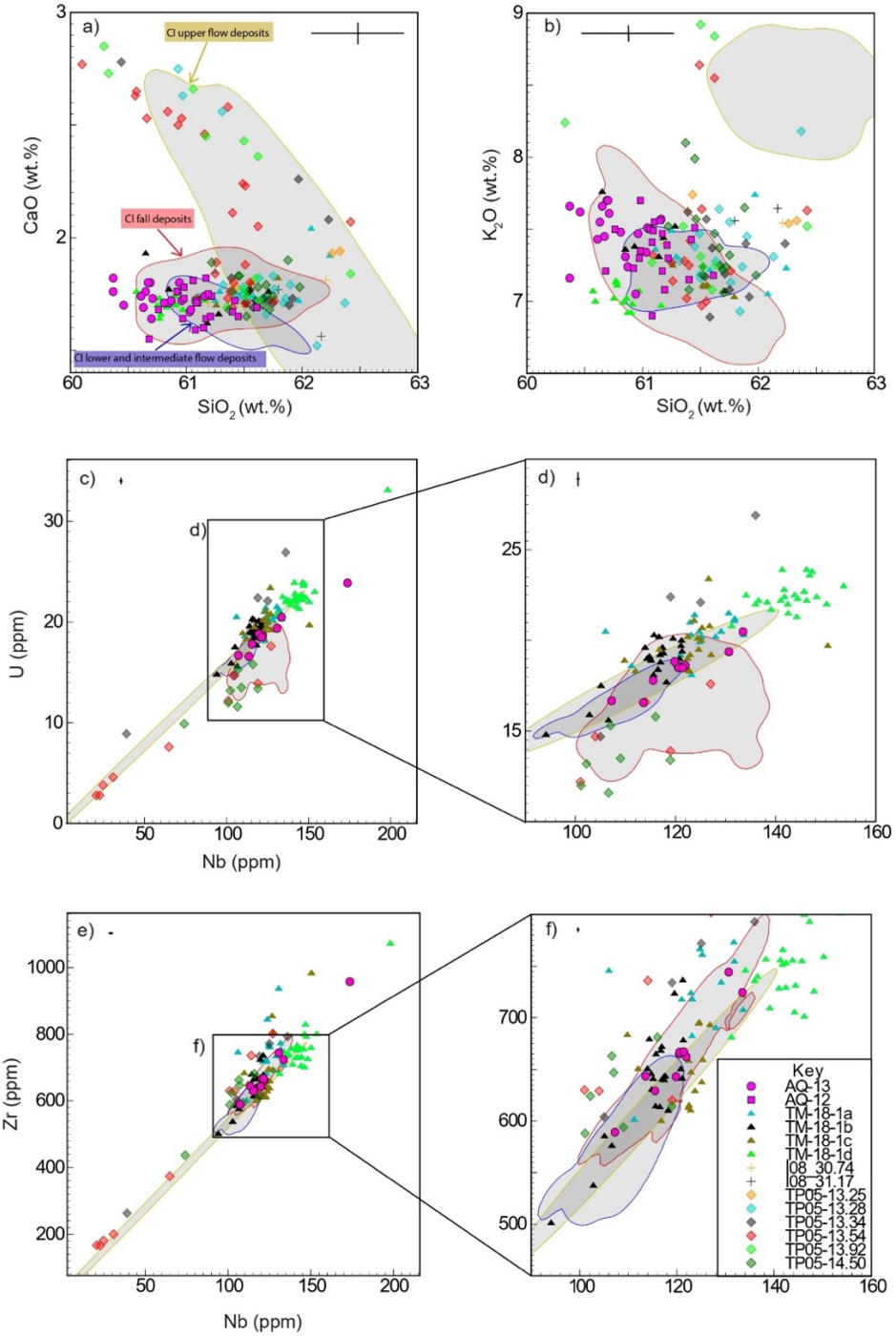


Figure 4.8: A,B) Major element plots of the Acquamorta Group D tephras (AQ-12 ad AQ-13) with the four tephras found directly beneath the CI in the LGdM sequence (TM-18-1a, TM-18-1b, TM-18-1c and TM-18-1d; (Wutke et al., 2015), two cryptotephras between the Y6 and the CI from the Ioannina site (I08-30.74 and I0831.17; McGuire et al., 2022), and six tephras between 40,670 - 47,310 cal yr BP from Tenaghi Phillippon (Wulf et al., 2018). The field for the CI upper flow (red field), CI lower and intermediate flow (grey field) and the CI fall deposits (green field) is obtained from the literature (Tomlinson et al., 2012). C-F) Trace element of the Group D tephra units (AQ-12 and AQ-13) at Acquamorta with the four tephras found directly beneath the CI in the LGdM sequence (TM-18-1a, TM-18-1b, TM-18-1c and

TM-18-1d; (Wutke et al., 2015) alongside the data of the CI deposits (Tomlinson et al., 2012). Errors are 2 s.d. calculated using replicate analyses of MPI-DING StHs6/80 glass.

Other distal records located in northeast Greece — Ioannina (McGuire et al., 2002) and Tenaghi Philippon (Wulf et al., 2018) — have reported a total of eight cryptotephras beneath the CI with overlapping major element geochemical compositions to the CI (Figs. 4.1B and 4.8A,B). Seven of these cryptotephra deposits are believed to be reworked CI deposits (McGuire et al., 2022; Wulf et al., 2018). Wulf et al., (2018) has tentatively correlated one other cryptotephra deposit from Tenaghi Philippon (TP05-13.34) with the LGdM TM-18-1d tephra deposit due to major and trace element similarities. However, the TP05-13.34 glasses have higher K_2O and SiO_2 contents than the TM-18-1d glasses, and thus do not correlate. TP05-13.34 is compositionally similar to the younger TM-18-1-a-c tephra deposits, the I08-30.74 and 108-31.17 cryptotephra deposits preserved in Ioannina, and the AQ-12 and AQ-13 tephra deposits at Acquamorta (Fig. 4.8). Due to the compositional similarity both within the Acquamorta Group D glasses and glasses preserved just below the CI in distal sites, it is not possible to correlate particular units. These two Group D Acquamorta units are the first proximal deposits identified that are compositionally similar to the CI. These could possibly correlate to distal tephra units in Italy (LGdM; Wutke et al., 2015) and Greece (Tenaghi Philippon: Wulf et al., 2018; Ioannina: McGuire et al., 2022) or could be separate small eruptions prior to the CI. Ultimately the identification of the first proximal units displaying the same compositions as the TM-18-1a-c tephras that were erupted <600 years before the CI highlights that there were eruptions with similar glass compositions before the CI, and that records that assigned layers beneath the CI as reworked layers based on the chemistry may need to be revisisted (e.g. McGuire et al., 2022).

4.6.4. Eruption history

The Acquamorta outcrop is a unique record on the western sector of the CI caldera. The site records twelve eruption deposits between the MEGT (56 ka) and the CI (40 ka) eruptions; three from Ischia and nine from Campi Flegrei. We have not been able to correlate with tephra units elsewhere so we are unable to use these deposits to constrain the size or dispersal of the eruptions. The Acquamorta units from Campi Flegrei are typically thin (Fig. 4.3), which is consistent with prevailing westerly winds that indicate the position is unlikely to have been on the dispersal axis. Most mapped eruption dispersals extend toward the east with little or nothing preserved at Acquamorta (Costa et al., 2008; Rosi et al., 1999). Based on what is known about the size and the dispersal of other Campi Flegrei eruptions

(e.g., Smith et al., 2011a; D'Antonio et al., 1999), these tephra layers likely represent eruptions with volumes of ≥0.5 km^3 dry rock equivalent (DRE) and a Magnitude or VEI ≥5.

This study provides evidence for the tempo of volcanism of these two caldera systems both in the lead up to, and in the aftermath of caldera-generating eruptions and thus has hazard assessment implications for these closely spaced, highly active volcanic centres. Ultimately, these findings highlight the need for integration of records from the proximal through to distal settings in order to generate the most complete eruption histories possible (see Figs. 4.1 and 4.2).

4.6.4.1. Ischia

The three Ischia units that outcrop at Acquamorta highlight difficulties in in terms of chemically correlating and distinguishing eruption units, and thus obtaining a detailed record of the post-MEGT Ischia eruption frequency. Whilst the eruption stratigraphy of Ischia is better preserved in proximal locations than that of Campi Flegrei (e.g. Brown et al., 2008, 2014; Poli et al., 1987) and many of the Ischia units have been geochemically characterised (see Tomlinson et al., 2014), we have been unable to correlate any of the post-MEGT Ischia units preserved at Acquamorta to particular eruption deposits because the glass compositions of the tephra units are too similar. It is likely that the proximal deposits on Ischia, mostly outcropping in cliffs and coastal sections, represent a substantially incomplete record, lacking units that are in distal records. The Acquamorta Ischia units show overlap with the Schiappone tephra on major and trace element compositions, but do not display the full compositional range observed in the Schiappone unit sampled on Ischia (Tomlinson et al., 2014). The tight compositional group (Fig. 4.5C-F) may be due to changes in wind direction during the eruption and only part of the eruption deposit is preserved at Acquamorta. Nevertheless, all three Ischia units at Acquamorta show a greater degree of geochemical similarity to the TM-18-9a deposit preserved 130 km east in LGdM, which has varve age of 41,420 yrs. BP (Fig. 4.5C-F). The TM-18-9a is stratigraphically positioned above the distal equivalent of the MEGT (TM-19) and has not been correlated to a proximal equivalent (Tomlinson et al., 2014) and due to the homogenous compositions of the three units at Acquamorta, we are unable to identify which, if any, of these tephras is the proximal equivalent of this distal layer. The identification of these three proximal units with repeated chemical signatures suggests that it is not possible to correlate to a particular Ischia tephra within this time interval, unless they have the wider compositional range of the Schiappone, or are slightly distinct like the deposits from Agnone or Pietre Rosse eruptions.

Distal tephra deposits have been correlated to the Schiappone eruption using major element glass chemistry data. However, given the new proximal data generated by this study and the geochemical affinity with LGdM tephras, we argue that previous correlations to the Schiappone tephra need to be revisited, such as the PRAD-1752 cryptotephra preserved ~8 cm below the CI in the Adriatic Sea (Bourne et al., 2010) and to other Ischia deposits across the Mediterranean including the 20 cm thick SMP1-a tephra deposit preserved beneath the CI on the Sorrento Peninsula with the TM-18-1 cryptotephra deposit located 50 km east (Wutke et al., 2015). The lack of detailed geochemical characterisation of previously identified proximal post-MEGT Ischia units (i.e. Chiummano, La Roia and Capo Grosso) may result in miscorrelations, as has been argued for more widespread Ischia deposits (D'Antonio et al., 2021).

4.6.4.2. Campi Flegrei

The data presented in this study is a significant addition to the eruption history of the highly active Campi Flegrei caldera volcano. The identification of the nine Pre-CI Campi Flegrei tephra deposits between MEGT and CI marker units provides new insight into activity in the lead up to the CI super-eruption; a time-interval where a comprehensive long-term eruption history has been lacking (see Fig. 4.1). It is not possible to discern each of the deposits on the basis of geochemical data alone as many successive deposits have overlapping and repeating compositions. However, two compositional shifts are observed over time, denoting packages of units. These packages can be correlated over distance and provide some insight into the magmatic system feeding this extremely productive phase of the volcano.

This study pulls together evidence in the proximal and distal tephra record and demonstrates that there was heightened activity prior to the CI caldera-forming event, which has implications for hazard evaluation (Giaccio et al., 2017; Wutke et al., 2015; Tomlinson et al., 2012; Di Vito et al., 2008; Wulf et al., 2004; Di Vivo et al., 2001; Pappalardo et al., 1999). Further detailed stratigraphic and geochemical characterisation of proximal outcrops below the CI caldera is required to generate a more complete eruption history and refine hazard assessments for Campi Flegrei. Furthermore, this can be used to further constrain the magmatic processes preceding very large, caldera-forming eruptions.

4.6.5. Magmatic system

The compositional data presented here provides further insight into the magmatic systems beneath both Ischia and Campi Flegrei between 56 and 40 ka. The glass compositions of the deposits are evolved and largely homogenous suggesting that each eruption tapped a single magma batch. This is consistent with these Acquamorta deposits between the MEGT and CI being associated with eruptions with a VEI/M ≥5 as the large events from both Campi Flegrei and Ischia tend to tap multiple, homogeneous magma batches, such as the Campanian Ignimbrite (e.g. Smith et al., 2016) and Masseria de Monte (Albert et al., 2019b) from Campi Flegrei, and the Schiappone and MEGT from Ischia (Tomlinson et al., 2014).

The three post-MEGT Ischia units preserved at Acquamorta provide limited insight into the magmatic system beneath Ischia as there are at least six eruption deposits from Ischia in this time period (Fig. 4.1). Whole-rock and isotopic data from Brown et al. (2014) shows a shift after the MEGT with the influx of less evolved and isotopically distinct melt. The Capo Grosso, La Roia and Chiummano eruptions that followed the MEGT and preceded the Schiappone (Fig. 4.1, 4.5C-F) are distinct from each other and less evolved than the Schiappone, but the similar isotopic compositions indicate that they may have derived from the same parent magma, with each eruption tapping it at different stages of its evolution. Consistent with it being a larger eruption on Ischia, the Schiappone tephra is compositionally heterogeneous tapping multiple magma batches (Tomlinson et al., 2014). One of the Schiappone melt compositions is the same as that tapped by the three Ischia eruptions that are preserved at Acquamorta. It is not clear whether these deposits precede, succeed, or include the Schiappone eruption. In any case, since the major and trace element compositions are identical for these three Ischia deposits it shows that the melt in the system did not differentiate much between the eruptions.

Previous studies on the pre-CI Campi Flegrei magmatic system focussed on whole-rock and limited isotopic data from a few of the deposits (Pappalardo et al., 1999; Pabst et al., 2008) and did not provide a detailed insight into the system. Our new data shows that similar melt compositions are commonly erupted over successive events, and there were a couple of compositional shifts over time; between Group B and C, and Group C and D.

The two units in Group B share similar major elements and trace element compositions. The compositional change that occurs between Group B and C is an increase in Na_2O, Rb, Y, Zr, Nb, REE, Th, and U, and a decrease in K_2O, CaO, V, and Sr (Fig. 4.4,

4.6; Table 4.1). While the four units in Group C share similar major element compositions and the trace element compositions are homogeneous, the trace element compositions change through the sequence. The compositions of each unit extend to lower V concentrations, and higher Rb, Y, Zr, Nb, REE, Ta, Th concentrations than the previous unit (Table 4.1). These temporal changes are consistent with crystallisation and subtle evolution of the melt, while the lack of changes in the major elements suggests that the overall amount of crystallisation was limited. The shift between Group C and D is marked by a subtle change in major elements to slightly higher SiO_2 and lower Na_2O contents (Fig. 4.4). While the trace element ranges observed by Group C and D overlap, and the shift between the groups is marked by a return to concentrations that are observed at the start of Group B, i.e. melts with lower Rb, Y, Zr, Nb, REE, Ta, and Th concentrations. The two Acquamorta units in Group D are compositionally identical to each other and the melt that was tapped in the Plinian phase of the CI, which is not preserved at the Acquamorta site (Tomlinson et al., 2012; Smith et al., 2016). At least four eruptions occurred in Group D, given that four units directly below the CI in the LGdM record (TM-18-1a-d) have major and trace element compositions that are identical to our Group D composition at Acquamorta (Wutke et al., 2015; Fig. 4.8A-F). Whole-rock data from one of the pre-CI units presented in Pabst et al. (2008) indicates that at least one of the eruptions before the CI has similar isotope compositions, which suggests that the large homogeneous melt body that fed the first phases of the CI eruption was at least partly in place before the Group D eruptions. These pre-CI Group D eruptions would have only tapped relatively small portions of the melt, and the identical major and trace element compositions indicate there was little differentiation of this melt between these Group D eruptions and the caldera-forming CI. Given that the Group D and CI compositions are different to those erupted earlier (Group B and C) it implies that the CI magma that fed the Plinian phase and portions of the PDCs (>150 km^3 DRE; Marti et al., 2016) did not exclusively occupy the upper crust beneath Campi Flegrei in the 14 kyr prior to the CI eruption. In fact, the high-resolution chronology from the LGdM record suggests that the distally dispersed Group D magma was only erupted during the 600 years prior to the CI (Wutke et al., 2015).

Both Ischia and Campi Flegrei tap compositionally similar melts through time. This implies that there are extended periods during which the eruptions are only tapping portions of the melt in the homogenous magmatic system beneath each volcano. Although we do not have a precise chronology of the pre-CI events, the fact that there are well-developed paleosols between the deposits implies that the magmatic systems were similar over thousands of years. Similar patterns with successive eruptions tapping compositionally similar melts is observed at other times at Campi Flegrei, such as prior to and following the

NYT eruption (Albert et al., 2019b; Forni et al., 2018; Smith et al., 2011a). The main compositional shifts observed over time (i.e. between Group B and C, and Group C and D) likely correspond to the new input of melt into the upper crust beneath Campi Flegrei, and likely match the isotopic shifts that observed by Pabst et al. (2008) within the pre-CI deposits.

4.7. Conclusion

New major and trace element glass data for twelve tephra deposits preserved between the MEGT and CI within the Acquamorta outcrop located on the western side of the CI caldera wall have been acquired and are presented. We have been able to correlate all twelve deposits to a volcanic source within the CVZ; three units are from Ischia eruptions and nine units are from Campi Flegrei eruptions. The compositional data obtained indicates that successive eruptions from each volcano are broadly compositionally homogenous, with small compositional shifts over time observed in those from Campi Flegrei.

The three Ischia tephra deposits are compositionally indistinguishable at both the major and trace element level and have not been correlated to any proximal or distal tephra units. These are compositionally similar to the most evolved component of the Schiappone tephra, the largest post-MEGT Ischia eruption, with none showing the full compositional range that is diagnostic of this particular eruption deposit. Whilst we cannot rule out that one of these tephra deposits at Acquamorta may represent the Schiappone, there are another two other eruptions with a similar geochemical composition. Ultimately the identification of these geochemically indistinguishable units suggests that the post-MEGT eruption history for Ischia is not well resolved and may be incomplete, and care must be taken when correlating post-MEGT Ischia units.

We have shown that the nine pre-CI Campi Flegrei units from Acquamorta form three distinct geochemical clusters and demonstrate the ability to discern temporal differences in glass chemistry of the volcano through time. These data indicate the pre-CI Campi Flegrei eruptions were fed by highly, but differently, evolved magmas, similar to the post-NYT Campi Flegrei deposits (Smith et al., 2011a). These groups follow a general trend of becoming increasingly evolved in the lead-up to the CI, with the youngest units (Group D) very similar in composition to the magma erupted during the Plinian phase of the CI eruption (Fig. 3.8). Whilst trace element data was obtained for several units, they are not as useful as the major elements for discriminating the three pre-CI Campi Flegrei compositional groups (Fig. 3.4A-

H). The most useful elements for distinguishing the pre-CI Campi Flegrei deposits are Al_2O_3, CaO, Na_2O, K_2O, Nb and Th. We have identified multiple tephra deposits at Acquamorta with the same chemistry as both known proximal (Group B with the TLf tephra; Tomlinson et al., 2012) and distal (Group D with the TM-18-1a-c units; Wutke et al., 2015) tephra deposits. Thus, these correlations are not to particular eruptions and instead correlations can only be made to a package of tephra units with similar chemistry (i.e. a respective pre-CI Group), which erupted over the order of several thousand years.

The results highlight the need for further detailed chrono-stratigraphic and geochemical data from tephra deposits located across the CI caldera to generate more complete eruption histories and magmatic systems for the CVZ volcanoes and thus improve the hazard assessments for some of Europe's most active volcanoes. Once this has been undertaken it will be possible to combine proximal and distal records to establish a detailed tephrostratigraphy and ascertain which eruptions resulted in major tephra dispersal across the southern Mediterranean region.

CRediT **author statement**

S.O.V.: Conceptualisation; Resources; Data Collection; Methodology; Investigation; Formal analysis; Visualization; Writing-Original Draft; Writing-Review & Editing; Funding acquisition. **R.I.:** Data Collection; Writing-Review & Editing. **P.G.A.:** Formal Analysis; Writing-Review & Editing; Supervision. **R.J.B.:** Data Collection; Writing-Review & Editing. **V.C.S:** Conceptualisation; Resources; Data Collection; Writing-Review & Editing; Supervision; Funding acquisition.

Acknowledgements:

S.O.V is funded by NERC as part of the Environmental Research Doctoral Training Programme at the University of Oxford (NE/ S007474/1). V.C.S acknowledges funding from NERC (NE/S003584/1). P.G.A is funded through a UKRI Future Leader Fellowship (FLF) award (MR/S035478/1). In addition, V.C.S and P.G.A acknowledge funding from the John Fell Fund. We also thank Madeleine Humphreys, Michael Stock, Antony Hinchliffe and Jenny Riker for assistance in the field and Christina Manning for assistance with LA-ICP-MS analysis. Shane Cronin (editor), Steffen Kutterolf and an anonymous reviewer are thanked for their constructive comments that improved this paper.

See Appendix A for Supplementary Material.

Chapter 5: A detailed record of large explosive eruptions from Japan between ~120 and 50 ka preserved at Lake Suigetsu

Sophie O. Vineberg[a], Paul G. Albert[b], Danielle McLean[a], Takehiko Suzuki[c], Richard A. Staff[a,d,e], Keitaro Yamada[f,g], Ikuko Kitaba[f,h], Junko Kitagawa[i,j], Christina J. Manning[k], Hannah M. Buckland[b], Fumikatsu Nishizawa[l], SG14 Project Members[m], Takeshi Nakagawa[f] and Victoria C. Smith[a]

[a] Research Laboratory for Archaeology and the History of Art, School of Archaeology, University of Oxford, Oxford, OX1 3TG, UK
[b] Department of Geography, Swansea University, Swansea, SA2 8PP, UK
[c] Department of Geography, Tokyo Metropolitan University, Tokyo, 192-0397, Japan
[d] Scottish Universities Environmental Research Centre, University of Glasgow, East Kilbride, G75 0QF, UK
[e] The British Museum, London, WC1B 3DG, UK
[f] Research Centre for Paleoclimatology, Ritsumeikan University, Kusatsu, Shiga, 525-8577 Japan
[g] Institute for Geothermal Sciences, Kyoto University, Kyoto, 606-8224, Japan
[h] Research Center for Inland Seas, Kobe University, Kobe, 657-8501, Japan
[i] Varve Museum, Wakasa, Fukui, 919-1331, Japan
[j] Fukui Prefectural Satoyama-Satoumi Research Institute, Wakasa, Fukui, 919-1331, Japan
[k] Centre for Dynamic Earth and the Solar System, Department of Earth Sciences, Royal Holloway, University of London, Egham, Surrey, TW20 0EX, UK
[l] Kanagawa Prefectural Museum of Natural History, Odawara, 250–0031, Japan
[m] www.suigetsu.org

Highlights

- Forty-one crypto-/tephras identified Lake Suigetsu archive spanning ~120-50 ka.
- Tephras are mostly from volcanoes in Kyushu, with a few from Hokkaido and intraplate sources.
- Frequent explosive activity from Kirishima volcanic complex over a 19 kyr interval.
- Provide ages for the widespread SK (100.4 ± 3.1 ka) and Toya (108.1 ± 3.9 ka).

Abstract

We present the findings of a detailed non-visible (cryptotephra) tephra investigation of the Lake Suigetsu (Japan) sedimentary sequence spanning ~120 to 50 ka. Thirty-nine new cryptotephra and two visible tephra horizons are identified during this interval interspersed between visible tephra layers associated with large-magnitude eruptions and regional event markers (e.g., Aso-4, K-Tz, Ata). The newly identified volcanic deposits are geochemically analysed using major (EMP) and trace (LA-ICP-MS) element glass analyses, and the chemical fingerprints are used to trace these deposits to subduction related volcanoes located along the three main Japanese islands (Kyushu, Honshu and Hokkaido), as well as nearby intraplate volcanoes. Our findings provide geochemical, chronological and ash-fall

constraints on the activity at multiple volcanic centres; in particular, the Kirishima volcanic complex in the southern volcanic region of Kyushu. Furthermore, the Lake Suigetsu cryptotephra record reveals distal ash-fall from two notable large magnitude (≥M6.0) eruptions, the Plinian Sambe Kisuki (SK) eruption and the caldera-forming Toya eruption, both of which are important widespread tephrostratigraphic markers suitable for linking regional terrestrial and marine sequences. Using the Lake Suigetsu age-depth model, they are dated to 100.4 ± 3.1 ka (±1σ) and 108.1 ± 3.9 ka (±1σ), respectively. Finally, our investigation reveals numerous eruption deposits which have not yet been identified in near-vent sequences, indicating eruption under-recording. This research re-affirms Lake Suigetsu as the single most comprehensive ash-fall record of East Asian explosive volcanism over the past 150 kyr, and contributes significantly to our understanding of the timing and ash dispersals of pre-historic eruptions.

Keywords
Ash-fall; Cryptotephra; Lake Suigetsu; Tephrochronology; glass chemistry

5.1. Introduction

Large explosive eruptions have caused significant and incredibly widespread environmental and societal effects in history (Oppenheimer, 2003) and are therefore of substantial scientific interest/importance (e.g., Tambora 1815 CE and Krakatau 1883 CE eruptions). Although historical records and the high-resolution polar ice cores have provided detailed eruption archives for the last couple of millennia (e.g., Sigl et al., 2015), knowledge of eruptions further back in time (e.g., across the last glacial to interglacial cycle) are not particularly well constrained. A statistical re-analysis of the LaMEVE (Large Magnitude Explosive Eruptions; Crosweller et al., 2012) database suggested that almost 89% of medium-large sized (Volcanic Explosivity Index [VEI] or Magnitude [M] ≥4) eruptions are currently missing from the eruption record at ~100 ka (Kiyosugi et al., 2015). Detailed eruption histories across such timescales are essential for the development of robust hazard and risk assessments, providing insight into the frequency and behaviour of large events (e.g., caldera-forming eruptions) and their return intervals (e.g., Uesawa et al., 2022).

The East Asian Pacific region is home to over 30% of the global population (Cook et al., 2010) and has one of the greatest population densities living within 100 km of an active volcano (Brown et al., 2015). Japan alone has over 130 active volcanic centres, many of which have produced several of the largest magnitude volcanic eruptions in the last 200 ka

(Newhall et al., 2018; Machida and Arai, 2003). Sixteen Japanese volcanoes are considered candidates to produce a large eruption (VEI/M ≥7) in future millennia (Newhall et al., 2018). However, reconstructing the past eruption histories of these centres has proved difficult using near-vent (proximal) eruption records alone. This is partly due to the burial, destruction and subsequent erosion of eruption deposits around the productive volcanoes, and that Japan has a high degree of urbanisation, strong seasonality and dense vegetation in less developed areas. Distal sedimentary archives such as lacustrine and marine sediment cores can overcome such preservation and accessibility issues and may even capture separate medium-sized events (e.g., VEI/M ≥4) more clearly than their proximal counterparts (Chen et al., 2019; McLean et al., 2018; Wulf et al., 2018; Tomlinson et al., 2014).

The Lake Suigetsu sedimentary record (central Japan; location shown in Fig. 5.1) provides a key tephro-stratotype of explosive volcanism for Japan spanning the last 200 kyr. To date, seventy-six visible and non-visible (cryptotephra) deposits have been identified and geochemically characterised in the sediments (Albert et al., 2018, 2019a, 2024; McLean et al., 2016, 2018, 2020a, 2020b; Smith et al., 2011b, 2013). Whilst many of the tephra layers have been correlated to arc volcanoes located on Honshu and Kyushu (e.g., Albert et al., 2018, 2019a; Smith et al., 2013), several layers also originate from Japanese centres located >500 km north of Lake Suigetsu (e.g., Hokkaido), as well as the more distal intraplate volcanoes such as Ulleungdo in South Korea and Changbaishan on the border of China and North Korea (Albert et al., 2018, 2019a; McLean et al., 2016, 2018; Smith et al., 2011b). Investigations of cryptotephras within the Lake Suigetsu sediments have also been completed for the Holocene and Late Pleistocene (0-20 ka and 30-50 ka) and reveal volcanic deposits from an additional eight volcanic centres indicating that there are four times as many cryptotephra deposits preserved relative to visible tephra layers (Albert et al., 2024; McLean et al., 2018). The identification of these tephra within the well dated Lake Suigetsu sequence (Bronk Ramsey et al., 2012) provides tight age constraints for past eruptions and enabled the integration of regional tephrostratigraphies, as well as facilitating the first direct link to the Greenland ice cores (i.e., the B-Tm tephra, 946 CE; Oppenheimer et al., 2017; McLean et al., 2016; Sun et al., 2014).

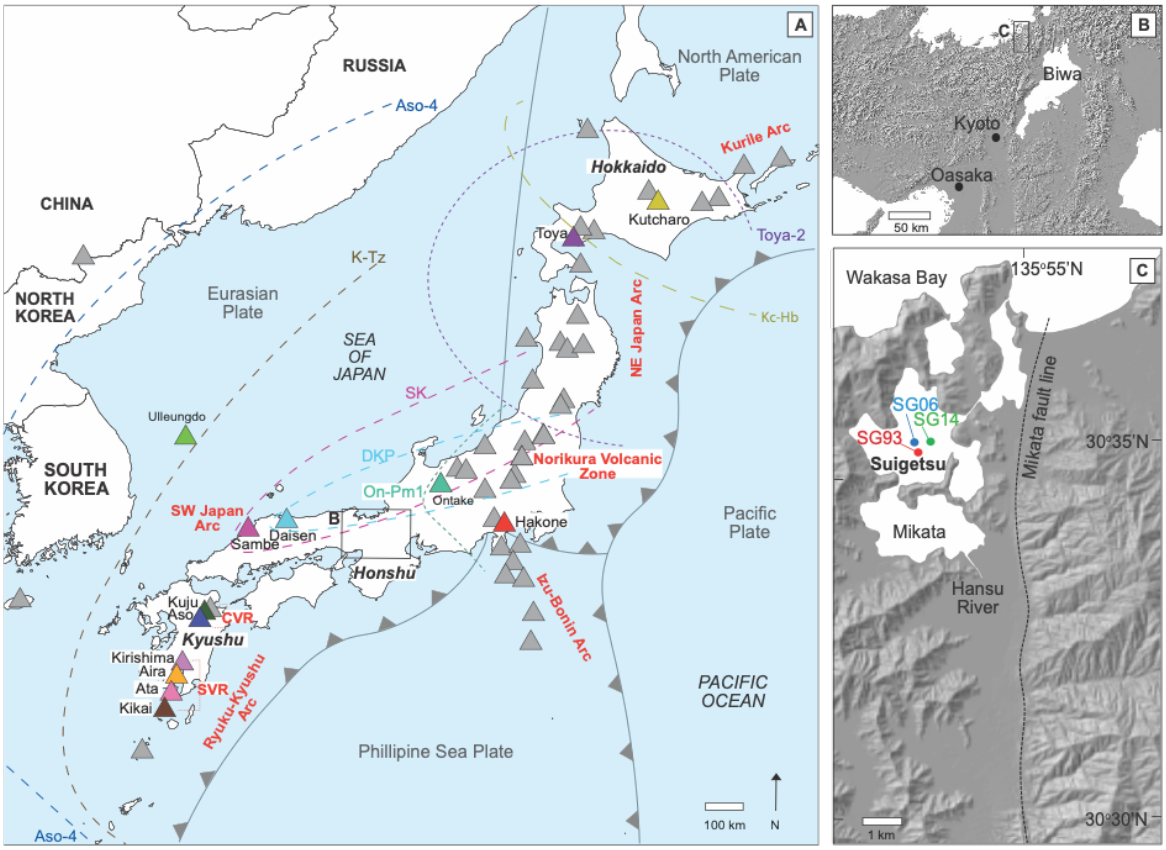


Figure 5.1: A) Volcanoes (triangles) that have been active in and around Japan in the Quaternary. The volcanoes that are mentioned in the text and likely sources of the tephra in Lake Suigetsu in this period are coloured. The dashed lines denote the ash dispersal boundaries for various widespread tephra layers (as labelled), which are from (Machida, 2002). The red labels are the volcanic arcs: SVR = Southern Volcanic Region; CVR = Central Volcanic Region; SWJA = SW Japan Arc; NVZ = Norikura Volcanic Zone; NEJA = NE Japan Arc. (B) Proximity of Lake Suigetsu to Lake Biwa and major Japanese cities. (C) Location of Lake Suigetsu as part of the five Mikata Lakes, adjacent to Wakasa Bay. The positions of all three coring campaigns are marked (B and C modified after Nakagawa et al., 2005).

To further refine the Late Quaternary tephrostratigraphic framework for the East Asian/Pacific region, we investigate the unexplored cryptotephra record preserved in the ca. 20 m of the Lake Suigetsu sediments (SG14 core) dated between ~120 and 50 ka (Bronk Ramsey et al., 2012; Schlolaut et al., 2012, 2018). The high-resolution sediments of Lake Suigetsu offer unprecedented insight into the timing, frequency and dispersal of ash-fall events dispersed over this now heavily populated region of East Asia.

5.2. Study Site

Lake Suigetsu is the largest of the of the 'Mikata Five Lakes' (4.3 km^2) and is in a small tectonic basin situated on the western side of the Mikata fault (Fig. 5.1C). These lakes are situated on central Honshu Island (35°35′0″N, 135°53′0″E, 0 m above present sea level), adjacent to Wakasa Bay on the Sea of Japan coast (Fig. 5.1). The principal tributary, the Hasu River, enters on the southeast edge of Lake Mikata which adjoins Suigetsu through a narrow channel (Fig. 5.1C). The low energy environment and deep-water column (34 m) hinder disturbance to the deposited sediments. This unique hydrological configuration means that the sedimentary environment is highly stable and dominated by fine-grained deposition as coarser material settles out upstream in Lake Mikata (Nakagawa et al., 2021). Lake Suigetsu is situated 150 km from the nearest active volcano (Ontake, Fig.5.1A) and thus, is not inundated with locally sourced volcanic glass, which would hinder the identification of low-concentrated cryptotephra from more distant volcanic sources.

5.3. Eruption histories of volcanoes in and around Japan between ~120 and 50 ka

Volcanism in Japan occurs via subduction along the Ryuku-Kyushu Arc, SW Japan Arc (SWJA), the NE Japan Arc (NEJA) and the Kurile Arc (Fig. 5.1). Intraplate volcanism is also relevant in this region with volcanoes located in South Korea (Halla on Jeju Island located off the south coast of South Korea and Ulleungdo located in the Sea of Japan) and on the North Korea/China border (Changbaishan) (Fig. 5.1A; Brenna et al., 2012). Many of these centres have been highly productive during the Late Quaternary (Fig. 5.2), several of which have produced some of the largest known caldera-forming eruptions (VEI/M ≥7; see Machida and Arai, 2003). An overview of the known eruption histories from these volcanic centres likely to be identified in Lake Suigetsu in the ~120 – 50 ka timeframe are provided in Table 5.1 and are discussed in brief in the following sections.

Table 5.1: Key East Asian eruption deposits reported in proximal and medial locations in the ~120 – 50 ka timeframe that are most likely to be preserved in the Lake Suigetsu sediments. Those in bold are widespread marker layers (Machida and Arai, 2003), and those previously identified in Lake Suigetsu sediments as visible tephras (layers noted by their SG labels; (Albert et al., 2018; 2019a; Smith et al., 2013).

Region	Volcano	Eruption	Tephra	SG label	Magnitude (M)	Tephra volume (km^3)	Dispersal	Age (cal. yrs BP/ ka)	(Ref.)
Kyushu (Central Volcanic Region; CVZ)									
	Aso	ACP-4	ACP-4	SG06-3912	4.6	0.43	E	49,974 ± 33[1]	1
		ACP-5	ACP-5	-	4.2	0.15	NE	>ACP-4	-
		ACP-6	ACP-6	-	4.3	0.21	E	~60	2
		Aso-4	**Aso-4**	**SG06-4963**	**7.8**	**600**	**-**	**86.4 ± 1.1[1*]**	**1**
		Aso-Y	Aso-Y	-	4	0.1	E?	>Aso-4	-
		Aso-ABCD	Aso-ABCD	SG06-5287	5	1	-	~96	3
		Aso-IK	Aso-IK	-	5	1	ENE	>100<123	1
		Aso-MN	Aso-MN	-	5	1	ENE	>Aso-IK	-
		Aso-3	**Aso-3**	**-**	**7.5**	**150**	**ENE**	**~123 – 135**	**4, 5**
	Kuju	Pumice 1/Handa	Kj-P1/Hd	SG06-4141	5.3	2	E	54.4 ± 1.6	6
		Kuju-D	Kj-D	-	-	-	-	>Kj-P1/Hd	-
		Miyagi	Kj-Mj	-	-	-	S	>Kj-P1; >Aso-3	-
Kyushu (Southern Volcanic Region; SVR)									
	Aira	Iwato	A-Iw	-	6	9.5	E	~55	7
		Fukuyama	A-Fk	-	-	-	EN	90	4
	Ata	**Ata**	**Ata**	**SG06-5353**	**7.5**	**350**	**NE**	**99.3 ± 6.0**	**1**
	Kikai	Tozurahara	K-Tz	SG06-5181	7.2	150	NE (radial)	94.5 ± 4.8	1
		Nagase	K-Ns	-	-	-	-	>K-Tz	4
	Kirishima	Awaokoshi	Kr-Aw	-	-	-	ENE	<Kr-Aw	-
		Iwaokoshi	Kr-Iw	-	-	-	ENE	40-45	4
Honshu (South West Japan Arc; SWJA)									
	Daisen	**Kurayoshi Pumice**	**DKP**	**SG06-4281**	**6.5**	**32**	**E**	**59.6 ± 5.5**	**6**
		Sekigane Pumice	DSP	SG06-4318	4.9	0.85	E	61.1 ± 5.8	6
		DNP	DNP	-	6.9	80	E	~80	4
		DHP	DHP	-	-	-	E	>DNP	-
		DMP	DMP	-	-	-	W	~125	3
	Sambe	Oda Pumice Flow	SoD	-	-	-	-	~53 ka	4
		Unan Pumice Fall	SuN	SG06-4124	6.1	13	-	53.8 ± 1.2	1
		Kisuki	**SK**	**-**	**6.3**	**20**	**NE**	**~100**	**4, 9**
Honshu (Norikura Volcanic Zone; NVZ)									
		Nagawa	On-Ng	-	-	-	NE	~83	4
		Ina	On-In	-	6	10	E	~93	4
		Katamachi	On-kt	-	-	-	NNE	~94	4
		Daiichi Pumice	O-Pm1	-	6.7	50	E	~95	4
Honshu/ Hokkaido (Northeast Japan Arc; NEJA)									
	Toya	**Toya**	**Toya**	**-**	**7.2**	**170**	**Radial**	**112-115 (MIS5d)/108**	4,10
Hokkaido (Kurile Arc)									
	Kutcharo	Kc-2/3	Kc-2/3	-	6.4	25	N-NNEW	~85	8
		Kc-Hb/4	**Kc-Hb**	**-**	**7.2**	**175**	**W**	**120**	**11**
Intra-plate									
	Changbaisan	Baegdusan–Japan Basin tephra	B-J	-	-	-	-	50.67	12
		Baegdusan–Sado-oki tephra	B-Sado	-	-	-	-	67.68	13
		Baegdusan–Yamato Basin tephra	B-Ym	-	-	-	-	85.88	13
	Ulleungdo	Ulleung–Sado-oki tephra	U-Sado	-	-	-	-	61.18	13

Footnote: Dispersal and tephra volume estimates are from Machida and Arai (2003) and the LaMEVE database (Crosweller et al., 2012; and references therein). The magnitude (M) of each eruption has been calculated using the published tephra volumes and the equation of Pyle (2000), assuming a magma density of 2300 kg/m^3 and tephra density of 1000 kg/m^3. * indicates $^{40}Ar/^{39}Ar$ age. Eruption age references as follows: 1: Albert et al. (2019a); 2: Miyabuchi (2011); 3 Hayakawa (2023); 4 Machida and Arai (2003); 5 Kaneko et al. (2015); 6 Albert et al. (2018); 7 Ikehara et al (2006); 8 Smith et al. (2013); 9 Kimura et al. (1999); 10 Ito (2014); 11 Hasegawa et al. (2016); 12 Ikehara et al. (2004); 13 Lim et al. (2013).

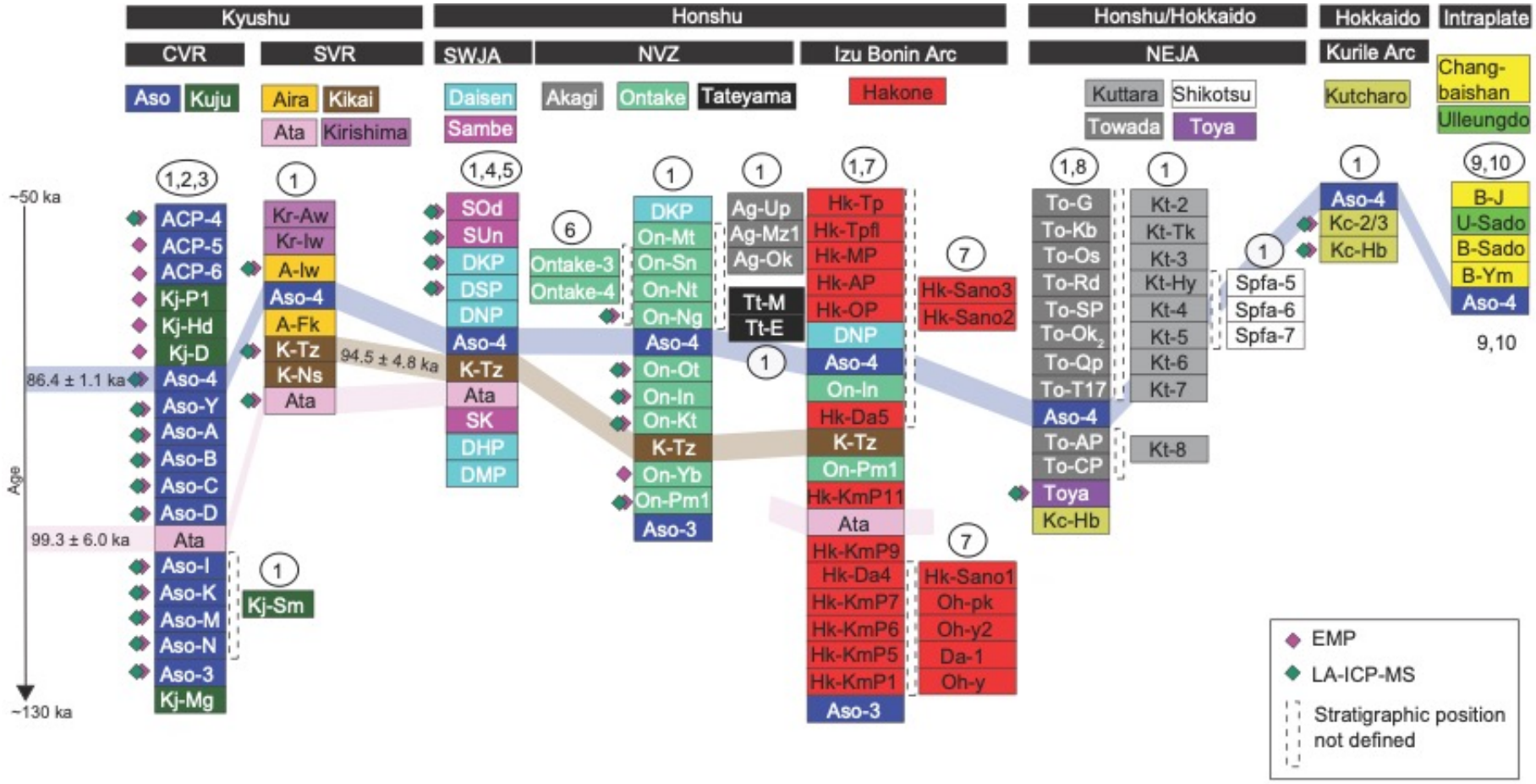


Figure 5.2: Relative stratigraphic order of known eruptions (~130 – 50 ka), based largely on the proximal stratigraphies, in and around Japan. The key widespread marker layers that link several of the stratigraphies include the Ata (from Aira volcano), K-Tz (Kikai) and Aso-4 (Aso) tephras. The ages of Ata and K-Tz are modelled ages based on their position the Lake Suigetsu sediments (Smith et al., 2013; Albert et al., 2019a), and Aso-4 has been directly dated via $^{40}Ar/^{39}Ar$ (Albert et al., 2019a). References: 1. Machida and Arai (2003); 2. Albert et al. (2019a); 3. Kamata et al. (1998); 4. Albert et al. (2018); 5. Nagaoka et al. (2001); 6. Hayakawa (1985); 7. Kobayashi and Koyoma (1996); 8. Matsu'ura et al. (2014). Medial marine records: 9. Ikehara et al. (2004); 10. Lim et al. (2014).

5.3.1. The Central Volcanic Region (CVR) associated with the Ryuku-Kyushu Arc

The CVR is located in northeast Kyushu and notably includes the Aso caldera and the Kuju volcanic complex (Fig. 5.1A). Aso has been highly productive during the Late Quaternary with numerous Plinian eruptions of ≥M4 (Table 5.1). The present caldera is one of the largest on Earth and is a product of at least four M6-8 eruptions (Machida and Arai, 2003; Miyabuchi, 2009). The Aso-4 eruption is the most recent caldera-forming event and is dated to 86.4 ± 1.1 ka ($^{40}Ar/^{39}Ar$; Albert et al., 2019a), and resides within sediments associated with MIS 5b (Aoki et al., 2008). It provides a key widespread tephrostratigraphic marker and is frequently identified in distal records across East Asia (Figs. 5.2 and 5.3). The proximal stratigraphies from outcrops close to the caldera indicate that there were a series of post-caldera Plinian fall eruptions from central cones following the Aso-4 eruption, which span ~60 – 50 ka (Miyabuchi, 2009). ACP4 is the most widely traced of these eruptions with a visible ash layer identified in Lake Suigetsu, SG06-3912 (49,974 ± 33 cal. BP; Albert, et al., 2019a). The pre-Aso-4 deposits are buried under the tephra from the caldera-generating eruption (Fig. 5.2; Table 5.1) and the number of eruptions are still unclear. At least four eruptions (several with multiple phases) are observed beyond the caldera walls, two units (Aso-Y and Aso-ABCD; SG06-5287) occur above the widespread Ata marker tephra, while multiple units are recognised between Ata and the Aso-3 (caldera-forming) eruption deposits (Table 5.1; Fig. 5.2; Hoshizumi et al., 2022; Albert et al., 2019a).

The Kuju volcanic complex lies North of Aso and consists of over twenty small stratovolcanoes and lava domes (Kawanabe et al., 2015), and has produced some widely dispersed tephras (Machida and Arai, 2003). Kuju activity at ~55 – 53 ka includes three deposits: Kj-D, Kj-P1 and Kj-Hd (Fig. 4.2). Both the Kj-Hd (Handa) ignimbrite and Kj-P1 Plinian fall deposits are considered to have erupted contemporaneously (Okuno et al., 2017) and have been identified distally in Lake Suigetsu (SG06-4141; Albert et al., 2019a). Older Kuju deposits that have been reported: Kj-Sm at 110 ± 4.0 ka (Fig. 5.2); and Miyagi (Kj-Mg), which is beneath Aso-3 and considered to be >150 ka (Hayakawa 2023; Kaneko et al., 2015; Machida and Arai, 2003). Glass compositions of the CVR tephras are well established; most notably for the eruptions from Aso. Glasses from Aso erupted between 135 and 50 ka range from trachy-dacite through to rhyolites, and plot on a distinctive K_2O evolutionary trend relative to those erupted from many other Japanese volcanic centres, including Kuju (Fig. 5.2; McLean et al., 2020b; Albert et al., 2019a; Kimura et al., 2015; Machida and Arai, 2003). In contrast, glasses from Kuju are rhyolitic and cannot be discriminated from those erupted from volcanoes in the SWJA using major or trace element compositions (Matsu'ura et al., 2021). Geochemical data are available for four of the Kuju deposits that are listed in Fig. 5.2.

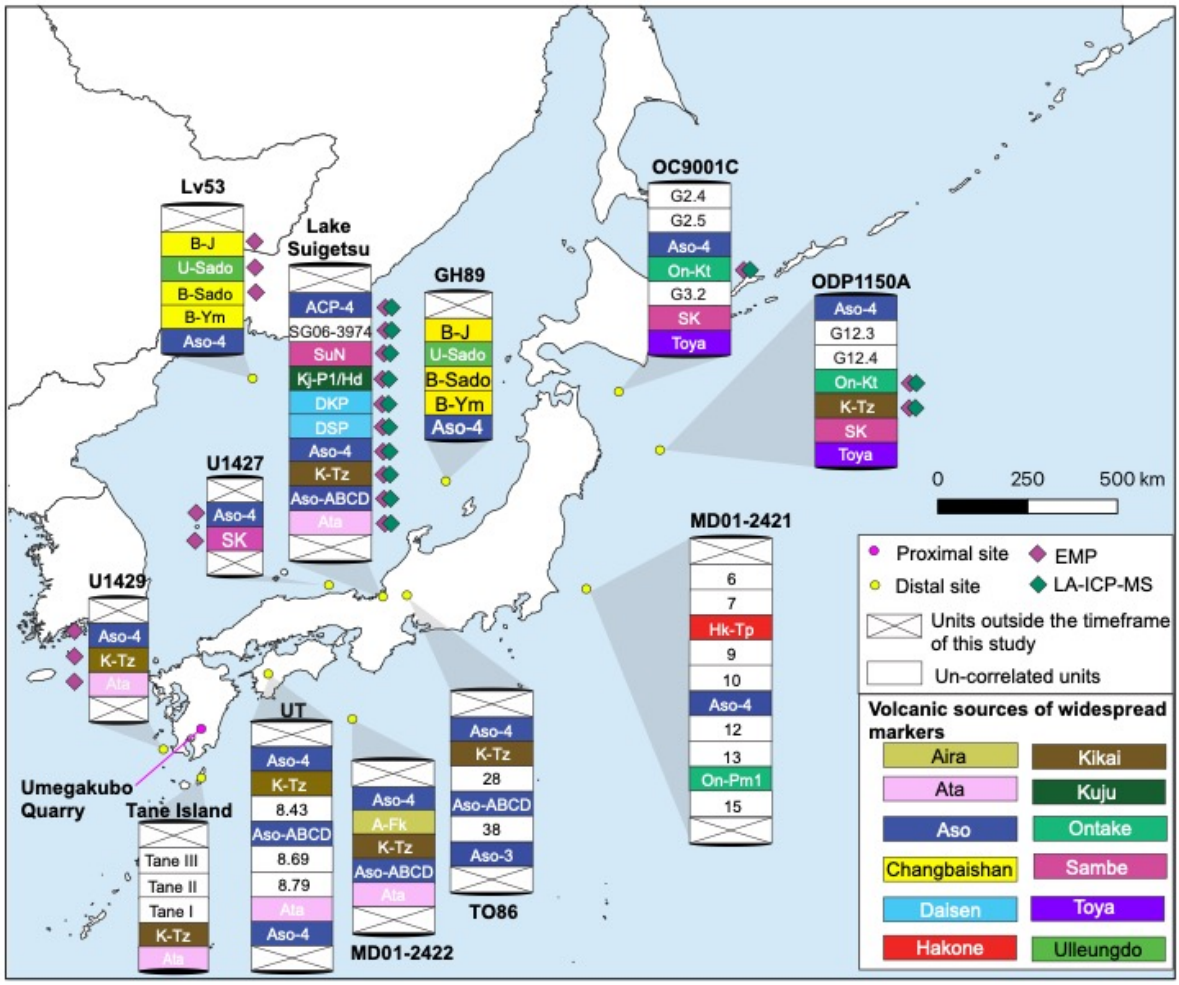


Figure 5.3: Sedimentary records that contain identified and correlated tephras in the ~120 – 50 ka interval. The terrestrial records include Lake Suigetsu (SG06/SG14; Smith et al., 2013; Albert et al., 2018, 2019a) and Lake Biwa (TO86; Nagahashi et al. 2004); and the marine records include: OC9001C and ODP1150A (Matsu'ura and Komatsubara, 2024); GH89 (Ikehara et al., 2004; Lim et al., 2013); MD012422 (Matsu'ura et al., 2021); Lv-53 (Derchachev et al., 2019); UT (Tsuji et al 2018); U1427 and U1429 (Sagawa et al., 2018). The purple and green diamonds show which deposits have been characterised via EMP, or LA-ICP-MS in previous studies and can be used for comparison in this study.

5.3.2. The Southern Volcanic Region (SVR) associated with the Ryuku-Kyushu Arc

The SVR is located on southern Kyushu and includes the Ata, Kikai and Aira calderas, and the Kirishima volcanic complex furthest north (Fig. 5.1A). The submerged Ata caldera beneath Kagoshima Bay was partly created during the M7.5 Ata eruption which generated 350 km^3 of tephra (Machida and Arai, 2003) and is found across Kyushu and Honshu beneath the Aso-4 deposit (Figs. 5.2 and 5.3). Kikai caldera is the product of two large magnitude eruptions occurring in the last ca. 100 ka: the Kikai Akahoya (K-Ah), which is one of the largest Holocene eruptions (M7.3), and the older M7.2 Kikai Tozurahara (K-Tz; Table 5.1) eruption. Further Kikai eruptions are documented between the Ata and K-Tz

deposits, the Kikai Nagase (K-Ns; Fig. 5.2; Machida and Arai, 2003) as well as the younger post-K-Tz Tane tephras (Fig. 5.2; Okuno and Kobayashi, 1994).

Aira has been active since 100 ka (Nagaoka 1988; Nagaoka et al., 2001) and the caldera was generated during the enormous M7.9 Aira Tanzawa (AT) eruption that produced a widespread tephra. The AT tephra is ~35.1 cm thick in the Lake Suigetsu sediments (the thickest tephra recorded at the site) and has been assigned an age of 30,078 ± 96 cal. BP based on the Lake Suigetsu age-depth model (Smith et al., 2013). Prior to the AT tephra, two Aira deposits, the older Fukuyama eruption (A-Fk) and the younger Iwato eruption (A-Iw), are identified in proximal exposures interspaced by the Aso-4 tephra (Fig. 5.2). The Kirishima complex comprises multiple small stratovolcanoes and pyroclastic cones that are known to have been active over the last 60 ka, including the Iwaokoshi (Kr-Iw) and Awaokoshi (Kr-Aw) tephras (Nagaoka et al., 2011). Of the SVR units in this timeframe, only the Ata and K-Tz tephras are particularly widespread and found in marine and terrestrial sediments around Kyushu and southern and central Honshu (Figs. 5.2 and 5.3). They have been identified in Lake Suigetsu with modelled ages of 99.3 ± 6.0 ka and 94.5 ± 4.8 ka, respectively (Albert, et al., 2019a; Smith et al., 2013).

Previous Lake Suigetsu tephra investigations have identified eighteen SVR crypto-/tephra deposits (Albert et al., 2019a, 2024; McLean et al., 2018, 2020a; Smith et al., 2013). Geochemical characterisation of these units and proximal units around the volcanoes has generated detailed compositional fingerprints for the centres within the SVR (e.g., Albert et al., 2019a). Glasses erupted from Kirishima are compositionally distinct from other SVR glasses, plotting along a well-defined SiO_2 vs. K_2O trend and containing higher Th contents (Albert et al., 2024). Glasses erupted from Ata, Aira and Kikai share similar major element compositions (Albert et al., 2019a), but trace element concentrations are useful for discrimination. Glasses erupted from Aira have lower Y and Zr and extend to higher Th than those from Kikai and Ata, and Nb contents can distinguish products from Kikai and Ata (Albert et al., 2019a).

5.3.3. SW Japan Arc (SWJA)

The SWJA relates to back arc volcanism in SW Honshu and includes the stratovolcanoes of Daisen and Sambe (Fig. 5.1). The explosively erupted products are well documented, yet inconsistencies exist in the volcanic histories, and the frequency of recorded events decreases further back in time (Albert et al., 2018). There were at least

eight eruptions between 125 and 60 ka, three of which have been identified in Lake Suigetsu (Table 5.1); the most widespread are the 59.6 ka Daisen Kurayoshi Pumice (DKP; Albert et al., 2018; Machida and Arai 2003) and the ca. 100 ka Sambe Kisuki (SK; Machida and Arai 2003; Kimura et al., 1999).

The proximal deposits of Daisen and Sambe are often heavily weathered and altered (e.g., Furusawa, 2008) and consequently, only limited reliable volcanic glass data are available to characterise the tephras (e.g., Albert et al., 2018; Kimura et al., 2015). The SWJA glasses are characterised by lower Y contents at given Th contents relative to other Japanese centres (Albert et al., 2018). Geochemically distinguishing the two volcanoes is possible, as Sambe tephras typically exhibit higher CaO at a given SiO_2 content and are more depleted in Zr relative to those from Daisen (Albert et al., 2018). Notably, glasses show partial overlap at major and trace element levels with those erupted at Kuju (Albert et al., 2019a).

5.3.4. Izu Bonin Arc

The Izu Bonin Arc lies on the eastern margin of the Philippine plate and extends south from Hakone volcano into the Pacific Ocean (Fig. 5.1). Volcanic centres along the Izu Bonin Arc are typically stratovolcanoes, with few experiencing caldera-forming eruptions (Machida, 1999). Only Hakone was active in the interval relevant to this study (Fig. 5.2).

Despite the number of volcanic systems located along the Izu-Bonin Arc (sixteen centres; Tatsumi et al., 2016), only limited geochemical glass data exists for the Kawagodaira, Niijima, Kozushima and Hakone volcanoes (see: Albert et al., 2019a; Suzuki et al., 2018; McLean et al., 2018). Quaternary explosive volcanism at the Izu-Bonin Arc is typically rhyolitic (Tamura and Tatsumi, 2002) and is predominantly represented by low-K tholeiites (<1 wt.% K_2O) that are highly depleted in Th (Byrant et al., 2003). The Hakone glasses can be distinguished from other tholeiitic deposits from other arc settings as they have lower Al_2O_3 and higher FeO_t contents, and are extremely low in Th (<2 ppm) and Rb (<30 ppm; Albert et al., 2019a). Although more than twenty eruptions occurred from Hakone pre-50 ka, none of the glasses in these units have been subjected to detailed geochemical characterisation (Fig. 5.2).

5.3.5. Norikura Volcanic Zone (NVZ)

The NVZ is located at the southern edge of the NE Japan arc (NEJA) in central Honshu and includes several stratovolcanoes such as Haruna, Akagi, Asama, Tateyama and Ontake (Fig. 5.1). These are known to have produced several large explosive ≤M6 eruptions (Albert, et al., 2019a) but only deposits from the Akagi, Ontake and Tateyama have been reported prior to 50 ka (Fig. 5.2; Machida and Arai, 2003). The largest known eruption is the ca. 95 ka Ontake Daiichi (On-Pm1) that occurs in MIS 5c (Machida amd Arai, 2003). At least ten eruptions occurred at Ontake between 95 ka and 60 ka (Table 5.1; Machida and Arai, 2003), and several widespread key markers (K-Tz and Aso-4) have been identified between some of these Ontake derived units (Fig. 5.2). Notably, several Ontake tephras have been recognised in marine sediments of the western Pacific Ocean (Fig. 5.3). Akagi stratovolcano, located to the northwest of Ontake, also produced a series of large Plinian eruptions during the Pleistocene, and three are identified between the Aso-4 and DKP marker layers (Fig. 5.2; Machida and Arai, 2003).

Major element compositions of the Ontake glasses are like other Japanese centres, but they can be distinguished based on Th and Zr content (Albert et al., 2019a). Matsu'ura and Komatsubara (2024) geochemically characterised five units relevant to this study and indicate that Hf and Zr abundances are lower in the Ontake units below the K-Tz marker layer (Fig. 5.2). There are no published detailed geochemical data for the three Akagi and two Tateyama eruption deposits that occurred between Aso-4 and the DKP (Fig. 5.2).

5.3.6. NE Japan Arc (NEJA)

A series of Late Quaternary calderas are situated along the NEJA (Fig. 5.1), which include Towada (northern Honshu), Kuttara, Shikotsu, and Toya (Hokkaido), and have produced at least twenty-three known explosive volcanic eruptions between 100 and 50 ka (Fig. 5.2; Machida and Arai, 2003). One of the largest Late Quaternary eruptions to occur along the NEJA is associated with the formation of the Toya caldera (tephra volume 170 km^3, with a radial dispersal). The age of the Toya tephra remains poorly constrained using radiometric methods; for instance, U-Pb and U/Th dating of zircons has yielded an age of 108 ± 19 ka (Ito et al., 2014); similarly, single aliquot regeneration–red thermal luminescence (SAR–RTL) dating yielded ages of between 104 ± 30 and 118 ± 30 ka (Ganzawa and Ike, 2011). The Toya tephra is also chrono-stratigraphically constrained by its position in MIS5d sediments dated at around 115 – 105 ka (Machida and Arai, 2003; Matsu'ura et al., 2014).

The restricted Y, Rb and Th contents of glasses erupted from the NEJA are useful for discerning them from those from other Japanese arcs (Albert et al., 2019a). However, there are no geochemical data for Kuttara glasses. Glasses erupted from Towada, Shikotsu and Toya can be distinguished from each other by their CaO content (Albert et al., 2019a). Despite the number of NEJA deposits preserved in the proximal realm in the timeframe relevant to this study, geochemical data are only available for the Toya tephra (Fig. 5.2).

5.3.7. Kurile Arc

The Kurile Arc extends from northern Hokkaido to Kamchatka (Russia) and includes three Quaternary calderas (Akan, Mashu and Kutcharo) that form a cluster in eastern Hokkaido (Fig. 5.1). The Kutcharo caldera was formed by a series of major eruptions between 340 and 30 ka, including two large explosive eruptions (M6.4 and M7.2), Kutcharo-2/3 (Kc-2/3) and Kutcharo-Hb (Kc-Hb), which are both preserved beneath the widespread Aso-4 deposit (Fig. 5.2). Reported activity at both Akan and Mashu are much younger and thus not relevant to the timeframe of this study (Machida and Arai, 2003).

Glasses erupted from Kutcharo volcano are calc-alkaline and rhyolitic and can be discriminated from other Japanese volcanic centres using SiO_2 vs. K_2O plots owing to relatively low K_2O content (~1.5 wt.%) at a given SiO_2 content (Albert et al., 2019a). Most of the trace elements in the Kutcharo glasses are similar to Kikai, with the exception of lower Y content (Albert et al., 2019a). Major and trace element glass compositions are available for both the Kc-Hb and Kc-2/3 units (Fig. 5.2) and, whilst both show a degree of overlap, the younger Kc-2/3 glasses span a broader major element compositional range than the older Kc-Hb glasses (Albert et al., 2019a).

5.3.8. Intra-plate

The intra-plate volcanoes that have dispersed ash across Japan in the past include Changbaishan and Ulleungdo (Fig. 5.1; Kimura et al., 2015; Machida and Arai, 2003; McLean et al., 2016, 2018, 2020b; Smith et al., 2011b, 2013). Jeju (Halla), an island off the south coast of South Korea is known to have had explosive eruptions (Brenna et al., 2015), but the deposits have not been identified in distal records. The complete eruptive histories of these volcanoes are not well constrained due to poor exposure and inaccessibility.

The alkaline tephra deposits from Ulleungdo and Changbaishan can be easily discriminated from other intraplate sources (e.g., Jeju volcano; Brenna et al., 2015) and from Japanese glasses by the absence of Nb and Ta depletions and more enriched Zr compositions (McLean et al., 2016, 2020b). Ulleungdo derived glasses are phonolite-trachytes and contain lower SiO_2 and higher Al_2O_3 and K_2O compared to other regional volcanic centres (McLean et al., 2016, 2020b). No geochemical data has been reported for the pre-50 ka Changbaishan or Ulleungdo eruption deposits sampled near the volcanoes; however, some major element glass data are available for deposits preserved in marine cores that are thought to come from these volcanoes (Fig. 5.3; Derkachev et al., 2019; Chun et al., 2007).

Three >50 ka Changbaishan tephras have been identified in marine records across the Sea of Japan: Baegdusan-Yamato Basin (B-Ym; ca. 85.8 ka), Baegdusan-Sado-Oki (B-Sado; ca. 67.6 ka), and Baegdusan-Japan Basin (B-J; ca. 50.6) (Fig. 5.3; Lim et al., 2013; Ikehara et al., 2004;). Similarly, the Ulleungdo derived U-Sado, also known as the SKP-II layer (Chun et al., 2007), has been reported in marine records and has an age of ~60.5 ka based on stratigraphy (Ikehara, 2015; Lim et al., 2013).

5.4. Materials and methods

5.4.1. Cryptotephra extraction techniques

To identify the cryptotephras preserved in the sediments spanning ~120 – 50 ka, the master SG14 core was contiguously sub-sampled at ca. 5 cm (low) resolution from 38.83 to 59.79 m composite depth (CD). Positions of elevated shard concentrations in the low-resolution samples were resampled at 1 cm (high) resolution, which were used to refine the stratigraphic positions of the cryptotephra peaks.

All samples were dried, weighed, and then wet sieved and the >25 μm fraction (alongside blanks to test for any laboratory contamination) were processed using the heavy liquid floatation method outlined by Turney (1998) and Blockley et al. (2005). This stepped floatation method is shown to reliably concentrate the glass shards in the Lake Suigetsu sediments so that cryptotephra peaks can be resolved (e.g., McLean et al., 2022). The extraction residues, i.e. those with the same density as glass, were mounted on slides using Canada Balsam. The glass shards in the sample were counted using a light microscope to quantify the number of shards per gram of dried sediment (shards/gram). Morphological features of the shards were also recorded as in McLean et al. (2018). Where background

shard concentrations were high, particularly in the sediments above visible tephra layers, differences in the morphological features and colour of the shards were also used to help identify the stratigraphic position of new primary ash-falls, for instance SG14-5099 and SG14-5367. Samples taken above visible tephra layers (e.g., following the 2.8 cm thick K-Tz tephra) have high shard concentrations due to subsequent (re-)mobilisation of the shards within the catchment (referred to as background). These samples were processed as outlined above and then spiked with a known quantity of *Lycopodium* pollen spores after the sample had been sieved and floated. Each *Lycopodium* tablet has a particular spore count (9666 spores per tablet from batch 3862). The tephra and *Lycopodium* solution was mounted on microscopic slides, and both were counted, and the concentration of glass shards was estimated using the following equation (Payne and Gehrels, 2010): number of glass shards counted / (number of *Lycopodium* spores counted / total number of *Lycopodium* spores added to the sample). The resulting counts are expressed as shards/gram using weights of the dry samples that were taken before sample processing, but were capped at 20,000 s/g as the accuracy of counting spiked samples is undetermined.

5.4.2. Reference tephra samples

To assess the volcanic sources of the newly recognised Lake Suigetsu cryptotephra deposits, the glasses were geochemically characterised and compared to the published Japanese volcanic glass datasets (e.g., Matsu'ura and Komatsubara 2024; Albert et al., 2018, 2019a, 2024; McLean et al 2016, 2018, 2020a; Suzuki et al., 2018; Kimura et al., 2015; Smith et al., 2011b, 2013). Additionally, new major and trace element glass data were obtained for the following temporally relevant eruptions: Kirishima (Kr-Iw and Kr-Aw) and Sambe (SK). These eruption deposits were sampled close to the volcanoes where the stratigraphy is clear; locations are reported in Chapter 2 and the glass compositions are reported in Table 5.4.

5.4.3. Glass compositions

Individual glass shards were manually picked using a syringe mounted on a micromanipulator (outlined in Lane et al., 2014), and subsequently mounted on to Struers Epoxy resin stubs. Samples with shard concentrations >10,000 shards/gram samples were directly pipetted onto stubs. The shards were then covered with a thin film of resin and placed in an oven at 50^{o}C for 4.5 hours to cure. The surfaces of the stubs were manually

sectioned using silicon carbide papers to expose the shards on a flat surface, polished with diamonds, and then carbon coated.

Major element compositions of individual glass shards were analysed using a JEOL JXA-8200 wavelength dispersive electron microprobe (WDS-EMP) equipped with 5 spectrometers located in the School of Archaeology, University of Oxford, UK. An accelerating voltage of 15 kV, 6 nA current, and a defocussed 10 μm beam were used. Peak counting times were 12 s for Na, 30 s for other major elements except for Mn, Cl and P, which were collected for 50 s. A suite of mineral standards was used to calibrate the microprobe, and the MPI-DING references glasses (Jochum et al., 2006) were run as secondary standards during each analytical session. All analyses presented have been normalised to 100% for comparative purposes and to account for variable hydration (Shane et al., 2008). Analyses with analytical totals <94% were discarded as they are not thought to be representative of the true melt composition.

The trace element compositions of individual glass shards were determined using an Agilent 8900 triple quadrupole LA-ICP-MS (laser ablation inductively coupled plasma mass spectrometry; ICP-QQQ) coupled to a Resonetics 193 nm ArF excimer laser-ablation device in the Department of Earth Sciences, Royal Holloway, University of London. A range of crater sizes was used (20 and 25 μm), depending on the area of the sectioned glass. The laser energy density on the target was 3.0 Jcm^{-2}, the repetition rate was 5 Hz. Ablation of the samples lasted 40 s on the sample, followed by 40 s during which there was no ablation, and this gas blank is used to subtract the background signal. The MPI-DING reference glasses were used to monitor analytical accuracy (Jochum et al., 2006). Typically, blocks of eight glass shards and one MPI-DING reference glass were bracketed by the NIST612 glass adopted as the calibration standard. The internal standard applied was ^{29}Si (determined by EMP-WDS analysis). LA-ICP-MS data reduction was performed in Microsoft Excel, as described in Tomlinson et al. (2010). Accuracies of LA-ICP-MS analyses were monitored using MPI-DING reference glasses, ATHO-G and StHs6/80-G, and accuracies were typically ≤ 5% for many elements measured (see Appendix B).

Error bars on plots represent reproducibility, calculated as ± 2 standard deviations of replicate analyses of MPI-DING StHs6/80-G glasses. Error bars on the trace element plots are typically smaller than the symbols. All major and trace element data and the secondary standards run alongside are included in Appendix B.

5.4.4. The Lake Suigetsu core and its chronology

Lake Suigetsu was drilled in 2006 (~250 m from an earlier [SG93] borehole; Fig. 5.1C) as part of the 'Lake Suigetsu Varved Sediment Project' with the aim of obtaining a complete 'master' sedimentary sequence by recovering overlapping cores from four parallel boreholes (Nakagawa et al., 2012). This ca. 73.2 m sequence, termed SG06, has an incredibly precise chronology for the last 50 ka as it is the longest continuously varved record from the Quaternary (Schlolaut et al., 2012, 2018). Moreover, ~800 macrofossils from the core have been radiocarbon dated (Bronk Ramsey et al., 2012, 2020; Staff et al., 2011). These chronological data have been incorporated into the international consensus radiocarbon calibration curve (i.e., IntCal13 and IntCal20; Reimer et al., 2013, 2020). In 2014, another coring campaign was undertaken (~320 metres east of the SG06 boreholes; Fig. 5.1C) from four additional boreholes, which have been integrated to form the composite SG14 master sequence. This sequence spans ~98 m (~25 m deeper than SG06) and reaches a thick basal gravel. The SG14 sequence has been precisely tied to the SG06 composite core (correlation model 28 October 2019) using 361 marker layers that include visible tephras. These correlations allow the high-precision SG06 chronology (Bronk Ramsey et al., 2020) to be transferred to the SG14 core. The SG14 composite core sequence was used for this cryptotephra investigation.

SG06 event-free depth(s) (EFD; version 13th Feb 2017) were used within the age model, which excludes instantaneous deposits >5 mm in thickness, i.e., event layers (Staff et al., 2011; Schlolaut et al., 2012). The software package developed to handle the correlation of parallel core sections, 'LevelFinder' (version 7.7.1, http://polsyems.rits-paleo.com), was used to linearly interpolate between the common marker layers to determine a composite depth (CD) or EFD for the cryptotephra layers. Down to the limit of radiocarbon dating (circa 52 cal. ka BP). For the deeper section of the stratigraphy examined in the present study, this chronology was extrapolated using a 'P_Sequence' deposition model within the Bayesian software package, OxCal (Bronk Ramsey, 2008), additionally including a single $^{40}Ar/^{39}Ar$-derived age of 86.4 ± 0.6 ka (±1σ) for the Aso-4 tephra, at a CD in SG14 of 4922.8 cm (Albert et al., 2019a; see below). The SG age model-derived ages for the tephra identified in this section of the SG core are reported in Table 2 and the ±1σ uncertainties are quoted throughout.

5.5. Results

5.5.1. Tephrostratigraphy

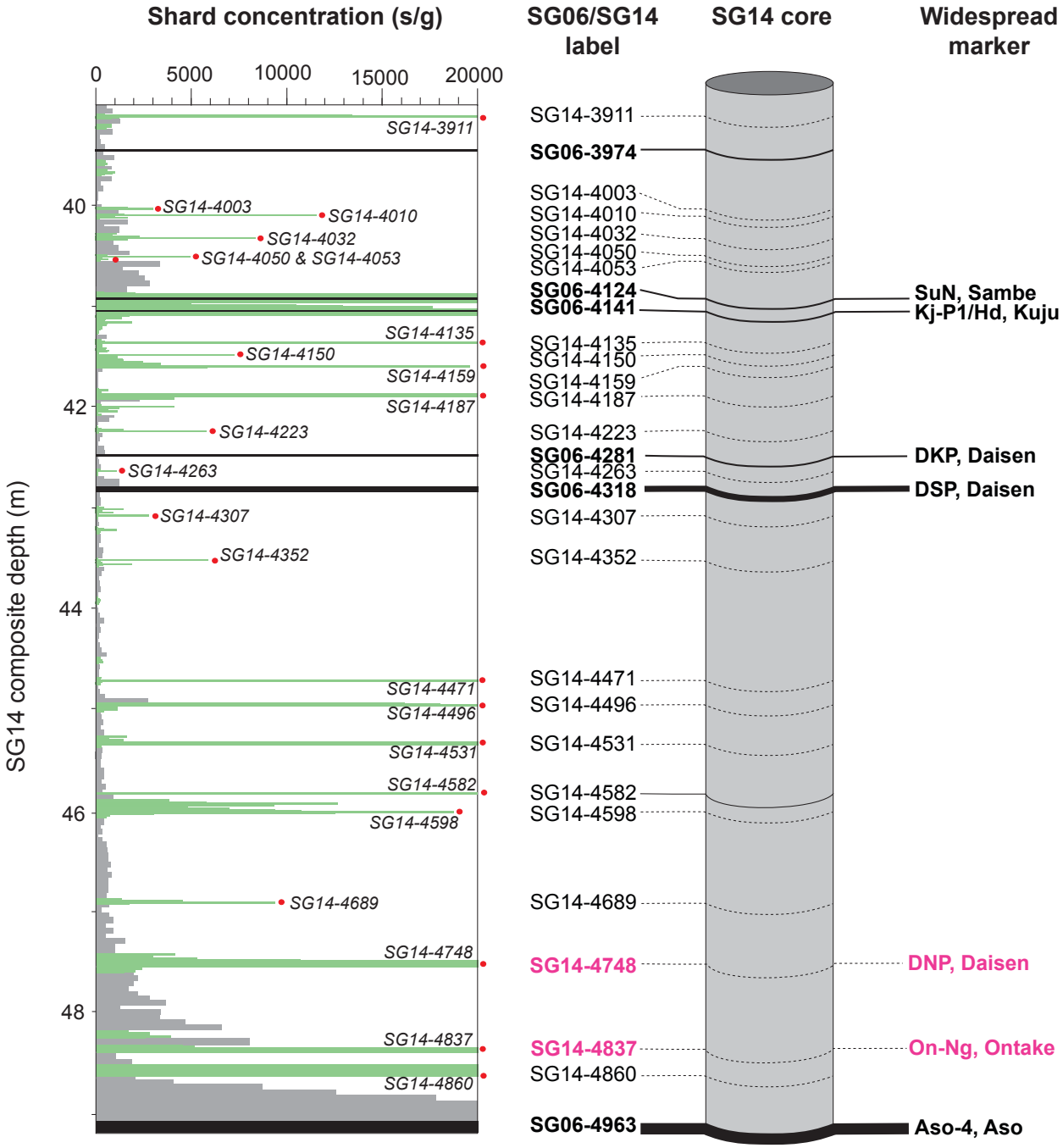
This detailed cryptotephra study identified a further forty-one eruption deposits in the 20 m of Lake Suigetsu sediments spanning ~120 to 50 ka. These deposits are in addition to the nine visible tephras that were previously reported across this interval (Table 5.2; Smith et al., 2013, Albert et al., 2018, 2019a). The newly identified crypto-/tephras are labelled herein using a SG14 prefix followed by the composite depth of the base of the tephra, rounded to the nearest integer (in cm; version 28th February 2019), in the 2014 core (Table 5.2). This labelling convention has been used for all the crypto-/tephras in Lake Suigetsu, including the visible tephra layers reported in SG06. Two new visible tephras are identified, SG14-4582 and SG14-5577, which are a 0.1 cm-thick fine-grained orange-brown ash, and a 0.8 cm thick fine-grained white ash, respectively. The details of all the visible tephra and cryptotephra identified are summarised in Table 5.2.

Table 5.2: Summary of the tephra layers (visible and cryptotephra) within the ~120 – 50 ka sediments of Lake Suigetsu (SG06/SG14 cores).

Tephra (SG14 Label)	v/c	v = thickness (cm)/ c = shards/gram	Average shard length	Glass shard morphology	Position in the SG14 master core (cm)	SG14 CD (cm) (ver. Feb 28, 2019)	SG06 CD (cm) (ver. Feb 28, 2019)	Modelled age (cal BP) (±1σ)	Correlation based on glass geochemistry (region, tephra, volcano)		M	Source to Suigetsu (km)
SG14-3911	C	24,890	50 – 100	F, MV	E-40 (44.5 – 45.5)	3911.1	3941.9	49.1 ± 0.2	CVR	Aso	-	525 SW
SG06-3974[1,2]	**V**	**0.3**	**-**	**-**	**E-40 (75.4 – 75.7)**	**3941.8***	**3974.1***	**49.6 ± 0.2**	**SWJA**	**Unknown, Daisen**	-	225 W
SG14-4002	C	300	70	MV, MI	E-41 (32.3 – 33.5)	4002.4	4040.8	50.5 ± 0.5	SVR	Kirishima	-	620 SW
SG14-4010	C	11,520	60	C, MI	E-41 (39.5 – 40.5)	4009.5	4047.8	50.7 ± 0.6	SVR	Kirishima	-	620 SW
SG14-4032	C	8,325	50	C, F	F-41 (9.0 – 10.0)	4031.7	4068.6	51.5 ± 0.9	CVR	Aso	-	525 SW
SG14-4050	C	49,50	70	B, C, MI	F-41 (27.0 – 28.0)	4049.7	4086.8	52.2 ± 1.1	CVR	Kuju	-	500 SW
SG14-4053	C	650	60	MI, V	F-41 (30.0 – 31.0)	4052.7	4089.7	52.4 ± 1.2	SVR	Kirishima	-	620 SW
SG06-4124[1,2]	**V**	**0.2**	**-**	**-**	**F-41 (67.5 – 67.7)**	**4089.9***	**4124.0***	**53.7 ± 1.5**	**SWJA**	**SuN, Sambe**	**-**	**225 W**
SG06-4141[1,2]	**V**	**1.4**	**-**	**-**	**E-42 (31.9 – 33.3)**	**4105.7***	**4141.2***	**54.3 ± 1.6**	**CVR**	**Kj-P1/Hd, Kuju**	**5.3**	**500 SW**
SG14-4135	C	>20,000	80	V	F-42 (30.9 – 31.9)	4135.4	4173.5	55.6 ± 1.7	CVR	Aso	-	525 SW
SG14-4150	C	7,290	70	C, V	F-42 (44.9 – 46.2)	4149.6	4188.2	56.2 ± 1.8	CVR	Kuju	-	500 SW
SG14-4159	C	19,510	70	B, C, MV	G-11 (22.4 – 23.4)	4158.7	4198.1	56.6 ± 1.9	CVR	Aso	-	620 SW
SG14-4187	C	>20,000	50	PU	G-11 (51.0 – 52.0)	4187.3	4224.4	57.6 ± 2.0	-	-	-	-
SG14-4223	C	5,775	80	B, V	G-11 (87.0 – 88.0)	4223.3	4259.7	59.0 ± 2.1	Intra-plate	Ulleungdo	-	500 NW
SG06-4281[1,2]	**V**	**0.3**	**-**	**-**	**F-43 (19.9 – 20.2)**	**4246.3***	**4281.1***	**59.9 ± 2.2**	**SWJA**	**DKP, Daisen**	**6.5**	**225 W**
SG14-4263	C	1,083	50	MI, MV	F-43 (36.2 – 37.2)	4262.8	4294.8	60.4 ± 2.2	SVR	Kirishima	-	620 SW
SG06-4318[1,2]	**V**	**1.7**	**-**	**-**	**F-43 (51.3 – 53.0)**	**4279.1***	**4318.4***	**61.3 ± 2.2**	**SWJA**	**DSP, Daisen**	**4.9**	**225 W**
SG14-4307	C	2,788	40 – 100	F, MV	E-44 (34.2 – 35.2)	4306.6	4343.8	62.3 ± 2.3	SVR	Kikai	-	750 SW
SG14-4352	C	5,883	70 – 100	PU	F-44 (25.8 – 26.8)	4351.9	4388.6	64.1 ± 2.4	CVR	Aso	-	525 SW
SG14-4471	C	1,333	40 – 100	B, MV, MI	F-45 (41.9 – 42.9)	4470.6	4509.0	68.7 ± 2.4	CVR	Aso	-	-
SG14-4496	C	30,717	50 – 100	C, V	F-45 (66.9 – 67.9)	4495.6	4533.1	69.7 ± 2.4	SVR	Kirishima	-	620 SW
SG14-4531	C	>20,000	70	C, MV	E-46 (46.5 – 48.0)	4531.0	4578.4	71.4 ± 2.4	-	-	-	-
SG14-4582	V	0.1	60	PU	F-46 (45.8 – 45.9)	4582.1*	4627.6*	73.4 ± 2.4	-	-	-	-
SG14-4598	C	18,650	70	C, MV	F-46 (61.4 – 62.4)	4598.1	4640.9	73.9 ± 2.3	SVR	Aira	-	-
SG14-4689	C	9,360	70	PU	F-47 (49.5 – 50.5)	4688.6	4716.8	76.9 ± 2.2	SWJA	-	-	-
SG14-4748	C	30,600	120	MI, PU	E-48 (63.0 – 64.0)	4748.1	4777.2	79.3 ± 2.0	SWJA	DNP, Daisen	-	225 W
SG14-4837	C	>20,000	120	B, MI	E-49 (49.6 – 50.6)	4837.0	4871.9	83.0 ± 1.5	NVZ	On-Ng,Ontake	-	225 E
SG14-4860	C	>20,000	>100	C, V	E-49 (72.6 – 73.6)	4860.0	4898.9	84.1 ± 1.3	NVZ	Ontake	-	225 E
SG06-4963[1,2]	**V**	**3.5**	**-**	**-**	**G-12 (57.2 – 60.7)**	**4922.8***	**4962.4***	**86.4 ± 0.6**	**CVR**	**Aso-4, Aso**	**7.7**	**525 SW**
SG14-5033	C	25,650	60	MI, MV	F-50 (90.0 – 91.0)	5033	5072.7	89.8 ± 1.6	Izu-Bonin Arc	Hakone	-	300 E
SG14-5071	C	49,225	60	C, F	F-51 (25.8 – 26.8)	5070.9	5113.1	91.2 ± 1.8	CVR	Aso	-	525 SW
SG14-5099	C	67,850	50 – 70	MI, V	F-51 (53.4 – 54.4)	5098.5	5138.5	92.0 ± 2.0	CVR	Aso	-	525 SW
SG06-5181[1,2]	**V**	**0.2**	**-**	**-**	**E-52 (55.3 – 55.5)**	**5142.2***	**5180.3***	**93.4 ± 2.2**	**SVR**	**K-Tz, Kikai**	**7.2**	**750 SW**
SG14-5183	C	20,000[S]	60 – 100	C, V	F-52 (37.4 – 38.4)	5182.0	5219.0	94.7 ± 2.4	-	-	-	-
SG14-5221	C	>20,000	80	C	F-52 (76.4 – 77.4)	5221.0	5257.0	95.9 ± 2.5	CVR	Aso	-	525 SW
SG06-5287[1,2]	**V**	**3.5**	**-**	**-**	**E-53 (52.5 – 56.0)**	**5252.1***	**5286.6***	**96.8 ± 2.7**	**CVR**	**Aso-ABCD, Aso**	**5.9**	**525 SW**
SG06-5353[1,2]	**V**	**1.5**	**-**	**-**	**G-14 (61.0 – 62.5)**	**5319.9***	**5354.2***	**99.0 ± 2.9**	**SVR**	**Ata, Ata**	**7.5**	**650 SW**
SG14-5367	C	20,000[S]	70	C, F, V	E-54 (68.9 – 69.9)	5366.9	5398.1	100.4 ± 3.1	SWJA	SK, Sambe	6.3	300 W
SG14-5406	C	11,100	>100	PU	G-15 (43.3 – 44.3)	5405.5	5447.1	102.1 ± 3.3	CVR	Kuju	-	500 SW
SG14-5469	C	2,217	70	C, V	E-55 (67.0 – 68.9)	5469.0	5515.8	104.4 ± 3.6	SVR	Ata	-	650 SW
SG14-5520	C	1,600	80	C	F-55 (57.2 – 58.2)	5519.8	5565.6	106.1 ± 3.7	SVR	-	-	-
SG14-5563	C	20,000[S]	90	PU, MV	E-56 (62.7 – 63.7)	5562.8	5611.5	107.6 ± 3.9	SWJA	Daisen	-	225 W
SG14-5575	C	>20,000[S]	70	C, F, V	E-56 (74.7 – 75.7)	5574.8	5626.4	108.1 ± 3.9	NEJA	Toya, Toya	7.3	950 NE
SG14-5579	V	0.8[S]	40 – 60	C, MV	G-16 (19.1 – 20.1)	5578.8	5631.1	108.3 ± 4.0	CVR	Aso	-	525 SW
SG14-5597	C	2,400	50	MV	G-16 (37.1 – 38.1)	5596.8	5649.9	108.9 ± 4.0	Izu-Bonin Arc	Hakone	-	700 NE
SG14-5616	C	18,950	40	MV	G-16 (56.1 – 57.1)	5615.8	5669.4	109.6 ± 4.1	Kurile Arc	Kutcharo	-	1250 NE
SG14-5648	C	>20,000[S]	70 – 100	MV	E-57 (46.2 – 47.2)	5648.3	5702.3	110.7 ± 4.2	CVR	Aso	-	525 SW
SG14-5851	C	5,400	60 – 90	C	E-59 (48.4 – 49.4)	5851.2	5908.0	117.7 ± 4.9	Izu-Bonin Arc	Hakone	-	300 E
SG14-5932	C	650	70	B	F-59 (67.3 – 68.3)	5932.4	5986.9	120.4 ± 5.1	SVR	Ata	-	650 SW
SG14-5950	C	250	50	PU	E-60 (46.3 – 47.3)	5950.1	6004.2	121.0 ± 5.2	-	-	-	-

Footnote: Depth given at the base of the visible tephra or at the identified midpoint of the 1 cm high-resolution for the cryptotephra. Previously reported visible tephra deposits are in bold, and the references for correlations to volcanic source and eruptions units are: 1. Smith et al. (2013), 2. Albert et al. (2019a). V/C = visible/cryptotephra. PU= Pumiceous, B=Blocky, C=Cuspate, F=Fluted, V=Vesicular, MV =Microvesicular, MI =Microlite Inclusions. Mil = million for samples spiked (S) with Lycopodium spores (see methodology). M = Magnitude (see Table 1).

The glass shards show considerable variance in terms of their physical characteristics (see Appendix B). Shard concentrations for all the cryptotephra identified peak above 200 shards/gram, with most exceeding 1500 shards/gram (Fig. 5.4, Table 5.2). Nineteen of these deposits exceed 20,000 shards/gram. The high background shard concentration observed between the SG14-5367 cryptotephra and the SG06-5353 (Ata) tephra are associated with the previously reported SG06-5385 tephra; however, the glasses are too weathered for geochemical analyses and have been discounted as representing an additional primary tephra deposit within the Lake Suigetsu record (see: Smith et al., 2013, Albert et al., 2019a).


Shard concentration (s/g)
SG06/SG14 label
SG14 core
Widespread marker
0
5000
10000
15000
20000
SG14 composite depth (m)
40
42
44
46
48
SG14-3911
SG14-4003
SG14-4010
SG14-4032
SG14-4050 & SG14-4053
SG14-4135
SG14-4150
SG14-4159
SG14-4187
SG14-4223
SG14-4263
SG14-4307
SG14-4352
SG14-4471
SG14-4496
SG14-4531
SG14-4582
SG14-4598
SG14-4689
SG14-4748
SG14-4837
SG14-4860
SG14-3911
SG06-3974
SG14-4003
SG14-4010
SG14-4032
SG14-4050
SG14-4053
SG06-4124
SG06-4141
SG14-4135
SG14-4150
SG14-4159
SG14-4187
SG14-4223
SG06-4281
SG14-4263
SG06-4318
SG14-4307
SG14-4352
SG14-4471
SG14-4496
SG14-4531
SG14-4582
SG14-4598
SG14-4689
SG14-4748
SG14-4837
SG14-4860
SG06-4963
SuN, Sambe
Kj-P1/Hd, Kuju
DKP, Daisen
DSP, Daisen
DNP, Daisen
On-Ng, Ontake
Aso-4, Aso

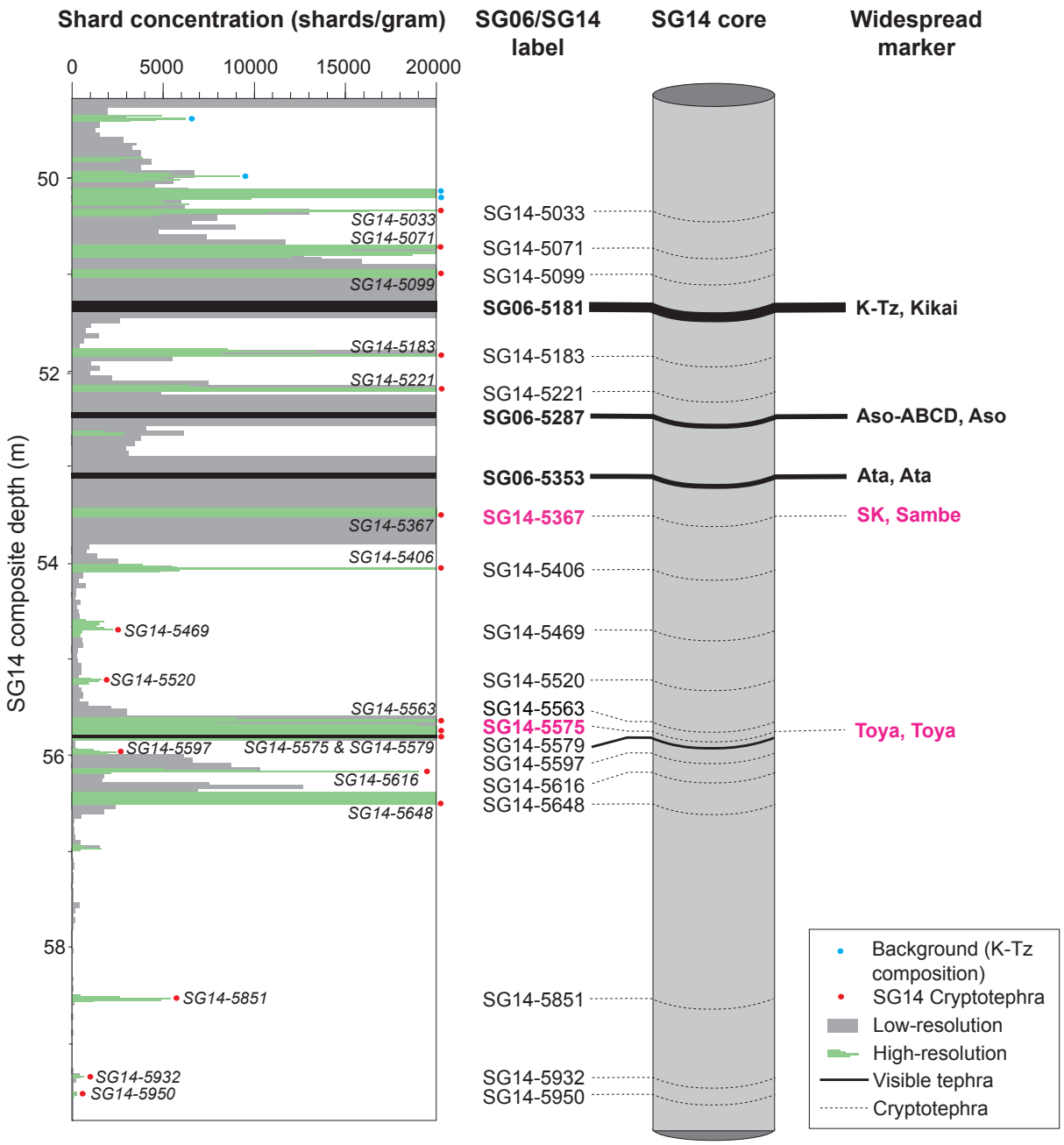


Figure 5.4: Glass shard concentrations in the sediments spanning ~120 – 50 ka of the Lake Suigetsu (SG14) core. These concentrations are capped at 20,000 shards/gram. Concentrations of glass shards in low-resolution (5 cm interval) samples are shown in grey on the LHS panel, whilst high-resolution (1 cm) sample counts are overlain in green. The red dots and labels denote the positions of the isochrons, which were sampled for chemical analysis. The blue dots represent where chemical analysis were conducted but consistent with the K-Tz tephra (i.e. background glass). Previously reported SG06 visible tephras are marked in bold black and new correlations are shown in bold pink.

5.5.2. Glass geochemical compositions

Major element and trace glass compositions of the forty-one SG14 deposits are presented in Table 5.3.

Table 5.3: Average major (EMP) and trace (LA-ICP-MS) element chemistry of the ~120 – 50 ka Lake Suigetsu crypto-/tephras. Major element glass data has been normalised (water free). <LoD refers to less than limit of detection. Full geochemical datasets are available in Appendix B.

Tephra	SG14-3911		SG14-4002		SG14-4010		SG14-4032		SG14-4050		SG14-4053		SG14-4135A		SG14-4135B		SG14-4150		SG14-4159		SG14-4187	
wt.%	Avg.	1 std. dev.	Avg.	1 std. dev.	Avg.	1 std. dev.	Avg.	1 std. dev.	Avg.	1 std. dev.	Avg.	1 std. dev.	Avg.	1 std. dev.	Avg.	1 std. dev.	Avg.	1 std. dev.	Avg.	1 std. dev.	Avg.	1 std. dev.
SiO_2	72.24	0.07	66.12	4.22	74.24	0.99	74.43	0.50	79.36	0.94	72.38	1.88	62.24	0.52	67.61	1.95	77.86	0.20	71.58	0.97	66.20	2.75
TiO_2	0.42	0.01	1.02	0.26	0.47	0.05	0.34	0.05	0.22	0.09	0.70	0.13	0.99	0.05	0.87	0.12	0.19	0.03	0.60	0.03	0.54	0.24
Al_2O_3	14.86	0.05	15.43	1.66	13.44	0.49	14.68	0.24	12.28	0.51	13.36	0.65	16.59	0.48	15.24	0.69	12.44	0.08	15.63	0.13	18.47	2.42
FeO	1.63	0.02	4.35	1.17	1.98	0.32	1.36	0.17	0.93	0.20	2.88	0.57	5.66	0.29	3.82	0.81	0.94	0.09	2.39	0.08	2.01	0.83
MnO	0.08	0.01	0.09	0.03	0.05	0.03	0.06	0.02	0.04	0.02	0.07	0.02	0.14	0.03	0.11	0.03	0.04	0.02	0.09	0.02	0.06	0.03
MgO	0.34	0.01	1.26	0.46	0.35	0.11	0.24	0.05	0.16	0.07	0.60	0.27	2.15	0.19	0.88	0.13	0.20	0.03	0.57	0.03	0.65	0.39
CaO	1.10	0.02	4.21	1.68	1.45	0.37	0.74	0.12	0.90	0.29	1.98	0.53	4.99	0.29	2.73	0.83	1.20	0.11	1.79	0.04	5.17	1.40
Na_2O	4.52	0.05	3.89	0.19	3.39	0.25	4.42	0.11	3.10	0.23	3.45	0.33	3.86	0.23	4.26	0.16	3.17	0.08	2.93	1.09	4.15	0.51
K_2O	4.66	0.04	3.24	0.79	4.46	0.24	4.96	0.13	4.30	0.41	4.35	0.27	3.05	0.20	4.20	0.27	3.77	0.09	4.22	0.07	2.47	0.55
P_2O_5	0.06	0.02	0.29	0.12	0.06	0.04	0.04	0.03	0.03	0.03	0.13	0.10	0.24	0.02	0.20	0.07	0.02	0.03	0.09	0.04	0.19	0.18
Cl	0.10	0.01	0.11	0.02	0.11	0.02	0.12	0.02	0.11	0.04	0.11	0.03	0.09	0.02	0.09	0.02	0.16	0.02	0.11	0.01	0.08	0.04
(n)	*27*		*9*		*16*		*19*		*28*		*11*		*14*		*6*		*12*		*26*		*10*	
ppm	**Avg.**	**1 std. dev.**	**Avg.**	**1 std. dev.**	**Avg.**	**1 std. dev.**	**Avg.**	**1 std. dev.**	**Avg.**	**1 std. dev.**	**Avg.**	**1 std. dev.**	**Avg.**	**1 std. dev.**	**Avg.**	**1 std. dev.**	**Avg.**	**1 std. dev.**	**Avg.**	**1 std. dev.**	**Avg.**	**1 std. dev.**
Rb	159	3.63	119	36.6	-	-	184	9.89	130	5.45	149	10.9	105	5.89	156	5.22	134	7.06	170	4.21	62.2	5.18
Sr	125	8.03	283	158	-	-	85.8	40.3	156	32.75	235	51.3	362	28.0	194	16.2	174	18.2	219	28.2	861	110
Y	34.5	0.94	24.7	2.70	-	-	36.2	0.90	6.75	1.40	29.4	1.92	27.5	0.97	32.0	0.12	6.82	0.96	32.4	2.43	18.7	1.13
Zr	295	8.14	245	44.7	-	-	305	9.28	94.0	10.0	321	9.35	202	11.0	298	7.16	93.5	8.79	303	20.5	157	6.85
Nb	16.6	0.31	10.7	1.40	-	-	16.9	0.44	11.5	0.39	14.1	0.58	12.61	0.56	17.0	0.39	11.8	0.40	16.1	0.79	21.0	1.57
Ba	820	20.14	651	93.0	-	-	769	38.9	927	78.87	877	18.2	558	27.9	726	12.0	970	33.9	799	29.5	767	42.1
La	32	0.93	27.4	3.78	-	-	34	0.99	23.2	1.27	34.1	0.96	23.9	1.04	29.5	0.64	23.8	1.11	32.4	2.05	29.0	1.75
Ce	70	1.84	58.5	7.90	-	-	74.9	2.27	41.8	3.13	71.7	2.60	54.1	1.94	65.5	0.31	43.8	2.45	69.6	3.42	61.4	3.61
Pr	8.05	0.27	6.62	0.89	-	-	8.62	0.28	3.70	0.41	8.15	0.34	6.46	0.24	7.91	0.03	3.93	0.07	7.90	0.34	6.73	0.43
Nd	33.4	1.16	26.8	3.11	-	-	35.1	2.22	12.2	1.66	32.5	2.22	27.8	1.65	33.4	0.24	12.2	0.57	32.4	1.31	27.5	1.25
Sm	7.43	0.33	5.95	0.58	-	-	7.45	0.66	2.30	0.54	6.92	0.67	6.24	0.63	6.96	0.61	<LOD	<LOD	6.58	0.40	5.15	0.34
Eu	1.27	0.08	1.18	0.34	-	-	1.14	0.13	0.54	0.10	1.22	0.18	1.40	0.09	1.30	0.04	<LOD	<LOD	1.28	0.19	1.51	0.19
Gd	6.12	0.41	4.69	0.54	-	-	6.25	0.57	<LOD	<LOD	5.60	0.65	5.45	0.52	6.16	0.96	<LOD	<LOD	6.03	0.46	4.24	0.46
Dy	5.92	0.29	4.52	0.46	-	-	6.37	0.40	<LOD	<LOD	5.34	0.49	5.11	0.29	5.99	0.50	<LOD	<LOD	5.50	0.72	3.39	0.29
Er	3.68	0.28	2.62	0.34	-	-	4.00	0.23	<LOD	<LOD	3.26	0.27	2.96	0.25	3.42	0.33	<LOD	<LOD	3.39	0.23	2.07	0.26
Yb	3.99	0.25	2.68	0.30	-	-	4.27	0.30	<LOD	<LOD	3.24	0.25	2.92	0.28	4.03	0.05	<LOD	<LOD	3.53	0.49	2.06	0.21
Lu	0.61	0.04	0.39	0.03	-	-	0.63	0.05	<LOD	<LOD	0.49	0.04	0.46	0.04	0.55	0.01	<LOD	<LOD	0.59	0.05	0.31	0.03
Hf	7.88	0.50	6.47	1.24	-	-	8.66	0.52	3.0	0.24	8.66	0.33	5.42	0.51	7.70	0.61	3.12	0.26	7.92	0.76	3.89	0.27
Ta	1.15	0.04	0.63	0.13	-	-	1.20	0.05	1.05	0.05	0.87	0.03	0.84	0.04	1.13	0.07	1.07	0.08	1.11	0.07	1.16	0.07
Pb	22.8	0.60	15.4	2.62	-	-	25.6	1.24	19.2	1.98	19.3	2.73	16.9	0.78	23.3	0.95	17.7	1.24	23.2	1.10	16.2	4.71
Th	14.0	0.62	9.85	2.57	-	-	16.3	0.72	12.8	0.82	13.6	0.68	9.49	0.49	14.0	0.46	12.4	0.73	15.6	0.87	5.78	0.35
U	4.18	0.21	2.16	0.49	-	-	4.80	0.22	2.85	0.14	2.77	0.14	2.75	0.24	4.28	0.13	2.90	0.35	4.34	0.51	1.55	0.11
(n)	*23*		*13*		*-*		*17*		*13*		*8*		*17*		*3*		*5*		*9*		*7*	

Tephra	SG14-4223		SG14-4263		SG14-4307		SG14-4352		SG14-4471A		SG14-4471B		SG14-4496		SG14-4531		SG14-4582		SG14-4598		SG14-4689	
wt.%	**Avg.**	**1 std. dev.**	**Avg.**	**1 std. dev.**	**Avg.**	**1 std. dev.**	**Avg.**	**1 std. dev.**	**Avg.**	**1 std. dev.**	**Avg.**	**1 std. dev.**	**Avg.**	**1 std. dev.**	**Avg.**	**1 std. dev.**	**Avg.**	**1 std. dev.**	**Avg.**	**1 std. dev.**	**Avg.**	**1 std. dev.**
SiO_2	59.08	0.39	72.43	0.80	74.27	0.38	65.78	1.12	65.71	1.08	72.86	0.43	72.61	0.78	60.72	0.24	79.44	0.26	78.17	0.32	77.88	2.16
TiO_2	0.69	0.08	0.67	0.04	0.57	0.03	0.81	0.07	1.14	0.27	0.42	0.04	0.59	0.05	1.33	0.05	0.19	0.05	0.16	0.03	0.26	0.05
Al_2O_3	19.72	0.17	13.58	0.23	12.76	0.26	16.62	0.61	15.42	0.37	15.20	0.11	13.84	0.28	16.64	0.10	12.40	0.14	12.37	0.17	13.20	1.50
FeO	3.92	0.14	2.75	0.29	2.72	0.12	4.58	0.50	5.49	0.75	1.48	0.05	2.57	0.29	6.64	0.19	1.04	0.07	1.04	0.09	0.91	0.25
MnO	0.16	0.02	0.05	0.02	0.07	0.02	0.16	0.03	0.13	0.03	0.09	0.01	0.06	0.03	0.17	0.02	0.04	0.02	0.04	0.02	0.03	0.02
MgO	0.73	0.08	0.60	0.10	0.58	0.04	1.29	0.26	1.46	0.32	0.33	0.02	0.57	0.09	2.24	0.07	0.18	0.03	0.16	0.03	0.16	0.10
CaO	2.20	0.22	2.24	0.27	2.38	0.13	3.48	0.50	3.96	0.58	1.07	0.05	2.14	0.27	5.18	0.15	1.18	0.17	1.32	0.15	1.44	0.68
Na_2O	6.64	0.16	3.26	0.45	3.90	0.26	4.53	0.20	2.84	0.94	3.99	0.65	3.41	0.49	4.13	0.15	3.30	0.27	3.36	0.12	3.22	0.44
K_2O	6.39	0.12	4.20	0.15	2.50	0.06	3.65	0.35	3.43	0.12	4.36	0.12	3.95	0.17	2.35	0.09	2.11	0.12	3.28	0.15	2.83	0.49
P_2O_5	0.27	0.14	0.10	0.03	0.11	0.04	0.35	0.10	0.33	0.11	0.08	0.02	0.14	0.06	0.51	0.06	0.11	0.03	0.02	0.02	0.06	0.03
Cl	0.21	0.02	0.12	0.02	0.12	0.03	0.08	0.02	0.11	0.02	0.12	0.01	0.12	0.01	0.09	0.01	0.01	0.01	0.09	0.01	0.01	0.02
(n)	*36*		*22*		*25*		*30*		*6*		*4*		*30*		*29*		*13*		*25*		*29*	
ppm	**Avg.**	**1 std. dev.**	**Avg.**	**1 std. dev.**	**Avg.**	**1 std. dev.**	**Avg.**	**1 std. dev.**	**Avg.**	**1 std. dev.**	**Avg.**	**1 std. dev.**	**Avg.**	**1 std. dev.**	**Avg.**	**1 std. dev.**	**Avg.**	**1 std. dev.**	**Avg.**	**1 std. dev.**	**Avg.**	**1 std. dev.**
Rb	169	9.71	155	7.54	72.7	2.08	139	16.8	94.3	19.1	157	22.5	147	9.86	69.9	1.36	166	0.32	138	4.97	125	33.0
Sr	345	96.9	155	25.4	128	9.28	378	117	426	67.3	195	67.8	154	24.3	498	12.5	164	2.12	86.7	9.46	257	151.9
Y	26.4	7.27	30.1	1.47	31.1	1.15	31.7	2.41	34.6	5.37	26.4	1.25	30.7	1.73	32.1	0.87	33.0	0.08	13.4	0.67	9.02	1.82
Zr	543	39.8	252	11.5	175	5.36	234	29.7	270	48.2	238	12.5	251	14.5	216	4.54	293	2.44	117	6.68	110	14.0
Nb	167	8.82	9.66	0.32	5.47	0.33	12.6	1.48	13.8	1.50	13.9	0.24	9.74	1.68	11.0	0.26	15.5	0.40	6.68	0.22	10.6	1.32
Ba	543	72.6	598	21.9	403	10.8	694	36.8	817	98.7	814	29.6	597	68.0	531	13.0	827	20.9	559	22.1	784	255
La	106	18.7	24.5	1.34	16.0	0.72	29.4	2.06	32.8	3.66	30.5	0.13	25.0	2.65	26.8	0.73	34.4	0.22	22.0	0.68	24.0	2.49
Ce	183	38.5	54.5	3.54	37.3	1.70	65.9	4.87	73.5	8.21	67.9	5.10	55.4	5.72	61.6	1.35	74.2	0.81	42.1	1.79	43.7	5.43
Pr	16.8	4.59	6.21	0.36	4.42	0.28	7.76	0.58	8.98	1.44	7.31	0.60	6.24	0.71	7.44	0.18	8.80	0.02	3.97	0.21	4.29	0.69
Nd	56.7	17.4	25.7	1.80	19.4	1.21	32.5	2.34	38.3	7.52	29.8	1.11	25.9	2.28	33.7	1.15	35.1	0.10	13.7	0.82	14.7	2.53
Sm	8.26	2.90	5.61	0.63	4.65	0.48	7.10	0.70	6.41	2.64	5.11	1.65	5.77	0.41	7.44	0.42	6.94	0.07	2.58	0.31	2.66	0.65
Eu	1.87	0.55	0.94	0.10	0.95	0.09	1.53	0.23	2.37	0.50	2.06	0.26	0.95	0.17	2.03	0.12	1.29	0.07	0.49	0.06	0.61	0.11
Gd	6.31	2.27	4.78	0.39	4.64	0.49	6.23	0.61	7.63	1.14	6.56	0.61	5.04	0.42	6.62	0.40	6.03	0.19	2.08	0.19	1.88	0.44
Dy	5.18	1.86	5.17	0.62	5.21	0.31	5.75	0.48	6.96	1.30	5.57	0.48	5.19	0.35	6.14	0.30	5.77	0.05	2.19	0.20	1.64	0.31
Er	2.86	0.83	3.48	0.34	3.44	0.36	3.35	0.36	4.28	0.45	3.24	0.07	3.30	0.29	3.51	0.19	3.56	0.07	1.50	0.16	1.00	0.20
Yb	2.74	0.59	3.38	0.34	3.72	0.30	3.46	0.32	4.01	0.81	3.93	0.42	3.49	0.30	3.28	0.23	3.92	0.26	1.79	0.14	1.38	0.23
Lu	0.40	0.08	0.50	0.07	0.56	0.04	0.52	0.06	0.59	0.06	0.61	0.01	0.52	0.04	0.50	0.03	0.60	0.01	0.29	0.03	0.20	0.04
Hf	11.0	1.19	7.01	0.60	4.70	0.33	6.23	0.92	7.77	1.23	7.30	0.24	7.18	0.48	5.64	0.26	7.89	0.51	3.48	0.28	3.38	0.61
Ta	8.54	0.49	0.71	0.04	0.38	0.03	0.91	0.11	0.78	0.09	1.06	0.07	0.74	0.13	0.61	0.01	1.16	0.03	0.64	0.02	0.91	0.11
Pb	13.4	1.14	21.9	1.77	19.3	2.07	20.9	1.94	20.1	4.85	20.5	3.53	22.7	1.07	11.4	0.54	27.2	4.44	19.5	0.85	19.1	3.40
Th	19.9	1.52	13.3	1.13	6.39	0.36	13.1	1.69	7.88	1.50	13.4	0.94	13.0	1.18	5.95	0.19	16.3	0.11	12.1	0.38	10.8	1.31
U	4.18	0.34	3.42	0.16	1.84	0.21	3.87	0.58	1.83	0.36	4.43	0.43	3.31	0.50	1.32	0.06	4.57	0.10	2.75	0.15	2.36	0.34
(n)	*12*		*10*		*13*		*18*		*5*		*2*		*13*		*14*		*4*		*12*		*12*	

Tephra	SG14-4748		SG14-4837		SG14-4860		SG14-5033		SG14-5071		SG14-5099		SG14-5183		SG14-5221		SG14-5367		SG14-5406		SG14-5469	
wt.%	**Avg.**	**1 std. dev.**	**Avg.**	**1 std. dev.**	**Avg.**	**1 std. dev.**	**Avg.**	**1 std. dev.**	**Avg.**	**1 std. dev.**	**Avg.**	**1 std. dev.**	**Avg.**	**1 std. dev.**	**Avg.**	**1 std. dev.**	**Avg.**	**1 std. dev.**	**Avg.**	**1 std. dev.**	**Avg.**	**1 std. dev.**
SiO_2	71.03	0.40	75.16	0.28	76.82	1.20	72.66	0.16	72.71	0.26	68.89	0.81	77.25	0.62	70.33	0.18	76.66	0.16	77.95	0.93	75.07	0.66
TiO_2	0.35	0.03	0.26	0.02	0.23	0.02	0.69	0.03	0.35	0.03	0.62	0.10	0.07	0.04	0.62	0.03	0.05	0.03	0.10	0.03	0.61	0.04
Al_2O_3	15.32	0.31	13.68	0.24	12.93	0.87	13.33	0.17	14.90	0.16	16.61	0.99	13.49	0.49	15.32	0.12	13.95	0.12	12.68	0.67	13.43	0.25
FeO	2.26	0.09	1.39	0.12	1.07	0.22	3.57	0.07	1.33	0.09	2.12	0.52	0.64	0.19	2.24	0.05	0.50	0.05	0.63	0.11	2.44	0.09
MnO	0.06	0.02	0.05	0.02	0.06	0.03	0.13	0.02	0.10	0.02	0.10	0.04	0.07	0.02	0.10	0.02	0.10	0.02	0.08	0.02	0.10	0.02
MgO	0.69	0.07	0.24	0.08	0.20	0.14	0.77	0.06	0.26	0.03	0.54	0.27	0.11	0.04	0.60	0.02	0.12	0.02	0.08	0.05	0.53	0.02
CaO	2.67	0.20	1.62	0.13	1.21	0.41	3.02	0.08	0.96	0.06	2.36	0.49	0.62	0.22	1.78	0.04	0.68	0.06	1.04	0.25	2.04	0.06
Na_2O	4.71	0.13	3.67	0.11	3.42	0.37	4.49	0.14	4.54	0.11	4.72	0.21	3.93	0.44	4.44	0.12	3.91	0.22	3.22	0.36	2.88	0.89
K_2O	2.41	0.06	3.79	0.21	3.94	0.39	1.07	0.04	4.70	0.09	3.82	0.39	3.67	0.45	4.37	0.08	3.90	0.10	4.08	0.30	2.72	0.05
P_2O_5	0.11	0.03	0.03	0.02	0.05	0.02	0.14	0.03	0.05	0.03	0.13	0.06	0.06	0.02	0.12	0.04	0.07	0.04	0.05	0.02	0.07	0.02
Cl	0.38	0.03	0.11	0.02	0.09	0.02	0.13	0.03	0.10	0.02	0.08	0.02	0.10	0.05	0.10	0.02	0.07	0.01	0.10	0.02	0.12	0.02
(n)	*11*		*17*		*28*		*15*		*19*		*9*		*7*		*18*		*16*		*10*		*16*	
ppm	**Avg.**	**1 std. dev.**	**Avg.**	**1 std. dev.**	**Avg.**	**1 std. dev.**	**Avg.**	**1 std. dev.**	**Avg.**	**1 std. dev.**	**Avg.**	**1 std. dev.**	**Avg.**	**1 std. dev.**	**Avg.**	**1 std. dev.**	**Avg.**	**1 std. dev.**	**Avg.**	**1 std. dev.**	**Avg.**	**1 std. dev.**
Rb	76.5	1.04	132	6.72	143	5.44	15.9	1.88	13.8	3.99	10.8	1.28	-	-	37.7	1.86	118	5.46	144	14.0	99.3	1.22
Sr	502	17.3	266	21.38	178	36.5	216	35.83	168	15.7	106	29.4	-	-	157	1.74	85.9	32.6	254	90.6	129	5.03
Y	6.63	0.13	16.1	0.42	13.2	0.49	33.9	3.01	151	27.9	59.7	6.21	-	-	239	8.81	8.89	0.35	10.6	0.97	41.8	1.79
Zr	131	3.57	215	4.98	186	4.76	107	9.20	32.5	2.51	26.5	0.44	-	-	32.2	0.88	31.8	1.65	77.0	6.62	224	12.1
Nb	8.30	0.10	10.9	0.22	11.1	0.51	1.84	0.16	281	30.9	146	2.96	-	-	267	6.67	18.6	0.75	11.1	1.40	10.3	0.31
Ba	543	16.1	923	24.62	906	43.7	434	37.00	15.3	1.91	5.89	2.28	-	-	15.2	0.27	958	64.4	809	25.7	451	18.8
La	21.2	0.92	31.7	0.80	31.8	1.06	6.45	0.64	761	55.6	452	4.26	-	-	790	17.6	5.96	0.54	27.2	1.09	25.0	0.96
Ce	40.0	1.34	61.4	1.71	61.8	1.71	17.6	1.63	33.3	3.62	16.2	0.26	-	-	32.1	0.97	13.1	1.18	52.2	3.59	56.9	2.23
Pr	3.90	0.21	6.27	0.26	6.17	0.25	2.62	0.24	74.4	7.64	36.5	0.53	-	-	70.7	1.85	1.35	0.18	5.28	0.59	6.60	0.49
Nd	13.4	0.79	23.3	0.90	21.0	0.91	13.9	1.30	8.43	0.95	4.08	0.14	-	-	8.06	0.33	4.72	0.52	17.5	1.00	29.1	1.60
Sm	2.09	0.24	4.00	0.28	3.47	0.30	4.29	0.48	34.5	4.42	16.4	0.98	-	-	34.0	1.23	1.39	0.23	2.94	0.25	6.77	0.50
Eu	0.72	0.01	0.87	0.08	0.68	0.10	1.27	0.08	7.05	0.80	3.80	0.18	-	-	7.24	0.42	0.30	0.03	0.61	0.12	1.33	0.10
Gd	1.43	0.18	3.01	0.34	2.57	0.33	5.02	0.58	1.31	0.17	0.58	0.06	-	-	1.43	0.10	1.31	0.15	2.05	0.18	6.50	0.37
Dy	1.33	0.20	2.83	0.28	2.25	0.24	6.05	0.65	5.76	0.79	3.72	0.35	-	-	5.85	0.24	1.49	0.11	1.85	0.21	7.36	0.18
Er	0.67	0.10	1.71	0.14	1.45	0.17	3.78	0.43	5.84	0.58	4.43	0.41	-	-	5.57	0.51	0.93	0.07	1.09	0.14	4.64	0.36
Yb	0.82	0.06	1.96	0.16	1.63	0.23	3.93	0.43	3.52	0.25	3.00	0.19	-	-	3.41	0.20	1.08	0.13	1.36	0.21	4.86	0.35
Lu	0.13	0.01	0.29	0.02	0.28	0.03	0.59	0.06	4.00	0.35	3.40	0.27	-	-	3.65	0.33	0.14	0.02	0.20	0.03	0.70	0.03
Hf	3.40	0.10	5.56	0.28	4.94	0.51	3.26	0.35	0.57	0.07	0.51	0.02	-	-	0.55	0.04	1.59	0.22	2.53	0.28	6.34	0.15
Ta	0.53	0.01	0.73	0.03	0.79	0.04	0.13	0.01	7.34	0.75	4.40	0.35	-	-	7.18	0.40	1.48	0.07	0.83	0.06	0.71	0.05
Pb	12.0	0.16	18.4	1.03	19.8	0.92	8.08	0.70	1.11	0.15	0.46	0.15	-	-	1.07	0.05	16.2	1.74	20.9	0.59	22.0	0.90
Th	7.20	0.04	12.3	0.50	14.0	0.49	0.92	0.11	24.4	1.23	18.8	1.19	-	-	21.8	0.87	5.05	0.37	13.4	0.75	9.07	1.18
U	2.09	0.07	2.34	0.08	2.65	0.13	0.47	0.06	15.4	1.77	8.03	0.33	-	-	14.2	0.90	3.87	0.19	3.24	0.32	2.38	0.20
(n)	*3*		*22*		*9*		*20*		*18*		*6*		*-*		*14*		*13*		*8*		*6*	

Tephra	SG14-5520		SG14-5563A		SG14-5563B		SG14-5575		SG14-5579		SG14-5597		SG14-5616		SG14-5648		SG14-5851		SG14-5932		SG14-5950	
wt.%	Avg.	1 std. dev.	Avg.	1 std. dev.	Avg.	1 std. dev.	Avg.	1 std. dev.	Avg.	1 std. dev.	Avg.	1 std. dev.	Avg.	1 std. dev.	Avg.	1 std. dev.	Avg.	1 std. dev.	Avg.	1 std. dev.	Avg.	1 std. dev.
SiO_2	74.03	0.19	76.60	0.07	77.96	0.19	78.02	0.28	71.45	0.37	73.09	1.28	76.64	0.27	69.25	0.31	69.31	0.19	71.60	0.34	72.25	0.21
TiO_2	0.59	0.04	0.19	0.01	0.23	0.01	0.06	0.02	0.44	0.04	0.47	0.10	0.36	0.03	0.69	0.04	0.71	0.03	0.77	0.04	0.21	0.03
Al_2O_3	13.20	0.12	13.39	0.17	12.39	0.07	12.76	0.18	15.29	0.18	13.95	0.48	12.71	0.16	15.43	0.13	14.65	0.10	13.68	0.13	14.23	0.11
FeO	2.37	0.08	0.88	0.14	1.07	0.06	0.89	0.04	1.62	0.08	2.95	0.29	1.81	0.09	2.54	0.11	4.05	0.14	3.50	0.14	3.01	0.08
MnO	0.08	0.01	0.03	0.00	0.04	0.03	0.09	0.02	0.09	0.02	0.13	0.03	0.05	0.02	0.10	0.02	0.14	0.02	0.08	0.02	0.08	0.02
MgO	0.54	0.02	0.17	0.08	0.21	0.07	0.03	0.02	0.39	0.05	0.58	0.15	0.40	0.04	0.68	0.05	1.07	0.04	0.83	0.04	0.03	0.02
CaO	2.07	0.05	1.50	0.06	0.96	0.08	0.36	0.03	1.24	0.08	2.71	0.38	2.18	0.09	1.88	0.11	3.88	0.12	2.96	0.17	0.54	0.02
Na_2O	4.05	0.04	3.94	0.10	3.59	0.17	4.82	0.20	4.29	0.19	4.84	0.08	3.47	0.15	4.42	0.11	4.95	0.17	3.79	0.13	5.78	0.07
K_2O	2.86	0.06	3.07	0.06	3.28	0.04	2.82	0.10	5.04	0.09	1.02	0.09	2.17	0.07	4.72	0.11	0.94	0.02	2.64	0.11	4.98	0.10
P_2O_5	0.09	0.04	0.08	0.04	0.06	0.01	0.02	0.03	0.06	0.03	0.09	0.04	0.05	0.03	0.20	0.07	0.14	0.03	0.05	0.06	0.01	0.01
Cl	0.11	0.01	0.15	0.01	0.21	0.03	0.12	0.02	0.11	0.01	0.16	0.03	0.14	0.03	0.09	0.01	0.15	0.02	0.10	0.02	0.29	0.01
(n)	*10*		*3*		*4*		*57*		*22*		*14*		*11*		*40*		*12*		*29*		*11*	
ppm	**Avg.**	**1 std. dev.**	**Avg.**	**1 std. dev.**	**Avg.**	**1 std. dev.**	**Avg.**	**1 std. dev.**	**Avg.**	**1 std. dev.**	**Avg.**	**1 std. dev.**	**Avg.**	**1 std. dev.**	**Avg.**	**1 std. dev.**	**Avg.**	**1 std. dev.**	**Avg.**	**1 std. dev.**	**Avg.**	**1 std. dev.**
Rb	-	-	95.0	4.05	85.5	5.33	64.5	3.74	17.1	2.60	16.4	5.55	75.0	1.29	174	5.62	20.3	3.52	97.2	1.88	293	10.4
Sr	-	-	253	27.8	395	123	21.9	10.0	190	14.7	230	46.4	209	4.37	266	46.8	237	8.23	142	3.24	1.58	1.34
Y	-	-	4.86	0.35	5.35	1.03	58.9	4.10	182	12.2	29.0	3.73	21.9	0.84	33.0	1.14	31.3	0.97	42.2	0.99	88.6	2.66
Zr	-	-	124	8.42	125	7.71	79.2	4.72	32.5	1.16	97.0	18.1	175	7.08	292	10.3	100	2.48	235	3.13	861	31.2
Nb	-	-	10.2	0.54	9.26	0.66	5.23	0.27	324	20.2	1.95	0.37	7.37	0.41	16.9	0.67	1.65	0.15	11.1	0.27	225	8.62
Ba	-	-	641	20.8	617	55.7	974	48.7	17.4	1.35	374	53.5	666	27.0	824	51.3	392	19.8	444	9.56	6.96	6.85
La	-	-	23.5	1.26	23.2	0.54	14.9	0.82	818	38.7	6.29	0.94	21.5	1.42	35.2	1.27	6.06	0.15	24.9	0.38	166	4.85
Ce	-	-	43.2	1.85	42.2	0.73	37.7	2.38	36.1	1.24	16.8	2.01	45.5	2.40	77.5	2.59	16.4	1.02	59.2	1.21	315	9.11
Pr	-	-	3.94	0.27	4.03	0.45	4.93	0.33	78.3	3.06	2.48	0.41	4.91	0.41	8.93	0.28	2.46	0.20	6.88	0.23	30.8	1.27
Nd	-	-	13.2	1.11	13.5	1.83	22.4	1.57	8.85	0.47	11.8	1.30	20.3	0.75	35.9	1.24	13.7	1.90	29.7	0.88	114	6.82
Sm	-	-	2.15	0.19	<LOD	<LOD	6.83	0.59	35.4	1.43	3.92	0.67	4.25	0.44	7.57	0.71	<LOD	<LOD	7.08	0.78	21.7	1.07
Eu	-	-	<LOD	<LOD	<LOD	<LOD	0.58	0.16	7.29	0.50	1.22	0.11	0.96	0.10	1.50	0.15	<LOD	<LOD	1.40	0.11	0.30	0.13
Gd	-	-	<LOD	<LOD	<LOD	<LOD	7.78	0.78	1.29	0.09	4.13	0.79	3.99	0.25	6.70	0.47	<LOD	<LOD	6.66	0.72	17.2	1.76
Dy	-	-	<LOD	<LOD	<LOD	<LOD	9.75	1.05	5.88	0.52	5.01	0.28	3.96	0.30	6.31	0.20	<LOD	<LOD	7.50	0.41	17.6	0.97
Er	-	-	<LOD	<LOD	<LOD	<LOD	6.29	0.44	5.77	0.41	3.37	0.53	2.45	0.30	3.47	0.26	<LOD	<LOD	4.69	0.35	8.78	0.55
Yb	-	-	<LOD	<LOD	<LOD	<LOD	7.11	0.53	3.57	0.18	3.06	0.38	2.32	0.26	3.60	0.31	<LOD	<LOD	5.05	0.37	7.73	0.71
Lu	-	-	<LOD	<LOD	<LOD	<LOD	1.03	0.06	3.61	0.16	0.47	0.14	0.36	0.03	0.56	0.06	<LOD	<LOD	0.73	0.03	1.05	0.06
Hf	-	-	3.37	0.44	2.85	0.16	3.58	0.34	0.56	0.04	2.97	0.47	4.54	0.41	7.87	0.28	3.48	0.38	6.60	0.50	26.3	1.32
Ta	-	-	0.74	0.03	0.67	0.12	0.37	0.03	8.63	0.51	0.12	0.02	0.47	0.02	1.22	0.05	0.12	0.01	0.71	0.03	12.8	0.85
Pb	-	-	13.4	0.95	13.3	0.64	28.2	1.61	1.28	0.10	6.95	1.07	13.4	0.53	24.4	3.43	7.30	0.49	20.3	0.84	26.0	2.28
Th	-	-	10.5	0.66	9.51	0.87	5.86	0.42	26.1	1.21	0.85	0.23	5.94	0.39	16.5	0.73	1.09	0.12	8.87	0.41	35.4	1.93
U	-	-	2.94	0.27	2.77	0.26	2.49	0.21	18.2	1.61	0.43	0.02	1.30	0.17	4.87	0.16	0.79	0.13	2.32	0.21	7.14	0.45
(n)	*-*		*7*		*2*		*10*		*17*		*4*		*5*		*8*		*6*		*11*		*7*	

The glass compositions of the newly identified crypto-/tephras are generally homogenous, except for the following deposits which span broad compositional ranges: SG14-4002, SG14-4010, SG14-4187 and SG14-4860 (Fig. 5.5). The glass compositions of the deposits are predominantly rhyolitic residing on either a calc-alkaline or high-K calc-alkaline evolutionary trend (Fig. 5.5). Trachy-andesite and trachy-dacite tephra deposits are also observed along the high-K calc-alkaline evolutionary series (Fig. 5.5). The SG14-5033, SG14-5597 and SG14-5851 deposits all show a distinctive Low-K tholeiitic affinity, whilst the SG14-4223 is unique in displaying a shoshonitic affinity, residing on the phonolite-trachyte boundary (Fig. 5.5A).

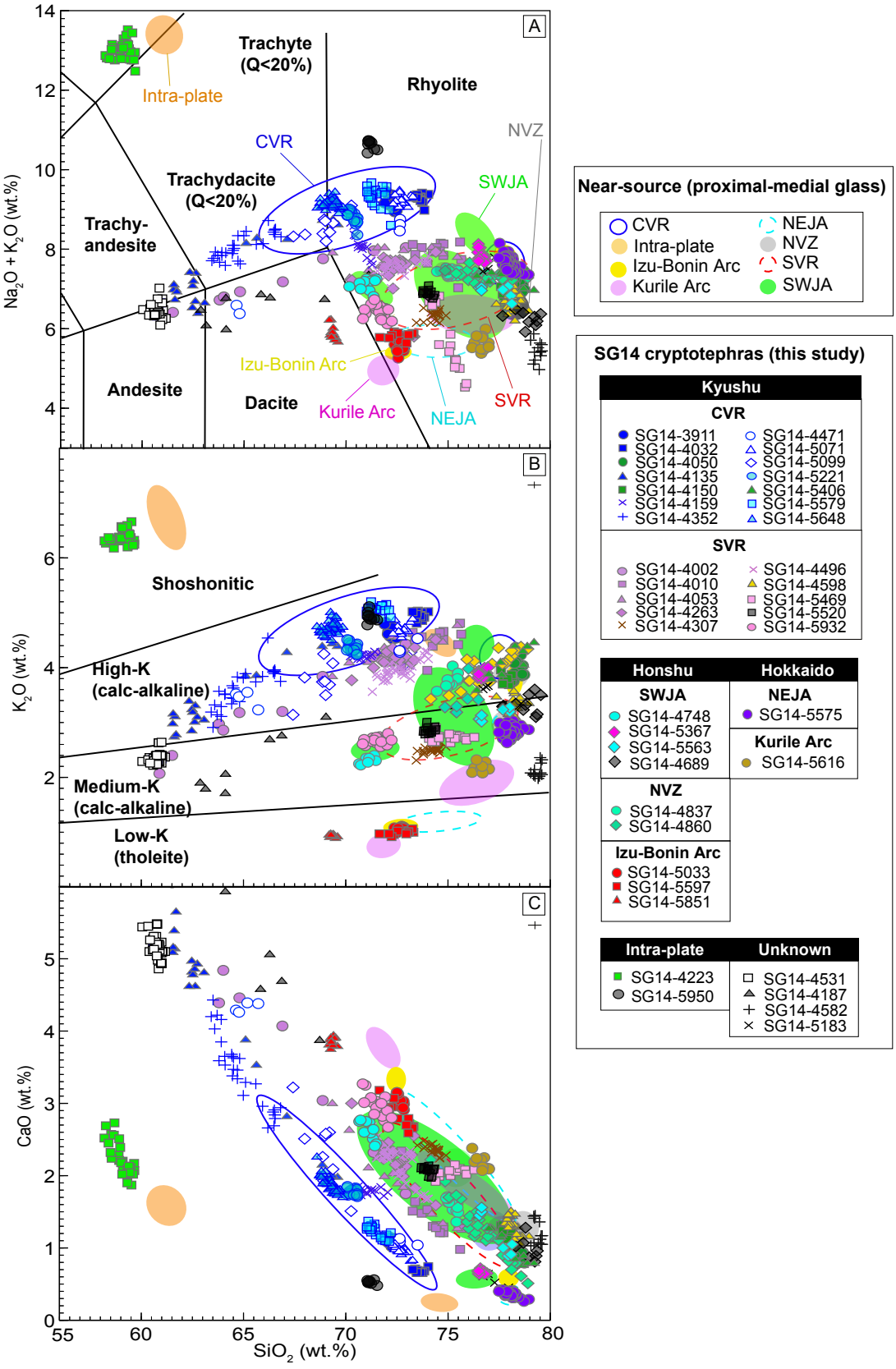


Figure 5.5: Major element glass compositions of the crypto-/tephras preserved in the SG14 sediments spanning ~120 – 50 ka. (A) K_2O classification fields follow

(Peccerillo and Taylor, 1976). Glass compositional fields/envelopes for the arcs are labelled in a-c, see Fig. 1 for locations. Compositional fields/envelopes for the following volcanic arcs are from data presented in previous studies for the CVR from Smith et al., 2013 (Aso-A, Aso-D, Aso-4), Albert et al., 2019a (Aso = ACP-3, ACP-4, ACP-5, ACP-6, Aso-4, Aso-Y, Aso-A, Aso-B, Aso-C, Aso-D Aso-I, Aso-K, Aso-M, Aso-N, Aso-3; Kuju = Kj-Mg, Kj-D, Kj-P1, Kj-Hd); McLean et al., 2020a (Aso = Aso-Kpfa); Intraplate proximal and Lake Suigetsu tephras for Changbaishan from McLean et al., 2018 (B-Tm) and Ulleungdo from Smith et al., 2011ab(U4/U-Oki); McLean et al., 2018 (U1, U2, U-3); McLean et al., 2020b (U-Ym); Izu-Bonin Arc from Albert et al., 2019a (Hakone = Tau8); Albert et al., 2024 (Nijima = Nj-Mt); Kurile Arc from Albert et al., 2019a (Kutcharo = Kc-Sr, Kc-2/3, Kc-Hb; Mashu = Ma-f); NEJA from Albert et al., 2019a (Shikotsu = Spfa-1; Towada = To-H; Toya = Toya); NVZ from Albert et al., 2019a (Ontake = On-Pm1) Albert et al., 2024 (Asama = As-K, As-UG, As-YP) Matsu'ura and Komatsubara 2024 (Ontake = On-Ng, On-Ot, On-In, On-Kt, On-Yb, On-Pm1); SVR from Smith et al., 2011b (Aira = AT); Smith et al. 2013 (Kikai = K-Ah) Albert et al., 2019a (Ata = Ata, AT, Ikeda; Aira = A-Iw; Kikai = K-Ah, K-Tz); Albert et al., 2024 (Aira = A-Moeshima, A-Tkn, Kr-Kb; Kirishima = Kr-Kb); McLean et al., 2020a (Aira = A-Fkm, A-Kn) and SWJA from Albert et al., 2018 (Daisen = DJs, DHg, DSs, DSP; Sambe = Th-pfl, S2-fl, Kr-fa, Uk-fa, Md-fl, U2, U1, Ht-fl, SI, Ikeda, SuN, Sod). Error bars on plots represent reproducibility, and 2 standard deviations of replicate analysis of MPI-DING StHs6/80-G standard.

Trace element data were obtained for all deposits apart from three, SG14-4010, SG14-5182, and SG14-5520, as the vesicularity and microlite inclusions precluded analyses (Table 5.3). Similarly to the major element compositional data, individual cryptotephras typically demonstrate relatively homogenous compositions. The phono-trachytic tephra, SG14-4223, displays the highest levels of incompatible trace element enrichment and the most heterogeneity (Fig. 5.6).

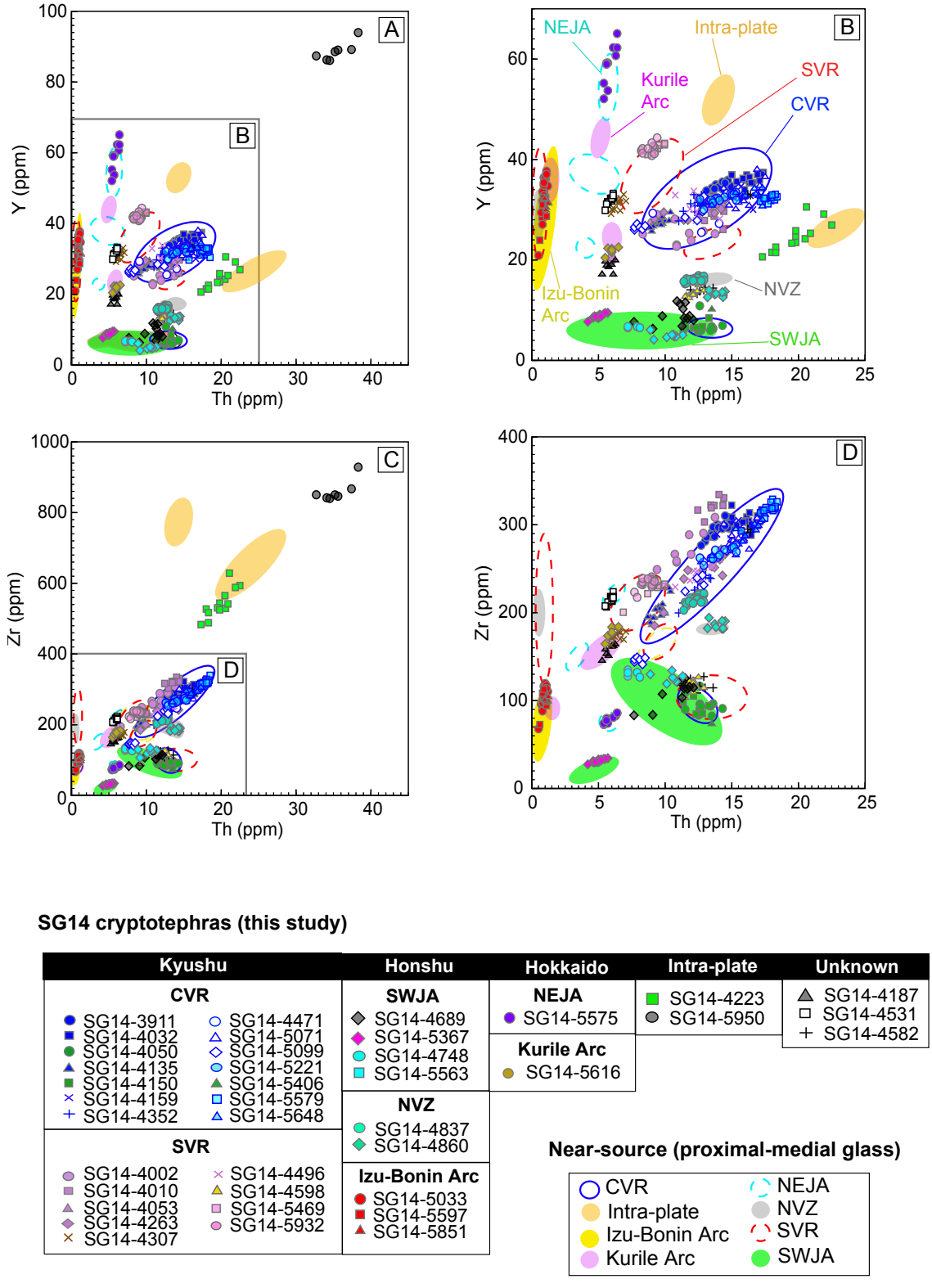


Figure 5.6: Trace element glass compositions of the crypto-/tephras preserved in the SG14 sediments spanning ~120 - 50 ka. Glass compositional fields/envelopes for the arcs are labelled in a-c, see Fig. 1 for locations. Compositional fields/envelopes for the following volcanic arcs are from literature data. Data for the CVR is from Albert et al., 2019a (Aso = ACP-3, ACP-4, Aso-4, Aso-Y, Aso-A, Aso-B, Aso-C, Aso-D Aso-I, Aso-K, Aso-M, Aso-N,

Aso-3; Kuju = Kj-Mg, Kj-P1, Kj-Hd) and McLean et al., 2020a (Aso = Aso-Kpfa); Intraplate proximal and Lake Suigetsu tephras for Changbaishan McLean et al., 2018 (B-Tm) and Ulleungdo from McLean et al., 2018 (U-3) and McLean et al., 2020b (U-Ym); Izu-Bonin Arc Albert et al., 2019a (Hakone = Tau8) and Albert et al., 2024 (Nijima = Nj-MtG); Kurile Arc from Albert et al., 2019a (Kutcharo = Kc-Sr, Kc-2/3, Kc-Hb; Mashu = Mashu-f); NEJA from Albert et al., 2019a (Shikotsu = Spfa-1; Towada = To-H; Toya = Toya); NVZ from Albert et al., 2019a (Ontake = On-Pm1), Albert et al., 2024 (Asama = As-K, As-UG, As-YP), and Matsu'ura and Komatsubara 2024 (Ontake = On-Ng, On-Ot, On-In, On-Kt, On-Yb, On-Pm1); SVR from Albert et al., 2019a (Ata = Ata, AT, A-Iw; Kikai = K-Ah, K-Tz), Albert et al., 2024 (Aira = A-Moeshima; Kirishima = Kr-Kb), and McLean et al., 2020a (Aira = A-Fkm, A-Kn); and SWJA from Albert et al., 2018 (Daisen = DSs and DSP; Sambe = SuN and Sod). Error bars on plots represent reproducibility, and 2 standard deviations of replicate analysis of MPI-DING StHs6/80-G standard.

5.6. Discussion

5.6.1. Provenance of the SG14 tephra layers erupted ~120 - 50 ka

The major and trace element glass compositions permit thirty-eight deposits to be attributed to their volcanic arcs, and thirty-four of these to specific volcanoes (Fig. 5.5, 5.6; Table 5.4). In summary, these deposits are from seven different Japanese volcanic arc settings (from the three main islands of Japan), and from intraplate sources (Fig. 5.5). Due to the number of deposits identified in this study, they have been grouped based on chemical affinities with volcanic sources and regions as listed below and in Table 5.2:

1) Kyushu Southern Volcanic Region (SVR): Kirishima (5); Aira (1); Ata (2) and Kikai (1)
2) Kyushu Central Volcanic Region (CVR): Aso (11) and Kuju (3)
3) SW Japan Arc (SWJA): Sambe (1) and Daisen (2)
4) Izu-Bonin Arc: Hakone (3)
5) Norikura Volcanic Zone (NVZ): Ontake (2)
6) NE Japan Arc (NEJA): Toya (1)
7) Kurile Arc: Kutcharo (1)
8) Intraplate: Ulleungdo (1)

There are another 7 eruption deposits that could not be reliably correlated to a particular arc or source volcano (Table 5.2).

Table 5.4: Average major element glass compositions of proximal tephra deposits analysed as part of this study to compare to the ~120 – 50 ka Lake Suigetsu crypto-/tephras. Major element glass data has been normalised. The SK (FLF04-1) tephra sample was collected from the base of Exp.346 U1427A Core 5H Section 7W (62 – 63 cm) and was first reported by Sagawa et al. (2018). Full geochemical datasets are available in the Appendix B.

Source	Sambe		Sambe		Kirishima		Kirishima		Kirishima		Kirishima	
Tephra	SK		SK		Kr-lw		Kr-lw		Kr-lw		Kr-Aw	
Material	Pumice		Pumice		Pumice		Pumice		Scoria		Scoria	
Deposit type	Fall		Fall		Fall		Fall		Fall		Fall	
Sample	FLF04		FLF133		FLF176		FLF177		FLF178		FLF181	
Location	IODP-U1427A		Kakeyacho Kakeyo		Umegakubo Quarry		Umegakubo Quarry		Umegakubo Quarry		Umegakubo Quarry	
(wt.%)	Avg.	1 std. dev.	Avg.	1 std. dev.	Avg.	1 std. dev.	Avg.	1 std. dev.	Avg.	1 std. dev.	Avg.	1 std. dev.
SiO_2	76.45	0.23	76.50	0.48	68.40	3.46	66.65	3.79	69.69	2.01	62.16	0.36
TiO_2	0.06	0.02	0.05	0.02	0.49	0.15	0.59	0.09	0.49	0.12	0.85	0.08
Al_2O_3	13.95	0.17	13.94	0.34	13.99	1.65	14.35	1.71	13.14	0.61	15.89	0.83
FeO	0.54	0.06	0.52	0.04	2.80	1.32	3.71	1.59	2.33	0.56	6.50	0.59
MnO	0.10	0.02	0.09	0.02	0.06	0.03	0.07	0.03	0.06	0.01	0.17	0.02
MgO	0.13	0.04	0.12	0.03	0.67	0.56	1.19	0.98	0.50	0.19	1.96	0.24
CaO	0.67	0.02	0.69	0.10	2.74	1.38	3.42	1.74	2.00	0.49	5.36	0.39
Na_2O	4.16	0.08	4.21	0.18	3.26	0.15	3.30	0.21	3.28	0.22	3.61	0.22
K_2O	3.80	0.08	3.74	0.11	3.58	0.59	3.35	0.78	3.90	0.30	1.75	0.16
P_2O_5	0.06	0.02	0.06	0.02	0.06	0.04	0.09	0.05	0.06	0.03	0.19	0.03
Cl	0.08	0.02	0.08	0.01	0.11	0.02	0.11	0.03	0.13	0.02	0.07	0.01
(n)	*15*		*19*		*11*		*14*		*14*		*11*	
(ppm)	Avg.	1 std. dev.	Avg.	1 std. dev.	Avg.	1 std. dev.	Avg.	1 std. dev.	Avg.	1 std. dev.	Avg.	1 std. dev.
Rb	112	5.58	103	1.24	140	24.1	116	36.6	123	18.1	60.3	2.37
Sr	118	5.51	112	2.76	198	66.6	293	162	180	125	330	18.9
Y	8.50	0.45	8.82	0.43	26.2	3.26	24.1	6.06	23.4	4.32	26.2	1.74
Zr	31.5	1.57	32.5	2.23	224	39.7	195	58.3	156	57	128	3.67
Nb	18.2	0.83	19.3	1.55	8.47	1.17	7.41	2.06	7.66	0.93	6.22	0.29
Ba	985	30.4	983	16.8	563	81.8	487	97.0	513	47.5	349	23.4
La	5.75	0.34	5.93	0.64	23.1	3.59	20.2	4.29	22.6	2.73	18.4	1.27
Ce	12.7	0.71	13.7	2.42	50.1	6.53	44.8	9.95	45.8	4.73	39.1	4.64
Pr	1.33	0.09	1.28	0.08	5.61	0.77	5.15	1.13	5.20	0.70	4.84	0.31
Nd	4.28	0.54	4.59	0.43	22.8	2.86	20.9	4.87	20.1	2.76	21.2	1.80
Sm	1.31	0.12	1.57	0.07	5.20	0.61	4.69	1.17	4.37	0.96	5.02	0.28
Eu	0.31	0.03	0.40	0.02	0.88	0.06	0.93	0.14	0.83	0.29	1.30	0.13
Gd	1.15	0.13	1.34	0.09	4.66	0.62	4.08	0.93	3.94	0.58	4.59	0.37
Dy	1.34	0.14	1.37	0.07	4.48	0.57	4.12	0.99	3.90	0.85	4.72	0.37
Er	0.94	0.09	0.90	0.11	2.81	0.35	2.61	0.70	2.54	0.61	2.92	0.24
Yb	0.97	0.12	1.10	0.15	3.07	0.47	2.72	0.70	2.68	0.65	2.79	0.34
Lu	0.14	0.02	0.14	0.01	0.44	0.07	0.40	0.11	0.41	0.08	0.42	0.02
Hf	1.49	0.07	1.53	0.03	6.07	1.33	5.41	1.56	4.59	1.52	3.65	0.22
Ta	1.46	0.03	1.54	0.10	0.62	0.11	0.54	0.16	0.60	0.07	0.41	0.02
Pb	17.5	0.74	24.81	13.5	20.7	2.17	21.2	7.85	19.7	1.84	13.3	1.38
Th	4.78	0.28	4.89	0.19	11.9	2.65	10.2	3.24	10.8	1.53	5.10	0.29
U	3.90	0.16	3.78	0.26	2.99	0.62	2.56	0.78	2.60	0.31	1.21	0.10
(n)	*9*		*3*		*11*		*15*		*6*		*12*	

5.6.1.1 Kyushu (SVR and CVR)

<u>Kirishima</u>

Five cryptotephras have compositions consistent with published and newly analysed deposits from the Kirishima volcanic complex: SG14-4002, SG14-4010, SG14-4053, SG14-4263 and SG14-4496. The SG14-4002 glasses span the broadest compositional ranges in both major and trace elements and extend to lower SiO_2 and Th contents (Fig. 5.7A-C). The younger two Kirishima deposits (SG14-4010 and SG14-4002) have higher Nb at a given Th contents and can be easily distinguished from older glasses (SG14-4263 and SG14-4496; Fig. 5.7C) indicating that they may have derived from different vents within the Kirishima complex.

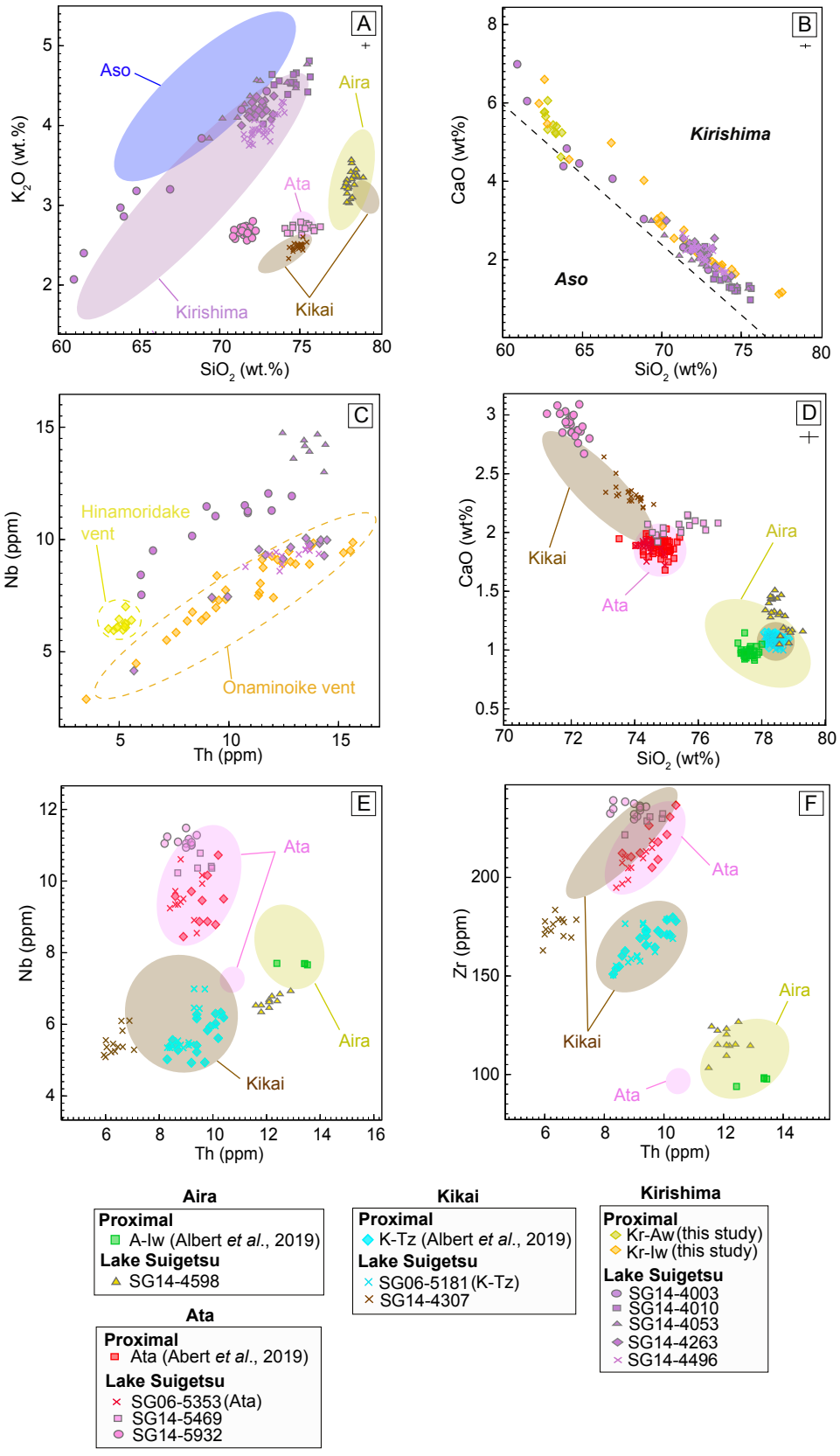


Figure 5.7: Major and trace element compositions of the SG14 cryptotephras (~120 – 50 ka) derived from the SVR in comparison for major eruptive SVR centres. Compositional fields/envelopes for the following volcanic centres are from proximal data presented in previous studies. Data for Aira is from Smith et al., 2011b (AT), McLean et al., 2020a (A-

Fkm, A-Kn), Albert et al., 2019a (A-Iw), and Albert et al., 2024 (A-Moeshima, A-Tkn); Ata from Albert et al., 2019a (Ata = Ata, AT, Ikeda); Kikai from Albert et al., 2019a (K-Ah, K-Tz) and Smith et al. 2013 (K-Ah); Kirishima from Albert et al., 2024 (Kr-Kb) and this study (Kr-Aw, Kr-Iw). Error bars represent 2x standard deviation of repeat analyses of the StHs6/80-G MPI-DING standard glass.

All five of the Kirishima cryptotephras share a geochemical affinity with the more evolved Kr-Iw glass compositions, which is stratigraphically older. SG14-4002 also shows partial overlap with the younger Kr-Aw glasses (Fig. 5.7B). At the trace element level, the oldest Kirishima cryptotephras (SG14-4496 and SG14-4263) show compositional overlap with the older Kr-Iw tephra, indicating that at least one of these is likely to equate to the Kr-Iw eruption. As both are separated by the widespread DSP tephra in Lake Suigetsu (SG06-4318), this offers a potential means for determining which is the distal equivalent of the Kr-Iw in future research. Whilst the SG14-4053 and SG14-4002 deposits do not chemically overlap with the younger Kr-Aw glasses analysed, they do reside on a trend of elevated Nb content relative to Th consistent with the source area of the Kr-Aw, probably the Hinamoridake edifice (Fig. 5.7C). Trace element data could not be obtained for the SG14-4010 cryptotephra. The findings of numerous Kirishima ash-fall layers in the SG14 record should prompt further near-source stratigraphic and chemical investigations at Kirishima, to establish more reliably the precise proximal counterparts of the different distal deposits.

Aira

The SG14-4598 cryptotephra deposit is preserved between Aso-4 (SG14-4963) and the DSP (SG06-4318) and has a SG age of 73.9 ± 2.3 ka (±1σ). It is correlated to Aira owing to higher Th (~12 ppm) and lower Zr (~117 ppm) contents, which is a distinguishing feature of Aira derived glasses (Fig. 5.7F). Of the two proximal Aira units in the relevant timeframe (A-Iw and A-Fk), the A-Iw is above the Aso-4 unit (Fig. 5.2). Whilst the SG14-4598 cryptotephra is in the same stratigraphic position as the A-Iw (Fig. 4.4), the glasses can be distinguished at both the major and trace element level (Fig. 5.7D-F). We are therefore currently unable to correlate the SG14-4598 Lake Suigetsu cryptotephra to a particular Aira tephra.

Ata

Two cryptotephras are interpreted as deriving from the Ata caldera: SG14-5469 and SG14-5932 (Table 5.2). The SG14-5932 glasses have lower SiO_2 and higher CaO content than the overlying SG14-5469 and the proximal and distal Ata deposits (SG06-5353) and are arguably more consistent with glasses erupted from the Kikai caldera at major element level (Fig. 5.7A,C). Both the SG14-5932 and SG14-5469 glasses are indistinguishable from each

other at the trace element level and have Nb contents (~10.5 ppm) which are consistent with glasses erupted from Ata (Albert et al., 2019a; Fig. 5.7E). We therefore interpret that both these cryptotephra deposits reflect pre-100 ka Ata activity. A potential candidate for one of these cryptotephras is the Ata Maimine eruption unit, however, its distribution is not extensively reported in the near-source setting and no geochemical data are currently available for comparison. Assuming the trace element link between these cryptotephras and Ata is robust, our data extends the compositional range of Ata erupted glasses.

Kikai

We have correlated the SG14-4307 cryptotephra dated to 62.3 ± 2.3 ka (±1σ) in Lake Suigetsuto an eruption from Kikai. The SG14-4307 glasses show overlap with glasses from near-vent Kikai units in major elements (Fig. 5.7A,C) and the lower Nb (~5 ppm) content is only consistent with Kikai tephra (Fig. 5.7E; Albert et al., 2019a). The SG14-4307 is 30 ka younger than the caldera-forming K-Tz eruption and has lower SiO_2 (ca. 4 wt.%) and Th (ca. 3.5 ppm) contents relative to the K-Tz (SG06-5181; Fig. 5.7D-F). The only other known Kikai tephra pre-50 ka is preserved beneath the K-Tz (Table 5.1; Machida and Arai, 2003). Given that SG14-4307 is younger (preserved between the Aso-4 [SG06-4963] and DSP [SG06-4318] tephras; Fig. 5.4), it provides evidence for an explosive eruption following the K-Tz eruption. The Tane I and Tane II tephras are thought to have erupted from Kikai. They are reported above the K-Tz and are ~65 ka based on their stratigraphic positions (Okuno and Kobayashi, 1994). However as Kikai is a submerged caldera, there are limited on land exposures near the volcano, with only patchy deposits, such as Tane II, outcropping on small islands. These tephras have not been geochemically characterised so we are unable to establish if SG14-4307 cryptotephra correlates with one of the Tane tephras.

Directly following the 2.8 cm thick visible K-Tz tephra, several cryptotephra peaks (>6000 shards/gram) are identified in the 1.5 m of sediment above (Fig. 5.4). These have been interpreted as reworked K-Tz deposits due to their similarity in geochemistry and shard characteristics. It is likely that these represent remobilisation of the K-Tz shards in the catchment during periods of high rainfall. Similar peaks in shard concentrations are observed following the deposition of other thick Kikai tephras, for example, following the 3 cm thick K-Ah tephra (ca. 7.3 ka) there are peaks in compositionally and physically similar shards in the 1 m of sediment above the visible unit (McLean et al. 2018).

Aso

Eleven crypto/-tephras from Aso have been identified in the studied Lake Suigetsu sediments (Table 5.2). Six of the cryptotephra deposits are preserved in the 10 m of

sediment above the Aso-4 tephra (SG06-4963; Table 5.2). The other five crypto-/tephras are preserved in the 7 m below: three between Aso-4 and Aso-ABCD (SG06-5287) and two beneath the latter (Table 5.2). The Aso glasses span the widest compositional range from any volcanic centre reported in this study and range from trachy-andesites through to rhyolites (Fig. 5.5; Table 5.3).

The five crypto-/tephras preserved in the 7 m of sediment beneath the Aso-4 layer are compositionally distinct from each other (Fig. 5.8). The SG14-5648 shows an affinity with Aso-I glasses in major element composition (Fig. 5.8D). However, many of the units have not been analysed (Aso-H, Aso-J and Aso-L; Hoshizumi et al., 2022) and it is likely that the SG14-5648 will correlate with one of the units preserved between Aso-3 and Aso-ABCD. Of the six post-Aso-4 cryptotephra deposits identified in this study, glasses from the younger SG14-4032 and SG14-3911 deposits form tight compositional clusters, whilst the others show a greater degree of variability, with the SG14-4135 and SG14-4471 spanning the broadest compositional ranges (Fig. 5.8C). Of the six deposits preserved in Lake Suigetsu between Aso-4 and the ACP4, only one shows potential correlation based on stratigraphic position and geochemistry: the SG014-3911 with the ACP4 (Fig. 5.8C). The ACP4 has previously been reported as a 1 mm thick visible tephra in Lake Suigetsu (SG06-3912; Table 5.2). The two deposits are separated by ~30 cm of sediment. is possible that ACP4 exhibited multiple phases of volcanic activity where magmas of similar composition were erupted, resulting in multiple tephras separated in time. None of the other five newly identified Aso cryptotephra deposits show a geochemical affinity with the Aso units reported for this timeframe (ACP6 and ACP5; Fig. 5.8C).

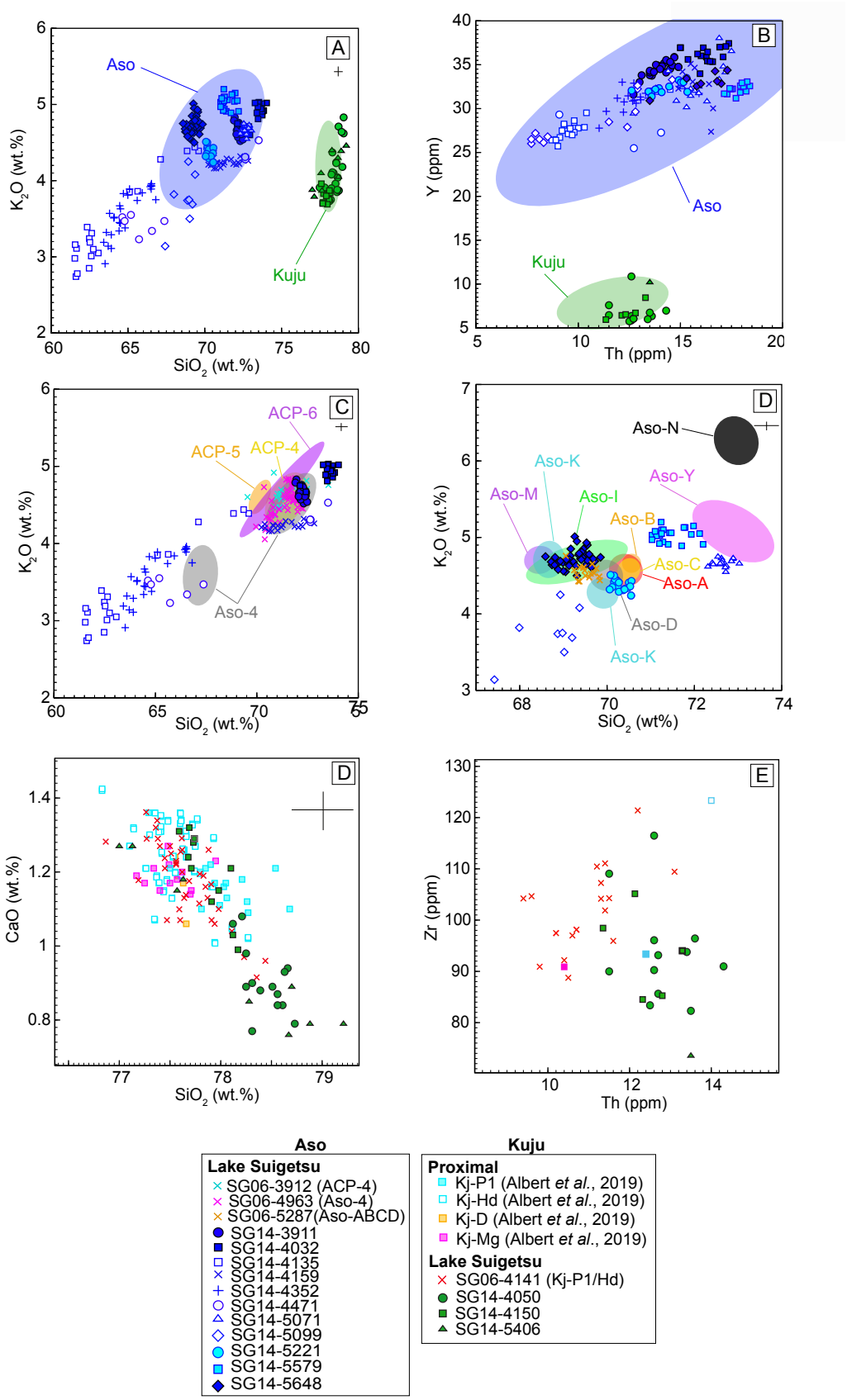


Figure 5.8: Major and trace element compositions of the SG14 crypto-/tephras (~120 – 50 ka) from the CVR. Compositional fields/envelopes for the following volcanic centres are from proximal data presented in previous studies. Data for Aso is from Smith et al., 2013 (Aso-A, Aso-D, Aso-4), Albert et al., 2019a (Aso = ACP-3, ACP-4, ACP-5, ACP-6, Aso-4, Aso-Y,

Aso-A, Aso-B, Aso-C, Aso-D Aso-I, Aso-K, Aso-M, Aso-N, Aso-3), and McLean et al., 2020a (Aso = Aso-Kpfa); and Kuju data arefrom Albert et al., 2019a (Kj-Mg, Kj-D, Kj-P1, Kj-Hd). Error bars represent 2x standard deviation of repeat analyses of the StHs6/80-G MPI-DING standard glass.

Kuju

Three cryptotephra deposits have glass compositions that are consistent with Kuju volcano: SG14-4050, SG14-4150 and SG14-5406, which have ages of 52.2 ± 1.1 ka, 56.2 ± 1.8 ka and 102.1 ± 3.3 ka, respectively (Table 5.2). These deposits demonstrate tightly clustered compositions and overlap with each other on major and trace element compositions (Fig. 5.8A-D). Two Kuju units (Kj-Mg and Kj-Sm) are reported beneath the widespread Ata, as is the SG14-5406 cryptotephra, whilst the Kj-D is found proximally between the Aso-4 and Kj-Hd tephra and in the same stratigraphic position as the SG14-4150 (Fig. 5.2; Table 5.2). Proximally, the Kj-D shows no evidence of being older than Kj-P1/Hd, although we observe 44 cm of sediment (equating to 2.5 kyr) separating the SG14-4150 cryptotephra and the overlaying visible SG06-4124 (Kj-P1/Hd). No prominent Kuju deposits have been reported in near-source sequences in the same stratigraphic position as SG14-4050 (Fig. 5.2). Given the similar geochemical compositions, the cryptotephras cannot be correlated to eruption units, but this provides the first evidence of at least four eruptions at Kuju which have deposited ash-fall as far away as central Honshu, and are geochemically indistinguishable spanning a 50 ka period.

5.6.1.2. Honshu (SWJA, Izu-Bonin Arc and NVZ)

Sambe

The SG14-5367 cryptotephra is preserved 47 cm beneath the visible Ata tephra (SG06-5353; Fig. 5.4) and has a very high shard concentration, with large distinct cuspate and fluted shards containing microvesicles (Table 5.2; Appendix B). These glasses have low Y, Zr, La and Th contents which are typical features of early Sambe activity (Table 5.3; Albert et al., 2018). The SG14-5367 glasses form a tight compositional cluster and show complete geochemical overlap with those from the SK tephra (Fig. 5.9). The SK is considered to be the largest eruption from the Sambe volcano erupting 20 km^3 of tephra and has a proposed age of ~100 ka based on: (1) its stratigraphic position beneath the Aso-4 tephra in marine sediments (102 ka; Sagawa et al., 2018) and (2) radiogenic measurements (100 ± 20 ka, Kimura et al. 1999; 110 ± 14 ka, Shitaoka et al. 2009). The Lake Suigetsu age model provides a date of 100.4 ± 3.1 ka (±1σ) for SG14-5367, which is consistent with the age of ~100 ka the SK eruption and has an easterly dispersal, that fits with it being

preserved in Lake Suigetsu (Fig. 5.1; Table 5.1). Based on the chronostratigraphic position and geochemical compositions, the SG14-5367 is the distal equivalent of the SK eruption. The SK may be a useful marker in terrestrial and marine sequences across Honshu and further afield due to high shard concentrations (Table 5.2; Fig. 5.3).

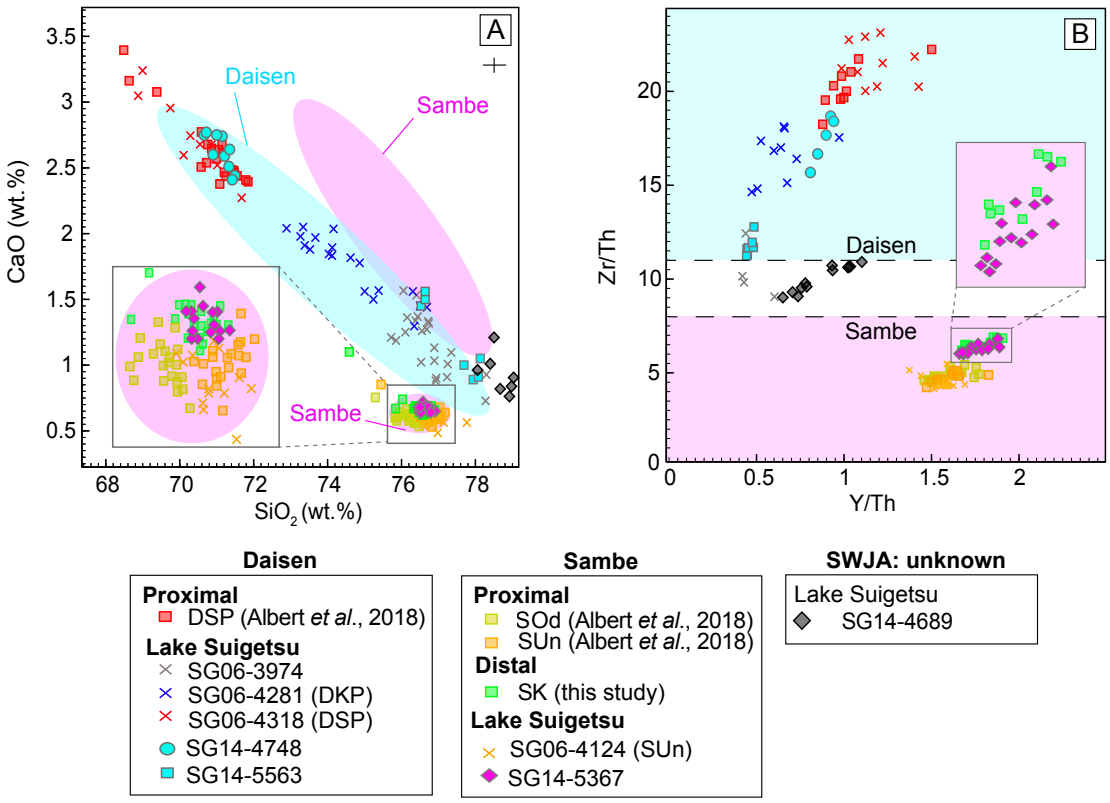


Figure 5.9: Major and trace element compositions of the SG14 cryptotephras (~120 – 50 ka) from the SWJA. Compositional fields/envelopes for the following volcanic centres are from proximal data presented in previous studies. Data for Daisen is from Albert et al., 2018 (DJs, DHg, DSs, DSP); and Sambe data arefrom Albert et al., 2018 (Th-pfl, S2-fl, Kr-fa, Uk-fa, Md-fl, U2, U1, Ht-fl, SI, Ikeda, SuN, Sod) and this study (SK – sampled from Sagawa et al., 2018). Error bars represent 2x standard deviation of repeat analyses of the StHs6/80-G MPI-DING standard glass.

Daisen

Two pumiceous cryptotephra deposits have been attributed to Daisen activity: the SG14-4748 which has an age of 79.3 ± 2.0 ka (±1σ); and the SG14-5563 with an age of 107.6 ± 3.9 ka (±1σ) (Table 5.2). The younger SG14-4748 is clearly from Daisen based on major elements, whilst the more rhyolitic (SiO_2 >76 wt.%) SG14-5563 glasses overlap with the Daisen and Sambe compositional fields (Fig. 5.9A). However, both deposits have >11 Zr/Th ratios, consistent with those from Daisen (Fig. 5.9B; Albert et al., 2018). The SG14-4748 is in the same chrono-stratigraphic position as the prominent DNP eruption unit (between Aso-4 and DSP; Fig. 5.2); however, in the absence of near-source glass chemistry

(see Albert et al., 2018) we can only tentatively correlate this unit to the Daisen eruption deposit. The SG14-5563 is more challenging to correlate. It is chrono-stratigraphically consistent with two older Daisen tephra units below the Aso-4 and SK marker layers, the DHP and DMP units (Fig. 5.2). Without fresh proximal deposits to establish their geochemical signature we are precluded from establishing more precise correlations between the Daisen eruption record and Lake Suigetsu.

Unknown SWJA tephra

The SG14-4689 cryptotephra forms a discrete peak of colourless pumiceous shards, stratigraphically located between the Aso-4 (SG06-4963) and DSP (SG06-4318) tephras in the Lake Suigetsu sediments (Fig. 5.4). The high SiO_2 contents (~77.88 wt.%) and Zr/Th ratios of 9 – 11 mean that these data do not plot precisely within the characterised compositional fields for SWJA, but the cryptotephra likely erupted from one of these sources (Fig. 5.9).

Hakone

The tholeiitic cryptotephras, SG14-5033, SG14-5597 and SG14-5851, are all dacite-rhyolites and are easily distinguished from other cryptotephra analysed in this study owing to low K_2O content (~1 wt.%) and low Th (<2 ppm) contents, and plot within the Izu-Bonin Arc compositional fields (Fig. 5.5 and 5.6). All three deposits show a geochemical affinity with glasses erupted from the Hakone volcano (Fig. 5.10) and are found beneath the Aso-4 marker layer (SG06-4963) and have ages of 89.8 ± 1.6 ka, 108.9 ± 4.0 ka and 117.7 ± 4.9 ka ($\pm 1\sigma$), respectively (Table 5.2). Whilst it is possible to distinguish the SG14-5851 using major element data, all three Hakone derived cryptotephra deposits are indistinguishable at the trace element level (Fig. 5.10). Although the SG14-5033 is in the same stratigraphic position as the only previously reported Hakone tephra between the K-Tz and Aso-4 marker tephras (Hk-Da-5; Fig. 5.2), there are currently no compositional data to test this potential correlation. Similarly, there are eleven Hakone tephras preserved beneath Ata in proximal outcrops (Fig. 5.2) and are likely to correlate with the SG14-5851 and SG14-5597 cryptotephras. The absence of any geochemical characterisation for any pre-50 ka Hakone near-vent units precludes any correlations. However, the glass chemistry of the Lake Suigetsu deposits indicate that the geochemical signatures of successive Hakone eruptions do not vary across at least a 28 kyr period and suggest that proximal glass compositions may not facilitate correlations to particular eruption units.

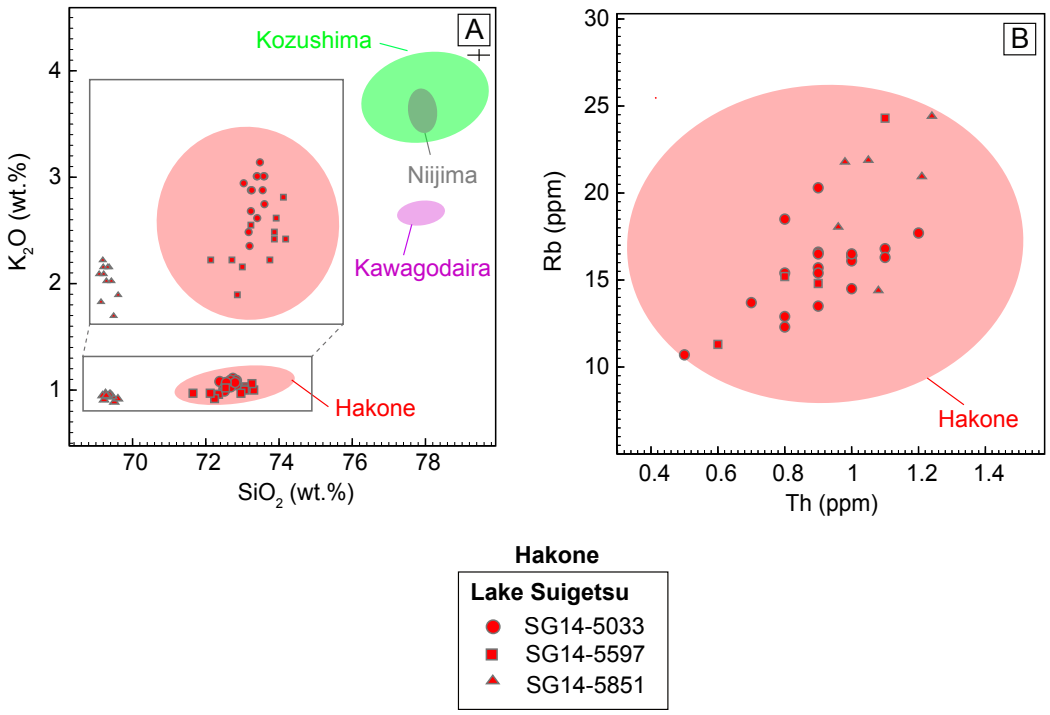


Figure 5.10: Major and trace element compositions of the SG14 cryptotephras (~120– 50 ka) erupted from the Izu-Bonin Arc compared to those of major eruptive centres located on this arc. Compositional fields/envelopes for the following volcanic centres are from proximal data presented in previous studies. Data for Hakone is from Albert et al., 2019a (Tau8); Kawagodaira from McLean et al., 2018 (KGP); Kozushima from Suzuki et al., 2016 (Iz-Kt); and Niijima from Albert et al., 2024 (Nj-Mt). Error bars represent 2x standard deviation of repeat analyses of the StHs6/80-G MPI-DING standard glass.

Ontake

The glasses represented by the SG14-4837 and SG14-4860 cryptotephras have Y and Zr contents typical of those produced from the NVZ (Fig. 5.5, 5.6). Both the SG14-4860 and SG14-4837 cryptotephra deposits are preserved within the ~90 cm of sediment above the Aso-4 tephra (SG06-4963; Fig. 5.4) and have respective ages of 83.0 ± 1.5 ka and 84.1 ± 1.3 ka (Table 5.2). The cryptotephras have high K_2O contents, which are consistent with eruption deposits from the Ontake volcano, although SG14-4860 marginally extends the known SiO_2 compositional range (Fig. 5.11B). The two cryptotephras show overlap with those from Ontake at the trace element level, with the younger (SG14-4837) more enriched in Zr (~35 ppm) relative to the older (SG14-4860) (Fig. 5.11D,E).

We correlate SG14-4837 to the On-Ng eruption of Ontake as the glass compositions and stratigraphic position are in excellent agreement (i.e., located between Aso-4 and DKP; Fig. 5.2, 5.4). This extends the dispersal of this eruption further west than previously reported (see Matsu'ura and Komatsubara, 2024). Using the Lake Suigetsu age model, the

age of the On-Ng tephra is now constrained to 83.0 ± 1.5 ka (±1σ). It is not yet possible to correlate SG14-4860 to specific eruption event of Ontake at ~84 ka (~1 ka prior to On-Ng), but we highlight that trace elements are essential to discriminating this event in other sedimentary records.

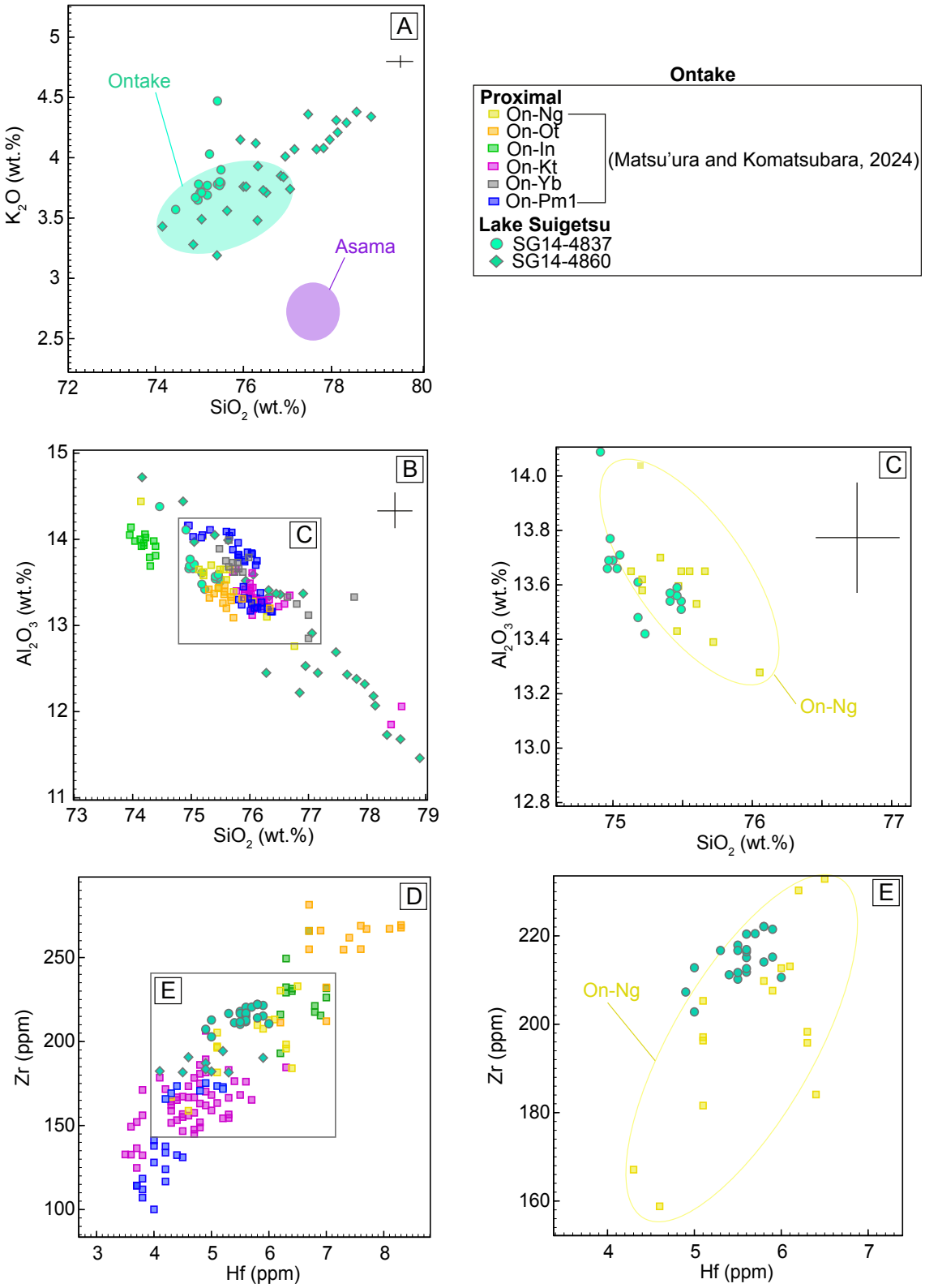


Figure 5.11: Major and trace element compositions of the SG14 cryptotephras (~120 – 50 ka) from the NVZ comparison to those of the major eruptive centres in the region. Compositional fields/envelopes for the following volcanic centres are from proximal data presented in previous studies. Data for Asama is from Albert et al., 2024 (As-K, As-UG, As-YP); and Ontake data arefrom Albert et al., 2019a (On-Pm1) and Matsu'ura and Komatsubara 2024 (On-Ng, On-Ot, On-In, On-Kt, On-Yb, On-Pm1). Error bars represent 2x standard deviation of repeat analyses of the StHs6/80-G MPI-DING standard glass.

5.6.1.3. Honshu/Hokkaido (NEJA and Kurile Arc)

Toya

The SG14-5575 cryptotephra deposit is stratigraphically positioned below two key widespread markers (Aso-4 [SG06-4963] and SK [SG14-5367]; Table 5.2) and has a high shard concentration (Table 5.2). Despite the generally high background concentrations during this period, the SG14-5575 shards were morphologically distinct (i.e., cuspate and fluted) from the two nearby tephras (both within 16 cm; Fig. 5.4).

The glass composition of the SG14-5575 deposit fall within the tight compositional field for the proximally characterised Toya deposit, with low FeO, CaO, high Na_2O, and moderate K_2O contents (Fig. 5.12A; Matsu'ura et al., 2014; Machida and Arai, 2003), but they extend to higher Th and Y contents than previously reported (Fig. 5.12B). Given the excellent chronostratigraphic position and geochemical agreement, SG14-5575 is correlated to the caldera-forming Toya eruption. An age of 108.1 ± 3.9 ka (±1σ) is estimated for the unit based on the Lake Suigetsu age-depth model, which is consistent with previously reported ages for the eruption, yet more precisely constrained (Table 5.1). This occurrence in Lake Suigetsu is the furthest south that the Toya tephra has been identified and extends the dispersal of this large eruption and allows sedimentary archives to be correlated across a wide geographical range (Fig. 5.3).

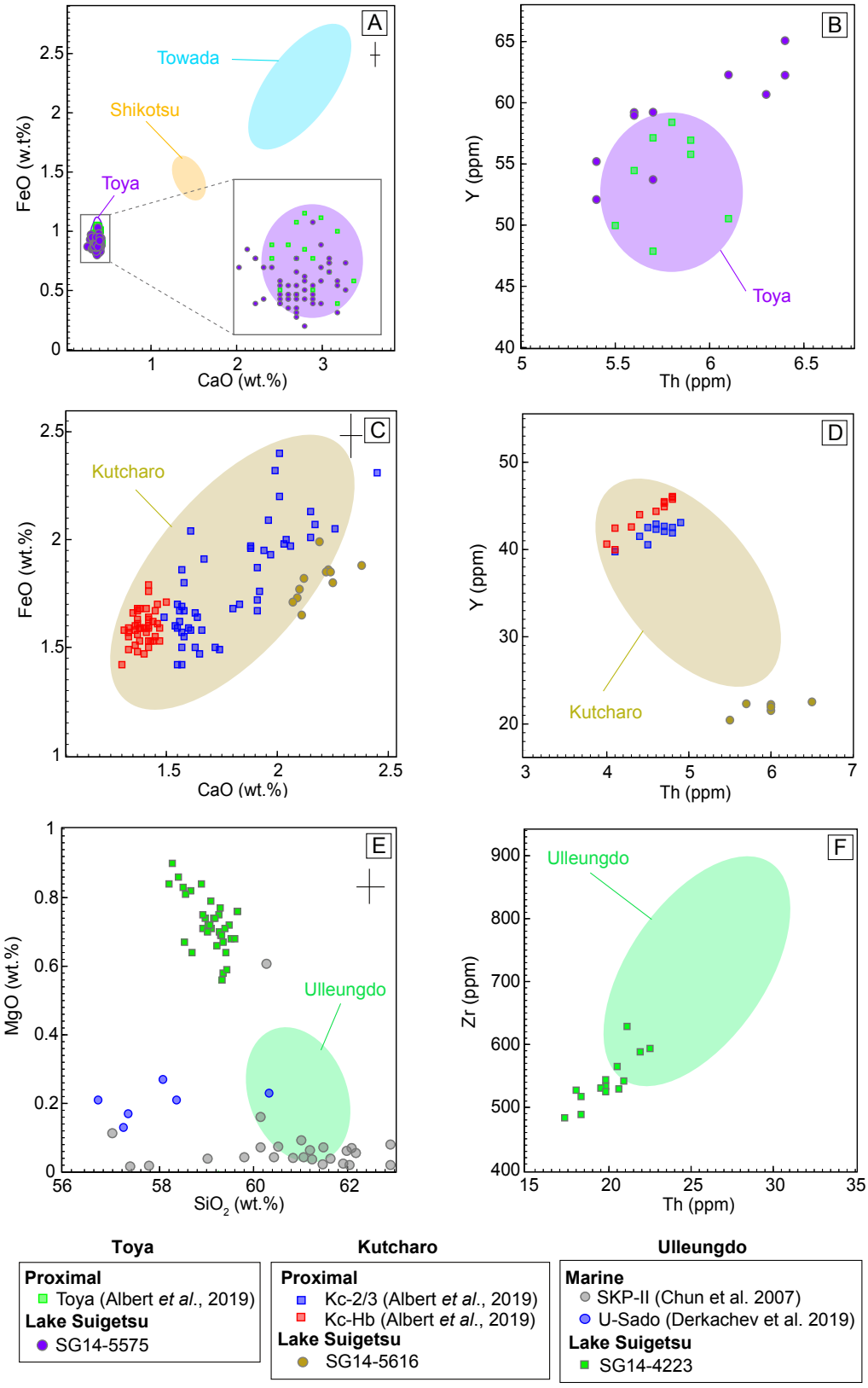


Figure 5.12: Major and trace element compositions of the SG14 cryptotephra deposits (~120 – 50 ka) from the NEJA (A,B), Kurile Arc (C,D) and Intraplate (E,F) volcanoes compared to major eruptive centres located in these regions. Compositional fields/envelopes for the following volcanic centres are from proximal data presented in previous studies. Data for Kutcharo is from Albert et al. (2019a) (Kc-Sr, Kc-2/3, Kc-Hb); Mashu from Albert et al. (2019a) (Ma-f); Shikotsu from Albert et al. (2019a) (Spfa-1); Towada from Albert et al.

(2019a) (To-H); Toya from Albert et al. (2019a) (Toya); and Ulleungdo, including other Lake Suigetsu tephras, is from Smith et al. (2011b)(U4/U-Oki), McLean et al. (2018), Smith et al. (2013) (U1, U2, U-3) and McLean et al., 2020b (U-Ym). Error bars represent 2x standard deviation of repeat analyses of the StHs6/80-G MPI-DING standard glass.

Kutcharo

The SG14-5616 cryptotephra is preserved beneath several widespread markers including Aso-4 and Toya (Fig. 5.4; Table 5.2). It is characterised as a discrete peak in shard concentration relative to the background (Fig. 5.4) and is comprised of shards that are small (40 μm in length), colourless and highly vesicular (Appendix B). Whilst it is challenging to ascribe a volcanic region based on major elements alone (Fig. 5.5), the trace concentrations show a clear affinity to those from the Kurile Arc (Th vs. Y; Fig. 5.6B). The only volcanic centre located along the Kurile Arc known to be active in this timeframe is Kutcharo (Fig. 5.2). Kutcharo produced at least two large eruptions (≥M6.0) at 120 ka (Kc-Hb/4) and 85 ka (Kc-2/3), which are beneath the Aso-4 unit (Fig. 5.2; Table 5.1). The SG14-5616 glasses possess subtly lower FeO_t content at a given CaO content relative to previously characterised Kutcharo tephras (Fig. 5.12C). Furthermore, the SG14-5616 glasses are easily discriminated from both the Kc-Hb/4 and Kc-2/3 glasses at the trace element level as the cryptotephra has much lower Y contents (~20 ppm; Fig. 5.12D) and thus likely represents another Kutcharo eruption at 109.6 ± 4.1 ka. Given the distance to Kutcharo (~1250 km), it is somewhat surprising that the eruption has not been identified in proximal sections, although the eruptive history of Kutcharo is not detailed, and our finding suggests that Kutcharo has had more large eruptions than previously reported.

5.6.1.4. Intraplate

Ulleungdo

The SG14-4223 cryptotephra deposit is stratigraphically preserved between the visible DKP (SG06-4281) and KjP1/Hd (SG06-4141) marker layers in the Lake Suigetsu archive and has a sharp peak in shard concentrations of 5775 shards/gram (Fig. 5.4). The shards are brown and blocky with microlite inclusions (Table 5.2; Appendix B). The glass chemistry of the SG14-4223 deposit is consistent with compositions erupted from Ulleungdo, but this older deposit has lower SiO_2 (~1 wt.%) than the previously reported Ulleungdo deposits (Fig. 5.12E; McLean et al., 2016, 2018, 2020b; Smith et al., 2013). The age for this deposit, based on the Suigetsu age model, is 59.0 ± 2.1 ka (±1σ). Due to its chronostratigraphic position and age, the SG14-4223 cryptotephra could be associated with the U-Sado/SKP-II tephra that has been previously reported in marine records (Fig. 5.3).

However, the SG14-4223 glasses are compositionally different from those units reported from the Sea of Japan with our data exhibiting much higher MgO content (Derkachev et al., 2019; Chun et al., 2007; Fig. 5.12E). These two compositionally distinct units indicate that there were at least two eruptions from Ulleungdo at ~60 ka.

5.6.1.5. Tephra that cannot be attributed to a source

Of the forty-one newly identified deposits, seven cryptotephras could not be correlated to specific arcs or volcanic centres based on their glass chemistry (Table 5.2). Of note is the lowermost (i.e., oldest) tephra identified in this study (SG14-5950), with an age of 121.0 ± 5.2 ka (±1σ), and with the lowest peak shard concentration (250 shards/gram) of any of the isochrons identified (Table 5.2). The glasses exhibit a distinct geochemical composition and only overlap with glasses erupted from the CVR in K_2O content (Fig. 5.5). Nonetheless, the glasses are highly enriched in Nb and Zr, which is indicative of intraplate volcanism (McLean et al., 2020b; Fig. 5.13B). The compositions are not like those erupted from Changbaishan or Ulleungdo which are, consequently, unlikely to represent the source. Jeju island (location shown in Fig. 5.1) was active from at least 88 ka based on $^{40}Ar/^{39}Ar$ dating (Brenna et al., 2015); however, no geochemical data are presently available of the eruption deposits for comparison.

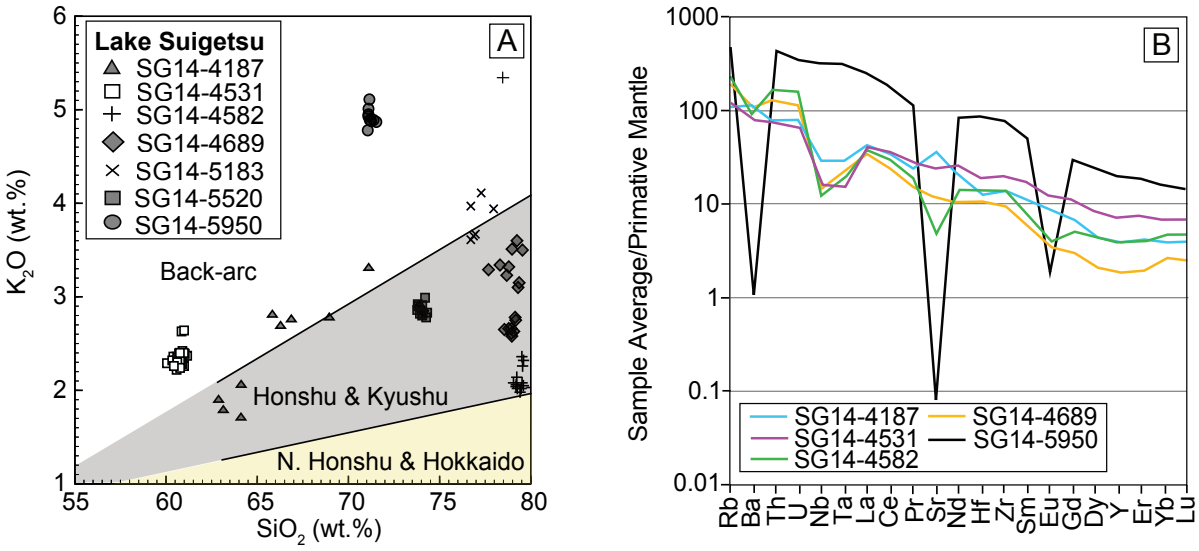


Figure 5.13: **(A)** Glass analyses are plotted on the whole-rock K-classification scheme of Peccerillo and Taylor (1976). The back-arc and intraplate volcanism produces high-K (shoshonitic) compositions, which contrast to the eruptive products from northern Honshu and Hokkaido, which have low-K (tholeiite) compositions. Error bars represent 2x standard deviation of repeat analyses of the StHs6/80-G MPI-DING standard glass. **(B)** Sample-averaged Primitive Mantle normalised trace element compositions of five Lake Suigetsu tephras identified within ~120 – 50 ka sediments which are uncorrelated to specific volcanic

sources. Trace element analyses of SG14-5182 and SG14-5520 could not be obtained due to their small shard sizes and/or abundance of microlite inclusions. Primitive mantle values used for normalisation follow Sun and McDonough (1989).

5.6.2. Identifying volcanic sources and eruptions of the Lake Suigetsu tephra

Of all the deposits preserved in Lake Suigetsu between ~120 and 50 ka, twelve (24%) of the layers identified can be correlated to a specific eruption, thirty-one (62%) are correlated to a volcano but not a particular eruption, three (6%) are correlated to a volcanic region only, and there are four (8%) layers for which the source is ambiguous. The reasons behind this difficulty in attribution are largely due to:

1. A lack of chemical data for various volcanoes and eruptions;
2. Poor eruption stratigraphies near the volcanoes due to burial and erosion, which mean that the volcanoes seem less productive than they have been in reality;
3. Successive eruptions from a particular volcano tapping similar melt compositions over long periods of time (as seen elsewhere, e.g., Campi Flegrei, Italy; Vineberg et al., 2023; Smith, et al., 2011a) so deposits cannot be reliably correlated to a particular event.

These points are discussed further below.

5.6.2.1. Limited glass geochemistry for eruption deposits

The major and trace element analyses of the distal Lake Suigetsu crypto-/tephras have been compared to the extensive glass datasets that have been produced for the East Asian volcanic systems, and supplemented by some proximal samples analysed for this study (Table 5.4). These data show that trace element compositions can help to identify the source of the tephra and reliably correlate the tephra to a particular eruption, especially when the major element compositions overlap. For example, eruption deposits from Ata and Kikai volcanoes share similar major elements but can be easily distinguished using Nb trace element contents (Fig. 5.7). Despite the availability of trace element data, some crypto-/tephras identified still cannot be correlated to particular sources (e.g., SG14-4582 and SG14-5932) as the glass compositions fall outside the currently known ranges for the arc regions and their volcanoes (Fig. 5.5, 5.6). Until these relatively distinct glass compositions are identified in other studies, no firm correlations can be established for the seven tephra layers that have been identified in Lake Suigetsu in the 120 – 50 ka timeframe.

5.6.2.2. Incomplete eruption stratigraphies

The identification of a significant Kutcharo deposit that is chemically distinct indicates that there were at least three eruptions from Kutcharo between 125 and 85 ka. Given that the volcano is located 1250 km northeast of Suigetsu, these eruptions are likely to have been much greater than M5.0. Such large eruptions are almost always preserved in near-vent stratigraphies as the deposits would have been incredibly thick. Nonetheless, only two large eruption deposits have yet been identified near Kutcharo in this time period: Kc-Hb/4 and Kc-2/3 (Hayakawa, 2023; Hasegawa and Nakagawa, 2016; Machida and Arai, 2003). It has been noted elsewhere that some large caldera-forming volcanoes are missing evidence for large magnitude events; e.g., the deposits of the M6.6 Masseria del Monte eruption that is linked to the Y-3 tephra, a widespread tephra layer across the central Mediterranean, are not well preserved close to the source volcano, the Campi Flegrei caldera, as subsequent explosive eruptions have destroyed and buried the deposits, and the proximal unit has only recently been identified (Albert et al., 2019b). It is possible that the more recent Kutcharo eruptions have buried or obscured the evidence for this third large Kutcharo eruption in this period. Cryptotephra analysis of high-resolution distal archives such as Lake Suigetsu provide additional information on these eruption events that appear to be lacking in the geological record (see Hayakawa, 2023). Further cryptotephra studies on other sediment cores should further constrain the explosive eruption history of volcanoes across Japan.

5.6.2.3. Similar melt compositions erupted from a volcano over long periods of time

This cryptotephra study further exemplifies that successive eruption deposits from the same volcano over long periods, 50 kyr in the case for Kuju, are frequently geochemically indistinguishable. The repeated chemistry of tephra deposits from Kirishima over a 19 kyr interval means that those of medium to large eruptions may be miscorrelated, particularly those with similar magnitudes and with poor chronological or stratigraphic control. These similar chemistries provide insight into the magmatic system and indicate that similar processes govern melt formation and evolution over prolonged periods of time. It is surprising that these medium to large eruptions do not show variation in trace element composition, which are particularly sensitive to crystallisation of crystals that would be modified by even subtle changes in the upper crustal architecture of the magmatic system. Due to the similar glass compositions of eruptions, there are periods when the tephra layers cannot be used as isochrons; however, they can still provide chronological constraints, albeit with broad uncertainties.

5.6.3. Tephra dispersal

The crypto-/tephras identified in Lake Suigetsu between ~120 and 50 ka are from at least twelve volcanoes situated across Japan and from intraplate settings to the west of Japan (Fig. 5.14). Unsurprisingly, most of the crypto-/tephras preserved in Lake Suigetsu are from volcanoes that are located southwest of Lake Suigetsu and the volcanic ash is carried by the prevailing westerly winds that are experienced across the full range of latitudes occupied by Japan. These volcanoes are also the main sources of cryptotephras in other sections of the core (Albert et al., 2024; McLean et al., 2018). The furthest known sources are 1250 km from Lake Suigetsu and, given that they are so distal, the tephra deposits would have covered extremely large areas, whilst the closest sources are 225 km away and the cryptotephra deposits associated with these eruptions typically represent eruptions that were considerably smaller (Fig. 5.14). The eruptions that are from sources more than 500 km away are likely to be ≥M5.0, while others from sources in central Honshu could be smaller ≤M4.0 (Sulpizio et al., 2024). However, this not only depends on the magnitude of the eruption but also on the wind directions and wind strength at the time of the eruption. This shows that eruptions of M4.0 and greater deposited ash over the region, which now hosts the densely populated cities of Tokyo, Osaka and Kyoto, every ~1,400 years.

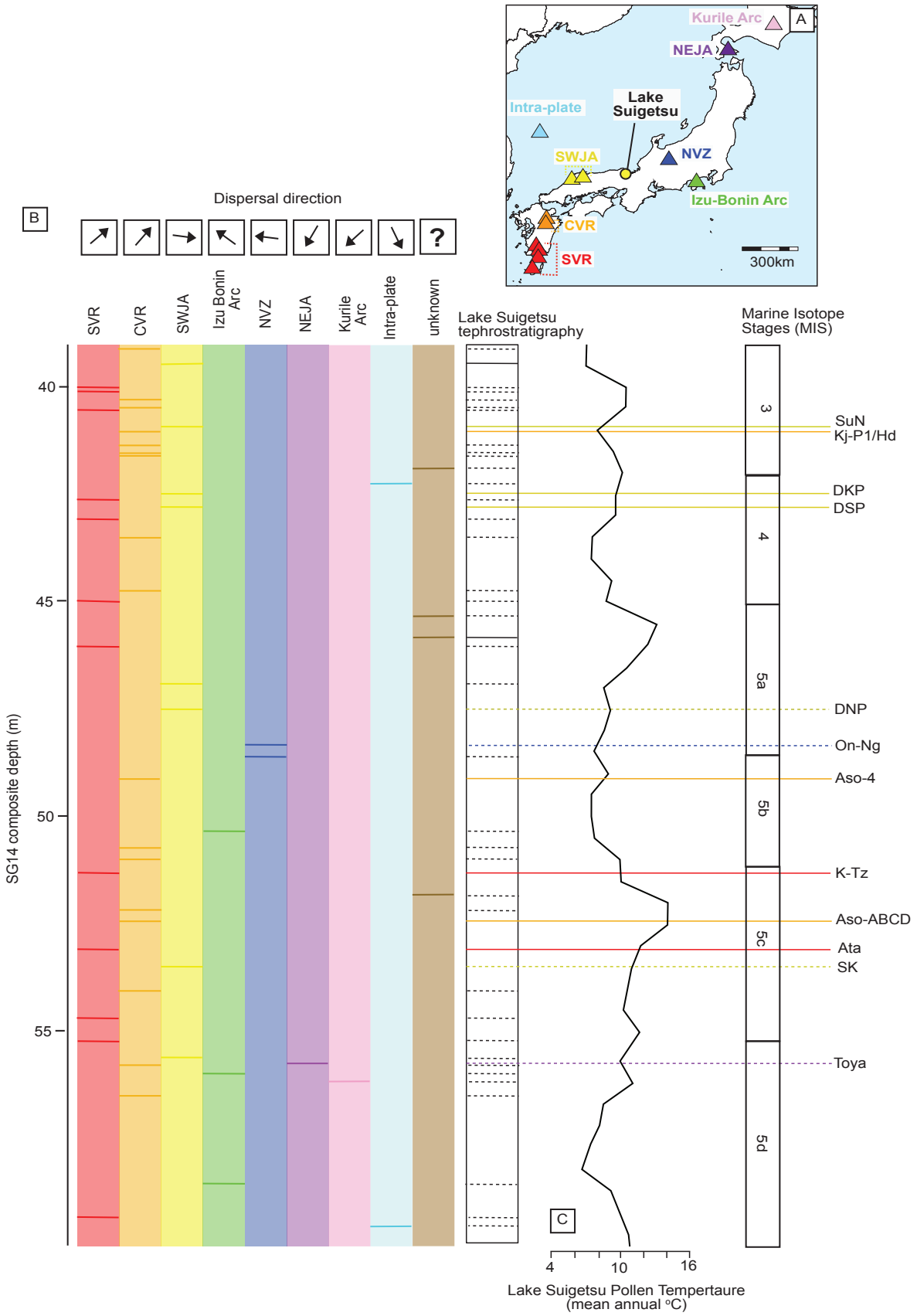


Figure 5.14: (A) Summary of the augmented Lake Suigetsu (SG14) tephrostratigraphy (visible and cryptotephra deposits) spanning ~120 – 50 ka. The distal deposits are correlated, where possible, to their volcanic arcs and specific eruptions using the composition of the volcanic glasses presented in this study. (B) Map showing the location of

the eight volcanic regions where deposits have been identified. (C) SG14 tephra layers plotted against the Lake Suigetsu pollen-based, mean 100 yr moving average, annual temperature reconstruction following on from the work of Nakagawa et al. (2021).

Based on the isopach maps produced by Machida and Arai (2003), the crypto-/tephra preserved in Lake Suigetsu are consistent with recorded thicknesses in the vicinity. In addition, where the identified deposits have not been observed in exposures near Lake Suigetsu, the layers are only present as cryptotephras, highlighting the reliability of the isopachs of Machida and Arai (2003). A great example is the isopach for the SK eruption from Sambe, which shows that dispersal was restricted to a tight ellipse extending northeast of the volcano with visible layers not observed as far east as Lake Suigetsu. In the Lake Suigetsu core, this SK tephra is only preserved as a cryptotephra (Fig. 5.4). In addition, the large caldera-forming Toya eruption has a broad and roughly circular isopach that testifies to weak winds during the eruption; the visible tephra layer had only been recorded as far south as ODP1150A (370 km SW from Toya) as a cryptotephra (see Matsu'ura and Komatsubara, 2024). The identification of Toya in Lake Suigetsu greatly increases the known dispersal of the eruption.

Key Japanese volcanic events missing from the Lake Suigetsu record include the A-Iw and Kc-2/3. Although eruptions were ≥M6.0, their ash dispersals were away from Lake Suigetsu. The A-Iw was dispersed to the east, whilst the was Kc-2/3 dispersed to the north-northeast (Table 5.1) and thus, it is unsurprising that no ash is preserved in Lake Suigetsu. Based on Sea of Japan tephra records, there are three eruptions from Changbaishan between around 86 and 50 ka (Lim et al., 2013; Ikehara et al., 2004). None of these eruptions are recorded in Lake Suigetsu, suggesting that the dispersal trajectory did not extend over southern Honshu and possibly lower magnitude than the 946 CE Millennium eruption, which is found as a very thin visible tephra layer in the uppermost metre of Suigetsu sediment (McLean et al., 2016). We surmise that if the isopachs show strong directionality, typically associated with strong winds, and directed away from Suigetsu, it is incredibly unlikely that the tephra will be preserved as even a cryptotephra.

This section of the high-resolution Lake Suigetsu record spans three MIS intervals (~70 ka; Fig. 5.14) and ideal for investigating relationships between volcanism and climate (Aubry et al., 2022 and references therein). However, no clear relationships in frequency or direction of ash dispersal are observed (Fig. 5.14). Although this study helps to understand the pacing of explosive volcanism from many volcanoes, its distal location relative to the

volcanoes means that it is highly unlikely to have captured all events and, thus does not provide a complete record to interrogate questions related to climate.

5.6.4. Widespread markers for tephra correlation

The presence of the Toya caldera-forming eruption (SG14-5575) and the SK tephra from Sambe (SG14-5367) expand the geographical limits of ash-fall events and can thus be used over wide areas to synchronise records in MIS 5d and MIS 5c, respectively. These marker layers could be used for the correlation of paleoenvironmental records, such as the two marine cores in the Pacific (OC9001C and ODP1150A) and the U1427 located in the Sea of Japan which all contain the SK tephras (Fig. 5.3; Matsu'ura and Komatsubara, 2024; Sagawa et al., 2018). Records that contain both Toya and SK can be used to examine the transition between these two stages, allowing an assessment of whether there is any temporal asynchrony. The Lake Suigetsu age model provides ages of 100.4 ± 3.1 ka (±1σ) and 108.2 ± 3.9 ka (±1σ) for the SK and Toya eruptions, respectively (Table 5.2). These are consistent with previous estimates. Twelve key widespread tephra layers have now been documented in Lake Suigetsu between 120 and 50 ka which will be invaluable in the correlation of the Lake Suigetsu to others (Fig. 5.14C).

5.7. Conclusions

The detailed cryptotephra investigation through the Lake Suigetsu sediments spanning ~120 to 50 ka and the resultant identification of numerous tephra layers provides important insight into the dispersal and tempo of East Asian volcanism. An additional forty-one crypto-/tephra deposits are identified in this timeframe, which is four times as many layers preserved as cryptotephra compared to visible layers. The geochemistry of the glass shards has enabled most of these distal tephra deposits to be correlated to their volcanic regions/arcs in Japan, and many correlations can be made to a specific volcano and a few to known eruption events. Twenty-seven of the tephras are from eruptive centres southwest of Lake Suigetsu, which is unsurprising given the prevailing westerly winds. The tephra record provides the first evidence for an intense period of explosive activity from Kirishima with five widespread ash dispersals between 69.7 ± 2.4 (±1σ) and 50.5 ± 0.5 ka (±1σ). In addition, the records indicates that tephra from calderas on Hokkaido (~1000 km away) have reached central Honshu (e.g., Kutcharo). Our findings significantly extend the ash dispersal for several known key Pleistocene marker layers, including the Toya ash, which is now

identified 950 km from its source, making it one of the most widespread Japanese isochrons. By conducting this detailed cryptotephra investigation we highlight that distal archives can greatly assist in constraining and augmenting the proximal stratigraphies of many of the productive Japanese volcanic centres.

CRediT **author statement**

S.O.V.: Conceptualisation; Resources; Data Collection; Methodology; Investigation; Formal analysis; Visualization; Writing-Original Draft; Writing-Review & Editing; Funding acquisition. **P.G.A.:** Conceptualisation; Resources; Data Collection; Writing-Review & Editing; Supervision; Funding acquisition. **D.M.:** Conceptualisation; Data Collection; Writing-Review & Editing; Supervision. **T.S.:** Resources; Writing-Review & Editing. **R.S.**: Formal analysis; Writing-Review & Editing. **K.Y.:** Data Collection. **I.K.**: Data Collection. **J.K.:** Resources. **C.J.M.**: Resources. **H.M.B:** Data Collection. Resources. **G.J.:** Resources. **F.N.:** Resources. **SG14 Project Members:** Resources. **T.N.:** Resources; Data Collection; Writing-Review & Editing; Funding acquisition. **V.C.S:** Conceptualisation; Resources; Data Collection; Writing-Review & Editing; Supervision; Funding acquisition.

Acknowledgements

S.O.V. is funded by NERC as part of the Environmental Research Doctoral Training Programme at the University of Oxford (NERC; NE/S007474/1). VCS and TN acknowledge funding from the Japan Society for the Promotion of Science (JSPS; KAKENHI-15H021443). The SG06 coring campaign was funded by the UK Natural Environmental Research Council (NERC; NE/ D000289/1) New Investigators Award to TN. The Fukui-SG14 coring campaign was funded by the Fukui Prefectural government, Japan. P.G.A., H.M.B and G.J. are funded through a UKRI Future Leader Fellowship award (FLF; MR/S035478/1). TS acknowledges funding from the Japan Society for the Promotion of Science (JSPS; KAKENHI-22H02380). FN acknowledges funding from the Japan Society for the Promotion of Science (JSPS; KAKENHI-JP19K13438.The Lake Suigetsu coring was conducted by the team of Seibushisui Co. Ltd Japan, led by Mr Atsumi Kitamura. This research used samples provided by the International Ocean Discovery Program (IODP), and we thank Dr Yusuke Kubo (IODP) Curator and the KCC (Kochi Core Center) for assistance with the sampling. We thank Giovanni Zanchetta, Sabine Wulf and an anonymous reviewer for their comments.

See Appendix B for Supplementary Material.

Chapter 6: Revealing the timing and dispersal of large explosive eruptions at Aso volcano (Japan) by integrating proximal and distal tephra records following the Aso-3 eruption

Sophie O. Vineberg[a], Paul G. Albert[b], Danielle McLean[a], Takehiko Suzuki[c], Yasuo Miyabuchi[d], Hideo Hoshizumi[e], Hannah M. Buckland[b], Gwydion Jones[b], Fumikatsu Nishizawa[f], Richard Staff[a,g], Keitaro Yamada[h], Ikuko Kitaba[i,], Junko Kitagawa[k], Christina J. Manning[l], SG14 Project Members[m], Takeshi Nakagawa[i] and Victoria C. Smith[a]

[a] Research Laboratory for Archaeology and the History of Art, School of Archaeology, University of Oxford, Oxford, OX1 3TG, UK
[b] Department of Geography, Swansea University, Swansea, SA2 8PP, UK
[c] Department of Geography, Tokyo Metropolitan University, Tokyo, 192-0397, Japan
[d] Centre for Water Cycle, Marine Environment and Disaster Management, Kumamoto University, Kurokami Chuo-ku Kumamoto 860-8555, Japan
[e] AIST, Geological Survey of Japan
fKanagawa Prefectural Museum of Natural History, Odawara, 250-0031, Japan
[g] Scottish Universities Environmental Research Centre, University of Glasgow, East Kilbride, G75 0QF, UK
[h] Institute for Geothermal Sciences, Kyoto University, Kyoto, 606-8224, Japan
[i] Research Centre for Paleoclimatology, Ritsumeikan University, Kusatsu, Shiga, 525-8577 Japan
[j] Fukui Prefectural Satoyama-Satoumi Research Institute, Wakasa, 919-1331 Japan
[k] Varve Museum, Wakasa, Fukui, 919-1331, Japan
[l] Department of Earth Sciences, Royal Holloway, University of London, Egham, Surrey, TW20 0EX, UK
[m] www.suigetsu.org

Highlights

- Comprehensive glass geochemical dataset for twenty silicic Aso tephra layers between ~130 – 30 ka.
- Ten Aso tephras can be correlated to tephra layers in the high-resolution Lake Suigetsu record.
- 400 years repose between the lower and upper phases of the ACP4 eruption.
- Aso produced at least four large explosive eruptions in the 10 kyr prior to the Aso-4 eruption.
- 5 kyr elapsed between the large Aso-4 and Aso-4X eruptions.

Key words: Aso, Aso-4, Geochemistry, Cryptotephra, Tephra, proximal-distal

Abstract

The Aso caldera in central Kyushu, SW Japan, is one of the largest and most active volcanoes in the world. The Aso system has experienced four caldera-forming eruptions (Aso-1 to -4) and inter-caldera activity from multiple central cones. This study provides detailed glass geochemistry of many previously uncharacterised, proximally preserved, pre-30 ka Aso units so that they can be correlated to layers in distally located records. In particular, the high-resolution Lake Suigetsu record, to better constrain the eruption frequency, chronology and dispersal of the Aso eruptions. This study contributes an extensive glass chemistry dataset of twenty eruption units between 130 ka and 30 ka. The glass chemistry of these large Aso eruptions typically straddle the trachy-dacitic to rhyolitic compositional boundary, with the exception of YmP7 and YmP6 which are trachy-andesites. Many of the units can be distinguished from each other using major (SiO_2, K_2O, CaO and FeO) and trace (Th and Sr) element compositions. The new proximal glass dataset has facilitated the correlation of a further seven tephra layers in the Lake Suigetsu record that is located 525 km away. Eleven of the twenty deposits in the Lake Suigetsu core with Aso glass compositions have now been correlated to particular eruption units and include: a post Aso-Kpfa ash, Aso-Kpfa, ACP4, ACP6, YmP5, Aso-4, Aso-4X, Aso-ABCD, Aso-EF and Aso-HI. Significantly, the identification of these tephra deposits in Lake Suigetsu provides better ages for many of these eruptions, and constrains repose periods between eruptions to 400 years between the two phases of ACP4 activity, and 5 kyr between the Aso-4X and Aso-4 caldera-forming eruption. This investigation reveals that there are seven eruption deposits in the Lake Suigetsu record that have not yet been identified in the exposed near-vent sequences, suggesting Aso has been more active than previously thought. This research demonstrates the merit of integrating the proximal-distal records for understanding of the timing and ash dispersals of pre-historic eruptions.

6.1. Introduction

Large explosive caldera-forming eruptions (i.e. those with volcanic explosivity index [VEI] or Magnitude [M] ≥6; Pyle, 2000; Newhall and Self,1982) have significant effects associated with the widespread ash-fall, voluminous ignimbrites, and landscape modification from the caldera collapse. Tephras erupted during such large eruptions are incredibly widespread, travelling 1000s km from vent and form key chronostratigraphic markers in the sediments in which they deposit. Once identified and geochemically characterised, these aid in the synchronisation and chronology of sedimentary sequences across large geographical areas (e.g. Davies et al., 2024; McLean et al., 2018, 2016; Sun et al., 2014; Lane et al.,

2013; Wulf et al., 2012). Accurately reconstructing the eruption histories at such volcanoes is an essential component of risk and hazard assessments. Whilst near-vent (proximal) eruption sequences are fundamental to the reconstruction of past volcanic histories by providing stratigraphic, chronological and geochemical constraints, they are often destroyed and/or buried by voluminous eruption deposits from caldera-forming events. Distal sedimentary archives (e.g. lacustrine and marine cores) overcome such preservation and accessibility issues and not only contain tephra deposits associated with the largest eruptions, they also often provide a record of small- and medium-sized eruptions (e.g. McLean et al., 2020a; Wutke et al., 2015; Bourne et al., 2010). Only once detailed geochemical characterisation of the corresponding proximal units are obtained, can these distal records be used to gain greater insights into tempo, frequency and repose periods (e.g. Campi Flegrei; Vineberg et al., 2023; Albert et al 2019b). Integration of the proximal-distal records is key to developing accurate tephrochronological frameworks of volcanic systems.

Volcanoes distributed across the heavily populated East Asian/Pacific region have been the source of some of the largest known caldera-forming events in the past 200 ka, blanketing Japan and the surrounding seas in ash (e.g. McLean et al., 2020a; Mahony et al., 2016; Schindlbeck et al., 2018; Smith et al., 2013; Machida and Arai, 2003). Furthermore, the high degree of urbanisation, strong seasonality and dense vegetation in less developed areas in Japan means only fragmentary eruption records are typically preserved/accessible at near-vent sites, hampering our ability to accurately reconstruct eruption histories. The Lake Suigetsu sedimentary archive (Fig. 6.1C) provides a key tephro-stratotype of explosive events for Japan (e.g., Vineberg et al.,2024; Albert et al., 2019a, 2024; McLean et al., 2016, 2018, 2020a, 2020b; Smith et al., 2013) and the unique high-precision chronology (e.g., Bronk Ramsey et al., 2012, 2020; Schlolaut et al., 2012; 2018) has created a strong chronostratigraphic control for the last 50 kyr. Eruption deposits associated with caldera-sized eruptions from volcanic systems located across the three main islands of Japan (Fig. 6.1A) have been identified throughout the ~200 kyr sediments of Lake Suigetsu as both visible tephra and non-visible tephra (cryptotephra) e.g. Ma-b, B-Tm, AT, Aso-4; K-Tz; Ata, Toya (Vineberg et al., 2024; Albert et al., 2019a; McLean et al., 2018; Smith et al., 2013). The preservation of cryptotephra deposits throughout the sequence has revealed events from these caldera systems (most notably Aso volcano) which have not been identified or characterised from the proximal realm (see: Vineberg et al., 2024; McLean et al., 2020a).

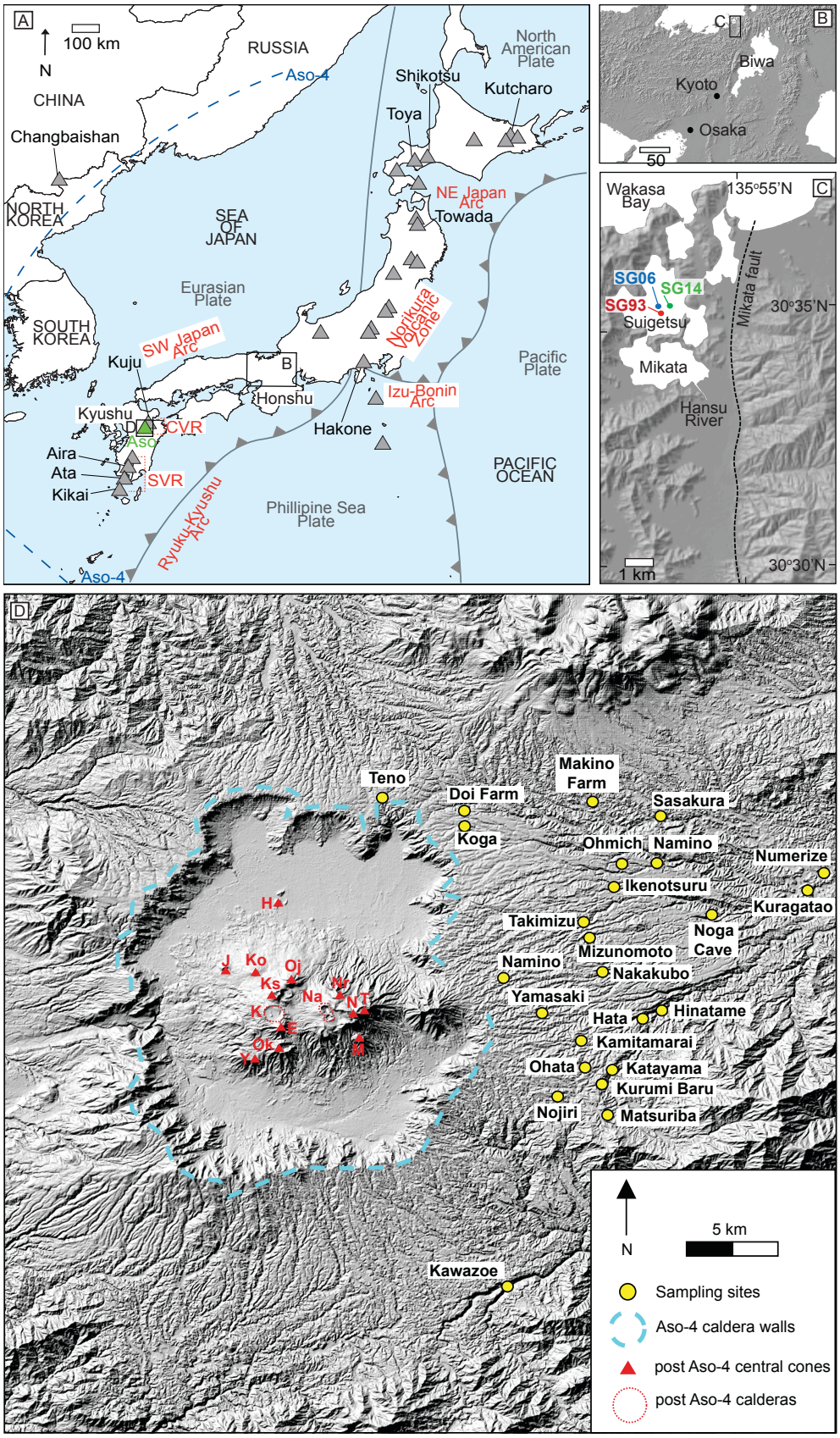


Figure 6.1: (A) Volcanoes (grey triangles) that have been active in and around Japan in the Quaternary. The Aso caldera is shown by a green triangle. The blue dashed line denotes the ash dispersal boundaries for the Aso-4 eruption which is from (Machida, 2002). The red

labels are the volcanic arcs: SVR = Southern Volcanic Region; CVR = Central Volcanic Region; SWJA = South West Japan Arc; NVZ = Norikura Volcanic Zone; NEJA = North East Japan Arc. (B) Proximity of Lake Suigetsu to Lake Biwa and major Japanese cities. (C) Location of Lake Suigetsu as part of the five Mikata Lakes, adjacent to Wakasa Bay. The positions of all three coring campaigns are marked (b and c modified after (Nakagawa et al., 2005). (D) Locations of stratigraphic sections discussed in this study (yellow circles). Blue dashed line denotes the Aso-4 caldera walls. Red triangles show peaks of the post Aso-4 central cones of Aso volcano: E: Eboshidake, J: Janoo, Ko: Komezuka, Ks: Kishimadake, M: Maruyama, N: Nakadake, Nr: Naraodake, Oj: Ojodake, Ok: Okamadoyama, T: Takadake, Tb: Takanoobane, Y: Yomineyama. Red dashed lines denote caldera walls from post Aso-4 central cone eruptions: K: Kusasenrigahama crater, Na: Nakadake caldera.

The Aso volcano, part of the Central Volcanic Region (CVR) located on Kyushu Island in the southwestern Japan Arc (Fig. 6.1A), is one of the most hazardous volcanic systems on Earth and is one of the most active volcanic complexes in Japan. The Aso caldera is 25 km wide north–south and 18 km east–west (Fig. 6.1D), and was formed and modified by four gigantic pyroclastic-flow eruptions (M 8) from ca. 270 – 90 ka and produced >850 km^3 of total deposits, including hundreds of cubic kilometres of pyroclastic deposits (e.g., Kaneko et al., 2015; Ono et al., 1985). The M 7.8 Aso-4 eruption is the most recent caldera-forming event and is dated to 86.4 ± 1.1 ka ($^{40}Ar/^{39}Ar$; Albert et al., 2019a), falling within Marine Isotope Stage (MIS) 5b (Aoki et al., 2008). The Aso-4 eruption produced 600 km^3 tephra volume and provides a key widespread tephrostratigraphic marker that is found interbedded within the eruption stratigraphies of other volcanic systems (e.g. Albert et al., 2018; Matsu'ura et al., 2014; Machida and Arai, 2003; Nagaoka et al., 2001) and is frequently identified in marine and terrestrial sedimentary records across East Asia (e.g. Matsu'ura and Komatsubara, 2024; Derchachev et al., 2019; Sagawa et al., 2018; Lim et al., 2014; Smith et al., 2013; Nagahashi et al. 2004). Near-vent eruptive stratigraphies associated with air fall tephra deposits from Aso are predominantly preserved and identified to the east of the caldera wall, interbedded between the ignimbrite deposits associated with caldera-forming events. Detailed tephrostratigraphic frameworks have been developed for the eruption units spanning approximately the last 135 kyr (e.g., Hoshizumi et al., 2022; Miyabuchi, 2011, Miyabuchi, 2009; Ono and Watanabe 1983; Ono, 1977). However, the lack of detailed geochemical characterisation of these units has prevented them being correlated across greater geographical areas. For instance, twenty volcanic deposits (four visible tephras and sixteen cryptotephras) have been identified in the Lake Suigetsu sediments spanning 120 – 30 ka, and geochemically correlated to Aso as their volcanic source (Vineberg et al., 2024; McLean et al., 2020a; Albert et al., 2019a; Smith et al., 2013). Only four of these deposits have been correlated to their proximal counterpart and thus, a particular eruption unit. These correlations between to Lake Suigetsu have constrained the ages of the following eruption deposits: Aso-Kpfa (SG14-2752; 32,512 ± 271 cal. BP;

McLean et al., 2020a), ACP4 (SG06-3911; 49,893 ± 668 cal. BP; Albert et al., 2019a) and Aso-ABCD (SG06-5287; 97.9 ± 6.0 ka; Smith et al., 2013; Albert et al., 2019a).

This study provides detailed geochemical characterisation of many of the previously uncharacterised proximally preserved Aso units to facilitate integration of proximal and distal records. In particular, this study aims to link Aso tephra preserved within the Lake Suigetsu record to particular eruptions to better constrain the eruption frequency, chronology and the dispersal of the Aso eruptions. All the Aso derived deposits preserved in Lake Suigetsu are preserved beneath the widespread Aira Tn ash (AT; Machida and Arai, 2003, 1983) at 30,078 ± 96 cal. BP (Albert et al., 2019a; Smith et al., 2013) that erupted from the Aira caldera located 200 km south of Aso. Whilst Aso eruption deposits have been identified above the AT ash in proximal sequences (see Miyabuchi, 2011), they have not been identified in Lake Suigetsu (see: Albert et al., 2024, 2019a; McLean et al 2018; Smith et al., 2013). Here we focus on the chemical characterisation of deposits associated with large explosive eruptions from Aso, as they are most likely to produced widespread ash dispersals, and potentially extended to Lake Suigetsu >500 km away (Fig. 6.1A). Consequently, our sample set is focused on the thickest units (>1 m around the vent) recorded in the relevant timeframe (135 – 30 ka), these typically correspond to the more silicic pumiceous eruption deposits, which are also better preserved in the near-source record, where more mafic, scoriaeous eruptions units have become heavily weathered (Miyabuchi, 2011).

6.2. 30 – 135 ka Aso eruption history

Here we outline the physical and, where applicable, the geochemical features of many of the fifty-six silicic tephras erupted from Aso between the Aso-3 (~123 – 135 ka; see below) and AT marker beds (Table 6.1) preserved in proximal outcrops to the east and north-east of the Aso caldera wall (Fig. 6.1D). It is from these outcrops we have sampled for geochemical data. All reported volumes are tephra volumes. For more detailed descriptions of the following units, and other mafic units, the reader is directed to Chapter 3.

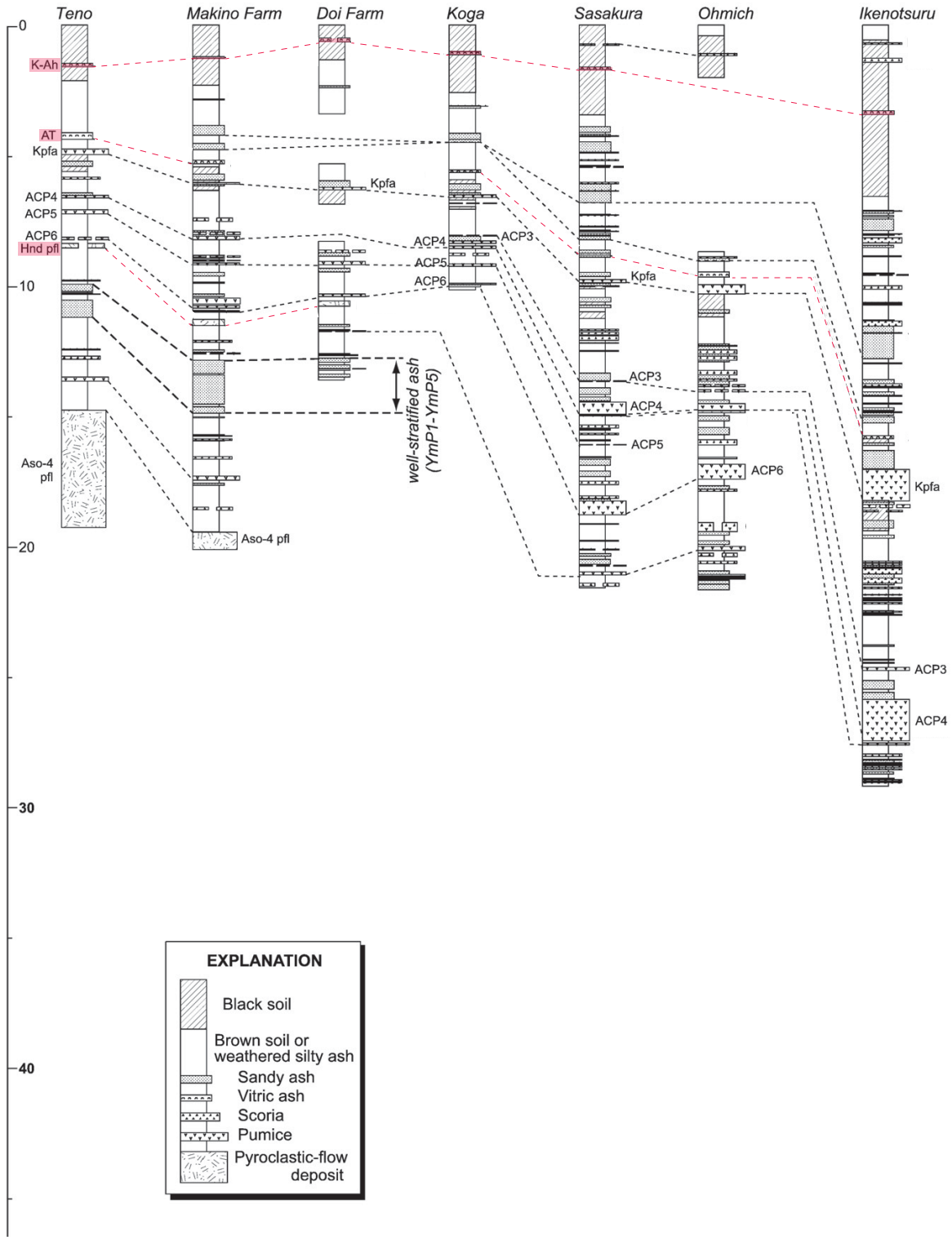
Table 6.1: Explosive eruptions defined from exposures around Aso volcano between Aso-3 and the AT (Aira). Dispersal and tephra volume estimates are from Machida and Arai (2003) and the LaMEVE database (Crosweller et al., 2012; and references therein). The magnitude (M) of each eruption has been calculated using the published tephra volumes and the equation of Pyle (2000), assuming a magma density of 2300 kg/m^3 and tephra density of 1000 kg/m^3. * indicates $^{40}Ar/^{39}Ar$ age. Eruption age references are as follows: a: Albert et al. (2019a); b: Miyabuchi (2009); c: Hoshizumui et al. (2022) d: Machida and Arai (2003); e: Kaneko et al. (2015).

Stage of activity	Eruption	Tephra	Previous correlation in Lake Suigetsu	Magnitude	Tephra Volume (km3)	Dispersal	Age
Post-caldera	Aso-Kpfa	Aso-Kpfa	SG14-2752	-	2.21	E and S	30,164 ± 217[a]
	ACP-3	ACP-3	-	-	0.07	ENE	>Aso-Kpfa;<ACP4
	ACP-4	ACP-4	SG06-3912	4.6	0.43	NE	49,974 ± 33[a]
	ACP-5	ACP-5	-	4.2	0.15	NE	>ACP4; <ACP6
	ACP-6	ACP-6	-	4.3	0.21	NE	~60[b]
	YmP-1-13	YmP-1-13	-	-	-	ESE - ENE	>ACP6; <NjP
	NjP	NjP	-	-	-	SE	84[b]
Aso-4	Aso-4	Aso-4	SG06-4963	7.8	600	-	86.4 ± 1.1[a]*
	Aso-4X	Aso-4X	-			-	>Aso-4; <Aso-Y
Stage 5	Aso-Y	Aso-Y	-	4.0	-	ENE	91.4[c]
Stage 4	Aso-ABCD	Aso-A	SG06-5287	5.0	8.10	ENE	97.9 ± 6.0[a]
		Aso-B					
		Aso-C					
		Aso-D					
	Aso-EF	Aso-E	-	-	1.70	-	99.2[c]
		Aso-F					
	Aso-G	Aso-G	-	-	0.40	-	100.5[c]
	Aso-G'	Aso-G'	-	-	1.00	-	101.2
	Aso-HI	Aso-H	-	5.0	5.00	ENE	102.6[c]
		Aso-I					
	Aso-JKL	Aso-J	-	5.0	2.10	ENE	103.3[c]
		As-K					
		Aso-L					
	Aso-M	Aso-M	-	5.0	2.50	ENE	104.7[c]
Stage 3	Aso-Z1-9	Aso-Z1-9	-	-	0.40 (total)	-	108.4 - 105.0[c]
Stage 2	Aso-10-26	Aso-10-26	-	-	1.20 (total)	-	114.1 - 108.4[c]
Stage 1	Aso-27-29	Aso-27-29	-	-	0.40 (total)	-	133.0 - 114.1[c]

6.2.1. Post-Aso-4

Post-caldera cones have developed near the centre of the caldera since the Aso-4 eruption (Ono and Watanabe, 1985). The total thickness of fallout tephra deposits after the Aso-4 eruption reaches about 100 m on the eastern caldera rim (Watanabe and Fujimoto, 1992). Nineteen silicic pumice- and ash-fall deposits have been reported in proximal

sequences between the Aso-4 and AT eruptions (Table 6.1). Five of these post-caldera units (ACP3, ACP4, ACP5, ACP6 and Aso-Kpfa) have been geochemically analysed from sections east of the caldera wall (see McLean et al., 2020a; Albert et al., 2019a). The ACP3 glasses were easily distinguished at the major element level due to higher SiO_2 content than the post-caldera units previously analysed (McLean et al., 2020a; Albert et al., 2019a). The ACP4 can be distinguished from the ACP3, ACP5 and ACP6 units as the ACP4 has subtly higher SiO_2 content and offset to higher Y content at a given Th content (Albert et al., 2019a). While the older ACP5 and ACP6 tephras show considerable geochemical overlap with each other and with the younger Aso-Kpfa at the major element level, making it difficult to distinguish them on geochemical data alone (McLean et al., 2020a; Albert et al., 2019a).


Teno
Makino Farm
Doi Farm
Koga
Sasakura
Ohmich
Ikenotsuru
0
10
20
30
40
K-Ah
AT
Kpfa
ACP4
ACP5
ACP6
Hnd pfl
Aso-4 pfl
well-stratified ash (YmP1-YmP5)
ACP3
EXPLANATION
Black soil
Brown soil or weathered silty ash
Sandy ash
Vitric ash
Scoria
Pumice
Pyroclastic-flow deposit

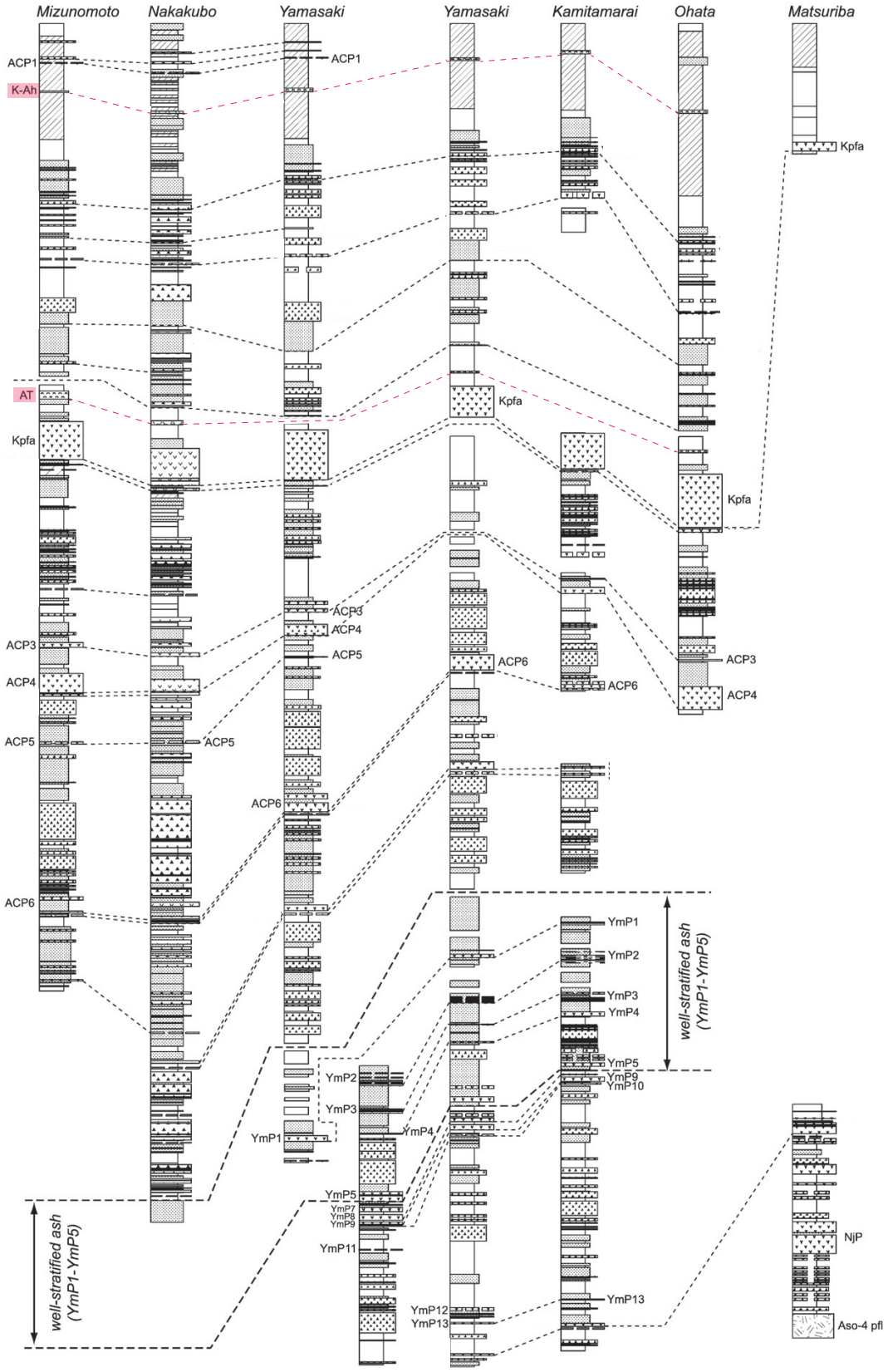


Figure 6.2: Post-Aso-4 stratigraphic relations of silicic Aso tephras. Key marker beds from other volcanic centres are highlighted red. Figure adapted from Miyabuchi (2009)

There are several minor scoria-fall deposits interspaced by weathered ash and soil between the Aso-4 and the Nojiri pumice (NjP) (Matsuriba; Fig. 6.2). The NjP is the first thick tephra deposit identified beyond the caldera-walls following the Aso-4 eruption and consist of extremely weathered pale-yellow pumice clasts, it is divided into a lower and upper parts by an olive-brown 10 cm thick silty ash (Miyabuchi, 2009). It is considered one of the largest eruption events to have occurred at the post-Aso central pumice cones (VEI 4 – 5) and is distributed along a SE-trending axis owing to its thickness (1.3 m) at Matsuriba located 6 km beyond the caldera rim (Fig. 6.1D), and absence at outcrops to the NE (Miyabuchi, 2009).

Directly above the NjP tephra, 4.5 m of alternating pumice and scoria layers, interbedded between paleosols are reported (Matsuriba; Fig. 6.2). Above this at Yamasaki, a series of pumices (termed the Yamasaki Pumices [YmP]; Miyabuchi, 2009) are identified in the overlying 15 m which comprise of primary tephra units, paleosols and silty ash layers (Fig. 6.2). This series of pumices has been divided into units related to thirteen different eruptions and labelled the YmP13 – 1 in ascending order and believed to span 77 – 61 ka (Miyabuchi et al., 2003). These deposits are subdivided by thin soil beds, indicating short repose intervals, and thicknesses indicate ESE to ENE dispersal (Miyabuchi et al., 2003). Most notably, the upper ~8 m is characterised by thick well-stratified ash layers including pumice beds and are divided into five units (YmP5–1) and by distinct soil layers (Fig. 6.2; Miyabuchi et al., 2003). The lowermost of these units (YmP5) is the thickest (2.3 – 2.5 m) with the lower section comprised of alternating ash and pumice beds, whereas middle and upper sections are characterised by scoria-fall deposits with thin ash layers (Miyabuchi et al., 2003). The YmP5 has been identified as the key marker of the Yamasaki pumice series (Miyabuchi, 2009; Miyabuchi et al., 2003).

Outcrops around the caldera wall reveal there were a series of post-caldera Plinian fall eruptions from central cones (Fig. 6.1D) termed the Aso central pumice cones (ACPs; Miyabuchi, 2009). Four of these units are preserved between the Yamasaki pumice series and the AT tephra and labelled ACP6 to ACP3 in ascending order spanning ~60 – 50 ka and are routinely identified in the proximal outcrops to the east of the caldera wall, whilst all have also been reported towards the NE (see Miyabuchi 2009, 2011). All four of these deposits are preserved at Koga (Fig. 6.1D and 6.2), varying in thickness and interspaced by layers of soils and mafic scoria, indicating periods of time between each of these eruption events (Fig. 6.2; Miyabuchi, 2009). The lowermost of these units is the ACP6 which is preserved directly above the widespread Kuju-Handa (Kj-Hd) tephra (SG06-4141) erupted 11 km north from Kuju (also located on the CVR) at 60 ka (Fig. 6.2) and is one of the key the post-caldera tephra layers (Takada, 1989). The ACP6 erupted a bulk volume of 0.21 km^3 and is

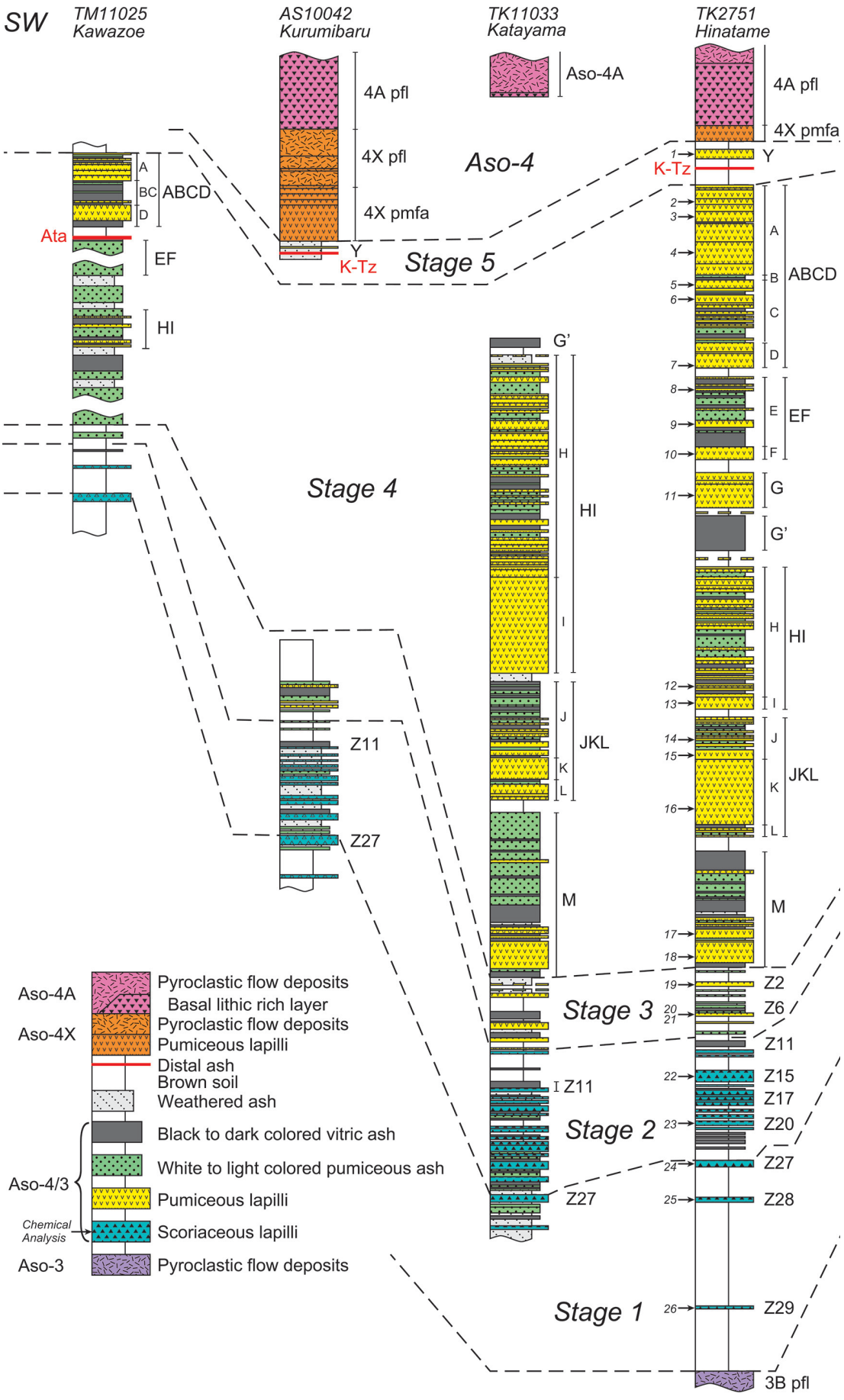
composed of poorly-sorted alternating beds of pumice and fine ash, divided into seven units; units 1, 3 and 6 are massive pumice deposits whereas units 2, 4, 5 and 7 are massive or stratified ash deposits; although the number of fall units differ between localities (Miyabuchi 2009, 2011). Several metres above the ACP6, the ACP5 is preserved in the eastern sections (Fig. 6.2). The ACP5 is another slightly smaller pumice-fall deposit with a bulk volume calculated at 0.15 km^3 (Miyabuchi, 2011; Miyabuchi, 2009). Two further M 4.0 silicic eruptions occurred in the western part of Aso caldera between 54 and 51 ka; ACP4 and ACP3 (Table 6.1). The ACP4 is the largest of these four pumice cone eruptions spanning the 60 – 50 ka time interval, with bulk volume calculated at 0.43 km^3 and the ACP4 unit is divided into four sub-units of yellow pumice and ash beds (see Miyabuchi, 2011). The ACP4 has been correlated to the SG06-3912 visible tephra in Lake Suigetsu and has a reported age of 48.7± 0.19 ka (Albert et al., 2019a). The overlaying ACP3 is preserved above a thick palaoesol and is believed to be precursory Plinian pumice fall to the overlaying lava flow which has been dated to 51 ± 5 ka and the smallest of these central cone eruptions (0.07 km^3 bulk volume; Miyabuchi, 2011). Geochemical data has been obtained for the ACP6 – 3 units from proximal outcrops at Mizunomoto and Namino (Fig. 6.1D; Albert et al., 2019a).

Above the ACP3, a series mafic scoria and soil layers are interbedded and overlain by the >1m thick Kusasenrigahama pumice (Aso-Kpfa; Watanabe et al., 1982) at Mizunomoto (Fig. 6.1D; Fig. 6.2; Miyabuchi, 2011). The Aso-Kpfa erupted from the Kusasenrigahama crater (Fig. 6.1D) and is divided into six fall units, all with S-E dispersals (Table 6.1). The Aso-Kpfa is the largest and most voluminous pumice-fall deposit from the post-caldera cones with bulk volumes of 2.39 km^3 and can be recognised in outcrops all around the Aso caldera (Miyabuchi, 2011). Geochemical data arepresented for the proximal Aso-Kpfa in McLean et al. (2020a), and it has been correlated to a cryptotephra deposit preserved in Lake Suigetsu located 525 km NE. The Lake Suigetsu age model (details below) provides an age of 32.7 ± 0.06 ka for the Aso-Kpfa eruption.

6.2.2. Pre-Aso-4

At least thirty-seven eruption units are deposited between the caldera Aso-3 and Aso-4 eruptions. The main units, from youngest to oldest, include: Aso-Y, Aso-ABCD, Aso-EF, Aso-G, Aso-G', Aso-HI, Aso-JKL, Aso-M and Aso-Z1 – 29. These have been divided into five stages of activity according to magma composition and erupted volume (Table 5.1; Hoshizumi et al., 2022). Several of these units have been correlated to previously identified units (Ono and Watanabe, 1983; Ono et al., 1977) and we will adopt the nomenclature

outlined in Hoshizumi et al. (2022). The exception is the Aso-Z2 tephra which has been correlated to the previously recorded Aso-N (see Hoshizumi et al., 2022), and as it is discussed in the wider literature by both names, we refer to this unit as Aso-N/Z2. Each of these tephra is typically comprised of multiple fall units. There are paleosols which represent time-gaps between the tephra units, and all Aso tephras are also interbedded between key widespread markers from other volcanoes on Kyushu: Ata (~30 ka Ata tephra) and Kikai (93 ka K-Tz tephra) (Fig. 6.3). Detailed stratigraphic descriptions of these units can be found in Hoshizumi et al. (2022). Here we provide a summary of the units and key physical and geochemical features of these units. Glass geochemistry was published for selected fall units: Aso-Y, Aso-ABCD (all units), Aso-K, Aso-I, Aso-M and Aso-N/Z2, by Albert et al., (2019a). The glasses erupted from the oldest (Aso-N/Z2) and youngest (Aso-Y) pre-Aso-4 tephras are distinctive from glass compositions of the intervening deposits as they both have high-K_2O content (~6.3 wt.%), with the Aso-N/Z2 glasses classified as Shoshonitic (Albert et al., 2019a). The Aso-M, Aso-K, Aso-I units all have similar major element chemistries, although the Aso-M glasses have subtly more elevated Sr. Moreover, these tephra deposits compositionally differ from the Plinian fall deposits stratigraphically above the Ata tephra, Aso-ABCD (Albert et al., 2019a). The Aso-ABCD is the only tephra layer where all fall units have been geochemically analysed and are all broadly overlapping, although the Aso-D sub-unit has higher CaO contents relative to the other sub-units (Albert et al., 2019a). Trace elements can further geochemically distinguish the Aso-ABCD sub-units; Aso-B and Aso-C have lower levels of enrichment (e.g. Th content), compared to those of Aso-A and Aso-D (Albert et al., 2019a).


SW
TM11025
Kawazoe
AS10042
Kurumibaru
TK11033
Katayama
TK2751
Hinatame
Aso-4A
4A pfl
4X pfl
4X pmfa
Aso-4
Stage 5
Stage 4
Stage 3
Stage 2
Stage 1
K-Tz
Y
Ata
A
BC
D
ABCD
EF
HI
G'
H
I
J
K
L
JKL
M
Z11
Z27
Z2
Z6
Z15
Z17
Z20
Z28
Z29
3B pfl
Aso-4X
Aso-3
Aso-4/3
Chemical Analysis
Pyroclastic flow deposits
Basal lithic rich layer
Pumiceous lapilli
Distal ash
Brown soil
Weathered ash
Black to dark colored vitric ash
White to light colored pumiceous ash
Scoriaceous lapilli

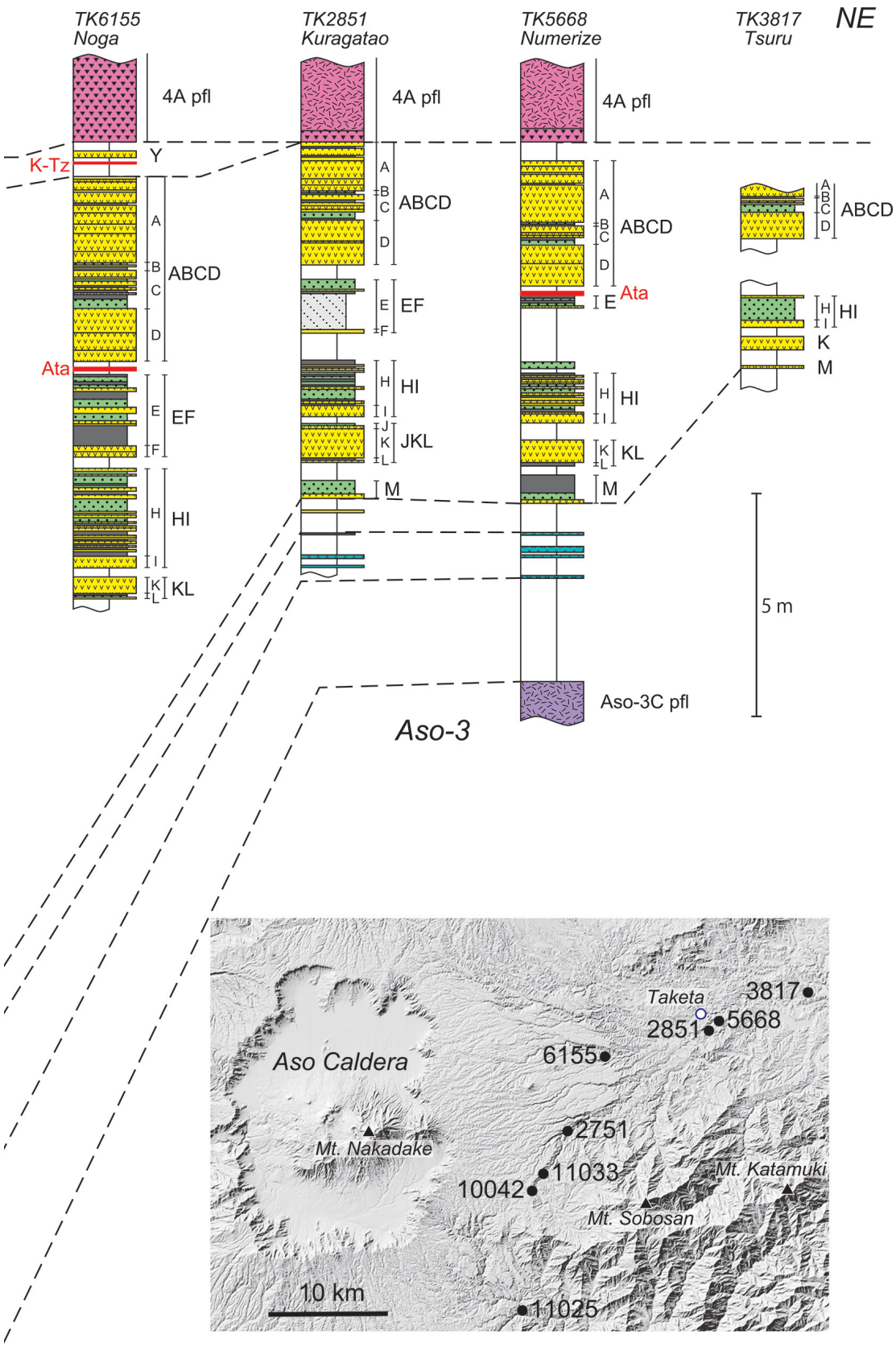


Figure 6.3: Stratigraphic relationships of the Aso units logged between Aso-3 and Aso-4 eruptions at sites east to the caldera walls. Figure taken from Hoshizumi et al. (2022).

The Aso-3 eruption is the penultimate caldera-forming eruption at ~123 – 135 ka with an ejecta volume of more than 150 km^3 consisting of Plinian fall and ignimbrite deposits (Ono et al., 1977). The tephra fall is clearly observed across a wide regional area of southwestern and central Japan, and thus is a prominent marker layer (Machida and Arai., 2003; Machida et al., 1985).

Following the Aso-3 eruption, there was an increase in eruptive activity of mostly mafic scoria- and ash-falls, during Stages 1 (133.0 – 114.1 ka) and 2 (114.1 – 108.4 ka), before more felsic eruptions in Stage 3 (108.4 – 104.7 ka; Hoshizumi et al., 2022). The three stages of activity only produced a collective total bulk volume of 2.1 km^3 in an ~18 kyr period and their dispersals are considered to be limited with E-SE trajectories (Table 6.1; Hoshizumi et al., 2022). The more silicic tephras erupted during Stage 3 are composed of nine pumice- and ash-fall layers (Aso-Z9 – 1) that are all considered M 3.0 – 4.0, and interbedded between soil layers at Katayama (Table 6.1; Fig. 6.3). Hoshizumi et al. (2022) note that the Aso-Z6 (a 27cm thick alternating pumice- and ash-fall unit) and the Aso-N/Z2 (an 11 cm thick white pumice fall layer) tephras are the most useful Stage 3 marker layers as they are frequently observed in outcrops to the east of the caldera rim (Fig. 6.3).

The most active phase of pre-caldera activity was Stage 4 (104.7 – 97.7 ka) with at least seven tephra units composed of numerous layers pumice- and ash-fall layers and interspaced by well-developed soils in a 7 kyr period: Aso-M, Aso-JKL, Aso-HI, Aso-G', Aso-G, Aso-EF and Aso-ABCD (Fig. 5.3; Hoshizumi et al., 2022). All of these units have been previously observed in proximal outcrops (see: Ono and Watanabe, 1983; Ono et al.,1977) with the exception of Aso-J, Aso-G', Aso-G and Aso-E which have only recently been identified by Hoshizumi et al. (2022) The Stage 4 eruptions are much larger than the eruptions in earlier post-Aso-3/pre-Aso-4 activity stages, and produced bulk volumes ranging from 0.4 – 8.1 km^3 and are considered M 5.0 except for the Aso-G' and Aso-G units which are considered to be an order of magnitude smaller (M4.0; Table 6.1; Hoshizumi et al., 2022). The oldest of these tephras (Aso-M) is a 3 m thick unit at Katayama (see Fig. 5.3) and comprised of stratified black ash and white pumice layers; although there is evidence of erosional contact in the base of the upper-ash layer, indicating it may reflect different eruptions separated in time (Hoshizumi et al., 2022).

Hoshizumi et al (2022) noted another previously unreported Aso-J sub-unit that they interpreted to be part of the Aso-KL eruption/tephra defined by Ono and Watanabe (1983), and estimate a total bulk volume 2.1 km^3 for Aso-JKL (Table 6.1). At Katayama, the Aso-JKL tephra is found directly above a 0.5 m thick soil separating it from the underlying Aso-M unit

(Fig. 6.3). The lowermost Aso-L unit is 0.7 m thick comprising of alternating layers of ash and pumice, which is overlain by the 0.7 m thick Aso-K unit, a white pumice layer. These are followed by the much thicker 2.0 m thick Aso-J unit which is again comprised of alternating pumice- and ash-layers (Fig. 6.3). Hoshizumi et al. (2022) observe at outcrops furthest east from the caldera (i.e. Noga cave, Numerize and Tsuru), the smaller Aso-J and Aso-L units are often unclear, which may explain why they were not documented in earlier studies (e.g. Ono and Watanabe, 1983; Ono et al., 1977).

At Katayama above the Aso-JKL tephra, there is a 0.3 m weathered ash layer upon which the 8.0 m thick Aso-HI is found (Fig. 6.3). The estimated volume of the Aso-HI eruption is 5.0 km^3, making it the second largest pre-caldera eruption and it is considered to have an easterly dispersal (Table 6.1; Hoshizumi et al., 2022). The lower Aso-I unit is defined as a 2.5 m thick pumice layer, whilst the overlaying Aso-H is a massive 5.5 m thick unit of alternating layers of pumice and ash (Fig. 6.3). Only the pumices from the lower Aso-I unit at Noga Cave and have been geochemically characterised (see Albert et al., 2019a).

The Aso-G' and subsequent Aso-G tephra units have only recently been identified by Hoshizumi et al. (2022) and these units are most prominent in proximal outcrops at Hinatame (11 km to the east of the caldera wall; Fig 6.1) but appear to be missing from sequences further northeast (Fig. 6.3). At Hitaname, the lower Aso-G' is a 1.0 m thick dark grey ash layer and has a volume of 1.0 km^3 dispersed to the SE. The overlaying Aso-G tephra, separated by well-developed soil, consists of three pumice layers and has an apparent volume of 0.4 km^3 and had a more E trajectory (Fig. 6.3; Hoshizumi et al., 2022). Neither the Aso-G' or the Aso-G tephras have been geochemically characterised.

Above a well-developed soil lies the Aso-EF unit which is most clearly preserved at Hinatame (Fig. 6.3). The apparent volume of the Aso-EF tephra layer is 1.7 km^3, despite the Aso-E unit previously unreported (see: Ono and Watanabe, 1983; Ono et al., 1977) and is frequently identified in outcrops around the caldera wall (Fig. 6.3; Hoshizumi et al., 2022). The older Aso-F unit is 0.5 m thick comprised of pumice-fall, whilst the overlaying Aso-E unit is a 1.5 m thick stratified ash layer with several thin pumice layers throughout; although the degree of stratification diminishes with increasing distance from the caldera (Fig. 6.3; Hoshizumi et al., 2022). The Aso-EF tephra has not been geochemically characterised.

The youngest of the Stage 4 tephras is the Aso-ABCD eruption that is comprised of numerous Plinian fall units, and it is the largest pre-caldera eruption (M5.9) producing a total volume of 8.1 km^3 of trachytic rhyolites (Hoshizumi et al., 2022; Albert et al., 2019a; Smith et

al., 2013). The Aso-ABCD tephra is preserved between Ata and K-Tz marker layers in proximal settings (Noga), and all constituent units are pumice-fall deposits except for the thinner (ca. 10 cm) Aso-B unit which is an ash-fall layer (Fig. 6.3). The Aso-ABCD measures 4.3 m in thickness at Noga cave, where the Aso-D and Aso-A are the thickest units (Fig. 6.3). Geochemical data has been obtained for all Aso-ABCD units, an on this basis, the 3.5 cm thick visible SG06-5287 tephra layer preserved in Lake Suigetsu has been tentatively correlated to the Aso-A unit of the Aso-ABCD layer and provides an age for this tephra layer of 96.8 ± 2.6 ka using the Lake Suigetsu age-model (Albert et al., 2019a). This age is in good agreement with the 97.7 ka estimated by loess-chronometry (Hoshizumi et al., 2022).

The Stage 5 activity is the final phase of activity prior to the Aso-4 eruption and is defined as the period between the Aso-ABCD tephra and the Aso-4 pyroclastic-flow (Hoshizumi et al., 2022). A significant drop in the eruption frequency is recorded in Stage 5 (97.7 – 88.0 ka), right before the Aso-4 event, erupting a single pumice-fall (Aso-Y) in almost 10 kyrs (Table 1; Hoshizumi et al., 2022). The abrupt drop in eruption frequency during stage 5 of the Aso-3/4 caldera cycle is suggested to be a typical characteristic of the evolution of a magmatic system in the fermentation phase of a caldera cycle (Keller et al., 2023; Hoshizumi et al., 2022; Bouvet de Maisonneuve et al., 2021). The Aso-Y tephra is a relatively small M 5.5 pre-caldera eruption with an apparent volume of 0.1 km^3 and measures just 0.2 m thick at Noga Cave (comprised of white pumices) and found stratigraphically above the widespread K-Tz marker from Kikai caldera 300 km south of Aso (Fig. 6.3; Hoshizumi et al., 2022). The Aso-Y unit at Noga Cave has been geochemically characterised (see Albert et al., 2019a).

At Kurumi Baru, above the Aso-Y tephra and a soil bed, there is another 3.0 m thick white pumice fall layer and is directly covered by Aso-4 pyroclastic-flow deposits (Fig. 6.3). The Aso-4X unit is therefore considered to be the basal Plinian fall of the Aso-4 pyroclastic-flow eruption (Hoshizumi et al., 2022), its glass chemistry has not been geochemically characterised. The massive M7.8 Aso-4 eruption is the second largest volcanic event experienced by the Earth within the last 100 ka, and the largest of the Aso caldera-forming eruptions, and produced a volume of 600 km^3, and the ignimbrite is found up to 50 km from the caldera wall and tephra fall is reported in terrestrial and marine cores across Japan (e.g. Matsu'ura et al., 2021; Tsuji et al 2018; Lim et al., 2013; Smith et al., 2013; Nagahashi et al. 2004). The Aso-4 ignimbrite has been precisely dated using Ar^{40}/Ar^{39} 86.4 ± 1.1 ka (Albert et al., 2019a). The Aso-4 ignimbrite deposits are distinctive owing to their compositional heterogeneity, proximal glasses from Noga Cave reveal three distinct glass populations, with two rhyolitic populations dominating and being most easily distinguished from each other using their CaO content (see Albert et al., 2019a). The glass chemistry of the 3.5 cm thick

visible tephra preserved in Lake Suigetsu (SG06-4963) shows good geochemical agreement with two rhyolitic components of the Aso-4 glasses (Smith et al., 2013). The $^{40}Ar/^{39}Ar$ age has been imported into the Lake Suigetsu age-depth model and provides a new chronological anchor for this deeper portion of the record (Albert et al., 2019).

6.3. Methods

6.3.1. Proximal tephra units

Seven outcrops located east the Aso-4 caldera, which have published stratigraphic logs, were sampled during field campaigns in 2022 and 2023. The nomenclature and stratigraphies of Hoshizumi et al. (2022) were followed for the pre-caldera eruptions (Noga Cave, Katyama and Kurumibaru), while Miyabuchi (2011; et al., 2009) were followed for the post-caldera (Koga and Yamasaki) eruption deposits. The remaining units were collected from east of the caldera near Hata (pre-caldera), Nojiri and Takimizu (post-caldera) after being correlated into the stratigraphic framework outlined at the localities above (Fig. 6.1D). At these locations, representative samples of the units were collected. The new 2022/23 samples collected for geochemical analysis were given a number and a FLF prefix, while those collected in previous field campaigns retain the prefix associated with earlier field sampling campaigns (e.g., A9746-B5/4; Miyabuchi, 2011 or ITJ94; Albert et al., 2019a). In the laboratory, these bulk representative samples of pumice clasts and ash were crushed and wet sieved to remove the fraction <25 μm. Samples were dried in an oven at ~60◦C and mounted in Struers Epoxy resin.

6.3.2. Distal Lake Suigetsu crypto-/tephra deposits from Aso

Various Aso derived tephra and the cryptotephra deposits preserved in Lake Suigetsu were identified in previous tephra/cryptotephra investigations (Vineberg et al., 2024; McLean et al., 2020a; Albert et al., 2019a; Smith et al., 2013).

SG06 event-free depth(s) (EFD; version 13th Feb 2017) were used within the age model, which excludes instantaneous deposits >5 mm in thickness, i.e., event layers (Staff et al., 2011; Schlolaut et al., 2012). The software package developed to handle the correlation of parallel core sections, 'LevelFinder' (version 7.7.1, http://polsyems.rits-paleo.com), was used to linearly interpolate between the common marker layers to determine a composite depth (CD) or EFD for the cryptotephra layers. Down to the limit of radiocarbon dating (circa 52 cal. ka BP). For the deeper section of the stratigraphy examined

in the present study, this chronology was extrapolated using a 'P_Sequence' deposition model within the Bayesian software package, OxCal (Bronk Ramsey, 2008), that also includes a single $^{40}Ar/^{39}Ar$-derived age of 86.4 ± 0.6 ka (±1σ) for the Aso 4 tephra, at a CD in SG14 of 4922.8 cm (Albert et al., 2019a; see below). The Lake Suigetsu age model-derived ages for the tephra identified in this section of the SG core are reported in Table 6.2 and the ±1σ uncertainties are quoted throughout.

6.3.3. Geochemical compositions of proximal tephra units

The surface of the resin stubs were manually sectioned using silicon carbide papers to expose the shards on a flat surface, polished with diamonds, and then carbon coated for chemical analyses.

Major element compositions of individual glass shards were analysed using a JEOL JXA-8200 wavelength dispersive electron microprobe (WDS-EMP) equipped with 5 spectrometers located in the School of Archaeology, University of Oxford, U.K. An accelerating voltage of 15 kV, 6 nA current and a defocussed 10 μm beam were used. Peak counting times were 12 s for Na, 30 s for other major elements except for Mn, Cl and P, which were collected for 50 s. A suite of mineral standards were used to calibrate the microprobe, and the MPI-DING references glasses (Jochum et al., 2006) were ran as secondary standards during each analytical session. Analyses with analytical totals <94% were discarded. All analyses presented have been normalised to 100% for comparative purposes.

The trace element compositions of individual glass were determined using an Agilent 8900 triple quadrupole LA-ICP-MS (laser ablation inductively coupled plasma mass spectrometry; ICP-QQQ) coupled to a Resonetics 193 nm ArF excimer laser-ablation device in the Department of Earth Sciences, Royal Holloway, University of London. Both 20 and 25 μm crater sizes were used depending on the size of the glass surface areas. The laser energy density on the target was 3.0 Jcm^{-2}, the repetition rate was 5 Hz. Ablation of the samples lasted 40 s on the sample, while 20 s of pre and 20 s of post ablation gas blank was used to subtract the background signal. The MPI-DING reference glasses were used to monitor analytical accuracy (Jochum et al., 2006). Typically, blocks of eight glass shards and one MPI-DING reference glass were bracketed by the NIST612 glass adopted as the calibration standard. The internal standard applied was ^{29}Si (determined by EMP-WDS analysis). LA-ICP-MS data reduction was performed in Microsoft Excel, as described in

Tomlinson et al. (2010). Accuracies of LA-ICP-MS analyses were monitored using MPI-DING reference glasses, ATHO-G and StHs6/80-G, and accuracies were typically ≤ 5% for most elements measured (see data in Appendix C). Error bars on plots represent reproducibility, calculated as ± 2 standard deviations of replicate analyses of MPI-DING StHs6/80-G glasses. Error bars on the trace element plots are typically smaller than the symbols. All major and trace element data for the Suigetsu tephras and the secondary standards run alongside, are available in Appendix C.

6.4. Results

Seventeen silicic tephra layers are preserved between the Aso-3 and Aso-4 units in sites located to the east of the Aso caldera wall (Fig. 6.2 and 6.3). We present geochemical data for nine of these tephra deposits, six of which have not previously been characterised. Many of these tephras have multiple eruption phases, and we present geochemical data for forty-eight samples from the twenty-four tephra sub-/units. Representative major and trace element analyses are reported in Table 6.2. Most glasses straddle the trachy-dacite – rhyolite boundary, except for the YmP7 and YmP6 glasses which are trachy-andesites through to trachytes and easily distinguishable from other glasses analysed in this study (Fig. 6.4A). All the Aso units collectively span a broad range in the major element compositions (Table 6.2), and individual deposits can be somewhat challenging to discriminate using major element data due to geochemical similarities (Fig. 6.4A). There is little heterogeneity within individual units (i.e. similar to analytical uncertainty) with only the ash above Aso-Kpfa, Aso-I, Aso-F units being heterogenous in composition and the YmP6 shows the greatest degree of variability in major elements (Fig. 5.4A; Table 6.2). Furthermore, the trachytic glasses of the YmP5 appear to be distinct from all other units analysed (Fig. 5.4A).

Table 6.2: Average major (EMP) and trace element (LA-ICP-MS) volcanic glass chemistry of the of the proximal Aso units sampled between Aso-3 and the AT marker beds. Major element glass data has been normalised (water free). Sampling locations are shown in Fig. 6.1D. Full geochemical datasets are available in Appendix C.

Tephra	Ash above K-pfa		Aso-KPfa		ACP-3		ACP-4 (basal)		ACP-4 (lower)		ACP-4 (middle)		ACP-4 (upper)		ACP-4 (lower)		ACP-4 (upper)		ACP-4 (bulk)		ACP6		YmP5	
Material	Ash		Pumice		Pumice		Pumice-lapilli		Pumice-lapilli		Pumice-lapilli		Pumice-lapilli		Pumice-lapilli		Pumice-lapilli		Pumice-lapilli		Pumice-lapilli		Pumice	
Sample	FLF57		FLF56		FLF58		FLF60		FLF61		FLF62		FLF63		FLF190		FLF191		FLF189		FLF186		A9746 P-B4	
Location	Takimizu		Takimizu		Takimizu		Takimizu		Takimizu		Takimizu		Takimizu		Koga		Koga		Koga		Koga		Yamasaki	
(wt.%)	Avg.	1 std. dev.	Avg.	1 std. dev.	Avg.	1 std. dev.	Avg.	1 std. dev.	Avg.	1 std. dev.	Avg.	1 std. dev.	Avg.	1 std. dev.	Avg.	1 std. dev.	Avg.	1 std. dev.	Avg.	1 std. dev.	Avg.	1 std. dev.	Avg.	1 std. dev.
SiO_2	66.01	2.08	69.40	0.65	74.04	0.53	71.89	0.31	71.94	0.96	71.53	0.66	71.82	0.77	71.71	0.96	72.34	2.83	72.17	0.69	72.99	0.40	66.19	0.95
TiO_2	0.91	0.06	0.73	0.03	0.33	0.05	0.45	0.05	0.47	0.12	0.48	0.08	0.46	0.05	0.48	0.22	0.44	0.35	0.45	0.05	0.33	0.07	0.76	0.17
Al_2O_3	15.12	0.42	15.05	0.40	14.00	0.42	14.99	0.20	14.95	0.41	15.07	0.24	14.93	0.35	14.86	0.18	14.64	2.30	14.73	0.21	14.58	0.48	16.10	1.01
FeO	4.63	0.69	2.74	0.27	1.24	0.12	1.69	0.11	1.71	0.29	1.82	0.30	1.78	0.14	1.75	0.45	1.57	1.59	1.60	0.44	1.33	0.10	3.98	0.59
MnO	0.13	0.03	0.11	0.02	0.07	0.05	0.09	0.05	0.07	0.03	0.08	0.05	0.07	0.04	0.08	0.04	0.07	0.10	0.07	0.04	0.07	0.02	0.16	0.04
MgO	1.17	0.28	0.66	0.07	0.19	0.05	0.38	0.08	0.34	0.10	0.42	0.10	0.36	0.08	0.36	0.10	0.32	0.65	0.36	0.19	0.21	0.05	1.09	0.33
CaO	3.01	0.59	1.88	0.11	0.68	0.10	1.22	0.06	1.17	0.25	1.29	0.20	1.20	0.20	1.20	0.38	0.98	0.85	1.10	0.08	0.75	0.14	2.91	0.59
Na_2O	4.56	0.23	4.86	0.27	4.27	0.19	4.57	0.19	4.60	0.32	4.58	0.27	4.68	0.15	4.71	0.27	4.61	1.07	4.66	0.10	4.47	0.19	4.52	0.42
K_2O	4.09	0.12	4.35	0.13	5.04	0.16	4.55	0.15	4.60	0.27	4.56	0.25	4.54	0.15	4.70	0.28	4.92	1.07	4.75	0.13	5.09	0.16	3.98	0.52
P_2O_5	0.29	0.10	0.11	0.03	0.02	0.03	0.05	0.04	0.05	0.04	0.06	0.04	0.05	0.02	0.06	0.11	0.05	0.04	0.05	0.02	0.04	0.03	0.22	0.06
Cl	0.08	0.01	0.11	0.07	0.11	0.02	0.11	0.04	0.10	0.02	0.10	0.03	0.11	0.04	0.10	0.05	0.06	0.07	0.08	0.03	0.12	0.03	0.10	0.02
(n)	*6*		*19*		*17*		*15*		*12*		*11*		*5*		*9*		*9*		*8*		*20*		*14*	
(ppm)	Avg.	1 std. dev.	Avg.	1 std. dev.	Avg.	1 std. dev.	Avg.	1 std. dev.	Avg.	1 std. dev.	Avg.	1 std. dev.	Avg.	1 std. dev.	Avg.	1 std. dev.	Avg.	1 std. dev.	Avg.	1 std. dev.	Avg.	1 std. dev.	Avg.	1 std. dev.
Rb	-	-	-	-	-	-	-	-	-	-	-	-	-	-	161	5.34	149	4.50	155	9.67	169	11.49	140	14
Sr	-	-	-	-	-	-	-	-	-	-	-	-	-	-	123	6.67	174	27.7	134	40.1	88.3	63.6	455	170.6
Y	-	-	-	-	-	-	-	-	-	-	-	-	-	-	35.1	0.41	35.5	3.94	35.3	2.02	35.3	2.20	30.3	3.95
Zr	-	-	-	-	-	-	-	-	-	-	-	-	-	-	310	6.63	299	23.0	308	12.6	312	38.6	233	29.9
Nb	-	-	-	-	-	-	-	-	-	-	-	-	-	-	17.0	0.28	16.3	0.97	16.8	0.60	16.7	1.55	12.6	1.56
Ba	-	-	-	-	-	-	-	-	-	-	-	-	-	-	799	26.0	774	98.8	828	29.8	772	106	737	61.7
La	-	-	-	-	-	-	-	-	-	-	-	-	-	-	32.1	0.60	31.6	1.22	31.9	1.91	32.9	2.40	28.8	2.74
Ce	-	-	-	-	-	-	-	-	-	-	-	-	-	-	70.6	1.83	70.0	2.85	71.9	4.84	72.1	6.83	63.3	6.70
Pr	-	-	-	-	-	-	-	-	-	-	-	-	-	-	8.30	0.17	8.44	0.61	8.22	0.77	8.39	0.72	7.65	1.45
Nd	-	-	-	-	-	-	-	-	-	-	-	-	-	-	34.2	0.64	33.7	2.08	33.7	2.33	33.8	3.47	32.0	3.72
Sm	-	-	-	-	-	-	-	-	-	-	-	-	-	-	7.19	0.31	7.12	1.54	7.14	1.31	7.24	0.77	7.02	0.71
Eu	-	-	-	-	-	-	-	-	-	-	-	-	-	-	1.26	0.08	1.47	0.21	1.35	0.14	1.18	0.30	1.66	0.34
Gd	-	-	-	-	-	-	-	-	-	-	-	-	-	-	6.16	0.35	6.46	0.27	6.22	0.53	6.22	0.81	5.96	1.62
Dy	-	-	-	-	-	-	-	-	-	-	-	-	-	-	6.22	0.34	6.18	0.95	6.09	0.55	6.36	0.73	5.47	1.15
Er	-	-	-	-	-	-	-	-	-	-	-	-	-	-	3.81	0.19	3.94	0.59	3.79	0.49	3.93	0.67	3.35	0.61
Yb	-	-	-	-	-	-	-	-	-	-	-	-	-	-	4.21	0.28	4.24	0.19	4.26	0.50	4.28	0.51	3.35	0.80
Lu	-	-	-	-	-	-	-	-	-	-	-	-	-	-	0.63	0.03	0.62	0.10	0.62	0.06	0.63	0.07	0.50	0.10
Hf	-	-	-	-	-	-	-	-	-	-	-	-	-	-	8.46	0.46	8.04	0.94	8.11	0.35	8.47	1.44	6.17	0.99
Ta	-	-	-	-	-	-	-	-	-	-	-	-	-	-	1.20	0.06	1.17	0.10	1.19	0.09	1.23	0.18	0.90	0.11
Pb	-	-	-	-	-	-	-	-	-	-	-	-	-	-	24.3	1.02	21.9	2.20	24.1	1.95	24.6	3.12	20.8	4.33
Th	-	-	-	-	-	-	-	-	-	-	-	-	-	-	14.5	0.45	14.3	1.20	14.2	0.63	16.18	2.50	12.6	1.72
U	-	-	-	-	-	-	-	-	-	-	-	-	-	-	4.30	0.11	4.15	0.35	4.25	0.22	4.63	0.58	3.70	0.42
(n)	-		-		-		-		-		-		-		*5*		*5*		*7*		*14*		*11*	

Tephra	YmP6		YmP7		YmP8		NjP		Aso-4X (lower)		Aso-4X (middle)		Aso-4X (upper)		Aso-Y		Aso-Y		Aso-D		Aso-E		Aso-E (lower)	
Material	Pumice		Pumice		Pumice		Pumice		Pumice		Pumice		Ash		Pumice		Ash		Pumice		Lapilli		Pumice-lapilli	
Sample	A9746 P-B5/4		A9746 P-B5		A9746 P-B6		FLF52		FLF194		FLF195		FLF196		FLF65		FLF248		FLF236		FLF74		FLF232	
Location	Yamasaki		Yamasaki		Yamasaki		Nojiri		Kurumi Baru		Kurumi Baru		Kurumi Baru		Noga Cave		Kurumi Baru		Hata		Noga Cave		Hata	
(wt.%)	Avg.	1 std. dev.	Avg.	1 std. dev.	Avg.	1 std. dev.	Avg.	1 std. dev.	Avg.	1 std. dev.	Avg.	1 std. dev.	Avg.	1 std. dev.	Avg.	1 std. dev.	Avg.	1 std. dev.	Avg.	1 std. dev.	Avg.	1 std. dev.	Avg.	1 std. dev.
SiO_2	61.89	4.05	61.12	0.80	68.03	0.72	67.04	0.06	72.38	0.89	72.40	0.76	71.84	0.73	72.61	0.56	73.27	0.55	69.58	0.58	70.92	0.23	70.48	0.48
TiO_2	0.88	0.25	0.91	0.07	0.65	0.09	0.61	0.05	0.37	0.15	0.36	0.07	0.36	0.04	0.35	0.07	0.33	0.07	0.61	0.06	0.60	0.02	0.60	0.02
Al_2O_3	16.41	1.45	16.69	0.66	15.87	0.57	16.52	1.32	15.05	0.71	14.96	0.48	14.96	0.32	14.84	0.29	14.62	0.26	15.62	0.38	15.00	0.12	15.09	0.47
FeO	6.13	2.37	6.30	0.40	3.08	0.30	3.26	0.76	1.40	0.25	1.38	0.18	1.48	0.23	1.31	0.13	1.26	0.15	2.35	0.17	2.10	0.16	2.11	0.11
MnO	0.16	0.07	0.17	0.05	0.12	0.04	0.15	0.04	0.09	0.03	0.09	0.03	0.10	0.02	0.09	0.04	0.08	0.04	0.10	0.04	0.09	0.02	0.10	0.01
MgO	1.97	1.04	2.14	0.21	0.78	0.25	0.93	0.28	0.29	0.07	0.31	0.10	0.33	0.07	0.26	0.07	0.24	0.05	0.70	0.07	0.49	0.03	0.55	0.03
CaO	4.72	1.62	4.87	0.46	2.31	0.34	2.81	0.47	1.00	0.13	1.01	0.17	1.06	0.22	0.94	0.11	0.86	0.12	1.97	0.14	1.43	0.05	1.51	0.20
Na_2O	4.05	0.53	4.11	0.38	4.38	0.27	4.63	0.15	4.40	0.30	4.43	0.21	4.67	0.24	4.33	0.37	4.23	0.27	4.44	0.20	4.37	0.12	4.57	0.19
K_2O	3.27	0.80	3.08	0.28	4.52	0.29	3.82	0.62	4.87	0.21	4.91	0.26	5.04	0.27	5.13	0.29	4.97	0.25	4.42	0.10	4.83	0.08	4.77	0.23
P_2O_5	0.44	0.18	0.51	0.12	0.16	0.04	0.14	0.06	0.03	0.04	0.04	0.06	0.05	0.02	0.04	0.04	0.03	0.04	0.09	0.06	0.07	0.03	0.09	0.01
Cl	0.08	0.04	0.08	0.03	0.10	0.02	0.09	0.04	0.10	0.04	0.11	0.03	0.11	0.02	0.10	0.02	0.10	0.03	0.11	0.03	0.09	0.01	0.10	0.01
(n)	*15*		*17*		*13*		*2*		*22*		*22*		*11*		*17*		*15*		*13*		*24*		*16*	
(ppm)	Avg.	1 std. dev.	Avg.	1 std. dev.	Avg.	1 std. dev.	Avg.	1 std. dev.	Avg.	1 std. dev.	Avg.	1 std. dev.	Avg.	1 std. dev.	Avg.	1 std. dev.	Avg.	1 std. dev.	Avg.	1 std. dev.	Avg.	1 std. dev.	Avg.	1 std. dev.
Rb	121	26.5	113	8.12	165	7.2	-	-	166	12.0	167	7.37	173	6.43	171	9.81	-	-	-	-	170	10.4	-	-
Sr	466	279	522	59.2	356	22.8	-	-	160	39.0	146	35.8	143	16.8	136	31.4	-	-	-	-	191	13.5	-	-
Y	27.9	10.7	28.1	4.2	31.2	2.72	-	-	33.3	2.04	33.8	2.02	33.7	3.64	33.4	4.09	-	-	-	-	35.5	1.96	-	-
Zr	187	31.6	190	32.3	286	24.4	-	-	301	15.4	302	22.4	299	37.9	294	34.1	-	-	-	-	298	17.4	-	-
Nb	10.10	0.77	9.9	1.24	15.1	1.02	-	-	16.2	1.69	16.1	0.83	16.1	1.31	15.8	1.71	-	-	-	-	16.8	0.90	-	-
Ba	593	79.3	607	76.2	852	100	-	-	806	48.4	808	32.8	796	66.6	762	92.2	-	-	-	-	874	55.6	-	-
La	25.3	5.37	25.8	4.31	31.8	2.69	-	-	33.6	2.28	34.4	2.21	34.3	3.74	33.9	4.53	-	-	-	-	35.1	2.50	-	-
Ce	56.6	13.9	59.6	12.4	69.1	13.3	-	-	72.6	7.14	73.8	4.84	73.6	6.29	73.4	10.4	-	-	-	-	75.5	7.07	-	-
Pr	6.81	2.08	6.97	1.58	8.0	0.42	-	-	8.65	0.53	8.56	0.54	8.65	0.83	8.50	0.87	-	-	-	-	8.94	0.80	-	-
Nd	29.6	11.1	31.5	5.15	33	2.04	-	-	35.2	1.75	35.1	2.66	35.3	4.43	33.7	5.76	-	-	-	-	36.8	2.66	-	-
Sm	6.62	2.92	7.37	1.27	7.58	1.52	-	-	7.00	0.77	7.10	0.97	7.10	1.15	7.08	1.58	-	-	-	-	8.02	0.80	-	-
Eu	1.56	0.79	1.80	0.33	1.56	0.29	-	-	1.31	0.18	1.31	0.17	1.29	0.30	1.21	0.27	-	-	-	-	1.47	0.28	-	-
Gd	5.51	2.19	5.92	1.33	5.85	1.04	-	-	5.87	0.63	6.18	0.92	6.14	0.74	5.90	1.06	-	-	-	-	6.37	0.67	-	-
Dy	5.07	1.98	5.27	1.65	5.50	0.87	-	-	5.81	0.78	5.93	0.77	5.89	0.86	5.78	0.95	-	-	-	-	6.32	0.59	-	-
Er	3.03	1.21	2.96	0.61	3.59	0.70	-	-	3.56	0.40	3.61	0.45	3.60	0.60	3.64	0.31	-	-	-	-	4.00	0.57	-	-
Yb	2.95	1.01	3.16	0.52	3.64	0.95	-	-	3.82	0.34	4.11	0.51	4.02	0.81	3.81	0.69	-	-	-	-	4.02	0.43	-	-
Lu	0.44	0.14	0.45	0.13	0.50	0.08	-	-	0.58	0.09	0.61	0.04	0.58	0.13	0.61	0.13	-	-	-	-	0.60	0.09	-	-
Hf	5.20	0.73	4.86	1.19	6.94	1.63	-	-	7.67	0.96	7.88	0.83	8.16	1.17	7.83	0.97	-	-	-	-	7.97	0.51	-	-
Ta	0.75	0.16	0.71	0.14	1.09	0.17	-	-	1.17	0.04	1.19	0.08	1.16	0.18	1.13	0.22	-	-	-	-	1.21	0.06	-	-
Pb	17.3	2.38	16.2	2.93	23.0	2.09	-	-	23.9	1.99	23.7	1.93	24.0	2.28	23.2	2.87	-	-	-	-	23.7	1.83	-	-
Th	10.8	1.63	10.1	2.74	15.5	2.78	-	-	16.06	1.66	16.63	1.14	15.9	3.12	16.15	2.80	-	-	-	-	16.7	1.86	-	-
U	3.26	1.09	3.08	0.53	4.51	0.60	-	-	4.79	0.29	4.84	0.31	4.83	0.67	4.85	0.85	-	-	-	-	4.85	0.31	-	-
(n)	*8*		*10*		*10*		*-*		*9*		*12*		*13*		*9*		*-*		*-*		*12*		*-*	

Tephra	Aso-E (middle)		Aso-E (upper)		Aso-F		Aso-F		Aso-G		Aso-H (base)		Aso-H (lower)		Aso-H (upper)		Aso-H (top)		Aso-I (basal)		Aso-I (top)	
Material	Ash		Ash-lapilli		Pumice-lapilli		Pumice		Pumice		Pumice		Pumice		Pumice		Ash		Pumice		Pumice	
Sample	FLF233		FLF234		FLF73		FLF230		FLF229		FLF208		FLF213		FLF217		FLF219		FLF206		FLF207A	
Location	Hata		Hata		Noga Cave		Hata		Hata		Katayama		Katayama		Katayama		Katayama		Katayama		Katayama	
(wt.%)	Avg.	1 std. dev.	Avg.	1 std. dev.	Avg.	1 std. dev.	Avg.	1 std. dev.	Avg.	1 std. dev.	Avg.	1 std. dev.	Avg.	1 std. dev.	Avg.	1 std. dev.	Avg.	1 std. dev.	Avg.	1 std. dev.	Avg.	1 std. dev.
SiO_2	70.74	0.41	71.03	0.78	71.17	0.44	73.15	0.74	70.23	0.55	68.34	0.33	69.07	0.49	69.14	0.34	69.32	0.41	69.51	0.58	69.45	0.44
TiO_2	0.61	0.01	0.60	0.02	0.46	0.07	0.34	0.05	0.60	0.06	0.70	0.06	0.67	0.07	0.67	0.07	0.67	0.05	0.65	0.07	0.66	0.09
Al_2O_3	14.95	0.28	14.89	0.30	15.24	0.33	14.54	0.53	15.45	0.47	15.58	0.33	15.43	0.14	15.36	0.23	15.31	0.28	15.40	0.30	15.42	0.15
FeO	2.06	0.10	2.08	0.26	1.78	0.48	1.28	0.16	2.28	0.12	2.86	0.22	2.63	0.25	2.65	0.14	2.61	0.14	2.43	0.21	2.50	0.39
MnO	0.10	0.01	0.10	0.01	0.08	0.05	0.09	0.04	0.10	0.04	0.12	0.03	0.10	0.05	0.11	0.04	0.11	0.04	0.10	0.04	0.10	0.04
MgO	0.53	0.07	0.51	0.04	0.40	0.07	0.24	0.07	0.58	0.06	0.83	0.06	0.71	0.10	0.71	0.07	0.70	0.09	0.65	0.07	0.66	0.07
CaO	1.43	0.11	1.33	0.12	1.30	0.15	0.88	0.16	1.64	0.24	2.26	0.13	1.97	0.14	1.95	0.14	1.86	0.13	1.86	0.17	1.86	0.16
Na_2O	4.54	0.20	4.35	0.42	4.26	0.46	3.99	0.44	4.11	0.85	4.41	0.18	4.36	0.23	4.27	0.22	4.26	0.28	4.34	0.20	4.30	0.16
K_2O	4.85	0.24	4.92	0.25	5.14	0.56	5.36	0.29	4.79	0.21	4.61	0.19	4.81	0.16	4.87	0.20	4.91	0.24	4.82	0.18	4.80	0.21
P_2O_5	0.09	0.01	0.09	0.01	0.07	0.04	0.03	0.03	0.11	0.02	0.18	0.06	0.16	0.09	0.17	0.10	0.16	0.07	0.12	0.08	0.14	0.10
Cl	0.09	0.01	0.10	0.03	0.11	0.02	0.11	0.03	0.11	0.08	0.10	0.03	0.10	0.02	0.09	0.02	0.09	0.01	0.10	0.03	0.10	0.03
(n)	*14*		*16*		*23*		*26*		*10*		*15*		*18*		*18*		*19*		*20*		*15*	
(ppm)	Avg.	1 std. dev.	Avg.	1 std. dev.	Avg.	1 std. dev.	Avg.	1 std. dev.	Avg.	2 std. dev.	Avg.	1 std. dev.	Avg.	1 std. dev.	Avg.	1 std. dev.	Avg.	1 std. dev.	Avg.	1 std. dev.	Avg.	1 std. dev.
Rb	-	-	-	-	182	14.1	-	-	172	8.61	164	8.87	166	8.73	168	3.35	170	10.3	182	6.45	-	-
Sr	-	-	-	-	197	25.8	-	-	214	10.5	278	56.7	241	45.0	244	16.2	244	13.1	244	24.2	-	-
Y	-	-	-	-	32.7	1.63	-	-	32.5	2.96	31.5	1.05	31.1	1.63	32.5	0.93	33.3	0.79	33.0	1.67	-	-
Zr	-	-	-	-	327	36.2	-	-	290	26.9	274	19.0	276	16.7	292	6.47	300	6.35	292	22.4	-	-
Nb	-	-	-	-	17.8	1.98	-	-	16.5	0.54	16.0	0.51	16.2	0.96	16.6	0.15	17.1	0.41	17.2	0.78	-	-
Ba	-	-	-	-	860	49.8	-	-	811	26.8	798	43.4	786	41.2	807	30.2	819	31.2	827	50.7	-	-
La	-	-	-	-	36.8	2.84	-	-	33.8	2.88	33.1	1.19	32.8	2.42	34.3	0.85	35.4	0.83	34.8	2.00	-	-
Ce	-	-	-	-	78.8	5.91	-	-	74.5	6.58	72.2	2.33	71.9	3.75	74.5	1.94	77.1	2.43	75.1	5.04	-	-
Pr	-	-	-	-	8.96	0.63	-	-	8.39	0.45	8.32	0.25	8.27	0.38	8.61	0.32	8.84	0.41	8.50	0.63	-	-
Nd	-	-	-	-	35.5	2.11	-	-	35.5	1.69	34.1	2.50	34.1	1.85	36.1	1.05	37.0	1.60	35.4	2.44	-	-
Sm	-	-	-	-	7.40	0.63	-	-	7.63	1.16	7.29	0.81	7.14	0.68	7.58	0.99	7.58	0.39	7.47	1.03	-	-
Eu	-	-	-	-	1.33	0.13	-	-	1.33	0.10	1.48	0.13	1.37	0.19	1.38	0.17	1.49	0.13	1.48	0.22	-	-
Gd	-	-	-	-	6.06	0.49	-	-	5.99	1.08	5.79	0.56	5.72	0.63	6.15	0.65	6.57	0.68	6.34	0.99	-	-
Dy	-	-	-	-	5.84	0.32	-	-	5.83	0.35	5.54	0.41	5.46	0.58	5.78	0.72	6.19	0.45	5.69	0.78	-	-
Er	-	-	-	-	3.62	0.32	-	-	3.47	0.37	3.49	0.22	3.38	0.49	3.56	0.36	3.67	0.39	3.54	0.37	-	-
Yb	-	-	-	-	3.78	0.27	-	-	3.68	0.57	3.38	0.30	3.52	0.45	3.73	0.37	3.93	0.32	3.90	0.30	-	-
Lu	-	-	-	-	0.58	0.04	-	-	0.54	0.09	0.54	0.05	0.52	0.09	0.55	0.05	0.57	0.04	0.55	0.08	-	-
Hf	-	-	-	-	8.72	1.12	-	-	7.44	1.34	7.35	0.59	7.38	0.71	7.83	0.66	7.97	0.54	7.62	0.87	-	-
Ta	-	-	-	-	1.31	0.18	-	-	1.17	0.12	1.12	0.11	1.13	0.12	1.20	0.05	1.23	0.04	1.20	0.13	-	-
Pb	-	-	-	-	25.5	2.54	-	-	23.3	1.22	22.0	1.31	23.0	2.19	23.0	1.27	23.4	1.62	24.0	2.35	-	-
Th	-	-	-	-	18.8	3.23	-	-	15.7	2.41	14.6	1.89	15.0	1.24	15.8	0.74	16.3	0.72	15.7	2.23	-	-
U	-	-	-	-	5.4	0.91	-	-	4.72	0.38	4.48	0.37	4.78	1.38	4.72	0.16	4.78	0.24	4.60	0.57	-	-
(n)	-		-		*10*		-		*4*		*8*		*11*		*8*		*7*		*15*		-	

Tephra	Aso-I (top)		Aso-J (basal)		Aso-J (middle)		Aso-K (lower)		Aso-K (upper)		Aso-L		Aso-L		Aso-M		Aso-N/Z2 (lower)		Aso-N/Z2 (upper)		Aso-Z6	
Material	Pumice		Pumice		Pumice		Pumice		Pumice		Pumice		Pumice		Pumice-lapilli		Pumice-lapilli		Ash		Pumice-lapilli	
Sample	FLF207B		FLF202		FLF203		FLF200		FLF201		FLF197		FLF-247		FLF72		FLF67		FLF69		FLF227	
Location	Katayama		Katayama		Katayama		Katayama		Katayama		Katayama		Noga Cave		Noga Cave		Noga Cave		Noga Cave		Katayama Upper	
(wt.%)	Avg.	1 std. dev.	Avg.	1 std. dev.	Avg.	1 std. dev.	Avg.	1 std. dev.	Avg.	1 std. dev.	Avg.	1 std. dev.	Avg.	1 std. dev.	Avg.	1 std. dev.	Avg.	1 std. dev.	Avg.	1 std. dev.	Avg.	1 std. dev.
SiO_2	70.68	0.15	68.37	0.36	68.69	0.26	68.42	0.37	68.44	0.28	69.52	0.39	69.49	0.23	67.88	0.55	72.90	0.25	73.01	0.23	67.12	0.77
TiO_2	0.52	0.05	0.72	0.06	0.72	0.09	0.72	0.06	0.72	0.05	0.66	0.06	0.65	0.07	0.72	0.04	0.28	0.03	0.26	0.04	0.63	0.09
Al_2O_3	15.17	0.12	15.55	0.23	15.48	0.21	15.58	0.21	15.55	0.18	15.42	0.25	15.62	0.23	15.82	0.24	14.15	0.30	14.10	0.20	15.96	0.98
FeO	2.05	0.17	2.89	0.15	2.84	0.16	2.89	0.14	2.88	0.15	2.49	0.18	2.43	0.13	3.03	0.21	1.83	0.16	1.82	0.12	3.47	0.66
MnO	0.10	0.02	0.11	0.04	0.11	0.04	0.12	0.04	0.12	0.04	0.09	0.05	0.09	0.06	0.11	0.03	0.05	0.04	0.06	0.03	0.10	0.04
MgO	0.47	0.04	0.81	0.05	0.76	0.05	0.79	0.06	0.80	0.07	0.63	0.06	0.64	0.11	0.84	0.07	0.15	0.04	0.14	0.05	0.88	0.40
CaO	1.41	0.11	2.21	0.09	2.11	0.20	2.24	0.17	2.21	0.10	1.81	0.05	1.77	0.06	2.24	0.18	0.82	0.03	0.83	0.04	2.65	0.48
Na_2O	4.26	0.18	4.34	0.23	4.21	0.25	4.32	0.27	4.30	0.16	4.19	0.22	4.24	0.46	4.42	0.19	3.40	0.17	3.37	0.29	3.99	0.28
K_2O	5.11	0.19	4.74	0.15	4.81	0.18	4.67	0.20	4.70	0.17	4.98	0.21	4.88	0.30	4.70	0.18	6.26	0.20	6.27	0.40	4.91	0.46
P_2O_5	0.11	0.09	0.18	0.07	0.18	0.07	0.16	0.08	0.18	0.06	0.14	0.07	0.11	0.05	0.16	0.07	0.02	0.03	0.03	0.03	0.19	0.04
Cl	0.11	0.02	0.10	0.03	0.08	0.03	0.09	0.02	0.09	0.02	0.08	0.03	0.08	0.03	0.10	0.05	0.13	0.03	0.12	0.03	0.09	0.03
(n)	*4*		*19*		*17*		*18*		*18*		*19*		*10*		*12*		*13*		*14*		*13*	
(ppm)	Avg.	1 std. dev.	Avg.	1 std. dev.	Avg.	1 std. dev.	Avg.	1 std. dev.	Avg.	1 std. dev.	Avg.	1 std. dev.	Avg.	1 std. dev.	Avg.	1 std. dev.	Avg.	1 std. dev.	Avg.	1 std. dev.	Avg.	1 std. dev.
Rb	181	7.83	178	14.7	-	-	-	-	169	5.53	-	-	-	-	-	-	-	-	-	-	-	-
Sr	248	33.7	287	26.4	-	-	-	-	294	11.9	-	-	-	-	-	-	-	-	-	-	-	-
Y	33.9	4.14	32.4	1.64	-	-	-	-	33.3	1.14	-	-	-	-	-	-	-	-	-	-	-	-
Zr	301	33.4	278	17.0	-	-	-	-	287	10.5	-	-	-	-	-	-	-	-	-	-	-	-
Nb	17.5	1.88	16.5	0.67	-	-	-	-	16.9	0.69	-	-	-	-	-	-	-	-	-	-	-	-
Ba	841	54.1	805	53.3	-	-	-	-	821	21.7	-	-	-	-	-	-	-	-	-	-	-	-
La	36.0	4.66	33.8	2.42	-	-	-	-	35.0	1.32	-	-	-	-	-	-	-	-	-	-	-	-
Ce	76.4	11.2	74.5	5.28	-	-	-	-	76.3	3.11	-	-	-	-	-	-	-	-	-	-	-	-
Pr	9.04	1.80	8.60	0.86	-	-	-	-	8.84	0.46	-	-	-	-	-	-	-	-	-	-	-	-
Nd	37.1	7.18	35.5	4.08	-	-	-	-	37.1	1.68	-	-	-	-	-	-	-	-	-	-	-	-
Sm	7.54	2.13	7.76	0.87	-	-	-	-	7.69	0.69	-	-	-	-	-	-	-	-	-	-	-	-
Eu	1.61	0.29	1.56	0.13	-	-	-	-	1.61	0.18	-	-	-	-	-	-	-	-	-	-	-	-
Gd	6.42	1.47	6.26	0.66	-	-	-	-	6.30	0.38	-	-	-	-	-	-	-	-	-	-	-	-
Dy	5.93	0.91	5.68	0.56	-	-	-	-	5.97	0.67	-	-	-	-	-	-	-	-	-	-	-	-
Er	3.66	0.86	3.50	0.45	-	-	-	-	3.57	0.38	-	-	-	-	-	-	-	-	-	-	-	-
Yb	3.87	0.59	3.54	0.67	-	-	-	-	3.65	0.55	-	-	-	-	-	-	-	-	-	-	-	-
Lu	0.57	0.11	0.52	0.12	-	-	-	-	0.55	0.05	-	-	-	-	-	-	-	-	-	-	-	-
Hf	7.83	0.62	7.33	0.73	-	-	-	-	7.61	0.69	-	-	-	-	-	-	-	-	-	-	-	-
Ta	1.19	0.13	1.17	0.13	-	-	-	-	1.20	0.05	-	-	-	-	-	-	-	-	-	-	-	-
Pb	24.0	2.56	23.3	2.18	-	-	-	-	24.0	1.15	-	-	-	-	-	-	-	-	-	-	-	-
Th	15.9	2.10	14.9	2.38	-	-	-	-	15.8	0.79	-	-	-	-	-	-	-	-	-	-	-	-
U	4.64	0.71	4.42	0.65	-	-	-	-	4.58	0.28	-	-	-	-	-	-	-	-	-	-	-	-
(n)	*9*		*10*		-		-		*10*		-		-		-		-		-		-	

Trace element data has been obtained for fifteen of the tephra units (Table 6.2). The compositions of the glasses are more easily distinguishable at the trace element level, particularly using Th vs. Sr plots (Fig. 6.4B). The YmP5 – 8 tephra units are most distinct as they much more enriched in Sr (>320 ppm) than the other units analysed (Fig. 6.4B). Again, the Aso-F glasses show are heterogenous composition at the trace element level and have a unique cluster of glasses at 24 ppm Th (Fig. 6.4B). The majority of the ACP6 glasses have a lower Sr content (<100 ppm), which may be a useful distinguishing feature of the glasses of this eruption (Fig. 6.4B). Here we further highlight the key compositional features of the units (including previous characterisations of units), and thus the diagnostic chemistry that can be used to aid correlations.

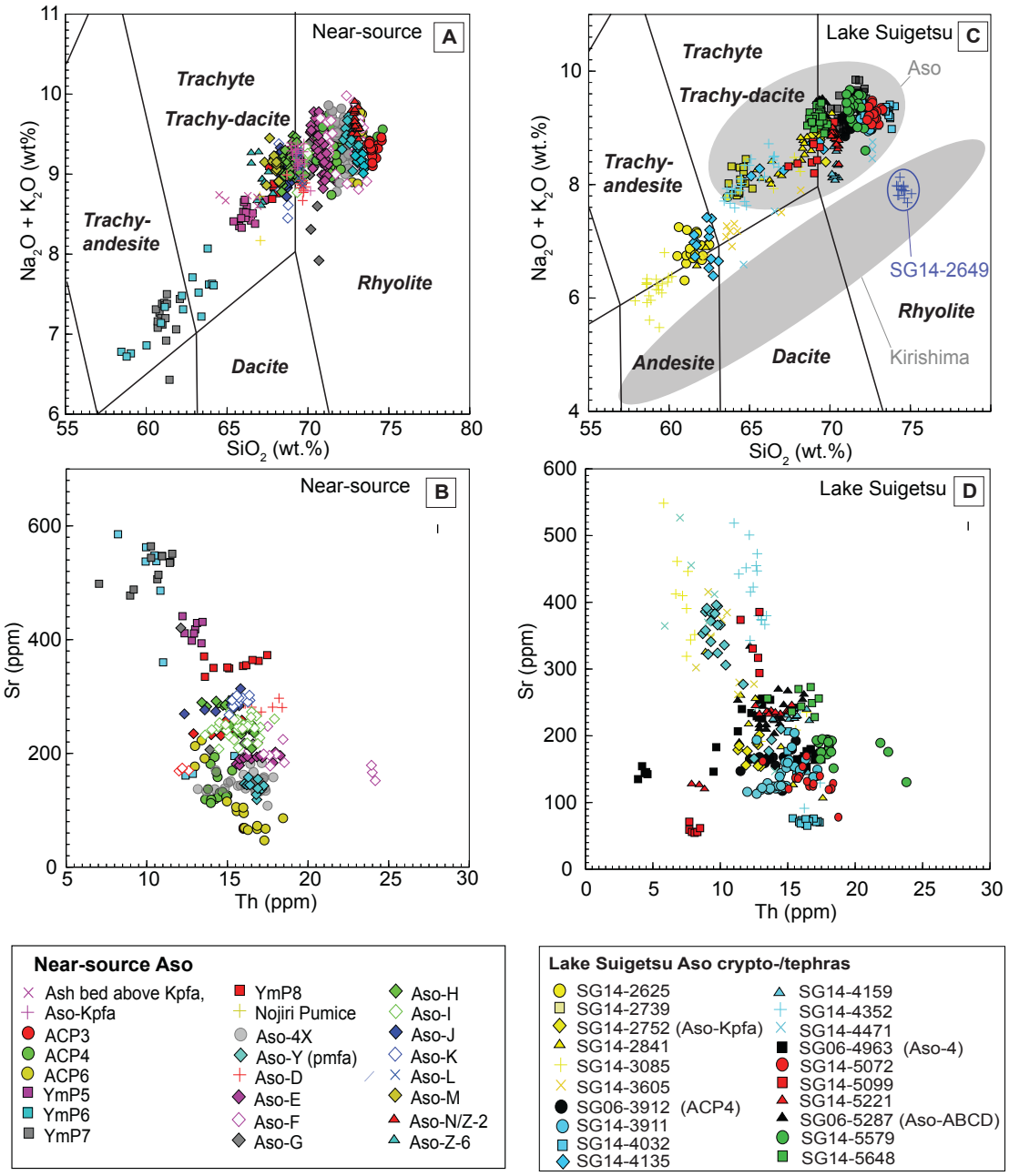


Figure 6.4: (A,B) Major and trace element glass compositions of the Aso tephra units preserved in proximal outcrops around the Aso caldera between the Aso-3 and AT marker beds. Compositional fields Aso and Kirishima are from proximal data presented in previous studies for Aso from Smith et al., 2013 (Aso-A, Aso-D, Aso-4), Albert et al., 2019a (Aso = ACP-3, ACP-4, ACP-5, ACP-6, Aso-4, Aso-Y, Aso-A, Aso-B, Aso-C, Aso-D Aso-I, Aso-K, Aso-M, Aso-N, Aso-3); McLean et al., 2020a (Aso = Aso-Kpfa) and for Kirishima from Albert et al., 2024 (Kr-Kb); Vineberg et al., 2024. (Kr-Aw, Kr-Iw). (C,D) Major and trace element glass compositions of the Aso crypto-/tephra deposits preserved in the SG14 sediments spanning 120 – 30 ka reported in: Vineberg et al. (2024); McLean et al. (2020a) Albert et al. (2019a) and Smith et al., (2013). Although the SG14-2649 was previously attributed to Aso activity (see McLean et al., 2020a) we re-assign the volcanic source to Kirishima.

6.4.1. Post-Aso-4

At Mizunomoto, 8 km east of the caldera wall, the deposit of the largest post-caldera eruption, Aso-Kpfa, is observed as a >1.0 m thick pumice-fall unit with occasional ash layers (Fig. 6.3; Miyabuchi, 2009). At Takimizu (1 km north of Mizunomoto; Fig. 6.1D), the Aso-Kpfa is also clearly observed, overlain by an ash bed, which is moderately-sorted, containing some fine pumice-lapilli. Both the Aso-Kpfa and overlying ash-bed were sampled for this study. The Aso-Kpfa has previously been characterised, although the location of this sampling site is unclear (see McLean et al., 2020a). The new major element data obtained from the tephra at Takimizu is consistent with earlier published data (Fig. 6.5A). We present the first trace element data for the Aso-Kpfa (Fig 6.5B). The ash bed above the Aso-Kpfa identified by this study can easily be distinguished from the Aso-Kpfa tephra as the younger ash, which is trachytic and in composition and has lower SiO_2 (64 – 67 wt.%) and greater FeO_t (>4 wt.%) contents (Fig. 6.5A).

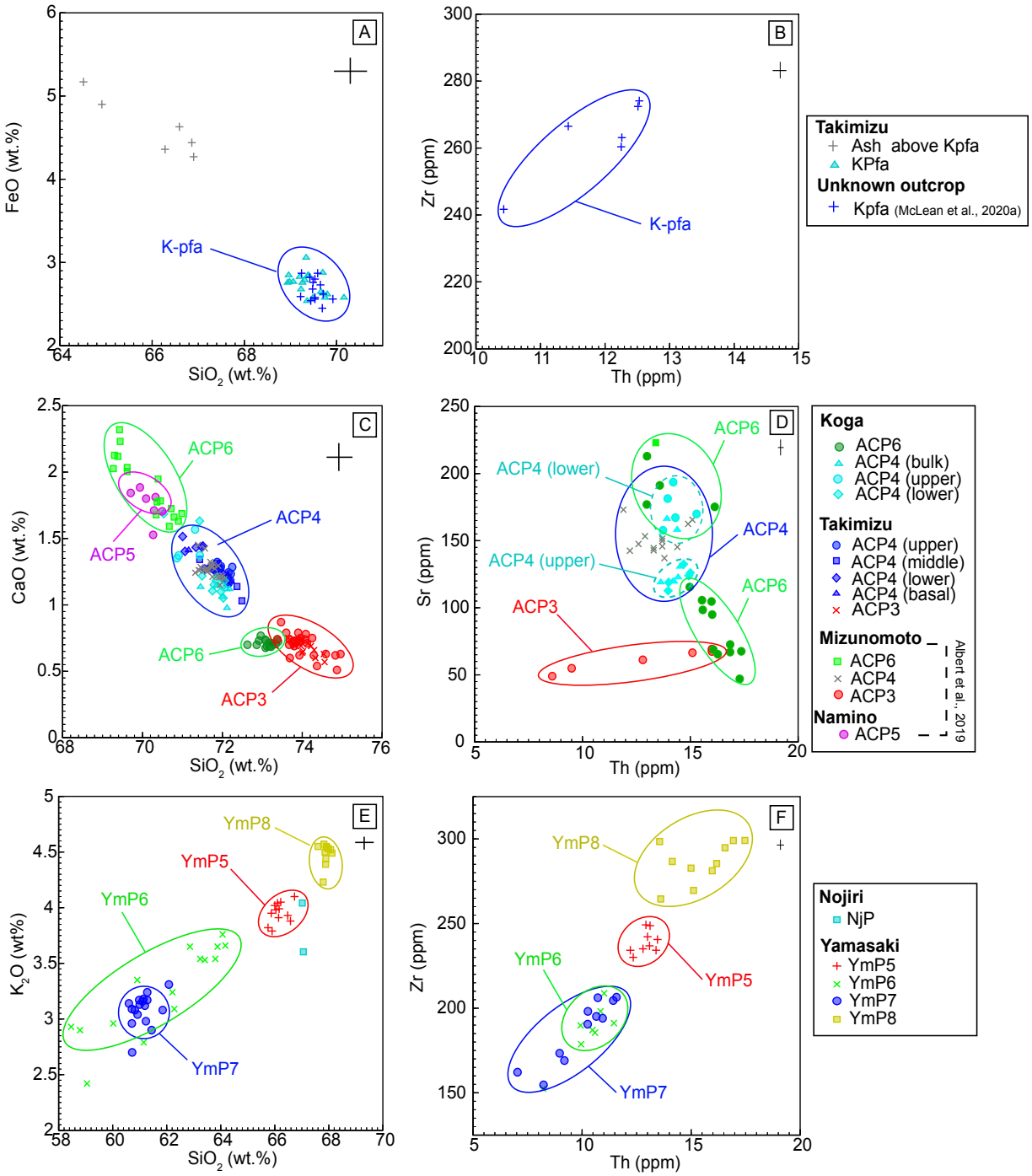


Figure 6.5: Major and trace element geochemical variability of volcanic glasses from large magnitude silicic eruptions between the Aso-4 and AT tephra layers preserved in outcrops to the east of the caldera wall (locations shown in Fig. 6.1) in comparison with other proximal deposits previously analysed (McLean et al., 2020a; Albert et al., 2019a). Error bars represent 2x standard deviation of repeat analyses of the StHs6/80-G MPI-DING standard glass.

Both the ACP3 and ACP4 tephras were observed and sampled at Takimizu, 1 km north of Mizunomoto (Fig. 5.1D). At Takimizu, the ACP3 is a 12 cm thick poor- to moderately-sorted pumice layer capped by a soil which is overlain by the 50 cm thick ACP4

which comprised of four sub-units: a 5 cm thick well-sorted fine pumice-lapilli (ACP4 base). Although the ACP5 has previously been reported in proximal outcrops at Koga (Fig. 6.3), the tephra was not clearly recognised in this outcrop and therefore not sampled. The ACP4 tephra at Koga is 39 cm thick and appears to be very weathered, and is subdivided into two units: 12 cm of scattered pumices within an ashy matrix (ACP4 lower) followed by 17 cm of coarser pumice-lapilli on top (ACP4 upper), which were both sampled. The ACP6 tephra at Koga measures 6 cm thick of well-sorted pumices and was also sampled. All four of the ACP3 – 6 tephras have previously been geochemically characterised from sites and Mizunomoto (ACP3, ACP4 and ACP6) 4 km SE from Namino (ACP5) (Albert et al., 2019a). The new major element data for the ACP3 and ACP4 tephras are broadly consistent with previously published data (Fig. 6.5C). In contrast, the ACP6 tephra sampled from Koga (NE of the caldera) is compositionally very distinct from the previously published ACP6 data from Mizunomoto east of the caldera wall (Albert et al., 2019a). The Koga ACP6 unit has higher SiO_2 content (ca. 73 wt.%), thus can easily be distinguished from overlying ACP5 and ACP4 glasses also preserved at Mizunomoto, as illustrated using SiO_2 vs. K_2O plot (Fig. 6.5C). Although Albert et al. (2019a) observed that the most silicic ACP deposit, ACP3, was distinguishable from ACP4 – 6, the new data for ACP6 reveals partial overlap with the ACP3 (Fig. 6.5C). Both glasses from the ACP3 and ACP6 tephras show partial compositional overlap with each other in both major and trace elements, although the older ACP6 glasses show a more constricted compositional range than the younger ACP3 glasses (Fig. 6.5C,D). Interestingly, at the trace element level, the ACP4 upper and lower samples from Koga can be discriminated at the trace element level where the ACP4 lower is more enriched in Sr at a given Th content relative to the overlaying ACP4 upper layer (Fig. 6.5D). As no trace element data was obtained from the four ACP4 sub-units at Takimizu, we cannot determine if this is replicated at sites further from the caldera wall. Nevertheless, the new data reveals two phases of the ACP4 eruption can be distinguished at the trace element level which has not previously been observed (Fig. 6.6D).

At Yamasaki, a series of thirteen pumice units (YmP) are identified within 15 m of sediment spanning 77 – 61 ka (Miyabuchi et al., 2003). We present the first glass data for the YmP5 – 8 tephras sampled from Yamasaki. The YmP5 is the thickest of the YmP eruptions and measures 2.3 – 2.5 m thick and is comprised of a lower pumice bed (analysed) and thin ash layers, overlain by scoria-fall (not analysed), whilst the YmP6 – 8 are pumice layers with no evidence of time between units (Fig. 6.2; Miybuchi et al, 2009). All four units span a broad silicic range (58 – 68 wt.% SiO_2) and are generally easily distinguished from other Aso units each other apart from YmP6 and YmP7 which show compositional overlap, although the younger YmP6 spans a broader compositional range (Table 6.2; Fig.

6.6E). Similarly, all tephras can be distinguished from each other at the trace element level, although YmP6 and YmP7 again show overlap, although YmP7 spans a broader range (Fig. 6.6F). All four units are easily distinguishable from other Aso units using major and/or trace element compositions (Fig. 6.4A,B).

The NjP is the first key tephra that erupted post-Aso-4 (Miyabuchi et al., 2003). At Nojiri, located 5 km east of the caldera wall, the NjP reaches a maximum thickness of 1.3 m an alternating pumice-lapilli and ash layer 50 cm from the base of the unit was sampled. However, the NjP appeared highly weathered, hindering the ability to obtain geochemical data for this tephra. Very limited major element (n = 2), show overlap with the YmP5 glasses (Fig. 6.5E) and no trace element data could be obtained.

6.4.2. Aso-4 and Aso-4X

The Aso-4 tephra has previously been analysed by Albert et al. (2019a) revealing the caldera-forming eruption erupted three geochemically distinct components at the major and trace element level (Fig. 6.6A,B). The Aso-4X observed at Kurumibaru is a 3.0 m thick unit and is directly overlain by Aso-4 pyroclastic-flow deposits and considered to be the basal Plinian fall of the Aso-4 pyroclastic-flow eruption (Fig. 6.3; Hoshizumi et al., 2022). Three samples were taken from throughout this unit (upper, middle and lower), and we present the first geochemical data for the Aso-4X tephra. There are no geochemical differences between the sub-units of the Aso-4X unit in major or trace element composition (Fig. 6.5A,B), although no trace element data has been obtained for the Aso-4X upper (Table 6.2). The Aso-4X glasses show overlap with the component 1 glasses of the Aso-4 eruption in both major and trace element composition, although extend to a broader range in Th content (13 – 18 ppm); more consistent with the Aso-Y glasses erupted during the older Stage-5 (Fig. 6.5B).

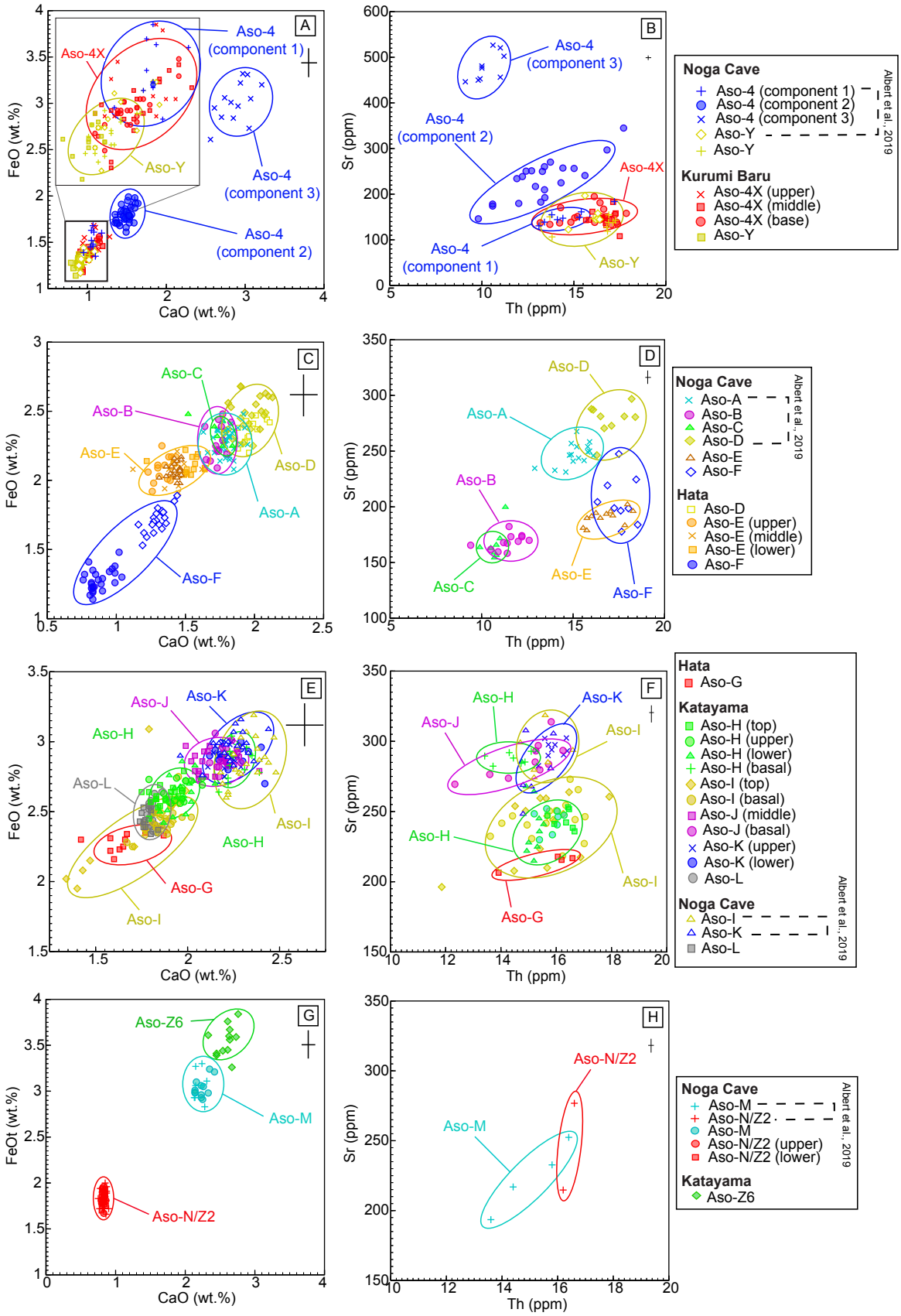


Figure 6.6: Major and trace element geochemical variability of volcanic glasses from large magnitude silicic eruptions between the Aso-3 and Aso-4 tephra layers preserved in outcrops to the east of the caldera wall (locations shown in Fig. 6.1) in comparison with other

proximal deposits previously analysed (Albert et al., 2019a). Error bars represent 2 x standard deviation of repeat analyses of the StHs6/80-G MPI-DING standard glass.

6.4.3. Stage 5 (Aso-Y)

The Aso-Y unit is a single pumice-fall eruption, and the only tephra between paleosols in the 10 kyr prior to the Aso-4 eruption (Table 6.1; Hoshizumi et al., 2022). Aso-Y was sampled both at Kurumi Baru and 11 km northeast at Noga Cave (Fig. 6.1D and 6.2) and has previously been geochemically analysed from Noga Cave (see Albert et al 2019a). The new data both from Noga Cave and Kurumi Baru show complete overlap with each other and previously published data (Fig. 6.6A,B). These Aso-Y compositions also share identical major and trace element compositions to the overlying Aso-4X and Aso-4 (component 1) (Fig. 6.6A,B).

6.4.4. Stage 4 (Aso-ABCD, Aso-EF, Aso-G, Aso-HI, Aso-JKL, Aso-M)

Here we discuss the geochemical features of the six units that make up the Stage 4 eruptions, many of which have not previously been analysed. The Aso-ABCD tephra is the largest pre-caldera eruption, and all units (Aso-A-D) have previously been characterised from an outcrop at Noga Cave (see Albert et al. 2019a). We provide additional major element data for the Aso-D unit sampled 7 km southeast of Noga Cave at Hata which is entirely consistent with previously published data (Fig. 6.6A).

We present the first geochemical data for the Aso-EF tephra (Fig 6.6C,D) from outcrops located at Hata and Noga Cave. The Aso-E unit is a thinner pumice-lapilli layer compared with the overlaying Aso-F unit, which is a thick package of alternating pumice- and ash-layers. At Hata, 8 km east of the caldera wall, the Aso-EF tephra measures 1.0 m thick whereas at Noga Cave, 18 km east of the caldera wall, the Aso-E unit is just 44 cm in thickness. Three samples were taken from the thicker Aso-E at Hata (upper, middle and lower) whilst one sample from the thinner unit preserved at Noga. All Aso-E glasses, regardless of their sampling site, are indistinguishable from each other at the major element level (Fig. 6.6C). Trace element data was only obtained from the Aso-E unit from Noga Cave, which can clearly be distinguished from the overlying Aso-ABCD tephra owing to lower Sr enrichment at a given Th content (Fig. 6.6D). The Aso-F glsses preserved at Hata and Noga Cave can be distinguished from each other at the major element level as the Noga Aso-F glasses are less evolved with lower SiO_2, FeO and CaO contents (Table 6.2; Fig. 6.6C). Only trace element data was obtained for the Aso-F glasses at Noga Cave. Whether sampled from Hata or Noga Cave, the glasses from the Aso-F and Aso-E units can be

distinguished from each other using CaO vs. FeO plot as the younger Aso-F deposit typically has glasses with lower CaO and FeO contents (Fig. 6.6C). However, discriminating the Aso-E and Aso-F units is somewhat challenging at the trace element level due to compositional overlap; although the glasses erupted during the Aso-F span a broader compositional range, for instance in Sr content (Table 6.2; Fig. 6.6D)

The Aso-G tephra has only recently been identified by Hoshizumi et al. (2022) and it is prominent in proximal outcrops at Hinatame (11 km to the east of the caldera wall), but missing from exposures further northeast (Fig. 6.3). We present the first geochemical data for the pumice erupted from Aso-G tephra, which was sampled from an outcrop located at Hata, 1 km southwest of Hinatame (Fig. 6.1D). The Aso-G glasses are relatively clustered (Fig. 6.6C–D), although show complete overlap with other units between Aso-3 and the AT tephras (Fig. 6.4A,B).

The Aso-HI eruptive succession is the second largest pre-caldera eruption, and measures at 8.0 m in thickness at Katayama, where Aso-I unit is defined as a 2.5 m thick pumice layer, overlain by Aso-H a 5.5 m thick package of alternating layers of pumice and ash beds, containing obsidian fragments (Fig. 6.3). Owing to the thickness of the Aso-H unit, at Katayama, for chemical characterisation, it was sub-divided into four sub-units labelled Aso-H1 – 4 (in ascending order) where he lowermost sub-units (Aso-H1 – 3) are all from pumice layers, whilst the uppermost sub-unit (Aso-H4) is from an ash layer.

The basal pumices (Aso-H1) have lower SiO_2, CaO and K_2O content relative to other Aso-H units (Aso-H2 – 4) which cannot be distinguished from each other (Table 6.2). Additionally, the Aso-H-1 can be distinguished from the overlying Aso-H2 – 4 sub-units at the trace element level owing to greater Sr enrichment (50 ppm) (Fig. 6.6F). Pumices from the upper and lower sections of the Aso-I unit from Katayama were analysed and cannot be distinguished from each other at the major or trace element level (Fig. 6.6E,F). The Aso-I unit was previously sampled at an outcrop at Noga Cave, 8 km northeast of Katayama (see Albert et al., 2019a). The glasses from the Aso-I unit at Noga Cave have higher CaO and FeO content, and greater Sr at a given Th content than the newly sampled Aso-I glasses from Katayama, and thus can easily be distinguished from each other using major and trace element compositions (Fig. 6.6E,F). This raises question marks over the stratigraphic correlation of Aso-I between Katayama and Noga. Interestingly, the basal pumice fall of Aso-H1 (basal pumice) at Katayama shows geochemical overlap with the glasses of the Aso-I unit previously sampled from Noga Cave at both the major trace element level (Fig. 6.6E,F). This might suggest that Aso-I is not actually recorded at Noga, and this fall deposit, resting

on a soil, corresponds to the earliest phase of the Aso-H eruption, as recorded at Katayama. Consequently, the earliest Aso-H fall deposit potentially offers a chemo-stratigraphic markers within the Aso-HI eruptive succession, given that the remaining Aso-H sub-units (Aso-H2 – 4) show partial overlap at major element and complete overlap at trace element level with the Aso-I unit at Katayama (Fig. 6.6E,F). Despite the thickness of the Aso-HI tephra, there is limited geochemical variation making correlations of specific sub-units challenging. The likely absence of Aso-I at Noga, and thinning between Katayama and Hinatame further north, might indicate that the plume of climatic Plinian phases of Aso-I, was predominantly dispersed towards the southeast.

The Aso-JKL tephra at Katayama measures a total thickness of 2.4 m where the lowermost Aso-L unit is 0.7 m thick and comprises alternating layers of ash and pumice. Aso-L is overlain by the 0.7 m thick Aso-K unit of white pumices, and followed by the much larger (2.0 m thick) Aso-J unit which is again comprised of alternating pumice and ash layers (Fig. 6.3; Hoshizumi et al., 2022). Upper and lower samples were taken from each of the Aso-J and Aso-K units, but there are no observable compositional differences within units (Fig. 6.6E). At Noga Cave, located 10 km northeast of Katayama (Fig. 6.1D), only the Aso-L (5 cm thick) and Aso-K (20 cm thick) units are seen (Fig. 6.3). The Aso-K unit from Noga Cave has been previously analysed (see Albert et al., 2019a), and here we present new data for the Aso-L unit. There are no geochemical differences between the Aso-K and Aso-L units sampled at Katyama and Noga Cave (Fig. 6.6E,F). The major element compositions of the younger units Aso-J and Aso-K show considerable overlap with each other, whilst the older Aso-L unit is easily distinguished owing to lower CaO (0.4.wt%) and FeO_t (0.4 wt.%) contents (Fig. 6.6E). At the trace element level, the Aso-J and Aso-K glasses show a high degree of similarity, although the younger Aso-J glasses extend from lower Th content (12 ppm; Fig. 6.6F).

The Aso-M tephra at Noga Cave is 9 cm thick comprised of well-sorted pumice-lapilli and has previously been analysed (see Albert et al., 2019a). The new data major element data obtained for Aso-M at Noga Cave is consistent with previously published glass data (Fig. 6.6G).

6.4.5. Stage 3 (Aso-N/Z-2, Aso-Z6)

The Aso-N/Z2 tephra at Noga Cave is 43 cm thick, comprised of a 19 cm of well-sorted, reversely graded pumice, followed by a 24 cm thick fine ash deposit with sporadic

pumices capped by a fine black ash. The lower pumice unit at Noga has previously been geochemically analysed (see Albert et al., 2019a). We analysed both the lower pumice and upper ash layers, but they cannot be distinguished from each other, and are consistent with previously published major element data for this unit (Fig. 6.6G).

At Katayama, the Aso-Z6 tephra is a 27 cm thick unit comprised of alternating pumice- and ash-layers (Fig. 6.3; Hoshizumi et al., 2022). We sampled a small 7 cm thick pumice-lapilli layer from Aso-Z6 at Katayama, and present the first major element data for this tephra. The Aso-Z6 tephra is compositionally distinct from the younger Stage 3 tephra Aso-N/Z2 as it has lower SiO_2 (6 wt.%) and higher CaO (2 wt.%) appearing to be less evolved (Table 6.2; Fig. 6.6G). No trace element data has been collected for the older Aso-Z6 tephra.

6.5. Discussion

6.5.2. Proximal-distal Aso correlations

Here we assess correlations between the proximal Aso tephras and the pre-30 ka tephra layers in Lake Suigetsu using the new glass geochemical data. Although some correlations have been previously made (McLean et al., 2020a; Albert et al., 2019a; Smith et al., 2013), many layers have not been correlated, particularly those prior to the Aso-4 eruption. Whilst McLean et al. (2020a) correlated the SG14-2649 cryptotephra to Aso, new data from Kirishima volcano suggests that it is a more likely source (Fig. 6.4C) and therefore, SG14-2649 is not discussed in this study.

The twenty Aso tephra and cryptotephra deposits preserved in Lake Suigetsu beneath the AT tephra (Table 6.3) are found interspaced between many widespread markers from across the islands of Japan, some of which occur in the volcanic stratigraphy of Aso. The Lake Suigetsu Aso deposits range from trachy-andesites through trachy-dacites to rhyolites (Fig. 6.4C). Four of these have previously been assigned to particular eruptions based on geochemical correlations to proximal deposits: SG142752 with Aso-Kpfa; SG06-3912 with ACP4; SG06-4963 with Aso-4; and SG06-5287 with Aso-ABCD (see: McLean et al., 2020a; Albert et al., 2019a; Smith et al., 2013). We focus on the six deposits beneath and thirteen above the Aso-4 tephra in Lake Suigetsu, with the aim of linking them to proximal units to help improve understanding of frequency, tempo and dispersal of Aso eruptions.

Table 6.3: Summary of the Aso derived crypto-/tephra layers identified in the sediments of the Lake Suigetsu (SG14 Core) between 120 – 30 ka.

Tephra (SG14 label)	V = thickness (cm)/ c = shards/gram		Glass shard morphology	Position in SG14 master core (cm)	SG14 CD (cm; ver. 28 Feb 2019)	SG06 CD (cm; ver. 28 Feb 2019)	IntCal20 yrs BP (median ± 1σ)	Major Element Glass Compositions (wt.%)				Trace Element Analyses	Aso correlation
								SiO2	K2O	CaO	n	n	
SG14-2625	C	9,838	MI, C, V	E-23 (6.0 – 7.0)	2624.7	2637.9	30.3 ± 0.05	60.51 - 65.12	2.61 - 3.88	3.57 - 5.48	21	-	-
SG14-2739	C	8,367	PL, MI	F-28 (62.8 – 63.8)	2738.9	2763.8	32.5 ± 0.05	63.70 - 65.18	3.58 - 3.92	3.39 - 4.20	16	-	Ash above Aso-Kpfa
SG14-2752	C	10,067	F, C, MV	F-28 (75.8 – 76.8)	2751.9	2776.3	32.7 ± 0.06	68.84 - 70.11	3.95 - 4.50	1.66 - 2.02	17	9	Aso-Kpfa
SG14-2841	C	2,850	PL, MI	E-30 (25.0 – 26.0)	2840.1	2861.4	35.00 ± 0.05	61.23 - 70.12	2.97 - 5.73	1.74 - 5.13	28	8	-
SG14-3085	C	4,400	PU	G-08 (52.0 – 53.0)	3084.0	3095.2	39.2 ± 0.06	57.89 - 68.16	1.88 - 4.55	2.56 - 6.95	28	12	-
SG14-3605	C	2,200	MI	E-37 (58.3 – 59.3)	3604.1	3629.3	45.5 ± 0.12	62.27 - 70.28	2.62 - 4.47	0.38 - 5.53	11	10	-
SG06-3912	V	0.1	F	F-39 (61.0 – 61.1)	3878.9	3911.6	48.7 ± 0.19	69.64 - 73.63	4.46 - 4.90	1.05 - 2.33	20	16	ACP4 (upper)
SG14-3911	C	24,890	F, MV	E-40 (44.5 – 45.5)	3911.1	3941.9	49.1 ± 0.1	71.90 - 72.48	4.52 - 4.83	1.02 - 1.15	27	23	ACP4 (lower)
SG14-4032	C	8,325	C, F	F-41 (9.0 – 10.0)	4031.7	4068.6	51.5 ± 1.1	72.13 - 74.03	4.60 - 5.03	0.66 - 1.02	19	17	ACP6
SG14-4135	C	>20,000	V	F-42 (30.9 – 31.9)	4135.4	4173.5	55.6 ± 1.7	61.54 - 69.60	2.74 - 4.44	1.98 - 5.65	20	20	-
SG14-4159	C	19,510	B, C, MV	G-11 (22.4 – 23.4)	4158.7	4198.3	56.6 ± 1.8	70.23 - 73.29	4.04 - 4.36	1.72 - 1.89	26	9	-
SG14-4352	C	5,883	PU	F-44 (25.8 – 26.8)	4351.9	4388.6	64.1 ± 2.3	63.42 - 66.81	2.91 - 4.54	2.66 - 4.43	30	18	YmP5
SG14-4471	C	1,333	B, MV, MI	F-45 (41.9 – 42.9)	4470.6	4509.0	68.7 ± 2.4	64.63 - 73.51	3.23 - 4.53	1.01 - 4.39	10	7	-
SG06-4963	V	3.5	F,V	G-12 (57.2 – 60.7)	4922.8	4962.4	86.4 ± 0.5	70.06 - 72.38	4.04 - 4.83	0.97 - 1.67	62	46	Aso-4
SG14-5071	C	49,225	C, F	F-51 (25.8 – 26.8)	5071.5	5113.6	91.2 ± 1.7	72.31 - 73.27	4.55 - 4.89	0.82 - 1.06	19	18	Aso-X
SG14-5099	C	67,850	MI, V	F-51 (53.4 – 54.4)	5098.5	5138.5	92.1 ± 2.1	67.42 - 70.26	3.14 - 4.43	1.51 - 3.22	9	6	-
SG14-5221	C	>20,000	C	F-52 (76.4 – 77.4)	5221.0	5257.0	96.0 ± 2.5	70.06 - 70.56	4.24 - 4.51	1.71 - 1.85	18	14	-
SG06-5287	V	3.5	MV	E-53 (52.5 – 56.0)	5250.6	5286.7	96.8 ± 2.6	69.19 - 69.88	4.43 - 4.65	1.69 - 1.92	18	21	Aso-ABCD
SG14-5577	V	0.8	C, MV	G-16 (19.1 – 20.1)	5578.8	5631.1	108.4 ± 4.1	71.03 - 72.20	4.89 - 5.20	1.09 - 1.37	22	17	Aso-EF
SG14-5648	C	>20,000[S]	MV	E-57 (46.2 – 47.2)	5648.3	5702.3	110.8 ± 4.1	69.85 - 68.59	4.50 - 5.01	1.70 - 2.26	40	8	Aso-HI

6.5.1.1. Post-Aso-4

Of the thirteen Aso deposits preserved in the 23 m of sediment above the Aso-4 in Lake Suigetsu, six can be correlated to proximal counterparts (Table 6.3). The SG14-2752 cryptotephra that is preserved 10 cm beneath the AT marker layer, was correlated by McLean et al. (2020a) to the Aso-Kpfa, the largest and most voluminous pumice-fall deposit erupted from the post-caldera cones (Fig. 6.7AB; McLean et al., 2020a). The SG14-2739 and SG14-2625 are preserved in the 1.3 m of sediment above the Aso-Kpfa (SG14-2752) that spans 2.3 ka (Table 6.3). Both deposits also plot at the trachy-andesite/andesite boundary (Fig. 6.4), and are less evolved than the older Aso-Kpfa. They can easily be distinguished from each other using major elements, becoming less evolved with time (Fig. 6.7A). The older SG144-2739 is preserved 13 cm above the Aso-Kpfa (SG14-2752) has an age of 32.5 ± 0.05 ka and shows partial overlap with the less evolved member of the newly identified ash bed above the Aso-Kpfa at Takimizu (Fig. 6.7A). We therefore tentatively correlate the SG14-2739 with this ash-bed above the Aso-Kpfa. On this basis, we determine there to be 300 yr between the eruptions responsible for the Aso-Kpfa and the overlying ash bed (Table 6.3). There are no obvious units in the proximal Aso sequences we investigated in the same stratigraphic position as the youngest Aso deposit in Lake Suigetsu (SG14-2625). In addition, nor does SG14-2625 show any geochemical overlap with any with Aso-Kpfa and the ash layer above the Aso-Kpfa (Fig. 6.7A). We therefore determine there to be at least one further compositionally distinct Aso eruption between Aso-KPfa and the AT tephra layers (Table 6.3).

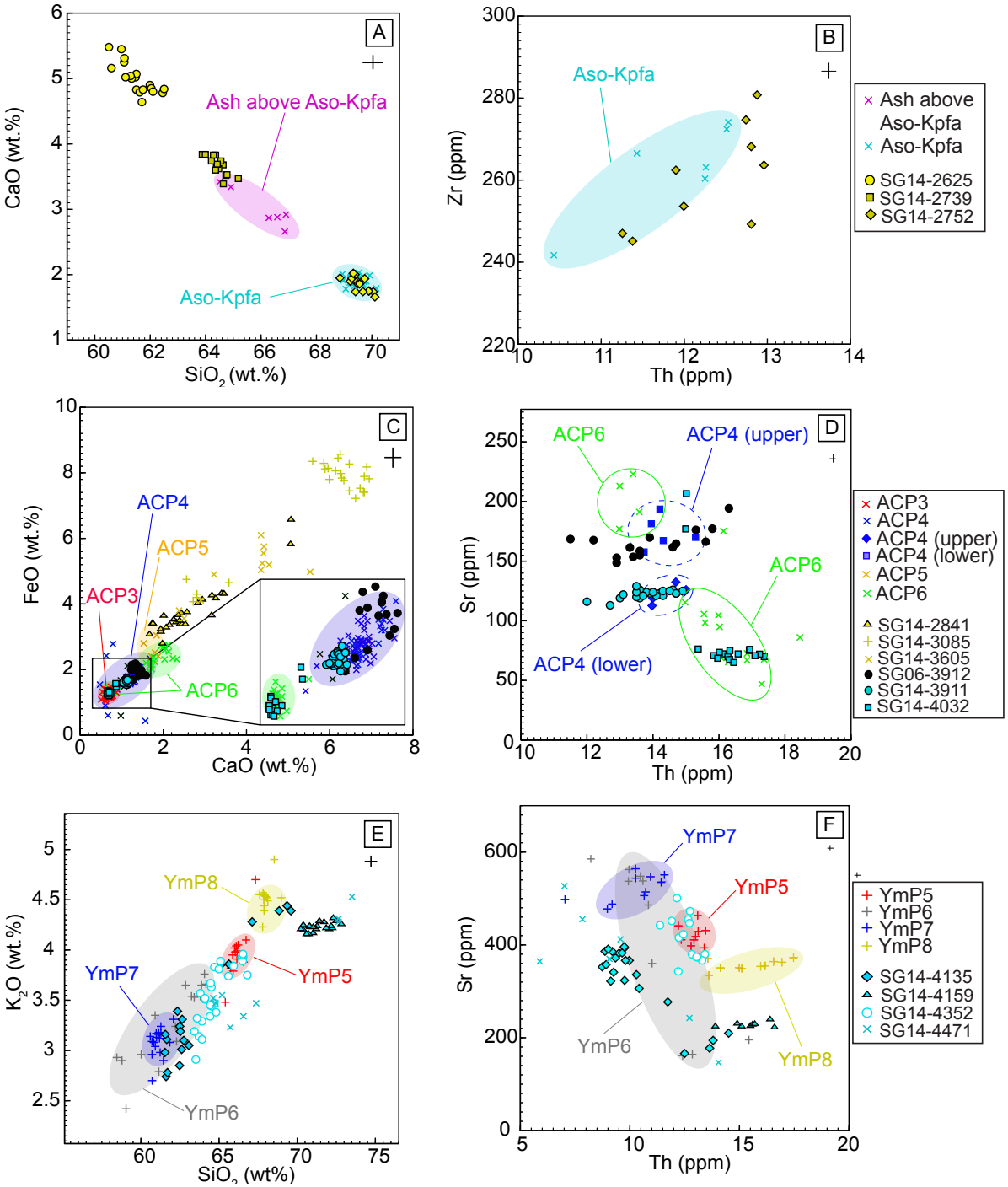


Figure 6.7: Major and trace element glass compositions of the Aso crypto-/tephra deposits preserved between the Aso-4 and AT tephra layers in the Lake Suigetsu sequence compared to reference chemical datasets produced for chrono-stratigraphically relevant eruption units. Reference chemical datasets obtained from proximal outcrops are from this Study, McLean et al., (2020a), and Albert et al. (2019a). Error bars represent 2x standard deviation of repeat analyses of the StHs6/80-G MPI-DING standard glass.

The three cryptotephra deposits SG14-3605, SG14-3085 and SG14-2841 are deposited within 11 kyr of each other and between the previously reported ACP4 (SG06-3912) and Aso-Kpfa (SG14-2752) tephras (Table 6.3). The younger SG14-2841 can be

distinguished from the older SG14-3085 and SG14-3605 deposits owing higher SiO_2 and lower Sr content (Fig. 6.4D), whereas the underlying can be discriminated from each other using CaO vs. FeO_t plots (Fig. 6.7C). Although these three deposits are at the same chronostratigraphic position as the ACP3 tephra (Fig. 6.3), there are no compositional similarities (Fig. 6.7C). All three of these Lake Suigetsu cryptotephras have relatively low shard concentrations (2,200 – 4,400 shards/gram; Table 6.3), and are indicative of smaller eruptions which may have been removed from the geologic record by the subsequent large Aso-Kpfa eruption or simply not preserved at the sites sampled, or different dispersal axes. We therefore determine there to be at least three further eruptions in addition to the ACP3 in the 16 kyr interval between the ACP4 and Aso-Kpfa eruptions (Table 6.3).

The ACP4 is a 1.0 mm thick visible tephra in Lake Suigetsu (SG06-3912) and has an age of 48.7 ± 0.19 ka (Table 6.3; Albert et al., 2019a). Vineberg et al. (2024) observed that the SG14-3911 cryptotephra also shares a geochemical affinity with the ACP4 in both major and trace element compositions (Fig. 6.7C,D). The two Lake Suigetsu SG14-3911 and SG06-3912 deposits are separated by ~30 cm of sediment, representing ~400 years and can be distinguished from each other both at the major and trace element level (Fig. 6.7C,D; Table 6.3). The acquisition of new trace element data for the upper and lower units of the ACP4 tephra allow the two units to be geochemically distinguished using Th vs. Sr (Fig. 6.7D). The older SG14-3911 cryptotephra glasses show a clear affinity with the ACP4 lower glasses whilst the younger SG06-3912 show an affinity with the ACP4 upper (Fig. 6.7D). This suggests that the two phases of ACP4 activity occurred over a 400 yr interval, not long enough for substantial soil development and hence why any hiatus in the eruption phases is not recorded in the proximal record (Table 6.3). The SG14-4032 cryptotephra is preserved 1.2 m beneath the ACP4 lower and show good overlap with the evolved member of the ACP6 tephra preserved at Koga (Fig. 6.7C). Glasses from both the SG14-4032 and ACP6 tephras are distinct at the trace element level owing to low Sr content (Fig. 6.4C,D) and are preserved in the same stratigraphic position, above the widespread Kuju-Hd/P1 marker (SG06-4141). Based on the good chronostratigraphic and geochemical agreement, we determine the SG14-4032 to represent the distal equivalent of the ACP6, and refine the age to 51.5 ± 1.1 ka using the Lake Suigetsu age model; 8 kyr younger than the age derived from the age-depth model presented in Miyabuchi (2009). Although the distal equivalents of the ACP3 and ACP5 have not been identified in the Lake Suigetsu sequence, we determine that the ACP3-6 eruptions occurred over a 23kyr interval, with the ACP3 and ACP5 erupting at 49 – 33 ka and 52 – 49 ka, respectively (Table 6.3).

In the 8.0 m of sediment between the Aso-4 (SG06-4963) and ACP6 (SG14-4032) eruption deposits there are four Aso cryptotephras preserved in Lake Suigetsu: SG14-4135, SG14-4159, SG14-4352, and SG14-4471 (Table 6.3). These four deposits span a 13 kyr interval and likely to correlate with the Yamasaki eruption units based on their chronostratigraphic position (Fig. 6.2). Only glasses from the SG14-4352 consistently show an affinity with the newly analysed Yamasaki pumices (Fig. 6.7E,F). The SG14-4352 show geochemical overlap with the glasses from the YmP5, but also some overlap with the older YmP6 (Fig. 6.7E,F). The YmP5 tephra is much thicker comprised of upper scoria-fall and lower pumice- and ash-layers, whereas the older YmP6 unit was a single thin pumice layer (Miyabuchi, 2009; Miyabuchi et al., 2003). Here only the lower pumice fall of the YmP5 was sufficiently well preserved for glass analysis, and given the upper portion of the YmP5 is comprised of scoria, its distal equivalent is likely to span a greater geochemical range than the YmP5 pumice sample analysed. The YmP5 is believed to have erupted over a relatively short period, and identified as the key post-caldera marker layer. Its ENE dispersal trajectory (Miyabuchi, 2009) suggests dispersal towards Lake Suigetsu 525 km away. Due geochemical agreement and the known dispersal axis, we provisionally correlate the SG14-4352 with the YmP5 tephra and revise the age of this eruption to 64.1 ± 2.3 ka using the Lake Suigetsu age model (Table 6.3). Whilst we are unable to correlate the three cryptotephra deposits (SG14-4032, SG14-4135 and SG14-4159) preserved above, and the one below (SG14-4471) the YmP5 (SG14-4352), in Lake Suigetsu to known Aso eruptions using geochemical data, we suggest these may be the distal deposits of eruptions in the YmP1-4 and YmP9 – 13 series, respectively. Due to the preservation of the YmP5 and ACP6 tephras in Lake Suigetsu, we are able to constrain the ages for the YmP1-4 eruptive series to between 64.1– 51.5ka. Likewise, the preservation of Aso-4 and YmP5 allows us to constrain the YmP6 – 13 eruptive series and the NjP eruption to between 86.4 ka and 64.1ka (Table 6.3). Further geochemical characterisation of the Yamasaki pumices is required to make further correlations with the Lake Suigetsu sequence, and provide further age constraints for these units. However, the preservation of many of these Yamasaki units is very poor, which makes chemical characterisation of the proximal deposits very challenging.

6.5.1.2. Pre-Aso-4

Of the six Aso eruption deposits preserved beneath Aso-4 in Lake Suigetsu, four can be correlated with their proximal counterpart (Table 6.3). Three Aso cryptotephra deposits are preserved in Lake Suigetsu between the previously identified Aso-ABCD (SG06-5387) and Aso-4 (SG06-4963) tephras preserved in Lake Suigetsu: SG14-5072, SG14-5099 and

SG14-5221 (Table 6.3). These three deposits chrono-stratigraphically correspond to the Stage 5 activity at Aso reported by Hoshizumi et al (2022), and these cryptotephra deposits all have shard concentrations exceeding 20,000 shards/gram (Table 6.3), indicating they are likely to have been large (≥M 5.5) eruptions in order to disperse ash 525 km northeast from source. Both the SG14-5072 and SG14-5099 cryptotephra deposits are preserved in the 0.7 m of sediment above the K-Tz deposit in Lake Suigetsu, and the SG14-5221 is identified 0.8 m beneath the K-Tz (Vineberg et al., 2024). Whilst the Aso-Y is preserved in proximal sequences in the same chronostratigraphic position as the SG14-5072 and SG14-5099 cryptotephra deposits (between the K-Tz and Aso-4 markers; Fig. 6.3), Vineberg et al. (2024) revealed these cryptotephra layers have lower K_2O contents than the Aso-Y glasses (Fig. 6.8A) and cannot be correlatives. The new glass data for Aso-Y presented here extends the compositional range, but the Lake Suigetsu deposits in the same stratigraphic position do not have the similar chemistry.

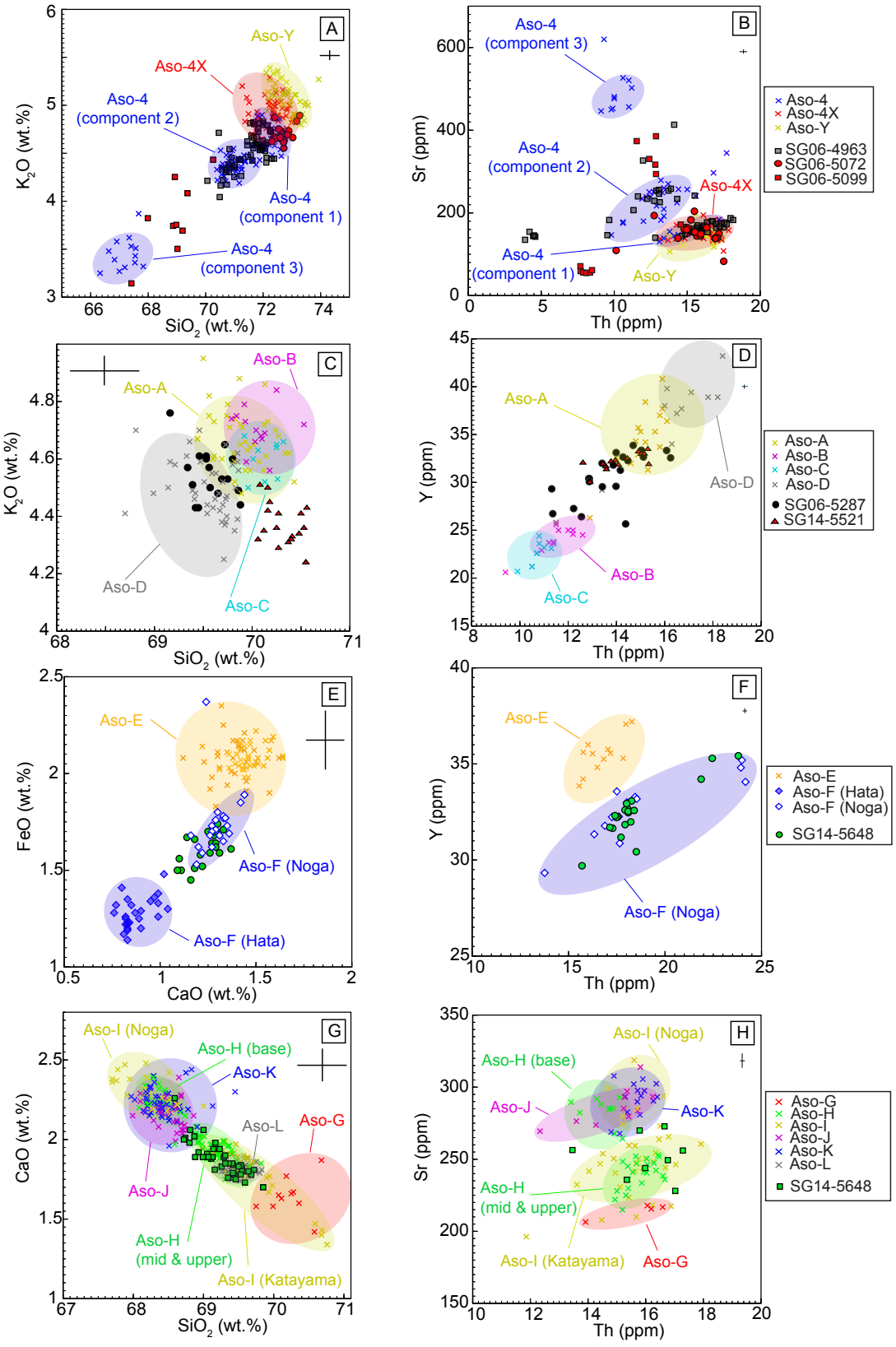


Figure 6.8: Major and trace element glass compositions of the Aso crypto-/tephra deposits preserved between the Aso-3 and Aso-4 tephra layers in the Lake Suigetsu sequence compared to reference chemical datasets produced for chrono-stratigraphically relevant eruption units. Reference chemical datasets obtained from proximal outcrops are from: This Study; McLean et al., 2020a and Albert et al., 2019a. Error bars represent 2 x standard deviation of repeat analyses of the StHs6/80-G MPI-DING standard glass.

The SG14-5072 cryptotephra is the final Aso eruptive deposit preserved 1.5 m beneath the 3.5 cm thick Aso-4 tephra (SG06-4963). The glass chemistry of SG14-5072 is similar to the component 1 of the Aso-4 ignimbrite glasses and the newly characterised Aso-4X glasses in both major and trace elements (Fig. 6.8A,B). We correlate the SG14-5072 with the Aso-4X tephra unit due to the compositional agreement and stratigraphic positioning and refine the age of the eruption to 91.2 ± 1.7 ka based on the Lake Suigetsu age model (Table 6.3). Although the Aso-4X unit is considered to be the basal Plinian fall of the Aso-4 pyroclastic-flow eruption (Hoshizumi et al., 2022), the fact that both are identified in Lake Suigetsu age, the age model indicates that 5 kyr elapsed between the Aso-4X and Aso-4 eruptions. Given that there is no clear evidence of a time break in near-vent records (i.e. soils), we suggest, owing to the Aso-4 eruption to have cut down into the underlying stratigraphy a multiple sites, and a sharp unconformity seen at the top of the Aso-4X tephra, that the Aso-4X tephra has been removed due to the erosive power of the massive M7.7 Aso-4 eruption.

The SG14-5221 sits 30 cm stratigraphically above the 3.5 cm thick visible SG06-5287 that has been correlated with Aso-ABCD (Albert et al., 2019a; Smith et al., 2013). The SG06-5287 glasses were tentatively correlated with those of the Aso-A sub-unit owing to similarities in Y and Th contents (Albert et al., 2019a). The SG14-5221 glasses show compositional overlap with both the Aso-A sub-unit and SG06-5287 at the trace element level (Fig. 6.8B), but has lower K_2O contents (Fig. 6.8A). Thus, SG14-5221 reflects younger activity post-Aso-ABCD.

The identification of three cryptotephra deposits in the ~10 kyr of sediment between Aso-ABCD and Aso-4 indicate there were three eruptions large enough to disperse ash 525 km away from source, including Aso-4X. Our new correlations indicate that Stage 5 activity includes Aso-Y, Aso-4X, and another two eruptions. We suggest that at least four eruptions occurred in the 10.4 kyrs prior to the Aso-4 eruption, which may be obscured in the proximal record due to burial and erosion by the subsequent Aso-4 eruption deposit.

The new glass geochemical data of proximal units has facilitated the correlation with two additional M 5.0 tephras erupted during Stage 4 of activity to those distally preserved in Lake Suigetsu: Aso-EF and Aso-HI. In the 4.2 m of sediment beneath the Aso-ABCD tephra (SG06-5287), Vineberg et al. (2024) identified two Aso deposits SG14-5577 and SG14-5648, dated to 108.4 ± 4.1 ka and 110.8 ± 4.1 ka, respectively (Table 6.3). Both deposits are preserved beneath the widespread markers of Ata, SK and Toya in Lake Suigetsu (see Fig. 6.9). The glasses from the 0.8 cm thick SG14-5577 tephra are distinct from other Aso

glasses preserved in Lake Suigetsu at the trace element level owing to a higher Th population (Fig. 6.4D). The SG14-5577 glasses show a clear geochemical affinity with the distinct Aso-F glasses sampled at Noga Cave, most notably both displaying high Th populations not present in any other geochemically analysed units (Fig. 6.8E,F). We therefore determine the SG14-5577 cryptotephra preserved in Lake Suigetsu to represent the distal equivalent to the Aso-EF eruptive sequence, and revise the age for this activity is 108.4 ± 4.1 ka, significantly which is older than the 99.2 ka estimate by Hoshizumi et al (2022) based on loess-chronometry. Based on the Lake Suigetsu age-model, a period of ~12 kyr elapsed between the Aso-EF and subsequent Aso-ABCD eruption.

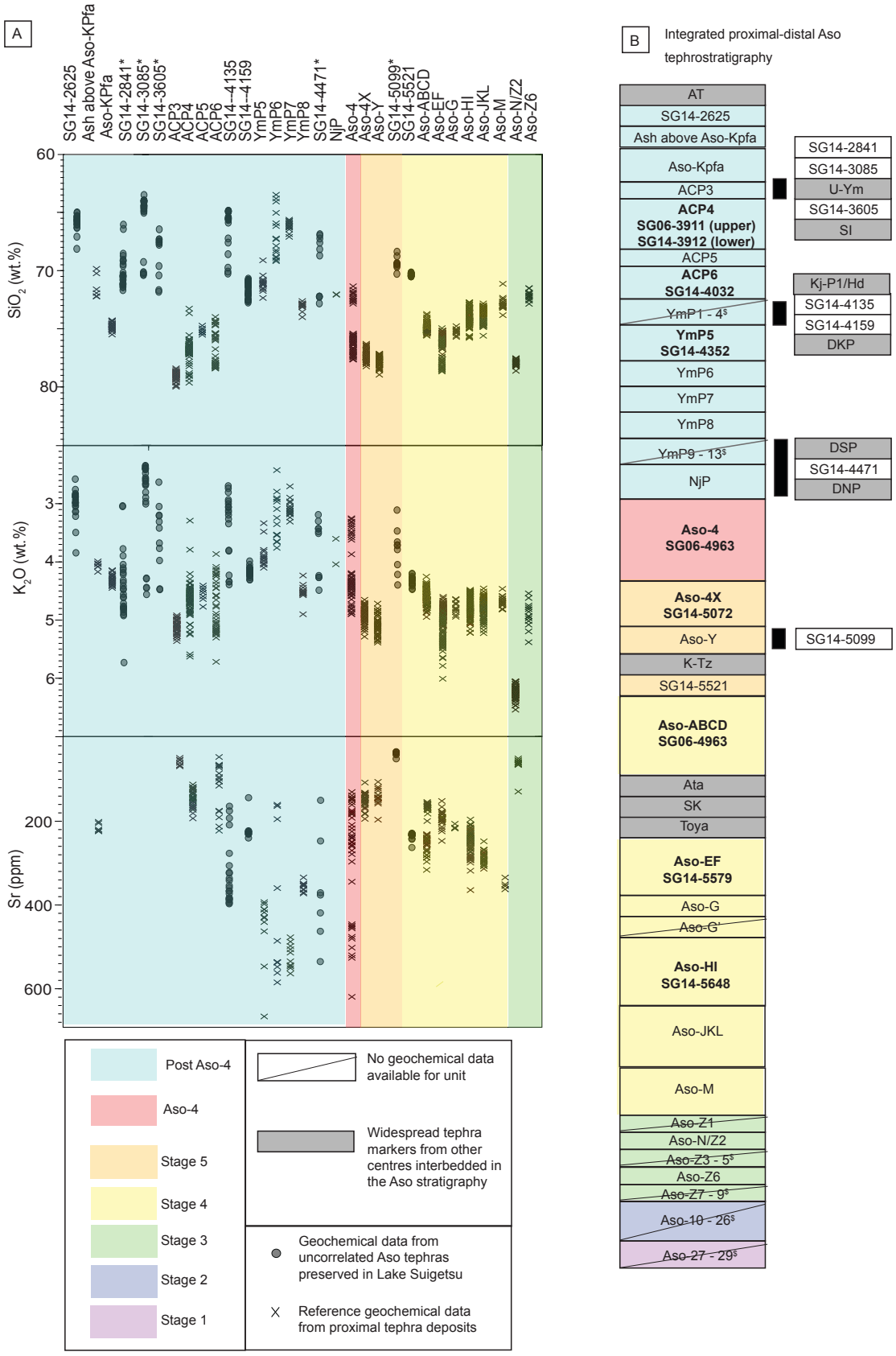


Figure 6.9: (A) Selected major and trace elements useful for recognising variations in the volcanic glasses erupted from tephra units preserved between the Aso-3 and AT tephras in outcrops around the caldera (black crosses) as well as uncorrelated Aso tephras identified in

the Lake Suigetsu archive (black circles) which have been geochemically analysed. * represents that the stratigraphic position may not be quite rights and may, for example be 1 unit too high, or 3 too low. $ represents multiple units. The height of boxes are indicative to the magnitude of eruption (i.e. larger boxes represent higher magnitude eruptions). Data for these units are from: This Study; McLean et al., 2020a; Albert et al., 2019a; Smith et al., 2013). (B) An integrated proximal-distal stratigraphy of Aso eruptions from proximal outcrops and Lake Suigetsu. The black bar represents the reltive stratigraphic position of Lake Suigetsu Aso tephras where their position is unclear. Stages 1 – 5 are as defined by Hoshizumi et al (2022) with the exception of Aso-4X which has been revised to Stage 5 by this study.

The SG14-5648 cryptotephra is the lowermost Aso deposit preserved in Lake Suigetsu, 69 cm beneath the Aso-EF (SG14-5579) tephra and has a high shard concentration of >20,000 shards/gram (Table 6.3; Vineberg et al., 2024). Vineberg et al. (2024) reported an affinity of the SG14-5648 glasses with those erupted during Aso-I, however new major element data indicate that the compositional overlap is with both Aso-HI and the older Aso-L glasses (from the Aso-JKL unit) on major elements (Fig. 6.8G). Using Th vs. Sr, the SG14-5648 cryptotephra glasses shows better affinity with the glasses from Aso-HI eruption preserved at Noga Cave owing to distinct Sr at a given Th content (Fig. 6.8H). The Aso-HI eruption was the second largest pre-caldera eruption with a volume of 5 km^3 and numerous pumice and ash beds that are 1.0 m thick, 35 km east of the caldera (Fig. 6.3; Hoshizumi et al., 2022). We determine the SG14-5648 cryptotephra to represent the distal equivalent to the Aso-HI eruption with an age of 110.8 ± 4.1 ka, which is broadly consistent with the 102.6 ka estimate by Hoshizumi et al (2022) based on their age-depth model.

6.6. Implications

6.6.1. Frequency, tempo and dispersal

Ten of the Aso tephras preserved in outcrops between the Aso-3 and AT tephras have been identified 525 km northeast of the volcano, in the Lake Suigetsu sequence. The following units have been identified in the 111 – 30 ka sediments: an ash bed above Aso-Kpfa, Aso-Kpfa, ACP4, ACP6, YmP5, Aso-4, Aso-4X, Aso-ABCD, Aso-EF and Aso-HI (Table 6.3.; Fig. 6.9). Six of these correlations have been facilitated through the new glass chemical data presented here, which includes data for an additional phases of the ACP4 eruptions.

The potential for erroneous correlations between near-source sections, only been revealed by chemically examining proximal units and integrating data with the distal record,

has implications for eruptive frequency. Many of volcanic deposits have been found interspaced with key tephras from other Japanese sources in the Lake Suigetsu sedimentary sequence (Fig. 6.9), which will help with the correlation to and the synchronisation with other records. For instance, the YmP5 tephra is preserved below the widespread DSP tephra from Daisen volcano, and the Aso-EF and Aso-HI tephras are beneath the massive M7.3 Toya caldera-forming eruption tephra (Fig. 6.9). The integration of the Aso proximal stratigraphy with the Lake Suigetsu record, a key tephro-stratotype for east Asian volcanism, is facilitated by the new glass chemistry for the deposits. It allows insights into the frequency, tempo and dispersal of eruptions in the lead up to and following caldera eruptions.

We determine that that the eruptions which produced the twenty Aso volcanic deposits Lake Suigetsu are likely to be ≥M 5.0 to have been dispersed tephra 525 km away from source (cf Sulpizio et al., 2024). The three post-Aso-4 tephras Aso-Kpfa, ACP4, ACP6 and YmP5 identified in Lake Suigetsu are all considered to be some of the largest post-caldera eruptions (Mitabuchi et al., 2003, 2009). Furthermore, the Aso-ABCD and Aso-HI eruptions that are also preserved in Lake Suigetsu are the two largest pre-caldera eruptions (Hoshizumi et al., 2022). There are nine Aso deposits preserved in Lake Suigetsu sediments that we have not been able to correlate to a specific eruption unit defined proximally. Although three of these distal layers (SG14-4471, SG14-4159 and SG14-4135) are in stratigraphic positions where there are recorded Aso eruption deposits (Yamasaki pumices), there are six distal layers (SG14-2625, SG14-2841, SG14-3085, SG14-3605, SG14-5099 and SG14-5521) preserved in Lake Suigetsu that are in positions where there are no units preserved in the exposures that have been studied. This suggests that the exposures studied by us and others are incomplete and indicate that Aso has been more active than previously thought in the in the ~10 kyr prior to the Aso-4 eruption.

Several of the eruptive deposits reported in outcrops to the east of the Aso-4 caldera wall are not in Lake Suigetsu (e.g. ACP3, ACP5, Aso-Y and Aso-G) indicating they were likely smaller eruptions given that dispersal are conducive to transport ash to Lake Suigetsu or they were erupted at times of the year when transport directions were unfavourable (Table 6.1). Moreover, although most silicic activity at Aso occurred pre-30 ka, eruptions have been reported above the AT tephra in proximal outcrops (Miyabuchi, 2009). None of these post-AT Aso eruptions have been identified in Lake Suigetsu (see Albert et al. 2024, 2019a; McLean et al., 2018, Smith et al., 2013). These more recent eruptions also have a ENE dispersal so the fact that they are not preserved in Lake Suigetsu must be due to their small tephra volumes (<1.0 km^3), corresponding to a M of 3. This study highlights that at locations ~500 km from vent and along the general dispersal axis, cryptotephra from the

eruptions may be preserved in sedimentary records if the tephra volumes >1 km^3 (i.e. M >3). This finding underscores the relationship between eruption size, dispersal distance and the potential for preserving volcanic ash in sedimentary records, which is essential for reconstructing volcanic histories.

6.6.2. Constrained eruption chronology

The Lake Suigetsu tephrostratigraphy provides detailed insights into Aso, one of the Japan's most active calderas and a possible candidate for the next VEI 7 eruption (Newhall et al., 2018). The integrated proximal-distal record reveals that Aso erupted explosively at least thirty-four times between 111 – 32 ka (Aso-HI – Aso-KPfa) (Fig. 6.9). The Lake Suigetsu age model constrains the age for six of these Aso eruptions: ACP6 51.5 ± 1.1 ka; YmP5 64.1 ± 2.3 ka; Aso-4X 91.2 ± 1.7 ka; Aso-EF 108.4 ± 4.1 ka and Aso-HI 110.8 ± 4.1 ka (Table 6.3). These ages from Lake Suigetsu are broadly consistent with earlier estimates (Table 6.1 and 6.3). The identification of the ACP6 in Lake Suigetsu further constrains the eruption age by ~8 ka to 51.5 ± 1.1 ka and thus, indicates that the four ACP3 – 6 eruptions occurred between 52 – 33 ka, which is more constrained than the 60 – 30 ka timeframe estimated by Miyabuchi (2009). Similarly, the new correlatives identified in this study have provided further age constraints for pre-caldera eruptions not preserved in Lake Suigetsu; 97 – 91 ka for the Aso-Y eruption, and 111 – 108 ka for the Aso-G and Aso-G' eruptions.

6.6.3. Geochemical compositions

The compositional data presented here provides further insight into the magmatic system beneath Aso between ~135 – 30 ka. Although many of the widespread eruption deposits identified have glasses that are rhyolites/trachytes, consistent with previous reports (Albert et al., 2019a), we have extended the known compositional range of the distal tephra to include trachy-andesites (Fig. 6.4B; Fig. 6.4C). The most distinct glasses erupted from Aso are those with low SiO_2 and K_2O contents associated with the Yamasaki pumice eruptions (Fig. 6.9). Although it is difficult to distinguish Aso deposits, trace elements offer another order of discrimination particularly Sr (Fig. 6.9). The glass chemistry of some eruption units varies between sites, e.g. ACP6, Aso-F and Aso-I (Fig. 6.5 and 6.6). This suggests that the eruption stratigraphy is probably more complex, and highlights the need for continued logging and geochemical characterisation of these proximal deposits to ensure correlations are robust. In the case of Lake Suigetsu, where correlations have been made to units that have different compositions at different sites (i.e. ACP6 and Aso-F; Fig. 6.5 and

6.6), the cryptotephra have compositions that are more similar to samples taken from the outcrops to the north, and northeast to the caldera. This implies that some eruptions sequentially tap different compositions through the eruption, and during which the wind direction may change. As expected, the distal sites have the compositions of the deposits that are found along the same dispersal axis. Thus, the findings from this study show how changing wind direction can influence the distribution of ash across different locations.

Whilst Aso glasses span a range of compositions and there are variations over time, there are no clear compositional shifts directly preceding or following the large caldera-forming eruptions (Fig. 6.9). This contrasts the magmatic shifts observed in the lead up to and following large caldera eruptions at Campi Flegrei, Italy (Vineberg et al., 2023; Pabst et al., 2008; Smith, et al., 2011a) and at the calderas in the Taupo Volcanic Zone (Pamukçu et al., 2020; Smith et al., 2005). However, only one of the twenty-nine tephras erupted in the early Stages 1 – 3 of activity have been analysed. Further characterisation of these earlier deposits is essential to the understanding of the detailed evolution of the magmatic system.

6.7. Conclusions

This study summarises the explosive volcanic activity of Aso volcano between 135 – 30 ka and provides glass compositional data for the largest and possibly widespread eruption deposits. This new data identifies further tie-points to the Lake Suigetsu record, which include: an ash bed above Aso-Kpfa, Aso-Kpfa, ACP4, ACP6, YmP5, Aso-4, Aso-4X, Aso-ABCD, Aso-EF and Aso-HI. These correlations provide invaluable insights into chronological constraints of these eruptions as well as the frequency, dispersal and tempo of activity. Most of the tephras correlated with their known counterpart in Lake Suigetsu are some of the largest pre- and post-caldera eruptions, producing vast amounts of tephra (volumes >1.7 km^3) capable of being dispersed over large geographical areas and are potentially useful markers for synchronising widespread distal records (e.g. Aso-HI, Aso-ABCD, ACP4 and Aso-Kpfa). Furthermore, the identification of an additional six tephras in Lake Suigetsu has provided better age constraints on these eruptions and thus refined understanding the tempo of activity. For example, the newly correlated ACP6 has meant that the four ACP3 – 6 eruptions occurred within an 11 kyr period. The ability to geochemically distinguish the upper and lower units of the ACP4 eruption have enabled both to be identified in Lake Suigetsu revealing 400 years occurred between these phases of one of the largest post-caldera eruptions. Moreover, significant insights into the activity in the lead-up to the cataclysmic Aso-4 eruption; in the 10 kyr prior to the Aso-4 eruption, there were at least

four eruptions (including Aso-Y and Aso-4X). Although the Aso-4X was considered contemporaneous with the Aso-4 eruption (Hoshizumi et al., 2022), we determine ~5 kyr occurred between these two eruptions using the Lake Suigetsu age-model. Similarly, at least three additional eruptions have likely been removed in near-vent sequences by the large post-caldera Aso-Kpfa eruption. Overall, this research expands the glass geochemical database for Aso tephra deposits. Furthermore, these glass data have helped integrate of the proximal-distal record update the tephrostratigraphry of one of the world's largest calderas. Future studies should continue to integrate the records to better constrain the magnitude and dispersal of the eruptions to better understand the magnitude and dispersal of the eruptions to inform future hazard and risk management strategies.

CRediT author statement

S.O.V.: Conceptualisation; Resources; Data Collection; Methodology; Investigation; Formal analysis; Visualization; Writing-Original Draft; Writing-Review & Editing; Funding acquisition. **P.G.A.:** Conceptualisation; Resources; Data Collection; Writing-Review & Editing; Supervision; Funding acquisition. **D.M.:** Conceptualisation; Data Collection. **T.S.:** Resources **Y.M.:** Resources; Data Collection. **H.H.:** Resources; Data Collection. **H.M.B:** Data Collection. Resources. **G.J.:** Resources. **F.N.:** Resources. **R.S.**: Formal analysis. **K.Y.:** Data Collection. **I.K.**: Data Collection. **J.K.:** Resources. **C.J.M.**: Resources. **SG14 Project Members:** Resources. **T.N.:** Resources; Data Collection; Funding acquisition. **V.C.S:** Conceptualisation; Resources; Data Collection; Writing-Review & Editing; Supervision; Funding acquisition.

Acknowledgements

S.O.V. is funded by NERC as part of the Environmental Research Doctoral Training Programme at the University of Oxford (NERC; NE/S007474/1). VCS and TN acknowledge funding from the Japan Society for the Promotion of Science (JSPS; KAKENHI-15H021443). The SG06 coring campaign was funded by the UK Natural Environmental Research Council (NERC; NE/ D000289/1) New Investigators Award to TN. The Fukui-SG14 coring campaign was funded by the Fukui Prefectural government, Japan. P.G.A., H.M.B and G.J. are funded through a UKRI Future Leader Fellowship award (FLF; MR/S035478/1). TS acknowledges funding from the Japan Society for the Promotion of Science (JSPS; KAKENHI-22H02380). FN acknowledges funding from the Japan Society for the Promotion of Science (JSPS; KAKENHI-JP19K13438. The Lake Suigetsu coring was conducted by the team of Seibushisui Co. Ltd Japan, led by Mr Atsumi Kitamura.

See Appendix C for Supplementary Material.

Chapter 7: General Discussion and Conclusions

In this final chapter, the main findings of this thesis are reviewed in the context of the aims and research questions outlined in Chapter 1. The findings from this thesis (Chapters 4 – 6) are discussed more broadly, and also includes recommendations for future crypto-/tephra studies in centres of intense volcanic activity, particularly in the context of Italy and Japan.

The overarching aim of this research project has been to refine the tephrostratigraphies of the very productive volcanic regions in both Italy and Japan through the integration of proximal and distal tephra records. This thesis has augmented the Campanian and Japanese tephrostratigraphic records through the use of both tephra and cryptotephra investigations of both proximally and distally located sequences. Detailed geochemical data (major and trace elements) were obtained for almost all crypto-/tephras identified in this thesis from Italy and Japan to correlate with their respective volcanic sources, and in some cases to specific eruptions (e.g. SK, Toya). Each results chapter (Chapters 4 – 6) has an individual discussion section, and thus this short chapter is designed to synthesise the results in view of the research questions set in Chapter 1, and place them in the wider tgephrochronological context.

7.1. Objective 1: Augment the tephrostratigraphic records of Campania (Italy) and Lake Suigetsu (Japan).

The absence of tephra layers from the geological record presents a significant challenge for reconstructing past volcanic events, and obscures key information about eruption history, dispersal, frequency, and magnitude of past eruptions. This becomes a bigger issue further back in time where almost 89% of medium-large sized (VEI or M ≥4) eruptions are currently missing from the eruption record at ~100 ka (Kiyosugi et al., 2015). The findings from this research of proximal and distal crypto-/tephra investigations conducted in Campania, Italy and in central and southern Japan, have identified numerous ash-fall deposits which have not previously been reported and provide new insights into some of the world's most dangerous volcanoes between ~120 – 40 ka. These outcomes show that even in fairly comprehensively studied regions, we do not yet have a very detailed understanding of the tempo of medium (and in some cases large) explosive events that have occurred over the Late Quaternary.

Revisiting previously logged proximal outcrops in Italy and Japan have identified further pyroclastic deposits (see Chapters 4 and 6). At Acquamorta, on the western edge of the Campi Flegrei caldera, twelve tephra units, separated by paleosols, were identified in the 6 m succession between the widespread 56 ka MEGT (Ischia) and the 40 ka CI (Campi Flegrei) tephra layers (Fig. 4.3). This is considerably more units than the four to six units which were previously identified in the same stratigraphic position at this outcrop (see Orsi et al., 1996; Perrotta and Scarpati, 1994; Rosi et al., 1988). Many of the tephra deposits identified at Acquamorta for this thesis are relatively thin despite their proximity to their volcanic sources, suggesting they may be small eruptions and may explain why they have not been previously identified (see Fig. 4.3). However, even large magnitude events erupted from Campi Flegrei are not always well preserved close to source, Japan, (see Albert et al., 2019b). Re-evaluation of outcrops to the east of the Aso caldera has identified further fall layers (see Hoshizumi et al., 2022) as well as an additional deposit identified during fieldwork in 2023 (ash layer abover the Aso-Kpfa, Chapter 6). Logging proximal outcrops for tephra, and being diligent in the process, is critical for building an accurate and detailed record of events, and has implications for calculating the total tephra volumes erupted.

Despite the number of outcrops with pyroclastic deposits preserved beneath the CI and NYT beyond the caldera wall (see Orsi et al., 1996), these sequences have not undergone robust geochemical characterisation. The findings from this thesis provide further evidence for compositional shifts at Campi Flegrei between caldera eruptions (Chapter 4; Smith et al., 2011a). With further such detailed stratigraphic and geochemical studies will it be possible to constrain the tempo of volcanic activity of these centres between the large caldera-forming eruptions to make correlations more robust for deposits in distal archives (e.g. McGuire et al., 2022; Wutke et al., 2015; Tomlinson et al., 2014; Wulf et al., 2004, 2008).

The cryptotephra investigation of the Lake Suigetsu sediments beyond 50 ka has significantly extended the tephrostratigraphic record of Japanese volcanism and provides new insights into lower magnitude and more distal eruptions. Visual inspections of the SG14 core identified 2 further visible macro-tephra deposits, however, the use of a stepped density-separation extraction procedure enabled many more cryptotephra glass shards to be detected, at varying quantities, throughout the entire sedimentary sequence (see Fig. 5.4). A total of one-hundred-and-twenty-two isochrons have now been identified in the whole Lake Suigetsu sedimentary sequence spanning the last ~200 kyr; eighty-four cryptotephras and thirty-eight visible tephras (Fig. 7.1). This thesis has contributed a further forty-one isochronous markers to the Lake Suigetsu record. In the investigated sediments (~120 – 50

ka), at least one significant cryptotephra is detected in each metre of sediment, although periods of high concentrations may indicate periods of increased volcanic activity or favourable conditions for preservation. On average, events that form isochrons in Lake Suigetsu sediments occur between four to five times more frequently than large (M≥6.0) and occur more frequently, consistent with what is observed in the younger sections of the sequences (Albert et al., 2024; McLean et al., 2018, 2020a). This research re-affirms Lake Suigetsu as the single most comprehensive ash-fall record of East Asian explosive volcanism over the past 200 kyr period, and contributes significantly to our understanding of the timing and ash dispersals of pre-historic eruptions

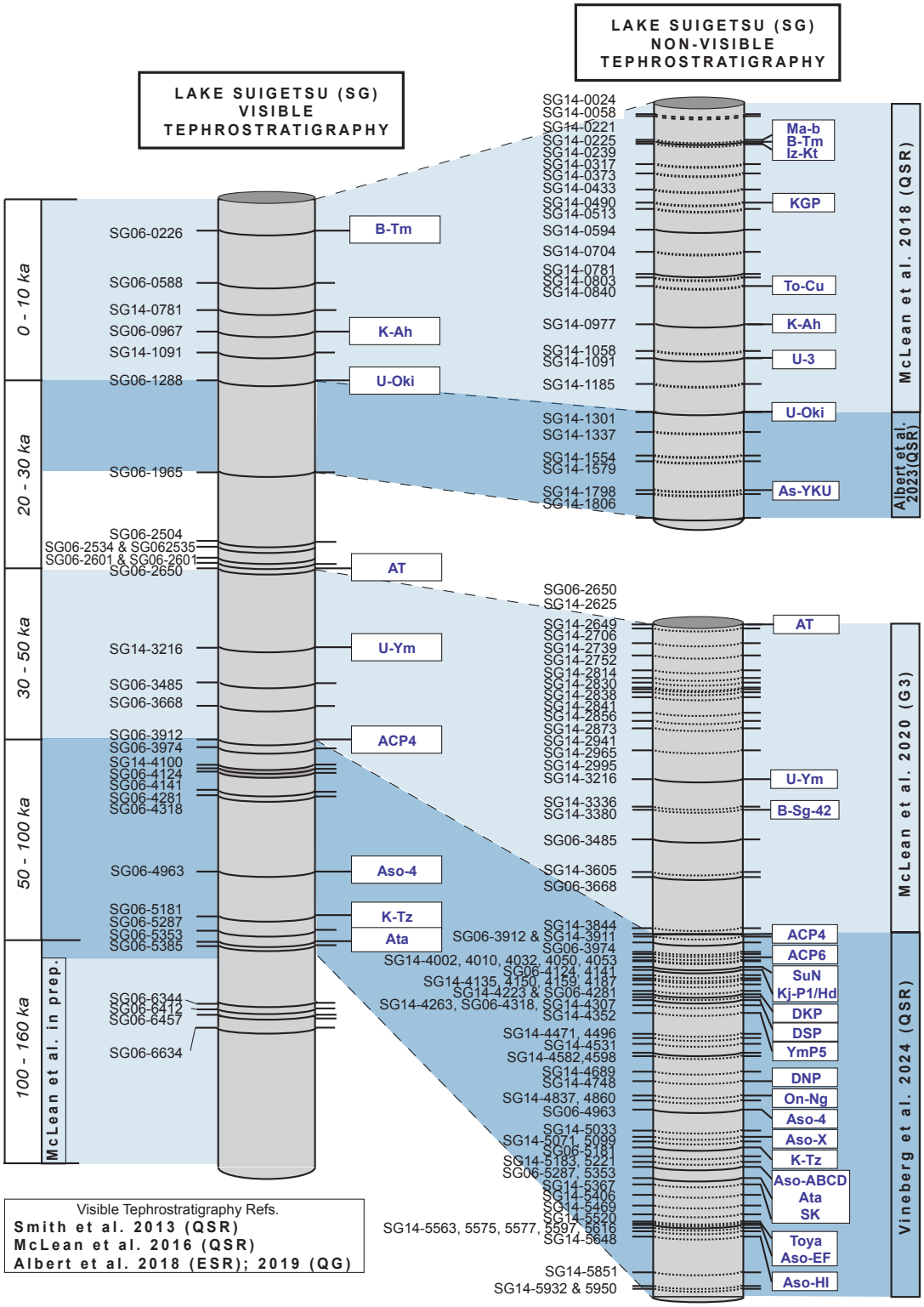


Figure 7.1: Summary of the Lake Suigetsu tephrostratigraphy and tephra research presented in this thesis (Albert et al., 2024; McLean et al., 2016; 2020a; Smith et al., 2013; Vineberg et al., 2024; Chapter 5). Non- visible (cryptotephra) layers are shown by a dashed line and solid lines represent visible tephras. All deposits are labelled with the respective SG06 or SG14 core depth and if correlated to widespread markers. Fifty isochrons were identified in the sediments of Lake Suigetsu dated between 120 and 50 ka (Chapters 4 – 5; Vineberg et al., 2024). Cryptotephra investigations are not possible above the 35 cm-thick AT tephra as background glass concentrations are too high between 30 and 25 ka.

This thesis has detected cryptotephra glass shards into the pre-50 ka section of the Lake Suigetsu sediments (Fig. 5.4). Conventional density-separation techniques are notoriously time consuming (>30 hours to process 1 m of sediment; McLean et al., 2022) and requires significant amount of core material thus it is not often feasible to undertake detailed cryptotephra investigations over long stratigraphic intervals. Even in the case for Greenland ice cores, where processing of material is less arduous as it is not necessary to sieve or carry out density extractions to remove host material, have only been assessed in part at low-resolution over certain time periods (e.g. Bourne et al., 2015; Davies et al., 2008, 2012, 2014; Abbott et al., 2012). The use of a stepped density-separation extraction procedure has enabled cryptotephra glass shards to be successfully detected, at varying quantities, throughout the entire Lake Suigetsu record and demonstrates what continuous investigations of high-resolution sequences can achieve (see Albert et al., 2024; Vineberg et al., 2024; McLean et al., 2018, 2020a). Timms et al. (2017) advocate for the use of 1 cm sampling of entire core sediments, rather than the traditional scan and resample methodology (as employed in Chapter 5), to identify the stratigraphic position of all cryptotephra horizons within a sedimentary sequence and thus eliminate subjective sampling methodologies. However, employing such a strategy for the whole ~98 m long SG14 sequence would be extremely time consuming, especially following the visible tephra layers given the high backgrounds of large eruptions (e.g. K-Ah, AT, K-Tz). Nonetheless, the findings from this study reinforce the calls for improvements in rapid non-destructive scanning techniques to enable the accurate and precise detection and characterisation of the actual number of cryptotephra horizons in a sequence (Kylander et al., 2012). Ultimately, near-future cryptotephra studies conducted in regions near highly active centres such as Japan should follow a similar stepped density-separation extraction procedure to ensure the detection of present cryptotephra deposits.

The ability to accurately identify and precisely locate the positions of isochrons within a sedimentary sequence is fundamental to crypto-/tephra studies as if erroneous they may alter the determinations of robust tephra correlations (e.g., Cook et al., 2018; McLean et al., 2018; Wulf et al., 2018). Sedimentary sequences located close to volcanic centres and in the sediments following large eruptions which blanket large areas, may produce large and persistent background concentrations of volcanic glass (e.g. McLean et al., 2018; Matsu-ura et al., 2017). As expected, high concentrations of glass shards are observed in the Lake Suigetsu core sediments following the visible ash layers, for example, after the 2.3 cm thick K-Tz tephra (SG06-5181) distinctive platy shards were continuously observed, in excess of 5,000 shards/gram, for several metres (Fig. 5.4). By conducting detailed morphological characterisations of cryptotephras in the high concentration ‘tails’ following visible

tephras/where high concentrations of shards occur, has helped ensure no other isochrons were missed. By employing the set of criteria outlined by McLean et al. (2018) involving morphological and geochemical techniques (see Fig. 1.2), we are confident that the additional 41 isochrons identified in the 70 kyr sediments investigated in this thesis do not represent re-worked events. However, this can only be tested once other high-resolution cryptotephra studies are conducted into deeper time (i.e. >50 ka) across Japan. Steps to begin outlining a framework for discriminating between reworked and primary cryptotephra or visible tephra layers have begun (McNamara et al., 2019; McLean et al., 2018; Bertrand et al., 2014) and may be advanced with experimental tephra focussing on how cryptotephra layers of different composition and size are preserved in different localities and over different timescales (e.g. Cutler et al., 2018; Dugmore et al., 2018). Advancing a framework to distinguish between reworked and primary cryptotephra deposits could benefit from targeted experimental studies which simulate tephra deposition under controlled conditions. This would help clarify how factors such as geochemical composition, particle size and environmental settings (e.g. local topography, weather conditions and vegetation) influence the presence or reworking of tephra over time. However, such progress is currently limited by the limited availability of long-term high-resolution monitoring of tephra in natural environments as well as the complexity and cost of experimental setups.

7.2. Objective 2: Provide detailed geochemical characterisation of the volcanic glasses. Use their major and trace element compositions to determine their source regions, volcanoes and specific eruptions.

This thesis has amassed huge glass geochemical datasets for Italian and Japanese volcanoes, facilitating new insights into the compositional features of many of these eruptive centres and events (Chapters 4 – 6). This thesis presents a total of *n = 2913* new geochemical analyses (*n = 2056* EMPA and *n = 857* LA-ICP-MS), contributing significantly to the geochemical databases of Italy (n = 453 EMPA and *n = 121* LA-ICP-MS) and Japan (*n = 1603* EMPA and *n = 736* LA-ICP-MS). Almost all distal volcanic deposits (visible tephras and cryptotephras) have been corelated to their respective volcanic centres by comparing to the proximal eruption datasets. All twelve of the Acquamorta were correlated to the Campanian sources of Campi Flegrei and Ischia through the comparison with previously published (Giaccio et al., 2017; Tomlinson et al., 2012, 2014, 2015) geochemical data for these centres (Fig. 4.4). The one-hundred and twenty-two crypto-/tephras preserved in the Lake Suigetsu sequence are from at least twenty-seven different volcanic centres, across three different geographic regions (Japan, North Korea China and South Korea) (Fig. 7.1).

The forty-one isochronous markers spanning 120 – 50 ka presented in this thesis are from a total of thirteen different volcanic centres located in Japan and South Korea (Table 5.2). The geochemistry of the glass shards has enabled most of these distal tephra deposits to be correlated to their volcanic regions/arcs in Japan, and many correlations can be made to a specific volcano and a few to known eruption events (Table 5.14).

All proximal and distal crypto-/tephras successfully underwent EMPA in this thesis (see Chapters 4 – 6). Despite several studies citing the precision of measurements using a 10 μm microbeam to be problematic for the EMPA of distal cryptotephra glass shards (e.g. Kuehn, 2016; Pearce et al., 2014; Hayward, 2012), glass shards from all the crytptotephra deposits were analysed in this thesis (Chapter 5). This may be in part due to the relatively high concentration of glass shards (typically >1000 s/g; Table 5.2) than in other cryptotephra studies conducted in other sequences, allowing more selective for glasses with larger, less vesicular shards with fewer microlite inclusions which meant they could easily be analysed by a 10 μm beam. Despite the high degree of precision afforded by EMPA (see Lowe et al., 2011; Hunt and Hill 1996; Westgate and Gorton 1981), many of the glasses analysed in this thesis (both proximal thick tephras and distally located cryptotephras) show repeated compositional overlap with each other at the major element level (Figs. 4.4 and 5.5). This thesis has further demonstrated that the sensitivity of EMPA is not always sufficient to discriminate compositionally similar tephra horizons and highlights the need for further diagnostic geochemistry techniques to distinguish many of the crypto-/tephras presented in this thesis (Chapters 4 – 6).

The utilisation of single-grain trace element analyses (i.e. LA-ICP-MS) has become increasingly popular in crypto-/tephra studies, particularly where discrimination between glasses which exhibit similar major-element geochemical compositions (e.g. Albert et al., 2018; Tomlinson et al., 2010, 2012). Almost all volcanic deposits underwent LA-ICP-MS to further characterise deposits, and the results further demonstrate that trace element data are particularly useful for discriminating different volcanic centres (see Chapters 4 – 6). For instance, the Ischia tephra units presented in Chapter 4 possess the lowest Th, Nb, Nd and Zr and higher Zr/Th and Y/Th relative to Campi Flegrei units identified at Acquamorta, and can easily separated using Th vs. Y and Th vs. Nd bi-variate plots (Fig. 4.4). Similarly, the varying Th, Zr, Sr and Y contents have enabled (through the use of bi-variate plots) the discrimination between volcanic centres located across Japan which cannot be distinguished using major element compositions alone (see Figs 5.5 and 5.6). However, since the size of the beam required for trace-elemental analysis is routinely 20 μm (Tomlinson et al., 2010), which was sometimes too big to analyse the cryptotephra glasses preserved in Lake

Suigetsu (see Chapter 5). Moreover, the acquisition of trace element data has not always enabled the geochemical differentiation of deposits with overlapping major element compositions (see Chapters 4 – 6). Nevertheless, continued efforts should be made to obtain trace element data to better characterise deposits and help avoid potential miscorrelations between sequences.

The need for further geochemical characterisation of proximal tephras into deeper time (beyond 40 ka) has been highlighted by this thesis. In Chapter 5, seven of the cryptotephra deposits preserved in Lake Suigetsu have not been correlated to a specific volcanic arc or centre (see Fig. 5.14). For example, the SG14-4223 glasses are unique in displaying a shoshonitic affinity, residing on the phonolite-trachyte boundary and appears to be from an intraplate source (Fig. 5.13) and do show compositional overlap with intraplate volcanoes which have deposits that have been geochemically characterised (e.g. Derkachev et al., 2019; McLean et al., 2018, 2020b; Brenna et al., 2014; Smith et al., 2013; Chun et al., 2007). This highlights the need for continuation characterisation of volcanic centres in East Asia, as this will allow to be correlated to their sources and provide information about frequency and dispersal of these centres. Additionally, several outcrops near Japanese volcanic centres have been logged but not geochemically analysed (e.g. Hakone; See Fig. 5.2), which may correlate with one or more of the cryptotephras preserved in Lake Suigetsu using many of the diagnostic features presented in this thesis (Fig. 5.10).

One of the key findings from this thesis reveals that successive eruptions from the same volcano may produce tephra units with very similar chemical signatures over several millennia or longer (Chapters 4 – 6). Previous studies on Pre-CI Campi Flegrei magmatic data focussed on whole rock and limited isotopic data from a few deposits and indicated successive eruptions appeared to tap into magma batches (Pabst et al., 2008; Pappalardo et al., 1999). The detailed characterisation of the Campanian deposits presented in Chapter 3 reveals numerous proximal units from both Ischia and Campi Flegrei have repeated chemical signatures (Fig. 4.4) and suggest that it is not always possible to correlate to distally located tephras with similar compositions. Thus, even where detailed major and trace element glass data are available, it is not always sufficient to geochemically distinguish separate tephra units. This has implications for differentiating eruptions, misinterpretation of eruption frequency and repose periods, complications in correlations between sites and potential for overestimating eruptive magnitude (e.g., Ponomareva et al., 2015). D'Antonio et al., (2021) demonstrate that the petrographic and mineral–chemical characterisations can be a useful for confidentially discriminating Ischia tephras. Whilst this may prove to be effective for proximal deposits, this may be more problematic in distally located cryptotephras where

there are no crystals. Ultimately the occurrence of repeated glass compositions demonstrates the need for other techniques are required to distinguish tephras to ensure proximal-distal and distal-distal correlations are robust.

This thesis reveals that in the lead-up to caldera-forming eruptions, we sometimes observe shifts in magma composition (e.g. Campi Flegrei; Chapter 4), but in other cases, the composition remains relatively stable (e.g. Aso, Chapter 6). The three compositional groups indicate the pre-CI Campi Flegrei eruptions were fed by highly, but differently, evolved magmas, similar to the post-NYT Campi Flegrei deposits (Smith et al., 2011a) and became increasingly evolved in the lead-up to the CI (Vineberg et al., 2023). Conversely, the integration of proximal-distal records of Aso tephra deposits reveal that glasses of variable compositions have erupted over time, however there are no clear compositional shifts directly preceding or following the large caldera-forming Aso-3 and Aso-4 eruptions (Fig. 6.9). Similar variability in other caldera-forming systems and how different magmatic processes are also observed such as mixing in Yellowstone, USA (Christiansen, 2001) and Taupo, New Zealand (Smith et al., 2005) or stability in Santorini, Greece (Flaherty et al., 2018). Ultimately each volcanic system is unique, and the behaviour of the magma prior to an eruption reflects the complex interplay of these processes. Our findings serve as a valuable springboard for volcanological research into some of the world's most dangerous systems (i.e. Campi Flegrei, Italy and Aso, Japan).

7.3. Objective 3: Identify key isochrons to aid the integration and synchronisation of proximal and distal records.

The identification of key widespread tephras within sedimentary sequences can aid the correlation and synchronisation of records over vast geographical areas and help reconstruct past volcanic activity and provide insights into regional environmental changes, aiding in understanding how such events impacted ecosystems and human societies over time. Throughout this thesis, numerous Campanian and Japanese widespread tephra markers have been discussed (see Chapters 4 – 6). At least seven widespread markers from Procida and Ischia are preserved between the MEGT and CI (Fig. 4.1), however, through the detailed geochemical characterisation of the units preserved at Acquamorta, none of these previously reported tephras (e.g. Schiappone from Ischia, Pietre Rosse, Agone and Vivara II from Procida) were identified (see Chapter 4). Thus, it was not possible to integrate the Acquamorta outcrop with other distally located sedimentary sequences with good chronologies (e.g. LGdM; Tomlinson et al, 2014) or help further constrain the eruption

history of the CVZ. In contrast, an additional ten widespread tephra markers in the Lake Suigetsu sediments have been identified to provide a total of eighteen tie-points for this 70 kyr period (see Fig. 7.1). Only by acquiring new major and trace element data for proximal tephras was it possible to identify their distal counterparts. Chapter 6 presented new major and/or trace element data for the SK and Toya tephras were presented (Table 5.4). These new data and the recent acquisition of the On-Ng (and other Ontake deposits) by Matsu'ura and Komatsubara (2024) have enabled confident correlations to the Lake Suigetsu record, providing tight age constraints for past eruptions and tempo of activity. In contrast, the SG14-4748 has been tentatively correlated with the Daisen DNP unit on the basis of its chrono-stratigraphic (between Aso-4 and DSP; Fig. 5.2) due to the absence of near-source glass chemistry as Daisen deposits are highly weathered (see Albert et al., 2018).

Aso is one of the largest and most active volcanoes in the world and has produced numerous caldera and inter-caldera eruptions (see: Hoshizumi et al., 2022; Miyabuchi 2009, 2011; Machida and Arai, 2003). The new geochemical data provided for many of the Aso units preserved in proximal sequences has enabled further integration with the Lake Suigetsu record located 525 km NE away. Eleven of the twenty deposits with Aso glass compositions preserved in the Lake Suigetsu sequence have now been correlated with a particular eruption unit exposed close to the volcano. This thesis has also further demonstrated the capacity for trace element data to distinguish individual phases of eruptions (e.g. ACP4; Chapter 6) having important implications for tephrochronology (e.g. Tomlinson et al., 2012). Significantly, the identification of these tephra deposits in Lake Suigetsu provides better ages for many of these eruptions, and constrains repose periods between eruptions for Aso activity (see Chapter 6). Whilst none of these newly identified have been reported in other distally located sequences, they offer potential future tie-points for records obtained from Kyushu and Honshu with the expansion of cryptotephra investigations across Japan. However, seven of the Aso eruption deposits in the Lake Suigetsu record that are not yet observed in the exposed near-vent sequences, indicating some deposits may have been removed or buried by subsequent large eruptions for instance the M7.8 Aso-4 caldera-forming eruption. This research demonstrates the merit of integrating the proximal-distal records for understanding of the timing and ash dispersals of pre-historic eruptions.

Despite the identification of further key widespread markers in the Lake Suigetsu record (see Chapters 5 and 6), none of these additional tephras have been radiometrically dated. Beyond the annually laminated and ^{14}C dated portion of the Lake Suigetsu sequence

(ca. 50 ka) the deeper section of the core has been extrapolated using a 'P_Sequence' deposition model within the Bayesian software package OxCal (Bronk Ramsey, 2008) and anchored by the $^{40}Ar/^{39}Ar$ age of the Aso-4 eruption at 86.4 ± 1.1 ka (Albert et al., 2019a). This has meant no further ages could be imported into the Lake Suigetsu age model using tephrochronology, and thus unable to further constrain the chronology of the lower part of SG14 and limiting the integration of this key paleoenvironmental archive for East Asia. Through the detailed characterisation of the physical properties of proximal tephras, this thesis identified that many tephras are suitable for $^{40}Ar/^{39}Ar$ with the inclusion of K-rich minerals (e.g. sanidine, biotite, hornblende apatite; see Chapter 3). Furthermore, the SK tephra sampled is suitable for zircon dating (see Chapter 3). Further investigation of the Campi Flegrei, Ischia and Aso tephras presented in this thesis may also contain zircons, which would not only be useful for dating these tephras but also allow greater understanding of the magma evolution (e.g. Strum et al., 2024; Danišík et al., 2020). Once radiometric dates have been obtained for some/all of these marker beds, their ages can be imported into the Lake Suigetsu age-model to provide further tie-points and helps to impose more precise age constraints on the linearly interpolated/extrapolated age estimates of tephra deposits in the deeper portion of the Suigetsu record. These ages could also be used to provide independent tie-points in other sequences with co-located markers (see Fig. 7.2).

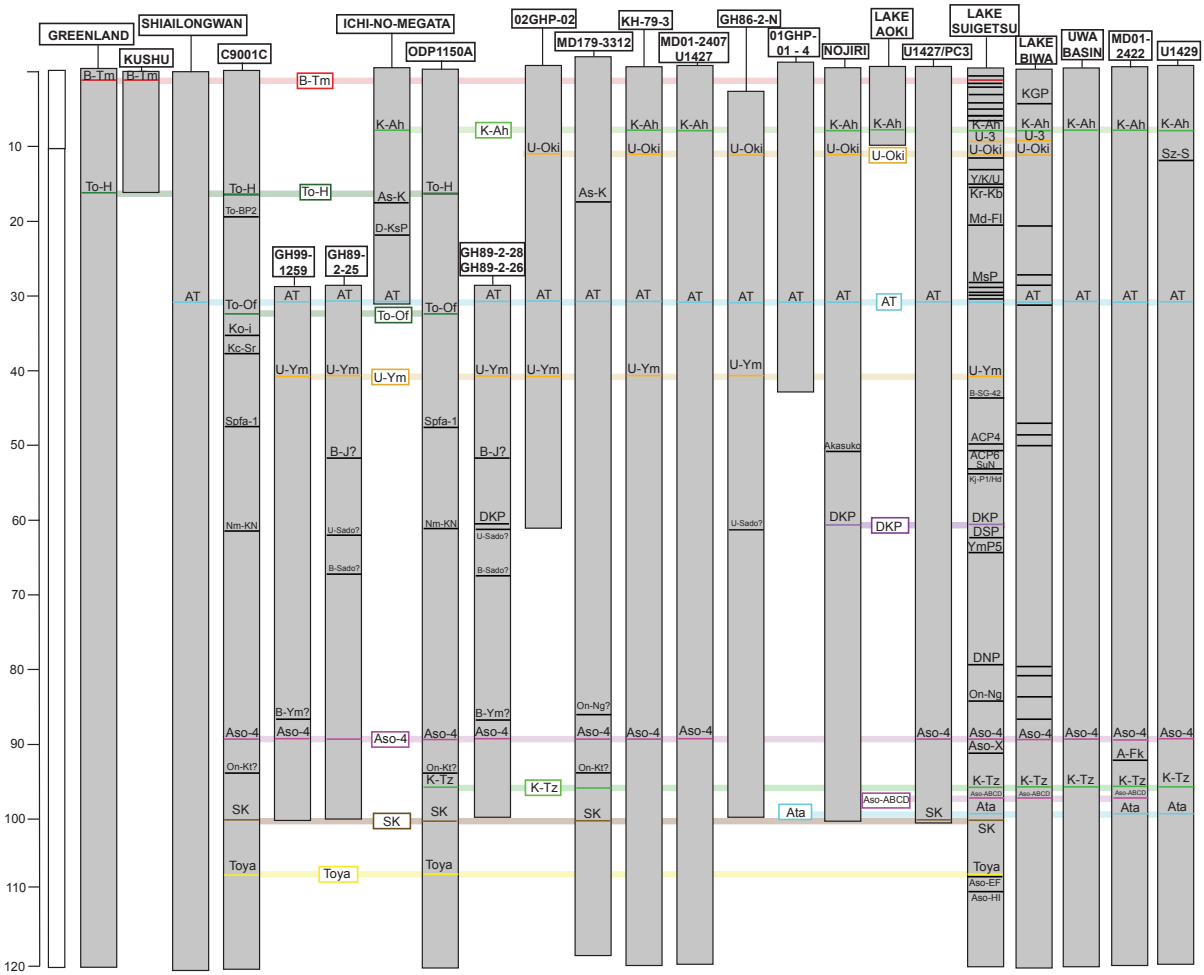


Figure 7.2: Tephrostratigraphic framework for Japan constructed for the past 120 ka (i.e., Late Pleistocene and Holocene). The framework is assembled using sedimentary records (locations shown in Figure 7.3 apart from Greenland) with tephra markers shown by a black (uncorrelated or regional marker) or coloured (key widespread marker layer) dash. Marker layers are plotted using approximate eruption ages to illustrate their synchronisation potential.

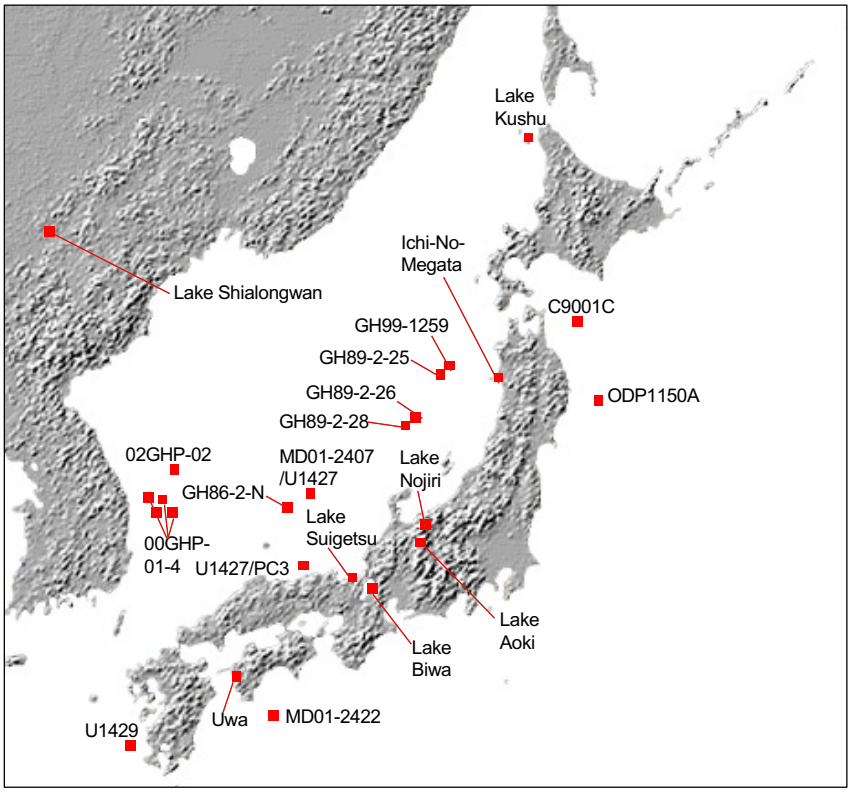


Fig. 7.3: Key sedimentary records (red squares) used to construct the tephrostratigraphic framework for Japan (see Figure 7.2. for tephra sequence and site reference).

Several key tephrostratigraphic markers were not identified or could not be confidently correlated to in this thesis. For example, key Japanese volcanic events missing from the Lake Suigetsu record include the M ≥6.0 A-Iw and Kc-2/3, however this is consistent with their ash dispersals that were away from Lake Suigetsu (see Machida and Arai, 2003). Moreover, we have identified potential widespread tephra markers in the correct ages and chronostratigraphic positions but owing to geochemical features, were unable to be robustly correlated. All three of the Acquamorta Ischia units presented in Chapter 4 are compositionally similar to the most evolved component of the widespread Schiappone tephra, with none showing the full compositional range that is diagnostic of this particular eruption deposit (Fig. 4.5; Tomlinson et al., 2014) and thus cannot confidently correlate one, if any, of the units to the Schiappone tephra. Similarly, due to its chronostratigraphic position and age, the SG14-4223 cryptotephra could be associated with the U-Sado/SKP-II tephra that has been previously reported in marine records, however glasses are compositionally different from those units reported from the Sea of Japan (Derkachev et al., 2019; Chun et al., 2007). We therefore recommended that more careful considerations are given when correlating to these specific eruptions, and that many of the previous correlations may need to be revised (e.g. Derchachev et al., 2019; Tomlinson et al., 2014; Bourne et al., 2010). These findings highlight the need for strong chronostratigraphic and geochemical data for

robust correlations. It may be prudent to consider a classification scheme to quantify the robustness of tephra correlations including information such as absolute chronology and geochemical characteristics.

Whilst it has been possible to integrate the tephrostratigraphic records of the Lake Suigetsu archive with the Greenland ice cores (see McLean et al., 2016), it is not yet been possible to extensively interlink this regional record to other neighbouring frameworks, such as the comprehensive Kamchatka eruption tephrostratigraphy (Bubenshchikova et al., 2024; Ponomareva et al., 2017, 2020; Derkachev et al., 2016; Plunkett et al., 2015). Despite sediment cores in the Sea of Okhotsk (located between the Kurile arc and Kamchatka) containing visible ash layers from several Hokkaido eruptions (e.g., Derkachev et al., 2016), they do not correspond with the Hokkaido cryptotephras identified in Lake Suigetsu. Future cryptotephra investigations of sediment cores in the Sea of Okhotsk may reveal further isochrons derived from northern Honshu and Hokkaido (such as the Toya tephra preserved in Lake Suigetsu and Pacific marine cores; Vineberg et al., 2024; Matsu'ura and Komatsubara, 2024) and will be key to extending the northernmost limits of this framework. This thesis has identified the first large magnitude event from Hokkaido to reach central Honshu, Japan (see Chapter 5). The Toya eruption event is established as potentially one of the most widespread Late Quaternary isochrons (Matsu'ura et al., 2014; Machida and Arai, 2003). The identification of the isochron as a cryptotephra almost 1000 km away from source and significantl extends the dispersal mapped for the eruption (Fig. 7.2; Matsu'ura and Komatsubara, 2024; Machida and Arai, 2003). It is not yet clear what eruption and climatic conditions are required for such large magnitude events erupted from Hokkaido to reach central Honshu. Furthermore, the preservation of the Toya eruption as a cryptotephra deposit within the Lake Suigetsu sediments will allow any changes in sediment composition or environmental proxies to be assessed as a result of this large eruption (e.g. Toba; Lane et al., 2013).

In light of recent identifications of Asian tephras in Greenland (Cook et al., 2018; ; Bourne et al., 2016;Sun et al., 2014), and the identification of Russian and Indonesian tephra in northern Japan (Chen et al., 2019), East Asia is an ideal region for the search of widespread tephra isochrons. However, the cryptotephra extraction method (e.g. Turney, 1998; Blockley et al., 2005) that is commonly employed in Europe and North Atlantic regions has had limited application thus far in East Asia. Thus far only the continuous sequences of Lake Suigetsu, central Honshu (Albert et al., 2024; McLean et al., 2018; 2020a,) and Lake Kushu, northern Hokkaido (Chen et al., 2019) have been systematically investigated for cryptotephra deposits. Investigations of these archives have revealed cryptotephra

extraction methods to be extremely useful for expanding the distribution of widespread tephra markers (Fig 7.2.) and a number of previously undocumented tephra horizons were reported from the studies (Fig. 7.2; Albert et al., 2024; Vineberg et al., 2024; McLean et. al., 2018, 2020a; Chen et al., 2019). This thesis demonstrates the need for further investigations of other sedimentary archives in and around Japan for the presence of cryptotephra deposits. Given the prevailing westerly winds, it may be prudent to further investigate marine cores off the east coast to improve tephrostratigraphic frameworks for east Asia (Fig. 7.2; Sagawa et al., 2018). However, several Pacific arc tephra layers have been identified in the Greenland ice core records are derived from medium magnitude events that are currently undocumented in the geological record (Bourne et al., 2016), once again highlighting the need for detailed geochemical characterisation of volcanic deposits to ensure robust proximal-distal correlations.

List of Consolidated References

Abbott, P. M., Griggs, A. J., Bourne, A. J., Chapman, M. R. and Davies, S. M. (2018) Tracing marine cryptotephras in the North Atlantic during the last glacial period: Improving the North Atlantic marine tephrostratigraphic framework. *Quaternary Science Reviews*. 189169–186.

Abbott, P.M., Bourne, A.J., Purcell, C.S., Davies, S.M., Scourse, J.D. and Pearce, N.J.G., (2016). Last glacial period cryptotephra deposits in an eastern North Atlantic marine sequence: exploring linkages to the Greenland ice-cores. *Quaternary Geochronology*, *31*, pp.62-76.

Abbott, P. M. and Davies, S. M. (2012). Volcanism and the Greenland ice-cores: the tephra record. *Earth-Science Reviews*, 115: 173-191

Albert, P. G., McLean, D., Buckland, H. M., Suzuki, T., Jones, G., Staff, R. A., Vineberg, S., Kitaba, I., Yamada, K., Moriwaki, H., Ishimura, D., Ikehara, K., Manning, C. J., Nakagawa, T., and Smith, V. C. (2024). Cryptotephra preserved in Lake Suigetsu (SG14 core) reveals the eruption timing and distribution of ash fall from Japanese volcanoes during the Late-glacial to early Holocene. *Quaternary Science Reviews,* 324, 108376. https://doi.org/10.1016/J.QUASCIREV.2023.108376

Albert, P. G., Giaccio, B., Isaia, R., Costa, A., Niespolo, E. M., Nomade, S., Pereira, A., Renne, P. R., Hinchliffe, A., Mark, D. F., Brown, R. J., and Smith, V. C. (2019a). Evidence for a large-magnitude eruption from Campi Flegrei caldera (Italy) at 29 ka. *Geology,* 47(7), 595–599. https://doi.org/10.1130/G45805.1

Albert, P. G., Smith, V. C., Suzuki, T., McLean, D., Tomlinson, E. L., Miyabuchi, Y., Kitaba, I., Mark, D. F., Moriwaki, H., and Nakagawa, T. (2019b). Geochemical characterisation of the Late Quaternary widespread Japanese tephrostratigraphic markers and correlations to the Lake Suigetsu sedimentary archive (SG06 core). *Quaternary Geochronology*. https://doi.org/10.1016/j.quageo.2019.01.005

Albert, P. G., Smith, V. C., Suzuki, T., Tomlinson, E. L., Nakagawa, T., McLean, D., Yamada, M., Staff, R. A., Schlolaut, G., and Takemura, K. (2018). Constraints on the frequency and dispersal of explosive eruptions at Sambe and Daisen volcanoes (South-West Japan Arc) from the distal Lake Suigetsu record (SG06 core). Earth-Science Reviews, 185, 1004–1028. https://doi.org/10.1016/j.earscirev.2018.07.003

Albert, P. G., Tomlinson, E. L., Smith, V. C., Di Roberto, A., Todman, A., Rosi, M., Marani, M., Muller, W. and Menzies, M. A. (2012). Marine-continental tephra correlations: volcanic glass geochemistry from the Marsili Basin and the Aeolian Islands, Southern Tyrrhenian Sea, Italy. *Journal of Volcanology and Geothermal Research*, 229: 74-94

Alessio, M., Bella, F., Improta, S., Belluomini, G., Calderoni, G., Cortesi, C. and Turi, B. (1976). University of Rome carbon-14 dates XIV. *Radiocarbon,* 18 (3), 321–349.

Allan, A.S.R., Baker, J.A., Carter, L. and Wysoczanksi, R.J. (2008). Reconstructing the Quaternary evolution of the world's most active silicic volcanic system: insights from an ~1.65 Ma deep ocean tephra record sourced from Taupo Volcanic Zone, New Zealand. *Quaternary Science Reviews*, 27 (25–26), 2341–2360.

Alloway, B.V., Andreastuti, S., Setiawan, R., Miksic, J. and Hua, Q., (2017). Archaeological implications of a widespread 13th Century tephra marker across the central Indonesian Archipelago. *Quaternary Science Reviews*, *155*, 86-99.

Alloway, B., Lowe, D.J., Barrell, D.J.A., Newnham, R.M., Almond, P.C., Augustinus, P.C., Bertler, N.A.N., Carter, L., Litchfield, N.J., McGlone, M.S., Shulmeister, J., Vandergoes, M.J. and Williams, P.W. (2007) Towards a climate event stratigraphy for New Zealand over the past 30 000 years (NZ-INTIMATE project). *Journal of Quaternary Science*. 22 (1), 9–35.

Aoki, K., (2008). Revised age and distribution of ca. 87 ka Aso-4 tephra based on new evidence from the northwest Pacific Ocean. *Quaternary International,* 178(1), 100-118. https://doi.org/10.1016/j.quaint.2007.02.005

Aoki, K. and Machida, H. (2006). Major element composition of volcanic glass shards in the late Quaternary widespread tephras in Japan—Distinction of tephras using K2O-TiO2 diagrams. *Bulletin of the Geological Survey of Japan*, *57*(7/8), 239-258.

Arai, F., Oba, T., Kitazato, H., Horibe, Y. and Machida, H. (1981). Late Quaternary tephrochronology and paleo-oceanography of the sediments of the Japan Sea. *The Quaternary Research (Daiyonki-Kenkyu)*. 20 (3), 209–230.

Arienzo, I., Civetta, L., Heumann, A., Woerner, G. and Orsi, G. (2009). Isotopic evidence for open system processes within the Campanian Ignimbrite (Campi Flegrei–Italy) magma chamber. *Bulletin of Volcanology*, *71*, 285-300.

Aubry, T.J., Farquharson, J.I., Rowell, C.R., Watt, S.F., Pinel, V., Beckett, F., Fasullo, J., Hopcroft, P.O., Pyle, D.M., Schmidt, A. and Sykes, J.S. (2022). Impact of climate change on volcanic processes: current understanding and future challenges. *Bulletin of Volcanology*, 84, 58. https://doi.org/10.1007/s00445-022-01562-8

Balascio, N.L., Francus, P., Bradley, R.S., Schupack, B.B., Miller, G.H., Kvisvik, B.C., Bakke, J. and Thordarson, T. (2015) *Investigating the Use of Scanning X-Ray Fluorescence to Locate Cryptoephra in Minerogenic Lacustrine Sediment: Experimental Results*. 305– 324.

Blockley, S.P., Edwards, K.J., Schofield, J.E., Pyne-O'Donnell, S.D., Jensen, B.J., Matthews, I.P., Cook, G.T., Wallace, K.L. and Froese, D., (2015). First evidence of cryptotephra in paleoenvironmental records associated with Norse occupation sites in Greenland. *Quaternary Geochronology*, *27*, 145-157.

Blockley, S.P.E., Bourne, A.J., Brauer, A., Davies, S.M., Hardiman, M., Harding, P.R., Lane, C.S., MacLeod, A., Matthews, I.P., Pyne-O'Donnell, S.D.F., Rasmussen, S.O., Wulf, S. and Zanchetta, G. (2014). Tephrochronology and the extended intimate (integration of ice-core, marine and terrestrial records) event stratigraphy 8-128kab2k. *Quaternary Science Reviews*.

Blockley, S.P.E., Lane, C.S., Hardiman, M., Rasmussen, S.O., Seierstad, I.K., Steffensen, J.P., Svensson, A., Lotter, A.F., Turney, C.S.M. and Bronk Ramsey, C. (2012). Synchronisation of paleoenvironmental records over the last 60,000 years, and an extended INTIMATE event stratigraphy to 48,000 b2k. *Quaternary Science Reviews*. 362–10.

Blockley, S.P.E., Lane, C.S., Lotter, A.F. and Pollard, A.M. (2007) Evidence for the presence of the Vedde Ash in Central Europe. *Quaternary Science Reviews*. 26 (25–28), 3030– 3036.

Blockley, S. P. E., Pyne-O'Donnell, S. D. F., Lowe, J. J., Matthews, I. P., Stone, A., Pollard, A. M., Turney, C. S. M., and Molyneux, E. G. (2005). A new and less destructive laboratory procedure for the physical separation of distal glass tephra shards from sediments.

Quaternary Science Reviews, 24(16–17), 1952–1960. https://doi.org/10.1016/J.QUASCIREV.2004.12.008

Beierle, B. and Bond, J. (2002). Density-induced settling of tephra through organic lakesediments. *Journal of Paleolimnology 2002 28:4*. 28 (4), 433–440.

Brauer, A., Hajdas, I., Blockley, S.P.E., Bronk Ramsey, C., Christl, M., Ivy-Ochs, S., Moseley, G.E., Nowaczyk, N.N., Rasmussen, S.O., Roberts, H.M., Spötl, C., Staff, R.A. and Svensson, A. (2014). The importance of independent chronology in integrating records of past climate change for the 60–8 ka INTIMATE time interval. *Quaternary Science Reviews*, 10647–66.

Bertrand, S., Daga, R., Bedert, R. and Fontijn, K., (2014). Deposition of the 2011–2012 Cordón Caulle tephra (Chile, 40 S) in lake sediments: Implications for tephrochronology and volcanology. *Journal of Geophysical Research: Earth Surface*, *119*(12), 2555-2573.

Bonadonna, C. and Houghton, B.F., (2005). Total grain-size distribution and volume of tephra-fall deposits. *Bulletin of Volcanology*, *67*, 441-456.

Bourne, A.J., Abbott, P.M., Albert, P.G., Cook, E., Pearce, N.J.G., Ponomareva, V., Svensson, A. and Davies, S.M., (2016). Underestimated risks of recurrent long-range ash dispersal from northern Pacific Arc volcanoes. *Scientific reports*, *6*(1), p.29837.

Bourne, A.J., Cook, E., Abbott, P.M., Seierstad, I.K., Steffensen, J.P., Svensson, A., Fischer, H., Schüpbach, S. and Davies, S.M. (2015). A tephra lattice for Greenland and a reconstruction of volcanic events spanning 25–45 ka b2k. *Quaternary Science Reviews*. 118122–141.

Bourne, A.J., Lowe, J.J., Trincardi, F., Asioli, A., Blockley, S.P.E., Wulf, S., Matthews, I. P., Piva, A., Vigliotti, L., (2010). Distal tephra record for the last ca 105,000 years from core PRAD 1-2 in the Central Adriatic Sea: implications for marine tephrostratigraphy. *Quaternary Science Reviews,* 29 (23–24), 3079–3094.

Brenna, M., Cronin, S. J., Kereszturi, G., Sohn, Y. K., Smith, I. E. M., and Wijbrans, J. (2015). Intraplate volcanism influenced by distal subduction tectonics at Jeju Island, Republic of Korea. *Bulletin of Volcanology,* 77(1), 1–16. https://doi.org/10.1007/S00445-014-0896-5/METRICS

Brenna, M., Cronin, S. J., Smith, I. E. M., Sohn, Y. K., and Maas, R. (2012). Spatio-temporal evolution of a dispersed magmatic system and its implications for volcano growth, Jeju Island Volcanic Field, Korea. *Lithos,* 148, 337–352. https://doi.org/10.1016/J.LITHOS.2012.06.021

Bronk Ramsey, C., Heaton, T.J., Schlolaut, G., Staff, R.A., Bryant, C.L., Brauer, A., Lamb, H.F., Marshall, M.H. and Nakagawa, T., (2020). Reanalysis of the atmospheric radiocarbon calibration record from Lake Suigetsu, Japan. *Radiocarbon*, *62*(4), pp.989-999. https://doi:10.1017/RDC.2020.18

Bronk Ramsey, C., Albert, P.G., Blockley, S.P.E., Hardiman, M., Housley, R.A., Lane, C.S., Lee, S., Matthews, I.P., Smith, V.C., and Lowe, J.J., (2015). Improved age estimates for key late Quaternary European tephra horizons in the RESET lattice. *Quaternary Science Reviews*, 118, 18–32.

Bronk Ramsey, C., Staff, R.A., Bryant, C.L., Brock, F., Kitagawa, H., Van Der Plicht, J., Schlolaut, G., Marshall, M.H., Brauer, A., Lamb, H.F. and Payne, R.L., (2012). A complete terrestrial radiocarbon record for 11.2 to 52.8 kyr BP. *Science*, 338(6105), 370-374. https://doi.org/10.1126/science.1226660

Bronk Ramsey, C., (2008). Deposition models for chronological records. *Quaternary Science Reviews*, 27(1-2), pp.42-60. https://doi.org/10.1016/j.quascirev.2007.01.019

Brown, S. K., Loughlin, S. C., Sparks, R. S. J., Vye-Brown, C., Barclay, J., Calder, E., Cottrell, E., Jolly, G., Komorowski, J.-C., Mandeville, C., Newhall, C., Palma, J., Potter, S., and Valentine, G. (2015). Chapter 2 Global volcanic hazard and risk. https://doi.org/10.1017/CBO9781316276273.004

Brown, R.J., Civetta, L., Arienzo, I., Moretti, R., Orsi, G., Tomlinson, E.L., Albert, P.G. and Menzies, M.A., (2014). Geochemical and isotopic insights into the assembly, evolution and disruption of a magmatic plumbing system before and after a cataclysmic caldera-collapse eruption at Ischia volcano (Italy). *Contributions to Mineralogy and Petrology*, 168, 1035.

Brown, R.J., Orsi, G. and de Vita, S. (2008). New insights into Late Pleistocene explosive volcanic activity and caldera formation on Ischia (southern Italy). *Bulletin of Volcanolgy*, 70 (5), 583–603.

Bryant, C.J., Arculus, R.J. and Eggins, S.M. (2003). The geochemical evolution of the Izu-Bonin arc system: A perspective from tephras recovered by deep-sea drilling. Geochemistry, Geophysics, Geosystems, 4(11).

Bubenshchikova, N., Ponomareva, V., Portnyagin, M., Nürnberg, D., Chao, W.S., Lembke-Jene, L. and Tiedemann, R., (2024). The Pauzhetka tephra (South Kamchatka): A key middle Pleistocene isochron for the Northwest Pacific and Okhotsk Sea sediments. *Quaternary Geochronology*, *79*, 101476.

Buchner, G., Italiano, A. and Vita-Finzi, C. (1996). Recent uplift of Ischia, southern Italy. *Geological Society, London, Special Publications*, *110*(1), 249-252.

Carey, S. and Sparks, R.S.J. (1986). Quantitative models of the fallout and dispersal of tephra from volcanic eruption columns. *Bulletin of Volcanology 1986 48:2*. 48 (2), 109–125.

Chen, X. Y., McLean, D., Blockley, S. P. E., Tarasov, P. E., Xu, Y. G., and Menzies, M. A. (2019). Developing a Holocene tephrostratigraphy for northern Japan using the sedimentary record from Lake Kushu, Rebun Island. *Quaternary Science Reviews*, 215, 272–292. https://doi.org/10.1016/j.quascirev.2019.05.017

Christiansen, R.L., (2001). *The quaternary and pliocene Yellowstone Plateau volcanic field of Wyoming, Idaho, and Montana* (Vol. 729). US Department of the Interior, US Geological Survey.

Chun, J. H., Cheong, D., Ikehara, K., and Han, S. J. (2007). Age of the SKP-I and SKP-II tephras from the southern East Sea/Japan Sea: Implications for interstadial events recorded in sediment from marine isotope stages 3 and 4. *Paleogeography, Paleoclimatology, Paleoecology*, 247(1–2), 100–114. https://doi.org/10.1016/J.PALEO.2006.11.024

Cioni, R., Santacroce, R., Sbrana, A., (1999). Pyroclastic deposits as a guide for reconstructing the multi-stage evolution of the Somma-Vesuvius Caldera. *Bulletin of Volcanology,* 61 (4), 207–222.

Civetta, L., Galati, R. and Santacroce, R., (1991). Magma mixing and convective compositional layering within the Vesuvius magma chamber. Bulletin of Volcanology, 53 (4), 287–300.

Costa, A., Dell'Erba, F., Vito, M.A., Isaia, R., Macedonio, G., Orsi, G., Pfeiffer, T., (2009). Tephra fallout hazard assessment at the Campi Flegrei caldera (Italy). *Bulletin of Volcanology*, *71*, 259-273.

Cook, E., Abbott, P.M., Pearce, N.J., Mojtabavi, S., Svensson, A., Bourne, A.J., Rasmussen, S.O., Seierstad, I.K., Vinther, B.M., Harrison, J. and Street, E., (2022). Volcanism and the Greenland ice cores: A new tephrochronological framework for the last glacial-interglacial transition (LGIT) based on cryptotephra deposits in three ice cores. *Quaternary Science Reviews*, *292*, 107596.

Cook, E., Portnyagin, M., Ponomareva, V., Bazanova, L., Svensson, A. and Garbe-Schönberg, D., (2018). First identification of cryptotephra from the Kamchatka Peninsula in a Greenland ice core: Implications of a widespread marker deposit that links Greenland to the Pacific northwest. *Quaternary Science Reviews*, *181*, 200-206.

Cook, E. R., Anchukaitis, K. J., Buckley, B. M., D'Arrigo, R. D., Jacoby, G. C., and Wright, W. E. (2010). Asian monsoon failure and megadrought during the last millennium. *Science*, 328(5977), 486–489. https://doi.org/10.1126/science.1185188

Costa, A., Di Vito, M.A., Ricciardi, G.P., Smith, V.C. and Talamo, P., (2022). The long and intertwined record of humans and the Campi Flegrei volcano (Italy). *Bulletin of Volcanology*, *84*, 1-27.

Costa, A., Smith, V.C., Macedonio, G. and Matthews, N.E. (2014). The magnitude and impact of the Youngest Toba Tuff super-eruption. *Frontiers in Earth Science*, *2*, 16.

Crosweller S. H., Arora, B., Brown, S. K., Cottrell, E., Deligne, N. I., Ortiz Guerrero, N., Hobbs, L., Kiyosugi, K., Loughlin, S. C., Lowndes, J., Nayembil, M., Siebert, L., Stephen, R., Sparks, J., Takarada, S., and Venzke, E. (2012). Global database on large magnitude explosive volcanic eruptions (LaMEVE). https://doi.org/10.1186/2191-5040-1-4

Cutler, N.A., Streeter, R.T., Marple, J., Shotter, L.R., Yeoh, J.S. and Dugmore, A.J., (2018). Tephra transformations: variable preservation of tephra layers from two well-studied eruptions. *Bulletin of Volcanology*, *80*, 1-15.

D'Antonio, M., Arienzo, I., Brown, R.J., Petrosino, P., Pelullo, C. andGiaccio, B., (2021). Petrography and mineral chemistry of Monte epomeo green tuff, ischia island, South Italy: Constraints for identification of the y-7 tephrostratigraphic marker in distal sequences of the central mediterranean. *Minerals* 11 (9), 955.

D'Antonio, M., Civetta, L., Orsi, G., Pappalardo, L., Piochi, M., Carandente, A., Vita, S.D.,Vito, M.A.D. and Isaia, R. (1999). The present state of the magmatic system of the Campi Flegrei caldera based on a reconstruction of its behavior in the past 12 ka. *Journal of Volcanology and Geothermal Research,* 91, 247–268.

Danišík, M., Schmitt, A.K., Stockli, D.F., Lovera, O.M., Dunkl, I. and Evans, N.J. (2017). Application of combined U-Th-disequilibrium/U-Pb and (U-Th)/He zircon dating to tephrochronology. *Quaternary Geochronology*. 4023–32.

Danišík, M., Lowe, D.J., Schmitt, A.K., Friedrichs, B., Hogg, A.G. and Evans, N.J., (2020). Sub-millennial eruptive recurrence in the silicic Mangaone Subgroup tephra sequence, New Zealand, from Bayesian modelling of zircon double-dating and radiocarbon ages. *Quaternary Science Reviews*, *246*, 106517.

Davies, S.M., Albert, P.G., Bourne, A.J., Owen, S., Svensson, A., Bolton, M.S., Cook, E., Jensen, B.J., Jones, G., Ponomareva, V.V. and Suzuki, T. (2024). Exploiting the Greenland volcanic ash repository to date caldera-forming eruptions and widespread isochrons during the Holocene. *Quaternary Science Reviews*, *334*, 108707.

Davies, S.M. (2015) Cryptotephras: The revolution in correlation and precision dating. *Journal of Quaternary Science*, 30 (2), 114–130.

Davies, S.M., Abbott, P.M., Meara, R.H., Pearce, N.J.G., Austin, W.E.N., Chapman, M.R., Svensson, A., Bigler, M., Rasmussen, T.L., Rasmussen, S.O. and Farmer, E.J. (2014) A North Atlantic tephrostratigraphical framework for 130–60 ka b2k: new tephra discoveries, marine-based correlations, and future challenges. *Quaternary Science Reviews*. 106101–121.

Davies, S.M., Elmquist, M., Bergman, J., Wohlfarth, B. and Hammarlund, D. (2007). Cryptotephra sedimentation processes within two lacustrine sequences from west central Sweden. *The Holocene*, *17*(3), 319-330.

De Astis, G., Pappalardo, L. and Piochi, M. (2004). Procida volcanic history: New insights into the evolution of the Phlegraean Volcanic District (Campania region, Italy). *Bulletin of Volcanology,* 66 (7), 622–641.

de Maisonneuve, C.B., Forni, F. and Bachmann, O., (2021). Magma reservoir evolution during the build up to and recovery from caldera-forming eruptions–a generalizable model?. *Earth-Science Reviews*, *218*, 103684.

De Vivo, B., Rolandi, G., Gans, P.B., Calvert, A., Bohrson, W.A., Spera, F.J., Belkin, H.E. and (2001). New constraints on the pyroclastic eruptive history of the Campanian volcanic Plain (Italy). *Mineralogy and Petrology,* 73 (1), 47–65.

Deino, A.L., Orsi, G., de Vita, S. and Piochi, M. (2004). The age of the Neapolitan Yellow Tuff caldera-forming eruption (Campi Flegrei caldera – Italy) assessed by 40Ar/39Ar dating method. *Journal of Volcanology and Geothermal Research*. 133 (1–4), 157–170.

Derkachev, A. N., Utkin, I. V., Nikolaeva, N. A., Gorbarenko, S. A., Malakhova, G. I., Portnyagin, M. V., Sakhno, V. G., Shi, X., and Lv, H. (2019). Tephra layers of large explosive eruptions of Baitoushan/Changbaishan Volcano in the Japan Sea sediments. *Quaternary International,* 519, 200–214. https://doi.org/10.1016/J.QUAINT.2019.01.043

Derkachev, A.N., Nikolaeva, N.A., Gorbarenko, S.A., Portnyagin, M.V., Ponomareva, V.V., Nürnberg, D., Sakamoto, T., Iijima, K., Liu, Y., Shi, X. and Lv, H., (2016). Tephra layers of in the quaternary deposits of the Sea of Okhotsk: Distribution, composition, age and volcanic sources. *Quaternary International*, *425*, 248-272.

Di Roberto, A., Smedile, A., Del Carlo, P., De Martini, P.M., Iorio, M., Petrelli, M., Pantosti, D., Pinzi, S. and Todrani, A. (2018). Tephra and cryptotephra in a~ 60,000-year-old lacustrine sequence from the Fucino Basin: new insights into the major explosive events in Italy. *Bulletin of Volcanology*, *80*, 1-23.

Di Renzo, V., Arienzo, I., Civetta, L., D'Antonio, M., Tonarini, S., Di Vito, M.A. and Orsi, G., (2011). The magmatic feeding system of the Campi Flegrei caldera: Architecture and temporal evolution. *Chemical Geology,* 281 (3–4), 227–241.

Di Vito, M.A., Sulpizio, R., Zanchetta, G., D'Orazio, M. (2008). The late Pleistocene pyroclastic deposits of the Campanian Plain: New insights into the explosive activity of Neapolitan volcanoes. *Journal of Volcanology and Geothermal Research,* 177 (1), 19–48.

Di Vito, M.A., Isaia, R., Orsi, G., Southon, J., De Vita, S., D'Antonio, M., Pappalardo, L., Piochi, M. (1999). Volcanism and deformation since 12,000 years at the Campi Flegrei caldera (Italy). *Journal of Volcanology and Geothermal Research,* 91 (2–4), 221–246.

Donato, P., Albert, P.G., Crocitti, M., De Rosa, R. and Menzies, M.A. (2016). Tephra layers along the southern Tyrrhenian coast of Italy: Links to the X-5 & X-6 using volcanic glass geochemistry. *Journal of Volcanology and Geothermal Research*, 317, 30–41.

Dugmore, A., Streeter, R. and Cutler, N., (2018). The role of vegetation cover and slope angle in tephra layer preservation and implications for Quaternary tephrostratigraphy. *Paleogeography, Paleoclimatology, Paleoecology*, *489*, 105-116.

Dugmore, A.J., Newton, A.J., Sugden, D.E. and Larsen, G., (1992). Geochemical stability of fine-grained silicic Holocene tephra in Iceland and Scotland. *Journal of Quaternary Science*, *7*(2),173-183.

Fedele, F., Giaccio, B., Isaia, R., and Orsi, G. (2003). The Campanian Ignimbrite Eruption, Heinrich Event 4, and Paleolithic Change in Europe: a High-Resolution Investigation. Geophys. Monograph Series 139, 301–325.

Flaherty, T., Druitt, T.H., Tuffen, H., Higgins, M.D., Costa, F. and Cadoux, A., (2018). Multiple timescale constraints for high-flux magma chamber assembly prior to the Late Bronze Age eruption of Santorini (Greece). *Contributions to Mineralogy and Petrology*, *173*, 1-21.

Fontijn, K., Rawson, H., van Daele, M., Moernaut, J., Abarzúa, A.M., Heirman, K., Bertrand, S., Pyle, D.M., Mather, T.A., de Batist, M., Naranjo, J.A. and Moreno, H. (2016). Synchronisation of sedimentary records using tephra: A postglacial tephrochronological model for the Chilean Lake District. *Quaternary Science Reviews*, 137234–254.

Forni, F., Degruyter, W., Bachmann, O., De Astis, G., Mollo, S. (2018). Long-Term magmatic evolution reveals the beginning of a new caldera cycle at Campi Flegrei. *Science Advances,* 4 (11).

Francus, P., Lamb, H., Nakagawa, T., Marshall, M. and Brown, E. (2009). The potential of high-resolution X-ray fluorescence core scanning: applications in paleolimnology.

Furukawa, R. And Nanayama, F. (2006). Holocene pyroclastic fall deposits along the Pacific coastal region of eastern Hokkaido. *Kazan*, *51*(6), 351-371.

Furusawa, A. (2008). Characterizing tephras by major-element analysis of glass inclusions in plagioclase phenocrysts: preliminary results from the DKP tephra of Daisen Volcano, Japan. *Journal Geological Societ. Japan,* 114, 618 – 631.

Furuta, T., Fujioka, K. and Arai, F. (1986) Widespread submarine tephras around Japan — Petrographic and chemical properties. *Marine Geology*, 72 (1–2), 125–142.

Ganzawa, Y. and Ike, M. (2011). SAR–RTL dating of single grains of volcanic quartz from the late Pleistocene Toya Caldera. *Quaternary Geochronology*, 6(1), 42-49. https://doi.org/10.1016/j.quageo.2010.07.001

Gehrels, M.J., Newnham, R.M., Lowe, D.J., Wynne, S., Hazell, Z.J. and Caseldine, C. (2008). Towards rapid assay of cryptotephra in peat cores: Review and evaluation of various methods. *Quaternary International*. 178 (1), 68–84.

Giaccio, B., Niespolo, E.M., Pereira, A., Nomade, S., Renne, P.R., Albert, P.G., Arienzo, I., Regattieri, E., Wagner, B., Zanchetta, G., Gaeta, M., Galli, P., Mannella, G., Peronace, E., Sottili, G., Florindo, F., Leicher, N., Marra, F. and Tomlinson, E.L. (2017). First integrated tephrochronological record for the last ~190 kyr from the Fucino Quaternary lacustrine succession, Central Italy. *Quaternary Science Reviews,* 158, 211–234.

Giaccio, B., Nomade, S., Wulf, S., Isaia, R., Sottili, G., Cavuoto, G., Galli, P., Messina, P., Sposato, A., Sulpizio, R. and Zanchetta, G., (2012). The late MIS 5 Mediterranean tephra markers: a reappraisal from peninsular Italy terrestrial records. *Quaternary Science Reviews,* 56, 31–45.

Giaccio, B., Isaia, R., Fedele, F.G., di Canzio, E., Hoffecker, J., Ronchitelli, A., Sinitsyn, A.A., Anikovich, M., Lisitsyn, S.N. and Popov, V. v. (2008) The Campanian Ignimbrite and Codola tephra layers: Two temporal/stratigraphic markers for the Early Upper Paleolithic in southern Italy and eastern Europe. *Journal of Volcanology and Geothermal Research*, 177 (1), 208–226.

Goldstein, J.I., Newbury, D.E., Michael, J.R., Ritchie, N.W., Scott, J.H.J. and Joy, D.C., (2017). *Scanning electron microscopy and X-ray microanalysis*. springer.

Gudmundsdóttir. R. E., Larsen, G. and Eiríksson, J., (2011). Two new Icelandic tephra markers: The Hekla Ö tephra layer, 6060 cal. yr BP, and Hekla DH tephra layer ,~ 6650 cal. yr BP. land-sea correlation of mid-Holocene tephra markers. *The Holocene*, *21*(4), 629-639.

Ha, K.J., Heo, K.Y., Lee, S.S., Yun, K.S. and Jhun, J.G. (2012). Variability in the East Asian Monsoon: A review. *Meteorological Applications,* 19 (2), 200–215.

Hall, K., (1982). Rapid deglaciation as an initiator of volcanic activity: an hypothesis. *Earth Surface Processes and Landforms*, *7*(1), 45-51.

Hansen, J. Lacis, A. Ruedy, R. and Sato, M. (1992). Potential climate impact of Mount Pinatubo eruption. *Geophysical Research Letters*, *19*(2), 215-218.

Hasegawa, T. and Nakagawa, M. (2016). Large scale explosive eruptions of Akan volcano, eastern Hokkaido, Japan: A geological and petrological case study for establishing tephro-stratigraphy and -chronology around a caldera cluster. *Quaternary International*, 397, 39–51. https://doi.org/10.1016/J.QUAINT.2015.07.058

Hayakawa, Y., (2023). Hayakawa's 2000-year Eruption Database and One Million Year Tephra Database. http://www.hayakawayukio.jp/database (Updated regularly).

Hayakawa, Y. (1985). Pyroclastic geology of Towada volcano. Bull. Earthq. Res. Inst. Univ. Tokyo 60, 507–592.

Hayward, C., (2012). High spatial resolution electron probe microanalysis of tephras and melt inclusions without beam-induced chemical modification. *The Holocene*, *22*(1), 119-125.

Hopkins, J.L., Bidmead, J.E., Lowe, D.J., Wysoczanski, R.J., Pillans, B.J., Ashworth, L., Rees, A.B. and Tuckett, F., (2021). TephraNZ: a major-and trace-element reference dataset for glass-shard analyses from prominent Quaternary rhyolitic tephras in New Zealand and implications for correlation. *Geochronology*, *3*(2), 465-504.

Hoshizumi, H., Miyabuchi, Y., Miyagi, I., Geshi, N. and Takarada, S. (2022). Tephrostratigraphy and eruptive history of Aso-4/3 tephra group, Aso volcano: preparatory process for Aso-4 ignimbrite eruption. *Bulletin of Volcanology Society of Japan*, 67(1), 91-112

Horwell, C.J. and Baxter, P.J. (2006). The respiratory health hazards of volcanic ash: a review for volcanic risk mitigation. *Bulletin of Volcanology*, *69*, 1-24.

Hunt, J.B. and Hill, P.G., (2001). Tephrological implications of beam size—sample-size effects in electron microprobe analysis of glass shards. *Journal of Quaternary Science: Published for the Quaternary Research Association*, *16*(2), 105-117.

Hunt, J.B. and Hill, P.G., (1996). An inter-laboratory comparison of the electron probe microanalysis of glass geochemistry. *Quaternary International*, *34*, 229-241.

Hunt, J.B. and Hill, P.G., (1993). Tephra geochemistry: a discussion of some persistent analytical problems. *The Holocene*, *3*(3), 271-278.

Ikehara, K. (2015). Marine tephra in the Japan Sea sediments as a tool for paleoceanography and paleoclimatology. *Progress in Earth and Planetary Science,* 2015 2:1, 2(1), 1–14. https://doi.org/10.1186/S40645-015-0068-Z

Ikehara, M., Murayama, M., Tadai, O., Hokanishi, N., Daido, N., Kawahata, H., Yasuda, H., (2006). Late quaternary tephrostratigraphy of two IMAGES cores taken from the off Shikoku in the northwest pacific. *The Paleontological Society of Japan*, vol. 79, 60–76.

Ikehara, K., Kikkawa, K., and Chun, J.-H. (2004). Origin and Correlation of Three Tephras That Erupted During Oxygen Isotope Stage 3 Found in Cores from the Yamato Basin, Central Japan Sea. *The Quaternary Research (Daiyonki-Kenkyu)*, 43(3), 201–212. https://doi.org/10.4116/JAQUA.43.201

Innes, H.M., Hutchison, W. and Burke, A., (2024). Geochemical analysis of extremely fine-grained cryptotephra: new developments and recommended practices. *Quaternary Geochronology*, 101553.

The Intergovernmental Panel on Climate Change (2021) IPCC, 2021: summary for policymakers. In: Masson-Delmotte V, Zhai P, Pirani A, et al. (eds) Climate Change 2021: The Physical Science Basis. *Contribution of Working Group I to the Sixth Assessment Report of the Intergovernmental Panel on Climate Change. Cambridge University Press*

Isaia, R., Vitale, S., Marturano, A., Aiello, G., Barra, D., Ciarcia, S., Iannuzzi, E. and Tramparulo, F.D.A. (2019). High-resolution geological investigations to reconstruct the long-term ground movements in the last 15 kyr at Campi Flegrei caldera (southern Italy). *Journal of Volcanology and Geothermal Research*, 385, 143–158.

Isaia, R., Marianelli, P., Sbrana, A. (2009). Caldera unrest prior to intense volcanism in Campi Flegrei (Italy) at 4.0 ka B.P.: Implications for caldera dynamics and future eruptive scenarios. *Geophysics Research Letters,* 36 (21).

Ito, H., (2014). Zircon U-Th-Pb dating using LA-ICP-MS: simultaneous U-Pb and U-Th dating on the 0.1 Ma Toya tephra. *Japan Journal of Volcanology and Geothermal Research,* 289, 210–223. https://doi.org/10.1016/J.QUAINT.2017.06.070

Iverson, N.A., Kalteyer, D., Dunbar, N.W., Kurbatov, A. and Yates, M., (2017). Advancements and best practices for analysis and correlation of tephra and cryptotephra in ice. *Quaternary Geochronology*, *40*, 45-55.

Jensen, B.J.L., Pyne-O'Donnell, S., Plunkett, G., Froese, D.G., Hughes, P.D.M., Sigl, M., McConnell, J.R., Amesbury, M.J., Blackwell, P.G., Bogaard, C. van den, Buck, C.E., Charman, D.J., Clague, J.J., Hall, V.A., Koch, J., Mackay, H., Mallon, G., McColl, L. and Pilcher, J.R. (2014) Transatlantic distribution of the Alaskan White River Ash. *Geology*. 42 (10), 875–878.

Jochum, K. P., Stoll, B., Herwig, K., Willbold, M., Hofmiann, A. W., Amini, M., Aarburg, S., Abouchami, W., Hellebrand, E., Mocek, B., Raczek, I., Stracke, A., Alard, O., Bouman, C., Becker, S., Dücking, M., Brätz, H., Klemd, R., De Bruin, D., Woodhead, J. D. (2006). MPI-DING reference glasses for in situ microanalysis: New reference values for element concentrations and isotope ratios. *Geochemistry, Geophysics, Geosystems, 7*(2). https://doi.org/10.1029/2005GC001060

Kaneko, K., Inoue, K., Koyaguchi, T., Yoshikawa, M., Shibata, T., Takahashi, T., and Furukawa, K. (2015). Magma plumbing system of the Aso-3 large pyroclastic eruption cycle at Aso volcano, Southwest Japan: Petrological constraint on the formation of a compositionally stratified magma chamber. *Journal of Volcanology and Geothermal Research,* 303, 41–58. https://doi.org/10.1016/J.JVOLGEORES.2015.07.016

Kawanabe, Y., Hoshizumi, H., Itoh, J. and Kamata, H. (1997). Tephra stratigraphy of the Kuju volcano before K-Ah tephra. *Programme and Abstracts the Volcanological Society of Japan* 1997, 2, 105.

Keller, F., Guillong, M., Geshi, N., Miyakawa, A. and Bachmann, O. (2023). Tracking caldera cycles in the Aso magmatic system–Applications of magnetite composition as a proxy for differentiation. *Journal of Volcanology and Geothermal Research*, *436*, 107789.

Keller, J., Ryan, W.B.F., Ninkovich, D., Altherr, R. (1978). Explosive volcanic activity in the Mediterranean over the past 200,000 yr as recorded in deep-sea sediments. *Geological Society of America Bulletin*, 89 (4), 591–604.

Kimura, J.-I., Nagahashi, Y., Satoguchi, Y., and Chang, Q. (2015). Origins of felsic magmas in Japanese subduction zone: Geochemical characterizations of tephra from caldera-forming eruptions <5 Ma. *Geochemistry, Geophysics, Geosystems,* 16(7), 2147–2174. https://doi.org/10.1002/2015GC005854

Kimura, J.-I., Okada, S., Nakayama, K., Umeda, K., Kusano, T., Asahara, A., Tateno, M., Danhara, T. (1999). Fission track ages of tephras from Daisen and Sambe volcanoes and their volcanological implications. *Quaternary Research*, 38, 145–155.

Kitagawa, H. and van der Plicht, J. (2000). Atmospheric radiocarbon calibration beyond 11,900 cal BP from Lake Suigetsu laminated sediments. *Radiocarbon*, 42: 370-381

Kitagawa, H. and van der Plicht, J. (1998) Atmospheric radiocarbon calibration to 45,000 yr B.P.: Late glacial fluctuations and cosmogenic isotope production. *Science*. 279 (5354), 1187–1190.

Kitagawa, H., Fukuzawa, T. Nakamura, M., Okumura, K., Takemura, A., Hayashida, A. and Yasuda, Y. (1995). AMS 14C dating of varved sediments from Lake Suigetsu, central Japan and atmospheric 14C change during the late Pleistocene, *Radiocarbon,* 37: 371- 378

Kiyosugi, K., Connor, C., Sparks, R. S. J., Crosweller, H. S., Brown, S. K., Siebert, L., Wang, T., and Takarada, S. (2015). How many explosive eruptions are missing from the geologic record? Analysis of the quaternary record of large magnitude explosive eruptions in Japan. *Journal of Applied Volcanology*, 4:1, 4(1), 1–15. https://doi.org/10.1186/S13617-015-0035-9

Kobayashi, M. and Koyama, M. (1996). Tephrochronology on the Western and Southern Foots of Hakone Volcano, Japan. *Journal of Geography (Chigaku Zasshi),* 105(4), 431-447.

Kuehn, S.C., Froese, D.G., Shane, P.A. and Participants, I.I., (2011). The INTAV intercomparison of electron-beam microanalysis of glass by tephrochronology laboratories: results and recommendations. *Quaternary International*, *246*(1-2), 19-47.

Kuehn, S.C., Froese, D.G., Carrara, P.E., Foit Jr, F.F., Pearce, N.J. and Rotheisler, P., (2009). Major-and trace-element characterization, expanded distribution, and a new chronology for the latest Pleistocene Glacier Peak tephras in western North America. *Quaternary Research*, *71*(2), 201-216.

Kumon, F., Kawai, S. and Inouchi, Y. (2003) Climate Changes between 25, 000 and 6, 000yrsBP Deduced from TOC, TN, and Fossil Pollen Analyses of a Sediment Core from Lake Nojiri, Central Japan. *The Quaternary Research (Daiyonki-Kenkyu)*, 42 (1), 13–26.

Kutterolf, S., Schindlbeck, J.C., Robertson, A.H.F., Avery, A., Baxter, A.T., Petronotis, K. and Wang, K.-L. (2018) Tephrostratigraphy and Provenance From IODP Expedition 352, Izu-Bonin Arc: Tracing Tephra Sources and Volumes From the Oligocene to Recent. *Geochemistry, Geophysics, Geosystems*. 19 (1), 150–174.

Kylander, M.E., Lind, E.M., Wastegård, S. and Löwemark, L. (2011) Recommendations for using XRF core scanning as a tool in tephrochronology. *The Holocene,* 22 (3), 371–375. *http://dx.doi.org/10.1177/0959683611423688*

Lane, C. and Woodward, J. (2017). Tephrochronology. In *Encyclopedia of Geoarchaeology* (pp. 1-7). *Cham: Springer International Publishing*.

Lane, C.S., Brauer, A., Martín-Puertas, C., Blockley, S.P.E., Smith, V.C. and Tomlinson, E.L. (2015). The Late Quaternary tephrostratigraphy of annually laminated sediments from Meerfelder Maar, Germany. *Quaternary Science Reviews*. 122192–206.

Lane, C. S., Cullen, V. L., White, D., Bramham-Law, C. W. F., and Smith, V. C. (2014). Cryptotephra as a dating and correlation tool in archaeology. *Journal of Archaeological Science* 42, 1, 42–50. https://doi.org/10.1016/j.jas.2013.10.033

Lane, C.S., Chorn, B.T. and Johnson, T.C. (2013). Ash from the Toba supereruption in Lake Malawi shows no volcanic winter in East Africa at 75 ka. *Proceedings of the National Academy of Sciences*. 110 (20), 8025–8029.

Lane, C.S., Blockley, S.P.E., Lotter, A.F., Finsinger, W., Filippi, M.L. and Matthews, I.P. (2012). A regional tephrostratigraphic framework for central and southern European climate archives during the Last Glacial to Interglacial transition: comparisons north and south of the Alps. *Quaternary Science Reviews*. 3650–58.

Lane, C.S., Andrič, M., Cullen, V.L. and Blockley, S.P.E. (2011). The occurrence of distal Icelandic and Italian tephra in the Lateglacial of Lake Bled, Slovenia. *Quaternary Science Reviews*. 30 (9–10), 1013–1018.

Larsen, G. and Eiríksson, J. (2008). Late Quaternary terrestrial tephrochronology of Iceland— frequency of explosive eruptions, type and volume of tephra deposits. *Journal of Quaternary Science*, 23 (2), 109–120.

León, A.C. de, Schindlbeck-Belo, J.C., Kutterolf, S., Danišík, M., Schmitt, A.K., Freundt, A., Pérez, W., Harvey, J.C., Wang, K.-L. and Lee, H.-Y. (2021) A history of violence: magma incubation, timing and tephra distribution of the Los Chocoyos supereruption (Atitlán Caldera, Guatemala). *Journal of Quaternary Science*, 36 (2), 169–179.

Lim, C., Toyoda, K., Ikehara, K., and Peate, D. W. (2013). Late Quaternary tephrostratigraphy of Baegdusan and Ulleung Volcanoes using marine sediments in the Japan Sea/East Sea. *Quaternary Research,* 80(1), 76–87. https://doi.org/10.1016/J.YQRES.2013.04.002

Lim, C., Ikehara, K. and Toyoda, K., (2008). Cryptotephra detection using high-resolution trace-element analysis of Holocene marine sediments, southwest Japan. *Geochimica et Cosmochimica Acta*, *72*(20), 5022-5036.

Lowe, D.J., Pearce, N.J., Jorgensen, M.A., Kuehn, S.C., Tryon, C.A. and Hayward, C.L., (2017). Correlating tephras and cryptotephras using glass compositional analyses and numerical and statistical methods: review and evaluation. *Quaternary Science Reviews*, *175*, 1-44.

Lowe, D.J. (2011) Tephrochronology and its application: A review. *Quaternary Geochronology*, 6 (2), 107–153.

Lowe, J.J., Ramsey, C.B., Housley, R.A., Lane, C.S., Tomlinson, E.L., Stringer, C., Davies, W., Barton, N., Pollard, M., Gamble, C., Menzies, M., Rohling, E., Roberts, A., Blockley, S., Cullen, V., Grant, K., Lewis, M., MacLeod, A., White, D., et al. (2015) The RESET project: Constructing a European tephra lattice for refined synchronisation of environmental and archaeological events during the last c. 100 ka. *Quaternary Science Reviews*, 1181–17.

Lowe, D.J., Shane, P.A.R., Alloway, B. v. and Newnham, R.M. (2008) Fingerprints and age models for widespread New Zealand tephra marker beds erupted since 30,000 years ago: a framework for NZ-INTIMATE. *Quaternary Science Reviews*, 27 (1–2), 95–126.

McCanta, M.C., Hatfield, R.G., Thomson, B.J., Hook, S.J. and Fisher, E. (2015). Identifying cryptotephra units using correlated rapid, nondestructive methods: VSWIR spectroscopy, X-ray fluorescence, and magnetic susceptibility. *Geochemistry, Geophysics, Geosystems*, *16*(12), 4029-4056.

Lowe, D.J., (1988). Stratigraphy, age, composition, and correlation of late Quaternary tephras interbedded with organic sediments in Waikato lakes, North Island, New Zealand. *New Zealand journal of geology and geophysics*, *31*(2), 125-165.

Machida, H. (2008) Geomorphology and geology in the south Kanto district during the last 420 ka: an overview. In: The Japan Association for Quaternary Research 2009. Digital Book: Progress in Quaternary Research in Japan. *Japan Association for Quaternary Research*, CD-ROM and booklet, 30p (in Japanese).

Machida, H., (2002). Volcanoes and tephras in the Japan area. *Global Environmental Research-English Edition*, 6(2), 19-28. (in Japanese).

Machida, H. and Arai, F., (2003). Atlas of Tephra in and around Japan. *University of Tokyo Presse*, *120*.

Machida, H., (1999). Quaternary Widespread Tephra Catalog in and around Japan Recent Progress. *The Quaternary Research (Daiyonki-Kenkyu),* 38(3), pp.194-201. (in Japanese).

Machida, H. and Arai, F. (1983). Extensive ash falls in and around the sea of Japan from large late quaternary eruptions. *Journal of Volcanology and Geothermal Research*. 18 (1–4), 151–164.

Mackay, H., Hughes, P.D.M., Jensen, B.J.L., Langdon, P.G., Pyne-O'Donnell, S.D.F., Plunkett, G., Froese, D.G., Coulter, S. and Gardner, J.E. (2016). A mid to late Holocene cryptotephra framework from eastern North America. *Quaternary Science Reviews*. 132101–113.

MacLeod, A., Palmer, A., Lowe, J. and Rose, J., (2008). Tephrostratigraphy of the Loch Laggan East lake sequence. *The Quaternary of Glen Roy and Vicinity, Field Guide. Quaternary Research Association, London*, 83-91.

Mahony, S.H., Sparks, R.S.J., Wallace, L.M., Engwell, S.L., Scourse, E.M., Barnard, N.H., Kandlbauer, J. and Brown, S.K. (2016). Increased rates of large-magnitude explosive eruptions in Japan in the late Neogene and Quaternary. *Geochemistry, Geophysics, Geosystems*. 17 (7), 2467–2479.

Mark, D.F., Petraglia, M., Smith, V.C., Morgan, L.E., Barfod, D.N., Ellis, B.S., Pearce, N.J., Pal, J.N. and Korisettar, R. (2014). A high-precision $^{40}Ar/^{39}Ar$ age for the Young Toba Tuff and dating of ultra-distal tephra: Forcing of Quaternary climate and implications for hominin occupation of India. *Quaternary Geochronology*. 21 (1), 90–103.

Marti, A., Folch, A., Costa, A., Engwell, S., (2016). Reconstructing the plinian and co-ignimbrite sources of large volcanic eruptions: a novel approach for the Campanian Ignimbrite. *Scientific Reports,* 1–11.

Martin-Jones, C., Lane, C.S., Blaauw, M., Mark, D.F., Verschuren, D., Van der Meeren, T., Van Daele, M., Wynton, H., Blegen, N., Kisaka, M. and Leng, M.J., 2024. The> 250-kyr Lake Chala record: A tephrostratotype correlating archaeological, palaeoenvironmental and volcanic sequences across eastern Africa. *Quaternary Science Reviews*, *326*, 108476

Matthews, I.P., Birks, H.H., Bourne, A.J., Brooks, S.J., Lowe, J.J., MacLeod, A. and Pyne-O'Donnell, S.D.F., (2011). New age estimates and climatostratigraphic correlations for the Borrobol and Penifiler Tephras: evidence from Abernethy Forest, Scotland. *Journal of Quaternary Science*, *26*(3), 247-252.

Matthews, R.K., (1968). Tectonic implications of glacio-eustatic sea level fluctuations. *Earth and Planetary Science Letters*, *5*, 459-462.

Matsu'ura, T., and Komatsubara, J. (2024). Ontake-Katamachi tephra: Marine-terrestrial correlation of a time marker of marine isotopic stage 5b in NE Japan, the Japan Sea, and the NW Pacific. *Journal of Asian Earth Sciences*, 259, 105876. https://doi.org/10.1016/j.jseaes.2023.105876

Matsu'ura, T., Ikehara, M., and Ueno, T. (2021). Late Quaternary tephrostratigraphy and cryptotephrostratigraphy of core MD012422: Improving marine tephrostratigraphy of the NW Pacific. *Quaternary Science Reviews,* 257. https://doi.org/10.1016/j.quascirev.2021.106808

Matsu'ura, T., Kimura, J.I., Chang, Q. and Komatsubara, J., (2017). Using tephrostratigraphy and cryptotephrostratigraphy to re-evaluate and improve the Middle Pleistocene age model

for marine sequences in northeast Japan (Chikyu C9001C). *Quaternary Geochronology*, *40*, 129-145.

Matsu'ura, T., Furusawa, A., Shimogama, K., Goto, N., and Komatsubara, J. (2014). Late Quaternary tephrostratigraphy and cryptotephrostratigraphy of deep-sea sequences (Chikyu C9001C cores) as tools for marine terrace chronology in NE Japan. *Quaternary Geochronology,* 23, 63–79. https://doi.org/10.1016/J.QUAGEO.2014.06.001

McCanta, M.C., Hatfield, R.G., Thomson, B.J., Hook, S.J. and Fisher, E., (2015). Identifying cryptotephra units using correlated rapid, nondestructive methods: VSWIR spectroscopy, X-ray fluorescence, and magnetic susceptibility. *Geochemistry, Geophysics, Geosystems*, *16*(12), 029-4056.

McGuire, A.M., Lane, C.S., Roucoux, K.H., Albert, P.G., Kearney, R., (2022). The dating and correlation of an eastern Mediterranean lake sediment sequence: a 46–4 ka tephrostratigraphy for Ioannina (NW Greece). Journal of Quaternary Science, 37 (8), 1313–1331.

McLean, D., Albert, P. G., Schlolaut, G., Lamb, H. F., Marshall, M. H., Brauer, A., Wade, J., Nakagawa, T., and Smith, V. C. (2022). How reliable is μXRF core scanning at detecting tephra layers in sedimentary records? A case study using the Lake Suigetsu archive (central Japan). Journal of Quaternary Science, 37(7), 1189–1206. https://doi.org/10.1002/JQS.3432

McLean, D., Albert, P. G., Suzuki, T., Nakagawa, T., Kimura, J., Chang, Q., Miyabuchi, Y., Manning, C. J., MacLeod, A., and Blockley, S. P. E. (2020a). Constraints on the timing of explosive volcanism at Aso and Aira calderas (Japan) between 50 and 30 ka: New insights from the Lake Suigetsu sedimentary record (SG14 core). Geochemistry, Geophysics, Geosystems, 21(8). https://doi.org/10.1029/2019GC008874

McLean, D., Albert, P. G., Suzuki, T., Nakagawa, T., Kimura, J.-I., Chang, Q., MacLeod, A., Blockley, S., Staff, R. A., and Yamada, K. (2020b). Refining the eruptive history of Ulleungdo and Changbaishan volcanoes (East Asia) over the last 86 kyrs using distal sedimentary records. *Journal of Volcanology and Geothermal Research,* 389, 106669. https://doi.org/10.1016/j.jvolgeores.2019.106669

McLean, D., Albert, P. G., Nakagawa, T., Suzuki, T., Staff, R. A., Yamada, K., Kitaba, I., Haraguchi, T., Kitagawa, J., and Smith, V. (2018). Integrating the Holocene tephrostratigraphy for East Asia using a high-resolution cryptotephra study from Lake Suigetsu (SG14 core), central Japan. *Quaternary Science Reviews,* 183, 36–58. https://doi.org/10.1016/j.quascirev.2017.12.013

McLean, D., Albert, P. G., Nakagawa, T., Staff, R. A., Suzuki, T., and Smith, V. C. (2016). Identification of the Changbaishan 'Millennium'(B-Tm) eruption deposit in the Lake Suigetsu (SG06) sedimentary archive, Japan: synchronisation of hemispheric-wide paleoclimate archives. Quaternary Science Reviews, 150, 301–307. https://doi.org/10.1016/j.quascirev.2017.12.013

McNamara, K., Rust, A.C., Cashman, K.V., Castruccio, A. and Abarzúa, A.M., (2019). Comparison of lake and land tephra records from the 2015 eruption of Calbuco volcano, Chile. *Bulletin of Volcanology*, *81*, 1-15.

Miyabuchi, Y., Okuno, M., Torii, M., Yoshimoto, M. and Kobayashi, T., (2014). Tephrostratigraphy and eruptive history of post-caldera stage of Toya Volcano, Hokkaido, northern Japan. *Journal of Volcanology and Geothermal Research*, *281*, 34-52.

Miyabuchi, Y. (2011). Post-caldera explosive activity inferred from improved 67-30 ka tephrostratigraphy at Aso Volcano, Japan. *Journal of Volcanology and Geothermal Research,* 205 (3–4), 94–113. https://doi.org/10.1016/j.jvolgeores.2011.05.004

Miyabuchi, Y. (2009). A 90,000-year tephrostratigraphic framework of Aso Volcano, Japan. *Sedimentary Geology,* 220(3–4), 169–189. https://doi.org/10.1016/J.SEDGEO.2009.04.018

Miyabuchi, Y., Hoshizumi, H., Takada, H., Watanabe, K. And Xu, S., (2003). Pumice-fall deposits from Aso volcano during the past 90,000 years, southwestern Japan. *Kazan*, *48*(2), 195-214.

Monaco, L., Palladino, D.M., Albert, P.G., Arienzo, I., Conticelli, S., Di Vito, M., Fabbrizio, A., D'Antonio, M., Isaia, R., Manning, C.J., Nomade, S., Pereira, A., Petrosino, P., Sottili, G., Sulpizio, R., Zanchetta, G., Giaccio, B., (2022). Linking the Mediterranean MIS 5 tephra markers to Campi Flegrei (southern Italy) 109–92 ka explosive activity and refining the chronology of MIS 5c-d millennial-scale climate variability. *Global Planetary Changes,* 211, 103785.

Monteath, A.J., Hughes, P.D.M. and Wastegård, S., (2019). Evidence for distal transport of reworked Andean tephra: Extending the cryptotephra framework from the Austral volcanic zone. *Quaternary Geochronology*, *51*, 64-71.

Munno, R. and Petrosino, P. (2007). The late Quaternary tephrostratigraphical record of the San Gregorio Magno basin (southern Italy). *Journal of Quaternary Science,* 22 (3), 247–266.

Nagahashi, Y., Yoshikawa, S., Miyakawa, C., Uchiyama, T. and Inouchi, Y., (2004). Stratigraphy and Chronology of Widespread Tephra Layers during the Past 430ky in the Kinki District and the Yatsugatake Mountains Major Element Composition of the Glass Shards Using EDS Analysis. *The Quaternary Research (Daiyonki-Kenkyu)*, *43*(1), 15-35.

Nagaoka, S. and Okuno, M., (2011). Tephrochronology and eruptive history of Kirishima volcano in southern Japan. *Quaternary International*, 246(1-2), 260-269. https://doi.org/10.1016/j.quaint.2011.06.007

Nagaoka, S., Okuno, M. and Arai, F., (2001). Tephrostratigraphy and eruptive history of the Aira caldera volcano during 100-30 ka, Kyushu, Japan. *Journal-Geological Society Of Japan*, 107(7), 432-450.

Nakagawa, T., Tarasov, P., Staff, R., Bronk Ramsey, C., Marshall, M., Schlolaut, G., Bryant, C., Brauer, A., Lamb, H., Haraguchi, T., Gotanda, K., Kitaba, I., Kitagawa, H., van der Plicht, J., Yonenobu, H., Omori, T., Yokoyama, Y., Tada, R., and Yasuda, Y. (2021). The spatio-temporal structure of the Lateglacial to early Holocene transition reconstructed from the pollen record of Lake Suigetsu and its precise correlation with other key global archives: Implications for paleoclimatology and archaeology. *Global and Planetary Change,* 202, 103493. https://doi.org/10.1016/J.GLOPLACHA.2021.103493

Nakagawa, T., Gotanda, K., Haraguchi, T., Danhara, T., Yonenobu, H., Brauer, A., Yokoyama, Y., Tada, R., Takemura, K., Staff, R. A., Payne, R., Bronk Ramsey, C., Bryant, C., Brock, F., Schlolaut, G., Marshall, M., Tarasov, P., and Lamb, H. (2012). SG06, a fully continuous and varved sediment core from Lake Suigetsu, Japan: stratigraphy and potential for improving the radiocarbon calibration model and understanding of late Quaternary climate changes. *Quaternary Science Reviews*, 36, 164–176. https://doi.org/10.1016/J.QUASCIREV.2010.12.013

Nakagawa, T., Kitagawa, H., Yasuda, Y., Tarasov, P. E., Gotanda, K., and Sawai, Y. (2005). Pollen/event stratigraphy of the varved sediment of Lake Suigetsu, central Japan from 15,701 to 10,217 SG vyr BP (Suigetsu varve years before present): Description, interpretation, and correlation with other regions. *Quaternary Science Reviews*, 24(14–15), 1691–1701. https://doi.org/10.1016/j.quascirev.2004.06.022

Nakagawa, T., Kitagawa, H., Yasuda, Y., Tarasov, P. E., Nishida, K., Gotanda, K., Sawai, Y., Yangtze River and Civilization Program members. (2003). Asynchronous Climate Changes in the North Atlantic and Japan During the Last Termination. *Science*, 299: 688-691

Nakamura, Y. (2016). Stratigraphy, distribution, and petrographic properties of Holocene tephras in Hokkaido, northern Japan. *Quaternary International*, 39752–62.

Newhall, C., Self, S., and Robock, A. (2018). Impacts of future VEI 7 eruptions *Geosphere,* 14(2). https://doi.org/10.1130/GES01513.1

Newhall, C.G. and Self, S. (1982). The volcanic explosivity index (VEI) an estimate of explosive magnitude for historical volcanism. *Journal of Geophysical Research: Oceans,* 87 (C2), 1231–1238.

Newhall, C., Self, S. and Robock, A. (2018). Anticipating future Volcanic Explosivity Index (VEI) 7 eruptions and their chilling impacts. *Geosphere*, *14*(2), 572-603.

Okuno, M., Nagaoka, S., Saito-Kokubu, Y., Nakamura, T., and Kobayashi, T. (2017). AMS Radiocarbon Dates of Pyroclastic-Flow Deposits on the Southern Slope of the Kuju Volcanic Group, Kyushu, Japan. Radiocarbon, 59(2), 483–488. https://doi.org/10.1017/RDC.2016.66

Okuno, M., Torii, M., Yamada, K., Shinozuka, Y., Danhara, T., Gotanda, K., Yonenobu, H. and Yasuda, Y. (2011). Widespread tephras in sediments from lake Ichi-no-Megata in northern Japan: Their description, correlation and significance. *Quaternary International*. 246 (1– 2), 270–277.

Okuno, M. and Kobayashi, T., (1994). Late Pleistocene tephra layers distributed on Tane Island, southwest Japan. The Quaternary Research (Daiyonki-Kenkyu), 33(2), 113-117.

Ono, K. and Watanabe, K., (1985). Geological map of Aso volcano. Geological map of volcanoes. *Geological Survey of Japan*, *4*. (in Japanese)

Ono, K. And Watanabe, H., (1983). Distribution and serological identification of Bacillus thuringi ensis isolated in Japan. *The Journal of Sericultural Science of Japan*, *52*(1), pp.47-50. (in Japanese)

Oppenheimer, C. (2003). Ice core and paleoclimatic evidence for the timing and nature of the great mid-13th century volcanic eruption. *International Journal of Climatology*, 23, 417–426. https://doi.org/10.1002/joc.891

Orsi, G., Di Vito, M.A., Isaia, R., (2004). Volcanic hazard assessment at the restless Campi Flegrei caldera. *Bulletin of Volcanology,* 66 (6), 514–530.

Orsi, G., De Vita, S., Di Vito, M., (1996). The restless, resurgent Campi Flegrei nested caldera (Italy): constraints on its evolution and configuration. *Journal of Volcanology and Geothermal Research*, 74 (3–4), 179–214.

Orsi, G., Gallo, G., Zanchi, A., (1991). Simple-shearing block resurgence in caldera depressions. A model from Pantelleria and Ischia. *Journal of Volcanology and Geothermal Research*, 47 (1–2), 1–11.

Pabst, S., Wörner, G., Civetta, L., Tesoro, R. (2008). Magma Chamber Evolution Prior to the Campanian Ignimbrite and Neapolitan Yellow Tuff Eruptions (Campi Flegrei, Italy). *Bulletin of Volcanology,* 70, 961-976.

Pamukçu, A.S., Wright, K.A., Gualda, G.A. and Gravley, D. (2020). Magma residence and eruption at the Taupo Volcanic Center (Taupo Volcanic Zone, New Zealand): insights from rhyolite-MELTS geobarometry, diffusion chronometry, and crystal textures. *Contributions to Mineralogy and Petrology*, *175*, 1-27.

Pappalardo, L., Civetta, L., D'Antonio, M., Deino, A., Di Vito, M., Orsi, G., Carandente, A., De Vita, S., Isaia, R., Piochi, M. (1999). Chemical and Sr-isotopical evolution of the Phlegraean magmatic system before the Campanian Ignimbrite and the Neapolitan Yellow Tuff eruptions. *Journal of Volcanology and Geothermal Research,* 91 (2–4), 141–166.

Park, M.H., Kim, I.S. and Shin, J.B. (2003) Characteristics of the late Quaternary tephra layers in the East/Japan Sea and their new occurrences in western Ulleung Basin sediments. *Marine Geology*, 202 (3–4), 135–142.

Paterne, M., Guichard, F. and Labeyrie, J. (1988). Explosive activity of the South Italian volcanoes during the past 80,000 years as determined by marine tephrochronology. J. Volcanol. Geotherm. Res. 34 (3–4), 153–172. *Journal of Volcanology and Geothermal Research, 443*

Paterne, M., Guichard, F., Labeyrie, J., Gillot, P.Y. and Duplessy, J.C., (1986). Tyrrhenian Sea tephrochronology of the oxygen isotope record for the past 60,000 years. *Marine Geology,* 72 (3–4), 259–285.

Payne, R., and Gehrels, M. (2010). The formation of tephra layers in peatlands: An experimental approach*. Catena,* 81(1), 12–23. https://doi.org/10.1016/J.CATENA.2009.12.001

Pearce, N.J.G., Abbott, P.M. and Martin-Jones, C. (2014). Microbeam methods for the analysis of glass in fine-grained tephra deposits: a SMART perspective on current and future trends. *Geological Society, London, Special Publications*. 398 (1), 29–46.

Pearce, N. J., Denton, J. S., Perkins, W. T., Westgate, J. A. and Alloway, B. V. (2007). Correlation and characterisation of individual glass shards from tephra deposits using trace element laser ablation ICP-MS analyses: current status and future potential. *Journal of Quaternary Science*, 22*:* 721-736

Pearce, N.J., Westgate, J.A., Preece, S.J., Eastwood, W.J. and Perkins, W.T., (2004). Identification of Aniakchak (Alaska) tephra in Greenland ice core challenges the 1645 BC date for Minoan eruption of Santorini. *Geochemistry, Geophysics, Geosystems*, *5*(3).

Peccerillo, A., and Taylor, S. R. (1976). Geochemistry of eocene calc-alkaline volcanic rocks from the Kastamonu area, Northern Turkey. Contributions to *Mineralogy and Petrology* 58(1), 63–81. https://doi.org/10.1007/BF00384745

Perrotta, A., Scarpati, C., Luongo, G., Morra, V., (2010). Stratigraphy and volcanological evolution of the southwestern sector of Campi Flegrei and Procida Island, Italy. *Stratigraphy and Geology of Volcanic Areas,* 171–191.

Perrotta, A., Scarpati, C., (1994). The dynamics of the Breccia Museo eruption (Campi Flegrei, Italy) and the significance of spatter clasts associated with lithic breccias. *Journal of Volcanology and Geothermal Research, 59* (4), 335–355.

Plunkett, G.M., Pilcher, J.R., McCormac, F.G. and Hall, V.A. (2016) New dates for first millennium BC tephra isochrones in Ireland. *The Holocene,* 14 (5), 780–786. http://dx.doi.org/10.1191/0959683604hl757rr.

Plunkett, G., Coulter, S.E., Ponomareva, V.V., Blaauw, M., Klimaschewski, A. and Hammarlund, D., (2015). Distal tephrochronology in volcanic regions: challenges and insights from Kamchatkan lake sediments. *Global and Planetary Change*, *134*, 26-40.

Poli, S., Chiesa, S., Gillot, P.Y., Gregnanin, A. and Guichard, F. (1987). Chemistry vs. time in the volcanic complex of Ischia (Gulf of Naples, Italy): evidence of successive magmatic cycles. *Contributions to Mineralogy and Petrology,* 95 (3), 322–335.

Ponomareva, V., Pendea, I.F., Zelenin, E., Portnyagin, M., Gorbach, N., Pevzner, M., Plechova, A., Derkachev, A., Rogozin, A. and Garbe-Schönberg, D., (2021). The first continuous late Pleistocene tephra record from Kamchatka Peninsula (NW Pacific) and its volcanological and paleogeographic implications. *Quaternary Science Reviews*, *257*, 106838.

Ponomareva, V., Portnyagin, M., Pevzner, M., Blaauw, M., Kyle, P. and Derkachev, A., (2015). Tephra from andesitic Shiveluch volcano, Kamchatka, NW Pacific: chronology of explosive eruptions and geochemical fingerprinting of volcanic glass. *International Journal of Earth Sciences*, *104*, 1459-1482.

Primerano, P., Giordano, G., Costa, A., de Vita, S. and di Vito, M.A. (2021). Reconstructing fallout features and dispersal of Cretaio Tephra (Ischia Island, Italy) through field data analysis and numerical modelling: Implications for hazard assessment. *Journal of Volcanology and Geothermal Research*, 415, 107248.

Pyle, D.M., Ricketts, G.D., Margari, V., van Andel, T.H., Sinitsyn, A.A., Praslov, N.D. and Lisitsyn, S. (2006). Wide dispersal and deposition of distal tephra during the Pleistocene 'Campanian Ignimbrite/Y5' eruption, Italy. *Quaternary Science Reviews*, 25 (21–22), 2713–2728.

Pyle, D.M., (2000). Sizes of volcanic eruptions. In: Sigurdsson, H., Houghton, B.F., McNutt, S.R., Rymer, H., Stix, J. (Eds.), Encyclopedia of Volcanoes. 257-264 *Academic Press, London*. https://doi.org/10.1016/B978-0-12-385938-9.00013-4

Pyle, D.M. (1995). Assessment of the minimum volume of tephra fall deposits. *Journal of Volcanology and Geothermal Research*, *69*(3-4), 379-382.

Pyle, D.M., (1989). The thickness, volume and grainsize of tephra fall deposits. *Bulletin of Volcanology*, *51*, 1-15.

Pyne-O'Donnell, S.D.F., Hughes, P.D.M., Froese, D.G., Jensen, B.J.L., Kuehn, S.C., Mallon, G., Amesbury, M.J., Charman, D.J., Daley, T.J., Loader, N.J., Mauquoy, D., Street- Perrott, F.A. and Woodman-Ralph, J. (2012). High-precision ultra-distal Holocene tephrochronology in North America. *Quaternary Science Reviews*, 526–11.

Rampino, M.R., Self, S. and Fairbridge, R.W., 1979. Can rapid climatic change cause volcanic eruptions?. *Science*, *206*(4420), 826-829.

Reimer, P. J., Austin, W. E. N., Bard, E., Bayliss, A., Blackwell, P. G., Ramsey, C. B., Butzin, M., Cheng, H., Edwards, R. L., Friedrich, M., Grootes, P. M., Guilderson, T. P., Hajdas, I., Heaton, T. J., Hogg, A. G., Hughen, K. A., Kromer, B., Manning, S. W., Muscheler, R., Talamo, S. (2020). The IntCal20 Northern Hemisphere Radiocarbon Age Calibration Curve (0–55 cal kBP). *Radiocarbon,* 62(4), 725–757. https://doi.org/10.1017/RDC.2020.41

Reimer, P.J., Bard, E., Bayliss, A., Beck, J.W., Blackwell, P.G., Ramsey, C.B., Buck, C.E., Cheng, H., Edwards, R.L., Friedrich, M. and Grootes, P.M., (2014). IntCal13 and Marine13 radiocarbon age calibration curves 0–50,000 years cal BP. *Radiocarbon*, *55*(4), 1869-1887.https://doi:10.2458/azu_js_rc.55.16947

Rex, C.L., Staff, R.A., Sanderson, D.C., Cresswell, A.J., Marshall, M.H., Hyodo, M., Horiuchi, D., Tada, R. and Nakagawa, T., (2022). Controls on luminescence signals in lake sediment cores: A study from Lake Suigetsu, Japan. *Quaternary Geochronology*, *71*, 101319.

Rolandi, G., Bellucci, F., Heizler, M.T., Belkin, H.E. and De Vivo, B. (2003). Tectonic controls on the genesis of ignimbrites from the Campanian Volcanic Zone, southern Italy. *Mineralogy and Petrology,* 79 (1), 3–31.

Rollinson, H.R. (2014) Using Geochemical Data: Evaluation, Presentation, Interpretation. *Using Geochemical Data*.

Rose, W.I. and Durant, A.J. (2009). Fine ash content of explosive eruptions. *Journal of Volcanology and Geothermal Research*,186 (1–2), 32–39.

Rosi, M., Sbrana, A., Vezzoli, L. (1988). Correlazioni tefrostratigraphiche di alcuni livelli di Ischia, Procida e Campi Flegrei. Mem. Soc. Geol. Ital. 41, 1015–1027. (In Italian)
Rosi, M., Vezzoli, L., Castelmenzano, A. and Grieco, G., (1999). Plinian pumice fall deposit of the Campanian Ignimbrite eruption (Phlegraean Fields, Italy). *Journal of Volcanology and Geothermal Research*, 91, 179–198.

Sagawa, T., Nagahashi, Y., Satoguchi, Y., Holbourn, A., Itaki, T., Gallagher, S. J., Saavedra-Pellitero, M., Ikehara, K., Irino, T., and Tada, R. (2018). Integrated tephrostratigraphy and stable isotope stratigraphy in the Japan Sea and East China Sea using IODP Sites U1426, U1427, and U1429, Expedition 346 Asian Monsoon. *Progress in Earth and Planetary Science,* 2018 5:1, 5(1), 1–24. https://doi.org/10.1186/S40645-018-0168-7

Santacroce, R., Cristofolini, R., La Volpe, L., Orsi, G. and Rosi, M., (2003). Italian active volcanoes. *Episodes Journal of International Geoscience*, 26 (3), 227–234.

Scandone, R., Bellucci, F., Lirer, L. andRolandi, G. (1991). The structure of the Campanian Plain and the activity of the Neapolitan volcanoes (Italy). *Journal of Volcanology and Geothermal Research*, 48 (1–2), 1–31.

Scarpati, C., Cole, P. and Perrotta, A. (1993). The Neapolitan Yellow Tuff—a large volume multiphase eruption from Campi Flegrei, southern Italy. *Bulletin of Volcanology*, *55*, 343-356.

Schindlbeck, J.C., Kutterolf, S., Straub, S.M., Andrews, G.D.M., Wang, K.-L. and Mleneck-Vautravers, M.J. (2018). One Million Years tephra record at IODP Sites U1436 and U1437: Insights into explosive volcanism from the Japan and Izu arcs. *Island Arc*, 27 (3), 12244.

Schlolaut, G., Staff, R. A., Brauer, A., Lamb, H. F., Marshall, M. H., Bronk Ramsey, C., and Nakagawa, T. (2018). An extended and revised Lake Suigetsu varve chronology from ~50 to

~10 ka BP based on detailed sediment micro-facies analyses. *Quaternary Science Reviews*, 200, 351–366. https://doi.org/10.1016/j.quascirev.2018.09.021

Schlolaut, G., Brauer, A., Marshall, M. H., Nakagawa, T., Staff, R. A., Ramsey, C. B., Lamb, H. F., Bryant, C.L., Naumann, R., Dulski, P., Brock, F., Yokoyama, Y., Tada, R., Haraguchi, T., Suigetsu 2006 project members. (2014). Event layers in the Japanese Lake Suigetsu 'SG06' sediment core: description, interpretation and climatic implications. *Quaternary Science Reviews.* 83: 157-170

Schlolaut, G., Marshall, M. H., Brauer, A., Nakagawa, T., Lamb, H. F., Staff, R. A., Bronk Ramsey, C., Bryant, C. L., Brock, F., Kossler, A., Tarasov, P. E., Yokoyama, Y., Tada, R., and Haraguchi, T. (2012). An automated method for varve interpolation and its application to the Late Glacial chronology from Lake Suigetsu, Japan. *Quaternary Geochronology,* 13, 52–69. https://doi.org/10.1016/j.quageo.2012.07.005

Schmidt, R., van den Bogaard, C., Merkt, J. and Müller, J., (2002). A new Lateglacial chronostratigraphic tephra marker for the south-eastern Alps: The Neapolitan Yellow Tuff (NYT) in Längsee (Austria) in the context of a regional biostratigraphy and paleoclimate. *Quaternary International*, *88*(1), 45-56.

Schmincke, H.U., Park, C. and Harms, E. (1999) Evolution and environmental impacts of the eruption of Laacher See Volcano (Germany) 12,900 a BP. *Quaternary International*. 61 (1), 61–72.

Shane, P., Nairn, I. A., Martin, S. B., and Smith, V. C. (2008). Compositional heterogeneity in tephra deposits resulting from the eruption of multiple magma bodies: implications for tephrochronology. *Quaternary International*, 178(1), 44–53.

Shane, P. (2000). Tephrochronology: a New Zealand case study. *Earth Science Reviews,* 49*:* 223-259

Shitaoka Y, Fukuoka T, Hasegawa A, Kusano T, Nagatomo T. (2009). Thermoluminescence dating of the pyroclastic deposits of the SanbeVolcano. *Bull Shimane Nat Mus Mt Sanbe (Sahimel)* 7:15–24

Sigl, M., Winstrup, M., McConnell, J. R., Welten, K. C., Plunkett, G., Ludlow, F., Büntgen, U., Caffee, M., Chellman, N., Dahl-Jensen, D., Fischer, H., Kipfstuhl, S., Kostick, C., Maselli, O. J., Mekhaldi, F., Mulvaney, R., Muscheler, R., Pasteris, D. R., Pilcher, J. R., Woodruff, T. E. (2015). Timing and climate forcing of volcanic eruptions for the past 2,500 years. *Nature*, 523(7562), 543–549. https://doi.org/10.1038/nature14565

Smith, R.E., Smith, V.C., Fontijn, K., Gebhardt, A.C., Wastegård, S., Zolitschka, B., Ohlendorf, C., Stern, C. and Mayr, C., (2019). Refining the Late Quaternary tephrochronology for southern South America using the Laguna Potrok Aike sedimentary record. *Quaternary Science Reviews*, *218*, 137-156.

Smith, V.C., Isaia, R., Engwell, S.L., Albert, P.G., (2016). Tephra dispersal during the Campanian Ignimbrite (Italy) eruption: implications for ultra-distal ash transport during the large caldera-forming eruption. *Bulletin of Volcanology*, 78.

Smith, V. C., Staff, R. A., Blockley, S. P. E., Bronk Ramsey, C., Nakagawa, T., Mark, D. F., Takemura, K., and Danhara, T. (2013). Identification and correlation of visible tephras in the Lake Suigetsu SG06 sedimentary archive, Japan: Chronostratigraphic markers for synchronising of east Asian/west Pacific paleoclimatic records across the last 150 ka. *Quaternary Science Reviews*. https://doi.org/10.1016/j.quascirev.2013.01.026

Smith, V. C., Isaia, R., and Pearce, N. J. G. (2011a). Tephrostratigraphy and glass compositions of post-15 kyr Campi Flegrei eruptions: Implications for eruption history and chronostratigraphic markers. *Quaternary Science Reviews*, 30(25–26), 3638–3660. https://doi.org/10.1016/j.quascirev.2011.07.012

Smith, V. C., Mark, D. F., Staff, R. A., Blockley, S. P. E., Ramsey, C. B., Bryant, C. L., Nakagawa, T., Han, K. K., Weh, A., Takemura, K., and Danhara, T. (2011b). Toward establishing precise 40Ar/39Ar chronologies for Late Pleistocene paleoclimate archives: An example from the Lake Suigetsu (Japan) sedimentary record. *Quaternary Science Reviews*. https://doi.org/10.1016/j.quascirev.2011.06.020

Smith, V.C., Shane, P., Nairn, I.A. and Williams, C.M., (2006). Geochemistry and magmatic properties of eruption episodes from Haroharo linear vent zone, Okataina Volcanic Centre, New Zealand during the last 10 kyr. *Bulletin of volcanology*, *69*, 57-88.

Smith, V. C., Shane, P. and Nairn, I. A. (2005). Trends in rhyolite geochemistry, mineralogy, and magma storage during the last 50 kyr at Okataina and Taupo volcanic centres, Taupo Volcanic Zone, New Zealand. *Journal of Volcanology and Geothermal Research*, 148: 372-406

Smith, D. G. W. and Westgate, J. A. (1968). Electron probe technique for characterising pyroclastic deposits. *Earth and Planetary Science Letters*, 5: 313-319

Sparks, R.S.J., (2003). Dynamics of magma degassing.

Sparks, R.S.J., Bursik, M.I., Ablay, G.J., Thomas, R.M.E. and Carey, S.N., (1992). Sedimentation of tephra by volcanic plumes. Part 2: controls on thickness and grain-size variations of tephra fall deposits. *Bulletin of Volcanology*, *54*, 685-695.

Staff, R.A., Sanderson, D.C., Rex, C.L., Cresswell, A., Hyodo, M., Kitaba, I., Marshall, M.H., Schlolaut, G., Yamada, K., Suzuki, Y. and Nowinski, V. (2024). A luminescence-derived cryptostratigraphy from the Lake Suigetsu sedimentary profile, Japan: 45,000–30,200 IntCal20 yr BP. *Quaternary Geochronology*, *83*, 101588.

Staff, R. A., Schlolaut, G., Ramsey, C. B., Brock, F., Bryant, C. L., Kitagawa, H., Van der Plicht, J., Marshall, M. H., Brauer, A., Lamb, H. F. and Payne, R. L. (2013). Integration of the old and new Lake Suigetsu (Japan) terrestrial radiocarbon calibration data sets. *Radiocarbon*, 55: 2049-2058

Staff, R. A., Ramsey, C. B., Bryant, C. L., Brock, F., Payne, R. L., Schlolaut, G., Marshall, M. H., Brauer, A., Lamb, H. F., Tarasov, P., Yokoyama, Y., Haraguchi, T., Gotanda, K., Yonenobu, H., and Nakagawa, T. (2011). New 14C Determinations from Lake Suigetsu, Japan: 12,000 to 0 Cal BP. *Radiocarbon*, 53(3), 511–528. https://doi.org/10.1017/S0033822200034627

Sturm, A., Schmitt, A.K. and Danišík, M., (2024). Updating the Eifel record: Zircon double-dating of tephras from Wehr volcano (East Eifel, Germany) as marker horizons for the European Pleistocene loess stratigraphy. *Quaternary Science Reviews*, *338*, 108810.

Sulpizio, R., Costa, A., Massaro, S., Selva, J., and Billotta, E. (2024). Assessing volumes of tephra fallout deposits: a simplified method for data scarcity cases. *Bulletin of Volcanology*, 86(7), 1–14. https://doi.org/10.1007/S00445-024-01753-5/FIGURES/3

Sulpizio, R., Zanchetta, G., D'Orazio, M., Vogel, H. and Wagner, B. (2010) Tephrostratigraphy and tephrochronology of lakes Ohrid and Prespa, Balkans. *Biogeosciences*, 7 (10), 3273–3288.

Sun, C., Plunkett, G., Liu, J., Zhao, H., Sigl, M., McConnell, J. R., Pilcher, J. R., Vinther, B., Steffensen, J. P., and Hall, V. (2014). Ash from Changbaishan Millennium eruption recorded in Greenland ice: Implications for determining the eruption's timing and impact. *Geophysical Research Letters*, 41(2), 694–701. https://doi.org/10.1002/2013GL058642

Sun, S., McDonough, W.F. (1989). Chemical and isotopic systematics of 630 oceanic basalts: implications for mantle composition and processes. In: Saunders, A.D., Norry, M.J. (Eds.), *Magmatism in Ocean Basins*, 631.

Suzuki, T., Saito, H., Kasahara, A., Kuriyama, E., Imaizumi, T. (2016). Late Quaternary tephrostratigraphy of underground sediments in the middle west part of Aizu Basin, Fukushima, northeast Japan. *Quaternary Research,* 55, 1–16 (In Japanese).

Takada, H., (1989). Preliminary report on tephra from Aso central cones*. Journal of the Kumamoto Geoscience Association*, 90: 8–11 (in Japanese)

Tamura, Y., and Tatsumi, Y. (2002). Remelting of an Andesitic Crust as a Possible Origin for Rhyolitic Magma in Oceanic Arcs: An Example from the Izu–Bonin Arc. *Journal of Petrology*, 43(6), 1029–1047. https://doi.org/10.1093/PETROLOGY/43.6.1029

Tatsumi, Y., Tamura, Y., Nichols, A. R. L., Ishizuka, O., Takahashi, N., and Tani, K.-I. (2016). Izu–Bonin Arc. *The Geology of Japan*, 175–199. https://doi.org/10.1144/GOJ.7

Thorarinsson, S., (1944). Tefrokronologiska studier på Island: Þjórsárdalur och dess förödelse. *Geografiska annaler*, *26*(1-2), 1-217. (in Icelandic)

Thunell, R., Federman, A., Sparks, S. and Williams, D. (1979). The Age, Origin, and Volcanological Significance of the Y-5 Ash Layer in the Mediterranean. *Quaternary Research*, 12 (2), 241–253.

Timms, R.G., Matthews, I.P., Palmer, A.P. and Candy, I. (2018). Toward a tephrostratigraphic framework for the British Isles: A Last Glacial to Interglacial Transition (LGIT c. 16-8 ka) case study from Crudale Meadow, Orkney. *Quaternary Geochronology*, *46*, 28-44.

Timms, R.G.O., Matthews, I.P., Palmer, A.P., Candy, I. and Abel, L., (2017). A high-resolution tephrostratigraphy from Quoyloo Meadow, Orkney, Scotland: Implications for the tephrostratigraphy of NW Europe during the Last Glacial-Interglacial Transition. *Quaternary Geochronology*, *40*, 67-81.

Tomlinson, E.L., Smith, V.C., Albert, P.G., Aydar, E., Civetta, L., Cioni, R., Çubukçu, E., Gertisser, R., Isaia, R., Menzies, M.A., (2015). The major and trace element glass compositions of the productive Mediterranean volcanic sources: tools for correlating distal tephra layers in and around Europe. *Quaternary Science Reviews,* 118, 48–66.

Tomlinson, E. L., Albert, P. G., Wulf, S., Brown, R. J., Smith, V. C., Keller, J., Orsi, G., Bourne, A. J., and Menzies, M. A. (2014). Age and geochemistry of tephra layers from Ischia, Italy: Constraints from proximal-distal correlations with Lago Grande di Monticchio. *Journal of Volcanology and Geothermal Research,* 287, 22–39. https://doi.org/10.1016/j.jvolgeores.2014.09.00

Tomlinson, E.L., Arienzo, I., Civetta, L., Wulf, S., Smith, V.C., Hardiman, M., Lane, C.S., Carandente, A., Orsi, G., Rosi, M., Müller, W., Menzies, M.A., (2012). Geochemistry of the Phlegraean Fields (Italy) proximal sources for major Mediterranean tephras: Implications for the dispersal of Plinian and co-ignimbritic components of explosive eruptions. *Geochim. Cosmochim.* Acta 93, 102–128.

Tomlinson, E. L., Thordarson, T., Müller, W., Thirlwall, M., and Menzies, M. A. (2010). Microanalysis of tephra by LA-ICP-MS — Strategies, advantages and limitations assessed using the Thorsmörk ignimbrite (Southern Iceland). *Chemical Geology*, 279(3–4), 73–89. https://doi.org/10.1016/J.CHEMGEO.2010.09.013

Ton-That, T., Singer, B. and Paterne, M. (2001). 40Ar/39Ar dating of latest Pleistocene (41 ka) marine tephra in the Mediterranean Sea: implications for global climate records. *Earth and Planetary Science Letters*. 184 (3–4), 645–658.

Tsuji, T., Ikeda, M., Furusawa, A., Nakamura, C., Ichikawa, K., Yanagida, M., Nishizaka, N., Ohnishi, K. and Ohno, Y. (2018). High-resolution record of Quaternary explosive volcanism recorded in fluvio-lacustrine sediments of the Uwa basin, southwest Japan. *Quaternary International*, 471, 278-297. https://doi.org/10.1016/j.quaint.2017.10.016

Turney, C.S., Lowe, J.J., Davies, S.M., Hall, V., Lowe, D.J., Wastegård, S., Hoek, W.Z. and Alloway, B., (2004). Tephrochronology of Last Termination sequences in Europe: a protocol for improved analytical precision and robust correlation procedures (a joint SCOTAV–INTIMATE proposal). *Journal of Quaternary Science*, *19*(2), 111-120.

Turney, C. S. M. (1998). Extraction of rhyolitic component of Vedde microtephra from minerogenic lake sediments. Journal of Paleolimnology 1998 19:2, 19(2), 199–206. https://doi.org/10.1023/A:1007926322026

Tyler, J., Kashiyama, Y., Ohkouchi, N., Ogawa, N., Yokoyama, Y., Chikaraishi, Y., Staff, R. A., Ikehara, M., Bronk Ramsey, C., Bryant, C. and Brock, F. (2010). Tracking aquatic change using chlorin-specific carbon and nitrogen isotopes: The last glacial-interglacial transition at Lake Suigetsu. *Geochemistry, Geophysics, Geosystems*, 11: 9

Uesawa, S., Toshida, K., Takeuchi, S. and Miura, D., (2022). Creating a digital database of tephra fallout distribution and frequency in Japan. *Journal of Applied Volcanology*, 11(1), 14. https://doi.org/10.1186/s13617-022-00126-x

Ukstins Peate, I. and Bryan, S.E., (2008). Re-evaluating plume-induced uplift in the Emeishan large igneous province. *Nature Geoscience*, *1*(9), 625-629.

van der Bilt, W.G., Lane, C.S. and Bakke, J., (2017). Ultra-distal Kamchatkan ash on Arctic Svalbard: towards hemispheric cryptotephra correlation. *Quaternary Science Reviews*, *164*, 230-235.

van den Bogaard C, Schmincke H-U. (2002). Linking the North Atlantic to central Europe: a high-resolution Holocene tephrochronological record from northern Germany. *Journal of Quaternary Science* 17: 3–20.

Vezzoli, L. (Ed.), 1988. Island of Ischia. Consiglio nazionale delle ricerche

Vineberg, S.O., Albert, P.G., McLean, D, Suzuki, T., Staff, R.A., Yamada, K., Kitaba, I., Kitagawa, J., Manning, C.J, Buckland, G. Jones, H.M, Nishizawa F., SG14 Project Members, Nakagawa, T. and Smith, V.C. (2024) A detailed record of large explosive eruptions from

Japan between ~120 and 50 ka preserved at Lake Suigetsu. *Journal of Quaternary Science*, 346 https://doi.org/10.1016/j.quascirev.2024.109021

Vineberg S.O., Isaia R., Albert P.G., Brown R.J, and Smith V.C. (2023). Insights into the explosive eruption history of the Campanian volcanoes prior to the Campanian Ignimbrite eruption. *Journal of Volcanology and Geothermal Research*, 443, https://doi.org/10.1016/j.jvolgeores.2023.107915

Vitale, S. and Isaia, R., (2014). Fractures and faults in volcanic rocks (Campi Flegrei, southern Italy): insight into volcano-tectonic processes. *International Journal of Earth Sciences*, *103*, 801-819.

Wagner, B., Sulpizio, R., Zanchetta, G., Wulf, S., Wessels, M., Daut, G. and Nowaczyk, N., (2008). The last 40 ka tephrostratigraphic record of Lake Ohrid, Albania and Macedonia: a very distal archive for ash dispersal from Italian volcanoes. *Journal of Volcanology and Geothermal Research*, *177*(1), 71-80.

Walcott, R.I., 1972. Past sea levels, eustasy and deformation of the earth. *Quaternary Research*, *2*(1), 1-14.

Westgate, J.A., Pearce, N.J.G., Perkins, W.T., Preece, S.J., Chesner, C.A. and Muhammad, R.F., (2013). Tephrochronology of the Toba tuffs: four primary glass populations define the 75-ka Youngest Toba Tuff, northern Sumatra, Indonesia. *Journal of Quaternary Science*, *28*(8), 772-776.

Westgate, J.A., Preece, S.J., Froese, D.G., Pearce, N.J., Roberts, R.G., Demuro, M., Hart, W.K. and Perkins, W., (2008). Changing ideas on the identity and stratigraphic significance of the Sheep Creek tephra beds in Alaska and the Yukon Territory, northwestern North America. *Quaternary International*, *178*(1), 183-209.

Westgate, J.A. and Gorton, M.P., (1981). Correlation techniques in tephra studies. In *Tephra Studies: Proceedings of the NATO Advanced Study Institute" Tephra Studies as a Tool in Quaternary Research", held in Laugarvatn and Reykjavík, Iceland, June 18–29, 1980*, 73-94.

Wilkins, K.L., Western, L.M. and Watson, I.M. (2016). Simulating atmospheric transport of the 2011 Grímsvötn ash cloud using a data insertion update scheme. *Atmospheric Environment*, *141*, 48-59.

Wulf, S., Hardiman, M. J., Staff, R. A., Koutsodendris, A., Appelt, O., Blockley, S. P. E., Lowe, J. J., Manning, C. J., Ottolini, L., Schmitt, A. K., Smith, V. C., Tomlinson, E. L., Vakhrameeva, P., Knipping, M., Kotthoff, U., Milner, A. M., Müller, U. C., Christanis, K., Kalaitzidis, S., Pross, J. (2018). The marine isotope stage 1–5 cryptotephra record of Tenaghi Philippon, Greece: Towards a detailed tephrostratigraphic framework for the Eastern Mediterranean region. *Quaternary Science Reviews*, 186, 236–262. https://doi.org/10.1016/J.QUASCIREV.2018.03.011

Wulf, S., Keller, J., Paterne, M., Mingram, J., Lauterbach, S., Opitz, S., Sottili, G., Giaccio, B., Albert, P.G., Satow, C., Tomlinson, E.L., Viccaro, M., Brauer, A., (2012). The 100-133 ka record of Italian explosive volcanism and revised tephrochronology of Lago Grande di Monticchio. *Quaternary Science Reviews*, 58, 104–123.

Wulf, S., Kraml, M., Keller, J. (2008). Towards a detailed distal tephrostratigraphy in the Central Mediterranean: the last 20,000 yrs record of Lago Grande di Monticchio. *Journal of Volcanology and Geothermal Research*. 177 (1), 118–132.

Wulf, S., Kraml, M., Brauer, A., Keller, J. and Negendank, J.F. (2004). Tephrochronology of the 100 ka lacustrine sediment record of Lago Grande di Monticchio (southern Italy). *Quaternary International*, *122*(1), 7-30.

Wutke, K., Wulf, S., Tomlinson, E.L., Hardiman, M., Dulski, P., Luterbacher, J., Brauer, A., (2015). Geochemical properties and environmental impacts of seven Campanian tephra layers deposited between 40 and 38 ka BP in the varved lake sediments of Lago Grande di Monticchio, southern Italy. *Quaternary Science Reviews,* 118, 67–83.

Yasuda, Y., Yamaguchi, T., Nakagawa, T., Fukusawa, K., Kitagawa, J. and Okamura, M. (2004). Environmental variability and human adaptation during the Lateglacial/Holocene transition in Japan with reference to pollen analysis of the SG4 core from Lake Suigetsu. *Quaternary International,* 123, 11-19

Appendix A: Supplementary Material for Article 1.

Table A1. Major element glass analyses of twelve Acquamorta tephra units between the MEGT and CI. (un-normalised)

Date of analysis	Unit	Sample	SiO_2	TiO_2	Al_2O_3	FeO_t	MnO	MgO	CaO	Na_2O	K_2O	P_2O5	Cl	Analytical Total
10/04/2021	**AQ-13**	CF282	57.33	0.44	17.81	3.09	0.27	0.32	1.67	6.33	6.80	0.04	0.88	94.97
10/04/2021	**AQ-13**	CF282	57.48	0.37	18.06	2.90	0.19	0.33	1.73	5.99	7.29	0.06	0.77	95.22
10/04/2021	**AQ-13**	CF282	58.39	0.43	18.50	2.72	0.21	0.31	1.64	6.20	7.36	0.03	0.79	96.58
10/04/2021	**AQ-13**	CF282	57.54	0.38	17.90	2.81	0.23	0.29	1.65	6.27	7.05	0.05	0.77	94.94
10/04/2021	**AQ-13**	CF282	57.38	0.39	17.96	2.71	0.22	0.26	1.60	6.19	7.15	0.05	0.75	94.64
10/04/2021	**AQ-13**	CF282	57.43	0.40	17.73	2.87	0.22	0.39	1.67	5.90	7.25	0.01	0.82	94.69
10/04/2021	**AQ-13**	CF282	58.07	0.38	18.10	2.82	0.25	0.33	1.72	6.13	7.13	0.01	0.78	95.71
10/04/2021	**AQ-13**	CF282	58.08	0.33	18.21	2.78	0.21	0.33	1.72	5.92	7.37	0.02	0.75	95.70
10/04/2021	**AQ-13**	CF282	57.81	0.41	17.90	2.87	0.19	0.30	1.56	6.07	7.33	0.02	0.77	95.24
10/04/2021	**AQ-13**	CF282	57.51	0.40	17.92	2.76	0.22	0.30	1.64	6.02	7.21	0.03	0.73	94.73
10/04/2021	**AQ-13**	CF282	58.30	0.46	18.12	2.79	0.22	0.32	1.64	5.99	7.17	0.03	0.85	95.87
10/04/2021	**AQ-13**	CF282	58.10	0.43	18.03	2.73	0.23	0.36	1.63	6.24	6.98	0.03	0.73	95.48
10/04/2021	**AQ-13**	CF282	57.27	0.42	17.84	2.63	0.22	0.30	1.62	6.11	6.81	0.03	0.86	94.08
10/04/2021	**AQ-13**	CF282	57.47	0.43	17.60	3.01	0.25	0.33	1.70	6.14	6.65	0.07	0.69	94.30
10/04/2021	**AQ-13**	CF282	59.50	0.42	18.41	2.75	0.21	0.25	1.68	6.18	7.29	0.03	0.86	97.60
10/04/2021	**AQ-13**	CF282	57.82	0.44	17.64	2.71	0.19	0.27	1.58	6.37	6.95	0.02	0.74	94.74
10/04/2021	**AQ-13**	CF282	57.87	0.38	17.80	2.77	0.18	0.32	1.59	6.06	7.12	0.04	0.69	94.81
05/08/2022	**AQ-12**	CF281	58.95	0.45	18.23	3.17	0.28	0.33	1.51	6.37	7.00	0.05	0.82	97.15
05/08/2022	**AQ-12**	CF281	58.74	0.49	18.52	2.83	0.22	0.28	1.62	5.99	7.25	0.08	0.65	96.68
05/08/2022	**AQ-12**	CF281	58.56	0.43	18.53	2.95	0.20	0.33	1.69	5.75	6.95	0.06	0.66	96.12
05/08/2022	**AQ-12**	CF281	58.98	0.45	18.24	2.97	0.23	0.34	1.59	6.15	7.06	0.05	0.69	96.74
05/08/2022	**AQ-12**	CF281	58.89	0.41	18.33	2.85	0.24	0.29	1.67	6.15	7.10	0.00	0.67	96.57
05/08/2022	**AQ-12**	CF281	60.14	0.45	18.64	2.98	0.25	0.36	1.76	5.80	7.59	0.07	0.60	98.63
05/08/2022	**AQ-12**	CF281	58.87	0.40	18.28	2.88	0.19	0.38	1.75	5.75	7.23	0.04	0.65	96.41
05/08/2022	**AQ-12**	CF281	58.93	0.44	18.36	2.85	0.22	0.33	1.66	5.81	7.15	0.07	0.68	96.48
05/08/2022	**AQ-12**	CF281	59.25	0.37	18.73	2.75	0.27	0.19	1.54	6.42	6.69	0.05	0.75	97.01
05/08/2022	**AQ-12**	CF281	59.09	0.43	18.29	2.75	0.23	0.31	1.65	6.05	7.24	0.05	0.65	96.72
05/08/2022	**AQ-12**	CF281	58.82	0.43	18.38	2.73	0.20	0.31	1.65	5.78	7.27	0.00	0.70	96.27

Date of analysis	Unit	Sample	SiO_2	TiO2	Al_2O_3	FeO_t	MnO	MgO	CaO	Na_2O	K_2O	P_2O5	Cl	Analytical Total
05/08/2022	**AQ-12**	CF281	59.01	0.37	18.23	2.92	0.19	0.33	1.54	5.94	7.30	0.01	0.68	96.50
05/08/2022	**AQ-12**	CF281	57.78	0.43	17.81	2.85	0.25	0.30	1.55	5.85	6.81	0.09	0.74	94.45
05/08/2022	**AQ-12**	CF281	61.05	0.46	18.85	3.02	0.18	0.36	1.82	5.95	7.46	0.04	0.62	99.80
05/08/2022	**AQ-12**	CF281	59.64	0.46	18.25	3.10	0.19	0.35	1.71	6.11	6.90	0.10	0.65	97.46
05/08/2022	**AQ-12**	CF281	59.65	0.42	18.45	2.85	0.23	0.27	1.61	6.06	7.20	0.05	0.64	97.45
05/08/2022	**AQ-12**	CF281	59.10	0.42	18.15	2.88	0.22	0.30	1.68	6.01	7.05	0.05	0.69	96.54
05/08/2022	**AQ-12**	CF281	61.30	0.47	18.85	2.95	0.23	0.28	1.67	6.20	7.14	0.03	0.72	99.83
05/08/2022	**AQ-12**	CF281	59.75	0.46	18.42	2.84	0.21	0.28	1.67	5.68	7.23	0.10	0.63	97.28
05/08/2022	**AQ-12**	CF281	61.13	0.43	18.56	2.97	0.23	0.29	1.64	6.01	7.47	0.04	0.72	99.48
05/08/2022	**AQ-12**	CF281	60.23	0.41	18.78	2.72	0.22	0.27	1.65	5.78	7.02	0.09	0.60	97.76
10/04/2021	**AQ-11**	CF280	59.44	0.52	17.77	2.26	0.19	0.31	1.33	6.15	6.76	0.04	0.62	95.40
10/04/2021	**AQ-11**	CF280	59.61	0.44	17.78	2.26	0.16	0.33	1.35	6.08	7.02	0.03	0.54	95.60
10/04/2021	**AQ-11**	CF280	59.27	0.46	17.92	2.27	0.15	0.29	1.39	5.66	7.12	0.04	0.48	95.03
10/04/2021	**AQ-11**	CF280	58.94	0.46	17.51	2.19	0.13	0.29	1.29	5.98	7.05	0.06	0.51	94.43
10/04/2021	**AQ-11**	CF280	59.33	0.48	17.65	2.26	0.17	0.26	1.27	6.27	6.64	0.06	0.63	95.02
10/04/2021	**AQ-11**	CF280	60.97	0.45	18.05	2.34	0.17	0.32	1.26	6.31	7.22	0.03	0.48	97.60
10/04/2021	**AQ-11**	CF280	59.20	0.41	17.69	2.19	0.16	0.30	1.39	5.78	7.04	0.08	0.51	94.77
10/04/2021	**AQ-11**	CF280	60.74	0.50	18.05	2.35	0.12	0.29	1.38	6.06	7.08	0.10	0.52	97.18
10/04/2021	**AQ-11**	CF280	59.57	0.46	17.73	2.27	0.17	0.32	1.40	5.96	6.87	0.02	0.50	95.27
10/04/2021	**AQ-11**	CF280	59.36	0.47	17.72	2.21	0.17	0.30	1.31	6.07	6.61	0.05	0.55	94.82
10/04/2021	**AQ-11**	CF280	60.06	0.49	17.98	2.15	0.16	0.27	1.34	6.41	6.47	0.03	0.57	95.92
10/04/2021	**AQ-11**	CF280	59.33	0.45	17.90	2.08	0.11	0.25	1.32	5.65	7.11	0.04	0.48	94.70
10/04/2021	**AQ-11**	CF280	59.25	0.43	17.64	2.21	0.16	0.25	1.24	6.05	6.71	0.03	0.60	94.55
10/04/2021	**AQ-11**	CF280	59.33	0.45	17.71	2.23	0.13	0.30	1.33	6.07	6.55	0.04	0.51	94.67
10/04/2021	**AQ-11**	CF280	59.20	0.52	17.42	2.20	0.14	0.33	1.36	5.76	6.97	0.01	0.50	94.41
10/04/2021	**AQ-11**	CF280	59.93	0.41	17.76	2.16	0.15	0.31	1.34	6.06	6.75	0.06	0.56	95.49
10/04/2021	**AQ-11**	CF280	59.75	0.49	17.70	2.12	0.18	0.28	1.25	6.18	6.55	0.00	0.63	95.10
10/04/2021	**AQ-11**	CF280	59.98	0.36	17.89	1.95	0.11	0.27	1.52	5.40	7.33	0.04	0.47	95.32
15/04/2021	**AQ-10**	CF279	57.20	0.44	18.34	3.04	0.31	0.17	1.64	7.31	6.27	0.04	0.90	95.66
15/04/2021	**AQ-10**	CF279	58.12	0.38	18.63	3.13	0.27	0.22	1.66	7.31	6.39	0.03	1.01	97.15

Date of analysis	Unit	Sample	SiO_2	TiO2	Al_2O_3	FeO_t	MnO	MgO	CaO	Na_2O	K_2O	P_2O5	Cl	Analytical Total
15/04/2021	**AQ-10**	CF279	57.08	0.46	18.22	3.07	0.31	0.21	1.57	7.18	6.32	0.02	0.94	95.39
15/04/2021	**AQ-10**	CF279	58.23	0.45	18.63	2.98	0.30	0.21	1.61	7.37	6.56	0.00	0.95	97.31
15/04/2021	**AQ-10**	CF279	58.08	0.42	18.46	3.08	0.32	0.28	1.58	7.33	6.49	0.02	0.96	97.02
15/04/2021	**AQ-10**	CF279	57.04	0.38	18.31	3.09	0.26	0.16	1.60	7.18	6.30	0.00	0.96	95.29
15/04/2021	**AQ-10**	CF279	58.82	0.43	18.56	3.24	0.30	0.20	1.47	7.48	6.65	0.04	0.99	98.19
15/04/2021	**AQ-10**	CF279	56.96	0.44	18.19	3.06	0.31	0.19	1.57	7.09	6.31	0.05	0.91	95.08
15/04/2021	**AQ-10**	CF279	58.83	0.41	18.61	3.12	0.25	0.24	1.62	7.49	6.50	0.01	0.96	98.05
15/04/2021	**AQ-10**	CF279	57.38	0.37	18.01	2.95	0.35	0.21	1.67	7.23	6.40	0.06	0.95	95.57
15/04/2021	**AQ-10**	CF279	57.11	0.39	18.21	2.98	0.33	0.19	1.66	7.06	6.21	0.01	0.95	95.10
15/04/2021	**AQ-10**	CF279	58.80	0.41	18.66	3.12	0.30	0.21	1.56	7.34	6.52	0.00	0.98	97.91
15/04/2021	**AQ-10**	CF279	57.86	0.42	18.46	3.05	0.25	0.19	1.64	7.15	6.33	0.00	0.91	96.28
15/04/2021	**AQ-10**	CF279	57.11	0.39	18.01	2.94	0.28	0.19	1.68	7.05	6.28	0.01	0.98	94.93
15/04/2021	**AQ-10**	CF279	56.77	0.42	17.91	2.97	0.27	0.21	1.55	6.79	6.29	0.00	0.97	94.14
02/06/2015	**AQ-9**	CF277	57.37	0.46	18.07	3.15	0.36	0.22	1.68	7.06	6.40	0.07	1.05	95.89
02/06/2015	**AQ-9**	CF277	58.30	0.44	18.59	3.15	0.34	0.24	1.67	7.03	6.56	0.05	1.08	97.45
02/06/2015	**AQ-9**	CF277	57.69	0.41	18.18	3.18	0.22	0.27	1.58	7.31	6.38	0.03	1.08	96.32
02/06/2015	**AQ-9**	CF277	56.56	0.46	17.70	3.22	0.25	0.12	1.65	7.14	6.39	0.00	1.07	94.57
02/06/2015	**AQ-9**	CF277	57.56	0.40	18.25	3.18	0.25	0.24	1.63	7.33	6.43	0.06	1.10	96.41
02/06/2015	**AQ-9**	CF277	56.74	0.39	18.05	2.95	0.36	0.26	1.50	7.02	6.29	0.06	1.07	94.68
02/06/2015	**AQ-9**	CF277	56.71	0.35	17.87	2.88	0.33	0.25	1.54	7.17	6.36	0.04	1.05	94.54
02/06/2015	**AQ-9**	CF277	58.75	0.44	18.88	3.54	0.32	0.26	1.53	7.15	6.57	0.02	0.84	98.28
03/02/2023	**AQ-9**	CF278A	57.71	0.41	18.41	3.11	0.26	0.24	1.61	7.12	6.57	0.05	1.10	96.59
02/06/2015	**AQ-9**	CF278A	59.17	0.41	18.97	3.29	0.35	0.24	1.60	7.20	6.51	0.00	1.17	98.90
02/06/2015	**AQ-9**	CF278A	58.30	0.42	18.76	3.20	0.32	0.27	1.73	7.42	6.58	0.00	1.08	98.07
02/06/2015	**AQ-9**	CF278A	57.27	0.41	17.99	3.02	0.26	0.21	1.63	6.79	6.30	0.05	1.04	94.97
02/06/2015	**AQ-9**	CF278A	57.17	0.42	17.92	3.04	0.25	0.24	1.69	6.39	6.19	0.05	1.04	94.40
02/06/2015	**AQ-9**	CF278A	58.78	0.40	18.93	3.18	0.22	0.28	1.60	7.25	6.51	0.00	1.14	98.28
02/06/2015	**AQ-9**	CF278A	58.74	0.40	18.78	3.35	0.18	0.22	1.51	7.16	6.41	0.08	1.17	97.99
02/06/2015	**AQ-9**	CF278A	59.05	0.43	18.86	3.11	0.34	0.27	1.61	7.48	6.64	0.03	1.02	98.83
02/06/2015	**AQ-9**	CF278A	58.00	0.44	18.45	3.02	0.28	0.28	1.68	6.94	6.48	0.00	1.11	96.70

Date of analysis	Unit	Sample	SiO_2	TiO2	Al_2O_3	FeO_t	MnO	MgO	CaO	Na_2O	K_2O	P_2O5	Cl	Analytical Total
02/06/2015	**AQ-9**	CF278A	57.60	0.42	18.29	3.38	0.29	0.31	1.53	6.84	6.33	0.00	1.11	96.09
02/06/2015	**AQ-9**	CF278A	59.12	0.40	19.12	3.31	0.29	0.24	1.59	7.45	6.77	0.03	1.06	99.37
02/06/2015	**AQ-9**	CF278A	57.98	0.42	18.53	3.22	0.27	0.20	1.64	7.31	6.42	0.02	0.99	97.01
02/06/2015	**AQ-9**	CF278A	57.06	0.33	18.09	2.76	0.31	0.24	1.62	6.49	6.43	0.10	1.09	94.53
03/02/2023	**AQ-9**	CF278A	59.08	0.43	19.09	3.05	0.28	0.23	1.61	7.74	6.54	0.00	0.75	98.81
03/02/2023	**AQ-9**	CF278A	57.13	0.45	18.55	3.13	0.32	0.18	1.58	7.14	6.20	0.02	0.83	95.53
03/02/2023	**AQ-9**	CF278A	59.21	0.41	19.71	3.08	0.27	0.24	1.68	7.21	6.25	0.03	0.83	98.89
03/02/2023	**AQ-9**	CF278A	57.43	0.46	18.39	3.09	0.28	0.24	1.73	7.29	6.14	0.04	0.83	95.93
03/02/2023	**AQ-9**	CF278A	57.40	0.40	18.45	3.09	0.32	0.25	1.65	7.15	6.21	0.05	0.84	95.82
03/02/2023	**AQ-9**	CF278A	59.15	0.43	18.92	3.20	0.29	0.22	1.65	7.57	6.39	0.01	0.92	98.73
03/02/2023	**AQ-9**	CF278A	58.92	0.48	18.73	3.14	0.26	0.27	1.69	7.50	6.44	0.04	0.89	98.35
03/02/2023	**AQ-9**	CF278A	58.92	0.42	18.80	3.11	0.28	0.26	1.81	7.36	6.41	0.05	0.86	98.26
03/02/2023	**AQ-9**	CF278A	57.54	0.43	18.43	3.19	0.31	0.21	1.54	7.08	6.43	0.04	0.76	95.94
03/02/2023	**AQ-9**	CF278A	58.20	0.43	18.54	3.15	0.28	0.21	1.71	7.35	6.37	0.05	0.78	97.05
03/02/2023	**AQ-9**	CF278A	58.54	0.40	18.82	3.07	0.29	0.25	1.65	7.35	6.30	0.00	0.93	97.60
03/02/2023	**AQ-9**	CF278A	58.52	0.52	18.74	3.19	0.31	0.20	1.66	7.16	6.36	0.01	0.91	97.57
03/02/2023	**AQ-9**	CF278A	58.75	0.49	18.60	3.23	0.31	0.20	1.65	7.33	6.47	0.04	0.87	97.94
03/02/2023	**AQ-9**	CF278A	59.06	0.48	18.81	3.23	0.33	0.25	1.63	7.29	6.40	0.00	0.90	98.37
03/02/2023	**AQ-9**	CF278A	59.13	0.43	18.83	3.25	0.28	0.21	1.74	7.34	6.42	0.02	0.84	98.48
03/02/2023	**AQ-9**	CF278A	57.90	0.45	18.52	3.01	0.28	0.21	1.60	7.31	6.29	0.01	0.85	96.42
03/02/2023	**AQ-9**	CF278A	58.56	0.40	18.75	3.01	0.29	0.20	1.61	7.39	6.44	0.03	0.83	97.52
03/02/2023	**AQ-9**	CF278A	59.68	0.46	19.05	3.05	0.29	0.22	1.71	7.53	6.56	0.02	0.78	99.35
03/02/2023	**AQ-9**	CF278A	59.24	0.48	18.48	3.27	0.25	0.23	1.64	7.58	6.55	0.01	0.88	98.60
03/02/2023	**AQ-9**	CF278A	59.57	0.46	18.92	3.55	0.38	0.24	1.56	7.52	6.04	0.07	0.79	99.09
02/06/2015	**AQ-9**	CF278B	58.71	0.50	19.20	3.43	0.34	0.24	1.64	7.22	6.63	0.04	1.03	98.98
02/06/2015	**AQ-9**	CF278B	58.31	0.40	18.61	2.89	0.25	0.27	1.61	6.61	6.50	0.00	0.96	96.42
02/06/2015	**AQ-9**	CF278B	58.04	0.47	18.56	3.41	0.43	0.26	1.55	7.29	6.57	0.00	1.06	97.65
02/06/2015	**AQ-9**	CF278B	59.62	0.41	19.10	3.23	0.25	0.18	1.62	6.95	6.80	0.00	1.17	99.34
02/06/2015	**AQ-9**	CF278B	57.45	0.39	18.42	2.89	0.32	0.17	1.60	6.62	6.65	0.11	1.08	95.72
02/06/2015	**AQ-9**	CF278B	59.18	0.50	18.88	3.19	0.31	0.25	1.70	7.35	6.62	0.07	1.15	99.19
02/06/2015	**AQ-9**	CF278B	56.12	0.41	18.13	3.26	0.24	0.17	1.58	6.82	6.53	0.06	0.90	94.23

Date of analysis	Unit	Sample	SiO_2	TiO2	Al_2O_3	FeO_t	MnO	MgO	CaO	Na_2O	K_2O	P_2O5	Cl	Analytical Total
02/06/2015	**AQ-9**	CF278B	58.36	0.40	18.85	2.99	0.30	0.23	1.66	7.15	6.72	0.05	1.12	97.84
02/06/2015	**AQ-9**	CF278B	58.27	0.49	18.79	3.32	0.31	0.27	1.68	7.23	6.68	0.03	1.10	98.17
02/06/2015	**AQ-9**	CF278B	57.86	0.42	18.72	3.15	0.39	0.21	1.67	6.70	6.53	0.00	1.06	96.73
02/06/2015	**AQ-9**	CF278B	58.32	0.49	18.92	3.14	0.25	0.21	1.70	6.91	6.46	0.00	1.11	97.51
02/06/2015	**AQ-9**	CF278B	59.26	0.50	19.11	3.28	0.29	0.24	1.69	7.34	6.61	0.03	1.07	99.42
04/06/2015	**AQ-9**	CF278B	56.30	0.39	18.18	3.08	0.27	0.30	1.60	6.59	6.46	0.02	1.10	94.28
04/06/2015	**AQ-9**	CF278B	58.44	0.42	18.99	3.37	0.25	0.27	1.62	7.33	6.59	0.09	1.04	98.42
03/02/2023	**AQ-9**	CF278B	59.16	0.37	19.03	2.96	0.24	0.22	1.64	7.57	6.38	0.04	0.78	98.38
03/02/2023	**AQ-9**	CF278B	59.19	0.43	18.67	3.22	0.29	0.21	1.59	7.53	6.50	0.03	0.75	98.41
03/02/2023	**AQ-9**	CF278B	56.58	0.39	18.01	3.02	0.25	0.24	1.58	6.97	6.17	0.00	0.85	94.06
03/02/2023	**AQ-9**	CF278B	58.11	0.41	18.57	3.05	0.25	0.22	1.61	7.06	6.33	0.02	0.83	96.45
03/02/2023	**AQ-9**	CF278B	58.77	0.48	18.64	3.05	0.29	0.18	1.62	7.22	6.37	0.02	0.85	97.49
03/02/2023	**AQ-9**	CF278B	57.59	0.37	18.47	2.82	0.22	0.22	1.65	7.12	6.30	0.06	0.73	95.54
03/02/2023	**AQ-9**	CF278B	59.64	0.48	19.09	3.32	0.28	0.24	1.66	6.96	6.36	0.03	0.87	98.92
03/02/2023	**AQ-9**	CF278B	59.55	0.40	18.80	3.10	0.28	0.22	1.66	7.29	6.44	0.01	0.92	98.66
03/02/2023	**AQ-9**	CF278B	57.12	0.46	17.81	2.99	0.32	0.26	1.60	7.00	6.25	0.01	0.78	94.60
03/02/2023	**AQ-9**	CF278B	57.68	0.42	18.46	2.89	0.26	0.23	1.64	6.83	6.28	0.00	0.81	95.50
02/06/2015	**AQ-8**	CF276	59.75	0.40	17.91	2.31	0.16	0.19	1.33	6.43	6.83	0.08	0.60	96.01
02/06/2015	**AQ-8**	CF276	59.33	0.47	17.87	2.24	0.10	0.38	1.39	5.86	6.67	0.05	0.54	94.91
02/06/2015	**AQ-8**	CF276	61.14	0.50	18.30	2.47	0.09	0.33	1.47	6.25	6.56	0.00	0.67	97.80
02/06/2015	**AQ-8**	CF276	60.59	0.44	18.20	2.23	0.15	0.25	1.31	6.07	6.94	0.09	0.67	96.92
02/06/2015	**AQ-8**	CF276	60.90	0.49	18.09	2.34	0.22	0.26	1.32	6.00	7.09	0.04	0.63	97.36
02/06/2015	**AQ-8**	CF276	60.67	0.52	18.27	2.19	0.13	0.30	1.42	5.82	7.01	0.00	0.64	96.96
02/06/2015	**AQ-8**	CF276	59.07	0.42	17.72	2.28	0.14	0.30	1.25	5.51	6.99	0.08	0.61	94.38
02/06/2015	**AQ-8**	CF276	60.04	0.51	17.71	2.42	0.17	0.29	1.18	6.05	6.66	0.05	0.69	95.76
02/06/2015	**AQ-8**	CF276	59.77	0.43	17.92	2.26	0.12	0.23	1.34	5.83	6.75	0.04	0.61	95.33
02/06/2015	**AQ-8**	CF276	60.71	0.44	17.97	2.18	0.20	0.23	1.30	6.22	6.86	0.06	0.63	96.79
02/06/2015	**AQ-8**	CF276	60.45	0.49	18.08	2.27	0.18	0.24	1.30	5.80	6.79	0.04	0.70	96.36
02/06/2015	**AQ-8**	CF276	59.70	0.28	17.88	2.06	0.11	0.27	1.19	5.74	6.89	0.03	0.59	94.73
02/06/2015	**AQ-8**	CF276	61.61	0.39	18.72	1.75	0.10	0.21	1.51	5.59	7.22	0.04	0.46	97.61
03/02/2023	**AQ-8**	CF276	60.63	0.45	18.29	2.21	0.17	0.27	1.31	6.22	7.11	0.02	0.56	97.23

Date of analysis	Unit	Sample	SiO_2	TiO2	Al_2O_3	FeO_t	MnO	MgO	CaO	Na_2O	K_2O	P_2O5	Cl	Analytical Total
03/02/2023	**AQ-8**	CF276	61.73	0.46	18.49	2.33	0.14	0.33	1.43	6.35	7.01	0.07	0.47	98.82
03/02/2023	**AQ-8**	CF276	60.32	0.49	17.97	2.37	0.15	0.27	1.41	5.93	7.03	0.03	0.48	96.46
03/02/2023	**AQ-8**	CF276	59.91	0.43	18.03	2.24	0.18	0.31	1.36	6.09	6.67	0.02	0.49	95.73
03/02/2023	**AQ-8**	CF276	59.99	0.53	17.97	2.18	0.17	0.26	1.29	6.16	6.71	0.07	0.51	95.82
03/02/2023	**AQ-8**	CF276	59.59	0.46	17.84	2.13	0.14	0.23	1.33	6.04	6.71	0.00	0.49	94.97
03/02/2023	**AQ-8**	CF276	60.12	0.46	17.75	2.28	0.16	0.28	1.42	5.99	6.83	0.00	0.50	95.80
03/02/2023	**AQ-8**	CF276	61.40	0.49	18.31	2.21	0.17	0.25	1.31	6.29	6.86	0.05	0.51	97.84
03/02/2023	**AQ-8**	CF276	59.37	0.44	17.88	2.04	0.16	0.28	1.30	5.97	6.58	0.05	0.53	94.59
03/02/2023	**AQ-8**	CF276	59.76	0.48	17.73	2.19	0.14	0.21	1.26	6.15	6.75	0.02	0.49	95.16
03/02/2023	**AQ-8**	CF276	59.51	0.45	17.82	2.20	0.10	0.24	1.32	5.94	6.61	0.03	0.48	94.70
03/02/2023	**AQ-8**	CF276	59.98	0.45	17.77	2.17	0.18	0.21	1.33	5.99	6.76	0.01	0.50	95.35
03/02/2023	**AQ-8**	CF276	60.05	0.50	18.07	2.09	0.15	0.26	1.29	5.73	6.75	0.05	0.49	95.42
03/02/2023	**AQ-8**	CF276	59.83	0.40	17.99	1.83	0.10	0.27	1.49	5.59	7.12	0.03	0.43	95.07
03/02/2023	**AQ-8**	CF276	59.70	0.47	17.78	2.12	0.14	0.21	1.29	6.04	6.55	0.03	0.51	94.83
03/02/2023	**AQ-8**	CF276	59.75	0.44	17.86	2.09	0.10	0.23	1.39	5.95	6.58	0.00	0.46	94.87
03/02/2023	**AQ-8**	CF276	61.05	0.45	17.99	2.23	0.12	0.26	1.38	5.76	7.09	0.00	0.46	96.79
04/06/2015	**AQ-7**	CF275	57.82	0.41	18.36	3.09	0.32	0.20	1.53	6.72	7.09	0.03	1.05	96.62
04/06/2015	**AQ-7**	CF275	58.13	0.41	18.40	3.06	0.33	0.24	1.67	6.87	6.83	0.02	1.05	97.02
04/06/2015	**AQ-7**	CF275	56.55	0.37	17.80	3.04	0.26	0.31	1.68	6.67	6.60	0.05	1.04	94.36
04/06/2015	**AQ-7**	CF275	58.20	0.45	18.46	3.15	0.26	0.31	1.56	6.85	6.67	0.06	1.09	97.03
04/06/2015	**AQ-7**	CF275	59.27	0.45	18.49	3.13	0.23	0.33	1.53	7.25	7.06	0.00	1.04	98.79
04/06/2015	**AQ-7**	CF275	57.77	0.45	18.10	3.23	0.32	0.19	1.54	6.76	6.79	0.05	1.09	96.27
04/06/2015	**AQ-7**	CF275	57.85	0.40	18.18	3.14	0.31	0.25	1.66	6.71	6.73	0.00	1.10	96.34
04/06/2015	**AQ-7**	CF275	57.75	0.38	18.13	3.11	0.30	0.28	1.36	6.98	6.83	0.04	1.00	96.15
04/06/2015	**AQ-7**	CF275	57.25	0.44	17.84	2.89	0.27	0.28	1.54	6.79	6.81	0.10	1.04	95.25
04/06/2015	**AQ-7**	CF275	58.02	0.46	18.20	3.01	0.19	0.28	1.62	6.93	6.65	0.03	1.01	96.40
04/06/2015	**AQ-7**	CF275	58.31	0.39	18.12	3.17	0.21	0.24	1.69	6.73	6.76	0.04	1.03	96.71
04/06/2015	**AQ-7**	CF275	57.23	0.41	17.89	3.16	0.32	0.26	1.77	6.26	6.36	0.00	0.87	94.51
03/02/2023	**AQ-7**	CF275	57.13	0.42	18.13	3.05	0.26	0.25	1.64	6.98	6.64	0.02	0.98	95.50
03/02/2023	**AQ-7**	CF275	58.38	0.45	18.72	3.20	0.27	0.29	1.70	6.83	6.54	0.00	0.89	97.27
03/02/2023	**AQ-7**	CF275	58.96	0.44	18.42	3.32	0.25	0.30	1.54	7.11	6.90	0.04	0.92	98.20

Date of analysis	Unit	Sample	SiO_2	TiO2	Al_2O_3	FeO_t	MnO	MgO	CaO	Na_2O	K_2O	P_2O5	Cl	Analytical Total
03/02/2023	**AQ-7**	CF275	58.86	0.45	18.56	3.15	0.25	0.26	1.69	7.16	6.56	0.02	0.88	97.85
03/02/2023	**AQ-7**	CF275	59.24	0.45	18.93	3.10	0.27	0.27	1.60	6.61	6.81	0.00	0.80	98.09
03/02/2023	**AQ-7**	CF275	59.68	0.43	18.89	3.06	0.26	0.22	1.63	7.26	6.47	0.06	0.84	98.81
03/02/2023	**AQ-7**	CF275	57.52	0.39	18.10	3.02	0.21	0.25	1.67	6.67	6.57	0.01	0.81	95.22
03/02/2023	**AQ-7**	CF275	59.66	0.46	18.96	3.23	0.26	0.26	1.57	6.58	6.93	0.01	0.80	98.71
03/02/2023	**AQ-7**	CF275	57.97	0.44	18.35	2.95	0.29	0.19	1.59	6.67	6.57	0.00	0.81	95.84
04/06/2015	**AQ-6**	CF274	58.47	0.43	18.63	3.17	0.24	0.28	1.69	6.86	6.93	0.08	1.04	97.82
04/06/2015	**AQ-6**	CF274	56.77	0.43	17.80	3.05	0.20	0.27	1.61	6.63	6.85	0.07	1.04	94.69
04/06/2015	**AQ-6**	CF274	57.78	0.49	18.30	3.11	0.19	0.27	1.58	6.74	6.83	0.05	1.01	96.35
04/06/2015	**AQ-6**	CF274	58.53	0.40	18.51	3.27	0.30	0.27	1.61	6.66	6.92	0.05	1.07	97.60
04/06/2015	**AQ-6**	CF274	58.37	0.46	18.40	3.09	0.19	0.26	1.74	6.73	6.92	0.06	1.02	97.25
04/06/2015	**AQ-6**	CF274	58.92	0.40	18.54	2.98	0.28	0.21	1.81	6.91	7.09	0.00	0.99	98.12
04/06/2015	**AQ-6**	CF274	57.19	0.44	17.96	3.09	0.24	0.24	1.66	6.53	6.84	0.00	1.01	95.20
04/06/2015	**AQ-6**	CF274	57.92	0.45	18.02	3.12	0.24	0.30	1.65	6.69	6.84	0.03	1.05	96.33
04/06/2015	**AQ-6**	CF274	57.33	0.38	17.91	3.04	0.23	0.28	1.59	6.69	6.74	0.00	1.01	95.18
04/06/2015	**AQ-6**	CF274	58.07	0.40	18.19	3.04	0.23	0.37	1.63	6.40	7.01	0.05	1.01	96.38
04/06/2015	**AQ-6**	CF274	57.98	0.43	18.10	3.09	0.20	0.29	1.59	6.39	7.03	0.07	1.00	96.15
04/06/2015	**AQ-6**	CF274	57.96	0.44	17.96	3.00	0.27	0.29	1.67	6.45	6.71	0.07	1.05	95.88
03/02/2023	**AQ-6**	CF274	59.11	0.43	18.91	2.97	0.28	0.32	1.72	7.05	6.74	0.05	0.88	98.46
03/02/2023	**AQ-6**	CF274	58.48	0.47	18.37	3.17	0.25	0.31	1.62	6.83	6.77	0.00	1.04	97.32
03/02/2023	**AQ-6**	CF274	58.86	0.42	18.69	3.05	0.29	0.28	1.75	6.91	6.67	0.02	0.80	97.75
03/02/2023	**AQ-6**	CF274	57.53	0.43	18.33	2.98	0.24	0.30	1.63	6.50	6.59	0.00	0.84	95.36
03/02/2023	**AQ-6**	CF274	57.95	0.42	18.24	3.02	0.26	0.30	1.68	6.65	6.69	0.04	0.82	96.06
03/02/2023	**AQ-6**	CF274	57.85	0.43	18.43	3.03	0.20	0.31	1.63	6.39	6.73	0.06	0.80	95.86
03/02/2023	**AQ-6**	CF274	59.45	0.44	18.72	3.12	0.28	0.25	1.66	6.97	6.68	0.06	0.82	98.45
03/02/2023	**AQ-6**	CF274	59.56	0.47	18.85	3.03	0.26	0.30	1.70	6.82	6.79	0.03	0.78	98.57
03/02/2023	**AQ-6**	CF274	58.98	0.48	18.50	3.11	0.25	0.24	1.65	6.61	6.86	0.02	0.78	97.48
03/02/2023	**AQ-6**	CF274	59.61	0.48	18.92	2.95	0.21	0.27	1.76	6.74	6.76	0.00	0.82	98.51
03/02/2023	**AQ-6**	CF274	59.90	0.45	18.93	3.08	0.25	0.32	1.68	6.78	6.70	0.05	0.83	98.94
03/02/2023	**AQ-6**	CF274	57.11	0.40	18.10	2.88	0.24	0.25	1.57	6.42	6.50	0.08	0.77	94.31
03/02/2023	**AQ-6**	CF274	58.88	0.44	18.48	3.08	0.21	0.25	1.67	6.63	6.65	0.00	0.81	97.10

Date of analysis	Unit	Sample	SiO_2	TiO2	Al_2O_3	FeO_t	MnO	MgO	CaO	Na_2O	K_2O	P_2O5	Cl	Analytical Total		
03/02/2023	**AQ-6**	CF274	59.52	0.44	18.87	3.09	0.26	0.32	1.63	6.41	6.83	0.02	0.79	98.16		
03/02/2023	**AQ-6**	CF274	58.80	0.47	18.42	3.02	0.22	0.28	1.67	6.48	6.74	0.07	0.78	96.93		
03/02/2023	**AQ-6**	CF274	58.93	0.46	18.53	2.94	0.22	0.28	1.67	6.45	6.77	0.01	0.77	97.03		
03/02/2023	**AQ-6**	CF274	58.23	0.48	18.13	2.96	0.24	0.28	1.63	6.23	6.80	0.05	0.81	95.84		
03/02/2023	**AQ-6**	CF274	58.34	0.36	18.14	2.95	0.21	0.28	1.67	6.51	6.66	0.07	0.80	95.98		
03/02/2023	**AQ-6**	CF274	57.38	0.40	18.21	2.89	0.26	0.28	1.69	6.08	6.35	0.02	0.74	94.29		
04/06/2015	**AQ-5**	CF272	59.34	0.53	17.73	2.35	0.27	0.32	1.30	6.20	7.00	0.06	0.64	95.73		
04/06/2015	**AQ-5**	CF272	60.99	0.47	18.01	2.74	0.21	0.30	1.33	6.63	6.72	0.06	0.67	98.13		
04/06/2015	**AQ-5**	CF272	60.76	0.43	17.96	2.66	0.15	0.26	1.27	6.53	6.82	0.04	0.68	97.55		
04/06/2015	**AQ-5**	CF272	61.76	0.49	18.42	2.41	0.20	0.29	1.29	6.10	7.03	0.05	0.71	98.77		
04/06/2015	**AQ-5**	CF272	58.80	0.42	17.15	2.43	0.21	0.24	1.21	6.25	6.64	0.02	0.66	94.02		
04/06/2015	**AQ-5**	CF272	59.97	0.43	17.82	2.15	0.17	0.35	1.27	6.19	6.83	0.07	0.65	95.89		
04/06/2015	**AQ-5**	CF272	59.60	0.44	17.62	2.32	0.11	0.26	1.29	6.10	6.83	0.05	0.68	95.29		
04/06/2015	**AQ-5**	CF272	58.96	0.41	17.15	2.28	0.11	0.28	1.27	6.40	6.74	0.06	0.56	94.21		
04/06/2015	**AQ-5**	CF272	59.87	0.45	17.53	2.36	0.13	0.29	1.31	6.29	6.65	0.06	0.72	95.65		
04/06/2015	**AQ-5**	CF272	60.56	0.45	17.83	2.43	0.16	0.31	1.31	6.10	6.80	0.07	0.65	96.67		
04/06/2015	**AQ-5**	CF272	59.83	0.51	17.47	2.17	0.22	0.38	1.31	5.94	6.91	0.02	0.59	95.36		
04/06/2015	**AQ-5**	CF272	59.30	0.44	17.45	2.28	0.11	0.21	1.30	5.95	6.69	0.04	0.68	94.47		
04/06/2015	**AQ-5**	CF272	58.79	0.51	17.48	2.39	0.15	0.29	1.30	5.94	6.67	0.02	0.67	94.21		
04/06/2015	**AQ-5**	CF272	58.67	0.47	17.33	2.24	0.25	0.29	1.23	6.15	6.63	0.01	0.65	93.94		
03/02/2023	**AQ-5**	CF272	58.90	0.51	17.57	2.16	0.20	0.27	1.32	6.22	6.50	0.06	0.54	94.24		
03/02/2023	**AQ-5**	CF272	60.29	0.48	17.94	2.49	0.16	0.25	1.23	6.32	6.45	0.00	0.67	96.30		
03/02/2023	**AQ-5**	CF272	61.93	0.49	18.43	2.27	0.18	0.30	1.36	6.37	6.85	0.06	0.53	98.76		
03/02/2023	**AQ-5**	CF272	60.32	0.47	18.00	2.28	0.15	0.31	1.31	6.02	6.78	0.00	0.50	96.13		
03/02/2023	**AQ-5**	CF272	59.85	0.50	17.83	2.18	0.17	0.30	1.31	5.81	6.72	0.09	0.51	95.28		
03/02/2023	**AQ-5**	CF272	62.68	0.47	18.46	2.35	0.14	0.30	1.39	6.30	6.78	0.03	0.54	99.43		
03/02/2023	**AQ-5**	CF272	60.79	0.47	18.00	2.28	0.16	0.27	1.31	5.80	6.75	0.02	0.54	96.41		
03/02/2023	**AQ-5**	CF272	59.32	0.44	17.48	2.25	0.14	0.25	1.23	5.97	6.51	0.01	0.49	94.09		
03/02/2023	**AQ-5**	CF272	60.61	0.43	17.89	2.25	0.16	0.25	1.38	5.24	7.11	0.02	0.51	95.86		
04/06/2015	**AQ-4**	CF192	56.58	0.38	17.66	2.97	0.15	0.25	1.82	6.46	7.08	0.05	0.80	94.21		

Date of analysis	Unit	Sample	SiO_2	TiO2	Al_2O_3	FeO_t	MnO	MgO	CaO	Na_2O	K_2O	P_2O5	Cl	Analytical Total
04/06/2015	**AQ-4**	CF192	56.65	0.47	17.92	2.98	0.21	0.33	1.74	6.63	6.95	0.06	0.97	94.92
04/06/2015	**AQ-4**	CF192	56.45	0.44	17.66	2.89	0.33	0.32	1.94	6.44	6.93	0.02	0.88	94.31
04/06/2015	**AQ-4**	CF192	57.04	0.40	17.82	2.89	0.14	0.33	1.70	6.50	7.13	0.06	0.89	94.90
04/06/2015	**AQ-4**	CF270	59.38	0.44	18.80	2.96	0.30	0.30	1.80	6.70	7.36	0.08	1.11	99.21
04/06/2015	**AQ-4**	CF270	59.56	0.44	18.88	3.23	0.27	0.24	1.82	6.64	7.33	0.05	1.07	99.53
04/06/2015	**AQ-4**	CF270	58.03	0.45	18.43	3.08	0.29	0.37	1.80	6.48	7.26	0.04	1.06	97.29
04/06/2015	**AQ-4**	CF270	57.14	0.45	18.15	3.23	0.32	0.31	1.71	6.14	6.97	0.05	1.00	95.46
04/06/2015	**AQ-4**	CF270	58.35	0.44	18.32	3.11	0.26	0.29	1.71	6.29	7.23	0.01	1.00	97.00
04/06/2015	**AQ-4**	CF270	58.68	0.42	18.56	3.13	0.24	0.30	1.71	6.51	7.16	0.00	1.08	97.81
04/06/2015	**AQ-4**	CF270	58.42	0.44	18.50	3.20	0.32	0.38	1.80	6.41	7.24	0.06	0.97	97.74
04/06/2015	**AQ-4**	CF270	59.46	0.43	18.65	3.14	0.22	0.27	1.73	6.43	7.25	0.00	1.08	98.68
04/06/2015	**AQ-4**	CF270	58.27	0.49	18.41	3.19	0.24	0.29	1.72	6.31	7.04	0.03	1.01	97.00
04/06/2015	**AQ-4**	CF270	58.67	0.45	18.69	3.27	0.19	0.27	1.71	6.17	7.08	0.06	1.02	97.58
04/06/2015	**AQ-4**	CF270	57.24	0.39	17.98	3.06	0.24	0.27	1.71	5.93	6.90	0.09	1.10	94.89
04/06/2015	**AQ-4**	CF270	58.01	0.38	18.33	3.00	0.20	0.33	1.67	5.88	7.24	0.04	1.04	96.12
04/06/2015	**AQ-4**	CF270	59.16	0.44	19.09	3.14	0.31	0.29	1.76	6.62	7.22	0.08	1.11	99.22
14/11/2013	**AQ-4**	CF270	57.19	0.46	18.30	2.98	0.34	0.28	1.78	6.08	7.19	0.03	1.05	95.68
14/11/2013	**AQ-4**	CF270	57.80	0.42	18.23	3.23	0.25	0.40	1.76	6.06	7.19	0.03	1.06	96.43
03/02/2023	**AQ-4**	CF270	57.43	0.50	18.20	3.13	0.25	0.34	1.68	6.34	6.86	0.11	0.81	95.65
03/02/2023	**AQ-4**	CF270	58.19	0.49	18.55	3.11	0.18	0.30	1.71	6.51	6.99	0.05	0.80	96.88
03/02/2023	**AQ-4**	CF270	58.21	0.44	18.51	2.98	0.23	0.31	1.69	6.69	6.88	0.07	0.83	96.86
03/02/2023	**AQ-4**	CF270	57.05	0.49	18.35	2.94	0.21	0.28	1.68	6.10	6.81	0.08	0.82	94.81
03/02/2023	**AQ-4**	CF270	58.23	0.44	18.48	3.01	0.22	0.28	1.75	6.55	6.89	0.05	0.76	96.67
03/02/2023	**AQ-4**	CF270	57.77	0.38	18.22	3.13	0.24	0.26	1.59	6.67	6.84	0.01	0.77	95.88
03/02/2023	**AQ-4**	CF270	57.27	0.41	18.22	2.84	0.23	0.29	1.67	6.58	6.66	0.04	0.84	95.02
03/02/2023	**AQ-4**	CF270	57.89	0.45	18.28	2.98	0.23	0.19	1.71	6.50	6.96	0.06	0.78	96.02
03/02/2023	**AQ-4**	CF270	57.70	0.50	18.34	2.96	0.24	0.26	1.76	6.20	6.84	0.05	0.79	95.63
03/02/2023	**AQ-4**	CF270	57.40	0.41	18.19	2.99	0.19	0.29	1.72	6.27	6.81	0.04	0.83	95.12
03/02/2023	**AQ-4**	CF270	57.98	0.40	18.39	3.02	0.27	0.27	1.71	6.34	6.71	0.06	0.86	96.02
14/11/2013	**AQ-4**	CF271	57.98	0.49	18.38	3.04	0.20	0.32	1.70	6.61	6.93	0.01	1.00	96.66
14/11/2013	**AQ-4**	CF271	59.18	0.41	18.80	3.13	0.25	0.26	1.71	6.94	7.15	0.05	1.07	98.95

Date of analysis	Unit	Sample	SiO_2	TiO2	Al_2O_3	FeO_t	MnO	MgO	CaO	Na_2O	K_2O	P_2O5	Cl	Analytical Total
14/11/2013	**AQ-4**	CF271	58.61	0.50	18.13	3.11	0.18	0.28	1.84	6.38	7.11	0.00	0.95	97.09
14/11/2013	**AQ-4**	CF271	58.43	0.45	18.32	2.94	0.19	0.31	1.72	6.56	7.02	0.05	1.09	97.07
14/11/2013	**AQ-4**	CF271	57.88	0.38	18.24	3.02	0.28	0.31	1.64	6.29	7.12	0.00	1.04	96.20
14/11/2013	**AQ-4**	CF271	58.93	0.35	18.59	3.34	0.28	0.29	1.87	6.78	7.23	0.06	1.04	98.72
14/11/2013	**AQ-4**	CF271	58.00	0.43	18.27	3.31	0.16	0.29	1.78	6.45	6.89	0.05	1.02	96.65
02/06/2015	**AQ-4**	CF271	58.10	0.44	18.41	3.17	0.19	0.34	1.66	6.42	6.82	0.04	1.11	96.71
02/06/2015	**AQ-4**	CF271	59.54	0.41	18.90	3.43	0.34	0.32	1.69	6.67	7.04	0.07	1.08	99.49
02/06/2015	**AQ-4**	CF271	58.86	0.39	18.24	2.87	0.29	0.31	1.77	6.69	7.21	0.09	0.93	97.63
02/06/2015	**AQ-4**	CF271	58.87	0.40	18.51	3.25	0.26	0.33	1.67	6.72	7.09	0.07	1.09	98.27
02/06/2015	**AQ-4**	CF271	59.07	0.41	18.71	3.12	0.26	0.29	1.76	6.70	7.11	0.00	1.09	98.53
02/06/2015	**AQ-4**	CF271	59.70	0.45	18.88	3.38	0.25	0.30	1.73	6.91	7.27	0.08	1.08	100.03
02/06/2015	**AQ-4**	CF271	57.37	0.40	18.33	3.21	0.29	0.29	1.65	6.50	7.03	0.06	1.05	96.18
02/06/2015	**AQ-4**	CF271	58.33	0.46	18.38	3.18	0.31	0.29	1.75	6.62	7.07	0.00	1.07	97.48
02/06/2015	**AQ-4**	CF271	56.53	0.33	17.75	3.06	0.20	0.34	1.67	6.45	6.74	0.07	1.04	94.17
02/06/2015	**AQ-4**	CF271	58.64	0.46	18.72	3.05	0.25	0.32	1.64	6.85	7.22	0.01	1.01	98.19
02/06/2015	**AQ-4**	CF271	57.04	0.45	18.06	3.17	0.23	0.31	1.79	6.27	7.01	0.02	0.99	95.34
02/06/2015	**AQ-4**	CF271	59.30	0.38	18.80	3.18	0.35	0.31	1.66	6.43	7.21	0.06	1.06	98.71
02/06/2015	**AQ-4**	CF271	59.74	0.42	18.94	3.05	0.28	0.29	1.69	6.44	7.09	0.04	0.97	98.94
02/06/2015	**AQ-4**	CF271	58.03	0.38	18.19	3.08	0.28	0.30	1.73	6.35	7.20	0.04	1.02	96.60
02/06/2015	**AQ-4**	CF271	58.31	0.37	18.50	3.01	0.21	0.38	1.80	6.43	7.12	0.07	1.10	97.29
03/02/2023	**AQ-4**	CF271	58.76	0.45	18.93	3.06	0.23	0.27	1.73	6.75	7.01	0.05	0.82	98.07
03/02/2023	**AQ-4**	CF271	59.76	0.47	19.02	3.21	0.23	0.36	1.74	6.98	6.94	0.07	0.85	99.64
03/02/2023	**AQ-4**	CF271	58.51	0.50	18.76	3.06	0.23	0.33	1.75	6.49	7.06	0.01	0.84	97.53
03/02/2023	**AQ-4**	CF271	58.86	0.45	18.70	3.18	0.25	0.33	1.77	6.69	6.99	0.06	0.77	98.06
03/02/2023	**AQ-4**	CF271	58.68	0.50	18.61	3.09	0.21	0.23	1.73	6.70	7.10	0.07	0.80	97.72
03/02/2023	**AQ-4**	CF271	58.36	0.48	18.65	3.15	0.25	0.30	1.73	6.61	6.82	0.04	0.81	97.19
03/02/2023	**AQ-4**	CF271	59.42	0.46	18.91	3.13	0.25	0.27	1.79	6.69	7.09	0.08	0.86	98.93
03/02/2023	**AQ-4**	CF271	59.08	0.43	18.81	3.07	0.25	0.27	1.75	6.77	7.05	0.04	0.83	98.33
03/02/2023	**AQ-4**	CF271	58.25	0.43	18.49	3.19	0.25	0.27	1.76	6.52	6.92	0.03	0.81	96.92
03/02/2023	**AQ-4**	CF271	58.43	0.42	18.47	3.06	0.21	0.30	1.82	6.46	7.01	0.04	0.86	97.08
03/02/2023	**AQ-4**	CF271	59.41	0.41	19.04	3.05	0.24	0.29	1.75	6.66	6.98	0.03	0.85	98.70
03/02/2023	**AQ-4**	CF271	58.56	0.49	18.41	3.04	0.25	0.31	1.79	6.84	6.72	0.00	0.83	97.23

Date of analysis	Unit	Sample	SiO_2	TiO2	Al_2O_3	FeO_t	MnO	MgO	CaO	Na_2O	K_2O	P_2O5	Cl	Analytical Total
03/02/2023	**AQ-4**	CF271	58.48	0.46	18.53	3.03	0.28	0.27	1.73	6.63	6.78	0.02	0.87	97.10
03/02/2023	**AQ-4**	CF271	59.70	0.43	18.98	3.17	0.23	0.30	1.77	6.29	7.30	0.05	0.85	99.08
03/02/2023	**AQ-4**	CF271	59.54	0.49	18.74	2.99	0.25	0.29	1.72	6.85	7.06	0.02	0.86	98.81
03/02/2023	**AQ-4**	CF271	59.87	0.48	18.94	3.03	0.25	0.37	1.76	6.79	6.94	0.00	0.82	99.24
03/02/2023	**AQ-4**	CF271	59.18	0.45	18.55	3.19	0.26	0.28	1.71	6.55	6.87	0.05	0.87	97.98
03/02/2023	**AQ-4**	CF271	59.73	0.46	18.91	3.17	0.26	0.26	1.76	6.31	6.93	0.06	0.88	98.73
03/02/2023	**AQ-4**	CF271	59.59	0.42	18.81	2.97	0.28	0.24	1.80	6.57	6.96	0.05	0.80	98.48
04/06/2015	**AQ-3**	CF269	57.80	0.43	18.82	3.10	0.20	0.35	1.99	5.80	7.97	0.03	0.98	97.49
04/06/2015	**AQ-3**	CF269	56.01	0.41	17.84	3.06	0.19	0.35	1.80	5.67	7.88	0.04	0.95	94.19
04/06/2015	**AQ-3**	CF269	57.11	0.35	18.39	3.04	0.25	0.37	1.90	5.73	7.95	0.05	0.90	96.04
04/06/2015	**AQ-3**	CF269	57.58	0.45	18.43	3.16	0.24	0.40	1.90	5.72	8.04	0.02	0.88	96.80
04/06/2015	**AQ-3**	CF269	59.38	0.43	19.12	3.24	0.24	0.41	1.93	5.86	8.09	0.06	0.96	99.72
04/06/2015	**AQ-3**	CF269	57.13	0.39	18.27	3.14	0.18	0.30	2.09	5.70	7.64	0.09	0.89	95.80
04/06/2015	**AQ-3**	CF269	58.24	0.38	18.57	2.94	0.28	0.37	1.90	5.78	8.13	0.05	0.95	97.58
04/06/2015	**AQ-3**	CF269	56.82	0.43	18.23	2.80	0.21	0.32	1.93	5.61	7.86	0.07	0.91	95.21
04/06/2015	**AQ-3**	CF269	59.32	0.37	18.94	3.07	0.31	0.42	2.01	5.79	8.06	0.07	0.95	99.32
04/06/2015	**AQ-3**	CF269	57.28	0.37	18.40	2.91	0.22	0.45	1.92	5.53	7.80	0.05	0.97	95.89
04/06/2015	**AQ-3**	CF269	57.37	0.38	18.51	2.89	0.19	0.36	1.95	5.49	7.92	0.02	0.93	96.00
04/06/2015	**AQ-3**	CF269	57.36	0.40	18.43	3.21	0.16	0.30	1.92	5.36	7.84	0.06	0.94	95.99
04/06/2015	**AQ-3**	CF269	57.03	0.39	18.17	3.15	0.19	0.37	1.91	5.43	7.69	0.05	0.96	95.35
04/06/2015	**AQ-3**	CF269	57.41	0.38	18.14	3.09	0.33	0.36	1.91	5.47	7.91	0.10	0.87	95.97
04/06/2015	**AQ-3**	CF269	58.50	0.36	18.59	3.07	0.21	0.40	1.88	5.52	8.18	0.09	0.93	97.75
04/06/2015	**AQ-3**	CF269	58.86	0.42	18.83	2.98	0.21	0.30	1.92	5.44	8.39	0.06	0.90	98.31
04/06/2015	**AQ-3**	CF269	59.10	0.38	18.81	2.96	0.12	0.39	1.94	5.99	8.00	0.05	0.91	98.67
04/06/2015	**AQ-3**	CF269	59.17	0.35	19.03	3.22	0.23	0.30	1.90	5.38	8.25	0.03	0.95	98.78
04/06/2015	**AQ-3**	CF269	58.68	0.45	18.52	2.97	0.20	0.29	1.99	5.66	8.03	0.05	0.92	97.76
04/06/2015	**AQ-3**	CF269	57.50	0.30	18.28	2.74	0.28	0.38	2.01	5.46	7.87	0.07	0.87	95.76
03/02/2023	**AQ-3**	CF269	58.54	0.48	19.24	3.31	0.22	0.39	1.99	6.27	7.78	0.02	0.81	99.03
03/02/2023	**AQ-3**	CF269	58.04	0.43	18.89	3.11	0.21	0.35	2.00	5.82	8.01	0.03	0.99	97.89
03/02/2023	**AQ-3**	CF269	58.66	0.51	18.92	3.53	0.24	0.39	2.01	5.89	7.71	0.06	0.78	98.72
03/02/2023	**AQ-3**	CF269	59.02	0.42	19.37	3.14	0.20	0.41	2.06	5.83	7.92	0.01	0.74	99.13

Date of analysis	Unit	Sample	SiO_2	TiO2	Al_2O_3	FeO_t	MnO	MgO	CaO	Na_2O	K_2O	P_2O5	Cl	Analytical Total		
03/02/2023	**AQ-3**	CF269	58.31	0.43	19.02	3.15	0.24	0.35	2.11	5.71	7.83	0.04	0.74	97.93		
03/02/2023	**AQ-3**	CF269	58.89	0.45	19.11	3.18	0.22	0.37	1.97	5.89	7.83	0.05	0.74	98.70		
03/02/2023	**AQ-3**	CF269	58.52	0.41	18.77	3.16	0.25	0.35	2.00	5.23	8.56	0.07	0.73	98.05		
03/02/2023	**AQ-3**	CF269	57.80	0.43	18.54	3.13	0.19	0.35	1.96	5.83	7.80	0.08	0.75	96.84		
03/02/2023	**AQ-3**	CF269	59.00	0.39	19.09	3.21	0.23	0.39	2.02	5.80	7.88	0.08	0.70	98.78		
03/02/2023	**AQ-3**	CF269	58.52	0.42	18.94	3.12	0.19	0.30	2.01	5.78	7.90	0.04	0.72	97.96		
03/02/2023	**AQ-3**	CF269	57.85	0.38	18.71	3.09	0.21	0.37	2.01	5.67	7.77	0.04	0.73	96.82		
03/02/2023	**AQ-3**	CF269	59.32	0.43	19.17	3.02	0.18	0.40	2.00	5.80	8.10	0.06	0.74	99.22		
03/02/2023	**AQ-3**	CF269	59.04	0.37	19.05	3.14	0.21	0.38	1.96	5.57	7.96	0.05	0.81	98.53		
03/02/2023	**AQ-3**	CF269	57.03	0.43	18.28	3.00	0.22	0.35	1.94	5.51	7.66	0.05	0.72	95.18		
03/02/2023	**AQ-3**	CF269	57.14	0.42	18.36	2.99	0.16	0.35	1.94	5.26	7.96	0.01	0.71	95.32		
03/02/2023	**AQ-3**	CF269	59.44	0.45	19.17	3.16	0.21	0.36	2.00	5.73	7.86	0.07	0.65	99.10		
03/02/2023	**AQ-3**	CF269	58.48	0.41	18.76	2.87	0.21	0.31	2.02	5.81	7.84	0.04	0.73	97.48		
03/02/2023	**AQ-3**	CF269	57.29	0.45	18.45	3.00	0.18	0.32	1.97	5.45	7.58	0.07	0.74	95.49		
03/02/2023	**AQ-3**	CF269	58.66	0.40	18.66	3.06	0.17	0.37	1.97	5.75	7.83	0.06	0.78	97.71		
03/02/2023	**AQ-3**	CF269	56.93	0.40	18.33	2.95	0.18	0.33	1.92	5.11	7.87	0.05	0.76	94.84		
03/02/2023	**AQ-3**	CF269	58.42	0.42	18.87	2.98	0.22	0.32	1.96	5.49	7.86	0.03	0.76	97.32		
03/02/2023	**AQ-3**	CF269	57.55	0.38	18.31	3.08	0.22	0.37	1.94	5.41	7.76	0.09	0.74	95.84		
03/02/2023	**AQ-3**	CF269	58.73	0.38	18.70	3.10	0.18	0.33	1.99	5.88	7.71	0.01	0.74	97.76		
03/02/2023	**AQ-3**	CF269	59.71	0.42	19.01	2.98	0.19	0.33	2.10	5.91	7.95	0.06	0.67	99.32		
03/02/2023	**AQ-3**	CF269	56.72	0.46	17.93	3.22	0.17	0.40	1.84	5.71	7.52	0.06	0.77	94.81		
03/02/2023	**AQ-2**	CF270	58.57	0.39	18.96	2.90	0.23	0.35	2.01	5.70	7.98	0.00	0.78	97.86		
04/06/2015	**AQ-2**	CF268	57.65	0.46	18.67	3.33	0.29	0.47	2.07	6.11	7.88	0.11	0.96	98.00		
04/06/2015	**AQ-2**	CF268	55.95	0.48	18.27	3.12	0.20	0.39	1.98	5.80	7.81	0.09	0.96	95.02		
04/06/2015	**AQ-2**	CF268	58.20	0.42	18.87	3.41	0.23	0.41	2.10	6.02	8.03	0.06	1.01	98.77		
04/06/2015	**AQ-2**	CF268	57.79	0.42	18.79	3.28	0.24	0.37	2.03	6.09	8.00	0.08	0.98	98.07		
04/06/2015	**AQ-2**	CF268	58.44	0.39	18.96	3.32	0.28	0.37	2.11	6.04	8.13	0.08	0.98	99.09		
04/06/2015	**AQ-2**	CF268	58.19	0.45	19.13	3.35	0.24	0.38	2.00	5.88	8.06	0.01	0.97	98.66		
04/06/2015	**AQ-2**	CF268	56.32	0.40	18.36	3.08	0.19	0.34	1.95	5.86	7.89	0.07	1.00	95.46		
04/06/2015	**AQ-2**	CF268	56.50	0.34	18.47	3.29	0.13	0.40	2.01	5.88	7.62	0.11	1.00	95.76		
04/06/2015	**AQ-2**	CF268	57.79	0.36	18.68	3.18	0.14	0.38	2.05	6.13	7.94	0.06	1.05	97.74		

Date of analysis	Unit	Sample	SiO_2	TiO2	Al_2O_3	FeO_t	MnO	MgO	CaO	Na_2O	K_2O	P_2O5	Cl	Analytical Total
04/06/2015	**AQ-2**	CF268	57.04	0.34	18.56	3.23	0.26	0.40	2.01	5.80	7.65	0.12	1.00	96.40
04/06/2015	**AQ-2**	CF268	56.70	0.36	18.47	3.10	0.25	0.35	2.02	5.79	7.68	0.07	1.03	95.82
04/06/2015	**AQ-2**	CF268	57.22	0.39	18.47	3.24	0.26	0.42	2.02	5.84	7.72	0.12	1.02	96.69
04/06/2015	**AQ-2**	CF268	56.98	0.41	18.40	3.23	0.13	0.40	2.00	5.77	7.86	0.06	0.99	96.25
04/06/2015	**AQ-2**	CF268	56.69	0.43	18.23	3.42	0.11	0.33	2.00	5.94	7.56	0.07	0.98	95.76
04/06/2015	**AQ-2**	CF268	58.66	0.48	18.85	3.22	0.28	0.33	2.13	6.05	7.87	0.05	1.04	98.95
04/06/2015	**AQ-2**	CF268	57.21	0.40	18.43	3.07	0.20	0.28	2.02	5.95	7.98	0.06	0.90	96.50
04/06/2015	**AQ-2**	CF268	57.87	0.40	18.56	3.22	0.22	0.40	2.11	5.87	7.84	0.07	1.02	97.57
04/06/2015	**AQ-2**	CF268	55.83	0.39	18.09	3.14	0.19	0.37	2.00	5.76	7.39	0.04	0.93	94.13
03/02/2023	**AQ-2**	CF268	58.30	0.43	19.18	3.28	0.18	0.40	2.08	6.04	8.02	0.06	0.78	98.74
03/02/2023	**AQ-2**	CF268	56.42	0.42	18.51	3.16	0.23	0.36	1.97	5.79	7.82	0.06	0.78	95.53
03/02/2023	**AQ-2**	CF268	56.64	0.46	18.64	3.26	0.19	0.39	1.97	5.97	7.43	0.05	0.80	95.81
03/02/2023	**AQ-2**	CF268	57.03	0.46	18.72	3.31	0.25	0.41	2.00	5.61	7.79	0.08	0.76	96.42
03/02/2023	**AQ-2**	CF268	58.70	0.43	19.29	3.46	0.23	0.37	2.10	6.15	7.72	0.04	0.73	99.24
03/02/2023	**AQ-2**	CF268	57.45	0.44	18.75	3.30	0.22	0.42	2.10	5.84	7.75	0.04	0.76	97.05
03/02/2023	**AQ-2**	CF268	56.48	0.41	18.52	3.06	0.19	0.36	2.02	5.95	7.40	0.08	0.80	95.26
03/02/2023	**AQ-2**	CF268	58.32	0.39	19.09	3.12	0.25	0.30	2.14	6.00	7.75	0.06	0.79	98.22
03/02/2023	**AQ-2**	CF268	56.64	0.41	18.36	3.16	0.22	0.35	1.95	5.95	7.44	0.08	0.81	95.36
03/02/2023	**AQ-2**	CF268	57.49	0.41	18.84	3.22	0.20	0.32	2.08	5.90	7.55	0.00	0.76	96.79
03/02/2023	**AQ-2**	CF268	58.23	0.51	18.88	3.31	0.18	0.32	2.05	5.74	7.91	0.07	0.80	98.02
03/02/2023	**AQ-2**	CF268	58.10	0.36	18.89	3.21	0.23	0.37	2.10	5.97	7.71	0.07	0.78	97.79
03/02/2023	**AQ-2**	CF268	57.25	0.41	18.73	3.16	0.18	0.36	2.10	5.76	7.58	0.03	0.78	96.34
03/02/2023	**AQ-2**	CF268	57.83	0.45	18.60	3.24	0.25	0.35	2.04	6.28	7.44	0.03	0.81	97.30
03/02/2023	**AQ-2**	CF268	56.50	0.40	18.12	3.14	0.24	0.37	2.12	5.68	7.55	0.09	0.78	94.99
03/02/2023	**AQ-2**	CF268	56.80	0.40	18.40	3.18	0.24	0.35	2.02	5.71	7.58	0.04	0.75	95.48
03/02/2023	**AQ-2**	CF268	57.59	0.45	18.72	3.10	0.21	0.34	2.01	5.96	7.64	0.06	0.72	96.79
03/02/2023	**AQ-2**	CF268	56.51	0.43	18.64	2.96	0.17	0.32	1.98	5.85	7.29	0.04	0.77	94.96
03/02/2023	**AQ-2**	CF268	58.13	0.42	18.82	3.11	0.22	0.34	2.13	5.95	7.77	0.01	0.75	97.65
03/02/2023	**AQ-2**	CF268	57.60	0.45	18.73	3.20	0.20	0.39	2.06	5.16	7.93	0.02	0.76	96.52
03/02/2023	**AQ-2**	CF268	56.59	0.42	18.72	3.17	0.22	0.34	1.98	5.81	7.52	0.04	0.76	95.58

Table A2. Major element glass analyses of the MPI-DING reference glass (StHs6/80-G, GOR132-G and ATHO-G)

Date of analysis	Label	SiO_2	TiO_2	Al_2O_3	FeO_t	MnO	MgO	CaO	Na_2O	K_2O	P_2O5	Cl	Analytical Total
14/11/2013	**ATHO_G**	75.91	0.27	12.46	3.18	0.16	0.09	1.79	3.92	2.72	0.02	0.05	100.57
14/11/2013	**ATHO_G**	75.38	0.24	12.50	2.98	0.10	0.11	1.62	4.21	2.65	0.00	0.05	99.84
14/11/2013	**ATHO_G**	75.64	0.30	12.45	3.18	0.17	0.11	1.66	4.21	2.75	0.01	0.04	100.52
14/11/2013	**ATHO_G**	75.09	0.29	12.20	3.15	0.16	0.08	1.69	4.19	2.74	0.01	0.06	99.65
14/11/2013	**ATHO_G**	74.87	0.20	12.02	3.34	0.11	0.10	1.76	4.28	2.78	0.02	0.05	99.52
14/11/2013	**ATHO_G**	76.13	0.23	12.35	3.14	0.12	0.08	1.71	4.05	2.66	0.01	0.04	100.51
02/06/2015	**ATHO_G**	74.25	0.22	12.29	3.18	0.18	0.12	1.62	4.16	2.68	0.10	0.03	98.84
02/06/2015	**ATHO_G**	75.65	0.24	12.32	3.08	0.11	0.11	1.72	4.24	2.68	0.02	0.04	100.21
02/06/2015	**ATHO_G**	74.96	0.26	12.25	3.13	0.11	0.09	1.66	4.04	2.85	0.04	0.04	99.43
02/06/2015	**ATHO_G**	74.56	0.31	12.23	3.00	0.13	0.13	1.71	4.12	2.73	0.02	0.04	98.98
02/06/2015	**ATHO_G**	75.29	0.21	12.20	3.22	0.06	0.07	1.64	4.10	2.82	0.00	0.06	99.68
02/06/2015	**ATHO_G**	75.21	0.23	12.24	3.15	0.10	0.07	1.65	4.12	2.84	0.01	0.04	99.68
02/06/2015	**ATHO_G**	75.34	0.28	12.36	3.16	0.09	0.06	1.63	3.86	2.75	0.04	0.05	99.61
02/06/2015	**ATHO_G**	75.27	0.22	12.33	3.20	0.09	0.10	1.62	4.08	2.74	0.00	0.03	99.69
04/06/2015	**ATHO_G**	75.83	0.28	12.21	3.04	0.11	0.10	1.72	3.96	2.71	0.00	0.03	99.99
04/06/2015	**ATHO_G**	75.27	0.21	12.19	3.31	0.11	0.13	1.62	4.09	2.82	0.00	0.03	99.76
04/06/2015	**ATHO_G**	75.33	0.28	12.21	3.05	0.12	0.14	1.66	4.26	2.75	0.00	0.05	99.83
04/06/2015	**ATHO_G**	75.44	0.26	12.39	3.18	0.11	0.05	1.69	4.29	2.70	0.01	0.03	100.15
04/06/2015	**ATHO_G**	75.48	0.20	12.20	3.21	0.11	0.13	1.63	4.05	2.84	0.02	0.05	99.93
04/06/2015	**ATHO_G**	75.36	0.26	12.20	3.18	0.08	0.08	1.64	4.33	2.69	0.03	0.03	99.88
04/06/2015	**ATHO_G**	75.40	0.29	12.33	3.40	0.08	0.10	1.56	4.13	2.72	0.01	0.04	100.05
04/06/2015	**ATHO_G**	75.28	0.24	12.17	3.18	0.12	0.19	1.69	4.04	2.79	0.00	0.02	99.71
04/06/2015	**ATHO_G**	75.33	0.25	12.19	3.18	0.11	0.11	1.67	4.30	2.76	0.03	0.04	99.97
04/06/2015	**ATHO_G**	75.00	0.27	12.19	3.15	0.15	0.10	1.55	4.13	2.65	0.00	0.05	99.24
10/04/2021	**ATHO_G**	74.74	0.22	12.24	3.17	0.11	0.10	1.73	4.16	2.75	0.05	0.03	99.30
10/04/2021	**ATHO_G**	74.76	0.25	12.11	3.25	0.11	0.11	1.73	4.15	2.72	0.01	0.04	99.25
10/04/2021	**ATHO_G**	74.27	0.22	12.17	3.18	0.09	0.07	1.71	4.06	2.76	0.00	0.06	98.59
10/04/2021	**ATHO_G**	74.81	0.23	12.15	3.23	0.11	0.06	1.67	4.20	2.72	0.03	0.05	99.26
10/04/2021	**ATHO_G**	74.29	0.28	12.17	3.18	0.13	0.09	1.80	4.24	2.66	0.04	0.03	98.91
10/04/2021	**ATHO_G**	74.54	0.31	12.06	3.23	0.06	0.08	1.74	4.17	2.61	0.01	0.03	98.83

Date of analysis	Label	SiO_2	TiO_2	Al_2O_3	FeO_t	MnO	MgO	CaO	Na_2O	K_2O	P_2O5	Cl	Analytical Total
10/04/2021	**ATHO_G**	74.27	0.27	12.03	3.16	0.11	0.09	1.72	4.11	2.64	0.05	0.06	98.51
10/04/2021	**ATHO_G**	74.42	0.24	12.07	3.15	0.11	0.05	1.72	3.98	2.69	0.02	0.05	98.50
10/04/2021	**ATHO_G**	74.66	0.23	12.12	3.15	0.14	0.13	1.74	4.14	2.69	0.03	0.05	99.09
10/04/2021	**ATHO_G**	74.34	0.31	12.12	3.15	0.13	0.08	1.73	4.16	2.65	0.04	0.07	98.79
10/04/2021	**ATHO_G**	74.40	0.24	12.28	3.12	0.11	0.08	1.73	4.20	2.71	0.06	0.03	98.95
15/04/2021	**ATHO_G**	74.56	0.24	12.18	3.12	0.11	0.08	1.72	4.19	2.76	0.03	0.03	99.02
15/04/2021	**ATHO_G**	74.73	0.21	12.15	3.22	0.14	0.09	1.70	4.08	2.69	0.01	0.05	99.06
15/04/2021	**ATHO_G**	74.91	0.22	12.22	3.12	0.12	0.11	1.77	4.01	2.65	0.00	0.06	99.19
15/04/2021	**ATHO_G**	74.66	0.25	11.99	3.10	0.11	0.13	1.71	4.18	2.70	0.01	0.03	98.87
05/08/2022	**ATHO_G**	75.70	0.32	12.31	3.19	0.11	0.08	1.73	4.23	2.65	0.02	0.02	100.36
05/08/2022	**ATHO_G**	76.00	0.26	12.25	3.18	0.07	0.04	1.66	4.12	2.66	0.02	0.04	100.30
05/08/2022	**ATHO_G**	75.60	0.26	12.29	3.16	0.08	0.09	1.73	4.16	2.59	0.03	0.02	100.01
05/08/2022	**ATHO_G**	75.75	0.22	12.40	3.31	0.09	0.13	1.68	4.13	2.63	0.01	0.05	100.40
05/08/2022	**ATHO_G**	75.31	0.32	12.19	3.12	0.13	0.10	1.72	4.03	2.69	0.04	0.04	99.69
05/08/2022	**ATHO_G**	75.60	0.29	12.26	3.13	0.12	0.09	1.68	4.01	2.67	0.00	0.01	99.85
05/08/2022	**ATHO_G**	74.98	0.29	12.35	3.25	0.10	0.10	1.70	4.34	2.72	0.07	0.03	99.92
05/08/2022	**ATHO_G**	75.67	0.28	12.30	3.20	0.10	0.08	1.69	4.34	2.72	0.03	0.06	100.46
05/08/2022	**ATHO_G**	75.52	0.31	12.35	3.20	0.11	0.11	1.70	4.18	2.67	0.00	0.03	100.18
05/08/2022	**ATHO_G**	76.05	0.27	12.36	3.12	0.11	0.07	1.67	4.03	2.69	0.04	0.04	100.44
05/08/2022	**ATHO_G**	75.80	0.30	12.34	3.17	0.09	0.11	1.65	4.19	2.66	0.04	0.03	100.39
05/08/2022	**ATHO_G**	76.03	0.26	12.29	3.08	0.10	0.10	1.70	4.10	2.65	0.00	0.04	100.36
05/08/2022	**ATHO_G**	75.58	0.26	12.49	3.09	0.09	0.07	1.63	4.23	2.64	0.05	0.04	100.17
05/08/2022	**ATHO_G**	75.58	0.23	12.20	3.21	0.08	0.10	1.70	4.06	2.71	0.00	0.02	99.89
05/08/2022	**ATHO_G**	75.59	0.25	12.14	3.07	0.08	0.09	1.70	4.23	2.71	0.02	0.03	99.91
05/08/2022	**ATHO_G**	75.42	0.24	12.39	3.09	0.12	0.10	1.67	4.20	2.66	0.01	0.02	99.93
05/08/2022	**ATHO_G**	76.00	0.24	12.37	3.27	0.10	0.11	1.64	4.17	2.69	0.00	0.01	100.59
05/08/2022	**ATHO_G**	75.47	0.26	12.28	3.08	0.11	0.03	1.65	4.03	2.71	0.03	0.04	99.69
05/08/2022	**ATHO_G**	75.69	0.25	12.19	3.23	0.12	0.14	1.72	4.12	2.72	0.01	0.03	100.23
05/08/2022	**ATHO_G**	75.39	0.27	12.28	3.19	0.09	0.05	1.67	4.26	2.69	0.00	0.03	99.92
05/08/2022	**ATHO_G**	76.25	0.27	12.37	3.19	0.09	0.11	1.66	4.32	2.68	0.03	0.04	101.00
05/08/2022	**ATHO_G**	76.27	0.24	12.43	3.20	0.11	0.08	1.67	4.05	2.73	0.00	0.03	100.81
05/08/2022	**ATHO_G**	75.39	0.24	12.34	3.26	0.11	0.13	1.68	4.17	2.68	0.00	0.03	100.02

Date of analysis	Label	SiO_2	TiO_2	Al_2O_3	FeO_t	MnO	MgO	CaO	Na_2O	K_2O	P_2O5	Cl	Analytical Total
05/08/2022	**ATHO_G**	75.75	0.26	12.32	3.14	0.09	0.07	1.68	4.02	2.70	0.03	0.05	100.11
05/08/2022	**ATHO_G**	76.02	0.23	12.50	3.21	0.11	0.06	1.69	4.34	2.73	0.00	0.05	100.94
03/02/2023	**ATHO_G**	75.70	0.32	12.31	3.19	0.11	0.08	1.73	4.23	2.65	0.02	0.02	100.36
03/02/2023	**ATHO_G**	76.00	0.26	12.25	3.18	0.07	0.04	1.66	4.12	2.66	0.02	0.04	100.30
03/02/2023	**ATHO_G**	75.60	0.26	12.29	3.16	0.08	0.09	1.73	4.16	2.59	0.03	0.02	100.01
03/02/2023	**ATHO_G**	75.75	0.22	12.40	3.31	0.09	0.13	1.68	4.13	2.63	0.01	0.05	100.40
03/02/2023	**ATHO_G**	75.31	0.32	12.19	3.12	0.13	0.10	1.72	4.03	2.69	0.04	0.04	99.69
03/02/2023	**ATHO_G**	75.60	0.29	12.26	3.13	0.12	0.09	1.68	4.01	2.67	0.00	0.01	99.85
02/06/2015	**GOR132-G**	45.50	0.37	10.82	10.42	0.18	22.23	8.34	0.85	0.01	0.07	0.00	98.78
02/06/2015	**GOR132-G**	45.40	0.31	10.77	10.35	0.22	22.35	8.50	0.81	0.01	0.07	0.01	98.80
02/06/2015	**GOR132-G**	46.20	0.31	10.81	10.22	0.18	21.93	8.43	0.65	0.03	0.01	0.01	98.78
02/06/2015	**GOR132-G**	45.65	0.31	11.04	10.22	0.20	22.18	8.60	0.76	0.02	0.05	0.00	99.03
02/06/2015	**GOR132-G**	46.13	0.29	10.92	10.14	0.13	22.24	8.39	0.73	0.04	0.07	0.00	99.10
02/06/2015	**GOR132-G**	45.98	0.25	10.88	10.50	0.08	22.41	8.46	0.87	0.03	0.08	0.00	99.54
02/06/2015	**GOR132-G**	45.35	0.30	10.99	10.13	0.19	22.30	8.39	0.71	0.06	0.05	0.02	98.48
02/06/2015	**GOR132-G**	45.70	0.26	10.88	10.30	0.12	22.15	8.35	0.67	0.02	0.06	0.00	98.52
02/06/2015	**GOR132-G**	45.28	0.34	11.00	9.73	0.26	22.12	8.21	0.75	0.01	0.14	0.00	97.84
02/06/2015	**GOR132-G**	45.66	0.32	11.00	9.94	0.13	21.92	8.43	0.83	0.05	0.09	0.00	98.37
04/06/2015	**GOR132-G**	45.43	0.24	11.11	10.06	0.09	22.23	8.28	0.91	0.03	0.07	0.01	98.47
04/06/2015	**GOR132-G**	45.52	0.32	11.15	10.08	0.16	22.16	8.23	0.80	0.03	0.01	0.01	98.47
04/06/2015	**GOR132-G**	45.56	0.35	10.96	10.02	0.13	22.12	8.39	0.89	0.02	0.01	0.02	98.46
04/06/2015	**GOR132-G**	45.60	0.30	10.98	10.61	0.19	22.23	8.41	0.74	0.05	0.03	0.01	99.16
04/06/2015	**GOR132-G**	45.96	0.31	11.03	10.35	0.15	22.14	8.37	0.84	0.05	0.05	0.00	99.25
04/06/2015	**GOR132-G**	45.59	0.32	11.01	9.93	0.13	22.19	8.43	0.68	0.07	0.09	0.00	98.44
04/06/2015	**GOR132-G**	45.78	0.32	11.00	10.43	0.16	22.63	8.35	0.83	0.02	0.09	0.00	99.61
04/06/2015	**GOR132-G**	45.87	0.27	11.02	10.03	0.16	22.26	8.36	0.69	0.04	0.00	0.01	98.71
04/06/2015	**GOR132-G**	45.83	0.25	11.13	10.14	0.16	22.08	8.22	0.82	0.01	0.00	0.01	98.65
04/06/2015	**GOR132-G**	45.61	0.35	10.86	9.90	0.23	22.28	8.59	0.72	0.00	0.00	0.00	98.54
05/08/2022	**GOR132-G**	45.61	0.31	10.79	10.26	0.16	22.06	8.54	0.78	0.05	0.02	0.00	98.57
05/08/2022	**GOR132-G**	45.49	0.26	10.82	10.29	0.20	22.31	8.61	0.85	0.03	0.00	0.00	98.86
05/08/2022	**GOR132-G**	45.44	0.31	10.80	10.44	0.13	22.24	8.50	0.84	0.03	0.00	0.01	98.74

Date of analysis	Label	SiO_2	TiO_2	Al_2O_3	FeO_t	MnO	MgO	CaO	Na_2O	K_2O	P_2O5	Cl	Analytical Total
05/08/2022	**GOR132-G**	45.57	0.30	10.99	10.49	0.17	22.28	8.50	0.86	0.03	0.04	0.01	99.25
05/08/2022	**GOR132-G**	45.46	0.34	10.80	10.30	0.12	22.34	8.57	0.87	0.03	0.00	0.00	98.84
05/08/2022	**GOR132-G**	45.58	0.29	10.87	10.23	0.17	22.37	8.59	0.79	0.04	0.00	0.00	98.94
05/08/2022	**GOR132-G**	45.53	0.32	10.85	10.48	0.15	22.39	8.41	0.86	0.04	0.03	0.00	99.07
05/08/2022	**GOR132-G**	45.57	0.28	10.95	10.33	0.18	22.20	8.64	0.85	0.06	0.00	0.00	99.07
05/08/2022	**GOR132-G**	45.56	0.35	10.99	10.15	0.16	22.54	8.55	0.80	0.05	0.01	0.00	99.15
05/08/2022	**GOR132-G**	45.31	0.30	10.96	10.25	0.17	22.42	8.54	0.85	0.01	0.03	0.00	98.84
05/08/2022	**GOR132-G**	45.56	0.37	11.07	10.28	0.18	22.59	8.55	0.89	0.04	0.03	0.03	99.58
05/08/2022	**GOR132-G**	45.50	0.31	11.20	10.24	0.13	22.34	8.51	0.90	0.02	0.02	0.00	99.17
05/08/2022	**GOR132-G**	45.47	0.30	10.89	10.33	0.14	22.54	8.41	0.85	0.02	0.08	0.00	99.03
05/08/2022	**GOR132-G**	45.67	0.38	10.77	10.29	0.15	22.38	8.53	0.81	0.04	0.06	0.00	99.09
05/08/2022	**GOR132-G**	45.54	0.31	10.95	10.19	0.15	21.90	8.64	0.72	0.04	0.00	0.01	98.44
05/08/2022	**GOR132-G**	45.44	0.32	10.99	10.17	0.16	21.91	8.49	0.80	0.03	0.04	0.00	98.34
05/08/2022	**GOR132-G**	45.57	0.31	10.92	10.22	0.12	22.32	8.53	0.83	0.02	0.05	0.00	98.90
05/08/2022	**GOR132-G**	45.06	0.32	10.90	10.28	0.17	22.40	8.66	0.87	0.02	0.06	0.00	98.75
05/08/2022	**GOR132-G**	45.53	0.32	10.90	10.30	0.17	22.49	8.52	0.77	0.00	0.02	0.00	99.02
05/08/2022	**GOR132-G**	45.39	0.30	10.93	10.34	0.14	22.52	8.49	0.91	0.02	0.00	0.00	99.05
05/08/2022	**GOR132-G**	45.87	0.30	11.01	10.07	0.16	22.32	8.56	0.78	0.04	0.04	0.00	99.16
05/08/2022	**GOR132-G**	45.23	0.33	11.02	10.42	0.14	22.34	8.63	0.79	0.03	0.03	0.00	98.97
05/08/2022	**GOR132-G**	45.64	0.29	10.97	10.29	0.17	22.52	8.58	0.79	0.05	0.01	0.01	99.32
05/08/2022	**GOR132-G**	45.19	0.28	11.00	10.32	0.16	22.52	8.48	0.74	0.01	0.01	0.01	98.73
05/08/2022	**GOR132-G**	45.66	0.34	10.92	10.23	0.15	22.61	8.53	0.79	0.04	0.04	0.01	99.32
05/08/2022	**GOR132-G**	45.56	0.35	10.92	10.33	0.18	22.49	8.55	0.84	0.05	0.01	0.00	99.29
05/08/2022	**GOR132-G**	45.67	0.26	11.03	10.25	0.13	22.25	8.57	0.88	0.00	0.01	0.00	99.06
03/02/2023	**GOR132-G**	45.61	0.31	10.79	10.26	0.16	22.06	8.54	0.78	0.05	0.02	0.00	98.57
03/02/2023	**GOR132-G**	45.49	0.26	10.82	10.29	0.20	22.31	8.61	0.85	0.03	0.00	0.00	98.86
03/02/2023	**GOR132-G**	45.44	0.31	10.80	10.44	0.13	22.24	8.50	0.84	0.03	0.00	0.01	98.74
03/02/2023	**GOR132-G**	45.57	0.30	10.99	10.49	0.17	22.28	8.50	0.86	0.03	0.04	0.01	99.25
03/02/2023	**GOR132-G**	45.46	0.34	10.80	10.30	0.12	22.34	8.57	0.87	0.03	0.00	0.00	98.84
03/02/2023	**GOR132-G**	45.58	0.29	10.87	10.23	0.17	22.37	8.59	0.79	0.04	0.00	0.00	98.94
14/11/2013	**StHs6/80-G**	63.60	0.66	18.00	4.18	0.19	1.90	5.30	4.38	1.35	0.07	0.02	99.64

Date of analysis	Label	SiO_2	TiO_2	Al_2O_3	FeO_t	MnO	MgO	CaO	Na_2O	K_2O	P_2O5	Cl	Analytical Total
14/11/2013	**StHs6/80-G**	63.09	0.72	17.52	4.37	0.15	2.00	5.33	4.58	1.29	0.13	0.00	99.18
14/11/2013	**StHs6/80-G**	63.32	0.71	17.53	4.35	0.15	2.04	5.12	4.40	1.31	0.08	0.01	99.01
14/11/2013	**StHs6/80-G**	62.35	0.69	17.37	4.61	0.15	1.97	5.18	4.67	1.43	0.08	0.02	98.51
14/11/2013	**StHs6/80-G**	63.45	0.68	17.65	4.31	0.13	1.93	5.23	4.48	1.35	0.13	0.02	99.35
14/11/2013	**StHs6/80-G**	63.94	0.71	17.69	4.41	0.16	1.91	5.30	4.54	1.31	0.05	0.00	100.03
02/06/2015	**StHs6/80-G**	63.10	0.72	17.60	4.26	0.12	1.88	5.17	4.55	1.30	0.16	0.03	98.89
02/06/2015	**StHs6/80-G**	63.82	0.73	17.63	4.41	0.06	1.96	5.29	4.52	1.37	0.21	0.01	100.00
02/06/2015	**StHs6/80-G**	63.15	0.71	17.73	4.51	0.09	2.02	5.24	4.49	1.34	0.14	0.00	99.42
02/06/2015	**StHs6/80-G**	62.72	0.64	17.58	4.32	0.04	1.92	5.32	4.50	1.34	0.16	0.02	98.57
02/06/2015	**StHs6/80-G**	62.94	0.69	17.67	4.40	0.04	1.96	5.36	4.37	1.26	0.15	0.01	98.84
02/06/2015	**StHs6/80-G**	63.05	0.73	17.85	4.32	0.04	1.96	5.27	4.34	1.34	0.19	0.00	99.10
02/06/2015	**StHs6/80-G**	62.91	0.72	17.72	4.65	0.11	1.97	5.27	4.39	1.33	0.22	0.02	99.31
02/06/2015	**StHs6/80-G**	63.65	0.73	17.72	4.40	0.04	1.97	5.11	4.21	1.26	0.20	0.01	99.27
02/06/2015	**StHs6/80-G**	63.62	0.76	17.60	4.25	0.13	2.06	5.21	4.59	1.31	0.22	0.01	99.76
02/06/2015	**StHs6/80-G**	63.34	0.71	17.78	4.53	0.09	2.02	5.50	4.59	1.38	0.15	0.02	100.10
04/06/2015	**StHs6/80-G**	63.49	0.64	17.67	4.33	0.08	1.89	5.24	4.68	1.32	0.18	0.01	99.52
04/06/2015	**StHs6/80-G**	63.57	0.77	17.61	4.27	0.12	1.97	5.09	4.38	1.28	0.15	0.00	99.22
04/06/2015	**StHs6/80-G**	63.47	0.72	17.63	4.34	0.09	1.89	5.22	4.68	1.29	0.12	0.02	99.46
04/06/2015	**StHs6/80-G**	63.60	0.72	17.84	4.59	0.11	2.07	5.24	4.69	1.29	0.13	0.02	100.31
04/06/2015	**StHs6/80-G**	63.29	0.70	17.83	4.26	0.07	1.87	5.30	4.32	1.30	0.15	0.00	99.08
04/06/2015	**StHs6/80-G**	63.37	0.66	17.78	4.53	0.12	1.84	5.34	4.54	1.30	0.15	0.00	99.64
04/06/2015	**StHs6/80-G**	63.23	0.64	17.67	4.46	0.07	1.89	5.19	4.34	1.37	0.22	0.02	99.11
04/06/2015	**StHs6/80-G**	63.15	0.71	17.58	4.51	0.11	1.87	5.34	4.57	1.27	0.19	0.00	99.30
04/06/2015	**StHs6/80-G**	63.89	0.75	17.86	4.54	0.11	1.94	5.17	4.74	1.32	0.16	0.00	100.46
04/06/2015	**StHs6/80-G**	63.55	0.72	17.71	4.33	0.05	1.98	5.16	4.78	1.31	0.22	0.02	99.83
10/04/2021	**StHs6/80-G**	62.74	0.71	17.81	4.22	0.10	1.88	5.21	4.59	1.29	0.12	0.04	98.70
10/04/2021	**StHs6/80-G**	62.21	0.61	17.77	4.41	0.06	1.92	5.35	4.73	1.33	0.15	0.02	98.56
10/04/2021	**StHs6/80-G**	62.98	0.74	17.87	4.19	0.05	1.87	5.20	4.58	1.28	0.12	0.03	98.90
10/04/2021	**StHs6/80-G**	62.54	0.73	17.55	4.16	0.10	1.87	5.35	4.64	1.29	0.19	0.03	98.45
10/04/2021	**StHs6/80-G**	62.70	0.69	17.64	4.30	0.12	1.91	5.30	4.59	1.26	0.20	0.03	98.74
10/04/2021	**StHs6/80-G**	63.02	0.70	17.38	4.34	0.10	1.96	5.27	4.67	1.30	0.04	0.00	98.78
10/04/2021	**StHs6/80-G**	62.96	0.69	17.23	4.26	0.06	1.89	5.30	4.71	1.29	0.00	0.01	98.41

Date of analysis	Label	SiO_2	TiO_2	Al_2O_3	FeO_t	MnO	MgO	CaO	Na_2O	K_2O	P_2O5	Cl	Analytical Total
10/04/2021	**StHs6/80-G**	62.93	0.69	17.22	4.27	0.13	1.90	5.22	4.58	1.29	0.05	0.01	98.28
10/04/2021	**StHs6/80-G**	62.92	0.69	17.12	4.11	0.06	1.86	5.21	4.63	1.32	0.07	0.02	98.00
10/04/2021	**StHs6/80-G**	63.23	0.66	17.44	4.39	0.07	1.92	5.26	4.77	1.31	0.05	0.01	99.11
10/04/2021	**StHs6/80-G**	62.97	0.70	17.37	4.28	0.09	1.94	5.25	4.71	1.31	0.02	0.00	98.64
15/04/2021	**StHs6/80-G**	62.80	0.67	17.64	4.23	0.10	1.89	5.27	4.57	1.31	0.19	0.00	98.67
15/04/2021	**StHs6/80-G**	62.89	0.77	17.71	4.36	0.09	1.95	5.37	4.36	1.29	0.14	0.02	98.95
15/04/2021	**StHs6/80-G**	62.84	0.73	17.62	4.24	0.06	1.90	5.29	4.72	1.28	0.14	0.01	98.84
15/04/2021	**StHs6/80-G**	62.60	0.76	17.67	4.31	0.07	1.95	5.34	4.66	1.30	0.14	0.02	98.82
15/04/2021	**StHs6/80-G**	63.33	0.72	17.59	4.26	0.09	1.91	5.36	4.41	1.30	0.15	0.01	99.12
05/08/2022	**StHs6/80-G**	63.76	0.76	17.64	4.51	0.03	1.93	5.28	4.62	1.24	0.13	0.01	99.91
05/08/2022	**StHs6/80-G**	63.21	0.67	17.65	4.51	0.08	1.93	5.29	4.80	1.27	0.07	0.03	99.51
05/08/2022	**StHs6/80-G**	63.41	0.79	17.96	4.45	0.07	1.91	5.30	4.74	1.26	0.11	0.00	100.00
05/08/2022	**StHs6/80-G**	63.68	0.79	17.72	4.56	0.09	1.88	5.32	4.72	1.28	0.16	0.00	100.21
05/08/2022	**StHs6/80-G**	63.32	0.72	17.78	4.28	0.06	1.93	5.24	4.54	1.27	0.16	0.01	99.32
05/08/2022	**StHs6/80-G**	63.52	0.80	17.71	4.37	0.09	1.91	5.27	4.82	1.26	0.13	0.00	99.88
05/08/2022	**StHs6/80-G**	63.79	0.71	17.64	4.41	0.02	1.92	5.31	4.59	1.29	0.11	0.00	99.79
05/08/2022	**StHs6/80-G**	63.60	0.73	17.71	4.56	0.09	1.93	5.32	4.66	1.28	0.13	0.02	100.03
05/08/2022	**StHs6/80-G**	63.68	0.72	17.91	4.45	0.10	1.93	5.25	4.64	1.25	0.15	0.04	100.11
05/08/2022	**StHs6/80-G**	63.84	0.70	17.63	4.40	0.07	1.94	5.26	4.67	1.27	0.12	0.01	99.91
05/08/2022	**StHs6/80-G**	62.69	0.77	17.50	4.27	0.06	1.86	5.20	4.67	1.33	0.13	0.01	98.50
05/08/2022	**StHs6/80-G**	63.44	0.77	17.66	4.40	0.09	2.02	5.33	4.68	1.26	0.12	0.03	99.80
05/08/2022	**StHs6/80-G**	63.89	0.76	17.83	4.43	0.07	1.91	5.31	4.55	1.32	0.21	0.01	100.29
05/08/2022	**StHs6/80-G**	63.54	0.78	17.94	4.33	0.05	1.99	5.34	4.42	1.24	0.13	0.02	99.79
05/08/2022	**StHs6/80-G**	63.78	0.73	17.47	4.37	0.08	1.88	5.25	4.69	1.27	0.13	0.01	99.65
05/08/2022	**StHs6/80-G**	63.86	0.73	17.75	4.40	0.05	1.95	5.30	4.63	1.27	0.16	0.00	100.11
05/08/2022	**StHs6/80-G**	63.20	0.76	17.94	4.46	0.10	1.94	5.25	3.61	1.33	0.10	0.00	98.70
05/08/2022	**StHs6/80-G**	63.37	0.72	17.34	4.41	0.07	1.91	5.24	4.90	1.28	0.06	0.00	99.29
05/08/2022	**StHs6/80-G**	63.89	0.76	17.64	4.51	0.06	1.93	5.21	4.71	1.31	0.10	0.01	100.13
05/08/2022	**StHs6/80-G**	63.78	0.78	17.73	4.48	0.06	1.90	5.24	4.48	1.29	0.08	0.00	99.82
05/08/2022	**StHs6/80-G**	63.99	0.76	17.47	4.45	0.06	1.92	5.29	4.64	1.31	0.05	0.00	99.95
05/08/2022	**StHs6/80-G**	64.07	0.75	17.49	4.49	0.05	1.92	5.21	4.71	1.30	0.03	0.03	100.06
05/08/2022	**StHs6/80-G**	63.68	0.72	17.44	4.32	0.07	1.90	5.24	4.65	1.26	0.06	0.00	99.35

Date of analysis	Label	SiO_2	TiO_2	Al_2O_3	FeO_t	MnO	MgO	CaO	Na_2O	K_2O	P_2O5	Cl	Analytical Total
03/02/2023	**StHs6/80-G**	63.76	0.76	17.64	4.51	0.03	1.93	5.28	4.62	1.24	0.13	0.01	99.91
03/02/2023	**StHs6/80-G**	63.21	0.67	17.65	4.51	0.08	1.93	5.29	4.80	1.27	0.07	0.03	99.51
03/02/2023	**StHs6/80-G**	63.41	0.79	17.96	4.45	0.07	1.91	5.30	4.74	1.26	0.11	0.00	100.00
03/02/2023	**StHs6/80-G**	63.68	0.79	17.72	4.56	0.09	1.88	5.32	4.72	1.28	0.16	0.00	100.21
03/02/2023	**StHs6/80-G**	63.32	0.72	17.78	4.28	0.06	1.93	5.24	4.54	1.27	0.16	0.01	99.32
03/02/2023	**StHs6/80-G**	63.52	0.80	17.71	4.37	0.09	1.91	5.27	4.82	1.26	0.13	0.00	99.88

Table A3. Trace element glass compositions of twelve Acquamorta tephra units between the MEGT and CI using LA-ICP-MS .

Date of analysis	Unit	Sample	Rb	Sr	Y	Zr	Nb	Ba	La	Ce	Pr	Nd	Sm	Eu	Gd	Dy	Er	Yb	Lu	Hf	Ta	Pb	Th	U
11/08/2021	**AQ-13**	CF282	469	39.2	66.3	744	131	72.4	148	276	29.1	100	17.8	1.28	13.7	11.7	6.64	6.64	1.04	15.6	6.20	54.9	60.4	19.4
11/08/2021	**AQ-13**	CF282	466	17.6	48.3	589	107	19.8	113	224	21.6	77.2	12.4	1.50	9.42	8.45	4.86	5.25	0.77	12.6	4.98	73.3	46.9	16.7
11/08/2021	**AQ-13**	CF282	465	18.6	54.4	665	120	11.8	127	243	24.3	84.6	14.6	1.35	10.7	9.80	5.56	5.59	0.81	14.3	5.68	64.8	51.8	18.6
11/08/2021	**AQ-13**	CF282	439	19.7	52.2	644	114	15.9	118	226	22.4	80.6	13.2	1.32	10.1	8.89	4.91	4.96	0.71	14.0	5.16	62.0	47.0	16.6
11/08/2021	**AQ-13**	CF282	570	10.0	77.2	958	174	4.78	171	336	32.4	113	18.3	1.14	13.5	12.9	7.60	6.46	1.11	19.8	7.58	76.3	67.0	23.9
11/08/2021	**AQ-13**	CF282	467	18.1	54.3	667	121	14.5	127	244	24.2	84.9	15.0	1.44	11.3	10.1	5.44	5.71	0.81	14.5	5.66	65.9	52.6	18.5
11/08/2021	**AQ-13**	CF282	472	17.9	54.4	662	122	13.0	127	244	24.4	86.2	15.0	1.33	11.1	9.26	5.44	5.50	0.75	13.8	5.62	63.5	51.2	18.6
11/08/2021	**AQ-13**	CF282	452	51.1	51.3	629	116	65.6	121	233	22.9	80.6	14.3	1.40	10.3	9.09	5.24	5.12	0.78	13.5	5.48	63.6	50.1	17.8
11/08/2021	**AQ-13**	CF282	461	19.7	52.5	643	120	13.1	123	239	23.7	83.3	14.4	1.34	11.0	9.34	5.33	5.52	0.82	13.6	5.59	64.5	51.5	18.8
11/08/2021	**AQ-13**	CF282	511	16.9	60.2	725	133	9.94	140	267	26.5	94.0	16.1	1.40	11.6	10.7	5.82	5.83	0.88	15.7	6.28	65.4	57.8	20.5
11/08/2021	**AQ-13**	CF282	472	20.1	55.2	667	121	14.7	129	245	24.7	85.8	15.5	1.44	11.5	9.59	5.54	5.40	0.81	14.2	5.74	66.1	53.4	18.5
11/08/2021	**AQ-11**	CF280	393	9.5	43.1	447	75	4.90	88.9	178	18.6	68.9	12.4	1.27	8.64	7.51	4.17	4.35	0.60	9.70	3.65	48.0	30.0	10.2
11/08/2021	**AQ-11**	CF280	339	57.3	32.1	346	54	58.0	74.7	140	15.1	51.1	8.9	1.44	7.07	6.02	3.18	2.73	0.49	8.46	2.74	49.4	26.0	6.8
11/08/2021	**AQ-11**	CF280	384	11.1	44.9	467	79	7.35	93.1	186	19.3	69.8	12.7	1.33	8.91	8.31	4.52	4.38	0.65	10.1	3.82	58.4	32.3	10.5
11/08/2021	**AQ-11**	CF280	361	24.8	40.2	414	67	14.7	85.6	166	17.7	64.7	11.8	1.46	9.33	7.39	3.95	4.03	0.62	9.44	3.39	50.3	29.5	9.0
11/08/2021	**AQ-11**	CF280	349	25.7	38.9	391	64	20.3	79.8	160	16.8	61.9	11.2	1.47	8.06	7.25	4.17	3.62	0.56	8.67	3.28	44.5	27.3	9.1
29/07/2021	**AQ-9**	CF278B	578	2.8	76.1	976	181	0.76	178	344	33.7	113	19.6	1.12	15.6	13.6	7.84	8.23	1.17	20.9	8.67	83.0	78.7	28.6
29/07/2021	**AQ-9**	CF278B	566	7.4	77.0	1001	185	5.53	179	342	34.2	115	19.8	1.20	15.6	13.5	7.59	8.22	1.16	20.0	8.55	79.8	76.5	28.1
29/07/2021	**AQ-9**	CF278B	565	3.5	75.2	966	179	1.18	177	341	33.7	115	19.2	1.21	15.8	13.9	7.57	8.05	1.17	20.8	8.59	82.3	78.8	28.6
29/07/2021	**AQ-9**	CF278B	586	2.9	76.5	980	181	1.17	179	343	33.8	115	19.6	1.31	16.0	14.1	7.67	7.99	1.20	20.8	8.75	85.7	79.4	28.8
29/07/2021	**AQ-9**	CF278B	466	7.7	64.5	852	155	2.19	157	295	29.0	98.4	17.0	1.31	13.4	12.0	6.51	6.72	1.00	17.7	7.51	75.6	67.8	24.6
29/07/2021	**AQ-9**	CF278B	590	3.4	73.0	943	178	1.08	172	333	32.9	112	19.2	1.19	14.9	12.8	7.38	7.67	1.15	19.8	8.45	79.2	75.5	28.2
29/07/2021	**AQ-9**	CF278B	587	4.0	77.3	987	178	1.46	179	342	34.0	116	19.5	1.29	16.2	14.1	8.28	8.45	1.19	20.7	8.62	75.6	79.4	28.6
29/07/2021	**AQ-9**	CF278B	571	6.5	77.2	984	179	3.29	182	349	34.4	115	19.9	1.20	15.9	13.8	7.95	8.23	1.16	19.7	8.35	78.9	78.1	27.6
29/07/2021	**AQ-9**	CF278B	538	8.7	65.2	821	154	4.83	154	295	29.0	99.3	17.0	1.33	13.5	11.7	6.57	6.87	1.00	17.3	7.29	74.1	65.4	23.5
29/07/2021	**AQ-9**	CF278A	502	8.1	75.2	954	180	2.26	177	338	33.1	112	19.3	1.23	15.2	12.9	7.43	8.05	1.14	20.4	8.45	81.5	75.3	27.5
29/07/2021	**AQ-9**	CF278A	591	5.4	74.0	959	179	1.44	173	330	32.4	110	19.3	1.16	15.6	12.8	7.96	7.34	1.17	20.9	8.54	79.9	76.7	28.7
29/07/2021	**AQ-9**	CF278A	574	5.7	71.2	938	176	1.90	169	322	31.2	106	18.9	1.23	14.4	12.9	7.17	8.01	1.12	21.0	8.44	79.5	74.5	27.0
29/07/2021	**AQ-9**	CF278A	583	5.3	72.2	929	177	1.83	170	330	32.0	108	18.4	1.21	15.2	13.0	7.65	7.79	1.15	19.5	8.22	86.3	73.0	27.4
29/07/2021	**AQ-9**	CF278A	572	4.5	70.2	904	174	1.77	167	320	30.9	105	18.5	1.15	13.7	12.3	7.33	7.12	1.08	18.5	7.99	76.3	70.5	26.0
29/07/2021	**AQ-9**	CF278A	576	5.1	75.3	962	178	1.94	176	335	33.0	114	19.5	1.17	15.8	13.1	7.56	7.81	1.10	19.7	8.18	76.2	73.3	26.5
29/07/2021	**AQ-8**	CF276	372	14.2	41.8	431	73	3.84	87.2	176	18.2	65.3	12.5	1.35	9.14	7.72	4.37	4.42	0.66	9.56	3.59	54.9	30.8	9.71
29/07/2021	**AQ-8**	CF276	370	14.5	42.2	424	70	8.62	88.2	175	18.5	65.8	11.9	1.44	9.50	7.91	4.31	4.31	0.66	9.80	3.55	47.4	30.2	9.52
29/07/2021	**AQ-8**	CF276	353	22.1	35.4	368	63	23.4	76.2	156	16.0	58.1	10.0	1.25	7.88	6.58	3.65	3.49	0.53	8.14	3.08	47.4	24.6	8.36
29/07/2021	**AQ-8**	CF276	359	17.6	41.7	420	69	6.01	87.1	173	18.1	66.4	11.9	1.40	8.96	7.96	4.34	4.34	0.60	9.40	3.47	47.6	29.4	9.39
29/07/2021	**AQ-8**	CF276	358	10.8	42.2	429	70	3.15	88.4	176	18.3	67.2	11.9	1.38	9.48	7.76	4.30	4.41	0.65	9.57	3.55	47.4	30.1	9.61
29/07/2021	**AQ-8**	CF276	360	40.2	40.4	412	68	28.9	84.1	166	17.2	63.1	11.2	1.37	8.67	7.57	4.07	4.35	0.62	9.11	3.34	45.6	28.7	9.19
29/07/2021	**AQ-8**	CF276	375	28.6	46.0	463	73	5.95	94.2	185	19.4	70.4	12.6	1.52	10.1	9.03	4.62	4.66	0.68	10.1	3.69	48.7	32.4	10.1
29/07/2021	**AQ-8**	CF276	350	16.1	40.9	421	67	5.95	86.4	171	18.2	65.0	11.7	1.44	9.14	7.58	4.25	4.37	0.65	9.22	3.45	47.3	29.9	9.40
29/07/2021	**AQ-8**	CF276	341	48.9	37.5	388	61	55.9	78.8	155	16.1	57.8	9.9	1.50	7.85	6.90	3.84	3.99	0.56	8.81	3.20	47.2	26.6	8.43
29/07/2021	**AQ-8**	CF276	378	13.6	38.3	382	65	6.92	80.5	161	16.7	61.1	11.0	1.20	8.23	7.00	3.85	3.83	0.58	8.42	3.21	59.1	26.7	8.72
29/07/2021	**AQ-8**	CF276	356	32.3	41.1	411	67	29.6	88.0	170	18.0	66.0	12.0	1.37	8.98	7.78	4.12	4.24	0.62	9.20	3.47	45.2	29.3	9.27
29/07/2021	**AQ-8**	CF276	247	20.1	43.0	430	63	13.4	90.8	182	18.8	69.3	12.6	1.25	9.61	8.05	4.61	4.26	0.68	9.54	3.64	45.8	31.3	9.85
29/07/2021	**AQ-8**	CF276	366	16.4	42.0	432	70	5.41	88.8	174	18.3	66.1	11.4	1.39	9.28	7.70	4.40	4.35	0.62	9.78	3.55	47.2	29.7	9.63
29/07/2021	**AQ-8**	CF276	348	74.8	38.1	390	63	108	77.9	152	16.5	57.3	10.6	1.47	8.46	6.84	3.68	3.98	0.58	8.84	3.22	44.6	26.6	8.66

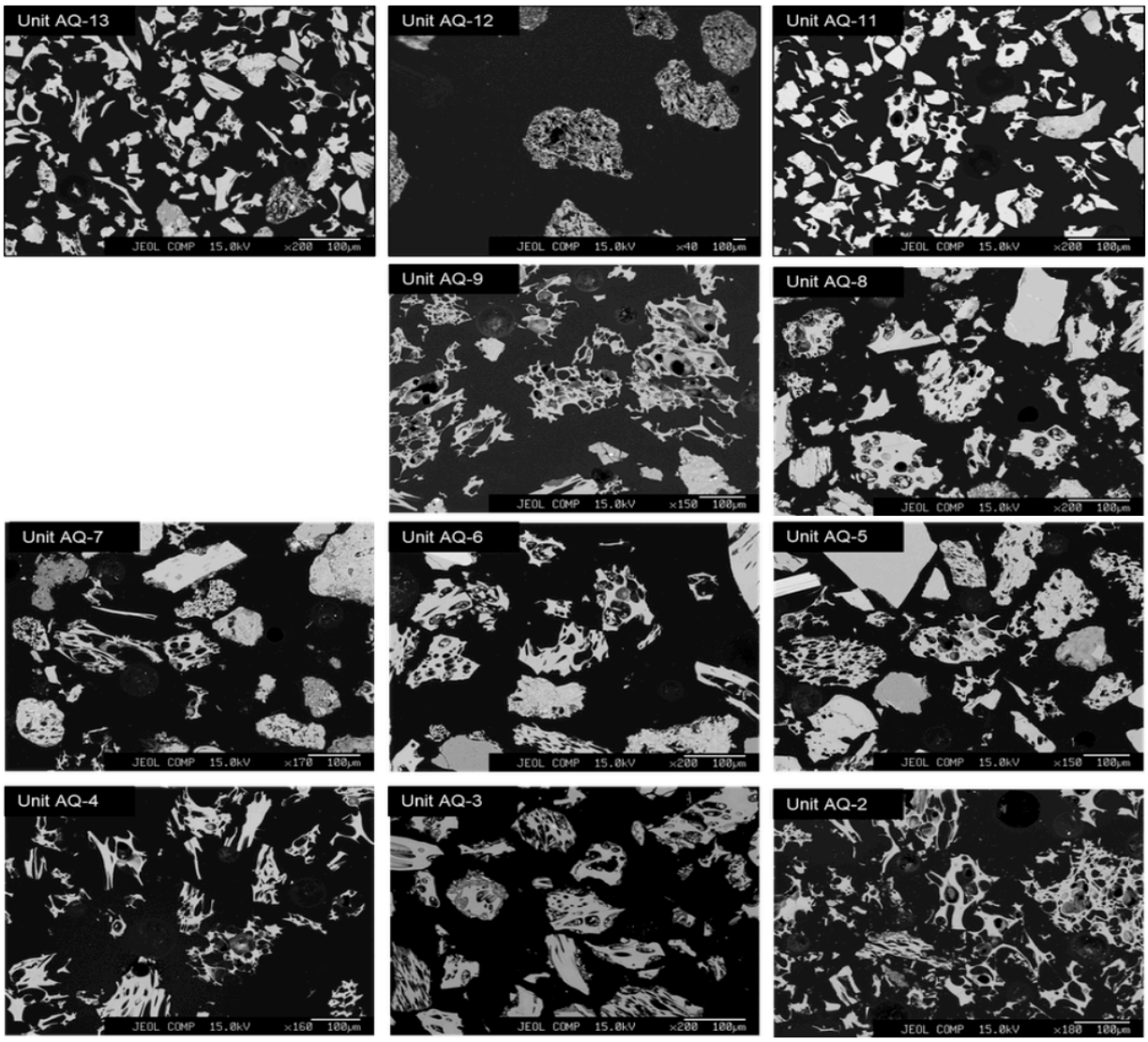
Date of analysis	Unit	Sample	Rb	Sr	Y	Zr	Nb	Ba	La	Ce	Pr	Nd	Sm	Eu	Gd	Dy	Er	Yb	Lu	Hf	Ta	Pb	Th	U
29/07/2021	**AQ-8**	CF276	338	77.6	38.2	384	62	115	80.8	161	16.8	60.1	10.6	1.46	8.39	7.14	4.04	3.93	0.59	8.87	3.15	45.5	27.2	8.38
29/07/2021	**AQ-8**	CF276	370	13.7	39.9	404	68	8.64	83.0	167	17.3	62.1	10.8	1.35	8.49	7.34	4.12	4.13	0.60	9.14	3.41	53.4	28.0	9.21
14/12/2021	**AQ-6**	CF274	476	13.5	62.5	764	142	10.9	144	273	27.4	97.1	15.8	1.32	12.0	11.6	6.30	6.60	0.92	16.1	6.71	71.4	61.1	21.7
14/12/2021	**AQ-6**	CF274	478	14.3	59.6	731	138	10.7	139	261	26.0	90.1	15.7	1.24	11.9	10.9	6.27	5.98	0.94	15.8	6.49	68.9	58.9	20.5
14/12/2021	**AQ-6**	CF274	363	25.3	51.6	509	91	2.77	133	256	26.3	92.3	14.9	1.99	11.6	9.65	4.81	5.38	0.76	11.1	4.13	62.5	42.5	13.5
14/12/2021	**AQ-6**	CF274	496	24.0	58.1	717	137	17.3	134	257	25.7	89.9	15.0	1.25	12.2	9.95	6.10	6.28	0.90	15.0	6.41	71.0	57.6	20.5
14/12/2021	**AQ-6**	CF274	472	13.7	61.6	755	142	11.3	143	273	27.1	95.5	16.5	1.35	12.2	10.9	6.30	6.78	0.93	16.6	6.78	71.2	62.1	21.7
14/12/2021	**AQ-6**	CF274	477	13.7	62.0	753	143	10.5	144	275	27.5	94.9	16.4	1.44	12.3	11.3	6.08	6.92	0.97	16.5	6.86	71.0	62.2	22.5
14/12/2021	**AQ-6**	CF274	467	20.5	59.8	737	137	17.1	138	262	25.7	90.4	15.8	1.34	12.4	10.5	5.74	6.29	0.89	15.5	6.58	69.9	59.3	21.4
14/12/2021	**AQ-6**	CF274	488	13.7	63.0	767	142	11.2	145	277	27.5	96.4	16.5	1.46	12.6	11.6	6.35	6.44	0.98	16.7	6.86	80.3	62.4	22.1
14/12/2021	**AQ-6**	CF274	345	25.7	48.9	487	85	5.39	126	244	24.9	87.0	15.7	2.28	11.1	9.30	4.89	4.74	0.70	10.8	3.87	60.8	40.7	12.5
29/07/2021	**AQ-5**	CF272	357	21.5	43.3	449	72	14.0	90.5	179	18.6	67.0	11.6	1.36	9.40	7.89	4.49	4.55	0.67	10.2	3.67	46.2	31.4	9.84
29/07/2021	**AQ-5**	CF272	368	14.5	42.0	443	73	6.83	87.9	174	18.0	64.3	11.2	1.21	9.11	7.84	4.23	4.13	0.62	9.8	3.59	47.9	29.7	10.1
29/07/2021	**AQ-5**	CF272	355	21.2	43.5	451	72	12.6	90.4	178	18.6	66.4	11.9	1.43	9.53	8.09	4.28	4.54	0.65	10.2	3.72	46.7	30.7	9.98
29/07/2021	**AQ-5**	CF272	353	21.9	43.2	446	72	15.0	89.8	178	18.5	65.2	12.0	1.37	9.44	8.13	4.45	4.56	0.67	10.4	3.72	49.3	31.1	10.0
29/07/2021	**AQ-5**	CF272	363	21.0	43.9	455	73	14.4	92.0	182	18.8	68.0	12.3	1.42	9.56	8.19	4.44	4.49	0.66	10.6	3.73	68.9	31.8	10.3
29/07/2021	**AQ-5**	CF272	356	21.1	43.7	453	72	13.1	90.1	180	18.2	66.0	12.5	1.36	9.48	8.35	4.46	4.37	0.67	10.1	3.68	47.4	31.0	10.0
29/07/2021	**AQ-5**	CF272	342	33.0	41.5	430	69	29.8	86.3	170	17.8	64.2	11.2	1.40	8.80	7.72	4.33	4.29	0.64	9.80	3.50	46.9	29.7	9.44
29/07/2021	**AQ-5**	CF272	390	11.8	38.3	397	68	6.09	80.3	157	16.6	58.2	10.7	1.06	7.34	6.85	3.79	4.14	0.52	8.06	3.08	43.6	25.0	8.45
29/07/2021	**AQ-5**	CF272	356	19.0	44.6	462	75	11.4	93.0	184	19.4	70.4	12.7	1.40	9.91	8.21	4.65	4.81	0.72	10.8	3.85	46.6	31.8	10.2
29/07/2021	**AQ-5**	CF272	365	19.0	39.7	415	70	12.5	83.1	167	17.3	62.5	10.9	1.23	8.66	7.21	3.95	3.99	0.63	9.50	3.52	53.6	28.4	10.0
29/07/2021	**AQ-5**	CF272	358	23.1	40.9	426	70	18.0	84.6	167	17.0	61.6	11.3	1.20	8.83	7.18	4.18	3.69	0.63	9.08	3.40	48.5	27.7	9.40
29/07/2021	**AQ-4**	CF271	470	6.0	53.6	656	126	2.60	125	239	24.4	82.2	14.4	1.33	10.9	9.68	5.23	5.26	0.71	13.0	5.47	64.5	47.8	17.7
29/07/2021	**AQ-4**	CF271	470	8.9	59.6	713	134	9.94	139	266	26.8	92.3	16.4	1.51	12.9	10.8	5.96	6.02	0.90	14.7	6.17	68.8	56.1	19.4
29/07/2021	**AQ-4**	CF271	473	6.2	58.4	701	132	2.15	137	262	26.5	91.9	15.2	1.42	12.1	10.7	5.78	6.04	0.85	14.5	6.17	68.4	55.2	20.0
29/07/2021	**AQ-4**	CF271	462	6.5	57.1	697	131	8.01	135	259	25.9	88.0	15.6	1.41	12.8	10.5	5.76	5.73	0.84	14.5	6.11	67.8	54.4	19.5
29/07/2021	**AQ-4**	CF271	477	5.0	58.4	710	134	1.25	138	265	26.4	90.6	16.0	1.48	12.6	10.8	5.77	5.85	0.87	15.1	6.23	71.5	55.7	20.1
29/07/2021	**AQ-4**	CF271	466	14.3	56.1	683	130	14.8	133	259	25.2	85.7	15.4	1.38	11.9	10.2	5.70	5.87	0.84	14.3	6.18	73.4	54.5	19.2
29/07/2021	**AQ-4**	CF271	463	9.2	60.6	743	140	6.55	143	276	27.1	95.7	16.5	1.50	13.1	11.2	6.12	6.15	0.91	15.9	6.57	72.8	60.4	20.6
29/07/2021	**AQ-4**	CF192	480	9.4	52.4	644	129	6.81	124	240	24.3	82.1	15.4	1.66	13.0	9.57	5.53	5.59	0.94	14.3	5.81	106.6	50.7	19.4
29/07/2021	**AQ-4**	CF192	471	11.4	55.3	678	130	3.44	131	253	25.1	85.9	15.3	1.46	11.9	10.3	5.93	5.80	0.86	14.1	6.06	71.5	54.7	19.8
29/07/2021	**AQ-4**	CF192	469	6.7	50.5	617	121	3.67	119	231	22.8	77.7	13.6	1.17	11.0	9.53	4.89	4.82	0.74	13.0	5.45	77.6	47.9	18.0
29/07/2021	**AQ-4**	CF192	455	11.4	53.0	663	129	10.4	126	246	24.2	81.0	15.9	1.48	12.0	9.00	5.22	5.27	0.77	13.6	5.82	70.8	50.0	18.4
29/07/2021	**AQ-4**	CF192	453	6.3	58.0	709	131	2.10	135	256	25.7	89.7	16.6	1.56	12.9	10.42	5.90	5.99	0.87	14.8	6.13	73.8	55.3	19.6
29/07/2021	**AQ-4**	CF192	466	8.2	54.6	670	128	2.73	130	248	24.9	84.1	15.2	1.46	11.9	9.84	5.61	5.75	0.85	14.0	5.87	68.2	51.3	18.9
29/07/2021	**AQ-4**	CF192	486	9.6	50.8	629	129	4.08	122	238	24.1	81.8	14.7	1.36	11.1	8.87	5.35	5.27	0.89	12.9	5.91	109.8	48.7	19.4
29/07/2021	**AQ-4**	CF192	456	9.3	54.6	652	126	10.2	129	261	25.3	86.1	20.3	2.27	20.5	10.7	6.50	6.24	1.73	14.9	5.85	132.9	49.1	18.6
29/07/2021	**AQ-4**	CF192	462	8.3	51.7	630	126	4.94	122	238	23.6	79.0	14.7	1.40	10.9	9.19	5.22	5.34	0.88	12.9	5.77	69.7	48.0	18.7
29/07/2021	**AQ-4**	CF192	457	7.4	53.6	657	127	3.02	127	241	24.5	82.9	15.4	1.39	10.9	9.75	5.34	5.71	0.81	14.0	5.82	67.1	50.9	18.8
29/07/2021	**AQ-4**	CF192	470	8.8	53.3	652	125	4.93	128	247	24.2	84.6	15.4	1.43	11.4	9.49	5.38	5.38	0.83	13.2	5.83	73.7	50.3	18.2
29/07/2021	**AQ-4**	CF192	484	8.6	54.8	657	129	9.89	127	246	24.4	82.5	15.1	1.46	11.5	9.75	5.61	5.89	0.79	13.5	5.87	77.6	50.3	19.7
29/07/2021	**AQ-3**	CF269	397	33.8	45.0	535	102	4.71	110	206	21.0	73.0	12.4	1.75	10.2	8.22	4.67	4.69	0.65	11.4	4.83	61.1	43.1	15.4

Date of analysis	Unit	Sample	Rb	Sr	Y	Zr	Nb	Ba	La	Ce	Pr	Nd	Sm	Eu	Gd	Dy	Er	Yb	Lu	Hf	Ta	Pb	Th	U
29/07/2021	**AQ-3**	CF269	403	36.7	47.0	559	105	12.5	111	213	21.5	73.6	12.5	1.73	10.3	8.35	4.70	4.91	0.70	11.9	4.98	61.8	43.6	15.1
29/07/2021	**AQ-3**	CF269	412	31.2	45.5	532	103	3.04	109	207	21.0	72.7	12.5	1.72	10.2	8.27	4.58	4.61	0.69	11.3	4.90	64.4	43.3	15.7
29/07/2021	**AQ-3**	CF269	409	34.5	43.2	508	100	5.39	104	197	19.9	70.3	11.7	1.69	9.83	7.61	4.43	4.36	0.64	10.7	4.63	63.3	39.9	14.8
29/07/2021	**AQ-3**	CF269	413	32.1	43.7	509	100	3.75	108	202	20.4	71.1	12.7	1.76	9.88	7.82	4.33	4.28	0.65	10.7	4.63	68.3	40.6	14.8
29/07/2021	**AQ-3**	CF269	407	38.5	45.6	535	102	12.0	109	207	20.9	72.7	12.8	1.75	10.0	8.26	4.45	4.64	0.68	11.4	4.80	62.3	42.4	14.7
29/07/2021	**AQ-3**	CF269	399	39.6	45.4	540	103	10.0	108	205	20.8	72.5	12.5	2.12	10.0	7.94	4.68	4.84	0.67	11.3	4.70	58.8	40.9	14.4
29/07/2021	**AQ-3**	CF269	409	44.4	45.9	549	107	12.8	111	205	21.3	73.7	14.2	1.81	10.2	8.47	4.61	4.57	0.69	11.6	4.82	65.0	42.7	14.4
29/07/2021	**AQ-3**	CF269	407	35.6	45.6	537	101	5.3	107	204	20.9	73.1	12.2	1.63	9.70	7.93	4.60	4.66	0.65	11.3	4.70	61.9	42.1	15.1
29/07/2021	**AQ-3**	CF269	388	55.8	45.2	556	107	31.2	107	206	20.4	72.4	12.3	1.71	9.59	8.00	4.66	4.75	0.70	11.1	4.81	68.1	42.1	13.5
29/07/2021	**AQ-3**	CF269	410	35.6	40.8	488	97	7.43	98.3	189	19.1	66.0	12.0	1.64	8.67	6.98	4.09	3.93	0.58	10.2	4.37	61.5	37.9	13.8
29/07/2021	**AQ-3**	CF269	415	32.5	45.0	532	102	3.31	108	205	20.7	71.4	12.7	1.57	9.61	8.35	4.59	4.60	0.67	11.0	4.77	63.4	42.3	15.4
29/07/2021	**AQ-3**	CF269	408	33.3	44.7	531	101	4.75	107	204	20.6	71.4	12.4	1.80	9.71	8.22	4.52	4.38	0.67	11.2	4.73	59.8	42.1	15.2
29/07/2021	**AQ-2**	CF268	417	26.5	48.0	579	110	7.17	115	220	22.0	75.5	13.4	1.67	10.5	8.84	4.80	4.92	0.73	11.8	5.17	63.9	45.5	16.3
29/07/2021	**AQ-2**	CF268	418	26.5	48.1	578	111	7.75	116	223	22.2	77.7	13.0	1.67	10.5	8.92	4.83	5.03	0.74	12.5	5.25	62.0	46.2	16.8
29/07/2021	**AQ-2**	CF268	421	29.2	49.0	585	111	7.84	116	227	22.2	78.1	13.3	1.69	10.7	9.00	5.08	5.05	0.74	12.3	5.16	61.3	46.2	16.3
29/07/2021	**AQ-2**	CF268	420	26.6	47.2	565	109	7.97	113	218	21.9	76.6	13.0	1.70	10.4	8.96	4.83	4.83	0.73	12.0	5.12	68.6	45.0	16.3
29/07/2021	**AQ-2**	CF268	409	28.2	49.2	585	111	7.20	116	225	22.3	78.0	13.4	1.64	10.7	9.09	4.87	5.04	0.77	12.2	5.27	63.2	46.9	16.1
29/07/2021	**AQ-2**	CF268	423	28.2	47.1	569	110	8.17	113	217	21.6	75.2	12.9	1.73	10.0	9.04	4.62	5.04	0.71	12.0	5.10	63.9	44.6	16.0
29/07/2021	**AQ-2**	CF268	411	28.2	45.6	559	108	7.83	110	212	20.6	72.3	13.3	1.38	9.80	8.23	4.78	4.66	0.65	11.6	4.81	58.4	41.3	15.3
29/07/2021	**AQ-2**	CF268	415	33.2	45.8	554	111	9.31	107	213	20.7	71.4	12.1	1.66	9.34	7.67	4.51	4.60	0.62	10.4	4.64	60.2	39.1	15.5
29/07/2021	**AQ-2**	CF268	422	26.2	48.8	579	111	7.32	112	218	21.0	74.5	14.0	1.65	9.56	9.06	4.88	5.01	0.71	12.0	5.06	63.8	44.5	16.1
29/07/2021	**AQ-2**	CF268	420	26.0	46.0	558	111	6.60	110	215	21.3	73.2	12.5	1.45	10.1	8.08	4.59	4.73	0.69	11.2	5.05	63.3	43.5	16.1
29/07/2021	**AQ-2**	CF268	419	26.5	47.8	580	113	6.91	115	221	22.0	76.3	13.1	1.66	10.6	9.12	4.83	4.83	0.72	12.0	5.30	62.1	46.3	17.0
29/07/2021	**AQ-2**	CF268	434	41.5	47.6	577	113	9.53	114	220	22.2	78.7	13.1	1.66	10.6	8.12	4.28	5.32	0.67	11.6	5.14	58.0	45.5	16.3
29/07/2021	**AQ-2**	CF268	417	26.1	46.5	562	109	6.64	110	212	21.2	74.0	13.1	1.67	9.87	8.04	4.59	4.72	0.68	11.4	4.94	62.6	42.6	15.7

Table A4. Trace element glass analyses of the MPI-DING reference glass (StHs6/80-G and ATHO-G)

Date of analysis	Label	Rb	Sr	Y	Zr	Nb	Ba	La	Ce	Pr	Nd	Sm	Eu	Gd	Dy	Er	Yb	Lu	Hf	Ta	Pb	Th	U
29/07/2021	**StHs6/80**	31.8	476	10.8	114	6.62	307	11.5	25.4	3.02	12.2	2.65	0.90	2.49	2.07	1.13	1.10	0.15	3.00	0.41	9.26	2.23	1.04
29/07/2021	**StHs6/80**	31.6	480	10.8	113	6.65	309	11.7	25.7	2.91	12.4	2.63	0.93	2.60	2.07	1.11	1.04	0.16	3.05	0.40	9.27	2.19	1.03
29/07/2021	**StHs6/80**	31.9	486	11.0	117	6.71	314	11.9	26.2	3.14	12.9	2.64	0.96	2.57	2.21	1.17	1.17	0.18	2.69	0.40	9.56	2.22	1.01
29/07/2021	**StHs6/80**	31.6	478	10.8	115	6.67	310	11.8	25.4	2.96	12.7	2.61	0.95	2.51	2.07	1.27	1.19	0.16	3.06	0.41	9.19	2.27	1.05
29/07/2021	**StHS6/80**	31.9	476	10.7	113	6.63	306	11.8	25.8	2.99	12.8	2.74	0.95	2.43	2.00	1.11	0.96	0.17	3.06	0.40	9.19	2.16	0.97
29/07/2021	**StHs6/80**	31.8	488	10.9	116	6.79	309	11.8	25.8	2.98	13.2	2.88	0.96	2.63	2.08	1.09	1.15	0.15	2.96	0.40	9.34	2.23	1.09
29/07/2021	**StHs6/80**	32.4	484	10.9	114	6.68	307	11.9	25.7	3.06	13.3	2.86	1.03	2.38	2.14	1.18	1.15	0.16	3.10	0.40	9.43	2.26	1.07
29/07/2021	**StHs6/80**	32.0	480	11.0	116	6.62	310	11.8	26.0	3.08	12.9	2.71	0.91	2.58	2.27	1.16	1.06	0.15	3.00	0.40	9.28	2.20	1.02
29/07/2021	**StHs6/80**	32.3	481	10.8	114	6.64	307	11.7	25.8	2.98	12.9	2.57	0.99	2.48	2.14	1.15	1.05	0.15	2.95	0.41	9.23	2.21	1.02
29/07/2021	**StHs6/80**	31.8	476	10.7	112	6.72	300	11.5	25.4	2.93	12.4	2.72	0.85	2.39	2.28	1.13	1.05	0.17	2.92	0.40	9.33	2.25	1.00
29/07/2021	**StHs6/80**	32.0	477	10.6	116	6.67	302	11.8	25.3	2.96	12.8	2.58	0.90	2.50	2.14	1.09	1.03	0.17	3.20	0.40	10.2	2.21	1.03
29/07/2021	**StHs6/80**	31.5	480	10.9	115	6.69	308	11.7	25.7	3.02	12.9	2.62	0.97	2.52	2.14	1.14	1.03	0.16	2.92	0.41	9.43	2.26	1.03
29/07/2021	**StHs6/80**	32.2	488	11.2	117	6.64	311	12.0	26.0	3.08	12.7	2.76	0.99	2.55	2.06	1.08	1.10	0.16	3.02	0.41	9.21	2.23	0.98
29/07/2021	**StHs6/80**	31.9	486	10.8	114	6.58	310	11.7	26.0	2.99	12.3	2.73	0.92	2.41	2.09	1.14	1.07	0.17	3.09	0.41	9.31	2.17	1.05
29/07/2021	**StHs6/80**	32.0	483	11.0	116	6.65	309	11.8	25.7	3.05	12.4	2.75	0.97	2.52	2.20	1.17	1.07	0.16	2.87	0.40	9.21	2.25	1.04
29/07/2021	**StHs6/80**	31.2	474	10.6	112	6.53	302	11.3	25.1	2.98	12.2	2.76	0.88	2.38	2.17	1.06	1.20	0.15	3.13	0.40	9.33	2.24	0.97
29/07/2021	**StHs6/80**	32.0	471	10.6	114	6.57	303	11.5	24.9	3.00	12.1	2.83	0.83	2.28	2.23	1.16	1.11	0.15	2.99	0.40	9.27	2.22	1.05
11/08/2021	**StHs6/80**	32.2	485	10.9	114	6.59	305	11.7	25.7	3.00	12.9	2.61	0.99	2.50	2.18	1.08	1.05	0.15	3.00	0.40	9.37	2.22	1.04
11/08/2021	**StHs6/80**	32.5	494	11.1	118	6.76	314	11.8	25.7	2.94	13.0	2.58	0.94	2.62	2.12	1.20	1.18	0.17	3.23	0.42	9.37	2.29	1.01
11/08/2021	**StHs6/80**	31.1	474	10.7	113	6.51	307	11.4	25.6	2.91	12.4	2.71	0.94	2.44	2.06	1.09	1.16	0.15	3.17	0.41	9.31	2.17	0.96
11/08/2021	**StHs6/80**	32.3	486	11.0	116	6.77	313	11.9	26.1	3.13	13.0	2.94	0.94	2.41	2.11	1.10	1.10	0.16	2.91	0.40	9.22	2.28	1.05
29/07/2021	**ATHO_G**	68.2	95.0	90.6	501	60.9	565	55.5	123.4	14.05	60.1	14.3	2.55	14.5	16.6	10.0	10.7	1.46	13.8	3.79	5.40	7.45	2.30
29/07/2021	**ATHO_G**	68.4	93.6	89.1	497	60.6	558	54.8	122.8	14.24	59.8	14.1	2.65	14.5	16.1	10.1	10.1	1.50	13.5	3.78	5.28	7.27	2.37
29/07/2021	**ATHO_G**	68.2	92.9	88.1	488	60.4	545	54.1	121.3	14.07	60.9	14.0	2.44	14.1	16.3	10.1	9.77	1.45	13.2	3.79	4.46	7.29	2.29
29/07/2021	**ATHO_G**	67.4	92.7	88.1	485	60.0	553	54.7	120.1	14.06	60.2	13.8	2.50	14.4	16.2	9.92	10.2	1.47	13.1	3.71	4.81	7.20	2.35
29/07/2021	**ATHO_G**	68.4	94.6	91.4	501	60.2	564	56.4	124.0	14.61	62.0	14.8	2.57	15.2	16.7	10.3	10.5	1.51	13.7	3.78	4.72	7.53	2.34
29/07/2021	**ATHO_G**	68.1	94.4	91.5	506	60.9	558	55.9	122.6	14.32	61.3	14.9	2.50	14.5	16.1	10.5	10.5	1.51	13.8	3.81	4.85	7.18	2.26
29/07/2021	**ATHO_G**	68.2	95.2	91.4	501	60.4	561	56.1	124.5	14.49	62.1	14.5	2.52	14.7	16.6	10.5	10.4	1.50	13.7	3.78	5.12	7.48	2.38
29/07/2021	**ATHO_G**	68.4	96.0	92.8	508	61.2	567	57.0	126.5	14.83	63.2	15.2	2.51	15.5	17.0	10.6	10.7	1.53	14.3	3.84	4.87	7.56	2.35
29/07/2021	**ATHO_G**	67.3	94.8	90.1	495	59.7	558	55.5	123.2	14.45	61.0	14.5	2.55	14.3	16.6	10.0	10.3	1.50	13.7	3.76	5.29	7.23	2.31
29/07/2021	**ATHO_G**	68.0	91.2	88.4	492	60.0	548	54.2	121.1	14.06	59.8	14.4	2.53	14.3	15.9	10.3	10.3	1.49	13.3	3.78	4.27	7.32	2.34
29/07/2021	**ATHO_G**	67.9	93.3	89.1	496	60.6	547	54.8	121.5	14.13	60.5	14.8	2.38	14.2	17.0	10.2	10.2	1.49	13.3	3.81	4.75	7.32	2.40
11/08/2021	**ATHO_G**	68.0	93.0	88.8	490	60.5	550	54.4	120.8	14.27	59.9	13.0	2.37	13.9	16.2	9.67	10.1	1.43	13.5	3.74	4.71	7.29	2.27
11/08/2021	**ATHO_G**	68.0	92.8	89.1	491	60.9	550	54.8	122.1	14.48	60.7	13.8	2.39	13.8	16.1	9.76	10.2	1.51	13.6	3.76	4.70	7.16	2.43
11/08/2021	**ATHO_G**	68.6	94.7	89.1	491	60.5	564	55.4	123.3	14.41	60.3	14.9	2.39	14.2	16.3	10.2	9.94	1.51	13.4	3.73	4.91	7.28	2.34

Figure A1. Shard images from the tephra units at Acquamorta using SEM.



Appendix B: Supplementary Material for Article 2.

Table B1. Major element glass analyses of the crypto-/tephra units preserved in Lake Suigetsu between 120 and 50 ka. (un-normalised)

Date of analysis	SG Label	SiO_2	TiO_2	Al_2O3	FeO_t	MnO	MgO	CaO	Na_2O	K_2O	P_2O_5	Cl	Analytical Total
24/08/2022	**SG14-3911**	69.91	0.38	14.20	1.50	0.06	0.33	1.07	4.38	4.50	0.07	0.10	96.51
24/08/2022	**SG14-3911**	70.07	0.42	14.24	1.52	0.07	0.37	1.03	4.37	4.47	0.12	0.09	96.77
24/08/2022	**SG14-3911**	70.29	0.39	14.32	1.62	0.08	0.33	1.10	4.32	4.53	0.04	0.08	97.09
24/08/2022	**SG14-3911**	70.07	0.45	14.30	1.51	0.07	0.32	1.07	4.56	4.38	0.02	0.14	96.91
24/08/2022	**SG14-3911**	69.97	0.42	14.30	1.54	0.05	0.34	0.99	4.48	4.60	0.06	0.11	96.86
24/08/2022	**SG14-3911**	70.38	0.41	14.42	1.69	0.08	0.33	1.10	4.59	4.53	0.00	0.09	97.62
24/08/2022	**SG14-3911**	70.14	0.38	14.35	1.59	0.08	0.34	1.10	4.43	4.53	0.05	0.11	97.10
24/08/2022	**SG14-3911**	70.18	0.39	14.35	1.60	0.07	0.35	1.03	4.46	4.49	0.00	0.09	97.01
24/08/2022	**SG14-3911**	70.42	0.41	14.49	1.61	0.07	0.35	1.07	4.53	4.73	0.10	0.10	97.88
24/08/2022	**SG14-3911**	69.32	0.43	14.20	1.62	0.08	0.34	1.04	4.28	4.42	0.08	0.08	95.89
24/08/2022	**SG14-3911**	69.65	0.36	14.26	1.49	0.07	0.29	1.08	4.36	4.51	0.08	0.09	96.25
24/08/2022	**SG14-3911**	70.20	0.44	14.39	1.59	0.08	0.29	1.10	4.39	4.46	0.06	0.10	97.09
24/08/2022	**SG14-3911**	69.77	0.42	14.33	1.61	0.08	0.34	1.06	4.38	4.42	0.06	0.11	96.59
24/08/2022	**SG14-3911**	69.48	0.42	14.28	1.53	0.10	0.31	1.02	4.36	4.47	0.03	0.09	96.10
24/08/2022	**SG14-3911**	69.74	0.44	14.37	1.53	0.07	0.34	1.05	4.39	4.58	0.04	0.11	96.68
24/08/2022	**SG14-3911**	69.52	0.44	14.28	1.59	0.09	0.29	1.07	4.17	4.42	0.07	0.11	96.06
24/08/2022	**SG14-3911**	70.84	0.44	14.62	1.57	0.08	0.33	1.09	4.43	4.61	0.08	0.09	98.18
24/08/2022	**SG14-3911**	70.84	0.45	14.64	1.64	0.09	0.34	1.06	4.49	4.58	0.07	0.09	98.28
24/08/2022	**SG14-3911**	69.53	0.37	14.34	1.62	0.09	0.31	1.09	4.25	4.58	0.00	0.09	96.29
24/08/2022	**SG14-3911**	69.72	0.40	14.39	1.63	0.06	0.30	1.06	4.48	4.42	0.08	0.08	96.62
24/08/2022	**SG14-3911**	69.41	0.36	14.28	1.47	0.06	0.33	1.07	4.24	4.35	0.08	0.10	95.76
24/08/2022	**SG14-3911**	69.71	0.44	14.41	1.53	0.08	0.38	1.11	4.28	4.51	0.06	0.10	96.62
24/08/2022	**SG14-3911**	69.93	0.44	14.48	1.62	0.10	0.30	1.06	4.34	4.53	0.03	0.10	96.93
24/08/2022	**SG14-3911**	69.66	0.41	14.41	1.54	0.06	0.30	1.06	4.25	4.56	0.03	0.09	96.38
24/08/2022	**SG14-3911**	70.19	0.37	14.54	1.56	0.08	0.29	1.01	4.32	4.47	0.05	0.11	96.99
24/08/2022	**SG14-3911**	69.62	0.38	14.58	1.60	0.05	0.32	1.07	4.37	4.45	0.08	0.10	96.62
24/08/2022	**SG14-3911**	70.09	0.42	14.78	1.64	0.08	0.32	1.11	4.26	4.67	0.04	0.09	97.49

Date of analysis	SG Label	SiO_2	TiO_2	Al_2O3	FeO_t	MnO	MgO	CaO	Na_2O	K_2O	P_2O_5	Cl	Analytical Total
06/07/2023	**SG14-4002**	70.30	0.58	12.82	2.45	0.06	0.52	1.68	3.48	4.27	0.08	0.15	96.39
06/07/2023	**SG14-4002**	70.29	0.68	13.40	2.94	0.06	0.75	2.29	3.70	4.14	0.13	0.12	98.49
06/07/2023	**SG14-4002**	65.78	0.88	13.78	3.42	0.06	0.93	2.90	3.74	3.67	0.25	0.09	95.50
06/07/2023	**SG14-4002**	62.25	1.19	14.22	5.23	0.10	1.67	4.28	3.60	3.05	0.36	0.11	96.06
06/07/2023	**SG14-4002**	62.07	1.34	14.88	5.79	0.10	1.79	4.27	3.65	2.89	0.39	0.11	97.30
06/07/2023	**SG14-4002**	63.49	0.87	14.95	3.60	0.09	0.93	3.86	3.78	3.04	0.20	0.09	94.90
06/07/2023	**SG14-4002**	63.00	1.19	15.57	5.05	0.12	1.57	4.77	3.88	2.82	0.36	0.09	98.42
06/07/2023	**SG14-4002**	60.33	1.09	17.37	4.92	0.11	1.51	5.94	3.93	2.36	0.43	0.09	98.09
06/07/2023	**SG14-4002**	59.59	1.07	17.73	4.61	0.12	1.29	6.84	4.17	2.03	0.32	0.09	97.86
24/08/2022	**SG14-4010**	73.01	0.40	12.28	1.60	0.04	0.22	0.95	3.25	4.65	0.05	0.14	96.58
24/08/2022	**SG14-4010**	71.78	0.45	12.56	1.81	0.05	0.34	1.21	3.47	4.37	0.02	0.11	96.16
24/08/2022	**SG14-4010**	72.51	0.43	12.70	1.81	0.05	0.28	1.17	3.37	4.52	0.02	0.11	96.96
24/08/2022	**SG14-4010**	72.68	0.42	12.79	1.91	0.04	0.32	1.25	3.23	4.38	0.05	0.11	97.20
24/08/2022	**SG14-4010**	71.65	0.44	12.67	1.90	0.11	0.31	1.26	3.38	4.36	0.06	0.12	96.26
24/08/2022	**SG14-4010**	72.70	0.42	12.85	1.90	0.07	0.34	1.18	3.22	4.52	0.16	0.10	97.46
24/08/2022	**SG14-4010**	72.98	0.47	12.84	1.82	0.05	0.28	1.30	2.52	4.27	0.02	0.11	96.67
24/08/2022	**SG14-4010**	71.98	0.51	12.94	2.01	0.05	0.32	1.26	3.44	4.26	0.08	0.10	96.94
24/08/2022	**SG14-4010**	72.43	0.53	13.01	1.97	0.02	0.29	1.25	3.30	4.42	0.04	0.09	97.34
24/08/2022	**SG14-4010**	73.51	0.37	13.01	1.20	0.03	0.19	1.23	3.04	4.48	0.05	0.06	97.17
24/08/2022	**SG14-4010**	71.15	0.49	13.02	2.04	0.08	0.38	1.42	3.36	4.40	0.10	0.09	96.52
24/08/2022	**SG14-4010**	73.65	0.51	13.44	2.16	0.06	0.41	1.52	3.68	3.93	0.04	0.13	99.53
24/08/2022	**SG14-4010**	71.24	0.47	13.36	2.19	0.06	0.37	1.46	3.39	4.51	0.06	0.11	97.23
24/08/2022	**SG14-4010**	70.48	0.46	13.20	2.14	0.05	0.40	1.57	3.22	4.33	0.06	0.11	96.03
24/08/2022	**SG14-4010**	70.69	0.54	13.55	2.67	0.07	0.69	2.23	3.36	4.01	0.02	0.10	97.92
24/08/2022	**SG14-4010**	70.63	0.43	14.47	1.59	0.00	0.26	2.28	3.39	3.90	0.09	0.10	97.12
02/06/2023	**SG14-4032**	69.75	0.29	13.02	1.20	0.03	0.23	0.70	4.11	4.73	0.04	0.11	94.22
02/06/2023	**SG14-4032**	70.30	0.31	13.54	1.15	0.06	0.21	0.64	4.19	4.77	0.06	0.12	95.36
02/06/2023	**SG14-4032**	69.68	0.32	13.50	1.27	0.05	0.20	0.64	4.12	4.68	0.01	0.11	94.60
02/06/2023	**SG14-4032**	69.73	0.27	13.57	1.21	0.08	0.25	0.63	4.19	4.64	0.06	0.12	94.74
02/06/2023	**SG14-4032**	70.37	0.31	13.75	1.21	0.09	0.17	0.63	4.11	4.64	0.00	0.16	95.43

Date of analysis	SG Label	SiO_2	TiO_2	Al_2O3	FeO_t	MnO	MgO	CaO	Na_2O	K_2O	P_2O_5	Cl	Analytical Total
02/06/2023	**SG14-4032**	69.60	0.27	13.63	1.26	0.09	0.17	0.64	4.05	4.67	0.00	0.11	94.50
02/06/2023	**SG14-4032**	70.18	0.32	13.72	1.21	0.05	0.24	0.65	3.86	4.67	0.00	0.15	95.04
02/06/2023	**SG14-4032**	69.88	0.30	13.68	1.21	0.04	0.21	0.62	4.05	4.65	0.01	0.09	94.76
02/06/2023	**SG14-4032**	70.06	0.32	13.77	1.20	0.08	0.22	0.65	4.05	4.79	0.02	0.11	95.28
02/06/2023	**SG14-4032**	69.77	0.35	13.74	1.15	0.06	0.21	0.65	4.31	4.57	0.05	0.10	94.96
02/06/2023	**SG14-4032**	70.13	0.28	13.80	1.22	0.05	0.19	0.63	4.07	4.70	0.04	0.11	95.22
02/06/2023	**SG14-4032**	70.04	0.24	13.88	1.18	0.08	0.20	0.68	4.26	4.66	0.09	0.12	95.44
02/06/2023	**SG14-4032**	69.89	0.29	13.85	1.14	0.02	0.22	0.66	4.14	4.77	0.03	0.10	95.11
02/06/2023	**SG14-4032**	69.69	0.31	13.82	1.19	0.03	0.19	0.62	4.10	4.71	0.08	0.12	94.86
02/06/2023	**SG14-4032**	69.49	0.32	13.84	1.24	0.08	0.19	0.66	4.07	4.76	0.07	0.12	94.85
02/06/2023	**SG14-4032**	69.26	0.36	13.99	1.41	0.07	0.23	0.83	4.26	4.48	0.05	0.11	95.05
02/06/2023	**SG14-4032**	69.42	0.33	14.03	1.50	0.07	0.27	0.81	4.23	4.38	0.05	0.10	95.18
02/06/2023	**SG14-4032**	69.01	0.48	14.17	1.71	0.08	0.32	0.96	4.28	4.55	0.03	0.09	95.68
02/06/2023	**SG14-4032**	68.79	0.38	14.07	1.59	0.03	0.34	0.97	4.20	4.44	0.08	0.12	94.99
02/06/2023	**SG14-4050**	74.88	0.27	10.72	1.08	0.05	0.18	0.67	2.90	3.96	0.01	0.11	94.84
02/06/2023	**SG14-4050**	74.99	0.34	10.83	1.07	0.00	0.05	0.51	2.86	4.49	0.05	0.07	95.27
02/06/2023	**SG14-4050**	75.93	0.15	10.91	0.70	0.05	0.11	0.70	2.88	3.83	0.07	0.16	95.49
02/06/2023	**SG14-4050**	75.15	0.31	10.90	1.00	0.01	0.10	0.54	2.75	4.42	0.00	0.06	95.24
02/06/2023	**SG14-4050**	74.53	0.22	10.78	0.84	0.00	0.02	0.40	2.42	4.83	0.01	0.06	94.11
02/06/2023	**SG14-4050**	74.86	0.23	10.93	0.87	0.01	0.09	0.53	2.52	4.57	0.04	0.06	94.72
02/06/2023	**SG14-4050**	74.58	0.15	11.38	0.77	0.02	0.17	0.83	2.96	4.02	0.00	0.05	94.93
02/06/2023	**SG14-4050**	74.56	0.13	11.41	0.81	0.05	0.18	0.79	3.08	3.65	0.04	0.16	94.85
02/06/2023	**SG14-4050**	75.06	0.21	11.47	0.68	0.05	0.13	0.42	2.32	4.87	0.05	0.04	95.29
02/06/2023	**SG14-4050**	74.89	0.16	11.51	0.77	0.04	0.15	0.80	2.83	4.03	0.06	0.07	95.32
02/06/2023	**SG14-4050**	74.98	0.23	11.56	0.75	0.02	0.14	0.84	3.06	3.92	0.02	0.13	95.65
02/06/2023	**SG14-4050**	75.30	0.17	11.57	0.68	0.05	0.13	0.90	2.94	3.86	0.00	0.12	95.72
02/06/2023	**SG14-4050**	75.03	0.15	11.59	0.77	0.04	0.15	0.85	3.07	3.79	0.00	0.14	95.57
02/06/2023	**SG14-4050**	75.28	0.11	11.63	0.76	0.09	0.11	0.76	2.99	3.70	0.02	0.17	95.62
02/06/2023	**SG14-4050**	74.77	0.11	11.63	0.71	0.04	0.13	0.74	3.01	4.17	0.02	0.15	95.48
02/06/2023	**SG14-4050**	73.19	0.43	11.65	1.49	0.07	0.20	0.78	2.83	4.43	0.10	0.08	95.25
02/06/2023	**SG14-4050**	74.32	0.15	11.61	0.75	0.02	0.15	0.85	2.95	3.90	0.07	0.13	94.90

Date of analysis	SG Label	SiO_2	TiO_2	Al_2O3	FeO_t	MnO	MgO	CaO	Na_2O	K_2O	P_2O_5	Cl	Analytical Total
02/06/2023	**SG14-4050**	74.36	0.15	11.63	0.81	0.06	0.18	0.93	3.06	3.71	0.02	0.12	95.02
02/06/2023	**SG14-4050**	74.93	0.19	11.68	0.70	0.05	0.14	0.89	2.90	3.70	0.00	0.12	95.29
02/06/2023	**SG14-4050**	74.24	0.20	11.71	0.97	0.06	0.18	1.06	3.10	3.73	0.05	0.11	95.41
02/06/2023	**SG14-4050**	74.85	0.12	11.78	0.75	0.06	0.13	0.86	3.06	3.90	0.00	0.15	95.66
02/06/2023	**SG14-4050**	78.20	0.18	12.35	0.70	0.02	0.30	2.34	3.31	1.87	0.03	0.02	99.34
02/06/2023	**SG14-4050**	73.47	0.23	11.81	1.16	0.06	0.30	1.08	2.88	3.71	0.04	0.08	94.83
02/06/2023	**SG14-4050**	74.29	0.15	11.85	0.75	0.05	0.18	1.02	2.95	3.56	0.04	0.13	94.98
02/06/2023	**SG14-4050**	74.07	0.17	11.83	0.81	0.05	0.18	1.01	3.03	3.54	0.01	0.12	94.81
02/06/2023	**SG14-4050**	75.84	0.24	12.77	0.94	0.02	0.31	1.30	3.06	4.68	0.07	0.03	99.26
02/06/2023	**SG14-4050**	73.34	0.21	12.55	1.04	0.04	0.21	1.65	3.50	3.71	0.01	0.13	96.38
02/06/2023	**SG14-4050**	72.34	0.34	12.73	1.14	0.05	0.16	1.37	3.11	4.00	0.04	0.12	95.41
07/07/2023	**SG14-4053**	71.29	0.50	11.85	1.83	0.05	0.26	1.20	2.86	4.51	0.07	0.06	94.47
07/07/2023	**SG14-4053**	71.62	0.50	12.13	2.16	0.04	0.39	1.29	3.28	4.28	0.03	0.10	95.81
07/07/2023	**SG14-4053**	70.11	0.55	11.96	2.29	0.05	0.38	1.39	3.32	4.29	0.07	0.08	94.49
07/07/2023	**SG14-4053**	67.66	0.70	12.44	3.61	0.09	1.26	2.01	3.21	3.90	0.20	0.08	95.15
07/07/2023	**SG14-4053**	70.00	0.69	12.69	2.59	0.05	0.51	1.77	3.50	4.16	0.06	0.11	96.12
07/07/2023	**SG14-4053**	68.00	0.68	12.77	2.88	0.07	0.61	2.14	3.58	4.06	0.07	0.17	95.03
07/07/2023	**SG14-4053**	71.07	0.70	13.26	2.89	0.05	0.56	2.00	3.02	4.49	0.13	0.11	98.28
07/07/2023	**SG14-4053**	70.76	0.69	13.18	2.78	0.07	0.52	1.84	3.07	4.45	0.13	0.08	97.57
07/07/2023	**SG14-4053**	68.97	0.63	13.13	2.78	0.06	0.60	1.91	3.53	4.19	0.04	0.10	95.94
07/07/2023	**SG14-4053**	67.98	0.91	13.46	3.67	0.13	0.69	2.54	3.09	3.96	0.30	0.14	96.88
07/07/2023	**SG14-4053**	65.40	0.82	13.93	2.86	0.08	0.56	2.83	3.84	3.62	0.26	0.11	94.32
04/05/2023	**SG14-4135A**	61.79	0.99	15.84	5.68	0.13	2.06	4.55	4.03	3.26	0.21	0.10	98.64
04/05/2023	**SG14-4135A**	60.54	0.94	15.61	5.51	0.09	1.94	4.61	3.46	2.93	0.25	0.10	95.99
04/05/2023	**SG14-4135A**	62.15	1.00	16.27	5.53	0.11	2.26	4.79	3.82	3.22	0.22	0.09	99.47
04/05/2023	**SG14-4135A**	62.24	1.01	16.36	5.67	0.20	2.03	4.61	4.02	3.38	0.22	0.09	99.84
04/05/2023	**SG14-4135A**	61.64	0.96	16.18	5.48	0.15	2.31	4.78	3.62	2.96	0.28	0.09	98.44
04/05/2023	**SG14-4135A**	62.71	0.98	16.49	5.55	0.15	2.11	4.79	4.02	3.20	0.23	0.08	100.31
04/05/2023	**SG14-4135A**	61.62	0.99	16.43	5.98	0.17	2.30	5.14	3.88	3.11	0.26	0.07	99.94
04/05/2023	**SG14-4135A**	61.70	1.01	16.19	5.58	0.15	2.25	4.85	3.24	3.05	0.22	0.09	98.33

Date of analysis	SG Label	SiO_2	TiO_2	Al_2O3	FeO_t	MnO	MgO	CaO	Na_2O	K_2O	P_2O_5	Cl	Analytical Total
04/05/2023	**SG14-4135A**	61.14	1.01	16.39	6.08	0.16	2.26	5.06	3.97	2.96	0.26	0.07	99.36
04/05/2023	**SG14-4135A**	60.97	1.06	16.49	5.66	0.13	2.26	5.11	3.91	3.13	0.25	0.07	99.04
04/05/2023	**SG14-4135A**	61.73	0.98	16.56	5.64	0.09	2.13	4.91	3.64	2.82	0.21	0.10	98.81
04/05/2023	**SG14-4135A**	61.30	0.96	16.89	5.68	0.16	2.16	5.36	3.97	2.73	0.21	0.07	99.50
04/05/2023	**SG14-4135A**	61.76	0.86	18.08	4.84	0.09	1.61	5.66	4.15	2.78	0.20	0.08	100.10
04/05/2023	**SG14-4135B**	66.27	1.02	14.23	4.75	0.12	1.07	2.78	3.92	4.23	0.26	0.08	98.73
04/05/2023	**SG14-4135B**	68.87	0.72	14.73	3.01	0.13	0.70	1.96	4.19	4.34	0.16	0.14	98.94
04/05/2023	**SG14-4135B**	65.72	0.75	14.22	2.84	0.11	0.74	1.89	4.08	4.21	0.12	0.08	94.77
04/05/2023	**SG14-4135B**	67.82	0.78	14.84	3.22	0.05	0.82	2.12	4.28	4.32	0.16	0.09	98.51
04/05/2023	**SG14-4135B**	65.73	0.93	15.73	4.59	0.10	0.96	3.54	4.43	3.87	0.19	0.08	100.15
04/05/2023	**SG14-4135B**	63.66	0.91	16.00	4.10	0.10	0.88	3.80	4.20	3.76	0.30	0.08	97.78
20/11/2023	**SG14-4150**	75.64	0.20	12.01	0.91	0.04	0.25	1.18	3.28	3.61	0.04	0.18	97.34
20/11/2023	**SG14-4150**	73.86	0.17	11.78	0.98	0.06	0.21	1.25	2.95	3.77	0.00	0.17	95.19
20/11/2023	**SG14-4150**	75.28	0.14	11.98	0.98	0.03	0.21	1.24	3.05	3.71	0.07	0.16	96.85
20/11/2023	**SG14-4150**	75.43	0.19	11.96	0.83	0.03	0.19	1.17	3.02	3.62	0.00	0.14	96.58
20/11/2023	**SG14-4150**	74.66	0.21	11.92	1.07	0.05	0.17	1.24	2.97	3.56	0.00	0.18	96.03
20/11/2023	**SG14-4150**	75.19	0.17	11.94	0.77	0.04	0.15	0.95	3.16	3.69	0.00	0.12	96.18
20/11/2023	**SG14-4150**	75.09	0.13	11.97	0.81	0.04	0.14	0.99	3.05	3.72	0.04	0.14	96.13
20/11/2023	**SG14-4150**	74.64	0.20	11.93	0.84	0.03	0.19	1.10	3.05	3.53	0.03	0.17	95.72
20/11/2023	**SG14-4150**	74.06	0.18	11.87	0.86	0.07	0.17	1.07	3.03	3.61	0.01	0.13	95.06
20/11/2023	**SG14-4150**	74.58	0.20	12.05	0.95	0.01	0.22	1.26	3.03	3.56	0.00	0.14	96.00
20/11/2023	**SG14-4150**	74.94	0.23	12.16	0.87	0.05	0.21	1.19	3.07	3.57	0.07	0.13	96.48
22/07/2023	**SG14-4159**	68.60	0.58	14.74	2.27	0.07	0.58	1.76	2.78	4.09	0.07	0.11	95.64
22/07/2023	**SG14-4159**	67.52	0.54	14.80	2.27	0.08	0.50	1.74	4.16	4.07	0.13	0.11	95.91
22/07/2023	**SG14-4159**	67.97	0.56	14.75	2.25	0.08	0.56	1.73	3.21	4.04	0.09	0.11	95.36
22/07/2023	**SG14-4159**	67.84	0.57	14.80	2.12	0.09	0.53	1.69	3.71	3.98	0.08	0.11	95.53
22/07/2023	**SG14-4159**	67.18	0.58	14.79	2.34	0.06	0.54	1.74	3.97	4.00	0.11	0.11	95.42
22/07/2023	**SG14-4159**	68.26	0.55	14.95	2.30	0.07	0.57	1.72	3.71	4.07	0.09	0.09	96.38
22/07/2023	**SG14-4159**	67.89	0.56	14.93	2.39	0.09	0.58	1.78	3.55	4.19	0.07	0.13	96.15
22/07/2023	**SG14-4159**	66.95	0.55	14.70	2.24	0.11	0.52	1.72	3.57	4.01	0.09	0.11	94.57

Date of analysis	SG Label	SiO_2	TiO_2	Al_2O3	FeO_t	MnO	MgO	CaO	Na_2O	K_2O	P_2O_5	Cl	Analytical Total
22/07/2023	**SG14-4159**	67.92	0.61	14.83	2.14	0.11	0.56	1.71	3.33	4.01	0.07	0.08	95.37
22/07/2023	**SG14-4159**	68.16	0.58	14.94	2.29	0.10	0.58	1.68	3.41	4.06	0.06	0.10	95.96
22/07/2023	**SG14-4159**	68.79	0.56	14.72	2.30	0.05	0.55	1.72	1.55	4.02	0.11	0.08	94.45
22/07/2023	**SG14-4159**	67.12	0.56	14.90	2.22	0.07	0.51	1.68	4.26	4.02	0.13	0.10	95.57
22/07/2023	**SG14-4159**	68.09	0.59	15.02	2.36	0.11	0.52	1.67	3.77	4.00	0.01	0.12	96.26
22/07/2023	**SG14-4159**	67.95	0.51	14.73	2.20	0.10	0.53	1.67	2.39	3.97	0.12	0.13	94.31
22/07/2023	**SG14-4159**	68.51	0.61	15.17	2.29	0.08	0.60	1.68	3.84	4.03	0.13	0.11	97.05
22/07/2023	**SG14-4159**	67.97	0.59	14.90	2.21	0.10	0.59	1.72	2.86	4.08	0.05	0.10	95.17
22/07/2023	**SG14-4159**	68.67	0.60	14.89	2.21	0.09	0.54	1.69	2.22	4.01	0.04	0.10	95.04
22/07/2023	**SG14-4159**	69.31	0.60	14.98	2.31	0.09	0.58	1.69	1.80	4.10	0.04	0.10	95.60
22/07/2023	**SG14-4159**	68.21	0.60	14.85	2.37	0.10	0.53	1.72	1.91	4.00	0.11	0.12	94.52
22/07/2023	**SG14-4159**	67.28	0.51	15.00	2.26	0.07	0.57	1.69	3.80	4.16	0.02	0.10	95.46
22/07/2023	**SG14-4159**	69.01	0.58	15.12	2.38	0.10	0.52	1.65	2.41	4.05	0.10	0.11	96.03
22/07/2023	**SG14-4159**	69.35	0.56	14.99	2.34	0.11	0.54	1.73	1.36	3.94	0.10	0.09	95.11
22/07/2023	**SG14-4159**	69.23	0.58	15.11	2.38	0.11	0.48	1.74	1.82	4.13	0.08	0.08	95.75
22/07/2023	**SG14-4159**	68.85	0.59	14.90	2.32	0.06	0.54	1.72	1.30	3.87	0.09	0.11	94.33
22/07/2023	**SG14-4159**	69.58	0.60	15.03	2.16	0.09	0.53	1.80	0.92	4.00	0.14	0.09	94.95
22/07/2023	**SG14-4159**	68.82	0.57	14.95	2.29	0.06	0.54	1.73	1.18	3.81	0.06	0.11	94.11
04/05/2023	**SG14-4187**	70.09	0.64	15.15	1.77	0.04	0.34	3.03	3.99	3.26	0.17	0.09	98.56
04/05/2023	**SG14-4187**	64.77	0.78	16.04	3.47	0.10	1.33	4.50	3.98	2.77	0.53	0.12	98.39
04/05/2023	**SG14-4187**	64.88	0.80	15.88	3.23	0.09	1.26	4.55	3.02	2.67	0.48	0.16	97.02
04/05/2023	**SG14-4187**	66.74	0.84	15.97	2.12	0.10	0.70	3.69	3.83	2.69	0.06	0.05	96.79
04/05/2023	**SG14-4187**	65.54	0.48	18.16	2.00	0.08	0.65	5.00	4.05	2.66	0.18	0.08	98.88
04/05/2023	**SG14-4187**	61.22	0.52	20.26	1.88	0.06	0.49	6.42	4.45	1.85	0.16	0.06	97.37
04/05/2023	**SG14-4187**	63.63	0.19	20.84	1.20	0.07	0.64	5.89	5.02	1.70	0.05	0.03	99.24
04/05/2023	**SG14-4187**	63.22	0.32	20.79	1.06	0.02	0.23	6.89	3.87	2.03	0.11	0.05	98.59
04/05/2023	**SG14-4187**	62.35	0.29	21.34	1.34	0.00	0.33	6.96	4.24	1.77	0.03	0.09	98.74
03/06/2023	**SG14-4223**	57.31	0.65	18.77	3.83	0.18	0.76	2.13	6.64	6.25	0.25	0.21	96.99
03/06/2023	**SG14-4223**	57.68	0.65	18.77	3.74	0.15	0.73	2.10	6.41	6.11	0.15	0.21	96.70
03/06/2023	**SG14-4223**	56.89	0.58	18.84	3.60	0.14	0.62	2.64	6.48	6.11	0.82	0.21	96.93

Date of analysis	SG Label	SiO_2	TiO_2	Al_2O3	FeO_t	MnO	MgO	CaO	Na_2O	K_2O	P_2O_5	Cl	Analytical Total
03/06/2023	**SG14-4223**	56.69	0.68	18.84	3.82	0.13	0.65	2.49	6.59	6.15	0.60	0.22	96.86
03/06/2023	**SG14-4223**	57.81	0.59	19.02	3.75	0.14	0.67	1.97	6.87	6.31	0.16	0.19	97.49
03/06/2023	**SG14-4223**	56.66	0.83	18.98	4.04	0.17	0.87	2.62	6.36	6.10	0.41	0.20	97.24
03/06/2023	**SG14-4223**	57.31	0.83	19.12	3.98	0.14	0.80	2.50	6.43	6.04	0.38	0.18	97.71
03/06/2023	**SG14-4223**	57.75	0.63	19.18	3.79	0.13	0.70	2.46	6.52	6.19	0.46	0.20	98.01
03/06/2023	**SG14-4223**	57.99	0.61	19.20	3.81	0.17	0.64	2.00	6.67	6.44	0.17	0.22	97.93
03/06/2023	**SG14-4223**	57.72	0.64	19.10	3.75	0.14	0.69	2.02	6.46	6.35	0.29	0.20	97.38
03/06/2023	**SG14-4223**	57.47	0.69	19.03	3.83	0.14	0.73	1.96	6.38	6.32	0.21	0.20	96.97
03/06/2023	**SG14-4223**	57.84	0.77	19.30	3.95	0.17	0.82	2.24	6.52	6.26	0.17	0.18	98.22
03/06/2023	**SG14-4223**	57.45	0.70	18.97	3.52	0.17	0.66	1.81	6.54	6.43	0.10	0.18	96.51
03/06/2023	**SG14-4223**	57.83	0.70	19.18	3.83	0.14	0.75	2.00	6.53	6.25	0.12	0.19	97.53
03/06/2023	**SG14-4223**	58.47	0.67	19.48	3.99	0.15	0.73	2.06	6.62	6.33	0.19	0.18	98.86
03/06/2023	**SG14-4223**	56.91	0.67	19.03	3.90	0.15	0.71	2.31	6.22	6.12	0.27	0.21	96.50
03/06/2023	**SG14-4223**	56.95	0.67	18.83	3.78	0.16	0.72	1.97	5.95	5.96	0.22	0.23	95.45
03/06/2023	**SG14-4223**	57.12	0.64	19.04	3.68	0.16	0.72	2.05	6.46	6.22	0.24	0.19	96.52
03/06/2023	**SG14-4223**	58.10	0.70	19.40	3.78	0.17	0.70	2.07	6.70	6.24	0.26	0.18	98.31
03/06/2023	**SG14-4223**	58.65	0.55	19.53	4.06	0.18	0.58	2.01	6.73	6.15	0.20	0.18	98.82
03/06/2023	**SG14-4223**	57.04	0.71	19.13	3.84	0.14	0.72	2.14	6.48	6.17	0.23	0.19	96.81
03/06/2023	**SG14-4223**	56.20	0.61	18.67	3.75	0.14	0.68	1.99	6.04	6.02	0.16	0.22	94.48
03/06/2023	**SG14-4223**	58.29	0.69	19.43	3.80	0.13	0.66	2.00	6.57	6.23	0.21	0.21	98.21
03/06/2023	**SG14-4223**	58.11	0.51	19.35	3.81	0.17	0.63	2.04	6.41	6.28	0.28	0.21	97.80
03/06/2023	**SG14-4223**	57.54	0.64	19.30	3.77	0.18	0.70	2.12	6.36	6.41	0.24	0.22	97.48
03/06/2023	**SG14-4223**	58.22	0.69	19.58	3.87	0.15	0.69	2.15	6.67	6.27	0.15	0.20	98.64
03/06/2023	**SG14-4223**	58.06	0.57	19.43	3.81	0.17	0.55	2.04	6.69	6.07	0.26	0.21	97.86
03/06/2023	**SG14-4223**	56.50	0.83	19.27	4.16	0.14	0.82	2.45	6.37	6.12	0.24	0.20	97.09
03/06/2023	**SG14-4223**	57.58	0.80	19.53	4.03	0.16	0.80	2.20	6.65	6.21	0.20	0.18	98.34
03/06/2023	**SG14-4223**	56.29	0.73	19.12	3.91	0.16	0.80	2.23	6.44	6.09	0.26	0.19	96.22
03/06/2023	**SG14-4223**	58.07	0.65	19.44	3.83	0.13	0.70	2.08	6.20	6.30	0.20	0.19	97.79
03/06/2023	**SG14-4223**	57.22	0.66	19.09	3.62	0.15	0.65	1.94	6.27	5.99	0.18	0.24	96.01
03/06/2023	**SG14-4223**	55.96	0.57	18.82	3.38	0.15	0.55	1.92	6.15	6.06	0.37	0.22	94.17
03/06/2023	**SG14-4223**	56.98	0.83	19.50	3.99	0.11	0.84	2.39	6.26	6.22	0.28	0.19	97.57
03/06/2023	**SG14-4223**	56.99	0.61	19.22	3.62	0.14	0.66	1.83	6.29	6.33	0.19	0.20	96.08

Date of analysis	SG Label	SiO_2	TiO_2	Al_2O3	FeO_t	MnO	MgO	CaO	Na_2O	K_2O	P_2O_5	Cl	Analytical Total
03/06/2023	**SG14-4223**	56.10	0.64	19.02	3.60	0.14	0.69	1.91	6.18	6.22	0.28	0.19	94.98
09/02/2023	**SG14-4263**	70.40	0.53	12.33	1.82	0.00	0.36	1.50	3.24	4.27	0.07	0.10	94.61
09/02/2023	**SG14-4263**	71.58	0.64	13.04	2.49	0.03	0.62	2.17	3.43	4.13	0.09	0.13	98.36
09/02/2023	**SG14-4263**	69.82	0.61	12.67	2.31	0.06	0.42	1.74	3.20	4.16	0.03	0.12	95.15
09/02/2023	**SG14-4263**	69.15	0.66	12.68	2.59	0.02	0.50	1.89	3.18	4.09	0.10	0.11	94.97
09/02/2023	**SG14-4263**	68.75	0.61	12.60	2.41	0.03	0.48	2.01	3.23	3.95	0.08	0.11	94.26
09/02/2023	**SG14-4263**	68.94	0.66	12.68	2.63	0.05	0.50	1.94	3.22	4.04	0.08	0.11	94.85
09/02/2023	**SG14-4263**	68.86	0.64	12.75	2.47	0.05	0.52	1.98	3.25	4.08	0.09	0.13	94.80
09/02/2023	**SG14-4263**	71.59	0.60	13.29	2.56	0.06	0.57	2.14	3.48	4.08	0.09	0.12	98.58
09/02/2023	**SG14-4263**	69.04	0.66	12.95	2.69	0.08	0.59	2.19	3.18	3.95	0.10	0.10	95.53
09/02/2023	**SG14-4263**	69.71	0.64	13.03	2.55	0.04	0.58	2.08	3.22	4.06	0.09	0.11	96.12
09/02/2023	**SG14-4263**	70.27	0.72	13.23	2.78	0.07	0.64	2.39	2.96	4.19	0.12	0.12	97.48
09/02/2023	**SG14-4263**	68.70	0.67	12.95	2.56	0.03	0.54	2.22	3.33	4.02	0.09	0.08	95.18
09/02/2023	**SG14-4263**	69.09	0.64	12.99	2.46	0.07	0.58	2.05	3.36	4.00	0.02	0.12	95.38
09/02/2023	**SG14-4263**	69.33	0.70	13.18	2.79	0.09	0.55	2.15	3.49	4.02	0.10	0.11	96.50
09/02/2023	**SG14-4263**	70.80	0.72	13.48	2.95	0.05	0.63	2.38	3.39	4.06	0.08	0.11	98.66
09/02/2023	**SG14-4263**	68.18	0.62	12.97	2.60	0.06	0.58	2.17	3.25	4.06	0.08	0.11	94.68
09/02/2023	**SG14-4263**	69.43	0.63	13.00	2.63	0.05	0.61	2.17	2.23	3.87	0.10	0.12	94.84
09/02/2023	**SG14-4263**	67.97	0.64	12.98	2.76	0.05	0.62	2.19	3.27	3.88	0.10	0.13	94.58
09/02/2023	**SG14-4263**	69.98	0.67	13.15	2.76	0.04	0.62	2.44	1.58	3.95	0.15	0.10	95.44
09/02/2023	**SG14-4263**	70.11	0.65	13.45	2.83	0.06	0.61	2.27	2.57	4.23	0.08	0.10	96.97
09/02/2023	**SG14-4263**	67.42	0.63	13.12	3.01	0.08	0.69	2.40	3.14	3.78	0.10	0.11	94.48
09/02/2023	**SG14-4263**	68.91	0.67	13.79	3.40	0.07	0.86	2.94	3.38	3.70	0.19	0.13	98.04
31/05/2023	**SG14-4307**	71.56	0.57	11.85	2.58	0.06	0.53	2.18	3.61	2.44	0.05	0.11	95.54
31/05/2023	**SG14-4307**	71.61	0.54	11.99	2.67	0.06	0.57	2.15	3.69	2.53	0.10	0.09	96.01
31/05/2023	**SG14-4307**	70.50	0.56	11.95	2.63	0.08	0.59	2.29	4.16	2.42	0.15	0.10	95.42
31/05/2023	**SG14-4307**	72.21	0.51	12.18	2.60	0.09	0.54	2.29	3.78	2.44	0.15	0.11	96.89
31/05/2023	**SG14-4307**	72.74	0.55	12.33	2.56	0.08	0.62	2.31	3.86	2.47	0.08	0.11	97.71
31/05/2023	**SG14-4307**	71.80	0.57	12.19	2.63	0.08	0.62	2.31	3.72	2.42	0.07	0.11	96.51
31/05/2023	**SG14-4307**	72.73	0.56	12.41	2.72	0.07	0.62	2.39	3.82	2.41	0.11	0.10	97.95

Date of analysis	SG Label	SiO_2	TiO_2	Al_2O3	FeO_t	MnO	MgO	CaO	Na_2O	K_2O	P_2O_5	Cl	Analytical Total
31/05/2023	**SG14-4307**	71.74	0.62	12.32	2.73	0.07	0.52	2.31	4.35	2.38	0.05	0.10	97.19
31/05/2023	**SG14-4307**	72.99	0.55	12.42	2.55	0.08	0.53	2.29	3.88	2.43	0.13	0.11	97.96
31/05/2023	**SG14-4307**	71.60	0.58	12.27	2.63	0.08	0.57	2.24	3.90	2.42	0.12	0.11	96.51
31/05/2023	**SG14-4307**	71.74	0.58	12.24	2.57	0.02	0.56	2.26	3.67	2.41	0.08	0.09	96.24
31/05/2023	**SG14-4307**	71.81	0.56	12.31	2.68	0.06	0.58	2.35	3.77	2.44	0.13	0.12	96.81
31/05/2023	**SG14-4307**	71.81	0.58	12.45	2.60	0.12	0.61	2.37	4.55	2.42	0.09	0.11	97.69
31/05/2023	**SG14-4307**	71.13	0.55	12.19	2.47	0.05	0.60	2.21	3.67	2.40	0.09	0.09	95.45
31/05/2023	**SG14-4307**	73.70	0.59	12.77	2.85	0.09	0.57	2.47	4.03	2.48	0.21	0.10	99.86
31/05/2023	**SG14-4307**	70.69	0.51	12.16	2.66	0.06	0.56	2.24	3.48	2.40	0.10	0.11	94.98
31/05/2023	**SG14-4307**	70.84	0.55	12.19	2.56	0.06	0.54	2.14	3.52	2.32	0.14	0.11	94.97
22/11/2023	**SG14-4307**	71.98	0.53	12.44	2.75	0.06	0.55	2.30	3.71	2.42	0.11	0.11	96.95
22/11/2023	**SG14-4307**	73.01	0.58	12.70	2.79	0.08	0.58	2.38	3.61	2.45	0.17	0.11	98.45
22/11/2023	**SG14-4307**	73.52	0.56	12.85	3.05	0.07	0.58	2.63	3.73	2.41	0.13	0.11	99.62
22/11/2023	**SG14-4307**	71.82	0.55	12.53	2.58	0.08	0.57	2.25	3.69	2.43	0.12	0.10	96.72
22/11/2023	**SG14-4307**	72.77	0.58	13.53	2.42	0.10	0.48	2.80	3.81	2.29	0.18	0.12	99.07
02/06/2023	**SG14-4352**	61.90	0.82	15.15	5.30	0.19	1.88	3.52	3.94	3.40	0.40	0.11	96.61
02/06/2023	**SG14-4352**	64.86	0.83	15.43	4.55	0.15	1.14	2.91	4.23	3.78	0.43	0.07	98.38
02/06/2023	**SG14-4352**	65.31	0.76	15.47	4.02	0.13	1.06	2.74	4.49	3.86	0.24	0.08	98.16
02/06/2023	**SG14-4352**	65.46	0.68	15.68	4.06	0.14	1.11	2.83	4.44	3.86	0.15	0.09	98.51
02/06/2023	**SG14-4352**	62.06	0.86	15.39	4.84	0.15	1.42	3.54	4.38	3.22	0.37	0.10	96.34
02/06/2023	**SG14-4352**	65.57	0.81	15.80	3.95	0.15	1.02	2.65	4.48	3.89	0.24	0.06	98.63
02/06/2023	**SG14-4352**	63.73	0.87	15.83	4.93	0.18	1.45	3.43	4.33	3.58	0.40	0.06	98.79
02/06/2023	**SG14-4352**	63.97	0.87	15.91	4.98	0.20	1.51	3.36	4.26	3.64	0.46	0.06	99.24
02/06/2023	**SG14-4352**	63.35	0.87	15.95	5.45	0.20	1.81	3.56	4.07	3.54	0.42	0.06	99.29
02/06/2023	**SG14-4352**	62.39	0.87	15.41	4.56	0.13	0.77	3.15	4.37	3.73	0.39	0.08	95.85
02/06/2023	**SG14-4352**	65.91	0.67	15.88	3.65	0.12	1.02	2.90	4.50	3.70	0.22	0.07	98.65
02/06/2023	**SG14-4352**	65.75	0.73	15.95	3.85	0.12	1.05	2.87	4.43	3.85	0.16	0.09	98.85
02/06/2023	**SG14-4352**	65.23	0.73	15.82	3.63	0.17	1.12	2.78	4.45	3.88	0.17	0.07	98.04
02/06/2023	**SG14-4352**	64.77	0.78	15.96	4.16	0.19	1.22	3.23	4.32	3.69	0.31	0.08	98.73
02/06/2023	**SG14-4352**	63.40	0.86	15.87	4.81	0.14	1.02	3.27	4.42	3.75	0.38	0.07	97.99
02/06/2023	**SG14-4352**	65.93	0.77	16.18	3.87	0.17	1.05	2.65	4.16	4.52	0.21	0.09	99.61

Date of analysis	SG Label	SiO_2	TiO_2	Al_2O3	FeO_t	MnO	MgO	CaO	Na_2O	K_2O	P_2O_5	Cl	Analytical Total
02/06/2023	**SG14-4352**	63.87	0.80	16.02	4.78	0.17	1.41	3.57	4.18	3.33	0.34	0.08	98.55
02/06/2023	**SG14-4352**	64.31	0.83	16.12	4.58	0.13	1.19	3.08	4.48	3.77	0.39	0.07	98.94
02/06/2023	**SG14-4352**	62.77	0.83	15.87	4.72	0.18	1.34	3.36	4.11	3.37	0.39	0.10	97.02
02/06/2023	**SG14-4352**	63.71	0.82	16.27	5.09	0.17	1.39	3.51	4.36	3.49	0.50	0.06	99.38
02/06/2023	**SG14-4352**	63.82	0.78	16.41	4.50	0.16	1.17	3.59	4.61	3.41	0.40	0.09	98.94
02/06/2023	**SG14-4352**	63.80	0.76	16.66	4.44	0.16	1.15	3.61	4.60	3.42	0.33	0.07	99.00
02/06/2023	**SG14-4352**	60.86	0.79	16.14	4.30	0.16	1.38	3.67	4.33	3.13	0.36	0.10	95.22
02/06/2023	**SG14-4352**	63.04	0.79	16.95	4.38	0.11	1.33	4.17	4.65	3.11	0.35	0.06	98.95
02/06/2023	**SG14-4352**	62.87	0.77	17.09	4.52	0.12	1.64	4.16	4.48	3.16	0.29	0.04	99.13
02/06/2023	**SG14-4352**	62.82	0.63	17.14	4.07	0.11	1.24	4.09	4.73	3.06	0.34	0.07	98.29
02/06/2023	**SG14-4352**	63.05	0.74	17.35	4.38	0.09	1.22	4.00	4.57	3.29	0.40	0.07	99.15
02/06/2023	**SG14-4352**	62.60	0.63	17.89	3.92	0.14	0.96	4.37	4.79	2.87	0.34	0.06	98.57
24/08/2022	**SG14-4471A**	60.82	1.21	14.18	5.64	0.11	1.49	4.04	2.89	3.31	0.36	0.08	94.12
24/08/2022	**SG14-4471A**	61.65	1.24	14.42	5.62	0.13	1.61	4.06	2.76	3.30	0.30	0.08	95.17
24/08/2022	**SG14-4471A**	61.48	1.24	14.31	5.75	0.14	1.59	4.14	1.86	3.35	0.35	0.11	94.32
21/11/2023	**SG14-4471A**	62.10	1.29	14.51	5.57	0.16	1.62	4.13	1.49	3.05	0.45	0.12	94.49
21/11/2023	**SG14-4471A**	66.23	0.79	15.76	4.55	0.09	1.06	3.19	4.17	3.32	0.22	0.12	99.50
21/11/2023	**SG14-4471A**	64.42	0.74	15.25	4.27	0.10	0.99	3.09	3.17	3.32	0.18	0.11	95.62
24/08/2022	**SG14-4471B**	70.50	0.46	14.63	1.40	0.08	0.31	0.98	4.31	4.18	0.06	0.13	97.03
24/08/2022	**SG14-4471B**	69.12	0.37	14.45	1.35	0.07	0.33	1.04	4.13	4.07	0.09	0.13	95.15
21/11/2023	**SG14-4471B**	69.23	0.40	14.50	1.44	0.10	0.33	1.07	3.96	4.11	0.05	0.12	95.31
21/11/2023	**SG14-4471B**	70.02	0.40	14.61	1.46	0.08	0.28	0.99	2.90	4.32	0.09	0.10	95.25
02/12/2022	**SG14-4496**	72.11	0.56	12.99	2.05	0.05	0.43	1.64	3.35	4.20	0.12	0.10	97.61
02/12/2022	**SG14-4496**	72.86	0.49	13.11	2.15	0.00	0.42	1.66	3.33	4.22	0.11	0.14	98.47
02/12/2022	**SG14-4496**	71.72	0.49	12.93	2.11	0.04	0.40	1.69	3.34	4.10	0.17	0.12	97.12
02/12/2022	**SG14-4496**	71.80	0.48	12.93	1.91	0.00	0.40	1.63	3.56	4.03	0.12	0.13	96.97
02/12/2022	**SG14-4496**	71.71	0.51	13.18	2.03	0.08	0.43	1.68	3.46	4.03	0.12	0.13	97.37
02/12/2022	**SG14-4496**	70.84	0.50	13.11	2.15	0.06	0.43	1.72	3.36	3.99	0.13	0.12	96.41
02/12/2022	**SG14-4496**	70.45	0.57	13.33	2.36	0.08	0.50	2.00	3.46	3.87	0.16	0.14	96.93
02/12/2022	**SG14-4496**	71.00	0.59	13.58	2.67	0.11	0.55	2.35	3.52	3.89	0.16	0.11	98.54

Date of analysis	SG Label	SiO_2	TiO_2	Al_2O3	FeO_t	MnO	MgO	CaO	Na_2O	K_2O	P_2O_5	Cl	Analytical Total
02/12/2022	**SG14-4496**	70.05	0.60	13.24	2.30	0.07	0.50	1.82	3.49	3.77	0.09	0.13	96.05
02/12/2022	**SG14-4496**	70.28	0.56	13.32	2.44	0.02	0.53	1.96	3.45	3.76	0.20	0.10	96.62
22/11/2023	**SG14-4496**	71.15	0.63	13.72	2.95	0.06	0.68	2.23	3.95	3.87	0.15	0.13	99.52
22/11/2023	**SG14-4496**	71.79	0.60	13.74	2.56	0.05	0.62	2.31	3.61	4.05	0.07	0.10	99.50
22/11/2023	**SG14-4496**	70.55	0.53	13.40	2.53	0.06	0.50	1.90	3.48	3.81	0.09	0.13	96.98
22/11/2023	**SG14-4496**	68.99	0.58	13.23	2.64	0.06	0.56	2.13	3.56	3.74	0.09	0.11	95.70
22/11/2023	**SG14-4496**	70.75	0.51	13.50	2.45	0.09	0.54	1.95	3.52	3.92	0.17	0.12	97.51
22/11/2023	**SG14-4496**	71.53	0.60	13.77	2.68	0.05	0.60	2.27	3.64	3.86	0.24	0.13	99.37
22/11/2023	**SG14-4496**	71.59	0.59	13.57	2.58	0.04	0.64	2.18	2.43	3.92	0.06	0.15	97.75
22/11/2023	**SG14-4496**	69.95	0.61	13.42	2.49	0.06	0.53	1.97	3.45	3.81	0.14	0.11	96.55
22/11/2023	**SG14-4496**	69.55	0.61	13.46	2.75	0.07	0.59	2.25	3.47	3.70	0.17	0.10	96.73
22/11/2023	**SG14-4496**	70.93	0.55	13.55	2.29	0.03	0.46	2.23	3.37	3.76	0.08	0.10	97.34
22/11/2023	**SG14-4496**	69.69	0.61	13.49	2.72	0.05	0.66	2.20	3.43	3.66	0.27	0.12	96.88
22/11/2023	**SG14-4496**	70.87	0.66	13.71	2.76	0.05	0.58	2.25	3.59	3.70	0.03	0.15	98.34
22/11/2023	**SG14-4496**	71.30	0.59	13.81	2.68	0.05	0.56	2.24	3.61	3.86	0.22	0.09	98.99
22/11/2023	**SG14-4496**	70.57	0.61	13.69	2.73	0.04	0.64	2.28	3.00	3.86	0.16	0.13	97.72
22/11/2023	**SG14-4496**	69.52	0.56	13.37	2.73	0.08	0.59	2.18	1.99	3.74	0.12	0.13	95.00
22/11/2023	**SG14-4496**	71.26	0.57	14.08	3.07	0.08	0.77	2.68	3.71	3.55	0.05	0.13	99.94
22/11/2023	**SG14-4496**	68.94	0.55	13.56	2.65	0.04	0.57	2.15	3.67	3.59	0.13	0.12	95.97
22/11/2023	**SG14-4496**	72.06	0.67	14.00	2.77	0.06	0.69	2.31	1.91	3.75	0.20	0.10	98.51
22/11/2023	**SG14-4496**	69.28	0.63	13.63	2.78	0.08	0.64	2.21	2.40	3.76	0.10	0.13	95.64
22/11/2023	**SG14-4496**	71.71	0.59	14.56	2.36	0.09	0.59	2.56	3.62	3.84	0.17	0.14	100.24
24/08/2022	**SG14-4531**	60.61	1.38	16.49	6.92	0.17	2.28	5.22	4.06	2.36	0.47	0.09	100.06
24/08/2022	**SG14-4531**	61.27	1.34	16.58	6.81	0.14	2.23	5.10	3.99	2.35	0.53	0.10	100.46
24/08/2022	**SG14-4531**	60.44	1.42	16.62	7.07	0.14	2.37	5.47	4.21	2.30	0.50	0.10	100.64
24/08/2022	**SG14-4531**	61.70	1.31	16.68	6.58	0.20	2.29	5.14	3.93	2.39	0.55	0.10	100.88
24/08/2022	**SG14-4531**	61.12	1.37	16.57	6.56	0.16	2.21	5.10	4.10	2.39	0.46	0.10	100.15
24/08/2022	**SG14-4531**	61.05	1.33	16.64	6.72	0.21	2.24	5.34	3.94	2.41	0.53	0.12	100.53
24/08/2022	**SG14-4531**	61.00	1.35	16.60	6.49	0.17	2.20	4.87	4.40	2.64	0.46	0.08	100.25
24/08/2022	**SG14-4531**	60.68	1.35	16.59	6.73	0.17	2.20	5.19	4.25	2.31	0.54	0.10	100.12
24/08/2022	**SG14-4531**	61.31	1.45	16.66	6.50	0.16	2.19	4.96	4.13	2.65	0.44	0.08	100.52

Date of analysis	SG Label	SiO_2	TiO_2	Al_2O3	FeO_t	MnO	MgO	CaO	Na_2O	K_2O	P_2O_5	Cl	Analytical Total
24/08/2022	**SG14-4531**	61.05	1.32	16.63	6.38	0.15	2.19	5.13	4.24	2.43	0.63	0.09	100.25
24/08/2022	**SG14-4531**	60.40	1.37	16.60	6.92	0.18	2.31	5.10	4.15	2.36	0.53	0.08	100.00
24/08/2022	**SG14-4531**	60.94	1.33	16.59	6.54	0.15	2.28	5.22	3.97	2.26	0.55	0.08	99.91
24/08/2022	**SG14-4531**	60.65	1.34	16.63	6.78	0.17	2.23	5.28	4.08	2.29	0.57	0.09	100.12
24/08/2022	**SG14-4531**	60.61	1.23	16.64	6.87	0.15	2.34	5.12	4.23	2.32	0.47	0.09	100.08
24/08/2022	**SG14-4531**	61.07	1.36	16.68	6.77	0.21	2.30	5.19	3.83	2.29	0.50	0.08	100.29
24/08/2022	**SG14-4531**	61.40	1.31	16.79	6.78	0.17	2.23	5.24	4.11	2.31	0.43	0.08	100.87
24/08/2022	**SG14-4531**	60.89	1.33	16.67	6.71	0.18	2.26	5.20	4.10	2.37	0.33	0.10	100.14
24/08/2022	**SG14-4531**	60.51	1.29	16.63	6.74	0.18	2.32	5.26	4.09	2.22	0.52	0.11	99.89
24/08/2022	**SG14-4531**	61.26	1.29	16.82	6.78	0.16	2.20	5.29	4.27	2.32	0.52	0.10	101.03
24/08/2022	**SG14-4531**	60.27	1.40	16.64	6.68	0.19	2.31	5.44	4.02	2.32	0.49	0.11	99.87
24/08/2022	**SG14-4531**	60.69	1.28	16.69	6.57	0.20	2.23	5.31	4.15	2.35	0.55	0.10	100.13
24/08/2022	**SG14-4531**	60.49	1.31	16.62	6.62	0.16	2.27	4.96	4.10	2.29	0.55	0.10	99.47
24/08/2022	**SG14-4531**	61.04	1.30	16.80	6.68	0.16	2.22	5.26	3.99	2.40	0.59	0.09	100.53
24/08/2022	**SG14-4531**	61.20	1.40	16.87	6.47	0.17	2.11	5.23	4.27	2.34	0.54	0.10	100.70
24/08/2022	**SG14-4531**	60.53	1.27	16.74	6.71	0.20	2.32	5.12	4.04	2.30	0.52	0.09	99.85
24/08/2022	**SG14-4531**	60.94	1.35	16.81	6.17	0.14	2.11	5.49	4.39	2.25	0.53	0.09	100.27
24/08/2022	**SG14-4531**	61.19	1.25	16.84	6.49	0.14	2.22	4.96	4.26	2.41	0.49	0.09	100.34
24/08/2022	**SG14-4531**	60.85	1.28	16.82	6.35	0.17	2.28	5.05	4.36	2.40	0.50	0.09	100.16
24/08/2022	**SG14-4531**	61.15	1.37	17.09	6.60	0.23	2.09	5.32	4.40	2.29	0.57	0.08	101.19
11/07/2023	**SG14-4582**	75.49	0.21	11.57	1.06	0.06	0.18	1.02	3.63	1.96	0.14	0.01	95.32
11/07/2023	**SG14-4582**	75.59	0.22	11.66	1.06	0.04	0.19	1.02	3.37	1.88	0.13	0.02	95.18
11/07/2023	**SG14-4582**	75.55	0.21	11.65	0.89	0.01	0.14	0.99	3.37	1.94	0.14	0.02	94.91
11/07/2023	**SG14-4582**	75.66	0.16	11.78	1.06	0.05	0.19	1.34	3.12	2.04	0.08	0.00	95.49
11/07/2023	**SG14-4582**	75.12	0.27	11.67	0.96	0.04	0.17	0.99	3.14	1.97	0.13	0.00	94.46
11/07/2023	**SG14-4582**	75.67	0.20	11.68	0.93	0.03	0.19	0.91	2.86	1.92	0.14	0.00	94.52
11/07/2023	**SG14-4582**	74.85	0.13	11.67	0.90	0.04	0.14	1.10	2.94	2.18	0.08	0.00	94.04
11/07/2023	**SG14-4582**	75.94	0.09	11.88	0.92	0.01	0.12	1.07	3.13	2.26	0.09	0.00	95.51
11/07/2023	**SG14-4582**	74.63	0.15	11.72	1.04	0.07	0.17	1.37	3.01	1.90	0.09	0.00	94.15
11/07/2023	**SG14-4582**	76.04	0.17	11.95	0.94	0.04	0.16	1.11	2.93	2.16	0.07	0.02	95.59
11/07/2023	**SG14-4582**	74.76	0.17	11.76	1.07	0.04	0.18	1.28	2.78	1.90	0.11	0.02	94.07

Date of analysis	SG Label	SiO_2	TiO_2	Al_2O3	FeO_t	MnO	MgO	CaO	Na_2O	K_2O	P_2O_5	Cl	Analytical Total
11/07/2023	**SG14-4582**	74.68	0.24	11.81	0.98	0.05	0.20	0.98	3.43	1.97	0.14	0.00	94.47
11/07/2023	**SG14-4582**	75.94	0.14	12.18	1.03	0.02	0.22	1.38	2.95	1.96	0.09	0.00	95.90
04/02/2023	**SG14-4598**	75.51	0.14	11.52	0.93	0.02	0.14	1.11	2.96	3.20	0.03	0.07	95.62
04/02/2023	**SG14-4598**	74.56	0.11	11.49	0.89	0.02	0.14	1.11	3.30	3.23	0.04	0.08	94.97
04/02/2023	**SG14-4598**	74.47	0.13	11.56	0.86	0.03	0.10	1.11	3.20	3.17	0.00	0.10	94.73
04/02/2023	**SG14-4598**	75.04	0.16	11.68	1.07	0.03	0.15	1.24	3.14	3.12	0.00	0.08	95.70
04/02/2023	**SG14-4598**	75.26	0.13	11.72	0.88	0.04	0.12	1.10	3.19	3.23	0.03	0.08	95.79
04/02/2023	**SG14-4598**	74.80	0.17	11.76	1.01	0.04	0.21	1.37	3.35	3.09	0.02	0.09	95.91
04/02/2023	**SG14-4598**	74.09	0.15	11.63	0.97	0.04	0.11	1.23	3.20	3.24	0.02	0.07	94.75
04/02/2023	**SG14-4598**	74.98	0.10	11.73	0.89	0.01	0.15	1.01	3.24	3.29	0.00	0.09	95.49
04/02/2023	**SG14-4598**	74.77	0.16	11.74	0.92	0.00	0.17	1.07	3.27	3.37	0.00	0.08	95.55
04/02/2023	**SG14-4598**	74.30	0.12	11.68	0.93	0.05	0.12	1.00	3.32	3.39	0.00	0.07	94.99
04/02/2023	**SG14-4598**	74.66	0.13	11.76	0.92	0.02	0.15	1.13	3.11	3.21	0.10	0.09	95.28
04/02/2023	**SG14-4598**	74.86	0.15	11.82	0.98	0.04	0.13	1.26	3.14	3.19	0.02	0.09	95.68
04/02/2023	**SG14-4598**	73.99	0.20	11.74	1.04	0.03	0.18	1.43	3.20	2.87	0.02	0.08	94.76
02/06/2023	**SG14-4598**	74.93	0.13	11.90	1.01	0.06	0.20	1.27	3.27	3.10	0.04	0.08	95.99
02/06/2023	**SG14-4598**	74.68	0.18	11.88	1.06	0.04	0.14	1.38	3.32	3.02	0.04	0.08	95.80
02/06/2023	**SG14-4598**	73.26	0.18	11.68	1.12	0.04	0.17	1.26	3.26	3.04	0.05	0.13	94.18
02/06/2023	**SG14-4598**	74.62	0.16	11.87	0.98	0.07	0.14	1.27	3.33	3.17	0.04	0.07	95.71
02/06/2023	**SG14-4598**	74.69	0.15	11.86	1.07	0.01	0.17	1.38	3.21	2.94	0.00	0.08	95.57
02/06/2023	**SG14-4598**	75.10	0.13	11.92	1.13	0.04	0.20	1.41	2.97	2.97	0.00	0.08	95.94
02/06/2023	**SG14-4598**	74.60	0.19	11.93	0.94	0.05	0.16	1.22	3.35	3.18	0.00	0.09	95.72
02/06/2023	**SG14-4598**	73.99	0.16	11.91	1.16	0.00	0.16	1.33	3.10	3.12	0.00	0.07	94.99
02/06/2023	**SG14-4598**	75.62	0.15	12.16	1.02	0.02	0.11	1.41	3.21	3.11	0.04	0.08	96.94
02/06/2023	**SG14-4598**	74.16	0.13	11.97	1.05	0.06	0.22	1.39	3.16	2.89	0.03	0.08	95.15
02/06/2023	**SG14-4598**	73.86	0.21	12.28	1.05	0.00	0.10	1.56	3.01	3.31	0.02	0.07	95.47
11/07/2023	**SG14-4689**	76.77	0.31	10.48	1.23	0.06	0.40	0.64	2.63	2.76	0.09	0.00	95.37
11/07/2023	**SG14-4689**	75.49	0.30	11.04	1.12	0.06	0.33	0.44	2.73	3.32	0.07	0.01	94.91
11/07/2023	**SG14-4689**	76.10	0.23	11.30	0.72	0.03	0.07	0.56	2.64	3.51	0.05	0.04	95.23
11/07/2023	**SG14-4689**	78.86	0.19	11.69	0.87	0.04	0.12	1.51	2.52	2.54	0.06	0.00	98.39

Date of analysis	SG Label	SiO_2	TiO_2	Al_2O3	FeO_t	MnO	MgO	CaO	Na_2O	K_2O	P_2O_5	Cl	Analytical Total
11/07/2023	**SG14-4689**	75.67	0.28	11.64	0.86	0.03	0.16	0.85	2.86	2.96	0.09	0.03	95.42
11/07/2023	**SG14-4689**	75.87	0.25	11.72	0.92	0.05	0.08	1.31	2.91	2.63	0.10	0.00	95.84
11/07/2023	**SG14-4689**	74.30	0.26	11.75	1.10	0.04	0.26	1.76	2.90	3.14	0.08	0.05	95.64
11/07/2023	**SG14-4689**	75.74	0.24	11.79	0.86	0.06	0.07	1.23	2.96	2.66	0.09	0.00	95.70
11/07/2023	**SG14-4689**	75.87	0.30	11.89	0.95	0.03	0.23	0.84	2.56	3.37	0.03	0.00	96.07
11/07/2023	**SG14-4689**	75.23	0.28	11.79	1.00	0.02	0.24	1.09	3.03	2.46	0.11	0.03	95.28
11/07/2023	**SG14-4689**	75.56	0.29	11.83	0.58	0.02	0.02	0.91	2.90	3.00	0.08	0.02	95.20
11/07/2023	**SG14-4689**	77.72	0.30	12.50	1.81	0.04	0.26	1.82	3.75	1.83	0.00	0.00	100.03
11/07/2023	**SG14-4689**	78.35	0.27	12.53	0.55	0.03	0.08	0.80	2.67	3.56	0.03	0.00	98.87
11/07/2023	**SG14-4689**	75.10	0.21	12.07	0.92	0.06	0.11	0.97	3.10	2.53	0.08	0.00	95.15
11/07/2023	**SG14-4689**	77.15	0.20	12.44	0.85	0.02	0.14	0.99	3.13	2.56	0.10	0.00	97.57
11/07/2023	**SG14-4689**	77.49	0.17	12.57	0.87	0.03	0.16	1.18	3.16	2.62	0.09	0.02	98.36
11/07/2023	**SG14-4689**	76.85	0.21	12.51	0.78	0.04	0.14	1.27	3.33	2.59	0.09	0.01	97.83
11/07/2023	**SG14-4689**	77.84	0.21	12.63	0.85	0.03	0.15	1.04	3.21	2.57	0.09	0.01	98.61
11/07/2023	**SG14-4689**	75.68	0.27	12.35	0.64	0.01	0.04	1.03	3.04	3.10	0.01	0.00	96.18
11/07/2023	**SG14-4689**	74.82	0.23	12.25	0.63	0.05	0.12	1.22	2.47	3.15	0.03	0.00	94.97
11/07/2023	**SG14-4689**	74.92	0.25	12.41	0.75	0.01	0.11	0.98	3.02	3.19	0.03	0.00	95.67
11/07/2023	**SG14-4689**	75.06	0.23	12.81	0.84	0.05	0.15	1.52	3.27	2.31	0.07	0.02	96.33
11/07/2023	**SG14-4689**	73.53	0.27	13.55	0.83	0.03	0.19	1.58	3.52	2.71	0.05	0.00	96.26
11/07/2023	**SG14-4689**	74.25	0.15	14.37	0.78	0.00	0.19	2.47	3.55	2.11	0.06	0.01	97.93
11/07/2023	**SG14-4689**	71.92	0.29	15.06	1.09	0.03	0.34	2.60	3.61	2.39	0.02	0.00	97.35
11/07/2023	**SG14-4689**	71.90	0.23	15.45	0.57	0.02	0.02	2.22	3.80	2.76	0.03	0.06	97.06
11/07/2023	**SG14-4689**	72.29	0.16	15.72	0.68	0.03	0.12	2.91	4.07	1.75	0.05	0.01	97.79
11/07/2023	**SG14-4689**	70.15	0.37	15.44	1.02	0.00	0.02	2.23	2.87	2.75	0.06	0.04	94.96
11/07/2023	**SG14-4689**	69.12	0.27	15.80	0.80	0.00	0.07	2.46	3.93	2.34	0.07	0.00	94.87
03/06/2023	**SG14-4748**	69.07	0.36	14.57	2.19	0.09	0.63	2.43	4.65	2.35	0.12	0.37	96.84
03/06/2023	**SG14-4748**	69.22	0.37	14.66	2.29	0.06	0.75	2.66	4.46	2.32	0.13	0.37	97.29
03/06/2023	**SG14-4748**	67.73	0.33	14.41	2.21	0.05	0.64	2.63	4.60	2.32	0.05	0.43	95.40
03/06/2023	**SG14-4748**	70.27	0.32	14.88	2.18	0.04	0.59	2.40	4.75	2.38	0.10	0.40	98.30
03/06/2023	**SG14-4748**	69.55	0.36	14.86	2.12	0.05	0.67	2.53	4.65	2.38	0.13	0.38	97.67
03/06/2023	**SG14-4748**	68.78	0.34	14.82	2.24	0.08	0.73	2.53	4.60	2.38	0.16	0.36	97.01

Date of analysis	SG Label	SiO_2	TiO_2	Al_2O3	FeO_t	MnO	MgO	CaO	Na_2O	K_2O	P_2O_5	Cl	Analytical Total
03/06/2023	**SG14-4748**	69.98	0.37	15.02	2.28	0.05	0.64	2.59	4.31	2.37	0.12	0.35	98.07
03/06/2023	**SG14-4748**	69.22	0.36	14.89	2.08	0.04	0.58	2.34	4.57	2.41	0.10	0.32	96.92
03/06/2023	**SG14-4748**	69.05	0.29	15.09	2.30	0.06	0.72	2.68	4.66	2.33	0.15	0.40	97.73
03/06/2023	**SG14-4748**	68.42	0.35	14.96	2.24	0.08	0.79	2.68	4.49	2.29	0.11	0.34	96.76
03/06/2023	**SG14-4748**	67.96	0.32	15.64	2.02	0.03	0.60	3.05	4.64	2.20	0.06	0.34	96.87
31/05/2023	**SG14-4837**	73.52	0.26	13.11	1.34	0.02	0.21	1.50	3.68	3.94	0.03	0.11	97.73
31/05/2023	**SG14-4837**	72.34	0.22	12.97	1.37	0.06	0.35	1.57	3.60	3.63	0.00	0.11	96.22
31/05/2023	**SG14-4837**	73.40	0.27	13.14	1.32	0.02	0.21	1.45	3.59	3.68	0.04	0.11	97.23
31/05/2023	**SG14-4837**	73.02	0.27	13.11	1.30	0.05	0.24	1.46	3.59	3.66	0.02	0.11	96.84
31/05/2023	**SG14-4837**	73.24	0.32	13.14	1.33	0.06	0.12	1.45	3.46	3.79	0.01	0.11	97.02
31/05/2023	**SG14-4837**	72.40	0.23	13.01	1.29	0.05	0.24	1.54	3.43	3.62	0.02	0.12	95.95
31/05/2023	**SG14-4837**	72.98	0.26	13.13	1.12	0.05	0.09	1.32	3.38	4.33	0.04	0.08	96.78
31/05/2023	**SG14-4837**	71.95	0.27	12.96	1.27	0.05	0.21	1.49	3.37	3.62	0.05	0.10	95.34
31/05/2023	**SG14-4837**	73.29	0.26	13.27	1.45	0.07	0.27	1.62	3.54	3.60	0.02	0.10	97.49
31/05/2023	**SG14-4837**	72.48	0.24	13.21	1.45	0.07	0.30	1.64	3.65	3.53	0.00	0.11	96.70
31/05/2023	**SG14-4837**	71.68	0.25	13.05	1.43	0.06	0.27	1.56	3.54	3.55	0.03	0.12	95.53
31/05/2023	**SG14-4837**	72.12	0.23	13.16	1.50	0.07	0.34	1.57	3.47	3.56	0.02	0.12	96.16
31/05/2023	**SG14-4837**	72.95	0.24	13.32	1.50	0.06	0.32	1.66	3.59	3.55	0.01	0.11	97.31
31/05/2023	**SG14-4837**	72.21	0.23	13.19	1.41	0.05	0.31	1.57	3.51	3.57	0.07	0.10	96.22
31/05/2023	**SG14-4837**	72.10	0.23	13.24	1.46	0.03	0.22	1.62	3.46	3.63	0.03	0.13	96.16
31/05/2023	**SG14-4837**	72.49	0.25	13.66	1.15	0.05	0.16	1.64	3.73	3.55	0.01	0.07	96.78
31/05/2023	**SG14-4837**	74.77	0.25	14.44	1.22	0.04	0.16	1.95	3.89	3.58	0.03	0.09	100.42
07/07/2023	**SG14-4860**	75.97	0.24	11.03	1.11	0.04	0.27	0.49	2.83	4.18	0.05	0.08	96.29
07/07/2023	**SG14-4860**	75.77	0.26	11.26	1.02	0.05	0.15	0.59	2.97	4.22	0.04	0.10	96.43
07/07/2023	**SG14-4860**	74.16	0.17	11.10	1.05	0.07	0.20	0.74	2.98	4.07	0.03	0.09	94.67
07/07/2023	**SG14-4860**	75.05	0.21	11.54	0.93	0.04	0.21	0.79	2.68	4.73	0.04	0.04	96.24
07/07/2023	**SG14-4860**	75.43	0.20	11.65	1.09	0.05	0.23	0.76	2.90	4.07	0.07	0.09	96.54
07/07/2023	**SG14-4860**	75.39	0.25	11.76	1.01	0.07	0.15	0.68	2.93	4.16	0.03	0.09	96.52
07/07/2023	**SG14-4860**	74.54	0.22	11.85	1.49	0.11	0.59	1.07	3.23	3.74	0.08	0.08	96.99
07/07/2023	**SG14-4860**	74.43	0.21	11.77	0.97	0.06	0.08	0.79	3.05	3.96	0.05	0.10	95.47

Date of analysis	SG Label	SiO_2	TiO_2	Al_2O3	FeO_t	MnO	MgO	CaO	Na_2O	K_2O	P_2O_5	Cl	Analytical Total
07/07/2023	**SG14-4860**	75.14	0.21	11.95	0.94	0.03	0.08	0.89	3.18	3.94	0.05	0.12	96.55
07/07/2023	**SG14-4860**	75.38	0.21	12.07	1.03	0.09	0.24	0.88	3.09	3.95	0.06	0.07	97.07
07/07/2023	**SG14-4860**	74.88	0.20	12.22	1.65	0.12	0.57	1.14	3.15	4.04	0.11	0.08	98.17
07/07/2023	**SG14-4860**	74.24	0.21	11.98	1.18	0.07	0.28	1.12	3.10	3.92	0.03	0.09	96.22
07/07/2023	**SG14-4860**	74.48	0.23	12.13	1.19	0.08	0.28	1.12	3.28	3.88	0.00	0.12	96.79
07/07/2023	**SG14-4860**	75.06	0.22	12.29	0.88	0.04	0.06	1.08	2.90	4.22	0.06	0.07	96.88
07/07/2023	**SG14-4860**	73.82	0.24	12.36	1.00	0.05	0.06	1.20	3.30	3.58	0.08	0.10	95.79
07/07/2023	**SG14-4860**	72.54	0.19	12.67	1.08	0.01	0.17	1.15	3.35	3.74	0.03	0.10	95.04
07/07/2023	**SG14-4860**	73.57	0.24	12.91	1.38	0.08	0.28	1.23	3.35	3.64	0.03	0.10	96.80
07/07/2023	**SG14-4860**	74.01	0.23	12.92	0.79	0.07	0.09	1.35	3.53	3.59	0.04	0.11	96.72
07/07/2023	**SG14-4860**	74.81	0.24	13.01	0.70	0.01	0.04	1.24	3.35	3.74	0.04	0.11	97.27
07/07/2023	**SG14-4860**	74.36	0.19	13.01	1.02	0.03	0.16	1.27	3.51	3.63	0.01	0.07	97.27
07/07/2023	**SG14-4860**	74.13	0.24	13.03	1.02	0.05	0.16	1.44	3.56	3.38	0.05	0.08	97.13
07/07/2023	**SG14-4860**	72.92	0.21	12.98	1.11	0.06	0.10	1.31	3.18	3.98	0.05	0.12	96.03
07/07/2023	**SG14-4860**	73.66	0.19	13.16	0.80	0.03	0.05	1.40	3.77	3.64	0.03	0.12	96.84
07/07/2023	**SG14-4860**	72.47	0.20	13.49	1.05	0.04	0.31	1.64	3.86	3.37	0.02	0.10	96.56
07/07/2023	**SG14-4860**	73.08	0.23	13.52	0.82	0.05	0.12	1.62	3.67	3.44	0.03	0.05	96.64
07/07/2023	**SG14-4860**	73.74	0.21	13.74	0.81	0.05	0.20	1.69	4.11	3.12	0.05	0.08	97.80
07/07/2023	**SG14-4860**	72.37	0.21	13.96	0.80	0.05	0.08	1.86	4.04	3.17	0.06	0.09	96.68
07/07/2023	**SG14-4860**	72.05	0.24	14.30	1.01	0.07	0.24	2.16	3.67	3.33	0.01	0.08	97.15
31/05/2023	**SG14-5033**	71.59	0.73	12.96	3.60	0.14	0.78	2.97	4.36	1.08	0.18	0.12	98.52
31/05/2023	**SG14-5033**	72.21	0.68	13.08	3.51	0.11	0.65	2.96	4.66	1.09	0.08	0.11	99.14
31/05/2023	**SG14-5033**	71.17	0.72	12.93	3.57	0.11	0.79	2.90	4.30	1.09	0.16	0.12	97.85
31/05/2023	**SG14-5033**	72.08	0.66	13.15	3.49	0.16	0.76	3.03	4.62	1.07	0.14	0.21	99.37
31/05/2023	**SG14-5033**	71.76	0.71	13.05	3.49	0.13	0.79	2.99	4.29	1.07	0.14	0.12	98.54
31/05/2023	**SG14-5033**	72.14	0.73	13.23	3.63	0.13	0.83	3.07	4.51	1.08	0.21	0.12	99.68
31/05/2023	**SG14-5033**	71.91	0.68	13.17	3.57	0.16	0.78	2.97	4.63	1.03	0.12	0.12	99.13
31/05/2023	**SG14-5033**	71.89	0.70	13.13	3.49	0.11	0.74	2.87	4.48	1.03	0.15	0.11	98.69
31/05/2023	**SG14-5033**	72.56	0.64	13.29	3.56	0.13	0.78	2.94	4.64	1.03	0.14	0.12	99.83
31/05/2023	**SG14-5033**	72.07	0.66	13.21	3.48	0.12	0.73	3.01	4.56	1.09	0.14	0.10	99.17
31/05/2023	**SG14-5033**	70.89	0.67	12.98	3.54	0.12	0.70	2.86	4.31	1.04	0.15	0.13	97.38

Date of analysis	SG Label	SiO_2	TiO_2	Al_2O3	FeO_t	MnO	MgO	CaO	Na_2O	K_2O	P_2O_5	Cl	Analytical Total
31/05/2023	**SG14-5033**	72.43	0.66	13.33	3.66	0.17	0.80	3.15	4.46	1.01	0.12	0.13	99.93
31/05/2023	**SG14-5033**	69.32	0.67	12.91	3.39	0.12	0.81	2.99	4.01	1.02	0.12	0.16	95.53
31/05/2023	**SG14-5033**	70.29	0.62	13.42	3.33	0.12	0.60	3.05	4.30	0.96	0.09	0.14	96.93
24/08/2023	**SG14-5071**	70.65	0.30	14.14	1.21	0.10	0.20	0.79	4.37	4.66	0.05	0.08	96.55
24/08/2023	**SG14-5071**	70.53	0.36	14.20	1.33	0.09	0.29	0.97	4.31	4.57	0.04	0.08	96.77
24/08/2023	**SG14-5071**	71.16	0.31	14.26	1.08	0.09	0.21	0.80	4.31	4.75	0.09	0.07	97.12
24/08/2023	**SG14-5071**	70.18	0.36	14.21	1.31	0.11	0.24	0.93	4.59	4.57	0.04	0.09	96.64
24/08/2023	**SG14-5071**	70.43	0.32	14.25	1.22	0.11	0.25	0.95	4.41	4.57	0.03	0.10	96.64
24/08/2023	**SG14-5071**	70.28	0.35	14.29	1.33	0.11	0.28	0.88	4.56	4.40	0.03	0.12	96.64
24/08/2023	**SG14-5071**	70.13	0.36	14.30	1.42	0.11	0.27	0.94	4.38	4.54	0.03	0.06	96.54
24/08/2023	**SG14-5071**	70.24	0.34	14.30	1.25	0.05	0.25	0.91	4.23	4.48	0.06	0.07	96.18
24/08/2023	**SG14-5071**	69.86	0.38	14.30	1.19	0.09	0.25	0.92	4.59	4.49	0.01	0.09	96.17
24/08/2023	**SG14-5071**	70.36	0.35	14.46	1.43	0.09	0.25	0.93	4.39	4.61	0.03	0.09	97.00
24/08/2023	**SG14-5071**	70.28	0.32	14.41	1.24	0.06	0.29	0.91	4.32	4.52	0.02	0.10	96.48
24/08/2023	**SG14-5071**	69.99	0.34	14.41	1.31	0.09	0.29	0.96	4.29	4.48	0.11	0.14	96.42
24/08/2023	**SG14-5071**	70.41	0.36	14.48	1.22	0.10	0.22	0.94	4.39	4.48	0.09	0.12	96.82
24/08/2023	**SG14-5071**	70.68	0.38	14.58	1.21	0.09	0.22	0.93	4.50	4.48	0.07	0.08	97.21
24/08/2023	**SG14-5071**	69.61	0.35	14.42	1.39	0.12	0.25	1.02	4.37	4.49	0.03	0.09	96.14
24/08/2023	**SG14-5071**	69.58	0.30	14.48	1.27	0.12	0.26	0.94	4.33	4.68	0.08	0.06	96.11
24/08/2023	**SG14-5071**	69.83	0.32	14.57	1.29	0.11	0.29	0.98	4.40	4.48	0.05	0.11	96.41
24/08/2023	**SG14-5071**	69.91	0.30	14.57	1.32	0.13	0.29	0.92	4.23	4.49	0.04	0.12	96.30
24/08/2023	**SG14-5071**	69.34	0.35	14.58	1.37	0.12	0.25	1.00	4.34	4.43	0.04	0.10	95.89
08/02/2023	**SG14-5099**	68.30	0.62	15.00	2.04	0.14	0.61	1.47	4.54	4.31	0.08	0.09	97.21
08/02/2023	**SG14-5099**	66.73	0.73	15.17	2.69	0.13	0.72	1.87	4.36	4.11	0.22	0.09	96.81
08/02/2023	**SG14-5099**	67.84	0.61	15.35	2.27	0.15	0.82	2.04	4.48	3.99	0.17	0.08	97.79
08/02/2023	**SG14-5099**	67.18	0.71	15.85	2.43	0.05	0.65	2.20	4.54	3.65	0.19	0.09	97.54
03/06/2023	**SG14-5099**	66.56	0.72	15.95	2.79	0.12	0.90	2.46	4.45	3.74	0.13	0.08	97.89
03/06/2023	**SG14-5099**	65.44	0.56	16.24	1.49	0.08	0.18	2.46	4.48	3.49	0.06	0.10	94.57
03/06/2023	**SG14-5099**	67.61	0.49	16.94	1.50	0.04	0.27	2.50	4.86	3.68	0.06	0.07	98.02
03/06/2023	**SG14-5099**	66.86	0.54	16.77	1.68	0.08	0.31	2.50	4.55	3.39	0.15	0.06	96.88

Date of analysis	SG Label	SiO_2	TiO_2	Al_2O3	FeO_t	MnO	MgO	CaO	Na_2O	K_2O	P_2O_5	Cl	Analytical Total
03/06/2023	**SG14-5099**	65.77	0.47	17.94	1.61	0.10	0.31	3.14	5.05	3.07	0.05	0.05	97.55
07/07/2023	**SG14-5183**	75.39	0.07	12.25	0.82	0.05	0.03	0.35	4.57	2.65	0.04	0.11	96.35
07/07/2023	**SG14-5183**	73.86	0.08	12.52	0.48	0.08	0.10	0.43	3.35	3.74	0.04	0.06	94.74
07/07/2023	**SG14-5183**	74.60	0.16	12.87	0.93	0.05	0.15	1.03	3.38	3.86	0.05	0.17	97.25
07/07/2023	**SG14-5183**	73.41	0.05	12.74	0.50	0.10	0.12	0.49	3.50	3.90	0.07	0.12	94.99
07/07/2023	**SG14-5183**	72.81	0.05	13.10	0.54	0.07	0.10	0.62	3.86	3.46	0.06	0.06	94.73
07/07/2023	**SG14-5183**	72.67	0.04	13.28	0.47	0.07	0.12	0.58	3.95	3.42	0.09	0.05	94.73
07/07/2023	**SG14-5183**	73.20	0.05	13.35	0.52	0.06	0.09	0.61	3.64	3.49	0.03	0.07	95.12
07/07/2023	**SG14-5221**	67.73	0.55	14.59	2.25	0.11	0.55	1.71	4.45	4.20	0.17	0.09	96.41
07/07/2023	**SG14-5221**	67.80	0.59	14.62	2.15	0.08	0.57	1.71	4.39	4.17	0.12	0.10	96.30
07/07/2023	**SG14-5221**	68.21	0.60	14.69	2.16	0.05	0.55	1.75	4.24	4.26	0.13	0.10	96.75
07/07/2023	**SG14-5221**	67.25	0.63	14.53	2.19	0.09	0.56	1.72	4.28	4.12	0.13	0.08	95.57
07/07/2023	**SG14-5221**	67.14	0.57	14.57	2.19	0.09	0.61	1.69	4.37	4.23	0.16	0.08	95.70
07/07/2023	**SG14-5221**	68.14	0.55	14.74	2.18	0.09	0.61	1.77	4.14	4.20	0.15	0.11	96.68
07/07/2023	**SG14-5221**	67.89	0.58	14.76	2.20	0.10	0.58	1.72	4.37	4.30	0.11	0.14	96.74
07/07/2023	**SG14-5221**	68.68	0.61	14.93	2.16	0.08	0.61	1.72	4.39	4.31	0.12	0.12	97.74
07/07/2023	**SG14-5221**	68.24	0.57	14.85	2.27	0.08	0.61	1.75	4.38	4.16	0.09	0.10	97.10
07/07/2023	**SG14-5221**	68.10	0.67	14.77	2.07	0.09	0.56	1.65	4.20	4.27	0.07	0.07	96.51
07/07/2023	**SG14-5221**	68.71	0.65	15.02	2.22	0.13	0.59	1.69	4.47	4.26	0.14	0.11	97.98
07/07/2023	**SG14-5221**	67.41	0.57	14.66	2.12	0.05	0.55	1.73	4.14	4.17	0.06	0.11	95.57
07/07/2023	**SG14-5221**	67.89	0.59	14.77	2.12	0.06	0.54	1.68	4.27	4.08	0.13	0.10	96.23
07/07/2023	**SG14-5221**	67.69	0.62	14.86	2.07	0.12	0.55	1.69	4.36	4.34	0.06	0.11	96.48
07/07/2023	**SG14-5221**	66.58	0.58	14.61	2.10	0.11	0.57	1.63	4.15	4.08	0.05	0.10	94.58
07/07/2023	**SG14-5221**	67.23	0.57	14.85	2.13	0.13	0.60	1.75	4.35	4.15	0.12	0.08	95.97
07/07/2023	**SG14-5221**	69.35	0.59	15.34	2.16	0.11	0.61	1.83	4.31	4.47	0.12	0.08	98.96
07/07/2023	**SG14-5221**	67.62	0.61	14.90	2.16	0.10	0.59	1.66	3.95	4.07	0.09	0.12	95.85
03/06/2023	**SG14-5367**	73.16	0.06	13.13	0.49	0.07	0.12	0.62	3.78	3.66	0.10	0.06	95.25
03/06/2023	**SG14-5367**	72.63	0.04	13.08	0.46	0.14	0.11	0.68	3.66	3.96	0.03	0.06	94.84
03/06/2023	**SG14-5367**	73.20	0.05	13.16	0.54	0.09	0.08	0.62	3.62	3.71	0.03	0.08	95.17

Date of analysis	SG Label	SiO_2	TiO_2	Al_2O3	FeO_t	MnO	MgO	CaO	Na_2O	K_2O	P_2O_5	Cl	Analytical Total
03/06/2023	**SG14-5367**	73.12	0.04	13.21	0.46	0.09	0.16	0.62	3.81	3.69	0.05	0.07	95.32
03/06/2023	**SG14-5367**	73.06	0.03	13.22	0.49	0.12	0.09	0.66	3.85	3.61	0.12	0.08	95.33
03/06/2023	**SG14-5367**	73.24	0.00	13.25	0.49	0.10	0.13	0.65	3.80	3.62	0.04	0.07	95.40
03/06/2023	**SG14-5367**	72.53	0.02	13.14	0.45	0.07	0.10	0.62	3.78	3.62	0.11	0.07	94.52
03/06/2023	**SG14-5367**	73.14	0.03	13.26	0.49	0.09	0.12	0.64	3.79	3.65	0.05	0.06	95.32
03/06/2023	**SG14-5367**	72.62	0.07	13.22	0.43	0.09	0.13	0.61	3.98	3.74	0.00	0.05	94.94
03/06/2023	**SG14-5367**	72.36	0.07	13.15	0.51	0.08	0.09	0.61	3.45	3.77	0.04	0.09	94.24
03/06/2023	**SG14-5367**	72.70	0.03	13.27	0.56	0.08	0.14	0.64	3.91	3.62	0.07	0.05	95.09
03/06/2023	**SG14-5367**	72.75	0.08	13.30	0.43	0.10	0.09	0.64	3.93	3.73	0.00	0.08	95.12
03/06/2023	**SG14-5367**	73.00	0.08	13.31	0.37	0.06	0.10	0.83	3.11	3.79	0.11	0.08	94.86
03/06/2023	**SG14-5367**	72.61	0.07	13.38	0.51	0.08	0.11	0.62	3.74	3.64	0.09	0.07	94.91
03/06/2023	**SG14-5367**	72.71	0.07	13.44	0.47	0.09	0.13	0.61	3.67	3.71	0.06	0.05	95.00
03/06/2023	**SG14-5367**	72.76	0.00	13.51	0.49	0.09	0.13	0.65	3.63	3.69	0.11	0.06	95.12
02/12/2023	**SG14-5406**	75.50	0.09	11.35	0.79	0.12	0.19	0.73	2.97	4.13	0.03	0.09	95.97
02/12/2023	**SG14-5406**	77.31	0.11	11.69	0.57	0.06	0.05	0.78	3.01	4.30	0.07	0.08	98.01
02/12/2023	**SG14-5406**	76.50	0.12	11.71	0.55	0.07	0.05	0.76	2.42	4.31	0.02	0.07	96.57
02/12/2023	**SG14-5406**	76.28	0.14	11.83	0.65	0.09	0.07	0.86	2.87	3.92	0.07	0.13	96.92
02/12/2023	**SG14-5406**	75.46	0.04	12.09	0.53	0.09	0.05	0.82	2.94	4.24	0.07	0.08	96.40
02/12/2023	**SG14-5406**	74.52	0.10	12.24	0.66	0.10	0.07	1.10	3.18	3.94	0.03	0.13	96.07
02/12/2023	**SG14-5406**	75.36	0.08	12.66	0.45	0.07	0.02	1.15	3.40	3.75	0.06	0.08	97.08
02/12/2023	**SG14-5406**	74.20	0.09	12.55	0.75	0.07	0.10	1.22	3.48	3.65	0.01	0.09	96.19
02/12/2023	**SG14-5406**	74.10	0.09	13.11	0.51	0.08	0.06	1.22	3.17	3.73	0.06	0.10	96.23
02/12/2023	**SG14-5406**	73.50	0.10	13.17	0.67	0.07	0.08	1.38	3.60	3.46	0.05	0.11	96.19
22/07/2023	**SG14-5469**	71.36	0.60	12.19	2.36	0.12	0.47	1.90	3.89	2.63	0.07	0.10	95.69
22/07/2023	**SG14-5469**	71.31	0.56	12.63	2.25	0.10	0.48	1.90	3.85	2.68	0.06	0.11	95.92
22/07/2023	**SG14-5469**	71.60	0.57	12.78	2.27	0.12	0.50	1.85	3.86	2.55	0.03	0.11	96.25
22/07/2023	**SG14-5469**	72.07	0.58	12.77	2.23	0.09	0.48	1.93	3.10	2.52	0.05	0.11	95.94
22/07/2023	**SG14-5469**	72.05	0.58	12.74	2.43	0.11	0.50	2.04	2.36	2.64	0.07	0.10	95.63
22/07/2023	**SG14-5469**	71.12	0.54	12.82	2.34	0.09	0.54	1.98	3.82	2.60	0.07	0.09	96.01
22/07/2023	**SG14-5469**	71.14	0.57	12.81	2.30	0.09	0.49	1.91	3.77	2.54	0.08	0.14	95.84

Date of analysis	SG Label	SiO_2	TiO_2	Al_2O3	FeO_t	MnO	MgO	CaO	Na_2O	K_2O	P_2O_5	Cl	Analytical Total
22/07/2023	**SG14-5469**	72.36	0.59	12.95	2.30	0.10	0.52	1.92	2.75	2.62	0.10	0.12	96.33
22/07/2023	**SG14-5469**	71.71	0.60	12.81	2.36	0.05	0.53	1.96	2.31	2.63	0.06	0.09	95.12
22/07/2023	**SG14-5469**	72.08	0.57	12.91	2.29	0.07	0.50	2.00	2.15	2.62	0.05	0.13	95.38
22/07/2023	**SG14-5469**	71.20	0.59	12.82	2.27	0.11	0.54	2.03	2.19	2.56	0.08	0.13	94.51
22/07/2023	**SG14-5469**	70.77	0.70	12.88	2.53	0.07	0.52	1.93	2.73	2.58	0.08	0.12	94.92
22/07/2023	**SG14-5469**	72.71	0.58	13.09	2.42	0.09	0.49	1.99	1.74	2.60	0.08	0.09	95.88
22/07/2023	**SG14-5469**	71.92	0.54	12.94	2.28	0.10	0.50	1.91	1.84	2.54	0.05	0.12	94.76
22/07/2023	**SG14-5469**	71.72	0.55	13.07	2.36	0.07	0.49	1.97	2.51	2.66	0.07	0.09	95.56
22/07/2023	**SG14-5469**	72.11	0.57	12.97	2.31	0.10	0.47	1.96	1.27	2.58	0.05	0.12	94.52
07/07/2023	**SG14-5520**	70.26	0.62	12.32	2.23	0.11	0.52	1.97	3.77	2.63	0.06	0.12	94.60
07/07/2023	**SG14-5520**	71.24	0.55	12.56	2.23	0.08	0.52	1.90	3.87	2.87	0.11	0.09	96.02
07/07/2023	**SG14-5520**	71.18	0.57	12.54	2.15	0.08	0.51	2.00	3.84	2.71	0.08	0.10	95.78
07/07/2023	**SG14-5520**	70.48	0.56	12.50	2.34	0.09	0.50	2.03	3.83	2.66	0.08	0.11	95.19
07/07/2023	**SG14-5520**	69.87	0.58	12.41	2.20	0.07	0.52	1.95	3.80	2.74	0.09	0.13	94.35
07/07/2023	**SG14-5520**	71.32	0.56	12.76	2.38	0.07	0.56	2.07	3.98	2.77	0.13	0.10	96.69
07/07/2023	**SG14-5520**	71.72	0.62	12.87	2.39	0.09	0.53	2.00	3.95	2.73	0.01	0.11	97.03
07/07/2023	**SG14-5520**	70.33	0.55	12.66	2.25	0.08	0.49	2.01	3.93	2.77	0.06	0.11	95.24
07/07/2023	**SG14-5520**	71.24	0.56	12.87	2.20	0.07	0.51	2.03	3.93	2.82	0.17	0.12	96.53
07/07/2023	**SG14-5520**	70.89	0.50	12.82	2.27	0.08	0.48	1.90	3.87	2.70	0.09	0.10	95.71
02/12/2023	**SG14-5563A**	73.98	0.18	12.81	0.99	0.03	0.25	1.40	3.84	2.95	0.10	0.14	96.67
02/12/2023	**SG14-5563A**	72.92	0.17	12.69	0.83	0.04	0.13	1.43	3.82	2.87	0.09	0.15	95.15
02/12/2023	**SG14-5563A**	74.14	0.20	13.14	0.73	0.03	0.10	1.51	3.70	3.03	0.04	0.13	96.74
02/12/2023	**SG14-5563B**	75.12	0.23	11.89	0.99	0.05	0.17	0.86	3.64	3.17	0.06	0.20	96.38
02/12/2023	**SG14-5563B**	74.06	0.23	11.76	1.09	0.06	0.29	0.96	3.52	3.14	0.06	0.16	95.32
02/12/2023	**SG14-5563B**	75.65	0.21	12.01	1.03	0.01	0.22	0.88	3.40	3.22	0.04	0.22	96.89
02/12/2023	**SG14-5563B**	74.30	0.20	11.88	0.99	0.01	0.14	1.00	3.23	3.07	0.06	0.21	95.10
31/05/2023	**SG14-5575**	75.91	0.07	11.66	0.90	0.12	0.02	0.27	4.32	2.76	0.04	0.09	96.15
31/05/2023	**SG14-5575**	75.40	0.03	11.78	0.93	0.07	0.07	0.28	4.44	2.83	0.03	0.11	95.98
31/05/2023	**SG14-5575**	75.37	0.06	12.02	0.80	0.07	0.06	0.39	4.87	2.65	0.03	0.11	96.42

Date of analysis	SG Label	SiO_2	TiO_2	Al_2O3	FeO_t	MnO	MgO	CaO	Na_2O	K_2O	P_2O_5	Cl	Analytical Total
31/05/2023	**SG14-5575**	75.97	0.07	12.08	0.84	0.08	0.00	0.25	4.31	2.79	0.00	0.13	96.51
31/05/2023	**SG14-5575**	73.86	0.06	11.88	0.84	0.10	0.05	0.36	4.71	2.72	0.05	0.11	94.75
31/05/2023	**SG14-5575**	75.15	0.05	12.08	0.90	0.10	0.06	0.32	4.70	2.66	0.03	0.12	96.17
31/05/2023	**SG14-5575**	74.68	0.07	11.99	0.89	0.09	0.01	0.31	4.53	2.73	0.05	0.10	95.44
31/05/2023	**SG14-5575**	75.54	0.08	12.15	0.82	0.09	0.04	0.30	4.55	2.92	0.00	0.12	96.62
31/05/2023	**SG14-5575**	74.83	0.07	12.04	0.90	0.09	0.03	0.29	4.60	2.64	0.04	0.10	95.65
31/05/2023	**SG14-5575**	75.94	0.03	12.22	0.83	0.11	0.04	0.31	4.48	2.71	0.03	0.11	96.81
31/05/2023	**SG14-5575**	74.45	0.07	12.06	0.84	0.06	0.00	0.33	4.80	2.78	0.01	0.13	95.52
31/05/2023	**SG14-5575**	74.40	0.06	12.05	0.98	0.09	0.02	0.36	4.47	2.77	0.03	0.11	95.33
31/05/2023	**SG14-5575**	74.46	0.07	12.07	0.81	0.09	0.00	0.37	4.87	2.55	0.03	0.09	95.41
31/05/2023	**SG14-5575**	75.24	0.05	12.19	0.81	0.07	0.01	0.34	4.55	2.78	0.07	0.13	96.23
31/05/2023	**SG14-5575**	73.70	0.06	11.97	0.81	0.08	0.00	0.36	4.69	2.73	0.00	0.12	94.51
31/05/2023	**SG14-5575**	74.68	0.06	12.16	0.94	0.07	0.02	0.37	4.56	2.88	0.01	0.11	95.86
31/05/2023	**SG14-5575**	74.44	0.01	12.09	0.91	0.11	0.03	0.30	4.39	2.82	0.02	0.14	95.26
31/05/2023	**SG14-5575**	75.24	0.06	12.20	0.83	0.08	0.05	0.34	4.48	2.65	0.02	0.14	96.09
31/05/2023	**SG14-5575**	75.19	0.06	12.24	0.87	0.06	0.06	0.33	4.69	2.66	0.02	0.10	96.28
31/05/2023	**SG14-5575**	74.37	0.00	12.08	0.81	0.05	0.03	0.33	4.54	2.64	0.06	0.13	95.03
31/05/2023	**SG14-5575**	73.98	0.10	12.01	0.81	0.09	0.04	0.35	4.21	2.76	0.01	0.12	94.49
31/05/2023	**SG14-5575**	74.30	0.06	12.09	0.84	0.10	0.02	0.33	4.53	2.64	0.03	0.14	95.08
31/05/2023	**SG14-5575**	73.44	0.07	12.05	0.84	0.07	0.02	0.40	4.89	2.83	0.02	0.10	94.72
31/05/2023	**SG14-5575**	74.93	0.05	12.27	0.85	0.09	0.06	0.39	4.96	2.69	0.00	0.10	96.40
22/11/2023	**SG14-5575**	73.90	0.07	12.06	0.81	0.08	0.05	0.32	4.51	2.67	0.00	0.14	94.60
22/11/2023	**SG14-5575**	74.37	0.09	12.18	0.85	0.08	0.02	0.33	4.76	2.73	0.00	0.08	95.48
22/11/2023	**SG14-5575**	75.31	0.07	12.35	0.83	0.10	0.01	0.34	4.86	2.60	0.08	0.12	96.67
22/11/2023	**SG14-5575**	74.57	0.08	12.27	0.87	0.05	0.02	0.36	4.80	2.70	0.00	0.14	95.85
22/11/2023	**SG14-5575**	74.69	0.05	12.28	0.83	0.09	0.05	0.33	4.68	2.64	0.10	0.12	95.86
22/11/2023	**SG14-5575**	74.95	0.06	12.31	0.83	0.05	0.03	0.34	4.63	2.77	0.01	0.12	96.10
22/11/2023	**SG14-5575**	74.88	0.08	12.34	0.90	0.09	0.02	0.39	4.80	2.64	0.01	0.09	96.25
22/11/2023	**SG14-5575**	74.62	0.11	12.32	0.90	0.08	0.06	0.39	4.69	2.71	0.05	0.11	96.05
22/11/2023	**SG14-5575**	74.51	0.07	12.29	0.89	0.10	0.03	0.37	4.57	2.78	0.02	0.13	95.76
22/11/2023	**SG14-5575**	75.01	0.05	12.33	0.86	0.10	0.00	0.39	4.61	2.58	0.02	0.13	96.10
22/11/2023	**SG14-5575**	74.72	0.08	12.30	0.79	0.09	0.02	0.34	4.71	2.68	0.00	0.12	95.86

Date of analysis	SG Label	SiO_2	TiO_2	Al_2O3	FeO_t	MnO	MgO	CaO	Na_2O	K_2O	P_2O_5	Cl	Analytical Total
22/11/2023	**SG14-5575**	75.23	0.10	12.42	0.83	0.11	0.06	0.33	4.61	2.83	0.06	0.12	96.70
22/11/2023	**SG14-5575**	74.66	0.08	12.32	0.85	0.10	0.00	0.35	4.86	2.55	0.04	0.11	95.92
22/11/2023	**SG14-5575**	74.23	0.04	12.27	0.76	0.09	0.08	0.35	4.76	2.68	0.05	0.11	95.41
22/11/2023	**SG14-5575**	74.70	0.05	12.28	0.81	0.07	0.02	0.37	4.38	2.71	0.00	0.11	95.51
22/11/2023	**SG14-5575**	74.01	0.05	12.24	0.83	0.11	0.06	0.35	4.75	2.53	0.05	0.12	95.08
22/11/2023	**SG14-5575**	75.24	0.07	12.42	0.81	0.10	0.00	0.35	4.67	2.60	0.04	0.09	96.41
22/11/2023	**SG14-5575**	74.84	0.07	12.39	0.80	0.11	0.08	0.35	4.82	2.60	0.01	0.10	96.17
22/11/2023	**SG14-5575**	75.37	0.06	12.47	0.84	0.09	0.04	0.35	4.67	2.70	0.00	0.13	96.70
22/11/2023	**SG14-5575**	74.00	0.04	12.24	0.85	0.09	0.04	0.35	4.37	2.70	0.00	0.14	94.82
22/11/2023	**SG14-5575**	74.73	0.04	12.39	0.86	0.08	0.06	0.38	4.76	2.55	0.01	0.10	95.96
22/11/2023	**SG14-5575**	76.01	0.04	12.58	0.85	0.12	0.02	0.33	4.50	2.69	0.07	0.11	97.31
22/11/2023	**SG14-5575**	74.40	0.09	12.39	0.90	0.11	0.07	0.40	4.70	2.60	0.00	0.11	95.77
22/11/2023	**SG14-5575**	75.35	0.06	12.56	0.89	0.07	0.02	0.35	4.81	2.68	0.00	0.11	96.90
22/11/2023	**SG14-5575**	75.15	0.06	12.52	0.86	0.12	0.05	0.35	4.56	2.74	0.04	0.11	96.58
22/11/2023	**SG14-5575**	74.25	0.06	12.38	0.83	0.09	0.01	0.36	4.66	2.71	0.01	0.11	95.48
22/11/2023	**SG14-5575**	74.04	0.02	12.39	0.91	0.10	0.03	0.34	4.35	2.81	0.00	0.14	95.12
22/11/2023	**SG14-5575**	74.71	0.05	12.52	0.91	0.05	0.02	0.38	4.64	2.53	0.03	0.09	95.92
22/11/2023	**SG14-5575**	73.26	0.07	12.38	0.87	0.08	0.04	0.38	4.69	2.66	0.00	0.11	94.54
03/06/2023	**SG14-5579**	68.42	0.43	14.02	1.43	0.09	0.28	1.12	4.20	4.90	0.09	0.09	95.06
03/06/2023	**SG14-5579**	68.81	0.38	14.43	1.44	0.10	0.29	1.06	4.27	4.92	0.05	0.10	95.85
03/06/2023	**SG14-5579**	68.25	0.39	14.43	1.56	0.09	0.36	1.21	4.23	4.84	0.09	0.10	95.55
03/06/2023	**SG14-5579**	68.79	0.43	14.48	1.39	0.07	0.38	1.11	4.12	4.92	0.06	0.10	95.86
03/06/2023	**SG14-5579**	68.78	0.37	14.45	1.49	0.04	0.33	1.05	4.13	4.82	0.04	0.12	95.62
03/06/2023	**SG14-5579**	68.31	0.45	14.47	1.58	0.10	0.37	1.13	4.14	4.84	0.09	0.10	95.58
03/06/2023	**SG14-5579**	68.24	0.44	14.63	1.64	0.14	0.43	1.24	4.26	4.82	0.04	0.11	95.98
03/06/2023	**SG14-5579**	68.30	0.41	14.65	1.57	0.07	0.44	1.23	4.20	4.89	0.00	0.10	95.86
03/06/2023	**SG14-5579**	68.16	0.39	14.44	1.42	0.09	0.30	1.03	3.72	4.77	0.06	0.12	94.51
03/06/2023	**SG14-5579**	67.88	0.42	14.55	1.63	0.10	0.37	1.21	4.01	4.86	0.10	0.10	95.21
03/06/2023	**SG14-5579**	68.10	0.42	14.67	1.45	0.06	0.33	1.17	4.27	4.97	0.06	0.09	95.59
03/06/2023	**SG14-5579**	68.66	0.45	14.84	1.53	0.08	0.43	1.22	4.41	4.86	0.09	0.10	96.66
03/06/2023	**SG14-5579**	69.10	0.47	14.87	1.66	0.05	0.37	1.29	4.05	4.75	0.08	0.09	96.78

Date of analysis	SG Label	SiO_2	TiO_2	Al_2O3	FeO_t	MnO	MgO	CaO	Na_2O	K_2O	P_2O_5	Cl	Analytical Total
03/06/2023	**SG14-5579**	68.56	0.39	14.81	1.68	0.10	0.35	1.25	4.13	4.85	0.08	0.09	96.28
03/06/2023	**SG14-5579**	68.07	0.45	14.73	1.60	0.10	0.44	1.23	4.15	4.81	0.00	0.12	95.69
03/06/2023	**SG14-5579**	68.05	0.40	14.72	1.52	0.10	0.41	1.26	4.12	4.83	0.04	0.09	95.51
03/06/2023	**SG14-5579**	68.57	0.42	14.74	1.59	0.07	0.35	1.09	3.94	4.68	0.04	0.12	95.62
03/06/2023	**SG14-5579**	69.14	0.45	14.97	1.65	0.10	0.42	1.25	4.09	4.79	0.05	0.08	96.99
03/06/2023	**SG14-5579**	67.96	0.45	14.75	1.63	0.08	0.39	1.19	4.16	4.70	0.03	0.12	95.45
03/06/2023	**SG14-5579**	68.57	0.43	14.93	1.55	0.08	0.40	1.32	4.08	4.90	0.09	0.10	96.44
03/06/2023	**SG14-5579**	69.10	0.36	14.82	1.51	0.06	0.32	1.16	3.53	4.70	0.04	0.12	95.72
03/06/2023	**SG14-5579**	68.40	0.50	14.93	1.56	0.09	0.39	1.24	4.30	4.78	0.01	0.10	96.30
03/06/2023	**SG14-5597**	73.60	0.26	12.36	2.45	0.10	0.24	1.86	4.65	1.25	0.06	0.15	96.98
03/06/2023	**SG14-5597**	73.79	0.28	12.70	2.08	0.08	0.29	1.79	4.83	1.10	0.02	0.13	97.08
03/06/2023	**SG14-5597**	73.11	0.48	13.71	2.94	0.13	0.54	2.67	4.86	1.00	0.13	0.16	99.73
03/06/2023	**SG14-5597**	71.51	0.51	13.66	3.14	0.14	0.73	3.03	4.90	0.95	0.14	0.12	98.84
03/06/2023	**SG14-5597**	69.14	0.45	13.14	2.92	0.09	0.51	2.58	4.54	0.97	0.04	0.19	94.58
03/06/2023	**SG14-5597**	72.88	0.47	13.85	2.89	0.15	0.56	2.64	4.80	1.06	0.04	0.14	99.49
03/06/2023	**SG14-5597**	71.09	0.41	13.68	2.76	0.12	0.59	2.71	4.71	0.99	0.10	0.15	97.30
03/06/2023	**SG14-5597**	71.66	0.50	13.89	3.05	0.18	0.63	2.75	4.81	1.01	0.13	0.16	98.80
03/06/2023	**SG14-5597**	71.37	0.48	13.84	2.86	0.12	0.58	2.53	4.74	0.98	0.02	0.17	97.69
03/06/2023	**SG14-5597**	70.02	0.47	13.62	2.89	0.14	0.53	2.60	4.48	0.93	0.10	0.19	95.97
03/06/2023	**SG14-5597**	72.32	0.52	14.33	3.13	0.12	0.67	2.95	4.92	0.92	0.08	0.16	100.12
03/06/2023	**SG14-5597**	71.81	0.63	14.38	3.25	0.14	0.77	3.19	4.82	0.97	0.10	0.15	100.22
03/06/2023	**SG14-5597**	72.04	0.56	14.40	3.11	0.12	0.70	2.93	4.79	0.96	0.16	0.12	99.89
03/06/2023	**SG14-5616**	72.39	0.36	12.06	1.76	0.04	0.42	2.10	3.08	2.00	0.08	0.17	94.46
03/06/2023	**SG14-5616**	72.94	0.31	12.07	1.71	0.03	0.38	2.14	3.14	2.08	0.09	0.13	95.02
03/06/2023	**SG14-5616**	72.59	0.38	12.27	1.89	0.02	0.39	2.08	3.31	2.07	0.01	0.15	95.14
03/06/2023	**SG14-5616**	73.00	0.35	12.45	1.80	0.06	0.39	2.28	3.29	2.00	0.04	0.16	95.83
03/06/2023	**SG14-5616**	73.52	0.38	12.22	1.78	0.04	0.41	2.13	3.20	2.08	0.07	0.12	95.96
03/06/2023	**SG14-5616**	74.15	0.34	12.05	1.71	0.05	0.34	2.02	3.35	2.08	0.08	0.14	96.31
03/06/2023	**SG14-5616**	74.21	0.39	12.04	1.59	0.06	0.34	2.03	3.58	2.20	0.01	0.12	96.58
03/06/2023	**SG14-5616**	74.97	0.31	12.39	1.69	0.03	0.38	2.03	3.30	2.10	0.05	0.12	97.36

Date of analysis	SG Label	SiO_2	TiO_2	Al_2O3	FeO_t	MnO	MgO	CaO	Na_2O	K_2O	P_2O_5	Cl	Analytical Total
03/06/2023	**SG14-5616**	73.95	0.33	12.11	1.76	0.04	0.41	2.04	3.60	2.00	0.07	0.12	96.43
03/06/2023	**SG14-5616**	72.31	0.35	12.04	1.61	0.09	0.31	1.95	3.37	2.08	0.04	0.16	94.32
03/06/2023	**SG14-5616**	74.90	0.32	12.50	1.81	0.08	0.41	2.20	3.43	2.28	0.03	0.07	98.05
22/11/2023	**SG14-5648**	66.71	0.67	14.57	2.42	0.10	0.60	1.75	4.14	4.70	0.16	0.09	95.91
22/11/2023	**SG14-5648**	67.13	0.67	14.78	2.22	0.09	0.57	1.92	4.42	4.71	0.44	0.10	97.05
22/11/2023	**SG14-5648**	66.97	0.63	14.70	2.48	0.12	0.66	1.77	4.29	4.56	0.18	0.09	96.46
22/11/2023	**SG14-5648**	67.21	0.64	14.77	2.43	0.09	0.63	1.77	4.24	4.49	0.28	0.11	96.66
22/11/2023	**SG14-5648**	66.61	0.67	14.61	2.39	0.10	0.64	1.73	4.15	4.48	0.07	0.09	95.55
22/11/2023	**SG14-5648**	67.94	0.66	14.92	2.34	0.11	0.66	1.73	4.17	4.60	0.28	0.09	97.51
22/11/2023	**SG14-5648**	66.33	0.64	14.61	2.41	0.08	0.63	1.74	4.13	4.56	0.21	0.10	95.44
22/11/2023	**SG14-5648**	66.87	0.68	14.76	2.44	0.10	0.68	1.69	4.35	4.55	0.16	0.09	96.37
22/11/2023	**SG14-5648**	67.51	0.68	14.87	2.49	0.12	0.63	1.74	4.23	4.56	0.14	0.09	97.06
22/11/2023	**SG14-5648**	66.59	0.64	14.69	2.42	0.06	0.66	1.70	4.31	4.54	0.17	0.11	95.90
22/11/2023	**SG14-5648**	67.50	0.61	14.93	2.54	0.02	0.63	1.71	4.47	4.65	0.19	0.09	97.34
22/11/2023	**SG14-5648**	66.45	0.64	14.74	2.56	0.10	0.68	1.74	4.21	4.57	0.28	0.10	96.08
22/11/2023	**SG14-5648**	66.32	0.67	14.66	2.34	0.10	0.67	1.76	4.29	4.50	0.15	0.09	95.55
22/11/2023	**SG14-5648**	67.92	0.62	15.01	2.40	0.06	0.56	1.71	4.49	4.74	0.18	0.09	97.79
22/11/2023	**SG14-5648**	66.53	0.64	14.75	2.44	0.11	0.66	1.76	4.04	4.81	0.24	0.09	96.05
22/11/2023	**SG14-5648**	66.56	0.70	14.81	2.58	0.11	0.66	1.84	4.37	4.39	0.31	0.08	96.40
22/11/2023	**SG14-5648**	66.91	0.69	14.90	2.68	0.12	0.67	1.83	4.36	4.53	0.18	0.10	96.98
22/11/2023	**SG14-5648**	67.38	0.70	14.98	2.56	0.10	0.69	1.89	4.26	4.59	0.20	0.10	97.45
22/11/2023	**SG14-5648**	67.67	0.66	15.03	2.32	0.10	0.66	1.74	4.36	4.69	0.16	0.08	97.48
22/11/2023	**SG14-5648**	67.49	0.60	14.90	2.25	0.10	0.63	1.64	4.17	4.58	0.17	0.09	96.62
22/11/2023	**SG14-5648**	66.88	0.64	14.90	2.44	0.11	0.69	1.87	4.25	4.52	0.21	0.10	96.61
22/11/2023	**SG14-5648**	66.52	0.71	14.74	2.35	0.07	0.64	1.72	4.10	4.41	0.17	0.10	95.53
22/11/2023	**SG14-5648**	66.89	0.62	14.83	2.46	0.11	0.59	1.66	4.18	4.60	0.09	0.08	96.12
22/11/2023	**SG14-5648**	66.85	0.61	14.92	2.49	0.10	0.65	1.82	4.34	4.47	0.14	0.08	96.48
22/11/2023	**SG14-5648**	66.97	0.69	15.00	2.60	0.12	0.65	1.82	4.27	4.51	0.17	0.09	96.89
22/11/2023	**SG14-5648**	65.98	0.70	14.80	2.45	0.07	0.65	1.80	4.37	4.42	0.11	0.09	95.44
22/11/2023	**SG14-5648**	67.14	0.62	15.03	2.45	0.07	0.65	1.84	4.40	4.35	0.20	0.10	96.86
22/11/2023	**SG14-5648**	66.97	0.63	15.11	2.51	0.13	0.71	1.96	4.51	4.52	0.28	0.09	97.42

Date of analysis	SG Label	SiO_2	TiO_2	Al_2O3	FeO_t	MnO	MgO	CaO	Na_2O	K_2O	P_2O_5	Cl	Analytical Total
22/11/2023	**SG14-5648**	66.89	0.59	14.98	2.34	0.10	0.63	1.78	4.16	4.62	0.25	0.09	96.43
22/11/2023	**SG14-5648**	66.37	0.67	14.87	2.28	0.06	0.59	1.77	4.12	4.74	0.22	0.08	95.75
22/11/2023	**SG14-5648**	66.46	0.69	15.00	2.50	0.08	0.73	1.94	4.26	4.50	0.24	0.10	96.51
22/11/2023	**SG14-5648**	66.33	0.65	14.82	2.26	0.09	0.58	1.70	4.08	4.70	0.10	0.08	95.39
22/11/2023	**SG14-5648**	66.61	0.74	15.00	2.35	0.11	0.64	1.82	4.33	4.54	0.19	0.10	96.44
22/11/2023	**SG14-5648**	66.51	0.67	15.02	2.45	0.11	0.70	1.85	4.31	4.52	0.28	0.07	96.49
22/11/2023	**SG14-5648**	65.72	0.71	14.90	2.56	0.10	0.70	1.91	4.28	4.48	0.21	0.06	95.64
22/11/2023	**SG14-5648**	67.00	0.62	15.21	2.61	0.11	0.77	1.92	4.31	4.52	0.21	0.09	97.39
22/11/2023	**SG14-5648**	67.43	0.70	15.27	2.50	0.13	0.71	2.02	4.32	4.46	0.12	0.08	97.72
22/11/2023	**SG14-5648**	66.60	0.66	15.15	2.61	0.10	0.66	1.99	4.20	4.59	0.14	0.09	96.79
22/11/2023	**SG14-5648**	66.19	0.77	15.10	2.48	0.08	0.77	2.18	4.14	4.58	0.13	0.09	96.51
22/11/2023	**SG14-5648**	65.16	0.65	14.85	2.48	0.10	0.67	1.78	4.28	4.33	0.18	0.12	94.60
03/02/2023	**SG14-5851**	69.68	0.74	14.56	4.00	0.18	1.07	3.96	4.92	0.97	0.19	0.14	100.40
03/02/2023	**SG14-5851**	68.19	0.71	14.35	4.20	0.14	1.05	3.82	4.86	0.90	0.15	0.15	98.52
03/02/2023	**SG14-5851**	69.56	0.75	14.66	4.11	0.15	1.05	3.93	4.97	0.96	0.10	0.17	100.42
03/02/2023	**SG14-5851**	69.47	0.74	14.60	4.03	0.12	1.05	3.91	4.88	0.89	0.12	0.15	99.95
03/02/2023	**SG14-5851**	69.06	0.66	14.60	3.96	0.17	1.03	3.74	5.25	0.97	0.13	0.15	99.72
03/02/2023	**SG14-5851**	67.62	0.71	14.33	3.79	0.14	1.10	3.72	5.15	0.93	0.12	0.14	97.74
03/02/2023	**SG14-5851**	67.97	0.71	14.33	3.97	0.13	1.00	3.70	4.64	0.90	0.16	0.15	97.66
03/02/2023	**SG14-5851**	67.38	0.64	14.25	3.92	0.16	1.02	3.78	4.64	0.91	0.19	0.14	97.03
03/02/2023	**SG14-5851**	68.77	0.71	14.57	3.87	0.14	1.04	3.77	5.02	0.95	0.15	0.15	99.14
03/02/2023	**SG14-5851**	68.82	0.69	14.63	4.02	0.14	1.04	3.82	4.93	0.94	0.09	0.15	99.26
03/02/2023	**SG14-5851**	68.89	0.71	14.81	3.97	0.15	1.08	3.83	4.81	0.94	0.12	0.13	99.43
31/05/2023	**SG14-5932**	70.41	0.72	13.16	3.27	0.10	0.79	2.80	3.78	2.59	0.14	0.10	97.85
31/05/2023	**SG14-5932**	69.22	0.80	13.02	3.48	0.05	0.78	2.75	3.71	2.59	0.12	0.06	96.57
31/05/2023	**SG14-5932**	70.57	0.81	13.29	3.49	0.13	0.78	2.91	3.88	2.60	0.02	0.07	98.55
31/05/2023	**SG14-5932**	66.98	0.76	12.75	3.56	0.12	0.85	3.07	3.59	2.43	0.14	0.14	94.39
31/05/2023	**SG14-5932**	69.90	0.74	13.15	3.29	0.09	0.83	3.00	3.56	2.53	0.00	0.10	97.19
31/05/2023	**SG14-5932**	71.01	0.75	13.45	3.50	0.06	0.84	2.89	3.79	2.72	0.00	0.10	99.11
31/05/2023	**SG14-5932**	70.48	0.81	13.36	3.45	0.11	0.84	2.80	3.78	2.62	0.00	0.07	98.32

Date of analysis	SG Label	SiO_2	TiO_2	Al_2O3	FeO_t	MnO	MgO	CaO	Na_2O	K_2O	P_2O_5	Cl	Analytical Total
31/05/2023	**SG14-5932**	70.86	0.74	13.44	3.48	0.08	0.84	2.83	3.63	2.61	0.00	0.09	98.61
31/05/2023	**SG14-5932**	69.27	0.71	13.19	3.46	0.09	0.84	2.86	3.66	2.58	0.02	0.09	96.75
31/05/2023	**SG14-5932**	71.23	0.73	13.51	3.32	0.08	0.79	2.84	3.78	2.66	0.03	0.10	99.08
31/05/2023	**SG14-5932**	69.20	0.71	13.21	3.38	0.08	0.79	2.93	3.72	2.54	0.13	0.10	96.80
31/05/2023	**SG14-5932**	70.78	0.73	13.44	3.41	0.12	0.75	2.72	3.73	2.68	0.00	0.11	98.48
31/05/2023	**SG14-5932**	70.50	0.72	13.44	3.38	0.04	0.78	2.94	3.86	2.60	0.00	0.09	98.35
31/05/2023	**SG14-5932**	71.03	0.77	13.57	3.46	0.10	0.76	2.90	3.79	2.68	0.13	0.10	99.29
11/07/2023	**SG14-5932**	69.19	0.73	13.18	3.42	0.08	0.77	2.72	3.65	2.56	0.00	0.09	96.39
11/07/2023	**SG14-5932**	70.66	0.77	13.55	3.58	0.08	0.87	2.98	3.82	2.69	0.00	0.07	99.08
11/07/2023	**SG14-5932**	71.41	0.76	13.64	3.54	0.09	0.86	2.93	3.72	2.68	0.00	0.07	99.70
11/07/2023	**SG14-5932**	68.08	0.67	13.03	3.41	0.07	0.79	2.84	3.51	2.43	0.03	0.09	94.96
11/07/2023	**SG14-5932**	68.58	0.84	13.19	3.27	0.08	0.73	2.82	3.72	2.62	0.00	0.09	95.93
11/07/2023	**SG14-5932**	67.93	0.72	12.98	3.27	0.04	0.72	2.73	3.33	2.44	0.03	0.14	94.32
11/07/2023	**SG14-5932**	69.55	0.75	13.44	3.44	0.06	0.84	3.01	3.87	2.60	0.00	0.08	97.63
11/07/2023	**SG14-5932**	70.89	0.79	13.67	3.47	0.05	0.81	2.83	4.02	2.66	0.00	0.09	99.30
11/07/2023	**SG14-5932**	69.51	0.73	13.28	3.19	0.08	0.76	2.58	3.55	2.70	0.00	0.06	96.44
11/07/2023	**SG14-5932**	70.73	0.75	13.70	3.31	0.09	0.86	3.52	3.99	2.10	0.12	0.07	99.24
11/07/2023	**SG14-5932**	68.86	0.84	13.42	3.67	0.05	0.88	2.92	3.68	2.62	0.09	0.09	97.12
11/07/2023	**SG14-5932**	70.16	0.72	13.52	3.39	0.10	0.82	2.93	3.49	2.59	0.00	0.08	97.80
11/07/2023	**SG14-5932**	68.57	0.75	13.14	2.98	0.07	0.77	2.66	3.33	2.55	0.01	0.09	94.92
11/07/2023	**SG14-5932**	68.98	0.77	13.69	3.58	0.07	0.79	3.18	3.55	2.54	0.14	0.10	97.39
02/06/2023	**SG14-5950**	67.52	0.25	13.11	2.74	0.08	0.03	0.45	5.31	4.60	0.00	0.30	94.39
02/06/2023	**SG14-5950**	67.40	0.19	13.20	2.81	0.10	0.07	0.48	5.48	4.62	0.00	0.27	94.61
02/06/2023	**SG14-5950**	67.25	0.19	13.22	2.89	0.08	0.04	0.50	5.40	4.74	0.00	0.27	94.59
02/06/2023	**SG14-5950**	67.25	0.22	13.23	2.79	0.08	0.02	0.51	5.31	4.83	0.01	0.27	94.51
02/06/2023	**SG14-5950**	67.45	0.23	13.29	2.89	0.06	0.06	0.49	5.41	4.67	0.04	0.27	94.87
02/06/2023	**SG14-5950**	67.18	0.15	13.26	2.89	0.05	0.01	0.51	5.46	4.62	0.00	0.26	94.39
02/06/2023	**SG14-5950**	67.71	0.18	13.36	2.74	0.06	0.03	0.53	5.34	4.64	0.00	0.28	94.86
02/06/2023	**SG14-5950**	67.13	0.20	13.33	2.79	0.07	0.00	0.50	5.45	4.68	0.00	0.27	94.42
02/06/2023	**SG14-5950**	67.19	0.21	13.51	2.89	0.09	0.02	0.52	5.34	4.52	0.01	0.26	94.55
02/06/2023	**SG14-5950**	68.93	0.41	14.27	1.36	0.10	0.31	1.01	4.53	4.33	0.11	0.11	95.48

Date of analysis	SG Label	SiO_2	TiO_2	Al_2O3	FeO_t	MnO	MgO	CaO	Na_2O	K_2O	P_2O_5	Cl	Analytical Total
02/06/2023	**SG14-5950**	68.29	0.42	14.70	1.55	0.10	0.41	1.24	4.58	3.86	0.09	0.10	95.33

Table B2. Major element glass analyses of the MPI-DING reference glass (StHs6/80-G, GOR132-G and ATHO-G) (un-normalised).

Date of Analysis	Label	SiO_2	Na_2O	Cl	K_2O	FeO_t	Al_2O_3	MgO	P_2O_5	CaO	MnO	TiO_2	Analytical Total
02/12/2022	**StHs/80-G**	64.04	4.69	0.01	1.32	4.41	17.43	1.89	0.04	5.28	0.07	0.67	99.86
02/12/2022	**StHs/80-G**	62.72	4.70	0.01	1.31	4.32	17.60	1.91	0.08	5.15	0.04	0.72	98.57
02/12/2022	**StHs/80-G**	63.85	4.51	0.01	1.26	4.36	17.90	1.96	0.16	5.32	0.10	0.71	100.13
02/12/2022	**StHs/80-G**	63.94	4.62	0.00	1.29	4.37	17.75	1.92	0.15	5.33	0.10	0.73	100.20
01/06/2023	**StHs/80-G**	63.32	4.60	0.02	1.24	4.31	17.72	1.97	0.14	5.24	0.09	0.63	98.03
01/06/2023	**StHs/80-G**	63.46	4.62	0.01	1.23	4.29	17.81	1.94	0.14	5.27	0.08	0.74	98.31
01/06/2023	**StHs/80-G**	63.84	4.66	0.02	1.22	4.17	18.07	1.92	0.13	5.31	0.07	0.69	98.82
01/06/2023	**StHs/80-G**	63.72	4.74	0.03	1.23	4.33	18.08	1.87	0.17	5.21	0.07	0.69	98.88
01/06/2023	**StHs/80-G**	63.46	4.51	0.04	1.24	4.32	17.88	1.91	0.06	5.31	0.06	0.69	98.21
02/06/2023	**StHs/80-G**	63.19	4.58	0.03	1.26	4.41	17.91	1.95	0.15	5.33	0.05	0.67	98.28
02/06/2023	**StHs/80-G**	63.60	4.62	0.02	1.23	4.25	17.87	1.99	0.19	5.28	0.06	0.70	98.54
02/06/2023	**StHs/80-G**	63.19	4.52	0.04	1.28	4.28	17.97	1.99	0.16	5.19	0.08	0.68	98.10
02/06/2023	**StHs/80-G**	63.43	4.65	0.02	1.27	4.34	17.80	1.97	0.16	5.26	0.07	0.72	98.42
02/06/2023	**StHs/80-G**	63.21	4.62	0.01	1.29	4.35	17.77	1.99	0.15	5.25	0.07	0.72	98.15
02/06/2023	**StHs/80-G**	63.57	3.40	0.02	1.29	4.39	17.88	2.07	0.15	5.30	0.07	0.72	97.59
02/06/2023	**StHs/80-G**	63.58	4.63	0.02	1.25	4.44	17.38	1.99	0.20	5.24	0.09	0.69	98.26
02/06/2023	**StHs/80-G**	63.92	4.51	0.01	1.24	4.45	17.81	1.98	0.16	5.26	0.05	0.73	98.85
02/06/2023	**StHs/80-G**	63.63	4.67	0.02	1.23	4.33	17.72	1.95	0.18	5.20	0.04	0.66	98.37
02/06/2023	**StHs/80-G**	63.62	4.36	0.01	1.27	4.40	17.48	1.99	0.06	5.15	0.05	0.68	97.80
02/06/2023	**StHs/80-G**	63.88	4.66	0.00	1.26	4.26	17.80	1.97	0.02	5.12	0.09	0.68	98.47
02/06/2023	**StHs/80-G**	64.42	3.10	0.01	1.26	4.49	17.35	1.94	0.06	5.21	0.05	0.72	97.34
02/02/2023	**StHs/80-G**	63.59	4.60	0.00	1.35	4.35	17.54	1.92	0.04	5.25	0.08	0.77	99.50
02/02/2023	**StHs/80-G**	63.86	4.74	0.00	1.28	4.48	17.28	1.88	0.08	5.25	0.09	0.77	99.72
02/02/2023	**StHs/80-G**	63.70	4.72	0.01	1.32	4.32	17.78	1.95	0.14	5.26	0.07	0.76	100.04
02/02/2023	**StHs/80-G**	62.96	4.65	0.01	1.24	4.30	17.56	1.93	0.16	5.32	0.08	0.71	98.92
02/02/2023	**StHs/80-G**	63.41	3.61	0.02	1.27	4.32	17.60	1.90	0.19	5.28	0.12	0.73	98.44
02/02/2023	**StHs/80-G**	63.76	4.69	0.00	1.29	4.28	17.52	1.97	0.15	5.29	0.07	0.71	99.73
02/06/2023	**StHs/80-G**	63.83	4.55	0.01	1.36	4.33	17.67	1.94	0.12	5.10	0.10	0.71	99.72
02/06/2023	**StHs/80-G**	64.08	4.58	0.00	1.35	4.13	17.69	1.94	0.09	5.10	0.10	0.70	99.75
02/06/2023	**StHs/80-G**	64.00	4.78	0.00	1.36	4.30	17.69	1.92	0.06	5.17	0.08	0.70	100.06

Date of Analysis	Label	SiO_2	Na_2O	Cl	K_2O	FeO_t	Al_2O_3	MgO	P_2O_5	CaO	MnO	TiO_2	Analytical Total
02/06/2023	**StHs/80-G**	63.52	4.54	0.01	1.36	4.36	17.71	1.98	0.10	5.18	0.10	0.73	99.59
02/06/2023	**StHs/80-G**	63.72	4.71	0.01	1.28	4.34	17.60	1.96	0.08	5.18	0.06	0.72	99.66
03/06/2023	**StHs/80-G**	63.13	4.55	0.03	1.29	4.21	17.93	2.05	0.15	5.27	0.05	0.69	99.35
03/06/2023	**StHs/80-G**	63.70	4.63	0.01	1.30	4.38	17.94	1.96	0.18	5.21	0.09	0.62	100.02
03/06/2023	**StHs/80-G**	63.43	4.53	0.01	1.28	4.30	17.82	1.94	0.21	5.32	0.06	0.68	99.58
03/06/2023	**StHs/80-G**	63.58	4.84	0.02	1.33	4.27	17.90	1.93	0.22	5.25	0.08	0.67	100.08
03/06/2023	**StHs/80-G**	63.65	4.55	0.01	1.33	4.38	17.92	2.02	0.19	5.28	0.09	0.70	100.13
03/06/2023	**StHs/80-G**	63.72	4.65	0.00	1.39	4.30	17.59	1.99	0.05	5.20	0.10	0.63	99.63
03/06/2023	**StHs/80-G**	63.88	4.46	0.01	1.38	4.26	17.78	1.92	0.10	5.24	0.05	0.69	99.78
03/06/2023	**StHs/80-G**	63.77	4.53	0.01	1.29	4.42	17.77	1.93	0.12	5.26	0.10	0.69	99.89
03/06/2023	**StHs/80-G**	63.66	4.64	0.00	1.32	4.39	17.71	1.96	0.15	5.34	0.09	0.69	99.95
03/02/2023	**StHs/80-G**	63.76	4.62	0.01	1.24	4.51	17.64	1.93	0.13	5.28	0.03	0.76	99.91
03/02/2023	**StHs/80-G**	63.21	4.80	0.03	1.27	4.51	17.65	1.93	0.07	5.29	0.08	0.67	99.51
03/02/2023	**StHs/80-G**	63.41	4.74	0.00	1.26	4.45	17.96	1.91	0.11	5.30	0.07	0.79	100.00
03/02/2023	**StHs/80-G**	63.68	4.72	0.00	1.28	4.56	17.72	1.88	0.16	5.32	0.09	0.79	100.21
03/02/2023	**StHs/80-G**	63.32	4.54	0.01	1.27	4.28	17.78	1.93	0.16	5.24	0.06	0.72	99.32
03/02/2023	**StHs/80-G**	63.52	4.82	0.00	1.26	4.37	17.71	1.91	0.13	5.27	0.09	0.80	99.88
04/02/2023	**StHs/80-G**	63.79	4.59	0.00	1.29	4.41	17.64	1.92	0.11	5.31	0.02	0.71	99.79
04/02/2023	**StHs/80-G**	63.60	4.66	0.02	1.28	4.56	17.71	1.93	0.13	5.32	0.09	0.73	100.03
04/02/2023	**StHs/80-G**	63.68	4.64	0.04	1.25	4.45	17.91	1.93	0.15	5.25	0.10	0.72	100.11
04/02/2023	**StHs/80-G**	63.84	4.67	0.01	1.27	4.40	17.63	1.94	0.12	5.26	0.07	0.70	99.91
04/02/2023	**StHs/80-G**	62.69	4.67	0.01	1.33	4.27	17.50	1.86	0.13	5.20	0.06	0.77	98.50
04/02/2023	**StHs/80-G**	63.44	4.68	0.03	1.26	4.40	17.66	2.02	0.12	5.33	0.09	0.77	99.80
04/02/2023	**StHs/80-G**	63.89	4.55	0.01	1.32	4.43	17.83	1.91	0.21	5.31	0.07	0.76	100.29
04/02/2023	**StHs/80-G**	63.54	4.42	0.02	1.24	4.33	17.94	1.99	0.13	5.34	0.05	0.78	99.79
04/02/2023	**StHs/80-G**	63.78	4.69	0.01	1.27	4.37	17.47	1.88	0.13	5.25	0.08	0.73	99.65
04/02/2023	**StHs/80-G**	63.86	4.63	0.00	1.27	4.40	17.75	1.95	0.16	5.30	0.05	0.73	100.11
04/02/2023	**StHs/80-G**	63.20	3.61	0.00	1.33	4.46	17.94	1.94	0.10	5.25	0.10	0.76	98.70
05/02/2023	**StHs/80-G**	63.37	4.90	0.00	1.28	4.41	17.34	1.91	0.06	5.24	0.07	0.72	99.29
05/02/2023	**StHs/80-G**	63.89	4.71	0.01	1.31	4.51	17.64	1.93	0.10	5.21	0.06	0.76	100.13
05/02/2023	**StHs/80-G**	63.78	4.48	0.00	1.29	4.48	17.73	1.90	0.08	5.24	0.06	0.78	99.82
05/02/2023	**StHs/80-G**	63.99	4.64	0.00	1.31	4.45	17.47	1.92	0.05	5.29	0.06	0.76	99.95

Date of Analysis	Label	SiO_2	Na_2O	Cl	K_2O	FeO_t	Al_2O_3	MgO	P_2O_5	CaO	MnO	TiO_2	Analytical Total
05/02/2023	**StHs/80-G**	64.07	4.71	0.03	1.30	4.49	17.49	1.92	0.03	5.21	0.05	0.75	100.06
05/02/2023	**StHs/80-G**	63.68	4.65	0.00	1.26	4.32	17.44	1.90	0.06	5.24	0.07	0.72	99.35
09/02/2023	**StHs/80-G**	63.42	4.59	0.01	1.29	4.23	17.34	1.85	0.09	5.15	0.09	0.71	98.76
09/02/2023	**StHs/80-G**	63.47	4.51	0.01	1.26	4.28	17.64	1.93	0.08	5.27	0.09	0.71	99.25
09/02/2023	**StHs/80-G**	63.32	4.62	0.02	1.30	4.26	17.54	1.91	0.15	5.27	0.10	0.74	99.22
09/02/2023	**StHs/80-G**	63.42	4.70	0.01	1.29	4.32	17.74	1.88	0.08	5.26	0.05	0.72	99.46
09/02/2023	**StHs/80-G**	63.48	4.64	0.01	1.28	4.37	17.54	1.88	0.15	5.26	0.07	0.74	99.40
09/02/2023	**StHs/80-G**	63.51	4.48	0.00	1.25	4.30	17.50	1.91	0.10	5.21	0.05	0.75	99.06
09/02/2023	**StHs/80-G**	63.87	4.49	0.01	1.28	4.22	17.59	1.91	0.09	5.25	0.07	0.77	99.55
09/02/2023	**StHs/80-G**	64.07	4.68	0.01	1.26	4.27	17.45	1.91	0.06	5.28	0.08	0.72	99.79
09/02/2023	**StHs/80-G**	63.65	4.43	0.02	1.31	4.37	17.67	1.89	0.03	5.27	0.08	0.76	99.48
09/02/2023	**StHs/80-G**	63.75	4.53	0.01	1.26	4.28	17.55	1.90	0.06	5.22	0.07	0.75	99.37
09/02/2023	**StHs/80-G**	63.94	4.65	0.00	1.28	4.35	17.57	2.06	0.08	5.25	0.04	0.68	99.90
09/02/2023	**StHs/80-G**	64.31	3.48	0.01	1.31	4.28	17.73	1.95	0.09	5.26	0.06	0.71	99.19
07/02/2023	**StHs/80-G**	64.08	4.45	0.00	1.27	4.22	17.53	1.96	0.08	5.18	0.07	0.72	99.10
07/02/2023	**StHs/80-G**	63.88	4.55	0.00	1.25	4.31	17.49	1.93	0.07	5.18	0.06	0.72	99.00
07/02/2023	**StHs/80-G**	63.80	4.54	0.01	1.32	4.27	17.66	1.95	0.13	5.12	0.05	0.70	99.09
07/02/2023	**StHs/80-G**	63.73	4.63	0.02	1.31	4.19	17.87	1.95	0.07	5.19	0.09	0.72	99.32
07/02/2023	**StHs/80-G**	63.43	4.48	0.00	1.29	4.26	17.64	1.99	0.12	5.19	0.10	0.73	98.77
08/02/2023	**StHs/80-G**	63.80	4.45	0.02	1.30	4.36	17.65	1.91	0.08	5.33	0.06	0.74	99.22
08/02/2023	**StHs/80-G**	64.07	4.34	0.01	1.28	4.36	17.43	1.89	0.11	5.25	0.09	0.72	99.08
08/02/2023	**StHs/80-G**	63.83	4.54	0.00	1.25	4.35	17.71	1.88	0.14	5.35	0.07	0.78	99.45
08/02/2023	**StHs/80-G**	63.86	4.61	0.00	1.29	4.22	17.80	1.92	0.13	5.34	0.04	0.78	99.54
08/02/2023	**StHs/80-G**	64.03	4.60	0.01	1.28	4.25	17.85	1.97	0.12	5.27	0.04	0.75	99.70
08/02/2023	**StHs/80-G**	63.96	4.58	0.01	1.31	4.30	17.67	1.93	0.10	5.28	0.09	0.80	99.57
30/05/2023	**StHs/80-G**	63.81	4.47	0.02	1.26	4.23	17.72	1.89	0.17	5.23	0.08	0.71	99.58
30/05/2023	**StHs/80-G**	64.11	4.50	0.02	1.27	4.13	17.97	1.93	0.13	5.28	0.09	0.67	100.09
30/05/2023	**StHs/80-G**	63.93	4.52	0.03	1.24	4.41	17.71	1.90	0.16	5.26	0.05	0.72	99.91
30/05/2023	**StHs/80-G**	63.79	4.74	0.03	1.23	4.26	17.88	1.93	0.13	5.28	0.08	0.74	100.08
30/05/2023	**StHs/80-G**	64.07	4.66	0.02	1.30	4.36	18.02	1.96	0.15	5.27	0.05	0.71	100.56
31/05/2023	**StHs/80-G**	63.32	4.56	0.02	1.27	4.36	18.00	1.97	0.16	5.27	0.08	0.64	99.65
31/05/2023	**StHs/80-G**	64.00	3.47	0.02	1.27	4.36	17.80	1.96	0.17	5.42	0.07	0.71	99.23

Date of Analysis	Label	SiO_2	Na_2O	Cl	K_2O	FeO_t	Al_2O_3	MgO	P_2O_5	CaO	MnO	TiO_2	Analytical Total
31/05/2023	**StHs/80-G**	63.52	4.63	0.03	1.25	4.20	17.80	1.95	0.22	5.36	0.11	0.66	99.73
31/05/2023	**StHs/80-G**	63.15	4.59	0.01	1.27	4.39	17.80	2.02	0.13	5.37	0.08	0.69	99.49
31/05/2023	**StHs/80-G**	63.83	4.58	0.02	1.29	4.32	18.01	1.91	0.13	5.29	0.08	0.72	100.18
31/05/2023	**StHs/80-G**	63.94	4.64	0.02	1.27	4.29	17.78	1.97	0.15	5.34	0.08	0.71	100.18
23/08/2022	**StHs/80-G**	63.51	4.65	0.02	1.27	4.37	17.84	1.89	0.12	5.27	0.05	0.72	99.72
23/08/2022	**StHs/80-G**	63.78	4.77	0.03	1.29	4.36	17.97	1.94	0.18	5.26	0.07	0.72	100.38
23/08/2022	**StHs/80-G**	63.25	4.70	0.03	1.30	4.29	17.61	1.92	0.18	5.25	0.07	0.70	99.30
23/08/2022	**StHs/80-G**	63.74	4.66	0.02	1.29	4.28	17.58	1.95	0.12	5.22	0.08	0.69	99.63
23/08/2022	**StHs/80-G**	63.92	4.45	0.01	1.22	4.34	17.78	1.88	0.13	5.21	0.05	0.70	99.70
24/08/2022	**StHs/80-G**	63.35	4.39	0.03	1.29	4.23	17.70	1.93	0.14	5.31	0.06	0.67	99.10
24/08/2022	**StHs/80-G**	63.62	4.53	0.02	1.30	4.36	17.91	1.97	0.17	5.29	0.08	0.73	99.99
24/08/2022	**StHs/80-G**	63.50	4.58	0.03	1.28	4.38	17.75	1.92	0.19	5.38	0.06	0.72	99.79
24/08/2022	**StHs/80-G**	63.42	4.50	0.03	1.31	4.26	17.81	2.00	0.14	5.29	0.07	0.67	99.50
24/08/2022	**StHs/80-G**	63.60	4.39	0.03	1.34	4.25	18.08	1.99	0.19	5.26	0.06	0.75	99.93
03/05/2023	**StHs/80-G**	64.15	4.74	0.01	1.34	4.21	17.57	1.93	0.09	5.25	0.06	0.74	100.09
03/05/2023	**StHs/80-G**	64.04	4.52	0.01	1.32	4.31	17.41	1.88	0.10	5.23	0.10	0.69	99.61
03/05/2023	**StHs/80-G**	63.79	4.54	0.00	1.34	4.21	17.47	1.87	0.07	5.25	0.06	0.73	99.33
03/05/2023	**StHs/80-G**	63.56	4.63	0.00	1.32	4.37	17.53	1.90	0.07	5.21	0.03	0.69	99.32
03/05/2023	**StHs/80-G**	64.05	4.47	0.01	1.35	4.22	17.61	1.90	0.05	5.16	0.09	0.74	99.66
04/05/2023	**StHs/80-G**	63.41	4.75	0.02	1.26	4.11	17.68	1.97	0.14	5.33	0.06	0.70	99.45
04/05/2023	**StHs/80-G**	63.64	4.46	0.02	1.27	4.21	17.79	1.94	0.15	5.29	0.09	0.66	99.52
04/05/2023	**StHs/80-G**	63.44	4.62	0.03	1.27	4.27	17.99	1.93	0.14	5.23	0.08	0.69	99.69
04/05/2023	**StHs/80-G**	63.42	4.45	0.01	1.28	4.10	17.64	1.95	0.13	5.26	0.05	0.71	99.01
04/05/2023	**StHs/80-G**	63.74	4.74	0.01	1.24	4.36	17.91	2.00	0.12	5.20	0.07	0.71	100.10
04/05/2023	**StHs/80-G**	63.49	4.73	0.02	1.29	4.23	17.98	1.97	0.11	5.29	0.10	0.69	99.91
04/05/2023	**StHs/80-G**	63.96	4.72	0.02	1.29	4.21	17.83	1.99	0.20	5.27	0.09	0.73	100.32
04/05/2023	**StHs/80-G**	63.65	4.54	0.01	1.32	4.29	17.69	1.92	0.16	5.33	0.08	0.75	99.74
04/05/2023	**StHs/80-G**	63.69	4.53	0.02	1.30	4.30	17.43	1.97	0.18	5.28	0.08	0.69	99.46
04/05/2023	**StHs/80-G**	63.91	4.61	0.00	1.27	4.27	17.73	1.89	0.17	5.26	0.10	0.70	99.93
04/05/2023	**StHs/80-G**	63.48	4.66	0.01	1.29	4.30	17.75	1.95	0.11	5.28	0.08	0.68	99.61
04/05/2023	**StHs/80-G**	63.04	4.67	0.01	1.27	4.30	17.67	1.93	0.13	5.24	0.09	0.72	99.06
04/05/2023	**StHs/80-G**	63.92	4.56	0.03	1.24	4.29	17.60	1.97	0.13	5.31	0.07	0.72	99.85

Date of Analysis	Label	SiO_2	Na_2O	Cl	K_2O	FeO_t	Al_2O_3	MgO	P_2O_5	CaO	MnO	TiO_2	Analytical Total
04/05/2023	**StHs/80-G**	64.11	3.50	0.01	1.27	4.33	17.99	1.92	0.11	5.29	0.08	0.70	99.32
01/12/2022	**ATHO-G**	75.67	3.96	0.01	2.86	3.23	12.29	0.09	0.04	1.60	0.08	0.25	100.09
01/12/2022	**ATHO-G**	75.69	3.97	0.04	2.78	3.31	12.32	0.12	0.00	1.68	0.12	0.23	100.28
01/12/2022	**ATHO-G**	75.63	3.97	0.04	2.80	3.21	12.32	0.08	0.09	1.64	0.07	0.23	100.09
01/12/2022	**ATHO-G**	75.94	4.03	0.03	2.78	3.12	12.33	0.04	0.01	1.68	0.07	0.24	100.29
02/12/2022	**ATHO-G**	75.46	3.98	0.03	2.69	3.10	12.35	0.07	0.01	1.70	0.11	0.25	99.74
02/12/2022	**ATHO-G**	76.65	4.08	0.02	2.79	3.21	12.55	0.09	0.00	1.70	0.13	0.28	101.50
02/12/2022	**ATHO-G**	75.29	4.10	0.04	2.75	3.22	12.39	0.12	0.00	1.72	0.11	0.26	100.00
02/12/2022	**ATHO-G**	74.48	4.23	0.03	2.72	3.24	12.12	0.10	0.08	1.65	0.11	0.24	99.00
02/12/2022	**ATHO-G**	76.09	1.35	0.02	2.80	3.22	12.06	0.08	0.01	1.69	0.10	0.26	97.68
01/06/2023	**ATHO-G**	76.09	3.78	0.03	2.57	3.27	12.18	0.09	0.04	1.69	0.13	0.23	98.68
01/06/2023	**ATHO-G**	75.42	4.15	0.05	2.52	3.24	12.25	0.09	0.04	1.65	0.09	0.26	98.37
01/06/2023	**ATHO-G**	76.19	4.20	0.03	2.51	3.16	12.33	0.13	0.04	1.72	0.11	0.28	99.29
01/06/2023	**ATHO-G**	75.41	4.09	0.02	2.56	3.42	12.13	0.10	0.05	1.71	0.09	0.19	98.36
01/06/2023	**ATHO-G**	75.37	4.10	0.03	2.50	3.27	12.27	0.08	0.03	1.72	0.11	0.25	98.33
02/06/2023	**ATHO-G**	74.99	4.07	0.05	2.54	3.23	12.14	0.09	0.07	1.72	0.12	0.27	97.89
02/06/2023	**ATHO-G**	75.77	3.95	0.03	2.58	3.27	12.24	0.11	0.00	1.73	0.10	0.29	98.67
02/06/2023	**ATHO-G**	75.84	4.22	0.03	2.51	3.21	12.34	0.09	0.00	1.76	0.11	0.20	98.92
02/06/2023	**ATHO-G**	75.66	3.99	0.03	2.57	3.11	12.22	0.10	0.00	1.75	0.14	0.28	98.44
02/06/2023	**ATHO-G**	75.36	4.13	0.03	2.53	3.30	12.29	0.09	0.02	1.69	0.10	0.23	98.37
02/06/2023	**ATHO-G**	75.82	4.01	0.05	2.54	3.20	12.25	0.10	0.00	1.68	0.08	0.26	98.59
02/06/2023	**ATHO-G**	75.70	4.05	0.04	2.59	3.32	12.23	0.10	0.00	1.71	0.08	0.20	98.61
02/06/2023	**ATHO-G**	75.47	4.14	0.04	2.54	3.16	12.34	0.09	0.02	1.74	0.10	0.27	98.53
02/06/2023	**ATHO-G**	75.67	4.20	0.04	2.67	3.22	12.33	0.08	0.03	1.71	0.14	0.24	98.93
02/06/2023	**ATHO-G**	75.51	4.10	0.04	2.62	3.23	12.33	0.12	0.03	1.70	0.13	0.21	98.63
02/02/2023	**ATHO-G**	75.72	4.19	0.02	2.64	3.23	12.38	0.11	0.02	1.67	0.07	0.29	100.34
02/02/2023	**ATHO-G**	75.63	4.13	0.03	2.71	3.10	12.31	0.10	0.02	1.66	0.09	0.24	100.03
02/02/2023	**ATHO-G**	75.70	4.06	0.04	2.68	2.97	12.36	0.09	0.00	1.68	0.10	0.26	99.93
02/02/2023	**ATHO-G**	75.52	4.28	0.02	2.70	3.13	12.01	0.10	0.03	1.65	0.10	0.24	99.79
03/02/2023	**ATHO-G**	76.16	3.91	0.04	2.66	3.16	12.33	0.10	0.00	1.66	0.10	0.23	100.36
03/02/2023	**ATHO-G**	75.70	4.18	0.04	2.70	3.19	12.33	0.12	0.00	1.67	0.11	0.28	100.32

Date of Analysis	Label	SiO_2	Na_2O	Cl	K_2O	FeO_t	Al_2O_3	MgO	P_2O_5	CaO	MnO	TiO_2	Analytical Total
03/02/2023	**ATHO-G**	75.88	4.17	0.03	2.70	3.18	12.38	0.08	0.03	1.63	0.09	0.31	100.48
03/02/2023	**ATHO-G**	75.76	4.24	0.03	2.79	3.18	12.25	0.07	0.00	1.60	0.10	0.24	100.26
03/02/2023	**ATHO-G**	75.23	4.11	0.04	2.71	3.23	12.20	0.11	0.00	1.53	0.07	0.28	99.51
02/06/2023	**ATHO-G**	75.39	4.13	0.03	2.74	3.22	12.01	0.09	0.01	1.69	0.07	0.25	99.63
02/06/2023	**ATHO-G**	75.30	4.11	0.05	2.67	3.26	12.13	0.13	0.02	1.75	0.09	0.27	99.78
02/06/2023	**ATHO-G**	75.64	4.19	0.04	2.72	3.25	12.42	0.11	0.05	1.68	0.10	0.25	100.44
02/06/2023	**ATHO-G**	75.46	4.15	0.06	2.73	3.30	12.25	0.09	0.04	1.67	0.12	0.22	100.08
02/06/2023	**ATHO-G**	75.40	4.18	0.05	2.73	3.21	12.31	0.09	0.07	1.70	0.12	0.24	100.10
03/06/2023	**ATHO-G**	75.30	4.09	0.04	2.71	3.28	12.26	0.08	0.04	1.69	0.12	0.23	99.83
03/06/2023	**ATHO-G**	75.26	4.08	0.03	2.78	3.28	12.45	0.11	0.06	1.71	0.08	0.23	100.08
03/06/2023	**ATHO-G**	75.54	4.04	0.03	2.66	3.22	12.23	0.12	0.00	1.71	0.12	0.25	99.92
03/06/2023	**ATHO-G**	75.16	4.13	0.03	2.72	3.24	12.14	0.08	0.00	1.67	0.11	0.22	99.49
03/06/2023	**ATHO-G**	75.62	4.09	0.05	2.68	3.17	12.36	0.06	0.02	1.71	0.11	0.25	100.11
03/06/2023	**ATHO-G**	75.63	4.00	0.03	2.69	3.25	12.33	0.11	0.10	1.72	0.10	0.21	100.17
03/06/2023	**ATHO-G**	76.05	4.08	0.05	2.64	3.32	12.34	0.10	0.00	1.74	0.11	0.24	100.68
03/06/2023	**ATHO-G**	75.73	3.93	0.04	2.73	3.26	12.51	0.08	0.04	1.81	0.10	0.20	100.44
03/06/2023	**ATHO-G**	75.84	4.02	0.04	2.70	3.29	12.38	0.09	0.05	1.75	0.13	0.26	100.55
03/06/2023	**ATHO-G**	75.23	4.03	0.02	2.72	3.30	12.28	0.10	0.00	1.78	0.07	0.20	99.72
03/02/2023	**ATHO-G**	75.70	4.23	0.02	2.65	3.19	12.31	0.08	0.02	1.73	0.11	0.32	100.36
03/02/2023	**ATHO-G**	76.00	4.12	0.04	2.66	3.18	12.25	0.04	0.02	1.66	0.07	0.26	100.30
03/02/2023	**ATHO-G**	75.60	4.16	0.02	2.59	3.16	12.29	0.09	0.03	1.73	0.08	0.26	100.01
03/02/2023	**ATHO-G**	75.75	4.13	0.05	2.63	3.31	12.40	0.13	0.01	1.68	0.09	0.22	100.40
03/02/2023	**ATHO-G**	75.31	4.03	0.04	2.69	3.12	12.19	0.10	0.04	1.72	0.13	0.32	99.69
03/02/2023	**ATHO-G**	75.60	4.01	0.01	2.67	3.13	12.26	0.09	0.00	1.68	0.12	0.29	99.85
04/02/2023	**ATHO-G**	74.98	4.34	0.03	2.72	3.25	12.35	0.10	0.07	1.70	0.10	0.29	99.92
04/02/2023	**ATHO-G**	75.67	4.34	0.06	2.72	3.20	12.30	0.08	0.03	1.69	0.10	0.28	100.46
04/02/2023	**ATHO-G**	75.52	4.18	0.03	2.67	3.20	12.35	0.11	0.00	1.70	0.11	0.31	100.18
04/02/2023	**ATHO-G**	76.05	4.03	0.04	2.69	3.12	12.36	0.07	0.04	1.67	0.11	0.27	100.44
04/02/2023	**ATHO-G**	75.80	4.19	0.03	2.66	3.17	12.34	0.11	0.04	1.65	0.09	0.30	100.39
04/02/2023	**ATHO-G**	76.03	4.10	0.04	2.65	3.08	12.29	0.10	0.00	1.70	0.10	0.26	100.36
04/02/2023	**ATHO-G**	75.58	4.23	0.04	2.64	3.09	12.49	0.07	0.05	1.63	0.09	0.26	100.17
04/02/2023	**ATHO-G**	75.58	4.06	0.02	2.71	3.21	12.20	0.10	0.00	1.70	0.08	0.23	99.89

Date of Analysis	Label	SiO_2	Na_2O	Cl	K_2O	FeO_t	Al_2O_3	MgO	P_2O_5	CaO	MnO	TiO_2	Analytical Total
04/02/2023	**ATHO-G**	75.59	4.23	0.03	2.71	3.07	12.14	0.09	0.02	1.70	0.08	0.25	99.91
04/02/2023	**ATHO-G**	75.42	4.20	0.02	2.66	3.09	12.39	0.10	0.01	1.67	0.12	0.24	99.93
04/02/2023	**ATHO-G**	76.00	4.17	0.01	2.69	3.27	12.37	0.11	0.00	1.64	0.10	0.24	100.59
04/02/2023	**ATHO-G**	75.47	4.03	0.04	2.71	3.08	12.28	0.03	0.03	1.65	0.11	0.26	99.69
04/02/2023	**ATHO-G**	75.69	4.12	0.03	2.72	3.23	12.19	0.14	0.01	1.72	0.12	0.25	100.23
05/02/2023	**ATHO-G**	75.39	4.26	0.03	2.69	3.19	12.28	0.05	0.00	1.67	0.09	0.27	99.92
05/02/2023	**ATHO-G**	76.25	4.32	0.04	2.68	3.19	12.37	0.11	0.03	1.66	0.09	0.27	101.00
05/02/2023	**ATHO-G**	76.27	4.05	0.03	2.73	3.20	12.43	0.08	0.00	1.67	0.11	0.24	100.81
05/02/2023	**ATHO-G**	75.39	4.17	0.03	2.68	3.26	12.34	0.13	0.00	1.68	0.11	0.24	100.02
05/02/2023	**ATHO-G**	75.75	4.02	0.05	2.70	3.14	12.32	0.07	0.03	1.68	0.09	0.26	100.11
05/02/2023	**ATHO-G**	76.02	4.34	0.05	2.73	3.21	12.50	0.06	0.00	1.69	0.11	0.23	100.94
09/02/2023	**ATHO-G**	75.63	4.01	0.03	2.65	3.36	12.29	0.08	0.04	1.66	0.11	0.26	100.13
09/02/2023	**ATHO-G**	75.37	4.08	0.03	2.66	3.11	12.35	0.09	0.01	1.69	0.11	0.21	99.70
09/02/2023	**ATHO-G**	75.70	4.22	0.04	2.63	3.13	12.31	0.06	0.03	1.71	0.10	0.25	100.17
09/02/2023	**ATHO-G**	75.50	4.15	0.03	2.71	3.29	12.26	0.05	0.02	1.72	0.10	0.32	100.14
09/02/2023	**ATHO-G**	75.39	4.20	0.02	2.66	3.12	12.27	0.08	0.04	1.69	0.08	0.27	99.80
09/02/2023	**ATHO-G**	75.24	4.23	0.04	2.71	3.22	12.42	0.09	0.00	1.68	0.11	0.30	100.05
09/02/2023	**ATHO-G**	75.86	4.08	0.04	2.68	3.26	12.37	0.03	0.01	1.67	0.11	0.31	100.41
09/02/2023	**ATHO-G**	75.68	4.08	0.03	2.74	3.21	12.30	0.09	0.01	1.71	0.13	0.26	100.23
09/02/2023	**ATHO-G**	75.56	4.14	0.04	2.68	3.15	12.34	0.11	0.07	1.71	0.08	0.28	100.16
09/02/2023	**ATHO-G**	75.56	4.10	0.02	2.68	3.12	12.27	0.09	0.02	1.71	0.09	0.30	99.95
09/02/2023	**ATHO-G**	75.38	4.14	0.04	2.68	3.19	12.30	0.10	0.01	1.68	0.11	0.28	99.90
07/02/2023	**ATHO-G**	75.16	4.10	0.03	2.67	3.24	12.15	0.13	0.00	1.69	0.12	0.27	99.13
07/02/2023	**ATHO-G**	75.57	3.98	0.04	2.65	3.08	12.37	0.09	0.01	1.72	0.06	0.23	99.37
07/02/2023	**ATHO-G**	75.16	3.95	0.03	2.65	3.11	12.08	0.10	0.01	1.64	0.11	0.26	98.68
07/02/2023	**ATHO-G**	75.44	4.16	0.02	2.65	3.05	12.21	0.07	0.00	1.74	0.10	0.23	99.23
07/02/2023	**ATHO-G**	75.01	4.32	0.02	2.66	3.18	12.22	0.09	0.02	1.69	0.10	0.25	99.12
08/02/2023	**ATHO-G**	75.48	4.12	0.03	2.66	3.11	12.19	0.13	0.01	1.70	0.08	0.28	99.35
08/02/2023	**ATHO-G**	75.31	4.24	0.04	2.66	3.10	12.24	0.10	0.01	1.70	0.09	0.25	99.31
08/02/2023	**ATHO-G**	75.39	4.00	0.02	2.67	3.10	12.41	0.07	0.00	1.68	0.11	0.30	99.32
08/02/2023	**ATHO-G**	75.70	4.11	0.05	2.70	3.18	12.37	0.05	0.00	1.67	0.09	0.22	99.71
30/05/2023	**ATHO-G**	75.21	4.02	0.04	2.67	3.28	12.27	0.08	0.04	1.75	0.11	0.26	99.72

Date of Analysis	Label	SiO_2	Na_2O	Cl	K_2O	FeO_t	Al_2O_3	MgO	P_2O_5	CaO	MnO	TiO_2	Analytical Total
30/05/2023	**ATHO-G**	75.80	3.99	0.05	2.65	3.25	12.30	0.10	0.04	1.68	0.10	0.21	100.17
30/05/2023	**ATHO-G**	75.39	4.02	0.04	2.68	3.28	12.21	0.11	0.03	1.76	0.10	0.22	99.84
30/05/2023	**ATHO-G**	75.35	4.14	0.04	2.71	3.31	12.13	0.12	0.01	1.72	0.09	0.30	99.92
30/05/2023	**ATHO-G**	75.60	4.20	0.03	2.74	3.26	12.23	0.12	0.02	1.72	0.09	0.22	100.24
23/08/2022	**ATHO-G**	75.76	4.08	0.04	2.63	3.17	12.38	0.08	0.02	1.70	0.09	0.22	100.16
23/08/2022	**ATHO-G**	75.38	3.94	0.03	2.61	3.26	12.27	0.09	0.00	1.68	0.10	0.26	99.61
23/08/2022	**ATHO-G**	75.73	4.01	0.04	2.62	3.26	12.23	0.09	0.02	1.74	0.11	0.24	100.09
23/08/2022	**ATHO-G**	75.93	3.97	0.05	2.61	3.28	12.31	0.10	0.00	1.67	0.11	0.28	100.32
23/08/2022	**ATHO-G**	75.91	4.06	0.04	2.63	3.33	12.26	0.10	0.00	1.64	0.13	0.29	100.38
24/08/2022	**ATHO-G**	75.79	3.97	0.05	2.60	3.30	12.18	0.10	0.03	1.73	0.13	0.22	100.10
24/08/2022	**ATHO-G**	75.61	3.99	0.05	2.65	3.25	12.36	0.07	0.02	1.68	0.10	0.23	100.00
24/08/2022	**ATHO-G**	75.43	4.05	0.06	2.67	3.33	12.39	0.12	0.07	1.72	0.06	0.28	100.19
24/08/2022	**ATHO-G**	75.88	4.01	0.05	2.68	3.19	12.36	0.09	0.01	1.70	0.15	0.22	100.34
24/08/2022	**ATHO-G**	75.64	3.83	0.03	2.66	3.26	12.33	0.12	0.03	1.72	0.13	0.24	99.99
03/05/2023	**ATHO-G**	75.43	4.11	0.04	2.74	3.20	12.22	0.07	0.04	1.67	0.07	0.23	99.81
03/05/2023	**ATHO-G**	75.57	4.15	0.05	2.67	3.27	12.26	0.13	0.03	1.72	0.12	0.23	100.18
03/05/2023	**ATHO-G**	75.79	4.06	0.04	2.73	3.17	12.08	0.10	0.02	1.70	0.12	0.25	100.06
03/05/2023	**ATHO-G**	75.53	4.13	0.04	2.74	3.25	12.26	0.09	0.06	1.73	0.12	0.19	100.14
03/05/2023	**ATHO-G**	75.53	4.09	0.04	2.69	3.18	12.19	0.07	0.02	1.72	0.12	0.22	99.86
04/05/2023	**ATHO-G**	75.97	4.17	0.04	2.68	3.12	12.32	0.15	0.00	1.67	0.11	0.28	100.51
04/05/2023	**ATHO-G**	75.40	4.09	0.03	2.71	3.21	12.25	0.08	0.00	1.72	0.10	0.29	99.87
04/05/2023	**ATHO-G**	75.57	4.00	0.05	2.65	3.21	11.85	0.12	0.03	1.74	0.09	0.23	99.54
04/05/2023	**ATHO-G**	75.49	4.09	0.05	2.64	3.07	12.22	0.11	0.02	1.74	0.09	0.22	99.72
04/05/2023	**ATHO-G**	75.79	4.18	0.04	2.63	3.18	12.43	0.14	0.05	1.71	0.10	0.25	100.50
04/05/2023	**ATHO-G**	75.50	4.18	0.03	2.67	3.17	12.23	0.08	0.04	1.68	0.08	0.27	99.92
04/05/2023	**ATHO-G**	75.56	4.05	0.03	2.74	3.15	12.26	0.13	0.06	1.68	0.13	0.30	100.09
04/05/2023	**ATHO-G**	75.95	4.14	0.03	2.74	3.14	12.33	0.10	0.00	1.68	0.10	0.26	100.47
04/05/2023	**ATHO-G**	75.56	4.00	0.04	2.69	3.09	12.19	0.09	0.02	1.71	0.11	0.25	99.75
04/05/2023	**ATHO-G**	75.35	4.15	0.05	2.71	3.14	12.19	0.13	0.00	1.68	0.12	0.24	99.75
01/12/2022	**GOR132**	45.35	0.86	0.00	0.02	10.41	11.07	22.51	0.07	8.60	0.16	0.30	99.35
01/12/2022	**GOR132**	45.62	0.88	0.00	0.02	10.31	10.94	22.44	0.07	8.48	0.17	0.28	99.21

Date of Analysis	Label	SiO_2	Na_2O	Cl	K_2O	FeO_t	Al_2O_3	MgO	P_2O_5	CaO	MnO	TiO_2	Analytical Total
01/12/2022	**GOR132**	45.29	0.76	0.00	0.02	10.29	11.11	22.36	0.01	8.60	0.14	0.29	98.87
01/12/2022	**GOR132**	45.53	0.81	0.00	0.01	10.24	10.94	22.37	0.10	8.58	0.15	0.22	98.94
02/12/2022	**GOR132**	45.81	0.77	0.02	0.04	10.15	10.91	22.51	0.00	8.67	0.16	0.31	99.34
02/12/2022	**GOR132**	45.83	0.62	0.01	0.05	10.24	10.82	22.28	0.01	8.63	0.13	0.31	98.92
02/12/2022	**GOR132**	45.07	0.87	0.00	0.04	10.19	10.81	22.38	0.04	8.47	0.13	0.28	98.30
02/12/2022	**GOR132**	45.23	0.84	0.00	0.04	10.31	11.20	22.34	0.08	8.60	0.18	0.29	99.10
01/06/2023	**GOR132**	45.49	0.83	0.00	0.01	10.33	11.16	22.36	0.04	8.45	0.16	0.29	98.19
01/06/2023	**GOR132**	45.79	0.79	0.00	0.05	10.21	10.95	22.30	0.08	8.46	0.14	0.29	98.11
01/06/2023	**GOR132**	45.68	0.87	0.01	0.04	10.22	11.09	22.20	0.07	8.50	0.17	0.32	98.21
01/06/2023	**GOR132**	45.45	0.83	0.00	0.03	10.17	11.05	22.37	0.01	8.37	0.15	0.29	97.77
01/06/2023	**GOR132**	45.62	0.81	0.00	0.03	10.19	10.92	22.10	0.05	8.42	0.14	0.32	97.67
02/06/2023	**GOR132**	45.23	0.78	0.00	0.04	10.11	10.95	22.68	0.07	8.56	0.13	0.31	97.95
02/06/2023	**GOR132**	45.55	0.82	0.01	0.04	10.25	10.79	22.62	0.00	8.50	0.14	0.33	98.09
02/06/2023	**GOR132**	45.53	0.81	0.00	0.02	10.28	10.84	22.70	0.07	8.51	0.19	0.28	98.31
02/06/2023	**GOR132**	45.39	0.84	0.01	0.03	10.07	10.94	22.78	0.03	8.35	0.17	0.32	98.00
02/06/2023	**GOR132**	45.48	0.88	0.02	0.03	10.06	10.96	22.54	0.02	8.38	0.14	0.31	97.86
02/06/2023	**GOR132**	45.52	0.70	0.00	0.05	10.32	11.10	22.76	0.04	8.42	0.15	0.33	98.45
02/06/2023	**GOR132**	45.58	0.86	0.00	0.04	10.22	10.90	22.63	0.04	8.46	0.17	0.31	98.27
02/06/2023	**GOR132**	45.93	0.82	0.01	0.04	10.30	10.89	22.60	0.03	8.43	0.11	0.31	98.54
02/06/2023	**GOR132**	45.66	0.72	0.00	0.03	10.31	10.93	22.52	0.00	8.43	0.16	0.30	98.12
02/06/2023	**GOR132**	45.49	0.83	0.01	0.02	10.53	10.90	22.72	0.00	8.39	0.18	0.30	98.42
02/06/2023	**GOR132**	45.60	0.83	0.00	0.05	10.24	11.01	22.72	0.00	8.47	0.12	0.27	98.37
02/06/2023	**GOR132**	45.66	0.89	0.01	0.03	10.46	11.03	22.57	0.05	8.51	0.15	0.27	98.68
02/02/2023	**GOR132**	45.63	0.92	0.00	0.03	10.07	10.91	22.32	0.02	8.64	0.12	0.32	98.98
02/02/2023	**GOR132**	45.61	0.79	0.01	0.02	10.04	10.93	22.35	0.04	8.49	0.15	0.31	98.74
02/02/2023	**GOR132**	45.61	0.87	0.00	0.02	10.10	10.89	22.44	0.01	8.67	0.16	0.31	99.07
02/02/2023	**GOR132**	45.58	0.74	0.00	0.04	10.19	10.98	22.44	0.00	8.63	0.15	0.32	99.07
02/02/2023	**GOR132**	45.38	0.84	0.00	0.02	9.94	11.15	22.38	0.04	8.56	0.15	0.33	98.79
02/02/2023	**GOR132**	45.63	0.80	0.01	0.03	9.99	10.83	22.34	0.04	8.61	0.12	0.35	98.74
02/02/2023	**GOR132**	45.66	0.82	0.00	0.03	10.22	11.05	22.60	0.00	8.41	0.13	0.30	99.22
02/02/2023	**GOR132**	45.45	0.79	0.00	0.01	10.32	10.96	22.56	0.00	8.50	0.16	0.36	99.11
03/02/2023	**GOR132**	45.61	0.84	0.00	0.02	9.98	11.00	22.37	0.01	8.41	0.18	0.30	98.71

Date of Analysis	Label	SiO_2	Na_2O	Cl	K_2O	FeO_t	Al_2O_3	MgO	P_2O_5	CaO	MnO	TiO_2	Analytical Total
03/02/2023	**GOR132**	45.64	0.72	0.01	0.03	10.16	11.13	22.30	0.00	8.28	0.18	0.34	98.78
03/02/2023	**GOR132**	45.57	0.86	0.00	0.06	10.17	10.80	22.51	0.05	8.29	0.14	0.32	98.76
03/02/2023	**GOR132**	45.60	0.88	0.01	0.05	10.14	10.87	22.36	0.05	8.31	0.14	0.30	98.71
03/02/2023	**GOR132**	45.35	0.77	0.00	0.03	10.02	10.85	22.53	0.02	8.16	0.13	0.35	98.21
03/02/2023	**GOR132**	45.64	0.86	0.02	0.05	10.06	11.08	22.72	0.03	7.99	0.13	0.27	98.85
03/02/2023	**GOR132**	45.29	0.86	0.00	0.03	10.09	10.85	22.55	0.04	8.08	0.13	0.34	98.26
02/06/2023	**GOR132**	45.74	0.79	0.01	0.04	10.23	10.91	22.64	0.03	8.40	0.15	0.29	99.24
02/06/2023	**GOR132**	45.59	0.72	0.00	0.02	10.14	10.86	22.71	0.02	8.37	0.16	0.30	98.90
02/06/2023	**GOR132**	45.66	0.81	0.00	0.03	10.33	10.99	22.58	0.02	8.33	0.14	0.29	99.19
02/06/2023	**GOR132**	45.46	0.91	0.00	0.03	10.48	10.91	22.49	0.02	8.46	0.14	0.32	99.22
02/06/2023	**GOR132**	45.61	0.79	0.00	0.02	10.22	10.83	22.61	0.01	8.48	0.17	0.33	99.07
03/06/2023	**GOR132**	45.14	0.90	0.00	0.04	10.39	10.80	22.70	0.06	8.46	0.15	0.30	98.93
03/06/2023	**GOR132**	45.46	0.87	0.01	0.03	10.24	11.08	22.73	0.06	8.48	0.18	0.31	99.45
03/06/2023	**GOR132**	45.54	0.87	0.00	0.02	10.23	11.02	22.62	0.06	8.53	0.14	0.33	99.35
03/06/2023	**GOR132**	45.58	0.86	0.01	0.03	10.43	10.94	22.55	0.05	8.48	0.12	0.29	99.33
03/06/2023	**GOR132**	45.67	0.93	0.01	0.03	10.37	11.06	22.60	0.07	8.52	0.19	0.33	99.79
03/06/2023	**GOR132**	45.29	0.86	0.00	0.02	10.24	10.71	22.63	0.05	8.50	0.16	0.29	98.74
03/06/2023	**GOR132**	45.47	0.74	0.00	0.04	10.02	10.99	22.40	0.04	8.47	0.15	0.34	98.65
03/06/2023	**GOR132**	45.85	0.75	0.00	0.03	10.19	11.15	22.51	0.04	8.53	0.16	0.27	99.47
03/06/2023	**GOR132**	45.84	0.86	0.01	0.03	10.31	10.86	22.56	0.01	8.54	0.13	0.33	99.48
03/02/2023	**GOR132**	45.61	0.78	0.00	0.05	10.26	10.79	22.06	0.02	8.54	0.16	0.31	98.57
03/02/2023	**GOR132**	45.49	0.85	0.00	0.03	10.29	10.82	22.31	0.00	8.61	0.20	0.26	98.86
03/02/2023	**GOR132**	45.44	0.84	0.01	0.03	10.44	10.80	22.24	0.00	8.50	0.13	0.31	98.74
03/02/2023	**GOR132**	45.57	0.86	0.01	0.03	10.49	10.99	22.28	0.04	8.50	0.17	0.30	99.25
03/02/2023	**GOR132**	45.46	0.87	0.00	0.03	10.30	10.80	22.34	0.00	8.57	0.12	0.34	98.84
03/02/2023	**GOR132**	45.58	0.79	0.00	0.04	10.23	10.87	22.37	0.00	8.59	0.17	0.29	98.94
04/02/2023	**GOR132**	45.53	0.86	0.00	0.04	10.48	10.85	22.39	0.03	8.41	0.15	0.32	99.07
04/02/2023	**GOR132**	45.57	0.85	0.00	0.06	10.33	10.95	22.20	0.00	8.64	0.18	0.28	99.07
04/02/2023	**GOR132**	45.56	0.80	0.00	0.05	10.15	10.99	22.54	0.01	8.55	0.16	0.35	99.15
04/02/2023	**GOR132**	45.31	0.85	0.00	0.01	10.25	10.96	22.42	0.03	8.54	0.17	0.30	98.84
04/02/2023	**GOR132**	45.56	0.89	0.03	0.04	10.28	11.07	22.59	0.03	8.55	0.18	0.37	99.58
04/02/2023	**GOR132**	45.50	0.90	0.00	0.02	10.24	11.20	22.34	0.02	8.51	0.13	0.31	99.17

Date of Analysis	Label	SiO_2	Na_2O	Cl	K_2O	FeO_t	Al_2O_3	MgO	P_2O_5	CaO	MnO	TiO_2	Analytical Total
04/02/2023	**GOR132**	45.47	0.85	0.00	0.02	10.33	10.89	22.54	0.08	8.41	0.14	0.30	99.03
04/02/2023	**GOR132**	45.67	0.81	0.00	0.04	10.29	10.77	22.38	0.06	8.53	0.15	0.38	99.09
04/02/2023	**GOR132**	45.54	0.72	0.01	0.04	10.19	10.95	21.90	0.00	8.64	0.15	0.31	98.44
04/02/2023	**GOR132**	45.44	0.80	0.00	0.03	10.17	10.99	21.91	0.04	8.49	0.16	0.32	98.34
04/02/2023	**GOR132**	45.57	0.83	0.00	0.02	10.22	10.92	22.32	0.05	8.53	0.12	0.31	98.90
04/02/2023	**GOR132**	45.06	0.87	0.00	0.02	10.28	10.90	22.40	0.06	8.66	0.17	0.32	98.75
04/02/2023	**GOR132**	45.53	0.77	0.00	0.00	10.30	10.90	22.49	0.02	8.52	0.17	0.32	99.02
04/02/2023	**GOR132**	45.39	0.91	0.00	0.02	10.34	10.93	22.52	0.00	8.49	0.14	0.30	99.05
05/02/2023	**GOR132**	45.87	0.78	0.00	0.04	10.07	11.01	22.32	0.04	8.56	0.16	0.30	99.16
05/02/2023	**GOR132**	45.23	0.79	0.00	0.03	10.42	11.02	22.34	0.03	8.63	0.14	0.33	98.97
05/02/2023	**GOR132**	45.64	0.79	0.01	0.05	10.29	10.97	22.52	0.01	8.58	0.17	0.29	99.32
05/02/2023	**GOR132**	45.19	0.74	0.01	0.01	10.32	11.00	22.52	0.01	8.48	0.16	0.28	98.73
05/02/2023	**GOR132**	45.66	0.79	0.01	0.04	10.23	10.92	22.61	0.04	8.53	0.15	0.34	99.32
05/02/2023	**GOR132**	45.56	0.84	0.00	0.05	10.33	10.92	22.49	0.01	8.55	0.18	0.35	99.29
05/02/2023	**GOR132**	45.67	0.88	0.00	0.00	10.25	11.03	22.25	0.01	8.57	0.13	0.26	99.06
09/02/2023	**GOR132**	45.09	0.84	0.00	0.04	10.00	10.96	22.21	0.02	8.39	0.11	0.37	98.02
09/02/2023	**GOR132**	45.58	0.85	0.00	0.03	10.02	10.91	22.66	0.02	8.59	0.15	0.27	99.07
09/02/2023	**GOR132**	45.45	0.75	0.00	0.05	10.15	10.87	22.33	0.00	8.50	0.14	0.25	98.50
09/02/2023	**GOR132**	45.37	0.80	0.01	0.02	10.18	10.73	22.51	0.00	8.60	0.14	0.33	98.69
09/02/2023	**GOR132**	45.57	0.86	0.01	0.03	9.94	11.05	22.26	0.02	8.42	0.14	0.31	98.61
09/02/2023	**GOR132**	45.49	0.85	0.00	0.04	10.08	10.93	21.95	0.01	8.60	0.13	0.29	98.37
09/02/2023	**GOR132**	45.66	0.78	0.00	0.04	9.99	11.02	22.31	0.01	8.58	0.12	0.37	98.88
09/02/2023	**GOR132**	45.83	0.91	0.00	0.01	10.29	11.05	22.57	0.05	8.52	0.13	0.32	99.69
09/02/2023	**GOR132**	45.66	0.91	0.00	0.01	10.03	11.05	22.45	0.03	8.61	0.17	0.37	99.29
09/02/2023	**GOR132**	45.76	0.89	0.00	0.05	10.15	10.95	22.56	0.02	8.65	0.16	0.33	99.52
09/02/2023	**GOR132**	45.60	0.94	0.00	0.03	10.34	11.00	22.53	0.03	8.55	0.17	0.34	99.52
09/02/2023	**GOR132**	45.56	0.78	0.00	0.01	10.06	10.94	22.48	0.06	8.55	0.17	0.27	98.87
07/02/2023	**GOR132**	45.79	0.82	0.02	0.03	10.03	11.00	22.34	0.01	8.48	0.15	0.34	98.19
07/02/2023	**GOR132**	45.56	0.69	0.01	0.03	9.88	10.89	22.31	0.08	8.44	0.12	0.30	97.51
07/02/2023	**GOR132**	45.65	0.71	0.00	0.02	9.99	10.81	22.23	0.00	8.51	0.13	0.33	97.57
07/02/2023	**GOR132**	45.59	0.77	0.00	0.03	10.30	11.26	22.37	0.04	8.49	0.15	0.32	98.51
07/02/2023	**GOR132**	45.28	0.85	0.00	0.06	10.20	10.65	22.33	0.05	8.49	0.19	0.37	97.64

Date of Analysis	Label	SiO_2	Na_2O	Cl	K_2O	FeO_t	Al_2O_3	MgO	P_2O_5	CaO	MnO	TiO_2	Analytical Total
08/02/2023	**GOR132**	45.61	0.76	0.00	0.05	10.09	11.11	22.35	0.00	8.63	0.10	0.28	98.15
08/02/2023	**GOR132**	45.69	0.84	0.01	0.03	9.98	11.14	22.38	0.05	8.57	0.14	0.37	98.39
08/02/2023	**GOR132**	45.61	0.81	0.01	0.05	10.21	11.16	22.35	0.04	8.52	0.16	0.31	98.42
08/02/2023	**GOR132**	45.46	0.76	0.00	0.02	10.34	10.95	22.44	0.04	8.53	0.14	0.33	98.21
08/02/2023	**GOR132**	45.50	0.80	0.01	0.04	10.11	11.32	22.55	0.04	8.52	0.17	0.34	98.58
08/02/2023	**GOR132**	45.46	0.87	0.01	0.04	10.23	11.02	22.42	0.00	8.52	0.17	0.31	98.24
08/02/2023	**GOR132**	45.31	0.76	0.00	0.00	10.15	11.08	22.37	0.00	8.58	0.10	0.29	97.84
08/02/2023	**GOR132**	45.84	0.87	0.00	0.03	10.14	10.95	22.36	0.07	8.46	0.12	0.32	98.35
08/02/2023	**GOR132**	45.43	0.88	0.00	0.03	10.25	10.98	22.62	0.00	8.52	0.18	0.33	98.40
08/02/2023	**GOR132**	45.73	0.83	0.01	0.02	10.05	11.14	22.63	0.01	8.55	0.17	0.33	98.63
08/02/2023	**GOR132**	45.27	0.82	0.00	0.02	10.03	11.02	22.44	0.00	8.57	0.17	0.31	97.85
08/02/2023	**GOR132**	45.75	0.78	0.00	0.01	10.05	11.04	22.54	0.04	8.54	0.11	0.37	98.42
30/05/2023	**GOR132**	45.26	0.81	0.00	0.02	10.10	10.88	22.28	0.06	8.49	0.14	0.32	98.36
30/05/2023	**GOR132**	45.58	0.81	0.00	0.03	10.26	10.92	22.44	0.04	8.44	0.12	0.26	98.90
30/05/2023	**GOR132**	45.52	0.86	0.02	0.04	10.06	10.89	22.34	0.03	8.58	0.08	0.28	98.70
30/05/2023	**GOR132**	45.59	0.77	0.00	0.02	10.22	10.99	22.24	0.02	8.54	0.18	0.35	98.94
30/05/2023	**GOR132**	45.83	0.81	0.01	0.05	10.13	10.83	22.32	0.03	8.67	0.17	0.29	99.15
30/05/2023	**GOR132**	45.70	0.80	0.00	0.03	10.28	10.93	22.34	0.04	8.59	0.14	0.33	99.18
31/05/2023	**GOR132**	45.55	0.72	0.01	0.02	10.14	10.82	22.34	0.02	8.51	0.16	0.30	98.59
31/05/2023	**GOR132**	45.23	0.83	0.03	0.02	10.20	10.93	22.60	0.00	8.65	0.13	0.27	98.89
31/05/2023	**GOR132**	45.22	0.93	0.00	0.03	10.00	10.89	22.49	0.04	8.55	0.17	0.26	98.57
31/05/2023	**GOR132**	45.09	0.83	0.00	0.05	10.05	10.97	22.35	0.06	8.57	0.14	0.32	98.43
31/05/2023	**GOR132**	45.60	0.86	0.01	0.04	10.35	10.84	22.56	0.03	8.53	0.17	0.29	99.29
23/08/2022	**GOR132**	45.67	0.82	0.00	0.02	10.34	11.06	22.40	0.03	8.38	0.15	0.31	99.17
23/08/2022	**GOR132**	45.54	0.87	0.00	0.04	10.29	11.01	22.59	0.02	8.48	0.14	0.30	99.28
23/08/2022	**GOR132**	45.33	0.92	0.01	0.03	10.11	10.85	22.21	0.04	8.45	0.15	0.24	98.35
23/08/2022	**GOR132**	45.37	0.88	0.00	0.03	10.45	10.95	22.36	0.03	8.34	0.11	0.32	98.84
23/08/2022	**GOR132**	45.51	0.75	0.00	0.02	10.23	10.82	22.42	0.00	8.39	0.15	0.31	98.60
24/08/2022	**GOR132**	45.47	0.87	0.00	0.05	10.28	10.91	22.62	0.05	8.45	0.16	0.27	99.13
24/08/2022	**GOR132**	45.68	0.75	0.00	0.01	10.26	10.82	22.34	0.07	8.51	0.17	0.31	98.91
24/08/2022	**GOR132**	45.39	0.82	0.00	0.04	10.27	10.98	22.38	0.03	8.56	0.16	0.31	98.94
24/08/2022	**GOR132**	45.70	0.84	0.01	0.02	10.33	10.92	22.33	0.05	8.49	0.08	0.32	99.10

Date of Analysis	Label	SiO_2	Na_2O	Cl	K_2O	FeO_t	Al_2O_3	MgO	P_2O_5	CaO	MnO	TiO_2	Analytical Total
24/08/2022	**GOR132**	45.64	0.80	0.01	0.02	10.03	10.70	22.36	0.04	8.55	0.15	0.32	98.62
03/05/2023	**GOR132**	45.57	0.80	0.00	0.07	10.03	10.93	22.24	0.02	8.61	0.14	0.31	98.70
03/05/2023	**GOR132**	45.65	0.82	0.00	0.05	10.01	10.89	22.24	0.00	8.49	0.18	0.24	98.56
03/05/2023	**GOR132**	45.39	0.93	0.00	0.02	9.90	10.96	22.41	0.00	8.51	0.15	0.39	98.65
03/05/2023	**GOR132**	45.27	0.69	0.02	0.03	10.10	10.97	22.22	0.04	8.46	0.15	0.28	98.22
03/05/2023	**GOR132**	45.72	0.84	0.00	0.04	10.16	10.89	22.43	0.05	8.56	0.16	0.29	99.13
04/05/2023	**GOR132**	45.09	0.87	0.00	0.05	9.96	10.67	22.48	0.06	8.47	0.17	0.31	98.12
04/05/2023	**GOR132**	45.61	1.01	0.02	0.03	10.38	10.90	22.64	0.02	8.40	0.11	0.33	99.45
04/05/2023	**GOR132**	45.76	0.77	0.00	0.02	10.16	10.89	22.49	0.00	8.40	0.16	0.26	98.93
04/05/2023	**GOR132**	45.33	0.98	0.01	0.03	10.15	10.91	22.52	0.02	8.56	0.16	0.30	98.96
04/05/2023	**GOR132**	45.40	0.85	0.00	0.02	10.22	10.90	22.37	0.01	8.42	0.17	0.32	98.68
04/05/2023	**GOR132**	45.50	0.87	0.01	0.01	10.23	11.07	22.52	0.04	8.41	0.11	0.27	99.03
04/05/2023	**GOR132**	45.55	0.84	0.00	0.03	9.91	10.87	22.15	0.01	8.45	0.15	0.30	98.27
04/05/2023	**GOR132**	45.59	0.94	0.02	0.05	10.25	10.85	22.47	0.03	8.55	0.18	0.30	99.22

Table B3. Trace element glass analyses of the crypto-/tephra units preserved in Lake Suigetsu between 120 and 50 ka.

Date of Analysis	SG Label	Rb	Sr	Y	Zr	Nb	Ba	La	Ce	Pr	Nd	Sm	Eu	Gd	Dy	Er	Yb	Lu	Hf	Ta	Pb	Th	U
24/11/2023	**SG14-3911**	156	119	33.0	281	16.3	787	30.7	67.9	7.49	32.5	6.77	1.32	5.95	5.80	3.18	3.84	0.63	7.13	1.12	23.5	13.0	3.78
24/11/2023	**SG14-3911**	157	119	33.7	292	16.1	800	31.1	69.9	7.86	33.3	7.42	1.24	6.60	5.79	3.25	3.87	0.65	7.43	1.16	23.0	13.6	3.99
24/11/2023	**SG14-3911**	156	123	34.9	300	16.8	828	32.5	71.7	8.24	34.2	7.54	1.24	6.00	5.79	3.54	3.97	0.56	8.18	1.15	23.0	13.9	4.37
24/11/2023	**SG14-3911**	154	113	31.6	277	15.6	771	29.1	66.1	7.54	30.9	7.65	1.17	5.44	5.39	3.56	3.95	0.61	6.80	1.04	22.8	12.7	3.94
24/11/2023	**SG14-3911**	154	123	35.2	304	16.7	830	32.1	71.5	8.29	35.1	7.34	1.34	6.22	6.33	3.81	4.35	0.65	7.96	1.16	23.1	14.2	4.02
24/11/2023	**SG14-3911**	161	123	35.9	308	16.9	842	33.2	73.4	8.45	35.0	7.69	1.17	6.23	5.64	3.60	4.27	0.66	7.90	1.22	23.4	14.7	4.27
24/11/2023	**SG14-3911**	159	124	35.0	296	16.8	822	31.5	70.9	7.83	32.8	7.39	1.30	6.91	6.08	3.83	4.01	0.57	7.39	1.16	23.3	13.8	4.23
24/11/2023	**SG14-3911**	152	144	34.5	310	17.1	852	33.3	73.4	8.46	35.1	7.29	1.31	6.32	6.09	3.46	4.24	0.67	8.48	1.19	22.1	14.5	4.59
24/11/2023	**SG14-3911**	159	116	29.8	254	16.1	722	27.8	63.6	7.36	29.8	5.80	1.19	6.10	5.01	3.27	3.52	0.53	5.86	1.02	25.8	12.0	4.18
24/11/2023	**SG14-3911**	156	121	34.1	299	16.6	808	31.7	71.2	7.98	32.9	7.38	1.28	6.79	5.84	3.81	4.21	0.63	7.75	1.16	22.9	14.3	4.54
24/11/2023	**SG14-3911**	155	121	34.8	299	16.6	819	31.4	70.9	8.09	33.4	7.54	1.24	5.56	5.93	3.81	3.57	0.54	7.92	1.14	22.2	14.1	4.05
24/11/2023	**SG14-3911**	162	120	33.8	291	16.5	834	31.1	69.0	8.12	33.0	7.42	1.17	5.72	5.24	3.49	3.67	0.55	7.43	1.12	23.7	13.5	4.20
24/11/2023	**SG14-3911**	158	126	34.9	297	16.7	822	32.0	71.7	8.05	34.2	7.31	1.28	6.17	6.29	3.96	3.86	0.63	8.04	1.15	23.4	14.6	4.22
24/11/2023	**SG14-3911**	157	126	34.2	297	16.6	819	31.4	71.6	8.07	31.6	7.14	1.25	6.04	5.87	3.48	3.90	0.58	7.39	1.10	22.8	13.6	4.19
24/11/2023	**SG14-3911**	160	124	34.1	287	16.4	816	30.8	69.6	7.87	32.4	7.50	1.16	5.77	5.49	3.41	4.22	0.60	7.42	1.07	21.7	13.5	3.83
24/11/2023	**SG14-3911**	158	124	34.5	297	16.7	815	31.9	71.8	8.44	34.4	7.44	1.18	6.10	6.14	3.97	3.98	0.59	7.90	1.18	22.1	14.0	4.39
24/11/2023	**SG14-3911**	165	129	34.3	288	16.6	844	32.4	70.4	8.04	33.2	8.05	1.40	5.99	5.74	3.33	4.05	0.56	7.93	1.13	22.4	13.5	4.29
24/11/2023	**SG14-3911**	161	125	35.5	296	16.5	823	32.5	70.5	8.27	34.1	8.05	1.27	6.57	6.09	3.90	4.52	0.56	8.86	1.20	23.4	14.3	4.30
24/11/2023	**SG14-3911**	156	125	34.7	296	16.5	804	31.7	68.8	7.96	32.0	7.37	1.31	5.76	6.29	4.00	3.81	0.63	8.11	1.15	23.1	14.9	4.06
24/11/2023	**SG14-3911**	161	152	34.8	302	16.7	855	32.4	71.3	8.21	34.7	7.41	1.46	6.13	5.92	3.52	3.74	0.61	8.27	1.16	21.7	14.9	4.28
24/11/2023	**SG14-3911**	166	121	34.2	286	16.3	806	31.2	67.8	7.84	33.2	7.02	1.29	5.45	6.00	3.89	3.53	0.62	8.11	1.12	22.1	13.7	3.87
24/11/2023	**SG14-3911**	159	123	35.8	296	16.8	815	32.6	71.0	7.91	34.4	8.00	1.28	6.79	6.16	3.76	4.28	0.62	8.62	1.17	23.5	14.7	4.20
24/11/2023	**SG14-3911**	162	122	33.8	286	16.6	800	31.3	67.4	7.74	32.1	6.74	1.22	6.05	5.98	3.58	4.01	0.61	7.68	1.16	22.9	13.1	4.23
24/11/2023	**SG14-3911**	163	125	35.3	299	16.9	838	32.5	71.1	8.34	34.0	7.41	1.33	6.26	6.18	4.38	3.92	0.64	8.44	1.16	23.3	14.5	4.28
19/02/2024	**SG14-4002**	149	105	25.2	308	11.7	715	31.1	64.8	7.27	28.0	5.92	0.49	4.25	4.52	2.87	3.02	0.38	8.24	0.79	18.3	13.7	2.87
19/02/2024	**SG14-4002**	206	150	25.3	289	12.1	704	30.2	65.0	7.09	28.6	5.79	0.95	5.01	4.90	2.74	2.73	0.39	7.36	0.78	14.3	11.8	2.48
19/02/2024	**SG14-4002**	101	343	29.0	249	11.0	661	28.5	63.4	7.49	31.5	6.41	1.71	5.61	5.19	3.14	3.00	0.43	6.58	0.66	15.7	9.39	2.06
19/02/2024	**SG14-4002**	75.5	514	24.8	195	9.51	532	23.2	51.5	6.87	26.2	5.89	1.54	4.64	5.02	2.95	2.42	0.43	4.97	0.51	13.5	6.54	1.27
19/02/2024	**SG14-4002**	137	162	23.9	266	11.3	725	29.0	61.2	6.78	26.4	5.64	0.97	4.41	4.37	2.70	2.75	0.37	7.58	0.69	19.2	11.9	2.60
19/02/2024	**SG14-4002**	136	173	25.7	290	11.9	785	31.4	65.8	7.35	28.4	6.08	1.02	4.61	4.73	2.60	2.66	0.38	8.15	0.76	18.8	12.9	2.68
19/02/2024	**SG14-4002**	107	276	25.2	232	10.2	620	25.8	56.6	6.02	25.6	5.81	1.23	4.87	4.25	2.85	2.50	0.40	5.48	0.51	13.9	8.32	1.84
19/02/2024	**SG14-4002**	66.8	629	19.9	164	7.54	478	20.0	42.5	4.86	21.2	4.66	1.45	3.98	3.64	1.87	2.15	0.37	4.61	0.42	11.2	6.01	1.55
19/02/2024	**SG14-4002**	84.7	429	20.6	171	8.43	506	21.2	44.2	4.90	22.2	5.70	1.42	3.76	4.02	2.33	2.51	0.38	4.58	0.43	11.6	5.98	1.59
19/02/2024	**SG14-4002**	133	170	23.0	257	11.3	693	28.1	58.7	6.63	25.2	5.54	0.91	4.44	4.46	2.39	2.47	0.35	6.41	0.69	13.2	10.9	2.27
19/02/2024	**SG14-4002**	103	288	27.4	241	11.5	640	27.6	60.8	7.15	29.8	7.07	1.50	4.94	4.88	2.57	2.73	0.42	6.86	0.66	16.4	8.98	2.02
19/02/2024	**SG14-4002**	114	281	28.1	266	11.5	706	31.1	66.6	7.46	30.5	6.64	1.24	5.52	4.82	2.81	3.33	0.43	6.85	0.69	16.1	10.7	2.24
19/02/2024	**SG14-4002**	134	164	22.7	259	11.2	698	28.5	59.0	6.21	24.1	6.23	0.93	5.00	3.94	2.29	2.58	0.38	6.43	0.64	17.2	10.9	2.58
02/02/2024	**SG14-4032**	185	70.0	37.4	314	16.7	771	35.6	76.0	8.65	37.4	7.42	1.11	5.81	6.61	4.24	4.88	0.68	9.29	1.28	26.8	17.4	4.78
02/02/2024	**SG14-4032**	187	72.0	37.1	317	17.2	791	34.3	77.2	9.04	35.6	6.59	1.09	5.92	6.54	4.10	4.52	0.72	8.81	1.24	25.4	17.2	4.83
02/02/2024	**SG14-4032**	190	72.3	36.9	309	17.1	760	33.6	72.7	8.97	34.3	7.27	1.12	7.17	6.39	4.15	4.37	0.68	8.59	1.19	25.7	16.1	4.89
02/02/2024	**SG14-4032**	200	69.8	35.9	304	16.2	758	33.8	74.8	8.60	32.3	7.16	1.21	6.80	6.42	4.46	3.95	0.59	9.10	1.17	25.6	16.3	5.08
02/02/2024	**SG14-4032**	185	75.2	37.0	309	17.2	784	34.3	76.7	8.91	37.2	7.79	1.15	6.32	6.43	4.00	4.40	0.62	9.07	1.24	25.9	16.9	4.99
02/02/2024	**SG14-4032**	186	67.5	35.4	300	16.8	744	33.3	75.0	8.24	34.0	7.43	1.15	6.53	6.23	3.85	4.33	0.65	8.38	1.20	24.9	16.3	4.69
02/02/2024	**SG14-4032**	185	70.8	35.9	303	16.6	762	33.4	75.0	8.57	35.2	7.64	1.07	5.77	6.77	4.01	4.03	0.64	8.21	1.22	27.0	17.1	4.82
02/02/2024	**SG14-4032**	187	76.3	35.6	299	16.8	773	33.1	73.5	8.78	32.8	6.65	1.09	5.99	6.13	3.91	3.69	0.60	8.33	1.19	25.8	15.4	4.80
02/02/2024	**SG14-4032**	191	76.0	37.0	310	17.3	786	35.2	77.2	8.93	38.6	7.86	1.17	7.30	6.27	4.09	4.14	0.63	9.38	1.23	26.0	16.9	5.16
02/02/2024	**SG14-4032**	188	73.6	36.0	304	16.8	776	33.5	74.6	8.70	35.8	7.31	1.01	5.83	5.92	4.05	4.45	0.61	8.40	1.19	25.3	16.0	4.67

Date of Analysis	SG Label	Rb	Sr	Y	Zr	Nb	Ba	La	Ce	Pr	Nd	Sm	Eu	Gd	Dy	Er	Yb	Lu	Hf	Ta	Pb	Th	U
02/02/2024	**SG14-4032**	189	70.8	36.2	303	17.1	760	33.4	74.1	8.52	33.7	7.62	1.05	5.87	5.79	3.85	4.49	0.62	8.24	1.20	25.2	15.8	4.81
02/02/2024	**SG14-4032**	188	72.3	35.3	295	16.9	769	32.9	75.2	8.46	33.8	7.96	1.06	6.03	6.31	3.73	4.23	0.64	9.17	1.26	26.0	16.6	4.95
02/02/2024	**SG14-4032**	174	68.5	34.0	288	15.8	710	31.8	68.6	8.11	30.9	6.49	1.03	5.69	5.60	3.72	3.87	0.53	7.41	1.04	25.1	16.0	4.59
02/02/2024	**SG14-4032**	185	75.2	36.5	314	17.0	767	33.2	76.1	8.40	35.5	7.55	1.13	6.14	6.83	4.25	4.15	0.70	9.28	1.22	25.3	16.3	5.05
02/02/2024	**SG14-4032**	162	207	36.9	309	17.4	890	35.1	78.2	8.70	37.0	7.97	1.52	7.31	6.55	4.10	4.14	0.65	8.82	1.20	28.6	15.0	4.21
02/02/2024	**SG14-4032**	185	65.1	35.4	288	16.4	706	32.4	72.2	8.14	33.3	6.70	1.02	5.56	6.26	3.47	4.18	0.59	8.38	1.22	25.2	16.4	4.79
02/02/2024	**SG14-4032**	161	177	36.9	322	17.4	768	34.4	75.7	8.86	38.7	9.19	1.34	6.19	7.28	3.98	4.72	0.57	8.37	1.19	22.3	15.0	4.58
20/12/2023	**SG14-4050**	130	166	6.34	96.4	11.6	992	23.0	40.7	3.70	11.3	2.08	0.42	-	-	-	-	-	2.66	1.02	18.6	13.6	2.72
20/12/2023	**SG14-4050**	126	165	6.36	96.1	11.4	972	23.2	41.4	3.47	11.6	1.92	0.50	-	-	-	-	-	3.15	1.01	18.2	12.6	2.76
20/12/2023	**SG14-4050**	179	71	11.0	105	5.61	764	8.50	18.8	2.18	8.49	2.01	0.47	-	-	-	-	-	3.51	0.77	80.7	5.1	1.02
20/12/2023	**SG14-4050**	129	142	5.85	90.2	11.3	913	22.9	41.2	3.31	10.7	1.71	0.48	-	-	-	-	-	3.10	1.05	18.7	12.6	3.01
20/12/2023	**SG14-4050**	135	147	6.46	90.0	11.5	961	23.9	42.8	3.48	11.8	2.01	0.58	-	-	-	-	-	2.92	1.02	20.1	11.5	2.71
20/12/2023	**SG14-4050**	127	174	10.9	116	12.2	1008	25.6	48.8	4.78	17.1	3.03	0.77	-	-	-	-	-	3.41	1.07	19.2	12.6	2.98
20/12/2023	**SG14-4050**	126	119	6.75	82.3	11.7	856	23.3	43.0	3.89	11.6	2.17	0.42	-	-	-	-	-	2.66	1.12	20.0	13.5	2.68
20/12/2023	**SG14-4050**	140	134	6.97	91.0	12.1	959	24.5	44.5	3.90	13.2	1.86	0.50	-	-	-	-	-	2.74	1.14	22.4	14.3	3.00
20/12/2023	**SG14-4050**	119	248	7.59	109	11.0	716	20.2	35.6	3.22	12.2	2.18	0.63	-	-	-	-	-	3.33	1.00	13.9	11.5	2.72
20/12/2023	**SG14-4050**	128	144	6.05	93.2	10.8	982	22.8	40.5	3.60	11.1	2.27	0.44	-	-	-	-	-	2.97	1.00	18.8	12.7	2.75
20/12/2023	**SG14-4050**	131	150	5.75	83.4	11.4	907	22.6	39.9	3.39	12.0	2.65	0.56	-	-	-	-	-	3.00	1.03	19.9	12.5	2.98
20/12/2023	**SG14-4050**	134	143	6.05	85.6	11.3	938	22.9	40.7	3.88	12.2	3.57	0.63	-	-	-	-	-	2.85	1.06	19.6	12.7	2.90
20/12/2023	**SG14-4050**	130	140	5.99	93.8	11.3	922	23.8	43.2	3.81	11.5	2.09	0.52	-	-	-	-	-	2.98	1.10	20.4	13.4	2.99
20/02/2024	**SG14-4053**	135	314	27.9	303	13.6	861	32.6	68.2	7.80	32.0	6.75	1.13	5.32	5.52	2.97	2.97	0.41	7.90	0.82	20.2	12.9	2.67
20/02/2024	**SG14-4053**	147	194	29.7	331	14.2	894	34.3	73.7	8.29	32.0	6.94	1.12	5.87	5.28	2.99	3.01	0.50	8.88	0.90	19.9	14.4	2.68
20/02/2024	**SG14-4053**	134	318	32.5	317	14.8	865	34.3	73.9	8.52	36.0	8.11	1.59	7.03	6.06	3.53	3.32	0.51	8.66	0.90	18.5	12.4	2.56
20/02/2024	**SG14-4053**	164	217	30.8	334	14.7	909	34.9	74.7	8.42	34.2	6.87	1.33	5.70	5.50	3.36	3.61	0.52	8.97	0.91	24.2	14.0	2.74
20/02/2024	**SG14-4053**	153	222	30.1	322	14.4	883	35.5	73.8	8.33	34.1	6.92	1.28	5.54	5.66	3.58	3.38	0.54	8.74	0.84	20.5	13.4	2.80
20/02/2024	**SG14-4053**	162	195	26.1	322	13.0	854	32.9	68.6	7.53	28.6	5.66	1.03	5.22	4.50	2.91	2.93	0.45	8.86	0.88	18.2	14.3	2.96
20/02/2024	**SG14-4053**	148	215	28.7	322	13.9	876	33.9	70.7	8.27	31.4	7.14	1.11	5.13	4.78	3.23	3.44	0.48	8.62	0.86	14.5	13.7	2.82
20/02/2024	**SG14-4053**	149	202	29.3	319	14.2	875	34.1	70.1	8.07	32.0	6.98	1.14	5.00	5.43	3.53	3.25	0.52	8.66	0.89	18.8	13.5	2.93
24/11/2023	**SG14-4135B**	162	177	32.0	303	17.0	728	28.9	65.4	7.94	33.6	6.51	1.34	7.26	5.65	3.79	4.08	0.55	7.01	1.08	23.6	13.6	4.42
24/11/2023	**SG14-4135B**	104	382	27.1	207	12.8	563	24.3	55.2	6.52	27.3	6.41	1.30	5.61	4.99	2.34	2.63	0.56	4.97	0.83	16.3	9.50	3.01
24/11/2023	**SG14-4135A**	102	372	28.1	205	12.7	549	24.5	54.3	6.35	26.4	7.45	1.53	5.41	5.13	2.98	2.48	0.46	5.57	0.82	17.6	9.34	2.56
24/11/2023	**SG14-4135A**	103	386	26.5	195	12.2	545	23.5	52.8	6.51	29.0	6.03	1.34	4.66	5.04	2.76	3.07	0.45	5.12	0.82	16.8	8.87	2.97
24/11/2023	**SG14-4135A**	106	353	26.4	195	12.7	537	23.1	52.9	6.43	26.5	6.64	1.30	5.47	4.66	2.72	2.73	0.45	5.23	0.79	17.5	8.74	2.67
24/11/2023	**SG14-4135B**	154	210	32.2	302	17.4	737	30.1	65.9	7.90	33.3	7.66	1.31	5.76	6.56	3.20	4.03	0.56	8.16	1.21	24.0	14.5	4.23
24/11/2023	**SG14-4135A**	104	366	27.8	199	12.4	554	23.5	54.8	6.67	29.4	6.30	1.40	5.55	4.92	3.13	2.64	0.45	5.57	0.80	17.1	9.97	2.87
24/11/2023	**SG14-4135A**	102	386	27.5	195	12.5	556	23.9	53.5	6.47	26.7	6.37	1.39	5.68	5.04	2.92	3.04	0.48	5.38	0.82	17.4	9.20	2.59
24/11/2023	**SG14-4135A**	114	306	29.5	224	13.9	597	25.9	58.2	6.85	31.5	6.73	1.39	6.53	5.47	3.35	3.52	0.46	6.70	0.92	17.9	10.4	3.27
24/11/2023	**SG14-4135A**	128	166	35.9	254	15.2	604	29.9	67.8	8.36	35.4	6.99	1.40	6.52	5.98	3.95	4.28	0.66	7.15	1.04	20.1	12.5	3.38
24/11/2023	**SG14-4135A**	103	394	28.4	205	12.6	574	24.9	55.7	6.41	29.5	6.50	1.52	5.57	4.98	2.90	3.01	0.56	5.91	0.86	17.1	9.76	2.84
24/11/2023	**SG14-4135A**	103	324	27.3	210	12.5	559	23.9	54.2	6.38	26.4	6.52	1.36	5.70	5.05	3.26	2.78	0.43	6.03	0.89	15.5	9.76	2.60
24/11/2023	**SG14-4135A**	105	383	27.7	205	12.7	559	24.0	54.6	6.45	27.7	6.68	1.46	5.70	5.19	2.96	3.01	0.47	5.05	0.84	17.0	9.65	2.45
24/11/2023	**SG14-4135B**	152	194	31.9	290	16.6	713	29.4	65.3	7.88	33.1	6.71	1.25	5.47	5.75	3.26	3.99	0.54	7.93	1.11	22.2	13.8	4.18
24/11/2023	**SG14-4135A**	107	322	26.7	194	12.0	535	22.7	52.2	6.21	27.6	6.13	1.19	4.65	5.57	2.81	2.85	0.42	5.07	0.79	16.9	9.13	2.71
24/11/2023	**SG14-4135A**	134	277	28.2	234	14.2	643	26.1	58.7	6.78	27.0	5.51	1.15	5.39	5.53	3.11	3.53	0.44	6.54	0.94	18.1	11.7	3.73
24/11/2023	**SG14-4135A**	103	396	27.0	197	12.8	566	23.8	53.1	6.44	26.7	5.28	1.40	4.72	5.70	3.04	2.74	0.42	5.39	0.88	16.7	9.74	2.62
24/11/2023	**SG14-4135A**	107	341	28.2	204	12.7	556	23.4	54.2	6.67	27.9	5.72	1.46	5.78	5.52	3.08	3.28	0.48	5.08	0.84	17.5	9.26	2.74
24/11/2023	**SG14-4135A**	95.0	391	25.7	186	11.5	515	22.1	49.9	5.75	25.8	4.98	1.45	4.77	4.83	2.88	2.88	0.43	4.51	0.81	14.9	9.01	2.40
24/11/2023	**SG14-4135A**	102	366	28.6	203	12.5	569	24.4	55.3	6.56	29.4	6.09	1.45	6.17	4.91	3.25	3.35	0.46	5.82	0.86	16.2	9.80	2.79

Date of Analysis	SG Label	Rb	Sr	Y	Zr	Nb	Ba	La	Ce	Pr	Nd	Sm	Eu	Gd	Dy	Er	Yb	Lu	Hf	Ta	Pb	Th	U
24/11/2023	**SG14-4135A**	123	336	27.9	228	13.7	635	25.9	56.8	6.75	28.9	6.94	1.35	5.09	4.91	3.23	2.65	0.45	5.57	0.90	17.2	10.3	3.13
24/11/2023	**SG14-4135A**	102	358	26.4	189	12.0	521	22.6	52.0	6.32	25.1	5.34	1.47	5.52	5.00	2.79	2.94	0.45	5.18	0.76	17.4	8.91	2.53
20/02/2024	**SG14-4150**	136	160	6.71	85.3	11.7	939	23.9	45.5	3.94	12.2	-	-	-	-	-	-	-	3.36	1.08	16.4	12.8	3.23
20/02/2024	**SG14-4150**	134	188	6.44	105	11.7	1016	23.3	43.9	3.93	11.5	-	-	-	-	-	-	-	3.19	1.07	17.6	12.1	3.12
20/02/2024	**SG14-4150**	122	198	5.95	98.4	11.3	991	22.4	40.7	3.83	13.1	-	-	-	-	-	-	-	2.72	1.00	16.8	11.3	2.53
20/02/2024	**SG14-4150**	140	169	8.45	94.0	12.4	965	25.5	46.9	4.01	12.2	-	-	-	-	-	-	-	3.32	1.18	18.8	13.3	3.11
20/02/2024	**SG14-4150**	138	156	6.54	84.5	11.7	937	23.7	42.3	3.95	12.2	-	-	-	-	-	-	-	3.00	1.00	19.2	12.3	2.51
19/12/2023	**SG14-4159**	179	145	27.4	354	14.1	767	37.3	77.3	8.59	31.6	6.05	0.99	5.64	4.73	3.08	2.62	0.50	9.5	0.94	21.9	16.5	3.06
19/12/2023	**SG14-4159**	168	225	34.2	304	16.2	826	32.2	68.9	7.83	32.1	6.13	1.35	6.58	6.47	3.55	3.67	0.55	8.0	1.12	24.1	15.1	4.57
19/12/2023	**SG14-4159**	174	226	35.1	305	16.6	852	33.6	72.3	7.90	34.0	7.06	1.41	6.01	6.41	3.38	3.35	0.63	8.4	1.15	24.7	15.5	4.48
19/12/2023	**SG14-4159**	167	223	30.0	301	16.2	819	32.1	66.1	7.47	33.6	6.38	0.95	5.57	4.32	3.07	3.60	0.55	7.5	1.09	21.5	16.6	4.37
19/12/2023	**SG14-4159**	165	231	32.3	284	16.0	803	30.9	68.6	7.78	31.7	6.54	1.40	6.61	5.49	3.37	3.46	0.58	7.1	1.14	22.9	14.9	4.50
19/12/2023	**SG14-4159**	169	229	33.1	296	16.3	794	31.5	69.8	7.67	33.8	6.68	1.31	5.62	5.40	3.32	3.32	0.62	7.5	1.14	23.6	15.6	4.79
19/12/2023	**SG14-4159**	169	225	32.4	289	16.0	762	30.4	66.6	7.61	30.7	7.00	1.40	6.62	5.23	3.43	3.62	0.60	8.0	1.10	24.4	13.9	4.15
19/12/2023	**SG14-4159**	171	230	34.7	294	16.5	790	31.3	67.7	8.17	30.9	7.08	1.25	5.59	5.41	3.82	4.53	0.65	7.0	1.12	23.3	15.7	4.65
19/12/2023	**SG14-4159**	171	240	32.8	296	16.8	777	32.0	69.1	8.08	33.6	6.32	1.47	6.00	6.08	3.45	3.59	0.60	8.3	1.18	22.7	16.4	4.49
19/02/2024	**SG14-4187**	61.1	809	20.0	164	20.9	767	29.2	61.5	7.04	29.2	5.53	1.65	5.02	3.52	2.01	1.99	0.33	4.22	1.20	14.6	6.26	1.59
19/02/2024	**SG14-4187**	60.8	799	17.2	146	19.2	730	26.5	56.5	6.13	25.6	4.63	1.36	4.04	3.29	1.85	2.11	0.26	3.78	1.09	12.9	5.27	1.47
19/02/2024	**SG14-4187**	72.6	702	17.2	162	24.0	857	32.1	68.1	7.45	28.2	5.06	1.51	3.59	3.31	1.70	1.76	0.28	3.79	1.26	26.4	6.11	1.71
19/02/2024	**SG14-4187**	64.1	896	19.7	158	21.6	757	28.9	61.4	6.87	28.5	5.07	1.71	4.57	3.86	2.19	2.05	0.31	4.18	1.16	17.5	5.52	1.47
19/02/2024	**SG14-4187**	60.9	914	19.1	162	21.4	767	29.7	62.9	6.68	26.6	5.46	1.30	4.04	3.24	2.40	1.90	0.33	3.84	1.19	14.7	5.98	1.63
19/02/2024	**SG14-4187**	59.5	854	18.9	153	20.2	753	27.8	60.0	6.49	27.4	5.45	1.31	4.08	2.95	2.01	2.44	0.35	3.45	1.11	13.6	5.60	1.56
19/02/2024	**SG14-4187**	56.1	1052	18.6	151	19.8	737	28.4	59.2	6.46	26.8	4.87	1.73	4.34	3.53	2.37	2.16	0.29	3.98	1.08	13.9	5.76	1.41
04/07/2023	**SG14-4223**	167	326	24.7	533	168	572	102	175	15.9	51.9	8.06	1.89	5.48	4.44	2.73	2.73	0.43	10.7	8.64	13.4	19.8	4.61
04/07/2023	**SG14-4223**	178	272	24.2	565	177	515	102	170	15.4	51.6	7.12	1.63	5.81	4.42	2.69	2.82	0.37	11.0	9.05	13.6	20.5	4.73
04/07/2023	**SG14-4223**	159	419	21.5	527	161	602	92.5	154	13.3	45.1	6.04	1.51	4.77	4.37	2.54	2.60	0.32	10.8	8.28	13.5	18.0	4.08
04/07/2023	**SG14-4223**	171	320	23.5	544	168	592	94.8	160	14.5	48.7	7.65	1.56	5.18	4.47	2.68	2.49	0.37	10.6	8.55	13.2	19.8	4.15
04/07/2023	**SG14-4223**	171	367	23.3	531	172	630	93.9	157	13.6	45.1	6.64	1.39	5.40	4.56	2.83	2.47	0.39	10.4	8.82	15.9	19.5	4.24
04/07/2023	**SG14-4223**	190	217	27.0	594	182	437	114	193	18.3	57.3	8.49	1.68	6.22	5.64	2.85	3.17	0.41	11.2	9.46	14.7	22.5	4.54
04/07/2023	**SG14-4223**	165	401	30.6	529	165	547	128	224	21.1	74.3	10.3	2.22	8.35	5.95	3.16	2.68	0.43	10.9	8.48	13.7	20.6	4.42
04/07/2023	**SG14-4223**	171	360	25.3	542	169	533	105	179	16.2	53.9	7.81	1.72	5.73	4.41	2.72	2.29	0.43	11.0	8.52	14.0	20.9	3.98
04/07/2023	**SG14-4223**	184	282	29.1	588	181	498	121	208	18.8	64.5	9.36	2.12	6.46	5.31	3.15	3.11	0.45	11.8	9.23	14.0	21.9	4.34
04/07/2023	**SG14-4223**	153	381	20.6	483	152	572	86.0	146	12.9	42.2	6.16	1.46	4.98	4.05	2.05	2.39	0.35	9.51	7.66	12.1	17.3	3.76
04/07/2023	**SG14-4223**	164	276	25.8	525	163	459	109	197	17.1	59.0	8.25	1.92	6.59	5.04	2.64	2.65	0.40	11.0	8.40	11.9	19.8	4.24
04/07/2023	**SG14-4223**	168	307	21.5	489	161	520	89.0	152	12.9	45.6	6.18	1.67	4.43	4.40	2.21	2.05	0.33	10.1	8.09	12.4	18.3	3.76
26/06/2023	**SG14-4263**	165	131	28.0	248	9.32	572	23.0	49.5	5.57	23.8	4.98	0.80	4.07	4.42	3.25	3.00	0.56	6.60	0.64	22.1	11.7	3.39
26/06/2023	**SG14-4263**	158	129	28.0	238	9.55	572	22.5	50.3	6.14	24.4	5.68	1.12	4.32	4.61	3.47	3.11	0.41	6.83	0.66	22.3	11.4	3.29
26/06/2023	**SG14-4263**	151	156	30.2	249	9.66	605	25.0	55.4	6.41	26.8	5.66	0.89	4.96	5.29	3.60	3.07	0.49	6.85	0.73	23.5	12.8	3.59
26/06/2023	**SG14-4263**	140	161	29.3	251	9.78	620	22.9	50.8	5.87	24.3	5.39	0.86	4.85	5.02	3.29	3.42	0.47	6.34	0.71	20.9	13.7	3.32
26/06/2023	**SG14-4263**	158	155	32.0	267	9.98	616	26.5	58.2	6.78	25.5	5.37	0.93	4.92	5.97	3.50	4.01	0.54	7.77	0.76	23.1	14.5	3.60
26/06/2023	**SG14-4263**	151	158	30.9	242	9.28	561	25.5	60.0	6.74	28.0	6.94	0.95	5.11	4.63	4.35	3.05	0.40	6.16	0.68	22.3	14.3	3.24
26/06/2023	**SG14-4263**	151	163	31.9	260	9.83	609	25.9	56.8	6.27	26.2	6.38	0.99	4.74	5.00	3.58	3.35	0.51	7.86	0.73	22.9	14.1	3.51
26/06/2023	**SG14-4263**	149	218	29.1	238	9.14	594	23.9	52.8	6.09	24.6	4.90	1.03	5.47	6.38	3.09	3.35	0.47	6.76	0.69	20.7	12.5	3.33
26/06/2023	**SG14-4263**	158	138	31.2	253	10.1	605	25.0	56.3	6.09	29.3	5.65	1.00	4.66	4.96	3.41	3.83	0.63	7.18	0.72	17.6	13.5	3.27
26/06/2023	**SG14-4263**	163	143	30.2	272	10.0	622	24.5	54.5	6.18	24.6	5.19	0.82	4.73	5.46	3.27	3.55	0.51	7.71	0.75	23.3	14.2	3.68

Date of Analysis	SG Label	Rb	Sr	Y	Zr	Nb	Ba	La	Ce	Pr	Nd	Sm	Eu	Gd	Dy	Er	Yb	Lu	Hf	Ta	Pb	Th	U
20/02/2024	**SG14-4307**	72.0	130	32.3	177	5.37	398	15.6	37.5	4.34	19.2	4.96	0.84	4.36	5.57	3.41	3.61	0.57	4.61	0.37	19.5	6.64	1.91
20/02/2024	**SG14-4307**	72.7	122	31.4	179	5.37	399	15.5	37.1	4.37	20.0	4.14	0.83	4.83	5.21	3.50	4.01	0.57	4.75	0.38	19.7	6.46	1.70
20/02/2024	**SG14-4307**	71.9	124	30.1	174	5.36	397	15.6	37.0	4.17	18.6	4.81	0.91	4.58	4.89	3.41	3.33	0.50	4.47	0.38	18.9	6.04	1.88
20/02/2024	**SG14-4307**	72.8	127	31.7	179	5.29	407	15.9	38.0	4.56	19.4	5.23	0.89	4.43	5.35	3.72	3.64	0.50	4.59	0.38	19.4	7.06	1.92
20/02/2024	**SG14-4307**	75.2	140	31.4	179	6.10	414	17.4	39.9	4.58	21.3	4.90	0.88	4.76	4.85	3.32	3.47	0.57	4.65	0.44	25.7	6.59	2.35
20/02/2024	**SG14-4307**	78.1	134	32.2	184	5.25	414	16.1	38.8	4.64	20.0	4.43	0.99	5.16	5.57	3.55	3.78	0.60	4.81	0.37	18.5	6.35	1.85
20/02/2024	**SG14-4307**	71.9	123	31.7	178	5.55	411	16.1	36.9	4.56	20.4	4.25	0.97	4.40	5.35	3.46	3.46	0.59	5.13	0.36	18.5	6.01	1.89
20/02/2024	**SG14-4307**	70.6	120	30.0	171	5.09	388	14.9	34.9	3.92	18.2	3.80	0.97	4.97	5.05	3.54	3.52	0.59	4.39	0.36	18.9	6.00	1.77
20/02/2024	**SG14-4307**	73.0	129	31.7	176	5.45	406	16.1	37.1	4.38	20.1	4.92	1.15	4.37	4.86	4.36	3.81	0.57	5.20	0.41	17.2	6.28	1.60
20/02/2024	**SG14-4307**	74.2	150	33.0	170	6.10	411	17.3	40.5	5.02	20.3	5.08	1.08	5.66	5.55	3.36	4.47	0.55	4.60	0.43	19.6	6.89	1.75
20/02/2024	**SG14-4307**	71.1	117	30.1	173	5.23	382	15.2	36.1	4.18	19.0	4.46	0.96	4.93	5.30	3.26	3.95	0.62	4.64	0.38	18.9	6.21	2.08
20/02/2024	**SG14-4307**	70.7	121	29.2	163	5.14	416	16.2	34.7	4.19	18.9	5.33	0.86	3.73	4.69	2.84	3.65	0.50	5.22	0.38	17.2	5.94	1.52
20/02/2024	**SG14-4307**	71.5	122	29.8	170	5.82	393	16.0	36.4	4.59	16.5	4.13	1.02	4.13	5.46	3.03	3.60	0.56	4.05	0.36	18.9	6.63	1.72
19/02/20224	**SG14-4352**	129	455	30.9	218	11.6	682	28.8	63.5	7.43	34.3	6.75	1.90	6.08	5.98	3.30	3.22	0.51	5.79	0.86	20.4	12.7	3.71
19/02/20224	**SG14-4352**	168	240	31.7	279	15.2	742	31.3	68.3	8.12	32.9	7.03	1.36	6.08	5.37	3.47	3.29	0.53	7.49	1.11	22.4	15.9	4.88
19/02/20224	**SG14-4352**	181	129	38.0	313	16.4	750	35.8	80.1	9.38	40.4	9.29	1.37	7.16	6.77	4.10	3.95	0.68	8.14	1.17	25.2	17.4	5.43
19/02/20224	**SG14-4352**	123	501	33.0	218	11.5	663	28.6	63.3	7.82	32.4	7.45	1.78	6.34	6.00	3.62	3.56	0.52	5.71	0.85	18.6	12.2	3.65
19/02/20224	**SG14-4352**	137	380	31.2	239	12.7	728	29.4	65.7	7.54	32.1	7.38	1.29	6.49	5.66	3.72	3.20	0.51	6.75	0.94	20.8	13.4	3.68
19/02/20224	**SG14-4352**	141	343	29.6	226	12.4	700	28.3	62.6	7.16	30.7	6.76	1.36	5.33	5.41	3.21	3.51	0.50	6.20	0.86	21.2	12.2	3.48
19/02/20224	**SG14-4352**	143	367	31.7	240	13.0	736	29.3	66.4	7.67	32.0	6.42	1.74	7.19	5.61	3.12	3.49	0.52	6.12	0.95	22.3	13.3	4.04
19/02/20224	**SG14-4352**	168	91	36.9	286	14.9	667	31.9	73.9	8.86	34.7	8.01	1.16	7.21	6.69	3.95	3.96	0.67	8.01	1.08	22.4	16.2	4.82
19/02/20224	**SG14-4352**	137	373	31.0	205	11.4	623	28.1	64.0	7.38	30.6	6.13	1.51	6.22	5.20	2.73	3.04	0.45	5.14	0.89	24.7	13.1	3.72
19/02/20224	**SG14-4352**	126	473	31.0	218	11.8	700	28.6	65.2	7.76	32.3	7.20	1.85	6.98	5.81	3.33	3.79	0.50	6.30	0.84	20.7	12.7	3.60
19/02/20224	**SG14-4352**	129	447	32.9	230	12.3	722	30.2	67.2	7.69	33.0	6.76	1.81	5.89	5.97	3.39	3.38	0.52	6.33	0.88	20.0	12.7	3.63
19/02/20224	**SG14-4352**	137	380	30.6	230	12.5	711	29.6	64.7	7.58	32.5	7.19	1.26	5.84	5.31	3.44	3.25	0.55	6.54	0.93	20.3	12.8	3.76
19/02/20224	**SG14-4352**	129	416	30.8	221	11.8	649	27.9	62.4	7.41	31.3	6.68	1.71	5.75	5.89	3.25	3.57	0.48	5.85	0.87	20.6	12.2	3.65
19/02/20224	**SG14-4352**	147	374	31.3	242	13.0	730	29.8	67.3	7.69	31.7	6.62	1.62	6.72	5.91	3.49	3.38	0.53	6.48	0.91	20.5	13.0	3.91
19/02/20224	**SG14-4352**	128	442	29.7	211	11.3	652	27.5	61.9	7.20	31.3	7.18	1.42	5.86	5.70	3.26	3.03	0.44	4.93	0.80	19.7	11.4	3.38
19/02/20224	**SG14-4352**	131	423	31.5	228	12.1	694	29.4	67.5	8.03	32.7	7.14	1.61	5.91	5.76	3.22	3.42	0.51	5.93	0.88	20.1	12.4	3.65
19/02/20224	**SG14-4352**	125	519	27.8	200	10.9	657	26.3	58.0	7.00	29.1	6.59	1.37	5.38	4.78	2.66	3.12	0.44	5.06	0.76	18.3	11.0	3.26
19/02/20224	**SG14-4352**	127	452	31.2	215	12.6	685	29.0	63.4	7.89	31.8	7.28	1.47	5.63	5.64	3.10	4.14	0.56	5.40	0.82	18.0	11.9	3.38
19/02/20224	**SG14-4471A**	109	412	38.4	333	15.9	864	37.7	82.6	10.4	40.3	4.34	2.41	8.87	7.47	4.67	4.55	0.65	9.32	0.88	19.4	9.57	2.34
19/02/20224	**SG14-4471B**	70.3	365	28.2	233	13.2	899	30.6	65.5	8.16	32.8	4.38	1.76	7.12	5.35	3.72	3.32	0.53	6.54	0.70	16.0	5.88	1.47
19/02/20224	**SG14-4471A**	112	370	29.3	235	12.3	754	30.1	66.2	7.02	29.1	4.76	2.01	6.00	5.82	3.95	3.48	0.56	7.50	0.77	19.4	9.07	2.07
19/02/20224	**SG14-4471B**	77.5	527	37.6	238	12.9	675	29.9	71.7	9.02	40.8	8.87	2.75	7.66	8.36	4.30	5.16	0.65	6.73	0.70	17.3	7.01	1.62
19/02/20224	**SG14-4471A**	103	455	39.4	311	14.8	895	35.8	81.7	10.3	48.4	9.69	2.95	8.51	7.80	4.74	3.52	0.56	8.75	0.86	28.3	7.84	1.66
19/02/20224	**SG14-4471A**	141	243	25.5	229	13.8	835	30.4	64.3	7.73	29.0	6.27	2.24	6.99	5.23	3.20	3.63	0.60	7.46	1.01	18.0	12.7	4.13
19/02/20224	**SG14-4471A**	173	147	27.3	247	14.1	793	30.6	71.5	6.88	30.6	3.94	1.88	6.13	5.91	3.29	4.23	0.61	7.13	1.11	23.0	14.0	4.74
20/02/2024	**SG14-4496**	150	144	30.9	252	9.56	592	24.8	54.5	6.06	25.9	6.04	0.96	5.16	5.18	3.32	3.60	0.52	7.50	0.72	23.2	13.5	3.31
20/02/2024	**SG14-4496**	149	149	31.4	254	9.50	582	24.7	55.3	6.32	26.5	5.82	1.01	4.96	5.06	3.65	3.74	0.51	7.32	0.71	23.0	13.7	3.38
20/02/2024	**SG14-4496**	141	160	33.7	248	9.44	567	25.1	57.3	6.36	27.5	6.49	0.95	6.03	5.91	3.63	3.66	0.57	7.38	0.75	22.4	12.2	3.23
20/02/2024	**SG14-4496**	157	159	32.2	287	15.2	813	33.3	72.8	8.43	31.9	6.19	1.37	5.22	4.87	3.48	3.81	0.59	7.75	1.15	23.8	15.5	4.71
20/02/2024	**SG14-4496**	153	148	31.7	261	9.72	609	25.5	56.7	6.41	27.1	6.01	0.98	4.91	5.09	3.64	3.30	0.52	7.72	0.73	23.3	13.6	3.24
20/02/2024	**SG14-4496**	149	147	31.1	251	9.54	596	24.8	55.3	6.12	25.2	5.69	0.89	4.99	5.48	3.25	3.60	0.54	6.98	0.73	22.8	13.5	3.15
20/02/2024	**SG14-4496**	142	180	29.7	238	8.90	567	24.0	52.3	6.10	24.5	5.54	0.87	4.71	5.38	3.34	3.64	0.49	6.74	0.68	21.8	12.4	2.95
20/02/2024	**SG14-4496**	156	121	29.5	247	9.27	573	23.9	52.7	5.74	24.8	5.40	0.72	5.08	4.70	2.94	2.91	0.50	7.84	0.66	20.7	12.4	3.08
20/02/2024	**SG14-4496**	162	103	28.2	261	9.36	601	24.4	52.9	5.87	22.5	4.99	0.69	4.86	5.01	2.94	3.51	0.46	7.30	0.69	22.8	14.1	3.66
20/02/2024	**SG14-4496**	147	161	29.9	253	9.34	593	24.5	54.9	5.97	25.8	5.92	1.01	5.13	5.33	3.11	3.37	0.53	7.22	0.72	22.5	13.2	3.53

Date of Analysis	SG Label	Rb	Sr	Y	Zr	Nb	Ba	La	Ce	Pr	Nd	Sm	Eu	Gd	Dy	Er	Yb	Lu	Hf	Ta	Pb	Th	U
20/02/2024	**SG14-4496**	124	175	27.8	240	8.59	533	21.9	48.0	5.53	23.3	5.21	0.99	4.20	4.74	2.83	3.11	0.47	6.65	0.68	25.0	12.3	2.90
20/02/2024	**SG14-4496**	137	198	32.9	229	8.79	555	23.8	53.0	5.91	25.5	5.98	1.08	5.43	5.63	3.55	3.91	0.55	6.35	0.68	22.6	10.8	2.66
20/02/2024	**SG14-4496**	144	157	30.2	237	9.34	583	24.3	53.9	6.34	25.9	5.73	0.89	4.90	5.12	3.17	3.15	0.54	6.59	0.70	21.4	11.9	3.21
26/06/2023	**SG14-4531**	69.8	505	32.3	218.3	11.0	532	26.6	61.2	7.27	33.4	8.03	2.10	6.77	5.87	3.35	3.06	0.51	5.98	0.61	11.2	5.94	1.38
26/06/2023	**SG14-4531**	69.9	509	32.8	217.8	11.2	531	27.0	62.2	7.46	33.5	7.95	1.98	6.17	6.39	3.76	3.31	0.46	5.98	0.60	12.1	6.13	1.30
26/06/2023	**SG14-4531**	69.2	501	32.5	218.3	11.1	539	27.3	62.8	7.66	34.0	7.78	2.02	6.92	6.14	3.43	3.34	0.49	5.62	0.62	11.3	6.07	1.26
26/06/2023	**SG14-4531**	69.3	514	33.2	223.7	11.1	544	27.3	62.9	7.67	34.0	7.48	2.19	6.41	6.44	3.61	3.36	0.55	5.38	0.62	11.2	6.11	1.30
26/06/2023	**SG14-4531**	70.6	506	32.7	217.3	11.3	537	27.8	63.3	7.29	34.5	6.94	2.22	6.73	6.49	3.69	3.42	0.51	5.40	0.61	11.1	6.10	1.38
26/06/2023	**SG14-4531**	70.0	502	32.8	218.3	11.2	545	27.2	61.9	7.13	34.7	7.20	2.15	7.25	6.41	3.55	3.72	0.50	5.47	0.60	11.0	6.12	1.33
26/06/2023	**SG14-4531**	69.7	499	31.8	217.8	11.2	531	26.8	61.3	7.41	33.6	7.25	1.91	6.96	6.21	3.48	3.46	0.47	5.55	0.64	11.5	5.99	1.31
26/06/2023	**SG14-4531**	70.4	499	32.1	216.9	11.3	542	27.0	62.7	7.55	34.4	7.12	1.98	6.45	6.03	3.72	3.05	0.49	5.78	0.61	11.1	5.96	1.22
26/06/2023	**SG14-4531**	73.6	496	32.2	213.4	10.8	524	26.2	62.0	7.47	33.6	7.64	1.93	6.03	6.08	3.75	3.29	0.48	5.94	0.63	11.4	5.97	1.42
26/06/2023	**SG14-4531**	67.8	507	31.5	212.0	10.8	521	26.1	60.4	7.37	33.5	6.56	2.04	6.73	5.71	3.29	3.05	0.50	5.81	0.59	10.6	5.73	1.31
26/06/2023	**SG14-4531**	69.2	484	31.1	206.6	10.6	513	26.2	60.3	7.44	32.1	7.52	1.91	6.07	6.25	3.27	2.98	0.45	5.17	0.60	12.7	5.64	1.34
26/06/2023	**SG14-4531**	69.0	465	29.9	207.5	10.5	498	24.9	58.1	7.17	30.6	7.11	1.79	6.22	5.42	3.20	3.08	0.50	5.39	0.60	11.8	5.53	1.22
26/06/2023	**SG14-4531**	68.4	493	32.3	215.7	11.1	538	27.2	61.6	7.64	34.6	7.86	2.10	7.23	6.18	3.62	3.64	0.53	5.92	0.61	11.1	5.96	1.29
26/06/2023	**SG14-4531**	71.1	487	32.8	217.1	11.2	535	27.0	62.2	7.58	34.8	7.70	2.11	6.67	6.37	3.46	3.21	0.49	5.59	0.60	11.0	6.10	1.43
20/12/2023	**SG14-4582**	151	80.3	13.3	108.6	6.62	555	21.9	42.2	3.89	13.9	2.54	0.38	1.96	2.04	1.34	1.90	0.29	3.04	0.65	21.3	12.4	2.81
20/12/2023	**SG14-4582**	148	83.2	14.4	114.5	7.03	580	23.9	48.5	4.38	15.4	3.23	0.58	2.83	2.28	1.59	1.96	0.27	3.42	0.68	20.7	13.6	2.93
20/12/2023	**SG14-4582**	146	85.6	13.8	116.3	6.73	584	23.3	43.8	4.29	14.9	2.47	0.45	2.05	2.35	1.56	1.97	0.28	3.39	0.67	20.4	12.6	2.89
20/12/2023	**SG14-4582**	153	79.2	14.5	114.4	6.93	596	27.4	64.0	4.28	15.9	2.66	0.60	2.14	3.29	1.58	1.90	0.26	3.54	0.64	20.8	13.0	2.80
20/12/2023	**SG14-4598**	133	94.2	13.0	124.4	6.53	551	21.8	40.4	3.82	12.3	2.44	0.55	1.90	2.38	1.32	1.76	0.26	3.14	0.64	17.9	11.6	2.46
20/12/2023	**SG14-4598**	139	87.9	13.5	114.6	6.79	577	22.5	43.3	4.06	14.6	2.77	0.44	2.03	2.29	1.47	1.90	0.30	3.25	0.66	18.7	12.2	3.02
20/12/2023	**SG14-4598**	137	91.7	13.3	123.3	6.64	554	21.8	41.6	3.79	13.4	2.59	0.54	2.01	1.92	1.33	1.57	0.29	3.89	0.62	19.0	12.1	2.67
20/12/2023	**SG14-4598**	134	91.7	13.0	122.3	6.53	544	21.1	41.1	3.77	13.7	2.50	0.37	2.03	2.30	1.41	1.79	0.27	3.51	0.65	19.2	11.8	2.74
20/12/2023	**SG14-4598**	145	75.7	14.0	114.6	6.94	593	23.0	44.1	4.34	15.3	2.66	0.55	2.10	2.45	1.43	1.82	0.30	3.31	0.67	20.4	12.9	2.96
20/12/2023	**SG14-4598**	140	101	13.8	115.3	6.65	585	22.7	44.5	3.96	13.9	2.04	0.48	2.26	2.10	1.78	1.69	0.31	3.55	0.65	21.0	12.4	2.74
20/12/2023	**SG14-4598**	136	88.5	13.6	115.0	6.47	569	22.2	42.4	4.07	13.5	2.54	0.51	2.23	2.10	1.48	1.92	0.29	3.82	0.65	19.8	12.1	2.89
20/12/2023	**SG14-4598**	133	74.9	12.7	103.4	7.14	546	20.8	40.4	3.68	13.6	2.40	0.00	1.96	2.14	1.59	1.73	0.25	3.11	0.62	19.5	11.5	2.63
20/12/2023	**SG14-4598**	130	90.5	12.5	115.1	6.35	513	21.2	38.6	3.74	12.4	2.50	0.49	1.93	1.95	1.25	1.77	0.26	3.49	0.61	19.4	11.8	2.71
20/12/2023	**SG14-4598**	145	67.5	13.4	109.6	6.69	562	22.6	43.3	4.06	14.0	2.61	0.42	2.05	1.99	1.58	1.69	0.28	3.21	0.64	19.8	12.1	2.76
20/12/2023	**SG14-4598**	141	90.9	15.0	126.8	6.85	571	22.4	43.9	4.30	14.2	3.40	0.00	2.56	2.51	1.73	2.12	0.33	3.83	0.68	20.5	12.5	2.81
20/12/2023	**SG14-4598**	141	85.7	13.1	120.4	6.63	541	22.0	41.2	4.02	13.6	2.55	0.52	1.91	2.15	1.59	1.74	0.33	3.66	0.63	19.4	12.1	2.62
19/02/2024	**SG14-4689**	116	188	6.82	103	10.5	946	22.1	38.9	3.64	11.9	1.79	0.62	1.46	1.27	0.97	1.37	0.17	3.50	0.91	18.4	11.3	2.46
19/02/2024	**SG14-4689**	120	158	8.38	113	11.3	987	22.9	43.2	3.92	13.4	2.01	0.50	1.42	1.61	0.94	1.35	0.19	3.46	0.94	21.6	11.7	2.50
19/02/2024	**SG14-4689**	148	163	11.8	122	11.4	464	25.5	49.7	5.14	18.4	3.47	0.58	2.55	2.22	1.28	1.50	0.27	3.61	0.96	17.8	10.9	2.27
19/02/2024	**SG14-4689**	84.0	441	6.31	83.7	8.24	787	20.1	36.0	3.35	11.3	2.21	0.72	1.47	1.43	0.74	1.11	0.12	2.63	0.75	15.0	9.07	1.94
19/02/2024	**SG14-4689**	112	209	10.3	121	11.3	1005	24.8	46.7	4.42	16.5	2.59	0.57	1.83	1.70	1.18	1.33	0.21	3.72	0.96	27.4	11.3	2.66
19/02/2024	**SG14-4689**	178	166	11.5	125	11.3	422	28.9	52.2	5.63	17.9	4.02	0.58	2.56	1.83	1.11	1.44	0.25	4.00	0.93	20.6	11.5	2.64
19/02/2024	**SG14-4689**	118	152	8.04	115	11.7	963	23.3	41.8	3.78	12.7	2.31	0.46	1.57	1.19	0.89	1.75	0.17	3.97	1.01	20.4	12.1	2.60
19/02/2024	**SG14-4689**	95.0	455	8.83	107	10.4	863	22.5	39.2	4.06	13.0	2.40	0.66	1.73	1.91	0.94	1.66	0.23	2.87	0.84	16.5	9.79	2.27
19/02/2024	**SG14-4689**	119	198	8.46	114	11.0	980	23.1	43.5	4.22	13.9	2.32	0.59	1.53	1.38	0.70	1.48	0.19	2.64	0.96	21.0	11.4	2.60
19/02/2024	**SG14-4689**	101	598	7.66	83.2	7.60	649	22.7	37.5	3.86	14.2	2.59	0.86	2.15	1.73	0.98	0.90	0.16	2.28	0.66	17.4	7.66	1.50
19/02/2024	**SG14-4689**	196	138	11.3	121	11.4	319	27.9	51.5	5.20	18.6	3.10	0.53	2.46	1.97	1.36	1.32	0.22	3.96	0.98	15.3	11.1	2.47
19/02/2024	**SG14-4689**	114	215	8.87	116	11.2	1023	24.6	43.8	4.29	14.2	3.11	0.67	1.86	1.41	0.89	1.30	0.18	3.91	0.97	17.7	11.8	2.44
04/07/2023	**SG14-4748**	75.3	486	6.49	128	8.19	526	20.5	38.8	3.75	12.5	1.83	0.72	1.22	1.44	0.74	0.88	0.14	3.44	0.53	12.0	7.23	2.01

Date of Analysis	SG Label	Rb	Sr	Y	Zr	Nb	Ba	La	Ce	Pr	Nd	Sm	Eu	Gd	Dy	Er	Yb	Lu	Hf	Ta	Pb	Th	U
04/07/2023	**SG14-4748**	77.1	520	6.67	135	8.37	558	22.2	41.4	4.14	13.9	2.31	0.72	1.55	1.10	0.72	0.79	0.13	3.29	0.52	11.8	7.22	2.15
04/07/2023	**SG14-4748**	77.1	499	6.74	132	8.35	546	20.9	39.8	3.81	13.7	2.13	0.71	1.53	1.46	0.55	0.79	0.11	3.47	0.54	12.1	7.16	2.10
24/11/2023	**SG14-4837**	133	278	16.9	221	11.0	958	32.2	63.0	6.47	22.3	3.97	0.81	2.85	3.35	1.75	1.98	0.31	5.85	0.72	19.1	12.5	2.33
24/11/2023	**SG14-4837**	132	333	15.2	212	10.5	943	30.6	61.3	5.63	22.4	3.32	0.98	1.81	2.77	1.27	1.77	0.29	5.57	0.73	19.0	11.5	2.39
24/11/2023	**SG14-4837**	132	269	16.3	218	11.2	952	31.8	62.7	6.05	22.6	3.69	0.99	3.10	2.43	1.67	2.06	0.25	5.46	0.69	17.9	12.2	2.30
24/11/2023	**SG14-4837**	143	255	16.6	217	11.2	915	31.4	61.4	6.48	23.5	3.96	0.93	3.01	2.94	1.51	2.00	0.32	5.54	0.75	18.9	12.7	2.30
24/11/2023	**SG14-4837**	136	242	16.2	217	10.9	932	31.4	61.6	6.04	24.0	4.08	0.83	3.01	2.84	1.71	2.09	0.31	5.34	0.69	16.3	11.9	2.25
24/11/2023	**SG14-4837**	133	263	16.5	220	11.3	948	32.7	62.6	6.74	24.3	4.13	0.83	3.07	3.04	1.70	1.75	0.28	5.63	0.79	19.3	12.9	2.52
24/11/2023	**SG14-4837**	135	269	16.4	222	11.2	970	32.3	63.6	6.46	23.5	4.14	0.88	3.18	2.85	1.83	1.67	0.32	5.80	0.77	19.1	12.8	2.43
24/11/2023	**SG14-4837**	131	278	16.2	220	11.0	948	32.1	62.9	6.47	23.5	4.13	0.86	3.16	2.80	1.76	2.31	0.28	5.67	0.77	19.0	12.5	2.22
24/11/2023	**SG14-4837**	129	296	15.8	215	10.7	922	31.5	61.4	6.05	22.5	3.86	0.80	2.94	2.48	1.80	1.99	0.29	5.63	0.73	18.3	12.1	2.41
24/11/2023	**SG14-4837**	129	255	16.3	207	10.6	891	31.7	62.8	6.48	25.9	4.30	1.01	3.47	3.55	2.01	2.02	0.25	4.93	0.67	16.6	11.6	2.36
24/11/2023	**SG14-4837**	127	285	15.8	216	10.7	929	32.5	61.8	6.17	23.0	4.08	0.87	2.63	2.94	1.70	1.96	0.29	5.63	0.76	17.8	12.6	2.26
24/11/2023	**SG14-4837**	132	270	16.8	222	11.3	939	33.7	63.9	6.69	24.5	4.52	1.04	3.32	2.97	1.72	2.07	0.29	5.75	0.77	18.3	12.9	2.43
24/11/2023	**SG14-4837**	131	272	16.4	217	10.8	937	32.2	62.8	6.45	23.6	4.35	0.80	2.89	2.74	1.78	1.78	0.30	5.62	0.73	17.5	12.4	2.31
24/11/2023	**SG14-4837**	124	260	15.8	215	10.8	900	31.1	60.8	6.23	23.0	4.47	0.86	2.89	2.91	1.75	2.02	0.30	5.87	0.74	18.6	12.4	2.30
24/11/2023	**SG14-4837**	127	254	15.8	214	10.8	914	31.7	61.8	6.24	23.2	3.78	0.79	2.90	2.88	1.74	1.86	0.30	5.80	0.74	19.2	12.8	2.41
24/11/2023	**SG14-4837**	130	266	16.0	213	11.0	897	31.4	59.7	6.09	23.6	3.99	0.82	3.30	2.45	1.90	1.85	0.30	5.65	0.71	17.8	12.9	2.35
24/11/2023	**SG14-4837**	123	265	16.1	211	10.7	902	30.7	60.0	6.30	21.8	3.84	0.92	3.33	2.75	1.66	1.82	0.30	5.45	0.73	18.1	12.1	2.39
24/11/2023	**SG14-4837**	155	223	15.4	210	10.7	910	29.9	56.9	5.86	22.6	3.89	0.75	2.88	3.02	1.69	2.08	0.26	5.51	0.74	20.8	11.6	2.24
24/11/2023	**SG14-4837**	131	266	16.1	213	10.9	908	31.6	60.8	6.24	23.2	3.65	0.85	3.34	2.49	1.85	2.30	0.29	5.02	0.73	19.6	11.8	2.37
24/11/2023	**SG14-4837**	132	250	15.9	212	11.0	902	31.0	59.2	6.05	24.2	4.06	0.86	2.83	2.70	1.64	1.94	0.33	5.48	0.74	18.9	12.7	2.44
24/11/2023	**SG14-4837**	127	255	15.7	203	10.6	873	31.4	59.0	6.40	23.2	4.04	0.85	3.18	2.85	1.67	1.84	0.31	5.04	0.67	17.7	11.4	2.29
24/11/2023	**SG14-4837**	129	249	15.9	211	10.8	924	31.7	60.1	6.28	22.4	3.82	0.84	3.16	2.44	1.57	1.92	0.27	6.01	0.72	17.3	12.1	2.24
20/02/2024	**SG14-4860**	142	192	13.0	181.6	10.8	919	31.7	61.6	5.86	20.0	3.85	0.81	2.16	2.09	1.37	1.66	0.32	5.34	0.74	19.7	14.4	2.68
20/02/2024	**SG14-4860**	136	232	13.3	181.7	10.2	917	33.2	61.1	6.37	21.5	3.59	0.66	2.21	2.01	1.37	1.91	0.27	4.48	0.78	19.5	14.3	2.51
20/02/2024	**SG14-4860**	146	185	12.6	182.4	11.4	976	33.2	64.2	5.95	20.3	3.01	0.76	2.64	2.71	1.59	2.06	0.22	4.14	0.82	21.2	14.3	2.70
20/02/2024	**SG14-4860**	146	159	14.0	194.3	11.8	895	30.4	61.7	6.24	20.5	3.38	0.65	2.88	2.33	1.72	1.29	0.29	5.22	0.77	21.3	13.3	2.92
20/02/2024	**SG14-4860**	141	136	13.7	190.3	11.3	899	32.3	62.5	6.55	22.0	3.76	0.57	2.96	2.01	1.22	1.56	0.23	5.86	0.87	20.0	14.5	2.52
20/02/2024	**SG14-4860**	135	183	12.6	182.2	10.7	886	30.6	58.0	5.86	19.8	3.69	0.73	2.88	2.34	1.27	1.60	0.29	5.00	0.75	19.7	13.2	2.76
20/02/2024	**SG14-4860**	151	118	13.1	187.1	11.6	817	31.2	61.9	6.02	21.1	3.40	0.48	2.24	1.98	1.40	1.52	0.32	4.89	0.80	19.0	13.7	2.53
20/02/2024	**SG14-4860**	139	176	13.6	190.7	11.3	945	32.7	63.2	6.30	22.5	3.48	0.69	2.82	2.34	1.53	1.64	0.30	4.62	0.80	19.4	14.3	2.68
20/02/2024	**SG14-4860**	148	219	13.3	183.6	11.0	904	31.1	62.2	6.35	20.9	3.05	0.77	2.32	2.41	1.64	1.43	0.26	4.87	0.78	18.6	13.8	2.57
04/07/2023	**SG14-5033**	12.9	267	28.3	90.6	1.59	421	5.33	15.2	2.30	11.9	4.09	1.33	4.30	4.93	3.31	3.12	0.53	3.08	0.12	6.70	0.77	0.43
04/07/2023	**SG14-5033**	16.6	187	36.4	116	1.99	479	6.78	18.5	2.71	15.7	4.21	1.22	6.17	6.50	4.43	4.14	0.63	3.61	0.13	8.60	0.94	0.47
04/07/2023	**SG14-5033**	16.4	178	36.0	111	1.88	444	6.64	18.6	2.66	14.0	4.94	1.30	4.96	5.99	4.18	3.97	0.63	3.03	0.13	8.87	0.95	0.47
04/07/2023	**SG14-5033**	16.4	197	36.5	116	1.96	477	6.78	18.9	2.88	14.7	4.70	1.28	5.61	6.08	4.25	4.58	0.66	3.46	0.13	8.90	0.97	0.45
04/07/2023	**SG14-5033**	16.4	188	36.1	114	1.92	476	6.79	18.7	2.85	15.9	4.72	1.29	5.67	6.64	4.25	4.11	0.66	3.82	0.13	8.61	1.00	0.47
04/07/2023	**SG14-5033**	16.1	195	35.9	116	1.94	473	6.96	18.5	2.83	15.2	4.61	1.19	5.35	6.31	4.13	3.91	0.61	3.29	0.14	8.40	0.98	0.51
04/07/2023	**SG14-5033**	20.3	258	33.8	103	1.76	417	6.30	16.9	2.55	13.5	3.98	1.33	5.25	6.12	3.48	4.21	0.57	3.30	0.12	8.63	0.88	0.41
04/07/2023	**SG14-5033**	15.4	186	31.8	100	1.76	404	5.79	16.2	2.33	12.9	4.09	1.29	4.68	5.09	3.48	3.80	0.49	2.85	0.11	7.30	0.79	0.00
04/07/2023	**SG14-5033**	13.7	256	29.4	95.9	1.50	360	5.26	14.7	2.30	12.7	3.63	1.23	4.56	5.10	3.07	3.31	0.57	2.72	0.12	6.79	0.74	0.47
04/07/2023	**SG14-5033**	17.7	211	34.7	110	1.93	448	7.49	20.5	3.05	15.6	5.00	1.28	5.43	6.65	3.77	4.03	0.64	3.54	0.13	8.76	1.15	0.64
04/07/2023	**SG14-5033**	18.5	240	33.6	97.2	1.69	386	6.20	16.3	2.63	13.7	4.38	1.24	4.31	5.86	3.50	3.62	0.51	3.26	0.10	7.61	0.79	0.35
04/07/2023	**SG14-5033**	13.5	224	31.4	102	1.69	391	5.96	16.6	2.29	12.2	3.41	1.22	4.16	5.96	3.45	4.21	0.59	2.78	0.12	7.66	0.95	0.44
04/07/2023	**SG14-5033**	16.5	183	36.4	119	1.94	457	6.90	18.4	2.72	15.5	4.12	1.24	5.16	6.61	3.86	3.77	0.63	3.50	0.13	8.38	0.97	0.50
04/07/2023	**SG14-5033**	16.5	179	34.9	111	1.97	449	6.86	18.2	2.57	14.2	4.82	1.15	5.25	6.34	3.69	4.17	0.55	3.45	0.13	8.22	0.86	0.43
04/07/2023	**SG14-5033**	16.8	199	37.7	117	2.05	475	7.09	18.7	2.85	14.1	4.67	1.39	5.07	6.49	4.19	4.64	0.66	3.53	0.13	8.31	1.06	0.50

Date of Analysis	SG Label	Rb	Sr	Y	Zr	Nb	Ba	La	Ce	Pr	Nd	Sm	Eu	Gd	Dy	Er	Yb	Lu	Hf	Ta	Pb	Th	U
04/07/2023	**SG14-5033**	14.5	232	32.7	103	1.83	419	6.42	17.1	2.59	14.0	3.69	1.10	4.45	6.36	3.87	3.51	0.56	3.25	0.12	8.12	0.96	0.54
04/07/2023	**SG14-5033**	12.3	308	27.1	88.1	1.54	371	5.47	14.8	2.18	11.6	3.63	1.26	3.98	4.45	2.91	3.13	0.47	2.46	0.10	6.93	0.80	0.38
04/07/2023	**SG14-5033**	16.3	193	37.1	114	1.99	463	7.29	20.1	2.88	15.0	4.67	1.29	5.24	6.85	3.88	4.39	0.65	3.63	0.15	8.69	1.05	0.50
04/07/2023	**SG14-5033**	15.7	194	35.4	110	1.95	447	6.53	18.2	2.69	13.1	4.61	1.37	5.46	6.38	4.34	3.83	0.58	3.41	0.14	7.92	0.94	0.45
04/07/2023	**SG14-5033**	15.4	239	32.8	105	1.85	427	6.21	17.0	2.65	13.3	3.88	1.39	5.40	6.26	3.67	4.21	0.61	3.32	0.13	8.23	0.85	0.48
02/02/2024	**SG14-5071**	168	138	33.4	298	15.6	758	34.6	77.5	8.62	34.9	7.19	1.33	6.07	6.25	3.66	4.24	0.60	7.75	1.17	24.5	16.9	5.01
02/02/2024	**SG14-5071**	167	144	32.1	287	15.6	756	33.1	76.0	8.48	33.7	7.26	1.35	5.37	5.60	3.62	3.44	0.56	7.34	1.18	25.6	15.7	4.77
02/02/2024	**SG14-5071**	174	161	30.9	278	15.7	772	32.7	74.6	8.21	33.6	6.50	1.28	5.42	5.42	3.27	4.10	0.54	7.05	1.14	23.8	14.8	4.59
02/02/2024	**SG14-5071**	180	164	30.8	272	14.9	780	33.4	74.0	8.70	34.5	7.36	1.25	6.43	6.37	3.43	4.49	0.50	6.68	1.10	24.4	16.3	4.07
02/02/2024	**SG14-5071**	168	144	31.8	284	15.5	755	33.4	75.6	8.41	33.2	7.13	1.21	6.42	5.53	3.65	3.90	0.63	7.57	1.17	25.4	15.9	4.50
02/02/2024	**SG14-5071**	115	109	27.5	172	7.87	569	20.0	46.0	5.09	19.3	4.48	0.75	3.76	4.57	3.08	3.87	0.53	4.97	0.58	24.5	10.1	3.17
02/02/2024	**SG14-5071**	168	154	31.5	278	15.2	757	32.0	73.6	8.21	34.4	6.08	1.60	5.07	5.78	3.70	3.68	0.56	7.64	1.09	22.8	15.5	4.44
02/02/2024	**SG14-5071**	177	82.9	36.6	312	16.8	695	36.6	82.4	8.90	38.5	7.49	1.27	6.55	6.34	3.80	4.59	0.65	8.15	1.27	25.9	17.5	5.49
02/02/2024	**SG14-5071**	172	149	34.2	305	16.3	785	35.3	78.1	8.90	36.1	7.11	1.39	6.61	6.34	3.55	3.86	0.62	7.90	1.19	24.8	17.2	4.81
02/02/2024	**SG14-5071**	166	149	32.5	282	15.6	752	32.7	75.8	8.68	35.9	6.69	1.29	5.60	5.93	3.23	3.85	0.61	7.90	1.17	26.2	15.9	5.25
02/02/2024	**SG14-5071**	168	164	32.5	282	15.5	787	33.9	72.2	8.40	34.2	6.95	1.23	5.57	5.25	3.42	4.03	0.58	7.17	1.16	25.7	15.1	4.66
02/02/2024	**SG14-5071**	156	204	32.3	285	15.5	814	34.0	76.3	8.71	35.3	7.46	1.47	6.04	5.82	3.18	3.93	0.63	7.41	1.16	23.5	15.5	4.57
02/02/2024	**SG14-5071**	172	139	34.8	304	16.2	797	35.9	80.0	9.08	38.1	7.07	1.33	6.31	6.41	3.81	4.74	0.57	8.16	1.24	25.4	17.1	4.96
02/02/2024	**SG14-5071**	183	138	38.1	308	16.2	812	37.2	80.3	9.71	39.2	8.15	1.50	5.48	7.07	3.36	4.00	0.70	7.86	1.16	23.9	16.9	4.95
02/02/2024	**SG14-5071**	171	139	34.3	301	15.6	785	35.4	76.5	8.76	39.7	7.26	1.37	6.55	6.12	4.03	4.12	0.59	7.51	1.09	22.9	14.4	4.56
02/02/2024	**SG14-5071**	160	194	29.5	258	15.2	783	32.8	71.7	7.53	31.7	7.14	1.38	4.52	5.48	3.37	4.10	0.44	6.70	1.01	21.7	12.7	4.20
02/02/2024	**SG14-5071**	191	183	30.2	266	16.3	753	33.0	73.0	8.36	32.8	7.45	1.33	5.33	5.47	3.51	3.48	0.47	7.54	1.08	24.9	15.3	4.37
02/02/2024	**SG14-5071**	166	160	32.7	288	15.8	797	34.0	75.6	8.93	36.4	8.04	1.29	6.62	5.33	3.76	3.65	0.46	6.73	1.08	23.2	15.0	4.56
02/02/2024	**SG14-5099**	165	71.2	26.0	144	10.5	447	16.3	36.6	3.96	15.8	3.75	0.67	3.52	4.21	3.28	3.30	0.47	3.95	0.76	17.8	7.68	2.40
02/02/2024	**SG14-5099**	93.9	59.1	26.5	147	5.11	453	16.5	36.8	4.31	15.6	3.94	0.54	3.84	4.96	2.86	3.29	0.54	4.32	0.41	19.2	7.70	2.43
02/02/2024	**SG14-5099**	91.3	55.9	27.2	149	5.05	453	16.5	36.4	3.94	17.7	3.89	0.64	3.72	4.64	2.80	3.03	0.51	4.97	0.40	19.2	7.88	2.31
02/02/2024	**SG14-5099**	91.8	54.5	26.5	146	4.94	448	16.0	36.1	4.09	16.4	4.02	0.54	3.24	4.42	3.13	3.41	0.51	4.31	0.42	19.6	8.09	2.15
02/02/2024	**SG14-5099**	98.1	55.7	26.1	141	4.57	452	15.9	35.7	4.15	15.4	3.66	0.50	3.68	3.77	2.85	3.57	0.50	4.22	0.38	17.0	8.34	2.27
02/02/2024	**SG14-5099**	92.5	61.6	26.8	149	5.16	459	16.3	37.2	4.03	17.5	3.53	0.58	4.30	4.58	3.07	3.82	0.52	4.63	0.40	20.2	8.48	2.41
02/02/2024	**SG14-5221**	155	245	32.1	262	14.9	780	31.9	72.2	7.43	34.8	8.01	1.35	5.89	4.39	3.05	3.85	0.51	7.15	0.96	20.5	12.6	3.96
02/02/2024	**SG14-5221**	158	233	32.5	272	15.7	798	31.6	71.5	8.20	34.6	7.17	1.39	5.88	5.30	3.30	3.42	0.53	7.07	1.09	20.8	14.5	4.39
02/02/2024	**SG14-5221**	159	234	32.3	263	15.3	799	31.8	71.1	8.08	34.7	7.46	1.43	5.38	5.53	3.25	3.54	0.55	7.16	1.10	21.8	14.0	4.20
02/02/2024	**SG14-5221**	161	237	33.2	272	15.5	813	33.1	72.3	8.35	33.7	6.79	1.49	5.98	5.73	3.87	3.72	0.52	7.66	1.12	23.2	14.9	4.48
02/02/2024	**SG14-5221**	156	246	33.5	277	15.4	832	34.4	74.2	8.39	35.2	7.91	1.52	5.91	6.64	3.57	4.24	0.60	7.99	1.15	22.5	15.3	4.40
02/02/2024	**SG14-5221**	157	233	30.0	254	14.9	767	30.5	67.3	7.63	31.9	6.75	1.52	5.44	4.98	3.40	3.29	0.56	6.36	1.00	21.0	12.9	3.61
02/02/2024	**SG14-5221**	156	238	32.2	271	15.3	790	32.2	71.0	8.13	34.3	7.24	1.50	5.94	5.72	3.45	3.55	0.52	6.84	1.07	22.3	13.8	4.22
02/02/2024	**SG14-5221**	157	236	31.7	262	15.0	770	31.7	69.2	7.80	33.0	6.62	1.51	5.72	5.24	3.52	4.07	0.54	6.96	1.04	22.1	13.6	3.83
02/02/2024	**SG14-5221**	154	236	33.0	274	15.3	786	32.5	71.5	8.16	34.3	6.90	1.62	6.17	5.68	3.35	3.45	0.57	7.58	1.15	22.2	15.0	4.33
02/02/2024	**SG14-5221**	156	237	31.9	262	15.1	780	32.1	68.7	8.06	32.6	7.35	1.30	5.74	5.57	3.46	3.93	0.59	6.94	1.02	22.1	13.4	4.03
02/02/2024	**SG14-5221**	156	232	31.4	261	15.0	781	30.7	69.3	7.80	33.5	7.13	1.36	5.98	5.74	3.40	3.00	0.52	6.90	1.06	20.4	13.6	4.23
02/02/2024	**SG14-5221**	159	235	31.9	266	14.8	773	31.6	69.0	7.91	31.9	7.01	1.26	5.97	5.71	3.37	3.88	0.52	7.16	1.07	21.5	14.1	4.19
02/02/2024	**SG14-5221**	158	236	33.0	274	15.5	790	32.8	72.6	8.74	35.2	7.58	1.38	6.24	5.97	3.17	3.74	0.59	7.36	1.10	22.0	15.2	4.31
02/02/2024	**SG14-5221**	159	266	31.9	269	15.5	799	32.2	70.0	8.15	35.7	7.48	1.44	5.68	5.72	3.60	3.47	0.63	7.40	1.10	22.9	15.3	4.11
26/06/2023	**SG14-5367**	113	117	8.56	30.6	18.3	996	5.59	12.1	1.38	4.81	1.17	0.30	1.23	1.60	1.04	1.08	0.15	1.93	1.45	16.9	4.88	3.90
26/06/2023	**SG14-5367**	111	113	8.51	29.9	17.9	1002	5.56	12.6	1.18	3.88	1.18	0.25	1.33	1.24	0.88	1.00	0.15	1.35	1.43	16.5	4.56	3.73
26/06/2023	**SG14-5367**	119	105	7.70	27.4	17.2	946	5.31	11.1	1.25	4.37	1.58	0.28	1.24	1.39	1.06	0.96	0.13	1.20	1.33	19.6	4.21	3.58
26/06/2023	**SG14-5367**	118	113	8.59	31.2	18.3	1005	5.75	12.2	1.26	4.87	1.40	0.31	1.28	1.46	0.85	1.05	0.12	1.48	1.44	16.7	4.57	3.76

Date of Analysis	SG Label	Rb	Sr	Y	Zr	Nb	Ba	La	Ce	Pr	Nd	Sm	Eu	Gd	Dy	Er	Yb	Lu	Hf	Ta	Pb	Th	U
26/06/2023	**SG14-5367**	113	121	8.44	30.1	18.1	1026	5.69	12.4	1.27	4.36	1.69	0.28	1.43	1.43	0.97	1.00	0.12	1.55	1.41	17.1	5.02	3.70
26/06/2023	**SG14-5367**	116	67	9.12	31.7	18.7	942	5.66	12.5	1.30	4.37	1.58	0.29	1.64	1.48	0.80	0.84	0.14	1.66	1.51	15.8	5.10	3.94
26/06/2023	**SG14-5367**	127	48	9.49	34.5	19.8	911	6.19	13.8	1.44	4.69	1.55	0.32	1.26	1.47	0.96	1.18	0.18	1.49	1.59	12.9	5.72	4.25
26/06/2023	**SG14-5367**	127	131	8.79	29.7	17.1	1061	5.58	12.5	1.28	4.78	0.97	0.35	1.24	1.51	0.93	1.17	0.12	1.35	1.38	19.5	4.65	3.65
26/06/2023	**SG14-5367**	118	45	8.95	33.0	18.8	853	5.85	13.5	1.37	4.98	1.59	0.00	1.19	1.55	0.91	0.98	0.14	1.43	1.55	16.2	5.18	4.08
26/06/2023	**SG14-5367**	111	115	8.73	30.1	17.7	1000	5.68	12.6	1.12	3.96	1.13	0.26	1.11	1.60	0.89	0.95	0.13	1.33	1.41	17.4	4.78	3.72
26/06/2023	**SG14-5367**	118	74	9.28	33.7	19.2	968	6.50	13.7	1.44	4.84	1.21	0.29	1.20	1.66	1.01	1.14	0.16	1.87	1.61	16.5	5.41	4.02
26/06/2023	**SG14-5367**	122	60	9.46	33.5	19.1	913	6.24	13.8	1.46	5.16	1.42	0.29	1.34	1.34	0.97	1.18	0.16	1.72	1.53	15.4	5.54	4.09
26/06/2023	**SG14-5367**	123	45	8.77	31.9	19.5	859	5.74	12.4	1.22	4.74	1.64	0.33	1.51	1.53	1.01	1.33	0.14	1.95	1.49	13.0	5.24	3.75
04/07/2023	**SG14-5406**	138	320	10.2	73.6	10.4	857	27.6	51.9	5.30	17.0	2.90	0.60	1.87	2.04	1.14	1.29	0.20	2.51	0.9	21.4	13.5	3.34
04/07/2023	**SG14-5406**	152	227	10.5	75.8	13.7	821	26.7	52.0	5.50	17.3	2.96	0.53	2.02	1.76	0.95	1.32	0.16	2.82	0.8	20.4	13.5	2.82
04/07/2023	**SG14-5406**	145	181	10.5	80.2	10.9	804	26.8	53.0	4.71	17.0	3.04	0.64	2.21	2.24	1.03	1.46	0.16	2.18	0.8	20.6	13.5	3.37
04/07/2023	**SG14-5406**	173	107	12.7	90.7	12.9	773	29.2	60.1	6.28	19.7	3.37	0.42	2.08	1.79	1.34	1.67	0.24	2.86	1.0	21.1	14.6	3.74
04/07/2023	**SG14-5406**	137	212	11.1	79.3	10.8	809	28.2	52.9	5.88	18.0	3.19	0.56	2.29	1.70	1.11	1.45	0.22	2.34	0.8	20.8	13.7	3.61
04/07/2023	**SG14-5406**	134	302	10.0	73.9	10.0	781	25.9	49.2	4.91	17.3	2.66	0.64	2.03	1.59	1.18	1.16	0.22	2.49	0.8	21.3	13.4	2.99
04/07/2023	**SG14-5406**	127	397	10.1	74.3	10.0	818	27.2	49.8	5.14	16.3	2.69	0.84	2.18	1.75	0.93	1.53	0.20	2.18	0.8	21.8	12.2	2.97
04/07/2023	**SG14-5406**	142	285	9.49	68.4	10.3	808	26.2	48.7	4.52	17.6	2.71	0.67	1.73	1.93	1.00	1.00	0.16	2.82	0.8	20.0	12.4	3.14
19/02/2024	**SG14-5469**	97.8	129	41.0	222	10.2	441	24.3	55.6	6.26	29.0	6.22	1.26	5.89	7.48	4.36	4.42	0.66	6.14	0.69	21.1	8.69	2.08
19/02/2024	**SG14-5469**	98.9	130	42.2	229	10.4	463	25.4	56.9	6.63	29.3	7.18	1.46	6.42	7.58	4.87	4.48	0.72	6.53	0.73	22.4	9.43	2.59
19/02/2024	**SG14-5469**	100	129	42.8	231	10.8	459	25.5	57.6	6.71	30.0	7.09	1.37	6.45	7.40	4.51	4.89	0.69	6.23	0.75	22.1	9.53	2.40
19/02/2024	**SG14-5469**	101	120	38.5	200	9.83	418	23.4	53.3	5.83	26.0	6.04	1.42	6.98	7.12	4.14	4.90	0.67	6.27	0.62	21.4	6.86	2.23
19/02/2024	**SG14-5469**	100	131	42.9	230	10.4	459	25.9	59.7	7.06	29.5	7.03	1.26	6.76	7.42	4.97	5.27	0.71	6.42	0.74	21.6	9.94	2.59
19/02/2024	**SG14-5469**	98.4	135	43.2	232	10.4	468	25.6	58.2	7.13	30.5	7.05	1.21	6.51	7.16	4.99	5.17	0.74	6.45	0.71	23.6	9.96	2.37
19/02/2024	**SG14-5563A**	90.9	250	4.75	124	9.91	665	23.2	43.5	4.25	13.8	1.86	-	-	-	-	-	-	3.47	0.74	12.39	10.7	2.95
19/02/2024	**SG14-5563A**	98.1	196	5.06	128	11.0	635	25.0	43.1	4.14	15.0	2.24	0.47	1.28	1.26	0.67	0.86	0.13	3.53	0.79	13.20	11.3	3.32
19/02/2024	**SG14-5563A**	91.7	280	4.14	107	9.27	600	20.9	39.4	3.42	11.5	2.27	-	-	-	-	-	-	2.50	0.69	13.94	9.15	2.48
19/02/2024	**SG14-5563A**	94.1	276	4.80	122	10.4	639	23.5	44.7	4.02	13.5	2.22	-	-	-	-	-	-	3.27	0.75	13.27	10.8	2.77
19/02/2024	**SG14-5563A**	93.8	257	5.14	124	10.1	645	23.5	43.2	3.78	12.4	0.00	-	-	-	-	-	-	3.68	0.77	12.26	10.7	3.13
19/02/2024	**SG14-5563A**	93.5	262	5.02	126	10.1	656	23.9	43.4	3.92	13.1	0.00	-	-	-	-	-	-	3.27	0.73	13.54	10.6	3.03
19/02/2024	**SG14-5563A**	103	254	5.10	134	10.4	649	24.2	45.2	4.02	13.0	0.00	-	-	-	-	-	-	3.86	0.74	15.06	10.5	2.93
19/02/2024	**SG14-5563B**	81.7	308	4.63	119	9.72	656	22.8	41.7	3.71	12.2	0.00	-	-	-	-	-	-	2.97	0.76	12.84	10.1	2.95
19/02/2024	**SG14-5563B**	89.3	482	6.08	130	8.79	577	23.6	42.8	4.35	14.8	1.92	0.55	1.85	1.26	0.70	0.88	0.10	2.74	0.59	13.75	8.89	2.59
26/06/2023	**SG14-5575**	65.1	23.2	60.7	82.7	5.20	1014	16.2	38.2	5.03	22.3	7.50	0.58	7.96	9.72	6.52	7.82	1.09	3.33	0.38	29.3	6.28	2.56
26/06/2023	**SG14-5575**	65.3	21.8	59.2	79.5	5.20	978	15.4	38.1	4.75	22.2	6.76	0.50	8.33	9.49	6.53	6.84	1.06	3.65	0.37	28.9	5.73	2.54
26/06/2023	**SG14-5575**	61.6	22.8	55.2	72.6	4.84	930	13.8	34.5	4.40	20.7	5.91	0.60	7.07	8.99	5.31	6.86	0.96	3.25	0.35	26.0	5.36	2.13
26/06/2023	**SG14-5575**	70.1	8.53	65.1	85.6	5.76	929	15.9	41.1	5.46	25.8	7.54	0.28	8.29	11.3	6.58	7.96	1.09	4.08	0.39	30.0	6.44	2.81
26/06/2023	**SG14-5575**	70.1	22.3	53.7	74.1	4.97	952	14.0	34.9	5.04	21.1	6.39	0.72	6.35	7.86	6.46	6.15	0.91	2.98	0.31	26.8	5.74	2.21
26/06/2023	**SG14-5575**	65.7	9.95	62.3	80.8	5.28	927	15.1	40.6	5.34	22.8	7.46	0.62	8.21	11.2	6.03	6.84	1.03	3.45	0.37	27.0	6.07	2.57
26/06/2023	**SG14-5575**	65.5	23.2	59.2	79.6	5.39	1009	14.4	37.2	4.86	23.0	6.11	0.47	8.72	9.88	6.42	6.94	1.03	3.87	0.37	31.1	5.56	2.44
26/06/2023	**SG14-5575**	60.9	23.4	62.3	86.0	5.45	966	15.3	39.5	5.10	23.5	7.25	0.62	8.43	10.46	6.72	7.46	1.10	3.89	0.42	28.3	6.43	2.62
26/06/2023	**SG14-5575**	58.9	45.6	52.1	74.0	5.01	1081	14.1	34.7	4.56	20.3	6.75	0.88	6.94	9.25	5.82	6.97	0.99	3.59	0.36	27.4	5.37	2.34
26/06/2023	**SG14-5575**	61.9	18.6	59.0	77.3	5.16	959	15.2	37.8	4.75	21.8	6.58	0.56	7.52	9.27	6.53	7.21	1.04	3.75	0.34	27.1	5.58	2.67
02/02/2024	**SG14-5579**	189	180	32.7	329	17.2	843	36.6	79.6	8.78	36.7	7.48	1.31	5.90	5.29	3.75	3.71	0.58	8.26	1.29	26.9	18.1	5.29
02/02/2024	**SG14-5579**	232	281	30.4	340	18.2	840	35.6	78.9	8.58	33.9	6.00	1.35	5.82	5.36	3.06	2.85	0.51	9.03	1.37	26.8	18.5	5.52
02/02/2024	**SG14-5579**	188	172	31.8	320	17.2	814	35.5	76.8	8.57	35.0	6.52	1.38	6.03	5.65	3.48	3.47	0.57	8.35	1.26	25.1	17.9	5.26
02/02/2024	**SG14-5579**	185	194	32.6	326	17.3	857	36.6	79.3	8.87	35.6	7.24	1.36	6.03	5.76	3.71	3.71	0.52	8.95	1.29	25.6	17.9	5.45

Date of Analysis	SG Label	Rb	Sr	Y	Zr	Nb	Ba	La	Ce	Pr	Nd	Sm	Eu	Gd	Dy	Er	Yb	Lu	Hf	Ta	Pb	Th	U
02/02/2024	**SG14-5579**	202	342	31.2	317	18.1	872	37.2	82.2	9.27	37.7	7.67	1.22	6.13	6.13	3.93	3.57	0.50	9.22	1.36	17.7	17.7	5.47
02/02/2024	**SG14-5579**	190	190	31.7	317	16.7	837	35.2	75.4	8.57	33.8	6.86	1.18	4.84	5.53	3.31	3.40	0.56	8.37	1.21	25.0	17.3	5.22
02/02/2024	**SG14-5579**	181	189	32.5	316	17.1	834	35.7	77.5	8.75	36.3	7.09	1.30	6.40	5.63	3.44	3.80	0.57	8.44	1.26	26.3	18.1	5.05
02/02/2024	**SG14-5579**	185	193	31.7	314	16.9	827	34.9	76.1	8.70	34.3	7.60	1.20	5.66	6.20	3.59	3.56	0.61	8.61	1.23	25.1	17.1	5.05
02/02/2024	**SG14-5579**	186	195	32.3	320	17.4	839	35.3	77.8	8.67	35.1	7.51	1.43	6.31	5.78	3.37	3.64	0.56	9.06	1.24	26.0	17.6	5.17
02/02/2024	**SG14-5579**	186	176	32.0	318	16.9	817	35.2	77.3	8.98	34.0	7.28	1.27	5.81	5.92	3.46	3.84	0.58	8.46	1.27	25.5	18.2	5.27
02/02/2024	**SG14-5579**	182	193	32.5	319	17.0	826	36.2	77.4	8.66	35.0	6.20	1.40	5.78	5.32	3.42	3.70	0.65	8.72	1.29	25.6	18.1	5.20
02/02/2024	**SG14-5579**	183	151	32.6	326	17.3	769	36.9	77.8	8.84	36.6	7.37	1.17	5.43	5.84	3.32	3.60	0.55	8.45	1.29	26.2	18.4	5.54
02/02/2024	**SG14-5579**	183	193	33.1	320	16.8	837	36.3	78.7	9.08	36.8	7.31	1.39	6.04	6.13	3.79	3.60	0.63	8.62	1.25	26.7	18.3	5.18
02/02/2024	**SG14-5579**	183	175	32.2	307	16.2	809	35.5	77.4	8.76	36.2	7.65	1.23	5.53	5.59	3.53	3.62	0.58	8.49	1.20	25.3	17.5	5.16
02/02/2024	**SG14-5579**	187	179	29.7	293	16.4	786	34.0	73.7	8.06	33.8	7.21	1.22	5.34	5.12	3.66	3.19	0.51	7.96	1.14	28.7	15.7	5.29
02/02/2024	**SG14-5579**	183	165	32.3	316	16.8	785	35.5	78.3	8.60	33.1	7.18	1.22	5.43	5.67	3.88	3.58	0.54	8.08	1.26	24.7	17.4	5.06
02/02/2024	**SG14-5579**	181	191	32.9	319	17.0	835	36.6	77.4	8.79	34.6	7.30	1.33	6.08	5.82	3.64	3.60	0.55	8.37	1.27	25.0	18.0	5.37
26/06/2023	**SG14-5597**	15.2	209	31.0	108	1.99	403	6.60	17.0	2.72	11.9	3.76	1.14	4.17	5.12	3.43	3.34	0.52	3.37	0.14	7.25	0.78	0.44
26/06/2023	**SG14-5597**	24.3	211	28.7	94.3	2.31	394	6.81	18.1	2.70	12.8	4.68	1.38	3.65	5.11	3.28	2.98	0.39	2.77	0.12	7.29	1.14	0.45
26/06/2023	**SG14-5597**	14.8	201	32.5	113	2.07	406	6.87	18.1	2.63	12.5	4.15	1.21	5.24	5.21	4.04	3.37	0.63	3.35	0.14	7.86	0.89	0.41
26/06/2023	**SG14-5597**	11.3	299	23.9	72.6	1.42	295	4.89	13.9	1.86	9.90	3.09	1.16	3.48	4.59	2.75	2.56	0.32	2.40	0.10	5.39	0.59	0.40
04/07/2023	**SG14-5616**	76.4	204	20.4	164	7.00	624	19.2	42.0	4.40	19.6	3.63	1.12	3.66	3.54	2.06	2.02	0.31	3.93	0.45	13.9	5.45	1.27
04/07/2023	**SG14-5616**	75.1	211	22.3	174	7.84	654	21.9	47.4	5.37	20.4	4.64	1.01	3.79	4.06	2.85	2.32	0.40	4.66	0.47	12.5	5.71	1.02
04/07/2023	**SG14-5616**	73.9	206	22.2	177	6.89	681	21.3	44.4	4.55	20.6	3.97	0.88	4.15	4.19	2.42	2.69	0.35	4.35	0.46	13.5	6.01	1.35
04/07/2023	**SG14-5616**	76.1	215	22.5	184	7.58	686	22.7	47.9	5.14	21.4	4.33	0.91	4.16	3.76	2.33	2.40	0.39	4.78	0.50	13.4	6.51	1.49
04/07/2023	**SG14-5616**	73.5	211	22.0	178	7.54	686	22.5	46.0	5.09	19.7	4.66	0.89	4.21	4.26	2.60	2.16	0.37	4.97	0.46	13.8	6.03	1.35
26/06/2023	**SG14-5648**	172	273	34.3	301	16.6	863	36.4	79.6	8.64	36.4	7.87	1.50	7.26	6.20	3.66	3.73	0.61	8.25	1.25	23.6	16.7	4.99
26/06/2023	**SG14-5648**	180	236	33.4	295	16.8	858	36.0	76.3	9.26	36.0	6.59	1.45	7.22	6.34	3.86	3.85	0.51	7.70	1.14	22.3	15.3	4.63
26/06/2023	**SG14-5648**	178	228	32.9	299	17.1	850	35.1	78.3	9.18	37.6	8.03	1.42	5.84	6.62	3.53	3.44	0.51	7.66	1.22	24.6	17.0	4.72
26/06/2023	**SG14-5648**	171	249	33.1	294	17.1	838	36.0	78.4	9.10	34.8	8.21	1.50	6.91	5.98	3.35	3.46	0.65	7.96	1.25	23.3	16.8	5.07
26/06/2023	**SG14-5648**	167	256	30.9	265	16.3	768	31.7	72.5	7.75	32.9	6.12	1.38	5.64	4.87	3.30	3.81	0.45	6.88	0.91	21.7	13.5	4.33
26/06/2023	**SG14-5648**	183	256	34.4	306	18.1	868	36.5	82.1	9.19	36.6	7.52	1.80	6.72	6.43	3.45	4.02	0.63	8.29	1.30	24.1	17.3	5.02
26/06/2023	**SG14-5648**	166	270	32.6	281	16.5	795	33.7	74.4	8.74	36.7	8.13	1.33	6.83	6.18	3.18	3.17	0.52	7.86	1.19	21.1	15.8	4.77
26/06/2023	**SG14-5648**	171	244	32.8	287	16.8	802	34.2	75.7	8.65	35.0	6.35	1.60	6.50	6.47	3.65	3.87	0.53	7.61	1.21	23.7	16.0	4.82
20/02/2024	**SG14-5851**	14.4	228	30.5	97.5	1.76	374	5.77	15.3	2.33	12.5	-	-	-	-	-	-	-	3.63	0.11	7.40	1.08	0.70
20/02/2024	**SG14-5851**	21.8	250	32.4	102	1.44	409	6.06	18.2	2.68	17.1	-	-	-	-	-	-	-	3.05	0.13	7.18	0.98	0.93
20/02/2024	**SG14-5851**	21.0	235	31.6	99.4	1.49	370	6.16	16.0	2.50	13.6	-	-	-	-	-	-	-	4.12	0.11	8.08	1.21	0.73
20/02/2024	**SG14-5851**	21.9	230	30.0	98.9	1.76	380	6.16	15.8	2.31	12.4	-	-	-	-	-	-	-	3.54	0.12	7.40	1.05	0.94
20/02/2024	**SG14-5851**	24.4	242	31.3	104	1.75	417	6.08	16.9	2.21	12.0	-	-	-	-	-	-	-	3.29	0.12	6.54	1.24	0.63
20/02/2024	**SG14-5851**	18.1	239	32.3	101	1.74	402	6.11	16.3	2.70	14.5	-	-	-	-	-	-	-	3.24	0.11	7.23	0.96	0.84
24/11/2023	**SG14-5932**	94.6	137	41.8	233	11.0	453	25.2	60.0	6.70	29.3	6.17	1.32	5.53	7.15	4.69	5.12	0.70	7.15	0.72	18.8	8.23	2.19
24/11/2023	**SG14-5932**	98.2	139	41.6	234	11.0	456	25.0	60.6	6.98	29.6	6.59	1.35	6.02	7.00	5.11	4.63	0.72	6.66	0.72	20.4	9.24	2.35
24/11/2023	**SG14-5932**	100	140	42.4	236	11.0	453	25.2	58.6	7.15	30.3	7.61	1.46	7.32	8.06	4.89	5.40	0.79	6.67	0.77	20.6	9.21	2.57
24/11/2023	**SG14-5932**	95.8	143	42.7	231	11.2	448	24.7	59.1	7.25	28.9	6.65	1.53	7.22	7.72	4.52	5.10	0.74	6.86	0.72	19.2	9.14	2.20
24/11/2023	**SG14-5932**	95.5	144	41.5	230	11.0	444	24.6	57.7	6.80	28.7	7.27	1.45	7.10	6.79	4.47	5.12	0.72	7.06	0.69	20.2	8.95	2.32
24/11/2023	**SG14-5932**	97.3	149	44.3	236	11.3	438	25.3	61.2	6.96	31.4	7.33	1.48	7.11	7.37	4.59	4.91	0.75	7.27	0.75	20.6	9.40	2.79
24/11/2023	**SG14-5932**	94.5	143	43.3	237	11.5	452	25.5	59.3	7.14	30.4	7.29	1.53	6.83	7.90	5.12	5.06	0.72	6.28	0.74	20.9	9.02	2.19
24/11/2023	**SG14-5932**	100	138	40.8	232	10.9	430	24.5	58.6	6.72	29.1	6.22	1.17	6.35	7.86	3.91	4.70	0.68	6.01	0.68	20.3	8.98	2.44
24/11/2023	**SG14-5932**	97.6	136	38.6	223	12.1	420	23.0	55.1	6.87	28.3	7.97	1.49	5.93	7.22	4.84	5.83	0.68	6.43	0.70	19.1	7.74	2.27
24/11/2023	**SG14-5932**	97.8	143	42.2	235	10.4	436	24.6	60.5	6.66	30.4	7.14	1.36	6.32	7.57	4.72	5.80	0.74	5.60	0.69	20.9	8.35	2.27

Date of Analysis	SG Label	Rb	Sr	Y	Zr	Nb	Ba	La	Ce	Pr	Nd	Sm	Eu	Gd	Dy	Er	Yb	Lu	Hf	Ta	Pb	Th	U
24/11/2023	**SG14-5932**	98.7	142	41.3	239	11.2	429	24.3	58.2	6.70	28.7	8.97	1.43	5.72	7.76	5.03	5.22	0.77	6.55	0.68	19.8	8.34	2.16
24/11/2023	**SG14-5932**	97.7	140	42.2	238	11.1	449	25.0	57.6	6.59	29.8	6.69	1.34	7.76	7.29	4.49	4.49	0.76	6.46	0.69	21.9	8.67	2.08
26/06/2023	**SG14-5950**	295	0.47	94.0	928	238	0.99	175	333	33.5	127	23.6	0.23	17.4	18.7	9.42	7.37	1.07	28.6	14.0	28.2	38.3	7.45
26/06/2023	**SG14-5950**	281	0.61	88.6	850	221	2.51	163	310	30.7	114	20.7	0.19	18.5	16.9	9.04	7.96	1.07	27.1	12.7	26.0	35.2	7.17
26/06/2023	**SG14-5950**	287	3.98	89.2	867	226	8.50	168	318	31.2	116	22.0	0.25	19.7	17.1	9.02	7.75	1.05	26.3	13.6	27.6	37.4	7.58
26/06/2023	**SG14-5950**	284	0.98	86.3	842	221	1.50	163	309	30.5	115	21.4	0.26	17.7	16.7	8.94	7.35	1.04	25.2	12.5	25.0	34.1	7.18
26/06/2023	**SG14-5950**	306	2.79	89.0	846	234	4.39	163	309	30.0	107	20.9	0.28	16.4	16.7	8.82	9.19	0.96	26.3	13.1	27.5	35.6	7.46
26/06/2023	**SG14-5950**	288	1.65	86.1	840	223	20.1	164	306	30.0	110	22.3	0.32	16.9	18.8	8.58	7.43	1.03	25.6	12.4	25.9	34.5	6.82
26/06/2023	**SG14-5950**	307	0.62	87.4	850	212	10.8	161	317	29.9	108	20.7	0.58	14.1	18.4	7.67	7.03	1.16	24.6	11.5	21.4	32.7	6.30

Table B4. Trace element glass analyses of the MPI-DING reference glass (StHs6/80-G and ATHO-G).

Date of Analysis	Label	Rb	Sr	Y	Zr	Nb	Ba	La	Ce	Pr	Nd	Sm	Eu	Gd	Dy	Er	Yb	Lu	Hf	Ta	Pb	Th	U
26/06/2023	**StHs6/80**	31.1	482	11.0	115	6.62	301	11.4	25.0	3.00	12.9	2.62	0.95	2.42	2.24	1.22	0.99	0.15	3.10	0.40	9.15	2.24	1.03
26/06/2023	**StHs6/80**	31.5	476	10.9	114	6.51	304	11.5	25.0	2.94	12.9	2.85	0.90	2.51	2.38	1.24	1.21	0.14	3.05	0.41	9.29	2.22	0.99
26/06/2023	**StHs6/80**	31.0	491	11.2	117	6.67	308	11.8	26.0	3.07	12.8	3.09	0.99	2.76	2.13	1.09	1.35	0.18	3.48	0.40	9.26	2.25	0.98
26/06/2023	**StHs6/80**	30.8	478	10.9	114	6.55	302	11.7	25.0	2.85	12.3	2.59	0.95	2.46	2.17	1.20	1.13	0.15	3.01	0.38	9.04	2.20	1.01
26/06/2023	**StHs6/80**	30.1	475	10.7	113	6.50	301	11.6	24.9	2.91	12.8	3.01	0.91	2.58	2.14	1.19	1.13	0.17	2.85	0.39	8.79	2.06	1.04
26/06/2023	**StHs6/80**	30.1	469	10.6	110	6.44	302	11.0	24.6	2.89	11.8	2.49	0.94	2.49	2.00	1.07	1.17	0.15	2.94	0.38	8.54	2.12	1.01
26/06/2023	**StHs6/80**	30.3	482	10.8	114	6.49	305	11.5	25.0	2.98	12.3	2.95	0.85	2.57	2.25	1.21	1.21	0.18	3.21	0.39	9.08	2.28	1.00
26/06/2023	**StHs6/80**	30.4	483	10.7	114	6.57	302	11.5	25.2	2.89	12.4	2.87	0.89	2.07	2.32	1.14	1.05	0.16	2.91	0.41	9.27	2.29	0.95
26/06/2023	**StHs6/80**	31.0	483	11.2	117	6.66	305	11.5	25.3	3.07	12.7	2.91	1.01	2.40	2.29	1.27	1.17	0.16	3.20	0.40	9.18	2.31	1.03
26/06/2023	**StHs6/80**	30.2	473	10.9	115	6.54	290	11.7	25.0	2.94	12.5	2.66	0.92	2.50	2.13	1.17	1.16	0.17	2.81	0.40	9.10	2.19	0.98
26/06/2023	**StHs6/80**	30.3	478	10.9	116	6.54	298	11.5	24.9	2.96	12.0	3.04	1.01	2.45	2.20	1.10	1.34	0.17	2.91	0.39	9.37	2.23	0.95
26/06/2023	**StHs6/80**	30.0	470	11.1	114	6.41	299	11.3	25.2	3.05	12.7	2.75	0.93	2.47	2.09	1.23	1.16	0.17	3.01	0.40	9.21	2.15	1.04
26/06/2023	**StHs6/80**	32.0	479	10.9	115	6.72	301	11.6	24.9	3.13	12.6	3.10	0.97	2.85	2.16	1.30	1.64	0.18	3.09	0.40	9.66	2.23	1.00
26/06/2023	**StHs6/80**	30.7	489	11.2	116	6.71	314	11.7	24.9	2.94	12.9	2.54	0.93	2.64	2.26	1.08	1.51	0.20	2.97	0.38	9.61	2.31	1.07
26/06/2023	**StHs6/80**	30.5	477	10.8	115	6.47	303	11.2	24.3	3.08	12.1	2.99	0.98	2.05	2.01	1.22	1.25	0.19	2.99	0.40	8.92	2.22	1.00
26/06/2023	**StHs6/80**	29.1	465	10.7	113	6.46	289	11.1	24.2	2.84	12.3	2.63	0.94	2.19	2.23	1.12	1.00	0.17	2.71	0.39	8.91	2.27	1.06
26/06/2023	**StHs6/80**	29.6	471	10.9	112	6.54	290	11.5	24.6	2.85	12.2	2.48	0.99	2.24	2.16	1.23	1.22	0.16	3.10	0.39	8.76	2.20	0.93
26/06/2023	**StHs6/80**	30.0	471	11.1	116	6.56	298	11.3	24.8	3.05	11.9	2.73	0.86	2.73	2.22	1.15	1.09	0.14	3.10	0.40	9.01	2.18	1.10
26/06/2023	**StHs6/80**	30.7	471	11.0	115	6.53	302	11.4	25.0	2.89	12.6	2.83	0.88	2.49	2.19	1.08	1.14	0.16	3.30	0.41	8.91	2.22	0.96
26/06/2023	**StHs6/80**	30.7	477	11.0	116	6.52	305	11.4	24.6	2.87	12.9	2.75	0.93	2.87	2.02	1.12	1.15	0.18	3.03	0.40	8.95	2.22	1.01
04/07/2023	**StHs6/80**	31.2	492	11.2	119	6.77	313	12.1	25.4	3.06	13.1	2.97	0.90	2.48	2.04	1.17	1.23	0.17	3.28	0.40	9.71	2.16	1.01
04/07/2023	**StHs6/80**	31.9	487	11.1	117	6.66	306	11.6	25.2	2.96	13.0	2.73	0.92	2.82	2.20	1.02	1.05	0.17	3.24	0.40	9.20	2.28	1.05
04/07/2023	**StHs6/80**	30.4	468	10.8	113	6.33	293	11.4	25.1	2.89	12.9	2.91	0.90	2.41	2.09	1.19	1.31	0.16	3.18	0.39	8.84	2.29	0.91
04/07/2023	**StHs6/80**	29.2	466	10.9	113	6.37	293	11.4	25.4	2.97	12.3	2.61	0.98	2.61	2.13	1.17	1.06	0.14	2.93	0.38	9.07	2.14	1.03
04/07/2023	**StHs6/80**	31.1	476	11.1	116	6.45	299	11.7	24.8	2.93	12.5	2.75	0.95	2.44	2.36	1.21	1.12	0.17	3.16	0.39	8.91	2.19	0.94
04/07/2023	**StHs6/80**	30.7	481	11.2	115	6.59	306	11.8	25.2	2.90	12.6	2.98	0.90	2.23	2.32	1.06	1.32	0.16	3.04	0.41	8.85	2.16	0.98
04/07/2023	**StHs6/80**	32.2	488	11.2	116	6.54	305	11.8	25.0	3.01	12.5	2.78	1.03	2.48	2.05	1.19	1.06	0.18	2.94	0.41	9.13	2.17	1.00
04/07/2023	**StHs6/80**	31.1	473	11.1	114	6.64	305	11.3	25.2	2.87	12.4	3.10	0.82	2.53	2.09	1.08	1.12	0.13	2.87	0.39	9.23	2.11	1.01
04/07/2023	**StHs6/80**	28.8	451	10.5	111	6.17	291	11.2	23.5	2.82	11.0	2.56	0.85	2.34	2.15	1.11	1.21	0.16	2.96	0.39	8.55	2.09	0.93
04/07/2023	**StHs6/80**	30.2	467	10.9	112	6.52	301	11.4	24.3	2.85	12.2	2.43	0.93	2.68	1.78	1.15	1.22	0.18	2.92	0.38	9.37	2.29	1.01
04/07/2023	**StHs6/80**	30.1	466	10.7	111	6.53	303	11.4	24.7	2.94	11.9	3.23	0.84	2.53	2.22	1.14	1.18	0.18	2.73	0.40	8.72	2.05	0.90
04/07/2023	**StHs6/80**	30.7	473	10.9	114	6.46	295	11.6	24.7	3.05	12.2	2.78	1.00	2.16	2.05	1.10	1.24	0.16	2.79	0.38	8.93	2.13	0.98
04/07/2023	**StHs6/80**	31.4	473	11.0	116	6.51	305	11.6	25.2	2.83	13.0	2.75	0.90	2.53	2.22	1.21	1.24	0.17	3.04	0.39	9.21	2.24	1.01
04/07/2023	**StHs6/80**	30.5	483	10.9	115	6.62	308	11.6	25.4	3.06	12.5	2.95	0.93	2.46	2.08	1.11	1.07	0.16	3.14	0.39	9.07	2.13	0.98
04/07/2023	**StHs6/80**	31.1	472	10.8	115	6.43	300	11.2	24.6	2.89	12.2	2.63	1.00	2.45	1.89	1.18	1.05	0.17	2.99	0.40	9.00	2.14	1.00
04/07/2023	**StHs6/80**	31.8	482	11.0	118	6.61	299	11.9	25.3	2.95	12.4	2.61	0.91	2.60	2.12	1.12	1.19	0.17	2.92	0.39	9.22	2.18	0.95
04/07/2023	**StHs6/80**	30.3	476	11.0	116	6.52	300	11.8	24.9	3.05	12.5	2.93	0.90	2.71	2.06	1.33	1.12	0.18	2.97	0.38	9.21	2.26	1.01
24/11/2023	**StHs6/80**	31.1	484	11.0	116	6.50	306	11.8	25.5	2.97	12.5	2.79	0.98	2.72	2.11	1.16	1.23	0.16	3.26	0.42	9.16	2.43	1.11
24/11/2023	**StHs6/80**	31.0	475	11.0	115	6.66	299	11.3	24.6	2.95	12.9	2.64	0.99	2.67	2.15	1.13	1.27	0.16	2.94	0.40	9.33	2.21	1.00
24/11/2023	**StHs6/80**	30.4	480	10.9	115	6.50	301	11.5	24.9	2.97	12.5	2.90	0.82	2.38	2.20	1.00	1.08	0.17	2.84	0.40	8.95	2.30	0.90
24/11/2023	**StHs6/80**	30.6	486	11.4	119	6.84	306	12.0	25.6	2.74	13.4	3.37	0.95	2.67	2.52	1.41	1.39	0.18	3.01	0.41	9.78	2.30	1.12
24/11/2023	**StHs6/80**	32.1	480	10.9	122	6.77	309	11.9	25.9	2.99	12.6	2.78	0.96	2.80	2.53	1.22	1.40	0.19	3.25	0.42	9.76	2.31	1.02
24/11/2023	**StHs6/80**	31.7	487	11.7	120	6.78	312	11.6	25.6	3.27	12.2	3.16	0.87	2.85	2.41	1.28	1.53	0.21	2.94	0.39	9.49	2.17	1.05
24/11/2023	**StHs6/80**	31.1	489	11.4	119	6.68	300	11.7	25.5	2.92	12.6	2.96	0.88	2.68	2.22	1.32	1.05	0.20	2.96	0.39	9.19	2.32	1.07
24/11/2023	**StHs6/80**	30.0	493	11.3	119	6.69	310	11.7	25.3	3.10	12.3	2.59	0.96	2.41	2.38	1.22	1.38	0.17	3.08	0.42	9.15	2.34	1.07
24/11/2023	**StHs6/80**	30.4	480	11.0	117	6.69	306	11.6	25.6	3.00	12.7	2.78	0.96	2.61	2.17	1.24	1.26	0.16	3.23	0.40	8.91	2.14	0.99
24/11/2023	**StHs6/80**	30.2	475	10.9	117	6.56	308	11.6	24.9	2.91	12.7	3.63	0.91	2.63	2.17	1.49	1.42	0.20	3.02	0.41	9.34	2.38	1.10
24/11/2023	**StHs6/80**	29.9	476	11.0	118	6.42	307	12.0	24.2	2.98	12.7	3.28	1.03	3.03	2.42	1.36	1.56	0.23	2.75	0.40	9.18	2.20	1.05

Date of Analysis	Label	Rb	Sr	Y	Zr	Nb	Ba	La	Ce	Pr	Nd	Sm	Eu	Gd	Dy	Er	Yb	Lu	Hf	Ta	Pb	Th	U
24/11/2023	**StHs6/80**	30.0	464	10.9	115	6.55	300	11.7	24.5	2.92	13.4	3.20	0.93	2.36	2.45	1.06	1.26	0.18	3.03	0.39	8.91	2.37	1.14
24/11/2023	**StHs6/80**	30.6	476	10.8	117	6.75	307	11.6	25.3	2.94	13.0	2.99	1.02	3.08	2.30	1.30	1.62	0.20	3.09	0.42	9.50	2.05	1.14
24/11/2023	**StHs6/80**	30.0	476	10.9	113	6.51	304	11.2	25.1	2.86	12.8	2.89	0.96	2.51	2.22	1.25	1.43	0.20	3.36	0.43	9.10	2.24	0.96
24/11/2023	**StHs6/80**	30.4	477	10.8	113	6.77	303	11.6	25.0	2.95	12.9	3.10	0.95	2.60	2.35	1.30	1.52	0.23	3.02	0.40	9.37	2.37	1.08
24/11/2023	**StHs6/80**	30.6	464	10.9	116	6.60	300	11.5	24.5	2.89	12.9	2.45	0.84	2.41	2.00	1.13	1.21	0.17	3.04	0.38	8.92	2.13	0.98
24/11/2023	**StHs6/80**	30.0	472	10.9	115	6.42	305	11.3	24.9	2.93	12.9	2.62	0.87	2.11	2.11	1.18	1.07	0.17	3.21	0.41	8.80	2.11	0.90
19/12/2023	**StHs6/80**	31.1	486	11.1	118	6.67	308	11.6	25.6	3.03	12.0	3.16	1.05	2.39	2.29	1.41	1.20	0.15	3.10	0.42	8.89	2.33	1.02
19/12/2023	**StHs6/80**	30.8	497	11.1	118	6.62	305	12.1	26.0	3.01	13.3	3.07	0.78	2.94	2.21	1.37	1.42	0.18	2.81	0.41	9.77	2.28	0.99
19/12/2023	**StHs6/80**	31.4	492	11.2	118	6.76	307	11.8	25.5	3.24	12.6	3.06	0.98	2.57	2.11	1.27	1.26	0.21	3.09	0.40	9.69	2.35	1.10
20/12/2023	**StHs6/80**	31.9	477	10.9	114	6.46	294	11.5	24.5	2.91	12.3	2.74	0.88	2.20	2.12	1.08	1.17	0.16	3.13	0.40	9.44	2.18	0.99
20/12/2023	**StHs6/80**	30.8	478	10.9	113	6.43	299	11.2	25.0	2.91	12.1	2.55	0.84	2.38	2.10	1.20	1.08	0.15	3.26	0.40	9.42	2.06	0.99
20/12/2023	**StHs6/80**	31.3	475	10.9	117	6.62	300	11.7	24.9	2.91	12.4	2.39	0.93	2.64	1.96	1.23	1.15	0.15	3.16	0.40	9.27	2.14	0.99
20/12/2023	**StHs6/80**	30.8	465	11.0	116	6.49	303	11.2	25.4	2.85	12.1	2.78	0.90	2.23	2.15	1.13	1.15	0.17	3.11	0.40	9.07	2.32	1.08
20/12/2023	**StHs6/80**	30.6	472	10.9	113	6.50	301	11.3	24.6	3.00	12.4	2.62	0.97	2.38	2.41	1.08	1.16	0.15	3.21	0.38	9.19	2.20	0.98
20/12/2023	**StHs6/80**	31.2	482	11.1	115	6.58	312	11.8	25.0	3.04	13.4	2.79	0.92	2.50	2.19	1.13	1.34	0.18	3.01	0.41	9.87	2.22	1.06
20/12/2023	**StHs6/80**	30.9	483	11.2	117	6.48	310	11.8	25.3	3.01	13.0	2.65	0.90	2.89	2.25	1.36	1.25	0.18	3.14	0.40	9.80	2.28	0.95
20/12/2023	**StHs6/80**	30.6	478	11.2	114	6.68	306	11.6	25.4	2.98	12.2	2.68	0.89	2.21	2.18	1.15	1.20	0.16	2.97	0.41	9.41	2.22	1.06
20/12/2023	**StHs6/80**	30.5	475	10.9	115	6.52	298	11.4	25.1	2.97	12.9	2.78	0.86	2.82	2.23	1.17	1.07	0.17	3.04	0.40	9.19	2.16	0.93
20/12/2023	**StHs6/80**	30.6	483	11.0	117	6.65	306	11.6	25.1	3.05	12.9	3.01	0.88	2.46	2.42	1.20	1.10	0.17	3.12	0.41	9.69	2.22	1.10
20/12/2023	**StHs6/80**	30.0	492	11.3	121	6.91	316	11.8	25.9	2.99	13.0	2.87	1.02	2.44	2.37	1.15	1.15	0.16	3.05	0.41	10.14	2.39	0.99
20/12/2023	**StHs6/80**	31.4	493	11.2	118	6.71	318	11.9	26.0	3.12	12.9	3.07	0.96	2.66	2.32	1.11	1.16	0.18	3.18	0.40	10.63	2.13	1.05
02/02/2024	**StHs6/80**	38.5	491	10.8	117	6.83	321	12.0	25.8	3.02	13.3	4.68	1.39	3.93	2.58	1.84	2.00	0.31	3.49	0.43	12.63	2.40	1.02
02/02/2024	**StHs6/80**	36.7	510	11.6	124	7.70	348	12.8	28.4	3.31	13.1	4.68	1.39	4.02	3.11	2.27	2.67	0.31	3.77	0.43	13.21	2.55	1.33
02/02/2024	**StHs6/80**	34.4	466	10.7	109	6.70	308	11.5	25.0	2.98	12.2	3.78	1.30	4.88	2.74	1.64	2.18	0.30	3.12	0.39	10.31	2.19	1.08
02/02/2024	**StHs6/80**	31.6	486	11.1	115	6.84	324	12.0	26.2	3.41	14.7	4.65	-	-	-	-	-	-	4.14	0.41	10.13	2.47	1.44
02/02/2024	**StHs6/80**	36.5	509	11.4	123	7.44	329	11.9	26.4	3.21	12.3	4.56	-	-	-	-	-	-	4.13	0.44	10.97	2.43	1.38
02/02/2024	**StHs6/80**	32.5	485	10.9	120	6.89	320	11.4	25.2	3.29	13.0	4.73	-	-	-	-	-	-	3.65	0.43	9.61	2.48	1.12
02/02/2024	**StHs6/80**	30.3	487	11.1	116	6.59	298	11.6	25.4	2.94	12.3	3.20	0.95	2.27	2.26	1.17	1.09	0.15	3.08	0.40	8.92	2.25	1.01
02/02/2024	**StHs6/80**	29.8	483	11.2	115	6.73	300	11.7	26.1	3.06	13.3	3.05	0.90	2.72	2.16	1.10	1.09	0.16	2.75	0.40	9.33	2.29	0.93
02/02/2024	**StHs6/80**	30.7	486	11.2	118	6.66	303	11.9	25.7	3.03	13.1	2.63	0.98	2.59	1.92	1.17	1.19	0.18	3.10	0.41	9.88	2.23	1.08
02/02/2024	**StHs6/80**	30.8	481	11.2	118	6.68	303	12.0	25.7	3.17	13.7	2.86	0.91	2.66	2.37	1.21	1.20	0.17	3.04	0.40	9.90	2.30	1.04
02/02/2024	**StHs6/80**	30.8	480	11.0	116	6.68	310	11.6	25.6	2.86	12.6	2.84	0.93	2.71	2.22	1.10	1.07	0.15	2.90	0.39	9.49	2.25	1.05
02/02/2024	**StHs6/80**	31.6	473	10.8	115	6.64	306	11.3	25.1	2.90	12.0	3.25	0.88	2.43	2.18	1.17	1.18	0.17	2.95	0.41	9.14	2.26	1.05
02/02/2024	**StHs6/80**	31.7	488	11.1	117	6.57	307	11.8	25.6	3.19	12.9	2.57	0.79	2.24	2.33	1.17	1.30	0.19	3.05	0.41	9.77	2.28	1.13
02/02/2024	**StHs6/80**	31.3	490	11.2	119	6.80	310	12.0	25.7	3.02	12.8	2.99	0.99	2.51	2.12	1.24	1.15	0.18	3.08	0.41	9.41	2.25	1.04
02/02/2024	**StHs6/80**	30.2	479	11.1	114	6.53	302	11.8	24.9	3.03	12.3	2.72	0.94	2.34	1.94	1.26	1.14	0.16	3.10	0.41	8.83	2.12	1.04
02/02/2024	**StHs6/80**	30.2	488	11.2	117	6.61	301	12.0	25.9	3.02	12.9	3.08	0.90	2.44	1.91	1.25	1.20	0.17	3.09	0.39	9.59	2.28	0.99
02/02/2024	**StHs6/80**	30.4	481	10.9	114	6.53	297	11.2	25.3	3.01	12.6	2.43	0.97	2.49	2.15	1.08	1.19	0.16	3.27	0.39	9.24	2.23	1.10
02/02/2024	**StHs6/80**	30.8	478	10.9	114	6.45	300	11.6	25.6	2.94	12.7	2.85	1.01	2.50	2.18	1.14	1.08	0.17	3.07	0.39	9.25	2.23	0.97
02/02/2024	**StHs6/80**	30.8	484	11.1	118	6.60	308	11.7	25.8	3.01	12.8	2.83	0.88	2.30	2.28	1.36	1.16	0.17	3.05	0.40	9.43	2.29	0.97
02/02/2024	**StHs6/80**	30.5	484	10.9	118	6.48	305	11.8	25.7	3.13	13.1	2.67	0.90	2.28	2.31	1.21	1.16	0.18	2.85	0.41	9.49	2.33	1.04
02/02/2024	**StHs6/80**	31.1	488	11.2	117	6.72	315	11.9	25.3	3.13	13.0	2.73	0.95	2.49	2.44	1.29	1.15	0.17	3.27	0.41	9.75	2.14	1.12
02/02/2024	**StHs6/80**	31.2	485	11.1	116	6.61	308	11.7	25.2	2.86	12.7	2.74	0.92	2.17	2.18	1.34	1.35	0.17	3.05	0.40	9.21	2.36	0.98
02/02/2024	**StHs6/80**	30.8	495	11.3	116	6.76	305	11.8	25.7	3.00	12.3	2.95	0.86	2.55	2.08	1.24	1.29	0.17	3.11	0.39	9.70	2.37	1.01
02/02/2024	**StHs6/80**	30.5	484	11.4	117	6.65	306	11.9	26.4	3.17	13.1	2.84	0.94	2.67	2.11	1.19	1.20	0.19	2.86	0.40	9.73	2.31	1.16
02/02/2024	**StHs6/80**	30.2	483	11.1	114	6.52	305	11.6	25.8	2.92	12.7	3.04	0.97	2.41	2.22	1.20	1.19	0.18	3.23	0.40	9.74	2.20	1.03
02/02/2024	**StHs6/80**	31.7	482	11.1	116	6.66	310	11.7	25.2	2.97	12.1	2.68	0.99	2.36	2.01	1.09	1.13	0.17	3.25	0.42	9.63	2.27	1.04
02/02/2024	**StHs6/80**	30.8	478	11.0	117	6.40	305	11.7	25.4	3.02	12.6	2.77	0.88	2.51	2.28	1.13	1.16	0.17	3.13	0.39	9.19	2.38	0.89
02/02/2024	**StHs6/80**	30.8	481	11.0	116	6.47	307	11.5	25.5	3.03	12.7	2.81	0.96	2.63	2.11	1.17	1.18	0.17	2.95	0.39	9.37	2.30	1.03
02/02/2024	**StHs6/80**	31.8	490	11.2	118	6.67	307	11.5	25.1	3.08	12.9	3.06	0.91	2.25	2.16	1.27	1.26	0.16	3.02	0.41	9.62	2.32	1.05

Date of Analysis	Label	Rb	Sr	Y	Zr	Nb	Ba	La	Ce	Pr	Nd	Sm	Eu	Gd	Dy	Er	Yb	Lu	Hf	Ta	Pb	Th	U
02/02/2024	**StHs6/80**	32.1	492	11.4	117	6.75	310	11.9	25.9	2.91	12.7	2.95	1.04	2.50	2.20	1.16	1.29	0.16	3.26	0.41	9.46	2.26	1.16
02/02/2024	**StHs6/80**	31.6	490	11.1	118	6.84	310	11.7	25.5	3.06	12.6	3.12	0.95	2.24	2.47	1.22	1.34	0.17	3.08	0.40	9.70	2.29	0.97
19/02/2024	**StHs6/80**	30.2	465	10.8	115	6.43	303	11.5	25.1	2.91	13.0	2.74	0.84	2.37	2.18	1.19	1.04	0.15	2.92	0.39	9.62	2.24	1.04
19/02/2024	**StHs6/80**	29.8	467	10.6	113	6.47	300	11.4	24.7	2.88	11.6	2.61	0.89	2.54	2.30	1.15	1.02	0.17	2.93	0.39	9.43	2.25	1.07
19/02/2024	**StHs6/80**	29.6	466	10.7	113	6.37	289	11.4	24.4	2.86	11.6	2.35	0.80	2.51	2.25	1.17	1.18	0.18	2.98	0.40	9.38	2.19	0.95
19/02/2024	**StHs6/80**	32.9	470	10.7	113	6.53	305	11.5	24.9	3.16	13.2	4.17	1.31	-	-	-	-	-	3.61	0.42	9.54	2.33	1.27
19/02/2024	**StHs6/80**	33.6	469	11.0	110	6.31	317	11.2	24.8	2.98	11.4	3.61	0.98	-	-	-	-	-	4.02	0.41	9.48	2.22	1.23
19/02/2024	**StHs6/80**	29.6	481	11.2	117	6.47	304	11.5	24.9	2.93	13.0	2.88	0.88	2.89	2.10	1.24	1.00	0.16	2.96	0.40	10.08	2.09	1.02
19/02/2024	**StHs6/80**	30.3	480	11.1	116	6.47	302	11.5	25.2	2.92	12.3	2.93	0.88	2.61	2.04	1.13	1.22	0.16	3.03	0.41	9.29	2.13	1.00
19/02/2024	**StHs6/80**	30.3	470	11.0	114	6.52	300	11.4	24.6	3.03	12.6	2.78	0.98	2.62	2.33	1.11	1.05	0.17	2.84	0.41	9.47	2.25	0.98
19/02/2024	**StHs6/80**	30.7	474	11.1	116	6.54	312	11.7	24.9	2.92	12.2	2.89	0.92	2.54	2.16	1.13	1.14	0.16	3.03	0.40	10.23	2.15	0.96
19/02/2024	**StHs6/80**	30.4	468	10.9	111	6.37	298	11.3	24.2	2.90	12.7	2.88	0.80	2.63	2.21	1.33	1.07	0.15	3.02	0.39	9.84	2.25	1.01
19/02/2024	**StHs6/80**	30.0	474	11.0	113	6.41	303	11.5	24.8	3.06	12.5	2.46	0.81	2.68	2.26	1.24	1.17	0.15	2.85	0.39	10.02	2.13	0.94
19/02/2024	**StHs6/80**	31.0	481	11.0	116	6.90	312	12.0	25.0	2.77	12.7	3.18	0.96	2.69	2.44	1.34	1.59	0.18	3.02	0.41	10.31	2.29	1.03
19/02/2024	**StHs6/80**	30.0	486	11.0	115	6.85	313	11.7	25.8	3.09	13.1	2.98	0.90	2.74	2.35	1.30	1.42	0.16	3.42	0.40	10.69	2.17	1.05
19/02/2024	**StHs6/80**	29.7	477	11.0	118	6.61	305	11.7	25.0	2.89	12.9	2.99	1.03	2.43	2.09	1.18	1.13	0.15	3.13	0.39	9.73	2.34	0.92
19/02/2024	**StHs6/80**	30.2	468	10.6	114	6.44	298	11.2	24.4	2.87	12.3	2.75	0.89	2.24	2.23	1.19	1.34	0.17	2.91	0.40	9.56	2.34	1.06
19/02/2024	**StHs6/80**	29.6	474	10.8	117	6.51	303	11.6	24.5	2.90	11.9	3.02	0.90	2.61	2.13	1.05	1.16	0.18	3.20	0.38	9.63	2.14	0.96
19/02/2024	**StHs6/80**	30.2	474	11.0	117	6.53	304	11.8	25.4	3.02	12.3	2.75	0.98	2.43	2.32	1.19	0.99	0.18	3.13	0.41	9.44	2.14	1.03
19/02/2024	**StHs6/80**	30.1	488	11.3	118	6.78	311	11.6	25.5	3.01	12.3	2.78	0.90	2.34	2.08	1.24	1.25	0.17	3.19	0.41	9.21	2.40	1.02
19/02/2024	**StHs6/80**	29.3	479	11.0	118	6.63	306	11.4	25.4	2.98	13.2	2.91	0.83	2.47	2.11	1.12	1.16	0.17	3.01	0.39	9.41	2.23	1.04
19/02/2024	**StHs6/80**	30.1	485	11.2	119	6.72	308	11.8	26.5	3.02	13.1	3.15	0.96	2.72	2.38	1.04	1.32	0.17	3.18	0.40	9.65	2.16	1.00
19/02/2024	**StHs6/80**	30.1	474	11.1	114	6.64	304	11.4	25.7	2.96	12.2	2.51	0.95	2.41	2.26	1.22	1.15	0.15	3.10	0.40	9.18	2.29	0.96
19/02/2024	**StHs6/80**	30.3	475	11.2	118	6.69	299	11.5	25.4	2.98	12.8	2.65	1.00	2.42	2.14	1.16	1.31	0.17	3.07	0.41	9.41	2.34	0.99
19/02/2024	**StHs6/80**	31.2	484	11.1	118	6.57	303	11.6	24.9	2.98	12.7	3.18	0.85	2.56	2.01	1.05	1.13	0.17	3.06	0.39	9.79	2.23	1.02
19/02/2024	**StHs6/80**	30.7	480	11.1	113	6.61	307	11.2	25.0	2.95	11.8	2.76	0.91	2.33	2.30	1.13	1.17	0.17	3.23	0.39	9.60	2.20	1.08
19/02/2024	**StHs6/80**	30.8	473	10.8	113	6.61	305	11.5	24.9	2.90	11.8	2.91	0.85	2.73	2.17	1.17	1.18	0.17	2.96	0.40	10.15	2.24	1.00
19/02/2024	**StHs6/80**	29.5	481	11.1	117	6.63	310	11.9	25.8	3.11	12.8	2.62	0.88	2.49	2.33	1.40	1.29	0.18	3.21	0.40	10.02	2.25	1.03
19/02/2024	**StHs6/80**	29.8	470	10.7	115	6.42	298	11.3	24.7	2.92	12.2	2.71	1.03	2.37	2.16	1.24	1.29	0.16	3.07	0.40	9.35	2.46	0.97
19/02/2024	**StHs6/80**	29.9	465	10.7	111	6.33	291	11.2	24.4	3.02	12.2	2.79	0.87	2.51	2.25	1.20	1.13	0.17	2.99	0.39	9.65	2.28	1.03
26/06/2023	**ATHO-G**	68.4	97.9	94.7	511	62.0	582	57.7	130	15.3	65.8	15.2	2.60	15.1	17.5	10.6	11.5	1.55	14.0	3.82	4.58	7.35	2.54
26/06/2023	**ATHO-G**	67.2	99.3	96.6	525	61.9	598	59.8	132	15.6	64.3	16.0	2.58	15.4	18.2	11.4	10.7	1.60	14.6	3.95	4.40	7.77	2.42
26/06/2023	**ATHO-G**	66.6	96.2	94.9	507	61.6	585	57.5	128	15.2	65.6	15.5	2.68	14.9	17.4	10.8	11.0	1.56	13.8	3.82	4.66	7.48	2.32
26/06/2023	**ATHO-G**	66.5	95.6	94.2	508	60.7	578	57.5	128	15.2	63.3	15.3	2.45	15.5	17.2	10.9	10.8	1.59	13.9	3.85	4.92	7.52	2.32
26/06/2023	**ATHO-G**	65.0	97.6	94.6	505	60.5	574	57.0	126	15.1	63.4	15.4	2.71	15.2	16.9	10.5	10.6	1.53	14.3	3.76	4.83	7.69	2.34
26/06/2023	**ATHO-G**	65.4	96.4	93.9	506	60.2	563	56.5	127	14.9	64.5	14.7	2.50	15.5	18.2	10.3	10.8	1.53	14.2	3.78	5.01	7.48	2.35
26/06/2023	**ATHO-G**	64.9	94.0	90.5	502	60.8	552	56.0	124	14.5	60.7	14.7	2.50	15.2	16.3	10.1	10.5	1.58	13.7	3.76	4.46	7.06	2.39
26/06/2023	**ATHO-G**	66.7	94.2	92.7	497	61.7	567	56.3	125	15.2	63.1	14.8	2.36	14.6	16.8	9.8	9.4	1.50	13.9	3.78	5.02	7.62	2.51
26/06/2023	**ATHO-G**	65.7	93.8	91.2	493	60.1	546	55.3	121	14.3	61.5	15.0	2.52	14.1	16.0	10.5	10.3	1.51	13.2	3.76	4.32	7.69	2.24
26/06/2023	**ATHO-G**	66.8	93.0	91.0	504	60.0	556	54.8	122	14.0	62.2	13.7	2.58	14.5	16.7	10.4	10.1	1.47	13.6	3.70	3.98	7.18	2.17
26/06/2023	**ATHO-G**	66.6	93.6	90.4	491	59.4	557	54.8	121	14.3	60.3	14.4	2.46	14.7	16.6	10.8	10.5	1.57	14.1	3.63	4.10	7.30	2.11
26/06/2023	**ATHO-G**	65.8	91.9	90.4	491	59.5	546	54.2	122	14.2	59.8	14.7	2.45	14.0	16.0	10.2	10.5	1.49	13.5	3.67	4.31	7.26	2.47
04/07/2023	**ATHO-G**	69.0	98.0	96.1	521	63.2	583	58.6	127	15.2	63.5	14.7	2.61	15.6	17.5	10.6	11.3	1.59	14.7	3.90	4.75	7.57	2.49
04/07/2023	**ATHO-G**	64.6	90.7	89.3	488	58.6	550	54.1	119	14.3	59.1	13.7	2.40	14.3	16.5	10.0	10.1	1.45	13.2	3.67	4.44	7.12	2.22
04/07/2023	**ATHO-G**	71.8	102	97.6	531	64.2	600	58.5	130	15.3	66.0	16.3	2.60	14.7	18.0	10.3	10.5	1.61	14.7	3.92	5.21	7.75	2.49
04/07/2023	**ATHO-G**	71.4	101	97.2	522	63.8	590	57.6	129	14.9	65.4	15.3	2.59	14.4	17.3	10.5	11.0	1.62	14.9	3.91	5.53	7.74	2.40
04/07/2023	**ATHO-G**	65.7	94.5	92.6	503	60.4	558	55.3	122	14.7	65.0	15.5	2.52	15.2	17.2	10.4	10.8	1.53	13.7	3.79	5.05	7.55	2.33
04/07/2023	**ATHO-G**	68.3	96.9	94.0	513	61.7	578	57.2	126	15.1	63.3	14.8	2.35	14.8	17.8	10.1	10.5	1.57	13.4	3.79	4.91	7.47	2.34
04/07/2023	**ATHO-G**	68.8	96.6	95.3	517	61.4	587	56.3	127	14.7	64.8	14.9	2.55	14.4	17.0	10.8	10.9	1.61	14.1	3.84	5.04	7.52	2.30

Date of Analysis	Label	Rb	Sr	Y	Zr	Nb	Ba	La	Ce	Pr	Nd	Sm	Eu	Gd	Dy	Er	Yb	Lu	Hf	Ta	Pb	Th	U
04/07/2023	**ATHO-G**	69.8	97.4	95.9	523	63.4	592	59.0	129	15.0	64.6	15.7	2.80	15.5	17.0	11.4	11.0	1.57	14.7	3.88	5.11	7.80	2.50
04/07/2023	**ATHO-G**	70.5	97.6	96.2	521	62.5	575	58.5	127	15.0	65.4	14.8	2.41	15.6	17.0	10.9	10.9	1.67	14.4	3.91	4.83	7.89	2.50
04/07/2023	**ATHO-G**	70.5	98.5	94.8	524	62.7	577	58.9	129	15.0	63.8	15.5	2.71	14.6	17.8	10.7	11.2	1.61	14.8	3.90	5.12	7.71	2.52
24/11/2023	**ATHO-G**	65.7	94.2	90.4	501	59.7	558	54.9	122	14.3	62.5	14.8	2.52	14.7	16.1	10.7	10.0	1.54	14.0	3.75	4.85	7.21	2.30
24/11/2023	**ATHO-G**	70.7	95.8	95.2	534	63.4	576	58.0	126	15.3	63.1	16.5	2.53	14.1	17.4	10.6	11.2	1.56	14.7	3.93	5.56	7.70	2.47
24/11/2023	**ATHO-G**	66.6	93.5	90.5	504	61.1	560	55.6	124	14.2	61.6	14.9	2.20	14.2	16.6	9.8	10.9	1.56	14.1	3.83	4.35	7.22	2.44
24/11/2023	**ATHO-G**	66.8	91.8	93.6	516	61.3	565	56.0	123	14.7	62.1	15.2	2.33	15.6	17.8	10.2	10.7	1.55	13.7	3.78	5.01	7.75	2.38
24/11/2023	**ATHO-G**	66.1	93.7	91.0	507	61.4	566	56.3	125	14.9	64.1	15.2	2.55	15.1	16.6	10.8	10.2	1.62	14.6	3.88	4.95	7.36	2.43
24/11/2023	**ATHO-G**	65.9	95.7	91.9	494	60.1	564	55.8	121	14.4	61.4	14.4	2.68	14.8	16.7	10.5	10.3	1.55	13.9	3.84	5.18	7.44	2.25
19/12/2023	**ATHO-G**	68.1	96.2	93.4	518	62.1	558	57.2	127	15.0	63.0	15.6	2.31	14.9	16.2	10.5	10.2	1.51	14.0	3.86	4.63	8.13	2.41
20/12/2023	**ATHO-G**	67.8	95.5	92.5	508	60.7	559	55.6	124	14.8	63.9	14.5	2.48	15.0	17.2	10.3	11.1	1.59	13.8	3.80	4.74	7.69	2.39
20/12/2023	**ATHO-G**	68.6	94.8	91.5	496	60.0	560	55.6	122	14.3	62.4	14.6	2.43	14.2	17.3	10.1	10.5	1.58	13.6	3.77	4.56	7.50	2.32
20/12/2023	**ATHO-G**	65.9	93.8	90.6	496	59.4	555	55.0	124	14.5	62.1	13.4	2.48	14.6	16.6	10.5	10.6	1.47	14.0	3.71	4.40	7.33	2.31
20/12/2023	**ATHO-G**	66.6	95.9	93.0	514	60.7	575	57.0	126	14.7	63.5	15.0	2.49	15.0	16.9	10.3	10.9	1.55	14.2	3.79	5.22	7.28	2.48
20/12/2023	**ATHO-G**	66.8	94.5	91.1	505	60.4	552	56.0	124	14.3	63.3	14.5	2.47	14.2	16.3	10.5	10.3	1.50	13.7	3.77	4.53	7.38	2.37
20/12/2023	**ATHO-G**	66.4	93.6	91.0	496	61.0	568	55.1	123	14.4	60.6	14.6	2.40	15.0	16.7	10.1	10.6	1.49	13.1	3.69	5.24	7.50	2.44
02/02/2024	**ATHO-G**	72.3	94.6	89.5	500	65.9	614	57.8	130	15.3	63.6	15.5	2.45	15.8	16.0	11.0	10.5	1.64	14.8	4.08	5.93	7.67	2.68
02/02/2024	**ATHO-G**	70.7	90.4	86.8	490	64.4	598	55.2	126	13.9	60.1	16.5	2.78	15.0	16.3	9.7	9.2	1.35	12.9	3.89	5.68	6.84	2.51
02/02/2024	**ATHO-G**	69.0	93.1	90.5	488	64.9	577	56.8	127	14.0	63.0	15.7	2.74	13.8	18.5	9.4	11.0	1.47	13.5	3.87	5.26	7.59	2.67
02/02/2024	**ATHO-G**	67.8	96.8	93.7	510	61.2	565	56.8	128	14.6	61.8	15.6	2.69	14.5	17.9	11.0	10.8	1.46	13.5	3.86	4.57	7.86	2.29
02/02/2024	**ATHO-G**	68.2	94.7	94.1	519	62.0	561	57.5	125	15.1	63.9	15.2	2.75	15.1	16.4	10.5	10.7	1.60	14.2	3.88	4.48	7.28	2.48
02/02/2024	**ATHO-G**	68.6	95.1	93.7	517	61.2	586	56.6	127	15.0	64.1	15.6	2.46	14.8	16.4	10.4	10.6	1.54	14.8	3.77	4.56	7.33	2.54
02/02/2024	**ATHO-G**	66.7	93.4	92.5	510	61.1	554	56.0	123	14.6	63.4	15.8	2.54	14.5	16.0	10.2	10.3	1.50	13.9	3.73	4.18	7.38	2.50
02/02/2024	**ATHO-G**	66.5	94.1	92.6	503	60.6	566	56.8	125	14.8	60.7	14.4	2.51	15.9	16.5	10.5	10.6	1.56	13.5	3.78	4.48	7.37	2.37
02/02/2024	**ATHO-G**	67.9	94.0	92.5	503	60.9	560	55.9	124	14.6	62.9	14.3	2.42	14.2	16.3	10.3	10.1	1.55	13.8	3.77	4.40	7.49	2.29
02/02/2024	**ATHO-G**	67.8	96.7	94.1	521	62.2	578	57.7	128	15.0	64.3	15.3	2.63	15.0	17.4	10.7	10.9	1.62	14.7	3.87	4.27	7.81	2.34
02/02/2024	**ATHO-G**	67.0	96.7	94.6	520	62.4	577	57.3	128	15.0	66.2	15.6	2.67	14.6	17.6	10.5	10.3	1.63	14.2	3.85	4.45	7.80	2.42
02/02/2024	**ATHO-G**	67.6	95.6	94.1	511	60.8	561	56.7	125	14.8	64.3	14.2	2.65	15.8	16.5	10.8	10.5	1.58	14.3	3.85	4.43	7.51	2.39
02/02/2024	**ATHO-G**	67.1	95.1	94.5	513	61.3	569	57.3	129	15.0	62.3	15.4	2.61	15.3	17.5	10.9	10.8	1.57	14.5	3.83	4.47	7.89	2.40
02/02/2024	**ATHO-G**	67.1	93.9	91.3	505	60.1	566	56.0	125	14.4	63.4	15.1	2.37	15.0	16.1	10.3	10.6	1.60	13.5	3.73	4.60	7.21	2.58
02/02/2024	**ATHO-G**	68.2	97.0	93.4	514	60.5	574	56.3	125	14.8	63.7	15.0	2.34	14.8	17.0	10.3	10.7	1.59	13.9	3.83	5.00	7.72	2.37
02/02/2024	**ATHO-G**	67.5	97.8	95.1	512	62.6	583	57.0	129	15.1	64.0	15.1	2.77	14.9	17.0	10.6	10.6	1.57	14.0	3.86	5.00	7.80	2.31
02/02/2024	**ATHO-G**	67.5	97.1	94.9	515	62.9	590	58.0	130	15.1	66.5	14.9	2.66	15.0	17.4	10.3	10.8	1.57	14.6	3.85	4.95	7.73	2.55
19/02/2024	**ATHO-G**	65.9	91.9	91.8	499	60.0	550	55.1	125	14.3	61.8	14.8	2.60	14.3	17.4	10.1	10.0	1.55	13.3	3.73	4.83	7.12	2.31
19/02/2024	**ATHO-G**	65.1	92.6	91.5	496	59.5	547	55.2	124	14.4	61.9	14.7	2.38	15.0	17.0	10.1	10.1	1.54	13.6	3.69	4.65	7.53	2.31
19/02/2024	**ATHO-G**	73.3	85.5	85.5	459	60.3	567	50.3	118	13.5	57.2	13.8	2.34	15.0	15.1	9.2	10.1	1.59	12.8	3.72	4.76	6.93	2.64
19/02/2024	**ATHO-G**	69.6	88.2	87.0	458	62.2	591	51.3	116	13.6	60.7	15.0	2.48	15.2	16.3	8.8	10.3	1.40	14.8	3.85	5.02	6.37	2.33
19/02/2024	**ATHO-G**	65.3	91.8	90.6	499	59.9	552	55.1	121	14.8	61.0	14.5	2.44	14.8	16.2	10.1	10.6	1.61	14.0	3.72	4.62	7.41	2.37
19/02/2024	**ATHO-G**	65.4	92.3	92.1	506	59.7	556	56.0	124	14.7	61.2	14.4	2.48	14.4	16.7	9.9	10.6	1.56	13.9	3.75	4.67	7.42	2.33
19/02/2024	**ATHO-G**	67.0	93.7	91.3	492	59.7	558	55.0	123	14.1	64.1	14.6	2.61	14.7	16.0	10.3	10.5	1.50	14.2	3.73	4.54	7.45	2.47
19/02/2024	**ATHO-G**	69.3	95.8	93.2	503	62.1	573	55.8	125	14.9	65.1	14.5	2.64	14.6	16.8	10.6	10.5	1.60	14.5	3.76	4.28	7.41	2.27
19/02/2024	**ATHO-G**	67.0	95.2	91.9	513	61.8	574	55.1	123	14.3	64.4	14.0	2.38	14.9	16.6	10.1	9.7	1.52	14.0	3.78	4.46	7.46	2.12
19/02/2024	**ATHO-G**	69.2	97.1	94.7	523	63.8	604	57.0	127	14.9	66.3	15.9	2.65	15.1	17.9	11.0	10.4	1.48	13.6	3.95	4.31	7.48	2.37
19/02/2024	**ATHO-G**	66.4	93.5	92.3	510	60.8	573	55.4	122	14.7	62.4	14.8	2.49	14.6	17.2	10.2	10.8	1.58	13.8	3.79	4.21	7.72	2.34
19/02/2024	**ATHO-G**	66.6	93.3	91.7	511	60.3	566	55.4	121	14.8	61.1	15.7	2.70	14.8	17.9	10.2	10.7	1.50	13.6	3.82	4.02	7.73	2.48
19/02/2024	**ATHO-G**	64.7	95.9	94.3	525	62.9	577	56.4	126	14.9	64.9	15.2	2.82	15.2	17.7	10.7	11.0	1.51	14.4	3.87	4.29	7.63	2.35
19/02/2024	**ATHO-G**	67.3	96.1	94.2	529	63.3	590	57.4	128	15.1	65.3	14.9	2.62	15.7	16.9	10.6	11.7	1.62	14.6	3.93	3.96	7.74	2.29
19/02/2024	**ATHO-G**	66.2	92.7	92.6	509	61.2	559	56.2	126	14.6	63.1	14.0	2.50	15.4	17.0	10.6	11.1	1.53	13.9	3.82	4.13	7.77	2.43
19/02/2024	**ATHO-G**	68.1	94.2	93.1	518	61.6	568	56.9	126	15.3	63.9	14.3	2.59	14.9	16.6	10.4	11.0	1.59	14.4	3.86	4.11	7.63	2.36
19/02/2024	**ATHO-G**	65.8	94.2	94.0	508	62.3	573	57.2	123	14.7	61.2	15.2	2.44	15.1	17.7	10.4	10.8	1.54	14.3	3.82	4.38	7.62	2.42

Date of Analysis	Label	Rb	Sr	Y	Zr	Nb	Ba	La	Ce	Pr	Nd	Sm	Eu	Gd	Dy	Er	Yb	Lu	Hf	Ta	Pb	Th	U
19/02/2024	**ATHO-G**	67.1	92.3	90.2	491	61.6	560	55.5	123	14.7	61.5	15.4	2.27	14.6	15.9	10.0	10.6	1.52	13.9	3.74	4.57	7.22	2.46
19/02/2024	**ATHO-G**	65.7	93.4	90.2	494	59.9	552	55.6	123	14.4	61.4	14.9	2.67	15.3	16.2	9.9	10.6	1.48	13.6	3.76	4.30	7.48	2.29
19/02/2024	**ATHO-G**	65.6	93.0	90.2	488	59.9	548	55.5	124	14.9	60.5	15.2	2.53	14.4	15.8	10.3	11.0	1.56	13.4	3.78	4.05	7.56	2.38

Table B5. Major element glass analyses of the proximal tephra units SK, Kr-Aw and Kr-lw.

Date of Analysis	Sample	Label	SiO_2	TiO_2	Al_2O_3	FeO_t	MnO	MgO	CaO	Na_2O	K_2O	P_2O_5	Cl	Analytical Total
04/08/2023	**SK**	FLF04-1	72.27	0.06	13.17	0.55	0.07	0.09	0.60	3.89	3.66	0.06	0.08	94.50
04/08/2023	**SK**	FLF04-1	72.90	0.04	13.36	0.49	0.11	0.08	0.63	3.94	3.55	0.06	0.09	95.25
04/08/2023	**SK**	FLF04-1	72.57	0.08	13.15	0.51	0.09	0.12	0.63	4.03	3.58	0.06	0.08	94.89
04/08/2023	**SK**	FLF04-1	72.80	0.03	13.19	0.54	0.11	0.12	0.62	3.99	3.53	0.00	0.06	94.98
04/08/2023	**SK**	FLF04-1	72.80	0.04	13.06	0.47	0.08	0.11	0.62	4.06	3.63	0.03	0.07	94.98
04/08/2023	**SK**	FLF04-1	72.64	0.07	13.24	0.46	0.10	0.10	0.64	3.85	3.65	0.07	0.06	94.86
04/08/2023	**SK**	FLF04-1	72.82	0.07	13.25	0.59	0.09	0.11	0.66	3.90	3.68	0.08	0.09	95.33
04/08/2023	**SK**	FLF04-1	72.23	0.07	13.40	0.63	0.10	0.23	0.70	3.78	3.72	0.05	0.09	95.00
04/08/2023	**SK**	FLF04-1	72.88	0.02	13.26	0.49	0.12	0.15	0.65	4.02	3.63	0.05	0.07	95.33
04/08/2023	**SK**	FLF04-1	72.68	0.07	13.15	0.49	0.09	0.09	0.62	3.86	3.64	0.05	0.05	94.79
04/08/2023	**SK**	FLF04-1	72.37	0.06	13.15	0.49	0.09	0.15	0.63	3.98	3.50	0.09	0.09	94.59
04/08/2023	**SK**	FLF04-1	72.34	0.02	13.24	0.52	0.05	0.17	0.63	3.98	3.65	0.09	0.09	94.77
04/08/2023	**SK**	FLF04-1	72.30	0.05	13.12	0.56	0.07	0.10	0.63	3.97	3.54	0.04	0.08	94.45
04/08/2023	**SK**	FLF04-1	72.22	0.06	13.07	0.52	0.11	0.14	0.64	3.92	3.45	0.09	0.06	94.28
04/08/2023	**SK**	FLF133	72.45	0.08	13.10	0.49	0.08	0.18	0.64	3.91	3.59	0.07	0.09	94.67
04/08/2023	**SK**	FLF133	72.76	0.05	12.94	0.47	0.10	0.13	0.63	3.83	3.57	0.05	0.09	94.62
04/08/2023	**SK**	FLF133	72.37	0.04	13.18	0.53	0.06	0.14	0.65	4.04	3.53	0.05	0.10	94.69
04/08/2023	**SK**	FLF133	72.58	0.07	13.06	0.48	0.09	0.12	0.62	3.87	3.52	0.05	0.07	94.53
04/08/2023	**SK**	FLF133	73.19	0.08	13.33	0.51	0.04	0.10	0.66	4.15	3.61	0.09	0.07	95.82
04/08/2023	**SK**	FLF133	72.09	0.03	13.12	0.53	0.07	0.12	0.63	3.97	3.49	0.02	0.07	94.13
04/08/2023	**SK**	FLF133	72.41	0.04	13.02	0.46	0.08	0.10	0.64	4.05	3.49	0.05	0.06	94.39
04/08/2023	**SK**	FLF133	72.67	0.02	13.14	0.47	0.07	0.08	0.63	3.98	3.60	0.04	0.04	94.74
04/08/2023	**SK**	FLF133	72.24	0.07	13.15	0.48	0.07	0.14	0.59	3.96	3.55	0.03	0.06	94.35
04/08/2023	**SK**	FLF133	72.57	0.04	13.17	0.47	0.10	0.09	0.61	3.87	3.65	0.09	0.07	94.75
04/08/2023	**SK**	FLF133	71.94	0.04	13.02	0.47	0.09	0.07	0.62	3.92	3.59	0.09	0.07	93.92
04/08/2023	**SK**	FLF133	72.04	0.05	13.17	0.52	0.11	0.11	0.65	3.89	3.46	0.09	0.09	94.17
04/08/2023	**SK**	FLF133	72.33	0.04	13.04	0.45	0.11	0.11	0.63	3.93	3.53	0.05	0.06	94.29
04/08/2023	**SK**	FLF133	72.97	0.08	13.00	0.56	0.12	0.10	0.66	3.92	3.52	0.03	0.06	95.02
04/08/2023	**SK**	FLF133	72.47	0.02	13.34	0.54	0.08	0.13	0.61	3.87	3.51	0.08	0.09	94.75

Date of Analysis	Sample	Label	SiO_2	TiO_2	Al_2O_3	FeO_t	MnO	MgO	CaO	Na_2O	K_2O	P_2O_5	Cl	Analytical Total
04/08/2023	**SK**	FLF133	72.18	0.09	13.10	0.50	0.09	0.12	0.64	4.06	3.49	0.04	0.08	94.38
04/08/2023	**SK**	FLF133	72.19	0.07	13.00	0.44	0.13	0.15	0.64	3.92	3.72	0.07	0.08	94.42
04/08/2023	**SK**	FLF133	72.97	0.02	13.19	0.56	0.09	0.09	0.60	3.97	3.58	0.07	0.08	95.22
17/10/2023	**Kirishima - Awaokoshi**	FLF181	62.11	0.84	16.42	6.43	0.17	1.89	5.61	3.69	1.69	0.18	0.07	99.09
17/10/2023	**Kirishima - Awaokoshi**	FLF181	62.08	0.75	17.22	5.88	0.15	1.70	5.72	3.84	1.53	0.20	0.07	99.15
17/10/2023	**Kirishima - Awaokoshi**	FLF181	62.36	0.95	14.15	7.79	0.20	2.45	4.53	3.22	2.03	0.21	0.10	98.00
17/10/2023	**Kirishima - Awaokoshi**	FLF181	61.65	0.83	16.16	6.48	0.16	1.92	5.68	3.73	1.61	0.18	0.08	98.48
17/10/2023	**Kirishima - Awaokoshi**	FLF181	61.98	0.69	17.05	5.52	0.14	1.69	5.98	3.86	1.52	0.16	0.07	98.68
17/10/2023	**Kirishima - Awaokoshi**	FLF181	62.39	0.87	15.68	6.60	0.19	2.03	5.14	3.56	1.79	0.18	0.09	98.53
17/10/2023	**Kirishima - Awaokoshi**	FLF181	62.14	0.87	15.59	6.97	0.20	2.12	5.27	3.62	1.94	0.15	0.08	98.94
17/10/2023	**Kirishima - Awaokoshi**	FLF181	61.85	0.86	15.67	6.09	0.16	1.59	5.09	3.76	1.73	0.22	0.06	97.09
17/10/2023	**Kirishima - Awaokoshi**	FLF181	62.06	0.96	15.51	6.66	0.18	2.11	5.15	3.36	1.80	0.21	0.05	98.06
17/10/2023	**Kirishima - Awaokoshi**	FLF181	62.06	0.86	15.56	6.36	0.20	1.98	5.35	3.76	1.86	0.22	0.07	98.27
17/10/2023	**Kirishima - Awaokoshi**	FLF181	63.02	0.88	15.75	6.74	0.17	2.09	5.38	3.35	1.80	0.22	0.06	99.46
17/10/2023	**Kirishima - Iwaokoshi**	FLF176	70.06	0.48	12.75	2.10	0.05	0.43	1.78	3.10	4.02	0.05	0.11	94.93
17/10/2023	**Kirishima - Iwaokoshi**	FLF176	75.14	0.11	12.02	1.40	0.01	0.17	1.14	3.40	3.33	0.00	0.12	96.85
17/10/2023	**Kirishima - Iwaokoshi**	FLF176	70.31	0.52	13.35	2.60	0.07	0.53	2.24	3.29	4.05	0.10	0.15	97.20
17/10/2023	**Kirishima - Iwaokoshi**	FLF176	70.25	0.46	13.36	2.47	0.09	0.56	2.02	3.26	4.08	0.06	0.13	96.74
17/10/2023	**Kirishima - Iwaokoshi**	FLF176	69.82	0.44	13.04	2.17	0.04	0.46	1.81	3.12	4.15	0.04	0.08	95.17
17/10/2023	**Kirishima - Iwaokoshi**	FLF176	66.89	0.63	14.07	3.40	0.10	0.83	2.92	3.42	3.38	0.16	0.12	95.94
17/10/2023	**Kirishima - Iwaokoshi**	FLF176	61.98	0.73	15.90	6.47	0.11	2.30	5.40	3.28	2.35	0.12	0.07	98.72
17/10/2023	**Kirishima - Iwaokoshi**	FLF176	67.84	0.58	13.04	2.37	0.03	0.46	2.04	3.18	3.78	0.05	0.11	93.49
17/10/2023	**Kirishima - Iwaokoshi**	FLF176	67.87	0.50	12.99	2.52	0.08	0.49	2.03	3.23	4.03	0.05	0.14	93.94
17/10/2023	**Kirishima - Iwaokoshi**	FLF177	68.98	0.55	13.24	2.32	0.06	0.50	2.01	3.39	3.87	0.04	0.11	95.06
17/10/2023	**Kirishima - Iwaokoshi**	FLF177	66.70	0.60	13.75	3.42	0.08	0.90	2.97	3.37	3.35	0.09	0.10	95.33
17/10/2023	**Kirishima - Iwaokoshi**	FLF177	61.75	0.77	15.62	6.72	0.14	2.82	5.94	2.98	2.17	0.18	0.09	99.18
17/10/2023	**Kirishima - Iwaokoshi**	FLF177	68.81	0.64	14.14	3.29	0.06	0.80	2.81	3.69	3.67	0.19	0.15	98.25
17/10/2023	**Kirishima - Iwaokoshi**	FLF177	68.70	0.51	13.06	2.32	0.06	0.47	2.02	3.19	4.12	0.07	0.14	94.66
17/10/2023	**Kirishima - Iwaokoshi**	FLF177	71.55	0.55	13.57	2.47	0.06	0.54	1.94	3.35	4.04	0.06	0.08	98.22

Date of Analysis	Sample	Label	SiO_2	TiO_2	Al_2O_3	FeO_t	MnO	MgO	CaO	Na_2O	K_2O	P_2O_5	Cl	Analytical Total
17/10/2023	**Kirishima - Iwaokoshi**	FLF177	69.55	0.48	12.77	2.48	0.03	0.44	1.86	3.14	4.10	0.04	0.13	95.02
17/10/2023	**Kirishima - Iwaokoshi**	FLF177	70.26	0.56	13.33	2.55	0.04	0.55	2.13	3.35	4.00	0.09	0.16	97.03
17/10/2023	**Kirishima - Iwaokoshi**	FLF177	63.44	0.57	15.06	6.14	0.10	3.17	4.51	3.17	2.54	0.10	0.08	98.87
17/10/2023	**Kirishima - Iwaokoshi**	FLF177	61.16	0.71	14.51	4.98	0.08	1.79	4.81	3.11	2.74	0.09	0.11	94.08
17/10/2023	**Kirishima - Iwaokoshi**	FLF178	70.87	0.42	12.51	1.93	0.05	0.30	1.56	3.03	4.12	0.04	0.13	94.95
17/10/2023	**Kirishima - Iwaokoshi**	FLF178	67.97	0.63	13.67	3.01	0.07	0.73	2.45	3.54	3.77	0.08	0.12	96.03
17/10/2023	**Kirishima - Iwaokoshi**	FLF178	69.92	0.57	13.36	2.52	0.06	0.51	2.12	3.41	4.01	0.03	0.14	96.66
17/10/2023	**Kirishima - Iwaokoshi**	FLF178	69.09	0.45	12.78	1.97	0.05	0.43	1.67	3.04	4.12	0.03	0.12	93.74
17/10/2023	**Kirishima - Iwaokoshi**	FLF178	70.23	0.59	13.73	2.80	0.07	0.66	2.30	3.57	3.88	0.06	0.13	98.03
17/10/2023	**Kirishima - Iwaokoshi**	FLF178	68.19	0.58	13.52	2.86	0.08	0.59	2.40	3.43	3.61	0.10	0.13	95.49
17/10/2023	**Kirishima - Iwaokoshi**	FLF178	68.84	0.50	12.90	2.44	0.05	0.50	1.92	3.12	3.97	0.10	0.11	94.45
17/10/2023	**Kirishima - Iwaokoshi**	FLF178	75.72	0.17	12.42	1.30	0.09	0.12	1.10	3.47	3.34	0.01	0.09	97.84
17/10/2023	**Kirishima - Iwaokoshi**	FLF178	68.73	0.56	13.97	2.37	0.04	0.58	2.66	3.35	3.79	0.07	0.15	96.27
17/10/2023	**Kirishima - Iwaokoshi**	FLF178	67.39	0.62	14.17	3.41	0.08	0.85	2.83	3.53	3.41	0.10	0.11	96.52
17/10/2023	**Kirishima - Iwaokoshi**	FLF178	70.71	0.39	12.54	1.74	0.05	0.32	1.63	3.02	4.34	0.04	0.16	94.94
17/10/2023	**Kirishima - Iwaokoshi**	FLF178	68.78	0.49	13.30	2.31	0.05	0.52	2.05	3.22	3.87	0.06	0.13	94.78
17/10/2023	**Kirishima - Iwaokoshi**	FLF178	69.38	0.42	12.43	1.88	0.05	0.39	1.54	3.04	4.27	0.03	0.14	93.57
17/10/2023	**Kirishima - Iwaokoshi**	FLF178	69.89	0.47	12.69	2.13	0.05	0.45	1.75	3.09	4.15	0.04	0.13	94.82

Table B6. Major element glass analyses of the MPI-DING reference glass (StHs6/80-G, GOR132 and ATHO-G) (unnormalised).

Date of Analysis	Label	SiO_2	TiO_2	Al_2O_3	FeO_t	MnO	MgO	CaO	Na_2O	K_2O	P_2O_5	Cl	Analytical Total
04/08/2023	**StHs6/80**	63.78	0.72	17.85	4.21	0.09	1.95	5.27	3.79	1.26	0.13	0.01	99.06
04/08/2023	**StHs6/80**	63.91	0.68	17.75	4.31	0.10	2.00	5.34	4.64	1.24	0.13	0.01	100.10
04/08/2023	**StHs6/80**	63.76	0.71	17.95	4.33	0.09	2.00	5.24	4.74	1.26	0.11	0.01	100.20
04/08/2023	**StHs6/80**	63.46	0.72	17.68	4.28	0.08	1.98	5.23	4.41	1.27	0.14	0.02	99.27
04/08/2023	**StHs6/80**	63.66	0.75	17.61	4.23	0.06	1.90	5.27	4.62	1.27	0.12	0.00	99.49
04/08/2023	**StHs6/80**	63.49	0.71	17.90	4.25	0.10	2.01	5.21	4.67	1.28	0.11	0.00	99.73
04/08/2023	**StHs6/80**	63.85	0.71	17.76	4.32	0.06	1.94	5.26	4.48	1.25	0.17	0.01	99.80
04/08/2023	**StHs6/80**	64.11	0.70	17.72	4.33	0.08	1.94	5.32	4.86	1.29	0.17	0.02	100.54
04/08/2023	**StHs6/80**	63.66	0.72	17.86	4.13	0.07	1.98	5.32	4.53	1.28	0.12	0.01	99.68
04/08/2023	**StHs6/80**	63.59	0.70	17.88	4.30	0.07	1.93	5.27	4.26	1.27	0.18	0.01	99.45
17/10/2023	**StHs6/80**	63.53	0.67	17.79	4.40	0.04	1.82	5.23	4.51	1.28	0.11	0.00	99.39
17/10/2023	**StHs6/80**	63.60	0.68	17.60	4.57	0.11	1.86	5.21	4.50	1.28	0.09	0.02	99.51
17/10/2023	**StHs6/80**	63.86	0.67	17.89	4.38	0.08	1.90	5.29	4.78	1.32	0.13	0.00	100.29
17/10/2023	**StHs6/80**	64.03	0.71	18.01	4.34	0.07	1.98	5.22	4.56	1.32	0.12	0.00	100.36
17/10/2023	**StHs6/80**	63.97	0.67	17.82	4.39	0.08	1.95	5.29	4.84	1.29	0.13	0.01	100.44
17/10/2023	**StHs6/80**	63.48	0.68	18.00	4.36	0.10	1.97	5.30	4.51	1.28	0.13	0.00	99.80
17/10/2023	**StHs6/80**	63.45	0.74	17.96	4.38	0.08	2.00	5.21	4.28	1.26	0.08	0.01	99.45
17/10/2023	**StHs6/80**	63.98	0.70	18.13	4.51	0.09	1.90	5.23	4.61	1.30	0.11	0.01	100.58
17/10/2023	**StHs6/80**	63.40	0.74	17.72	4.27	0.08	1.95	5.24	4.49	1.26	0.15	0.02	99.30
17/10/2023	**StHs6/80**	63.49	0.72	17.77	4.34	0.07	1.93	5.41	4.51	1.27	0.10	0.01	99.62
17/10/2023	**StHs6/80**	63.80	0.66	17.80	4.34	0.05	1.94	5.26	4.34	1.26	0.11	0.00	99.55
04/08/2023	**ATHOG**	75.69	0.28	12.14	3.11	0.10	0.09	1.73	4.09	2.65	0.03	0.06	99.96
04/08/2023	**ATHOG**	75.67	0.24	12.46	3.10	0.07	0.10	1.68	4.29	2.65	0.01	0.04	100.30
04/08/2023	**ATHOG**	75.58	0.25	12.30	3.26	0.12	0.08	1.70	4.14	2.58	0.03	0.05	100.09
04/08/2023	**ATHOG**	75.92	0.27	12.23	3.19	0.10	0.11	1.73	4.15	2.63	0.00	0.05	100.38
04/08/2023	**ATHOG**	75.94	0.28	12.33	3.20	0.10	0.12	1.67	4.05	2.62	0.03	0.02	100.37
04/08/2023	**ATHOG**	75.57	0.23	12.29	3.12	0.11	0.10	1.69	4.13	2.69	0.03	0.04	99.99
04/08/2023	**ATHOG**	75.70	0.23	12.29	3.33	0.14	0.12	1.68	4.15	2.71	0.07	0.03	100.45
04/08/2023	**ATHOG**	75.43	0.25	12.26	3.18	0.12	0.09	1.65	4.29	2.69	0.00	0.05	100.01

Date of Analysis	Label	SiO_2	TiO_2	Al_2O_3	FeO_t	MnO	MgO	CaO	Na_2O	K_2O	P_2O_5	Cl	Analytical Total
04/08/2023	**ATHOG**	75.48	0.21	12.24	3.26	0.10	0.09	1.67	4.20	2.65	0.05	0.04	99.99
04/08/2023	**ATHOG**	75.15	0.25	12.32	3.20	0.11	0.12	1.70	4.16	2.63	0.03	0.05	99.72
17/10/2023	**ATHOG**	76.08	0.26	12.25	3.28	0.09	0.07	1.69	4.31	2.69	0.00	0.02	100.74
17/10/2023	**ATHOG**	75.46	0.23	12.48	3.24	0.08	0.08	1.68	4.03	2.67	0.02	0.04	100.00
17/10/2023	**ATHOG**	74.76	0.24	12.45	3.17	0.07	0.04	1.69	5.79	2.66	0.00	0.03	100.91
17/10/2023	**ATHOG**	75.93	0.27	12.37	3.13	0.10	0.10	1.68	4.13	2.67	0.02	0.03	100.42
17/10/2023	**ATHOG**	76.10	0.29	12.46	3.23	0.12	0.09	1.71	4.15	2.68	0.02	0.04	100.88
17/10/2023	**ATHOG**	75.33	0.28	12.45	3.33	0.09	0.11	1.69	4.16	2.67	0.01	0.04	100.14
17/10/2023	**ATHOG**	75.86	0.28	12.40	3.09	0.08	0.08	1.66	3.95	2.66	0.00	0.03	100.08
17/10/2023	**ATHOG**	75.68	0.26	12.36	3.10	0.11	0.07	1.66	3.98	2.61	0.01	0.04	99.89
17/10/2023	**ATHOG**	75.71	0.23	12.34	3.12	0.07	0.10	1.70	3.69	2.67	0.02	0.04	99.69
17/10/2023	**ATHOG**	75.43	0.23	12.46	3.32	0.08	0.08	1.69	3.87	2.60	0.00	0.03	99.79
17/10/2023	**ATHOG**	75.72	0.24	12.42	3.21	0.12	0.16	1.66	3.83	2.61	0.00	0.04	100.00
04/08/2023	**GOR132**	45.76	0.29	10.97	10.01	0.16	22.67	8.46	0.88	0.04	0.01	0.01	99.24
04/08/2023	**GOR132**	45.55	0.35	10.94	9.99	0.16	22.56	8.64	0.86	0.02	0.04	0.01	99.11
04/08/2023	**GOR132**	45.54	0.30	11.04	9.86	0.16	22.60	8.53	0.78	0.02	0.02	0.00	98.85
04/08/2023	**GOR132**	45.73	0.29	11.00	9.97	0.16	22.53	8.51	0.75	0.03	0.06	0.02	99.03
04/08/2023	**GOR132**	45.00	0.34	10.97	10.15	0.13	22.62	8.59	0.79	0.03	0.06	0.00	98.67
04/08/2023	**GOR132**	45.43	0.34	10.91	10.25	0.16	22.38	8.53	0.78	0.03	0.04	0.00	98.84
04/08/2023	**GOR132**	45.33	0.31	10.81	9.89	0.14	22.40	8.51	0.83	0.04	0.03	0.00	98.29
04/08/2023	**GOR132**	45.68	0.26	10.68	10.12	0.15	22.49	8.55	0.81	0.03	0.05	0.00	98.81
04/08/2023	**GOR132**	45.26	0.28	11.01	9.93	0.13	22.56	8.49	0.86	0.02	0.00	0.01	98.55
04/08/2023	**GOR132**	45.47	0.31	10.99	10.06	0.15	22.64	8.46	0.87	0.02	0.06	0.01	99.03
17/10/2023	**GOR132**	45.55	0.30	10.96	10.15	0.15	22.34	8.52	0.86	0.03	0.00	0.00	98.86
17/10/2023	**GOR132**	45.38	0.31	11.03	10.46	0.14	22.42	8.52	0.81	0.04	0.01	0.00	99.11
17/10/2023	**GOR132**	45.51	0.30	11.07	10.16	0.14	22.46	8.52	0.81	0.03	0.00	0.02	99.02
17/10/2023	**GOR132**	45.85	0.29	11.00	10.26	0.15	22.32	8.51	0.93	0.05	0.01	0.01	99.38
17/10/2023	**GOR132**	45.49	0.31	10.80	10.43	0.16	22.43	8.59	0.84	0.02	0.02	0.00	99.08
17/10/2023	**GOR132**	45.49	0.29	11.20	10.24	0.13	22.33	8.64	0.75	0.04	0.02	0.01	99.15
17/10/2023	**GOR132**	45.67	0.32	11.07	10.20	0.18	22.39	8.67	0.70	0.03	0.01	0.00	99.23
17/10/2023	**GOR132**	45.32	0.29	11.11	10.16	0.17	22.67	8.61	0.84	0.07	0.04	0.02	99.29

Date of Analysis	Label	SiO_2	TiO_2	Al_2O_3	FeO_t	MnO	MgO	CaO	Na_2O	K_2O	P_2O_5	Cl	Analytical Total
17/10/2023	**GOR132**	45.59	0.33	11.02	10.29	0.14	22.32	8.60	0.73	0.03	0.02	0.00	99.06
17/10/2023	**GOR132**	45.25	0.33	11.11	10.40	0.14	22.27	8.60	0.82	0.03	0.03	0.02	99.01
17/10/2023	**GOR132**	45.22	0.27	10.93	10.30	0.19	22.45	8.58	0.81	0.03	0.05	0.01	98.82

Table B7. Trace element glass analyses of the proximal tephra units SK, Kr-Aw and Kr-Iw.

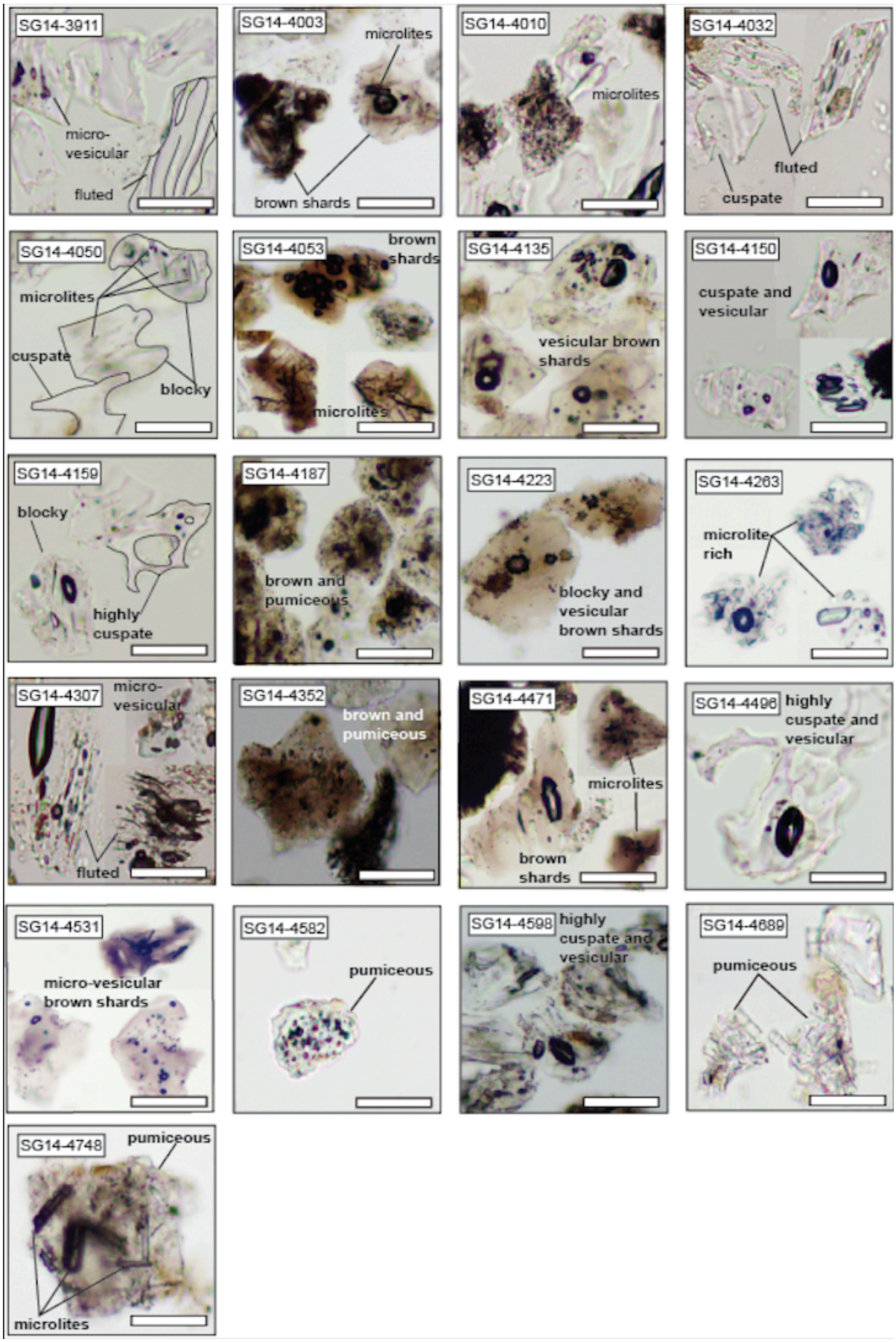
Date of Analysis	Sample	Label	Rb	Sr	Y	Zr	Nb	Ba	La	Ce	Pr	Nd	Sm	Eu	Gd	Dy	Er	Yb	Lu	Hf	Ta	Pb	Th	U
29/07/2024	**SK**	FLF133	96.1	109	11.0	40.8	23.9	930	7.81	19.6	1.70	5.50	1.32	0.27	1.57	1.63	0.96	1.04	0.17	2.36	2.00	16.7	5.78	4.41
29/07/2024	**SK**	FLF133	101	100	11.0	35.4	22.8	917	8.23	10.6	1.78	5.58	1.63	0.26	1.23	1.64	1.02	1.12	0.17	1.66	2.06	24.9	5.38	4.32
29/07/2024	**SK**	FLF133	109	114	8.62	29.8	17.9	1000	5.45	12.0	1.29	4.00	1.03	0.21	1.06	1.47	0.79	1.00	0.14	1.41	1.46	18.9	4.67	3.90
29/07/2024	**SK**	FLF133	105	109	8.93	31.8	18.5	997	6.29	12.3	1.51	4.55	1.42	0.23	1.41	1.55	0.85	1.07	0.15	1.62	1.50	16.7	4.91	3.91
29/07/2024	**SK**	FLF133	102	109	9.68	32.9	20.6	932	6.71	11.9	1.61	4.77	1.37	0.21	1.23	1.17	0.84	1.11	0.14	1.47	1.65	16.5	4.97	4.43
29/07/2024	**SK**	FLF133	103	109	9.53	35.1	19.9	959	6.84	12.1	1.68	5.15	1.31	0.25	1.06	1.64	0.83	1.06	0.15	1.90	1.70	17.7	5.06	4.08
29/07/2024	**SK**	FLF133	106	112	8.46	30.4	17.9	965	5.42	12.0	1.31	4.36	1.20	0.21	1.16	1.18	0.73	0.74	0.12	1.61	1.44	17.1	4.60	3.57
29/07/2024	**SK**	FLF133	105	116	8.64	38.1	20.2	1035	6.44	12.4	1.34	4.17	1.14	0.23	1.44	1.54	0.81	0.79	0.12	1.90	2.06	23.6	4.90	4.11
29/07/2024	**SK**	FLF133	97.6	100	10.9	34.8	19.0	859	7.09	10.3	1.68	7.04	2.74	0.57	1.48	1.61	1.06	1.54	0.22	1.34	1.59	17.4	4.28	3.79
29/07/2024	**SK**	FLF133	100	111	8.70	30.4	18.3	956	5.70	11.9	1.32	4.20	1.09	0.27	1.29	1.24	0.91	0.77	0.15	1.39	1.46	17.3	4.84	4.08
29/07/2024	**SK**	FLF133	103	112	9.55	34.4	19.5	961	6.51	11.9	1.45	5.42	1.33	0.26	1.02	1.55	0.80	1.24	0.12	1.91	1.63	16.2	5.20	4.10
29/07/2024	**SK**	FLF133	104	111	8.51	30.9	18.2	953	5.61	11.8	1.35	3.82	0.93	0.24	1.12	1.37	0.63	0.98	0.11	1.43	1.48	16.9	5.06	3.67
29/07/2024	**SK**	FLF133	98.3	97.3	10.1	38.8	22.5	803	7.38	14.8	1.47	6.19	1.99	0.42	1.33	1.87	0.95	1.34	0.18	1.87	1.77	16.1	5.30	4.18
29/07/2024	**SK**	FLF133	104	123	8.26	28.5	17.1	951	5.23	11.5	1.22	4.37	1.10	0.19	1.00	1.30	0.75	0.95	0.12	1.37	1.36	17.6	4.62	3.69
03/07/2023	**SK**	FLF04-1	113	119	8.93	32.8	18.6	1025	5.88	13.0	1.42	4.58	1.46	0.34	1.28	1.36	0.85	0.84	0.14	1.47	1.51	17.5	4.77	4.07
03/07/2023	**SK**	FLF04-1	107	114	8.33	31.1	17.2	966	5.62	11.9	1.34	4.44	1.34	0.27	0.95	1.19	0.96	0.99	0.13	1.51	1.45	17.5	4.50	3.91
03/07/2023	**SK**	FLF04-1	111	120	8.92	31.9	18.1	1011	5.81	12.9	1.28	4.61	1.50	0.30	1.00	1.50	0.88	1.15	0.13	1.42	1.47	16.6	4.98	4.07
03/07/2023	**SK**	FLF04-1	115	131	8.87	33.9	20.2	984	6.34	14.1	1.36	5.02	1.23	0.28	1.32	1.56	1.14	0.99	0.17	1.63	1.47	19.2	5.25	4.15
03/07/2023	**SK**	FLF04-1	109	115	8.28	30.8	17.9	960	5.19	12.0	1.27	4.11	1.28	-	1.16	1.18	0.90	0.82	0.12	1.47	1.47	17.5	4.95	3.72
03/07/2023	**SK**	FLF04-1	109	117	8.42	32.4	17.9	994	5.79	12.7	1.17	4.17	1.29	-	1.08	1.29	0.85	1.15	0.13	1.51	1.45	17.4	4.97	3.81
03/07/2023	**SK**	FLF04-1	107	117	8.64	31.0	18.1	1002	5.96	13.2	1.35	4.34	1.33	0.32	1.06	1.30	1.00	0.92	0.15	1.48	1.46	17.2	4.53	3.69
03/07/2023	**SK**	FLF04-1	109	118	8.57	30.9	18.1	1000	5.82	12.9	1.47	4.15	1.29	0.34	1.17	1.24	0.95	0.90	0.16	1.55	1.46	16.7	4.67	3.89
03/07/2023	**SK**	FLF04-1	125	112	7.50	28.4	17.9	925	5.35	12.0	1.33	3.06	1.10	-	1.28	1.43	0.89	1.02	0.14	1.38	1.39	17.5	4.37	3.79
23/11/2023	**Kirishima - Awaokoshi**	FLF181	63.2	322	25.9	129	6.23	355	18.5	40.0	4.81	21.2	5.21	1.16	4.54	4.75	2.71	2.49	0.40	3.33	0.39	12.6	5.30	1.26
23/11/2023	**Kirishima - Awaokoshi**	FLF181	58.2	340	26.3	127	6.08	351	18.7	41.3	4.92	22.2	4.93	1.31	4.82	4.86	3.02	2.58	0.44	3.80	0.41	14.3	5.29	1.23
23/11/2023	**Kirishima - Awaokoshi**	FLF181	59.3	330	25.5	125	5.95	357	18.8	40.2	4.97	20.9	5.09	1.29	4.78	4.29	2.84	3.04	0.44	3.99	0.39	11.6	4.75	0.93
23/11/2023	**Kirishima - Awaokoshi**	FLF181	62.5	344	26.1	128	6.45	361	18.7	40.9	4.98	21.9	5.29	1.43	4.17	4.86	2.80	2.63	0.41	3.53	0.41	14.0	4.99	1.32
23/11/2023	**Kirishima - Awaokoshi**	FLF181	63.6	323	26.2	129	6.27	359	18.4	39.0	4.82	23.4	5.17	1.40	4.75	4.73	2.77	2.59	0.45	3.89	0.43	13.4	5.27	1.19
23/11/2023	**Kirishima - Awaokoshi**	FLF181	58.2	357	26.1	128	6.07	355	19.3	41.0	4.92	21.5	5.15	1.18	4.37	4.84	2.87	3.10	0.41	3.61	0.38	13.5	4.88	1.23
23/11/2023	**Kirishima - Awaokoshi**	FLF181	60.8	288	22.4	119	6.02	282	14.5	27.2	3.89	15.9	4.40	1.05	3.82	3.74	2.44	2.20	0.39	3.53	0.42	10.0	4.51	1.20
23/11/2023	**Kirishima - Awaokoshi**	FLF181	62.6	319	30.4	131	7.01	329	18.4	32.1	4.86	20.6	4.52	1.45	5.22	4.82	3.39	3.49	0.43	3.52	0.42	12.6	5.29	1.18
23/11/2023	**Kirishima - Awaokoshi**	FLF181	58.6	337	26.0	124	5.97	349	18.5	43.1	4.96	21.2	5.09	1.17	4.32	4.78	3.05	2.69	0.44	3.52	0.39	14.2	5.17	1.18
23/11/2023	**Kirishima - Awaokoshi**	FLF181	60.6	315	27.0	132	6.41	365	19.2	41.6	5.08	21.4	5.23	1.36	4.66	5.17	2.97	2.95	0.43	3.94	0.42	14.6	5.56	1.23
23/11/2023	**Kirishima - Awaokoshi**	FLF181	60.5	339	26.9	131	6.12	370	19.3	41.6	5.03	22.0	4.95	1.33	4.85	4.77	3.07	3.00	0.43	3.35	0.43	14.6	5.24	1.33
23/11/2023	**Kirishima - Awaokoshi**	FLF181	55.9	352	26.1	128	6.10	350	18.6	41.0	4.83	21.7	5.20	1.43	4.76	5.01	3.09	2.76	0.42	3.74	0.42	14.2	4.93	1.23
23/11/2023	**Kirishima - Iwaokoshi**	FLF178	125	78.1	20.4	112	7.51	516	23.8	47.3	4.83	18.0	3.87	0.62	3.36	3.44	2.26	2.43	0.35	3.22	0.65	19.4	11.3	2.59
23/11/2023	**Kirishima - Iwaokoshi**	FLF178	144	185	31.1	249	9.26	573	25.2	51.0	6.52	25.0	5.79	1.09	4.63	5.18	3.70	3.98	0.55	7.13	0.61	22.4	12.0	3.01
23/11/2023	**Kirishima - Iwaokoshi**	FLF178	113	328	25.6	195	7.75	501	21.3	46.2	5.41	21.9	5.07	1.19	4.44	4.57	2.73	2.39	0.42	5.45	0.57	19.2	9.85	2.51
23/11/2023	**Kirishima - Iwaokoshi**	FLF178	133	78.3	20.1	110	7.64	533	24.1	46.0	4.93	18.4	3.51	0.60	3.80	3.16	2.19	2.55	0.35	3.31	0.63	19.3	11.4	2.54
23/11/2023	**Kirishima - Iwaokoshi**	FLF178	129	76.2	20.6	110	7.41	526	23.7	47.6	4.67	18.7	3.36	0.50	3.22	3.04	2.11	2.21	0.37	3.71	0.65	21.0	12.0	2.83
23/11/2023	**Kirishima - Iwaokoshi**	FLF178	91.9	337	22.5	161	6.37	429	17.7	36.9	4.81	18.9	4.61	0.96	4.20	3.99	2.24	2.51	0.38	4.74	0.47	17.0	8.10	2.10
23/11/2023	**Kirishima - Iwaokoshi**	FLF177	81.8	335	22.7	150	5.86	389	17.0	37.3	4.58	18.0	3.82	0.95	4.08	3.84	2.63	2.58	0.40	3.93	0.42	16.2	7.59	1.94
23/11/2023	**Kirishima - Iwaokoshi**	FLF177	134	195	29.6	238	8.93	554	23.9	52.7	6.07	25.4	6.36	1.03	5.11	5.10	3.46	3.17	0.49	6.02	0.66	22.0	12.5	3.06
23/11/2023	**Kirishima - Iwaokoshi**	FLF177	47.2	682	8.47	71.0	2.89	311	11.0	22.3	2.45	9.53	1.97	1.19	1.77	1.46	1.04	0.85	0.12	2.06	0.20	9.6	3.49	0.95

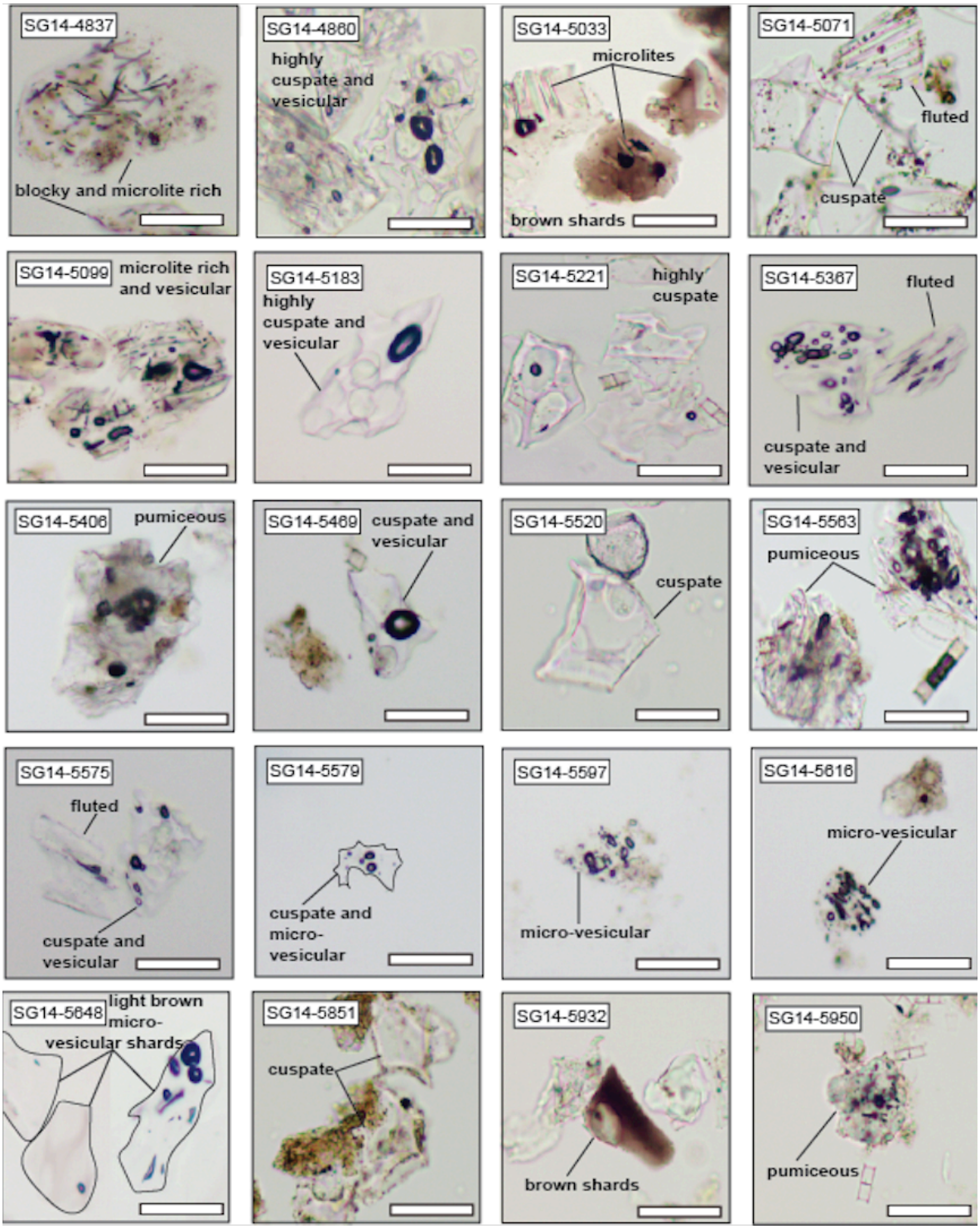
Date of Analysis	Sample	Label	Rb	Sr	Y	Zr	Nb	Ba	La	Ce	Pr	Nd	Sm	Eu	Gd	Dy	Er	Yb	Lu	Hf	Ta	Pb	Th	U
23/11/2023	**Kirishima - Iwaokoshi**	FLF177	153	153	29.2	255	9.70	583	24.3	54.5	6.15	24.8	5.10	0.91	4.34	4.78	2.78	3.41	0.46	7.09	0.70	23.5	13.74	3.37
23/11/2023	**Kirishima - Iwaokoshi**	FLF177	133	202	29.2	223	8.75	548	23.3	52.2	6.11	25.3	5.26	1.10	4.85	5.19	3.23	3.23	0.47	6.14	0.66	22.6	11.6	2.76
23/11/2023	**Kirishima - Iwaokoshi**	FLF177	100	319	22.2	168	6.59	443	18.8	42.6	5.02	19.2	4.19	0.93	4.30	3.99	2.25	2.88	0.37	4.94	0.48	16.3	8.96	2.24
23/11/2023	**Kirishima - Iwaokoshi**	FLF177	137	193	30.0	220	9.11	554	23.1	52.1	6.08	24.5	5.70	1.12	4.71	4.95	3.47	3.65	0.46	6.04	0.63	24.3	11.5	2.89
23/11/2023	**Kirishima - Iwaokoshi**	FLF177	151	155	27.1	241	9.10	583	22.8	50.8	5.75	23.1	5.00	0.77	4.31	4.73	3.04	2.90	0.45	6.79	0.65	23.2	12.2	3.17
23/11/2023	**Kirishima - Iwaokoshi**	FLF177	80.0	366	20.9	145	5.52	382	16.4	36.0	4.09	17.9	3.78	0.95	3.91	3.66	2.34	2.35	0.33	4.11	0.40	16.0	7.16	1.92
23/11/2023	**Kirishima - Iwaokoshi**	FLF177	114	304	22.8	184	7.30	476	19.7	44.2	5.11	20.1	5.01	0.96	4.05	3.50	2.22	2.69	0.40	5.02	0.51	19.9	9.54	2.38
23/11/2023	**Kirishima - Iwaokoshi**	FLF177	159	136	26.4	247	9.02	572	23.4	50.7	5.50	23.0	5.23	0.74	4.49	4.21	2.91	2.83	0.44	6.58	0.68	21.7	12.8	3.59
23/11/2023	**Kirishima - Iwaokoshi**	FLF177	68.0	565	14.6	112	4.48	342	12.8	28.7	3.30	12.3	2.98	0.74	2.26	2.77	1.47	1.85	0.23	3.35	0.33	13.6	5.77	1.53
23/11/2023	**Kirishima - Iwaokoshi**	FLF177	94.9	413	23.0	173	6.40	435	19.3	42.6	4.99	20.6	4.81	0.88	3.64	4.26	2.30	2.27	0.32	5.07	0.47	14.8	8.75	2.18
23/11/2023	**Kirishima - Iwaokoshi**	FLF177	122	248	27.2	220	8.05	527	22.6	48.7	5.71	23.9	6.09	0.97	4.95	4.58	2.75	2.82	0.44	6.12	0.58	32.5	11.4	2.78
23/11/2023	**Kirishima - Iwaokoshi**	FLF177	170	125	28.6	279	9.51	607	24.8	56.2	6.28	25.7	5.06	0.76	4.43	4.77	3.28	3.34	0.55	7.94	0.74	41.2	15.5	3.71
23/11/2023	**Kirishima - Iwaokoshi**	FLF176	159	140	29.2	274	9.41	614	25.1	56.1	6.39	26.0	5.78	0.86	5.62	5.06	2.82	3.42	0.44	7.65	0.74	23.4	15.2	3.79
23/11/2023	**Kirishima - Iwaokoshi**	FLF176	157	160	28.1	238	9.47	648	23.8	53.4	6.54	22.9	4.68	0.93	4.93	4.54	2.75	2.94	0.43	6.77	0.67	22.4	12.7	3.07
23/11/2023	**Kirishima - Iwaokoshi**	FLF176	152	176	28.0	248	8.90	579	23.5	53.2	5.96	23.9	5.33	0.89	4.45	5.05	2.85	2.93	0.51	7.30	0.68	21.2	13.7	3.27
23/11/2023	**Kirishima - Iwaokoshi**	FLF176	110	301	20.1	164	6.77	428	16.8	38.1	4.37	17.3	4.11	0.84	3.23	3.35	2.22	2.42	0.33	4.38	0.49	19.3	8.34	2.32
23/11/2023	**Kirishima - Iwaokoshi**	FLF176	155	166	29.8	263	9.84	618	24.6	55.1	6.17	26.2	5.57	0.83	5.01	4.76	3.51	3.87	0.57	7.27	0.76	23.0	13.9	3.55
23/11/2023	**Kirishima - Iwaokoshi**	FLF176	110	273	24.9	186	7.34	679	21.7	54.4	5.54	23.2	5.62	0.98	4.71	4.54	2.74	2.87	0.39	5.22	0.53	21.0	9.86	2.68
23/11/2023	**Kirishima - Iwaokoshi**	FLF176	174	120	29.1	274	9.87	617	25.1	56.7	6.33	24.8	5.39	0.83	4.76	5.21	3.05	3.48	0.49	7.38	0.73	21.8	15.7	3.96
23/11/2023	**Kirishima - Iwaokoshi**	FLF176	101	309	24.9	183	6.97	452	20.0	44.4	4.92	21.1	4.89	0.93	4.32	4.07	2.77	2.57	0.43	5.21	0.51	17.4	9.41	2.20
23/11/2023	**Kirishima - Iwaokoshi**	FLF176	147	167	28.6	240	8.91	553	22.9	52.7	5.82	25.3	6.19	0.85	4.75	4.75	3.16	3.37	0.46	6.60	0.67	19.8	13.0	3.18
23/11/2023	**Kirishima - Iwaokoshi**	FLF176	149	153	23.8	205	8.39	498	19.6	45.4	5.23	19.9	5.17	0.95	4.25	4.09	2.54	3.39	0.44	5.03	0.49	21.3	9.45	2.59
23/11/2023	**Kirishima - Iwaokoshi**	FLF176	126	216	22.1	190	7.36	511	30.5	41.3	4.47	20.0	4.50	0.77	5.21	3.91	2.49	2.48	0.35	3.96	0.53	16.8	9.27	2.30

Table B8. Trace element glass analyses of the MPI-DING reference glass (StHs6/80-G and ATHO-G)

Date of Analysis	Sample	Rb	Sr	Y	Zr	Nb	Ba	La	Ce	Pr	Nd	Sm	Eu	Gd	Dy	Er	Yb	Lu	Hf	Ta	Pb	Th	U
03/07/2023	**StHs6/80**	30.7	478	10.8	115	6.36	302	11.4	25.6	2.92	12.3	2.23	0.95	2.38	2.37	1.23	1.31	0.15	2.89	0.39	8.99	2.26	0.95
03/07/2023	**StHs6/80**	31.8	484	11.3	117	6.48	307	11.6	25.2	2.95	11.9	3.03	0.88	2.66	2.31	1.26	1.17	0.17	3.00	0.39	9.37	2.17	1.05
03/07/2023	**StHs6/80**	30.4	463	10.9	112	6.19	290	11.2	24.0	2.88	12.1	2.45	0.95	2.41	2.18	1.25	1.26	0.16	2.96	0.38	8.67	2.10	0.93
23/11/2023	**StHs6/80**	29.3	468	10.8	115	6.64	300	11.7	24.9	3.00	11.8	3.14	0.99	2.44	2.27	1.26	1.17	0.18	3.02	0.41	9.14	2.29	1.04
23/11/2023	**StHs6/80**	29.8	488	11.3	117	6.55	315	11.6	25.6	3.01	12.2	3.06	0.98	2.59	2.28	1.22	1.23	0.16	3.27	0.40	9.00	2.29	1.07
23/11/2023	**StHs6/80**	30.3	492	11.2	119	6.61	316	11.5	25.4	3.03	13.2	2.73	0.88	2.77	2.32	1.29	1.22	0.16	3.09	0.40	8.76	2.18	1.02
23/11/2023	**StHs6/80**	29.5	486	10.8	116	6.70	300	11.4	25.1	3.05	12.6	3.10	1.00	2.61	2.41	1.31	0.99	0.16	2.99	0.40	9.18	2.38	1.15
23/11/2023	**StHs6/80**	30.4	478	10.8	116	6.63	299	11.4	25.4	2.96	12.6	2.92	0.93	2.79	2.20	1.11	1.27	0.18	3.10	0.39	8.77	2.26	1.01
23/11/2023	**StHs6/80**	30.2	482	10.9	115	6.50	306	11.5	24.9	2.94	12.1	2.85	0.95	2.25	2.14	1.24	1.26	0.19	3.40	0.40	9.23	2.34	1.11
29/07/2024	**StHs6/80**	30.3	471	11.0	114	6.43	304	11.5	25.0	2.84	12.2	2.82	0.92	2.33	2.03	1.10	1.03	0.16	3.03	0.40	8.91	2.14	0.94
29/07/2024	**StHs6/80**	30.4	477	10.9	113	6.47	304	11.6	25.3	2.97	12.2	2.81	0.93	2.57	2.11	1.20	1.17	0.17	3.06	0.40	8.52	2.18	1.03
29/07/2024	**StHs6/80**	30.3	480	11.0	115	6.58	304	11.6	25.6	2.98	12.3	2.66	0.91	2.49	2.28	1.10	1.10	0.16	2.93	0.40	8.97	2.32	1.00
03/07/2023	**ATHO-G**	67.0	92.6	90.5	500	59.9	559	55.2	122	14.5	60.7	14.9	2.49	15.1	16.7	10.3	10.0	1.50	13.7	3.69	4.82	7.21	2.42
03/07/2023	**ATHO-G**	65.0	91.8	89.9	491	59.2	556	54.2	120	14.4	57.3	13.7	2.52	14.5	16.9	9.8	9.68	1.47	13.2	3.66	4.50	7.48	2.37
03/07/2023	**ATHO-G**	63.7	90.9	88.5	487	58.3	548	54.0	120	14.2	60.3	14.1	2.44	14.2	16.2	9.8	10.4	1.50	13.6	3.59	4.63	7.05	2.26
23/11/2023	**ATHO-G**	65.5	93.4	92.5	506	60.9	546	55.5	122	14.5	62.3	15.3	2.39	15.3	16.7	10.3	10.9	1.51	13.8	3.83	4.61	7.42	2.50
23/11/2023	**ATHO-G**	66.1	95.2	93.3	509	60.8	545	56.0	124	14.5	62.3	15.2	2.54	15.4	17.1	10.6	10.7	1.55	14.1	3.81	4.39	7.23	2.41
23/11/2023	**ATHO-G**	64.7	94.6	91.9	497	60.0	559	54.6	122	14.4	62.8	15.1	2.64	14.2	17.0	10.4	10.0	1.49	14.1	3.73	4.16	7.39	2.20
23/11/2023	**ATHO-G**	64.2	92.2	92.5	497	60.3	556	55.3	122	14.4	61.0	15.4	2.44	13.4	17.4	10.1	10.4	1.56	13.9	3.77	4.21	7.32	2.24
23/11/2023	**ATHO-G**	65.9	95.0	92.7	497	60.2	568	55.1	122	14.6	61.0	14.5	2.50	13.4	17.1	10.2	10.8	1.50	14.2	3.73	4.67	7.54	2.33
29/07/2024	**ATHO-G**	65.9	94.8	91.0	490	60.1	565	54.9	123	14.7	61.3	14.1	3.06	14.1	16.5	10.3	10.0	1.50	13.5	3.71	3.78	7.31	2.02
29/07/2024	**ATHO-G**	65.5	94.1	89.8	492	59.6	563	54.9	122	14.6	60.2	14.3	2.99	14.3	16.9	10.2	9.91	1.53	13.7	3.73	3.87	7.47	1.90
29/07/2024	**ATHO-G**	66.0	95.5	90.9	492	59.7	567	55.4	122	14.6	61.8	14.8	3.08	14.3	16.5	10.3	11.1	1.50	13.4	3.74	3.63	7.35	1.98

Figure B1: Annotated shard photos where white bar equates to 50 microns




SG14-4837
blocky and microlite rich
SG14-4860
highly cuspate and vesicular
SG14-5033
microlites
brown shards
SG14-5071
fluted
cuspate
SG14-5099
microlite rich and vesicular
SG14-5183
highly cuspate and vesicular
SG14-5221
highly cuspate
SG14-5367
fluted
cuspate and vesicular
SG14-5406
pumiceous
SG14-5469
cuspate and vesicular
SG14-5520
cuspate
SG14-5563
pumiceous
SG14-5575
fluted
cuspate and vesicular
SG14-5579
cuspate and micro-vesicular
SG14-5597
micro-vesicular
SG14-5616
micro-vesicular
SG14-5648
light brown micro-vesicular shards
SG14-5851
cuspate
SG14-5932
brown shards
SG14-5950
pumiceous

Appendix C: Supplementary Material for Article 3.

Table C1. Major element glass analyses of the proximal Aso tephra units

Date of Analysis	Sample	Label	SiO_2	TiO_2	Al_2O_3	FeO_t	MnO	MgO	CaO	Na_2O	K_2O	P_2O_5	Cl	Analytical Total
23/04/2024	**Ash bed above Aso-Kpfa**	FLF57	64.87	0.94	15.33	4.89	0.14	1.36	3.33	4.65	4.02	0.34	0.08	99.94
23/04/2024	**Ash bed above Aso-Kpfa**	FLF57	67.06	0.88	15.05	4.45	0.12	1.04	2.67	4.52	4.21	0.23	0.08	100.29
23/04/2024	**Ash bed above Aso-Kpfa**	FLF57	66.46	0.91	15.30	4.38	0.11	1.13	2.88	4.69	4.06	0.29	0.07	100.28
23/04/2024	**Ash bed above Aso-Kpfa**	FLF57	64.96	0.97	15.42	5.20	0.13	1.33	3.44	4.67	4.13	0.35	0.08	100.69
23/04/2024	**Ash bed above Aso-Kpfa**	FLF57	65.78	0.89	14.81	4.57	0.14	1.06	2.85	4.33	4.02	0.25	0.08	98.77
23/04/2024	**Ash bed above Aso-Kpfa**	FLF57	66.44	0.89	14.72	4.24	0.15	1.08	2.90	4.46	4.08	0.27	0.07	99.30
23/04/2024	**Aso-Kpfa**	FLF56	68.56	0.68	14.59	2.57	0.11	0.65	1.87	4.69	4.28	0.12	0.11	98.22
23/04/2024	**Aso-Kpfa**	FLF56	69.10	0.72	14.82	2.63	0.12	0.64	1.83	4.80	4.31	0.13	0.11	99.19
23/04/2024	**Aso-Kpfa**	FLF56	67.89	0.71	14.74	2.78	0.11	0.65	1.84	4.70	4.24	0.11	0.09	97.86
23/04/2024	**Aso-Kpfa**	FLF56	67.26	0.71	14.88	2.70	0.12	0.68	1.87	4.75	4.31	0.11	0.11	97.50
23/04/2024	**Aso-Kpfa**	FLF56	68.79	0.74	15.02	2.66	0.11	0.66	1.94	4.88	4.37	0.11	0.09	99.37
23/04/2024	**Aso-Kpfa**	FLF56	67.83	0.71	14.51	2.79	0.10	0.66	1.85	4.77	4.33	0.12	0.09	97.76
23/04/2024	**Aso-Kpfa**	FLF56	68.09	0.69	14.45	2.57	0.10	0.64	1.85	4.83	4.24	0.12	0.10	97.67
23/04/2024	**Aso-Kpfa**	FLF56	67.38	0.68	14.16	2.49	0.10	0.66	1.84	4.83	4.23	0.11	0.11	96.60
23/04/2024	**Aso-Kpfa**	FLF56	69.20	0.72	14.76	2.86	0.10	0.66	1.84	4.69	4.24	0.12	0.09	99.28
23/04/2024	**Aso-Kpfa**	FLF56	68.35	0.74	14.84	2.75	0.10	0.66	1.83	4.88	4.25	0.11	0.11	98.62
23/04/2024	**Aso-Kpfa**	FLF56	68.71	0.74	15.18	2.81	0.12	0.65	1.86	4.76	4.24	0.11	0.12	99.30
23/04/2024	**Aso-Kpfa**	FLF56	67.93	0.72	15.17	2.73	0.10	0.64	1.76	4.79	4.30	0.12	0.11	98.37
23/04/2024	**Aso-Kpfa**	FLF56	69.31	0.72	15.33	2.77	0.12	0.64	2.02	5.03	4.37	0.11	0.11	100.54
23/04/2024	**Aso-Kpfa**	FLF56	70.71	0.73	15.12	2.60	0.12	0.64	1.81	4.60	4.26	0.10	0.09	100.78
23/04/2024	**Aso-Kpfa**	FLF56	61.48	0.66	13.20	2.71	0.08	0.48	1.70	4.11	3.97	0.06	0.23	88.67
23/04/2024	**Aso-Kpfa**	FLF56	69.08	0.73	15.18	2.75	0.11	0.65	1.87	4.80	4.36	0.11	0.09	99.74
23/04/2024	**Aso-Kpfa**	FLF56	67.28	0.71	14.74	2.78	0.11	0.67	1.86	5.02	4.15	0.11	0.12	97.56
23/04/2024	**Aso-Kpfa**	FLF56	68.48	0.71	14.93	2.54	0.10	0.66	1.87	4.75	4.28	0.12	0.10	98.54
23/04/2024	**Aso-Kpfa**	FLF56	68.74	0.71	15.09	2.52	0.11	0.64	1.80	4.93	4.35	0.12	0.10	99.11
04/08/2023	**ACP3**	FLF58	70.21	0.33	13.53	1.19	0.05	0.20	0.60	3.94	4.70	0.02	0.11	94.88
04/08/2023	**ACP3**	FLF58	70.48	0.30	13.34	1.13	0.05	0.16	0.65	3.92	4.81	0.01	0.10	94.96
04/08/2023	**ACP3**	FLF58	70.19	0.29	13.52	1.27	0.07	0.18	0.71	4.18	4.75	0.02	0.12	95.30
04/08/2023	**ACP3**	FLF58	70.60	0.37	13.55	1.09	0.06	0.19	0.67	4.19	4.78	0.03	0.11	95.65

Date of Analysis	Sample	Label	SiO_2	TiO_2	Al_2O_3	FeO_t	MnO	MgO	CaO	Na_2O	K_2O	P_2O_5	Cl	Analytical Total
04/08/2023	**ACP3**	FLF58	70.54	0.33	13.15	1.20	0.06	0.21	0.67	3.98	4.89	0.01	0.10	95.15
04/08/2023	**ACP3**	FLF58	70.96	0.36	13.15	1.17	0.01	0.17	0.63	4.11	4.83	0.00	0.11	95.51
04/08/2023	**ACP3**	FLF58	71.17	0.29	13.30	1.16	0.03	0.15	0.57	4.01	4.91	0.03	0.12	95.75
04/08/2023	**ACP3**	FLF58	71.35	0.33	13.57	1.24	0.09	0.19	0.67	4.05	4.84	0.02	0.11	96.46
04/08/2023	**ACP3**	FLF58	70.68	0.30	13.46	1.15	0.06	0.19	0.62	4.03	4.87	0.02	0.11	95.49
04/08/2023	**ACP3**	FLF58	70.91	0.33	13.57	1.16	0.09	0.18	0.68	4.20	4.72	0.01	0.09	95.94
04/08/2023	**ACP3**	FLF58	71.44	0.30	13.05	1.10	0.04	0.15	0.55	4.15	4.88	0.03	0.13	95.81
04/08/2023	**ACP3**	FLF58	70.63	0.32	13.49	1.22	0.07	0.20	0.70	4.13	4.80	0.01	0.13	95.71
04/08/2023	**ACP3**	FLF58	70.73	0.34	13.55	1.18	0.08	0.19	0.69	4.01	4.73	0.00	0.10	95.61
04/08/2023	**ACP3**	FLF58	70.86	0.31	13.38	1.31	0.11	0.22	0.66	4.23	4.80	0.02	0.09	96.00
04/08/2023	**ACP3**	FLF58	70.31	0.29	13.43	1.19	0.05	0.15	0.70	4.03	4.83	0.06	0.11	95.14
04/08/2023	**ACP3**	FLF58	70.80	0.31	13.48	1.26	0.08	0.21	0.67	4.21	4.79	0.02	0.10	95.94
04/08/2023	**ACP3**	FLF58	71.40	0.28	12.93	1.15	0.07	0.16	0.61	4.05	5.01	0.03	0.10	95.78
04/08/2023	**ACP4**	FLF60	68.53	0.41	14.36	1.67	0.07	0.41	1.17	4.46	4.32	0.03	0.11	95.53
04/08/2023	**ACP4**	FLF60	67.60	0.44	14.19	1.57	0.10	0.37	1.08	4.20	4.16	0.04	0.09	93.82
04/08/2023	**ACP4**	FLF60	68.95	0.46	14.34	1.66	0.14	0.31	1.14	4.39	4.34	0.03	0.10	95.86
04/08/2023	**ACP4**	FLF60	68.56	0.43	14.13	1.67	0.12	0.35	1.18	4.45	4.50	0.06	0.08	95.53
04/08/2023	**ACP4**	FLF60	68.69	0.44	14.36	1.52	0.09	0.35	1.17	4.45	4.39	0.06	0.11	95.63
04/08/2023	**ACP4**	FLF60	69.40	0.40	14.45	1.65	0.10	0.35	1.17	4.31	4.28	0.05	0.11	96.26
04/08/2023	**ACP4**	FLF60	68.62	0.44	14.49	1.59	0.06	0.38	1.21	4.34	4.35	0.04	0.09	95.63
04/08/2023	**ACP4**	FLF60	68.98	0.43	14.23	1.67	0.08	0.31	1.21	4.29	4.23	0.03	0.10	95.55
04/08/2023	**ACP4**	FLF60	67.35	0.45	13.96	1.54	0.07	0.35	1.16	4.46	4.29	0.05	0.15	93.83
04/08/2023	**ACP4**	FLF60	69.01	0.43	14.43	1.55	0.09	0.33	1.12	4.29	4.37	0.02	0.10	95.74
04/08/2023	**ACP4**	FLF60	68.92	0.44	14.27	1.60	0.05	0.42	1.17	4.32	4.30	0.06	0.11	95.67
04/08/2023	**ACP4**	FLF60	69.20	0.41	14.56	1.72	0.07	0.38	1.20	4.31	4.36	0.02	0.11	96.34
04/08/2023	**ACP4**	FLF60	69.47	0.48	14.50	1.70	0.08	0.30	1.19	4.36	4.47	0.07	0.09	96.72
04/08/2023	**ACP4**	FLF60	70.77	0.42	14.73	1.65	0.13	0.42	1.19	4.64	4.54	0.08	0.09	98.66
04/08/2023	**ACP4**	FLF60	69.39	0.44	14.46	1.61	0.07	0.40	1.20	4.48	4.44	0.08	0.12	96.70
04/08/2023	**ACP4**	FLF61	70.25	0.36	13.89	1.33	0.08	0.24	0.86	4.12	4.69	0.05	0.10	95.97
04/08/2023	**ACP4**	FLF61	69.66	0.35	14.32	1.52	0.05	0.27	0.92	4.28	4.67	0.06	0.10	96.22
04/08/2023	**ACP4**	FLF61	68.69	0.46	14.32	1.70	0.09	0.37	1.19	4.49	4.39	0.04	0.10	95.84
04/08/2023	**ACP4**	FLF61	69.35	0.49	14.47	1.84	0.06	0.36	1.20	4.50	4.35	0.08	0.10	96.79
04/08/2023	**ACP4**	FLF61	68.96	0.47	14.40	1.60	0.09	0.34	1.17	4.55	4.39	0.02	0.11	96.10

Date of Analysis	Sample	Label	SiO_2	TiO_2	Al_2O_3	FeO_t	MnO	MgO	CaO	Na_2O	K_2O	P_2O_5	Cl	Analytical Total
04/08/2023	**ACP4**	FLF61	68.60	0.41	14.28	1.70	0.06	0.35	1.20	4.45	4.40	0.04	0.08	95.57
04/08/2023	**ACP4**	FLF61	70.73	0.46	14.75	1.75	0.06	0.38	1.24	4.57	4.52	0.03	0.10	98.59
04/08/2023	**ACP4**	FLF61	68.48	0.57	14.72	1.73	0.07	0.31	1.24	4.43	4.25	0.05	0.08	95.93
04/08/2023	**ACP4**	FLF61	69.40	0.51	14.40	1.86	0.06	0.28	1.18	4.75	4.35	0.03	0.10	96.92
04/08/2023	**ACP4**	FLF61	68.72	0.43	14.25	1.59	0.08	0.38	1.14	4.38	4.39	0.03	0.12	95.52
04/08/2023	**ACP4**	FLF61	68.70	0.47	14.22	1.61	0.07	0.37	1.13	4.39	4.34	0.06	0.10	95.48
04/08/2023	**ACP4**	FLF61	68.99	0.42	14.53	1.55	0.06	0.29	1.05	4.20	4.34	0.04	0.10	95.57
04/08/2023	**ACP4**	FLF62	68.14	0.44	14.55	1.99	0.06	0.47	1.40	4.42	4.36	0.05	0.09	95.96
04/08/2023	**ACP4**	FLF62	68.70	0.46	14.29	1.93	0.10	0.49	1.32	4.44	4.31	0.07	0.08	96.19
04/08/2023	**ACP4**	FLF62	69.16	0.45	14.47	1.56	0.06	0.39	1.17	4.28	4.43	0.07	0.12	96.17
04/08/2023	**ACP4**	FLF62	68.67	0.44	14.52	1.72	0.07	0.33	1.17	4.51	4.45	0.07	0.11	96.06
04/08/2023	**ACP4**	FLF62	70.61	0.27	13.36	1.20	0.06	0.20	0.70	4.07	4.94	0.00	0.10	95.52
04/08/2023	**ACP4**	FLF62	67.63	0.44	14.11	1.63	0.08	0.37	1.14	4.27	4.35	0.07	0.09	94.18
04/08/2023	**ACP4**	FLF62	66.97	0.42	14.00	1.63	0.06	0.38	1.12	4.14	4.49	0.07	0.10	93.38
04/08/2023	**ACP4**	FLF62	70.31	0.57	14.90	1.90	0.06	0.45	1.36	4.46	4.44	0.07	0.09	98.61
04/08/2023	**ACP4**	FLF62	70.07	0.53	14.85	1.90	0.08	0.45	1.33	4.80	4.45	0.03	0.11	98.60
04/08/2023	**ACP4**	FLF62	68.70	0.44	14.38	1.58	0.05	0.35	1.13	4.30	4.34	0.02	0.08	95.38
04/08/2023	**ACP4**	FLF62	71.92	0.27	13.74	1.16	0.05	0.20	0.60	4.13	4.93	0.02	0.11	97.13
04/08/2023	**ACP4**	FLF62	68.21	0.47	14.63	1.77	0.13	0.42	1.33	4.25	4.10	0.07	0.10	95.47
04/08/2023	**ACP4**	FLF62	68.74	0.46	14.42	1.59	0.09	0.38	1.18	4.53	4.45	0.08	0.09	96.02
04/08/2023	**ACP4**	FLF63	70.74	0.26	13.47	1.21	0.04	0.20	0.66	4.07	4.86	0.00	0.14	95.65
04/08/2023	**ACP4**	FLF63	70.46	0.44	14.53	1.74	0.06	0.34	1.09	4.52	4.57	0.06	0.10	97.89
04/08/2023	**ACP4**	FLF63	70.86	0.48	15.18	1.87	0.10	0.42	1.36	4.75	4.44	0.06	0.10	99.62
04/08/2023	**ACP4**	FLF63	69.01	0.47	14.26	1.74	0.05	0.30	1.12	4.56	4.34	0.06	0.08	95.99
04/08/2023	**ACP4**	FLF63	67.35	0.43	13.89	1.59	0.06	0.32	1.05	4.36	4.23	0.04	0.12	93.46
04/08/2023	**ACP4**	FLF63	69.21	0.40	14.27	1.66	0.09	0.38	1.17	4.42	4.36	0.03	0.11	96.10
05/02/2024	**ACP4**	FLF191	71.28	0.62	13.36	2.36	0.08	0.21	0.62	3.91	5.11	0.04	0.08	97.65
05/02/2024	**ACP4**	FLF191	69.55	0.57	13.63	2.69	0.10	0.36	0.77	4.26	4.74	0.06	0.06	96.78
05/02/2024	**ACP4**	FLF191	72.08	0.49	12.27	1.48	0.08	0.35	0.47	3.83	5.40	0.05	0.09	96.60
05/02/2024	**ACP4**	FLF191	67.78	0.48	14.40	1.80	0.07	0.38	1.30	4.26	4.24	0.08	0.09	94.88
05/02/2024	**ACP4**	FLF191	72.04	0.43	14.95	0.60	0.03	0.00	0.66	4.67	5.57	0.01	0.00	98.97
05/02/2024	**ACP4**	FLF191	69.94	0.18	14.88	1.73	0.16	1.03	1.33	5.07	4.31	0.04	0.03	98.70

Date of Analysis	Sample	Label	SiO_2	TiO_2	Al_2O_3	FeO_t	MnO	MgO	CaO	Na_2O	K_2O	P_2O_5	Cl	Analytical Total
05/02/2024	**ACP4**	FLF191	73.38	0.42	13.99	0.89	0.00	0.04	0.60	4.17	5.18	0.05	0.04	98.77
05/02/2024	**ACP4**	FLF191	71.70	0.12	16.86	0.44	0.00	0.00	1.58	5.57	4.23	0.03	0.02	100.54
05/02/2024	**ACP4**	FLF191	68.30	0.52	14.46	1.78	0.09	0.45	1.32	4.81	4.43	0.06	0.09	96.32
05/02/2024	**ACP4**	FLF190	71.46	0.45	14.64	1.76	0.05	0.40	1.18	4.58	4.80	0.04	0.11	99.47
05/02/2024	**ACP4**	FLF190	71.40	0.46	14.83	1.63	0.08	0.36	1.10	4.78	4.74	0.04	0.10	99.50
05/02/2024	**ACP4**	FLF190	71.36	0.43	14.83	1.66	0.11	0.36	1.09	4.53	4.66	0.05	0.08	99.15
05/02/2024	**ACP4**	FLF190	70.29	0.43	14.46	1.65	0.09	0.36	1.12	4.48	4.60	0.08	0.08	97.65
05/02/2024	**ACP4**	FLF190	70.16	0.76	14.86	2.32	0.06	0.24	1.68	4.78	4.35	0.19	0.08	99.48
05/02/2024	**ACP4**	FLF190	68.02	0.74	14.51	3.58	0.20	1.54	2.53	4.66	3.78	0.07	0.04	99.67
05/02/2024	**ACP4**	FLF190	68.13	0.43	14.28	1.57	0.06	0.37	1.16	4.74	4.39	0.03	0.15	95.30
05/02/2024	**ACP4**	FLF190	71.39	0.42	14.70	1.61	0.07	0.33	1.17	4.61	4.66	0.02	0.11	99.07
05/02/2024	**ACP4**	FLF190	70.86	0.44	14.58	1.72	0.07	0.41	1.14	4.68	4.70	0.01	0.09	98.70
05/02/2024	**ACP4**	FLF190	71.14	0.41	14.62	1.62	0.09	0.38	1.04	4.56	4.77	0.06	0.09	98.78
05/02/2024	**ACP4**	FLF189	69.67	0.47	14.44	1.70	0.10	0.31	1.18	4.58	4.36	0.06	0.07	96.93
05/02/2024	**ACP4**	FLF189	71.26	0.44	14.65	1.70	0.10	0.39	1.14	4.67	4.68	0.06	0.08	99.18
05/02/2024	**ACP4**	FLF189	71.39	0.45	14.65	1.66	0.05	0.34	0.97	4.56	4.79	0.03	0.10	98.99
05/02/2024	**ACP4**	FLF189	70.87	0.48	14.79	1.45	0.02	0.34	1.05	4.49	4.84	0.06	0.06	98.44
05/02/2024	**ACP4**	FLF189	71.17	0.46	14.30	1.69	0.08	0.38	1.11	4.59	4.70	0.02	0.11	98.61
05/02/2024	**ACP4**	FLF189	69.18	0.46	13.89	2.05	0.11	0.69	1.10	4.63	4.56	0.06	0.08	96.82
05/02/2024	**ACP4**	FLF189	71.14	0.39	14.51	1.72	0.09	0.34	1.11	4.44	4.81	0.02	0.10	98.67
05/02/2024	**ACP4**	FLF189	68.94	0.21	18.63	0.74	0.03	0.08	2.08	6.40	3.31	0.01	0.00	100.43
05/02/2024	**ACP4**	FLF189	73.55	0.35	14.76	0.58	0.00	0.02	0.98	4.71	4.68	0.05	0.00	99.68
05/02/2024	**ACP6**	FLF186	70.40	0.30	13.69	1.30	0.06	0.20	0.71	4.29	4.85	0.02	0.11	95.94
05/02/2024	**ACP6**	FLF186	69.41	0.27	13.61	1.33	0.04	0.20	0.65	4.31	4.87	0.03	0.12	94.84
05/02/2024	**ACP6**	FLF186	69.44	0.31	13.71	1.39	0.11	0.23	0.67	4.35	4.94	0.03	0.13	95.30
05/02/2024	**ACP6**	FLF186	69.38	0.33	13.62	1.14	0.07	0.18	0.70	4.39	4.91	0.05	0.16	94.92
05/02/2024	**ACP6**	FLF186	69.49	0.76	15.00	2.73	0.12	0.64	1.94	4.94	3.85	0.17	0.07	99.70
05/02/2024	**ACP6**	FLF186	67.06	0.27	14.40	1.23	0.08	0.20	0.63	3.81	4.40	0.02	0.11	92.21
05/02/2024	**ACP6**	FLF186	70.33	0.28	15.16	1.24	0.08	0.17	0.68	3.97	4.78	0.03	0.13	96.83
05/02/2024	**ACP6**	FLF186	69.56	0.31	13.71	1.27	0.03	0.23	0.70	4.43	4.99	0.05	0.13	95.39
05/02/2024	**ACP6**	FLF186	69.52	0.61	14.99	1.00	0.04	0.07	1.28	4.62	4.60	0.14	0.04	96.92
05/02/2024	**ACP6**	FLF186	69.81	0.31	13.68	1.29	0.06	0.22	0.66	4.34	4.97	0.01	0.12	95.47

Date of Analysis	Sample	Label	SiO_2	TiO_2	Al_2O_3	FeO_t	MnO	MgO	CaO	Na_2O	K_2O	P_2O_5	Cl	Analytical Total
05/02/2024	**ACP6**	FLF186	68.57	0.33	13.90	1.40	0.08	0.32	0.86	4.41	4.73	0.08	0.11	94.79
05/02/2024	**ACP6**	FLF186	66.15	0.69	14.21	2.58	0.11	0.71	1.78	4.02	5.48	0.11	0.08	95.91
05/02/2024	**ACP6**	FLF186	69.13	0.29	13.70	1.33	0.07	0.20	0.70	4.31	4.80	0.00	0.08	94.61
05/02/2024	**ACP6**	FLF186	69.59	0.27	13.42	1.26	0.03	0.18	0.67	4.27	4.98	0.09	0.12	94.89
05/02/2024	**ACP6**	FLF186	70.17	0.31	13.74	1.31	0.04	0.20	0.68	4.28	5.00	0.03	0.11	95.90
05/02/2024	**ACP6**	FLF186	69.86	0.32	13.64	1.27	0.06	0.22	0.65	4.31	4.92	0.06	0.11	95.41
05/02/2024	**ACP6**	FLF186	69.79	0.26	13.65	1.26	0.07	0.20	0.69	4.21	4.79	0.03	0.13	95.08
05/02/2024	**ACP6**	FLF186	68.83	0.34	13.55	1.17	0.06	0.22	0.72	4.31	5.00	0.04	0.10	94.34
05/02/2024	**ACP6**	FLF186	69.94	0.33	13.67	1.31	0.09	0.19	0.67	4.22	4.87	0.03	0.12	95.46
05/02/2024	**ACP6**	FLF186	70.20	0.29	13.91	1.20	0.07	0.20	0.68	4.27	4.98	0.04	0.10	95.96
05/02/2024	**ACP6**	FLF186	70.38	0.31	13.64	1.26	0.07	0.22	0.68	4.34	5.04	0.01	0.15	96.10
05/02/2024	**ACP6**	FLF186	71.25	0.33	14.80	1.34	0.09	0.24	0.66	3.89	4.77	0.04	0.10	97.50
02/02/2024	**YmP5**	A9746 P-B4	66.21	0.74	15.95	3.84	0.15	1.11	2.87	4.47	3.91	0.25	0.09	99.60
02/02/2024	**YmP5**	A9746 P-B4	63.49	0.70	15.46	3.75	0.17	1.05	2.77	4.35	3.88	0.16	0.10	95.88
02/02/2024	**YmP5**	A9746 P-B4	63.78	0.71	15.19	4.21	0.18	1.48	3.03	4.39	3.71	0.23	0.10	97.01
02/02/2024	**YmP5**	A9746 P-B4	65.75	0.72	16.07	3.94	0.15	1.12	2.87	4.65	3.96	0.22	0.10	99.56
02/02/2024	**YmP5**	A9746 P-B4	65.61	0.71	16.14	3.78	0.11	1.09	2.87	4.61	4.01	0.24	0.09	99.26
02/02/2024	**YmP5**	A9746 P-B4	63.86	0.71	15.82	3.94	0.16	1.11	2.93	4.40	3.68	0.20	0.10	96.91
02/02/2024	**YmP5**	A9746 P-B4	65.85	0.76	15.96	3.63	0.17	1.03	2.82	4.57	3.84	0.18	0.09	98.91
02/02/2024	**YmP5**	A9746 P-B4	63.37	0.67	14.55	5.08	0.26	3.26	3.63	4.13	3.30	0.53	0.08	98.87
02/02/2024	**YmP5**	A9746 P-B4	64.45	0.65	16.97	3.51	0.11	0.88	3.39	4.86	3.43	0.22	0.07	98.54
02/02/2024	**YmP5**	A9746 P-B4	66.02	0.76	16.28	3.92	0.14	1.06	2.94	4.53	3.90	0.18	0.09	99.83
02/02/2024	**YmP5**	A9746 P-B4	63.33	0.71	15.52	3.78	0.17	1.02	2.90	4.33	3.86	0.23	0.09	95.95
02/02/2024	**YmP5**	A9746 P-B4	63.90	0.97	14.05	4.55	0.16	0.73	1.97	3.77	4.47	0.25	0.09	94.91
02/02/2024	**YmP5**	A9746 P-B4	63.57	0.73	15.35	3.82	0.15	1.10	2.85	4.35	3.83	0.22	0.11	96.08
02/02/2024	**YmP5**	A9746 P-B4	64.82	0.78	15.60	3.75	0.15	0.97	2.58	4.15	3.98	0.23	0.10	97.13
02/02/2024	**YmP5**	A9746 P-B4	63.41	0.66	15.65	3.94	0.16	1.11	2.92	4.33	3.80	0.20	0.08	96.27
02/02/2024	**YmP6**	A9746 P-B5/4	61.69	0.82	17.21	5.22	0.15	1.66	4.58	4.17	3.06	0.40	0.08	99.05
02/02/2024	**YmP6**	A9746 P-B5/4	63.11	0.81	15.83	5.46	0.13	1.60	3.88	3.92	3.60	0.39	0.06	98.79
02/02/2024	**YmP6**	A9746 P-B5/4	62.03	0.93	16.01	5.83	0.18	1.71	3.82	4.01	3.60	0.47	0.08	98.69
02/02/2024	**YmP6**	A9746 P-B5/4	58.68	1.02	15.91	7.05	0.13	2.40	5.24	3.82	2.90	0.56	0.07	97.77
02/02/2024	**YmP6**	A9746 P-B5/4	56.88	1.00	15.65	7.91	0.17	2.66	5.87	3.74	2.85	0.48	0.06	97.28
02/02/2024	**YmP6**	A9746 P-B5/4	58.64	1.01	16.07	7.54	0.15	2.50	6.19	4.31	2.41	0.44	0.06	99.30

Date of Analysis	Sample	Label	SiO_2	TiO_2	Al_2O_3	FeO_t	MnO	MgO	CaO	Na_2O	K_2O	P_2O_5	Cl	Analytical Total
02/02/2024	**YmP6**	A9746 P-B5/4	59.40	0.73	15.36	5.21	0.15	1.65	3.80	3.73	3.33	0.45	0.12	93.93
02/02/2024	**YmP6**	A9746 P-B5/4	63.53	0.74	15.86	5.18	0.17	1.66	4.01	3.84	3.73	0.33	0.10	99.16
02/02/2024	**YmP6**	A9746 P-B5/4	60.08	1.05	15.31	7.34	0.24	2.53	4.33	3.73	3.31	0.61	0.09	98.64
02/02/2024	**YmP6**	A9746 P-B5/4	63.76	0.72	15.78	5.36	0.13	1.64	3.99	3.93	3.64	0.35	0.08	99.37
02/02/2024	**YmP6**	A9746 P-B5/4	62.90	0.77	15.63	5.77	0.14	1.99	4.40	3.66	3.50	0.32	0.10	99.20
02/02/2024	**YmP6**	A9746 P-B5/4	60.89	0.90	16.26	5.51	0.16	1.96	4.40	4.15	3.17	0.37	0.08	97.87
02/02/2024	**YmP6**	A9746 P-B5/4	57.42	0.98	15.94	7.70	0.19	2.62	5.64	3.73	2.84	0.54	0.08	97.68
02/02/2024	**YmP6**	A9746 P-B5/4	60.55	0.73	18.15	4.85	0.14	1.60	5.27	4.50	2.77	0.42	0.04	99.01
02/02/2024	**YmP6**	A9746 P-B5/4	63.35	0.82	17.09	4.43	0.11	0.89	4.14	4.50	3.51	0.37	0.08	99.30
02/02/2024	**YmP7**	A9746 P-B5	57.37	0.88	16.54	6.07	0.14	1.83	4.07	3.29	2.70	0.39	0.07	93.37
02/02/2024	**YmP7**	A9746 P-B5	60.33	0.83	17.08	5.93	0.14	2.00	5.09	4.15	3.05	0.51	0.08	99.20
02/02/2024	**YmP7**	A9746 P-B5	61.48	0.88	16.34	5.86	0.20	1.92	4.46	4.09	3.28	0.44	0.07	99.03
02/02/2024	**YmP7**	A9746 P-B5	60.06	0.89	16.05	5.89	0.20	2.05	4.62	3.87	2.99	0.43	0.07	97.12
02/02/2024	**YmP7**	A9746 P-B5	60.35	0.88	16.22	6.28	0.20	2.18	4.90	3.89	2.94	0.64	0.09	98.58
02/02/2024	**YmP7**	A9746 P-B5	60.24	0.90	16.23	6.47	0.20	2.20	4.87	4.11	3.01	0.56	0.10	98.90
02/02/2024	**YmP7**	A9746 P-B5	60.05	0.86	16.79	6.27	0.14	2.02	5.23	4.36	2.67	0.44	0.06	98.91
02/02/2024	**YmP7**	A9746 P-B5	59.93	0.82	16.38	6.35	0.19	2.27	5.06	4.12	3.10	0.55	0.11	98.89
02/02/2024	**YmP7**	A9746 P-B5	59.64	0.90	16.38	6.22	0.17	2.12	4.77	3.90	3.06	0.55	0.07	97.78
02/02/2024	**YmP7**	A9746 P-B5	60.49	0.89	16.34	6.03	0.16	2.06	4.71	4.21	3.20	0.55	0.08	98.72
02/02/2024	**YmP7**	A9746 P-B5	58.17	0.89	15.94	6.36	0.14	2.19	4.75	3.95	2.84	0.49	0.10	95.81
02/02/2024	**YmP7**	A9746 P-B5	59.88	0.94	16.21	6.23	0.20	2.16	4.80	4.13	3.11	0.48	0.06	98.19
02/02/2024	**YmP7**	A9746 P-B5	60.25	0.91	16.25	6.20	0.15	2.20	4.82	4.17	3.11	0.46	0.08	98.60
02/02/2024	**YmP7**	A9746 P-B5	60.19	0.90	16.35	6.19	0.17	2.13	4.72	4.11	3.13	0.48	0.08	98.45
02/02/2024	**YmP7**	A9746 P-B5	60.47	0.93	16.41	6.09	0.16	2.07	4.67	4.15	3.12	0.51	0.09	98.68
02/02/2024	**YmP7**	A9746 P-B5	60.34	0.91	16.43	6.48	0.18	2.26	5.09	4.04	3.07	0.51	0.08	99.39
02/02/2024	**YmP7**	A9746 P-B5	60.49	0.87	16.49	6.23	0.17	2.13	4.71	4.03	3.08	0.57	0.10	98.87
02/02/2024	**YmP8**	A9746 P-B6	65.44	0.61	15.02	3.01	0.11	0.85	2.27	4.19	4.31	0.18	0.08	96.07
02/02/2024	**YmP8**	A9746 P-B6	67.97	0.69	15.43	2.74	0.15	0.45	1.97	4.41	4.45	0.17	0.10	98.54
02/02/2024	**YmP8**	A9746 P-B6	65.98	0.65	15.51	3.11	0.14	0.74	2.21	4.33	4.27	0.15	0.10	97.21
02/02/2024	**YmP8**	A9746 P-B6	64.71	0.59	15.08	2.97	0.11	0.90	2.25	4.08	4.33	0.16	0.12	95.29
02/02/2024	**YmP8**	A9746 P-B6	65.43	0.63	15.32	2.89	0.13	0.81	2.30	4.14	4.36	0.11	0.09	96.23
02/02/2024	**YmP8**	A9746 P-B6	65.21	0.61	15.36	3.01	0.13	0.80	2.30	4.39	4.39	0.16	0.09	96.47
02/02/2024	**YmP8**	A9746 P-B6	64.10	0.60	14.96	2.91	0.13	0.74	2.23	3.99	4.26	0.14	0.10	94.17

Date of Analysis	Sample	Label	SiO_2	TiO_2	Al_2O_3	FeO_t	MnO	MgO	CaO	Na_2O	K_2O	P_2O_5	Cl	Analytical Total
02/02/2024	**YmP8**	A9746 P-B6	64.63	0.62	15.21	2.95	0.10	0.76	2.21	4.09	4.32	0.16	0.08	95.14
02/02/2024	**YmP8**	A9746 P-B6	64.27	0.51	15.78	2.65	0.08	0.58	2.45	4.23	4.01	0.16	0.09	94.82
02/02/2024	**YmP8**	A9746 P-B6	64.37	0.66	15.05	3.03	0.10	0.77	2.25	4.12	4.27	0.13	0.10	94.86
02/02/2024	**YmP8**	A9746 P-B6	65.60	0.63	15.19	3.02	0.12	0.78	2.28	4.44	4.42	0.15	0.09	96.73
02/02/2024	**YmP8**	A9746 P-B6	66.99	0.68	15.64	3.09	0.12	0.82	2.30	4.38	4.38	0.17	0.08	98.67
02/02/2024	**YmP8**	A9746 P-B6	67.31	0.67	15.13	3.23	0.13	0.80	1.88	4.04	4.81	0.14	0.09	98.22
03/08/2023	**Nojiri Pumice**	FLF52	66.43	0.59	16.83	2.96	0.16	0.83	2.94	4.53	3.57	0.12	0.10	99.07
03/08/2023	**Nojiri Pumice**	FLF52	65.99	0.62	15.81	3.47	0.13	1.02	2.60	4.61	3.98	0.16	0.08	98.46
24/04/2024	**Aso-4X**	FLF196	68.71	0.37	14.47	1.62	0.10	0.32	1.03	4.62	4.72	0.05	0.10	96.12
24/04/2024	**Aso-4X**	FLF196	69.25	0.30	14.23	1.43	0.09	0.28	0.90	4.18	5.07	0.05	0.10	95.87
24/04/2024	**Aso-4X**	FLF196	68.46	0.37	14.59	1.36	0.10	0.34	1.09	4.52	4.87	0.05	0.09	95.84
24/04/2024	**Aso-4X**	FLF196	68.20	0.34	14.03	1.29	0.10	0.26	0.90	4.41	4.76	0.04	0.12	94.43
24/04/2024	**Aso-4X**	FLF196	68.90	0.35	14.52	1.36	0.10	0.33	1.06	4.49	4.65	0.05	0.11	95.93
24/04/2024	**Aso-4X**	FLF196	68.88	0.35	14.40	1.60	0.10	0.33	1.06	4.59	4.84	0.05	0.12	96.33
24/04/2024	**Aso-4X**	FLF196	68.63	0.38	14.39	1.50	0.10	0.37	1.23	4.48	5.01	0.07	0.12	96.29
24/04/2024	**Aso-4X**	FLF196	68.59	0.36	14.43	1.30	0.10	0.34	1.03	4.55	4.66	0.06	0.11	95.53
24/04/2024	**Aso-4X**	FLF196	68.00	0.33	13.85	1.35	0.11	0.30	1.01	4.45	4.82	0.04	0.11	94.36
24/04/2024	**Aso-4X**	FLF196	68.57	0.34	14.05	1.47	0.10	0.30	0.91	4.32	4.79	0.04	0.11	95.00
24/04/2024	**Aso-4X**	FLF196	68.59	0.34	14.21	1.30	0.08	0.27	0.87	4.42	4.75	0.03	0.11	94.97
05/02/2024	**Aso-4X**	FLF195	69.46	0.35	14.18	1.34	0.09	0.23	0.87	4.20	4.75	0.03	0.08	95.59
05/02/2024	**Aso-4X**	FLF195	66.70	0.35	14.60	1.39	0.12	0.31	1.01	4.11	4.38	0.03	0.13	93.14
05/02/2024	**Aso-4X**	FLF195	67.21	0.35	14.24	1.37	0.06	0.34	1.12	4.38	4.50	0.01	0.10	93.68
05/02/2024	**Aso-4X**	FLF195	68.26	0.36	14.66	1.46	0.09	0.39	1.10	4.11	4.54	0.02	0.11	95.11
05/02/2024	**Aso-4X**	FLF195	70.07	0.35	14.13	1.27	0.08	0.24	0.86	4.19	4.81	0.02	0.09	96.12
05/02/2024	**Aso-4X**	FLF195	69.28	0.38	14.10	1.24	0.09	0.32	0.96	4.29	4.52	0.03	0.12	95.32
05/02/2024	**Aso-4X**	FLF195	68.63	0.34	14.05	1.34	0.08	0.31	0.97	4.18	4.58	0.05	0.10	94.63
05/02/2024	**Aso-4X**	FLF195	69.09	0.35	14.08	1.32	0.08	0.31	0.90	4.21	4.93	0.04	0.09	95.39
05/02/2024	**Aso-4X**	FLF195	68.45	0.37	14.14	1.33	0.10	0.30	0.92	4.06	4.75	0.00	0.10	94.53
05/02/2024	**Aso-4X**	FLF195	69.19	0.36	14.30	1.33	0.09	0.31	0.98	4.31	4.77	0.04	0.08	95.76
05/02/2024	**Aso-4X**	FLF195	68.85	0.30	14.25	1.38	0.08	0.30	0.96	4.15	4.67	0.08	0.10	95.12
05/02/2024	**Aso-4X**	FLF195	68.72	0.36	14.32	1.28	0.07	0.28	0.96	4.14	4.63	0.02	0.13	94.90
05/02/2024	**Aso-4X**	FLF195	69.40	0.24	14.17	1.12	0.08	0.17	0.90	4.34	4.73	0.02	0.11	95.27

Date of Analysis	Sample	Label	SiO_2	TiO_2	Al_2O_3	FeO_t	MnO	MgO	CaO	Na_2O	K_2O	P_2O_5	Cl	Analytical Total
05/02/2024	**Aso-4X**	FLF195	68.34	0.34	14.32	1.40	0.08	0.35	1.03	4.20	4.51	0.06	0.13	94.77
05/02/2024	**Aso-4X**	FLF195	69.53	0.34	14.29	1.31	0.10	0.27	0.92	4.30	4.70	0.03	0.10	95.89
05/02/2024	**Aso-4X**	FLF195	69.61	0.30	14.05	1.23	0.11	0.25	0.86	4.13	4.63	0.07	0.09	95.33
05/02/2024	**Aso-4X**	FLF195	68.80	0.34	14.40	1.30	0.08	0.31	0.99	4.10	4.51	0.02	0.08	94.93
05/02/2024	**Aso-4X**	FLF195	69.31	0.34	14.13	1.29	0.09	0.27	0.93	4.33	4.82	0.00	0.09	95.60
05/02/2024	**Aso-4X**	FLF195	68.75	0.35	14.10	1.31	0.11	0.28	1.00	4.16	4.60	0.07	0.09	94.83
05/02/2024	**Aso-4X**	FLF195	69.37	0.36	14.08	1.14	0.09	0.28	0.89	4.19	4.93	0.00	0.10	95.44
05/02/2024	**Aso-4X**	FLF195	69.24	0.31	14.17	1.31	0.09	0.27	0.85	4.19	4.81	0.00	0.12	95.36
05/02/2024	**Aso-4X**	FLF195	69.17	0.39	14.34	1.46	0.07	0.33	1.08	4.51	4.69	0.09	0.10	96.23
05/02/2024	**Aso-4X**	FLF194	69.30	0.33	14.35	1.35	0.09	0.26	0.94	4.35	4.71	0.03	0.08	95.77
05/02/2024	**Aso-4X**	FLF194	69.40	0.32	13.77	1.18	0.08	0.26	0.88	4.13	4.65	0.02	0.10	94.79
05/02/2024	**Aso-4X**	FLF194	68.37	0.30	14.80	1.32	0.09	0.27	0.97	4.31	4.69	0.02	0.10	95.23
05/02/2024	**Aso-4X**	FLF194	68.15	0.40	14.54	1.48	0.05	0.35	1.09	4.18	4.58	0.04	0.11	95.00
05/02/2024	**Aso-4X**	FLF194	68.35	0.32	14.13	1.29	0.08	0.25	0.96	4.22	4.71	0.01	0.09	94.42
05/02/2024	**Aso-4X**	FLF194	69.10	0.36	14.38	1.35	0.12	0.26	1.00	4.14	4.64	0.02	0.09	95.46
05/02/2024	**Aso-4X**	FLF194	69.09	0.34	14.11	1.36	0.08	0.28	0.99	4.53	4.66	0.01	0.10	95.54
05/02/2024	**Aso-4X**	FLF194	67.52	0.64	14.43	1.78	0.09	0.29	0.99	4.15	4.57	0.03	0.11	94.60
05/02/2024	**Aso-4X**	FLF194	68.02	0.44	15.23	1.31	0.10	0.29	0.95	3.85	4.48	0.03	0.07	94.77
05/02/2024	**Aso-4X**	FLF194	69.02	0.34	13.78	1.30	0.07	0.26	0.91	4.24	4.69	0.02	0.14	94.78
05/02/2024	**Aso-4X**	FLF194	68.60	0.34	14.13	1.33	0.10	0.28	1.00	4.05	4.72	0.06	0.09	94.71
05/02/2024	**Aso-4X**	FLF194	69.05	0.33	14.12	1.23	0.09	0.24	0.85	4.00	4.56	0.05	0.08	94.60
05/02/2024	**Aso-4X**	FLF194	69.03	0.31	14.14	1.30	0.11	0.28	0.91	4.21	4.88	0.02	0.09	95.28
05/02/2024	**Aso-4X**	FLF194	68.75	0.32	14.17	1.31	0.10	0.29	0.94	4.31	4.69	0.04	0.13	95.04
05/02/2024	**Aso-4X**	FLF194	69.29	0.31	14.55	1.32	0.11	0.28	0.93	4.04	4.68	0.00	0.10	95.61
05/02/2024	**Aso-4X**	FLF194	69.16	0.32	14.11	1.26	0.11	0.28	0.94	4.05	4.65	0.02	0.09	95.00
05/02/2024	**Aso-4X**	FLF194	68.63	0.33	14.23	1.26	0.09	0.26	0.87	4.25	4.63	0.01	0.10	94.64
05/02/2024	**Aso-4X**	FLF194	68.84	0.31	14.00	1.26	0.07	0.28	0.96	4.20	4.50	0.03	0.09	94.54
05/02/2024	**Aso-4X**	FLF194	66.74	0.31	13.74	1.27	0.07	0.26	0.88	4.15	4.50	0.02	0.11	92.05
05/02/2024	**Aso-4X**	FLF194	69.42	0.40	14.94	1.44	0.11	0.37	1.11	4.09	4.49	0.06	0.05	96.47
05/02/2024	**Aso-4X**	FLF194	68.20	0.34	14.53	1.29	0.10	0.29	0.92	4.03	4.45	0.06	0.11	94.33
05/02/2024	**Aso-4X**	FLF194	68.91	0.36	14.07	1.26	0.08	0.23	0.95	4.26	4.62	0.01	0.07	94.82
03/08/2023	**Aso-Y**	FLF65	69.03	0.39	14.30	1.20	0.08	0.28	0.91	4.26	4.88	0.05	0.09	95.47
03/08/2023	**Aso-Y**	FLF65	68.23	0.36	14.05	1.29	0.09	0.23	0.96	3.91	5.03	0.06	0.09	94.30

Date of Analysis	Sample	Label	SiO_2	TiO_2	Al_2O_3	FeO_t	MnO	MgO	CaO	Na_2O	K_2O	P_2O_5	Cl	Analytical Total
03/08/2023	**Aso-Y**	FLF65	69.13	0.30	13.93	1.27	0.08	0.30	0.93	4.16	5.11	0.02	0.10	95.35
03/08/2023	**Aso-Y**	FLF65	72.73	0.34	14.78	1.29	0.11	0.22	0.87	4.69	4.71	0.01	0.11	99.85
03/08/2023	**Aso-Y**	FLF65	67.82	0.32	13.96	1.26	0.10	0.27	0.90	3.65	4.77	0.03	0.11	93.19
03/08/2023	**Aso-Y**	FLF65	69.98	0.29	14.21	1.18	0.08	0.25	0.82	4.14	4.94	0.05	0.09	96.03
03/08/2023	**Aso-Y**	FLF65	68.68	0.37	14.25	1.38	0.11	0.30	0.99	4.15	4.82	0.00	0.09	95.14
03/08/2023	**Aso-Y**	FLF65	69.18	0.36	14.29	1.32	0.11	0.26	0.88	4.20	4.87	0.01	0.10	95.58
03/08/2023	**Aso-Y**	FLF65	69.58	0.31	14.07	1.18	0.08	0.21	0.85	4.23	4.88	0.04	0.10	95.52
03/08/2023	**Aso-Y**	FLF65	69.99	0.32	13.97	1.15	0.08	0.21	0.86	4.07	4.89	0.03	0.11	95.68
03/08/2023	**Aso-Y**	FLF65	69.24	0.37	14.06	1.25	0.11	0.25	0.87	4.12	4.88	0.04	0.08	95.28
03/08/2023	**Aso-Y**	FLF65	69.29	0.32	13.99	1.26	0.05	0.22	0.83	4.14	4.89	0.04	0.07	95.11
03/08/2023	**Aso-Y**	FLF65	69.69	0.34	14.19	1.17	0.09	0.25	0.88	4.18	4.92	0.03	0.10	95.83
03/08/2023	**Aso-Y**	FLF65	68.69	0.31	14.14	1.24	0.08	0.23	0.89	4.08	4.80	0.05	0.11	94.63
03/08/2023	**Aso-Y**	FLF65	69.01	0.31	14.18	1.20	0.09	0.20	0.89	4.30	4.92	0.06	0.10	95.27
03/08/2023	**Aso-Y**	FLF65	69.44	0.33	14.11	1.24	0.07	0.25	0.90	4.22	4.79	0.08	0.10	95.54
03/08/2023	**Aso-Y**	FLF65	68.07	0.39	14.30	1.29	0.11	0.31	0.97	3.75	5.04	0.05	0.11	94.39
05/02/2024	**Aso-Y**	FLF248	69.27	0.32	13.91	1.25	0.08	0.26	0.85	3.88	4.84	0.00	0.10	94.76
05/02/2024	**Aso-Y**	FLF248	69.72	0.33	13.83	1.22	0.07	0.24	0.75	4.02	4.80	0.04	0.10	95.13
05/02/2024	**Aso-Y**	FLF248	69.28	0.35	13.97	1.22	0.05	0.22	0.87	4.18	4.62	0.03	0.08	94.86
05/02/2024	**Aso-Y**	FLF248	69.43	0.34	14.09	1.20	0.07	0.22	0.88	4.03	4.66	0.03	0.07	95.01
05/02/2024	**Aso-Y**	FLF248	69.66	0.31	13.74	1.08	0.12	0.20	0.81	3.92	4.73	0.03	0.10	94.70
05/02/2024	**Aso-Y**	FLF248	69.52	0.33	13.80	1.20	0.09	0.20	0.82	3.84	4.73	0.02	0.09	94.65
05/02/2024	**Aso-Y**	FLF248	69.60	0.31	14.07	1.27	0.06	0.22	0.86	4.12	4.62	0.04	0.12	95.28
05/02/2024	**Aso-Y**	FLF248	69.78	0.32	13.85	1.16	0.09	0.20	0.78	4.13	4.67	0.02	0.10	95.10
05/02/2024	**Aso-Y**	FLF248	74.89	0.19	11.62	0.95	0.03	0.18	0.98	3.35	2.92	0.02	0.15	95.28
05/02/2024	**Aso-Y**	FLF248	68.56	0.32	13.79	1.29	0.09	0.26	0.83	3.97	4.71	0.05	0.12	94.00
05/02/2024	**Aso-Y**	FLF248	69.83	0.28	13.98	1.19	0.07	0.24	0.84	4.16	4.57	0.02	0.08	95.27
05/02/2024	**Aso-Y**	FLF248	70.67	0.31	13.69	1.03	0.08	0.19	0.67	3.82	5.03	0.00	0.10	95.59
05/02/2024	**Aso-Y**	FLF248	68.74	0.24	13.55	1.19	0.04	0.25	0.86	3.81	4.70	0.06	0.11	93.56
05/02/2024	**Aso-Y**	FLF248	69.32	0.35	13.78	1.26	0.09	0.22	0.84	4.19	4.66	0.04	0.10	94.85
05/02/2024	**Aso-Y**	FLF248	70.06	0.30	14.06	1.22	0.03	0.23	0.83	3.98	4.62	0.01	0.08	95.42
05/02/2024	**Aso-Y**	FLF248	68.51	0.37	13.77	1.18	0.08	0.25	0.82	4.04	4.74	0.04	0.12	93.91
05/02/2024	**Aso-D**	FLF236	66.78	0.56	14.91	2.13	0.10	0.68	1.80	4.20	4.30	0.08	0.10	95.64
05/02/2024	**Aso-D**	FLF236	64.34	0.61	14.62	2.09	0.06	0.64	1.76	3.93	4.08	0.13	0.10	92.34

Date of Analysis	Sample	Label	SiO_2	TiO_2	Al_2O_3	FeO_t	MnO	MgO	CaO	Na_2O	K_2O	P_2O_5	Cl	Analytical Total
05/02/2024	**Aso-D**	FLF236	66.98	0.60	14.71	2.07	0.09	0.68	1.85	3.51	4.23	0.11	0.08	94.91
05/02/2024	**Aso-D**	FLF236	65.15	0.59	15.30	2.31	0.08	0.69	1.98	4.34	4.19	0.11	0.09	94.82
05/02/2024	**Aso-D**	FLF236	66.17	0.60	14.83	2.25	0.08	0.62	1.92	4.27	4.23	0.09	0.10	95.15
05/02/2024	**Aso-D**	FLF236	66.84	0.56	14.87	2.18	0.13	0.64	1.85	4.30	4.16	0.11	0.09	95.73
05/02/2024	**Aso-D**	FLF236	65.36	0.58	14.59	2.26	0.09	0.62	1.87	4.13	4.10	0.03	0.10	93.74
05/02/2024	**Aso-D**	FLF236	66.07	0.60	14.76	2.31	0.10	0.67	1.85	4.39	4.26	0.05	0.11	95.18
05/02/2024	**Aso-D**	FLF236	66.23	0.53	14.74	2.35	0.11	0.72	1.91	4.21	4.20	0.12	0.12	95.23
05/02/2024	**Aso-D**	FLF236	66.39	0.62	14.90	2.10	0.13	0.62	1.87	4.18	4.19	0.08	0.11	95.19
05/02/2024	**Aso-D**	FLF236	66.29	0.55	14.70	2.30	0.09	0.67	2.01	4.19	4.25	0.06	0.10	95.21
05/02/2024	**Aso-D**	FLF236	66.31	0.58	14.79	2.26	0.09	0.64	1.79	4.32	4.16	0.11	0.10	95.14
05/02/2024	**Aso-D**	FLF236	66.11	0.60	14.70	2.19	0.11	0.70	1.85	4.20	4.15	0.11	0.10	94.82
05/02/2024	**Aso-D**	FLF236	66.05	0.58	14.95	2.20	0.10	0.67	1.86	4.14	4.29	0.05	0.13	95.03
04/08/2024	**Aso-E**	FLF74	66.50	0.54	14.04	1.94	0.05	0.46	1.33	4.20	4.48	0.10	0.10	93.73
04/08/2024	**Aso-E**	FLF74	66.38	0.56	14.10	1.98	0.10	0.46	1.33	3.98	4.43	0.06	0.09	93.46
04/08/2024	**Aso-E**	FLF74	66.05	0.56	14.05	1.89	0.10	0.44	1.33	3.99	4.52	0.03	0.07	93.03
04/08/2024	**Aso-E**	FLF74	67.50	0.60	14.48	2.06	0.10	0.47	1.36	4.26	4.57	0.08	0.10	95.58
04/08/2024	**Aso-E**	FLF74	67.16	0.58	14.24	1.93	0.09	0.49	1.37	4.12	4.54	0.07	0.08	94.68
04/08/2024	**Aso-E**	FLF74	66.59	0.55	14.20	1.89	0.07	0.40	1.22	3.88	4.62	0.09	0.07	93.59
04/08/2024	**Aso-E**	FLF74	67.54	0.60	14.23	1.89	0.10	0.51	1.39	4.30	4.50	0.03	0.10	95.19
04/08/2024	**Aso-E**	FLF74	67.32	0.62	14.42	1.99	0.09	0.46	1.39	4.18	4.67	0.07	0.09	95.30
04/08/2024	**Aso-E**	FLF74	67.25	0.53	14.20	1.92	0.05	0.42	1.37	4.26	4.61	0.06	0.08	94.75
04/08/2024	**Aso-E**	FLF74	67.43	0.57	14.10	1.94	0.09	0.48	1.39	4.26	4.53	0.03	0.08	94.91
04/08/2024	**Aso-E**	FLF74	67.38	0.57	14.20	2.00	0.13	0.46	1.33	4.08	4.70	0.10	0.08	95.04
04/08/2024	**Aso-E**	FLF74	66.78	0.57	14.01	1.95	0.09	0.47	1.37	4.04	4.52	0.05	0.09	93.93
04/08/2024	**Aso-E**	FLF74	66.81	0.55	14.14	1.90	0.07	0.47	1.34	3.99	4.67	0.08	0.09	94.11
04/08/2024	**Aso-E**	FLF74	67.76	0.53	14.61	1.96	0.05	0.44	1.35	4.36	4.65	0.12	0.09	95.92
04/08/2024	**Aso-E**	FLF74	65.92	0.54	13.93	2.65	0.07	0.48	1.47	4.10	4.41	0.12	0.08	93.76
04/08/2024	**Aso-E**	FLF74	67.36	0.56	14.34	1.95	0.08	0.48	1.32	4.34	4.63	0.06	0.07	95.19
04/08/2024	**Aso-E**	FLF74	66.83	0.56	14.04	1.97	0.10	0.49	1.27	3.89	4.54	0.08	0.09	93.87
04/08/2024	**Aso-E**	FLF74	66.26	0.57	14.07	2.00	0.11	0.44	1.34	3.93	4.39	0.04	0.12	93.26
04/08/2024	**Aso-E**	FLF74	67.24	0.57	13.99	1.92	0.09	0.52	1.29	4.04	4.57	0.06	0.07	94.36
04/08/2024	**Aso-E**	FLF74	67.20	0.55	14.18	1.91	0.08	0.46	1.36	4.18	4.51	0.04	0.07	94.54
04/08/2024	**Aso-E**	FLF74	67.25	0.58	14.26	2.06	0.12	0.44	1.40	4.12	4.64	0.03	0.09	95.00
04/08/2024	**Aso-E**	FLF74	67.42	0.58	13.95	1.96	0.05	0.47	1.38	4.27	4.50	0.08	0.09	94.76

Date of Analysis	Sample	Label	SiO_2	TiO_2	Al_2O_3	FeO_t	MnO	MgO	CaO	Na_2O	K_2O	P_2O_5	Cl	Analytical Total
04/08/2024	**Aso-E**	FLF74	67.70	0.57	14.26	2.12	0.06	0.50	1.38	2.56	4.50	0.03	0.10	93.78
04/08/2024	**Aso-E**	FLF74	66.06	0.56	14.00	1.84	0.09	0.46	1.34	4.08	4.43	0.06	0.10	93.02
04/08/2024	**Aso-E**	FLF74	67.48	0.56	14.19	2.05	0.12	0.46	1.40	4.30	4.76	0.10	0.12	95.53
12/03/2024	**Aso-E**	FLF 232	68.7403	0.59	14.44	2.06	0.11	0.54	1.53	4.49	4.69	0.09	0.11	97.39
12/03/2024	**Aso-E**	FLF 232	68.6555	0.59	14.78	1.99	0.10	0.55	1.50	4.65	4.48	0.09	0.11	97.49
12/03/2024	**Aso-E**	FLF 232	68.5904	0.58	14.43	2.01	0.10	0.54	1.51	4.29	4.55	0.09	0.10	96.80
12/03/2024	**Aso-E**	FLF 232	68.2354	0.57	14.99	1.98	0.10	0.54	1.44	4.46	4.49	0.08	0.09	96.99
12/03/2024	**Aso-E**	FLF 232	68.9012	0.58	14.97	2.04	0.10	0.54	1.61	4.39	4.61	0.09	0.11	97.94
12/03/2024	**Aso-E**	FLF 232	68.0054	0.58	14.62	2.12	0.10	0.54	1.53	4.33	4.56	0.08	0.10	96.56
12/03/2024	**Aso-E**	FLF 232	68.1131	0.57	14.72	2.06	0.10	0.54	1.38	4.41	4.70	0.09	0.10	96.80
12/03/2024	**Aso-E**	FLF 232	68.3503	0.58	14.78	2.16	0.10	0.54	1.46	4.46	4.81	0.09	0.10	97.44
12/03/2024	**Aso-E**	FLF 232	68.0758	0.59	14.12	2.09	0.10	0.55	1.53	4.53	4.84	0.10	0.09	96.62
12/03/2024	**Aso-E**	FLF 232	68.5461	0.58	14.75	1.99	0.10	0.54	1.47	4.55	4.54	0.09	0.10	97.25
12/03/2024	**Aso-E**	FLF 232	68.9218	0.60	14.44	2.07	0.09	0.48	1.18	4.30	4.70	0.09	0.10	96.97
12/03/2024	**Aso-E**	FLF 232	68.7245	0.58	14.89	2.12	0.11	0.55	1.51	4.38	4.66	0.08	0.10	97.71
12/03/2024	**Aso-E**	FLF 232	68.516	0.60	14.43	2.02	0.10	0.54	1.59	4.52	4.53	0.07	0.10	97.02
12/03/2024	**Aso-E**	FLF 232	68.42	0.59	14.73	2.06	0.11	0.54	1.38	4.46	4.59	0.09	0.08	97.05
12/03/2024	**Aso-E**	FLF 232	68.0285	0.58	14.34	2.00	0.10	0.53	1.46	4.45	4.65	0.08	0.11	96.32
12/03/2024	**Aso-E**	FLF 232	67.4686	0.58	14.89	1.99	0.10	0.53	1.44	4.36	4.68	0.07	0.10	96.21
12/03/2024	**Aso-E**	FLF 233	68.4657	0.59	14.13	1.88	0.10	0.51	1.39	4.32	4.54	0.09	0.09	96.10
12/03/2024	**Aso-E**	FLF 233	68.7656	0.58	14.61	2.01	0.10	0.51	1.42	4.58	4.98	0.08	0.10	97.73
12/03/2024	**Aso-E**	FLF 233	68.2223	0.59	14.38	2.00	0.09	0.51	1.33	4.35	4.76	0.08	0.09	96.41
12/03/2024	**Aso-E**	FLF 233	69.7542	0.60	14.00	2.02	0.09	0.41	1.09	4.31	4.82	0.09	0.10	97.28
12/03/2024	**Aso-E**	FLF 233	68.2246	0.59	15.06	1.85	0.10	0.45	1.53	4.68	4.58	0.08	0.08	97.23
12/03/2024	**Aso-E**	FLF 233	68.1013	0.59	14.26	1.84	0.10	0.51	1.39	4.40	4.71	0.08	0.08	96.07
12/03/2024	**Aso-E**	FLF 233	68.8326	0.58	14.69	2.15	0.09	0.51	1.39	4.04	4.61	0.09	0.10	97.08
12/03/2024	**Aso-E**	FLF 233	68.993	0.59	14.51	1.89	0.09	0.50	1.32	4.58	4.93	0.08	0.10	97.60
12/03/2024	**Aso-E**	FLF 233	68.6575	0.58	14.41	2.09	0.10	0.51	1.37	4.49	4.82	0.09	0.10	97.21
12/03/2024	**Aso-E**	FLF 233	68.9067	0.60	14.93	2.08	0.10	0.52	1.41	4.33	4.82	0.09	0.09	97.88
12/03/2024	**Aso-E**	FLF 233	68.7294	0.59	14.86	2.07	0.11	0.52	1.46	4.44	4.97	0.08	0.10	97.93
12/03/2024	**Aso-E**	FLF 233	68.2296	0.59	14.23	1.99	0.10	0.51	1.40	4.62	4.68	0.08	0.09	96.53
12/03/2024	**Aso-E**	FLF 233	67.9809	0.57	14.58	2.06	0.10	0.49	1.35	4.01	4.61	0.08	0.10	95.93
12/03/2024	**Aso-E**	FLF 233	70.1219	0.61	14.71	2.06	0.12	0.75	1.60	4.63	4.10	0.09	0.07	98.85

Date of Analysis	Sample	Label	SiO_2	TiO_2	Al_2O_3	FeO_t	MnO	MgO	CaO	Na_2O	K_2O	P_2O_5	Cl	Analytical Total
12/03/2024	**Aso-E**	FLF 234	68.54	0.58	14.47	2.05	0.10	0.51	1.26	4.51	4.67	0.09	0.09	96.87
12/03/2024	**Aso-E**	FLF 234	69.21	0.58	14.35	2.02	0.10	0.49	1.26	3.97	4.77	0.08	0.11	96.93
12/03/2024	**Aso-E**	FLF 234	68.47	0.58	14.25	1.85	0.08	0.43	1.22	4.32	4.91	0.08	0.04	96.25
12/03/2024	**Aso-E**	FLF 234	69.34	0.59	14.62	2.12	0.10	0.49	1.37	4.05	4.68	0.08	0.10	97.53
12/03/2024	**Aso-E**	FLF 234	68.86	0.58	14.14	2.10	0.09	0.51	1.39	4.28	4.72	0.08	0.09	96.85
12/03/2024	**Aso-E**	FLF 234	69.89	0.57	14.36	2.01	0.10	0.47	1.20	4.00	4.69	0.10	0.09	97.46
12/03/2024	**Aso-E**	FLF 234	68.86	0.58	14.54	1.94	0.10	0.50	1.35	4.31	4.86	0.09	0.09	97.22
12/03/2024	**Aso-E**	FLF 234	68.63	0.59	14.81	2.30	0.10	0.52	1.29	4.49	4.85	0.08	0.09	97.74
12/03/2024	**Aso-E**	FLF 234	68.84	0.58	14.50	1.95	0.10	0.50	1.33	4.41	4.67	0.08	0.09	97.05
12/03/2024	**Aso-E**	FLF 234	68.53	0.58	14.69	2.05	0.09	0.49	1.32	4.19	5.02	0.08	0.09	97.12
12/03/2024	**Aso-E**	FLF 234	68.84	0.58	14.31	2.03	0.10	0.49	1.36	4.09	4.61	0.08	0.10	96.58
12/03/2024	**Aso-E**	FLF 234	69.38	0.58	14.58	2.20	0.09	0.50	1.30	4.28	4.68	0.08	0.09	97.76
12/03/2024	**Aso-E**	FLF 234	68.42	0.60	14.24	2.09	0.11	0.52	1.33	4.16	4.77	0.08	0.11	96.44
12/03/2024	**Aso-E**	FLF 234	69.22	0.58	14.23	1.96	0.09	0.49	1.27	3.92	4.73	0.08	0.10	96.66
12/03/2024	**Aso-E**	FLF 234	69.84	0.57	14.69	1.94	0.09	0.48	1.24	4.02	4.90	0.08	0.09	97.93
12/03/2024	**Aso-E**	FLF 234	68.83	0.59	14.63	1.78	0.10	0.48	1.26	4.56	4.96	0.09	0.12	97.39
04/08/2024	**Aso-F**	FLF73	67.67	0.42	14.58	1.69	0.05	0.39	1.27	4.35	4.61	0.03	0.10	95.16
04/08/2024	**Aso-F**	FLF73	67.06	0.41	14.33	1.62	0.06	0.39	1.27	4.13	4.62	0.05	0.10	94.05
04/08/2024	**Aso-F**	FLF73	67.86	0.48	14.63	1.65	0.07	0.39	1.21	3.94	4.96	0.08	0.09	95.34
04/08/2024	**Aso-F**	FLF73	68.64	0.40	14.84	1.60	0.09	0.32	1.11	3.86	4.76	0.01	0.10	95.73
04/08/2024	**Aso-F**	FLF73	67.84	0.41	14.30	2.27	0.03	0.34	1.19	3.54	5.76	0.06	0.11	95.86
04/08/2024	**Aso-F**	FLF73	67.54	0.42	14.53	1.62	0.08	0.37	1.22	4.23	4.77	0.07	0.09	94.94
04/08/2024	**Aso-F**	FLF73	66.45	0.40	14.31	1.43	0.09	0.34	1.11	4.10	4.91	0.07	0.10	93.31
04/08/2024	**Aso-F**	FLF73	67.53	0.41	14.45	1.68	0.09	0.38	1.26	4.17	4.76	0.07	0.10	94.89
04/08/2024	**Aso-F**	FLF73	65.83	0.42	14.17	1.62	0.05	0.34	1.19	3.89	4.81	0.06	0.13	92.51
04/08/2024	**Aso-F**	FLF73	67.50	0.43	14.39	1.69	0.06	0.40	1.26	4.14	4.76	0.08	0.08	94.78
04/08/2024	**Aso-F**	FLF73	66.61	0.48	14.36	1.74	0.09	0.41	1.34	4.03	4.70	0.07	0.09	93.92
04/08/2024	**Aso-F**	FLF73	67.11	0.45	14.35	1.59	0.05	0.38	1.29	4.10	4.77	0.07	0.10	94.27
04/08/2024	**Aso-F**	FLF73	67.63	0.41	14.28	1.50	0.09	0.30	1.15	3.92	5.24	0.05	0.10	94.67
04/08/2024	**Aso-F**	FLF73	66.91	0.62	14.61	2.34	0.08	0.57	1.60	3.78	4.98	0.11	0.08	95.69
04/08/2024	**Aso-F**	FLF73	67.67	0.44	14.51	1.69	0.09	0.38	1.28	4.04	4.74	0.08	0.11	95.01
04/08/2024	**Aso-F**	FLF73	67.42	0.41	14.51	1.60	0.10	0.42	1.20	4.02	4.80	0.05	0.10	94.64
04/08/2024	**Aso-F**	FLF73	66.38	0.48	14.41	1.78	0.08	0.42	1.36	3.91	4.86	0.05	0.11	93.84
04/08/2024	**Aso-F**	FLF73	67.97	0.40	14.46	1.60	0.09	0.41	1.25	4.15	4.79	0.06	0.10	95.29

Date of Analysis	Sample	Label	SiO_2	TiO_2	Al_2O_3	FeO_t	MnO	MgO	CaO	Na_2O	K_2O	P_2O_5	Cl	Analytical Total
04/08/2024	**Aso-F**	FLF73	67.41	0.51	14.56	1.56	0.11	0.40	1.26	4.18	4.74	0.07	0.10	94.90
04/08/2024	**Aso-F**	FLF73	68.08	0.43	14.14	2.50	0.06	0.32	1.34	3.47	5.56	0.09	0.10	96.08
04/08/2024	**Aso-F**	FLF73	67.40	0.48	14.54	1.59	0.14	0.38	1.19	4.27	4.70	0.04	0.09	94.83
04/08/2024	**Aso-F**	FLF73	68.25	0.45	14.72	1.55	0.09	0.38	1.21	4.01	4.85	0.10	0.11	95.73
04/08/2024	**Aso-F**	FLF73	67.22	0.39	14.17	1.52	0.09	0.38	1.12	4.03	4.91	0.05	0.11	94.00
04/08/2024	**Aso-F**	FLF73	66.86	0.45	14.32	1.70	0.09	0.42	1.22	4.17	4.63	0.06	0.09	94.01
05/02/2024	**Aso-F**	FLF230	70.25	0.33	13.95	1.18	0.08	0.21	0.79	3.86	5.08	0.03	0.10	95.85
05/02/2024	**Aso-F**	FLF230	70.31	0.30	13.82	1.14	0.08	0.17	0.80	3.80	5.21	0.02	0.11	95.75
05/02/2024	**Aso-F**	FLF230	70.09	0.34	14.23	1.30	0.07	0.30	0.93	3.61	4.84	0.04	0.08	95.84
05/02/2024	**Aso-F**	FLF230	70.21	0.32	13.98	1.18	0.10	0.26	0.80	3.69	5.23	0.01	0.07	95.84
05/02/2024	**Aso-F**	FLF230	69.96	0.28	13.64	1.15	0.08	0.21	0.80	3.92	5.22	0.05	0.12	95.41
05/02/2024	**Aso-F**	FLF230	69.41	0.30	14.03	1.31	0.04	0.28	0.94	3.94	4.87	0.04	0.08	95.24
05/02/2024	**Aso-F**	FLF230	70.49	0.34	13.69	1.15	0.09	0.21	0.86	3.61	5.17	0.02	0.09	95.72
05/02/2024	**Aso-F**	FLF230	70.12	0.32	13.74	1.26	0.09	0.19	0.74	3.59	5.16	0.02	0.13	95.37
05/02/2024	**Aso-F**	FLF230	68.92	0.35	13.95	1.26	0.06	0.29	0.93	3.58	5.00	0.01	0.11	94.46
05/02/2024	**Aso-F**	FLF230	68.75	0.34	14.70	1.27	0.11	0.29	0.90	3.65	4.79	0.04	0.10	94.93
05/02/2024	**Aso-F**	FLF230	69.76	0.32	13.93	1.16	0.04	0.23	0.78	3.66	5.12	0.03	0.11	95.14
05/02/2024	**Aso-F**	FLF230	70.04	0.29	13.74	1.22	0.08	0.21	0.73	3.75	5.10	0.02	0.09	95.27
05/02/2024	**Aso-F**	FLF230	69.93	0.34	13.77	1.16	0.09	0.18	0.79	3.68	5.07	0.02	0.10	95.14
05/02/2024	**Aso-F**	FLF230	70.25	0.32	13.81	1.35	0.09	0.22	0.76	3.76	5.17	0.02	0.09	95.85
05/02/2024	**Aso-F**	FLF230	70.10	0.36	13.81	1.29	0.08	0.23	0.79	3.53	5.13	0.00	0.12	95.44
05/02/2024	**Aso-F**	FLF230	70.27	0.36	13.90	1.20	0.07	0.21	0.79	3.45	5.06	0.00	0.12	95.43
22/04/2024	**Aso-F**	FLF230	69.36	0.33	13.89	1.41	0.09	0.26	0.97	3.89	5.08	0.04	0.11	95.42
22/04/2024	**Aso-F**	FLF230	69.54	0.33	14.21	1.21	0.09	0.27	0.95	3.95	5.11	0.04	0.11	95.81
22/04/2024	**Aso-F**	FLF230	69.25	0.30	13.66	1.25	0.08	0.22	0.81	3.94	5.38	0.04	0.10	95.02
22/04/2024	**Aso-F**	FLF230	70.27	0.31	13.52	1.19	0.09	0.22	0.79	4.08	5.09	0.03	0.10	95.69
22/04/2024	**Aso-F**	FLF230	68.43	0.30	13.49	1.17	0.08	0.21	0.83	4.00	5.30	0.03	0.10	93.95
22/04/2024	**Aso-F**	FLF230	70.27	0.29	13.67	1.22	0.08	0.20	0.83	3.80	5.20	0.04	0.12	95.72
22/04/2024	**Aso-F**	FLF230	69.94	0.29	13.74	1.12	0.10	0.20	0.77	4.07	5.19	0.03	0.10	95.55
22/04/2024	**Aso-F**	FLF230	70.57	0.30	13.86	1.10	0.11	0.21	0.80	4.20	5.09	0.03	0.11	96.38
22/04/2024	**Aso-F**	FLF230	69.93	0.34	14.12	1.25	0.11	0.27	1.00	3.84	5.15	0.04	0.12	96.18
22/04/2024	**Aso-F**	FLF230	69.24	0.31	14.02	1.23	0.09	0.23	0.87	4.30	5.25	0.02	0.10	95.66
22/04/2024	**Aso-F**	FLF230	70.28	0.32	14.14	1.23	0.10	0.23	0.89	4.12	5.29	0.03	0.10	96.73

Date of Analysis	Sample	Label	SiO_2	TiO_2	Al_2O_3	FeO_t	MnO	MgO	CaO	Na_2O	K_2O	P_2O_5	Cl	Analytical Total
07/08/2023	**Aso-G**	FLF153	66.66	0.57	14.35	2.18	0.10	0.52	1.58	4.18	4.55	0.09	0.11	94.89
07/08/2023	**Aso-G**	FLF153	67.27	0.58	14.48	2.24	0.13	0.55	1.60	4.22	4.45	0.09	0.11	95.72
07/08/2023	**Aso-G**	FLF153	66.53	0.60	14.82	2.11	0.07	0.55	1.50	4.05	4.59	0.11	0.11	95.05
07/08/2023	**Aso-G**	FLF153	61.09	0.46	13.48	1.99	0.09	0.47	1.23	3.35	4.09	0.09	0.19	86.55
07/08/2023	**Aso-G**	FLF153	67.57	0.55	14.74	2.07	0.09	0.54	1.53	4.11	4.62	0.11	0.10	96.03
07/08/2023	**Aso-G**	FLF153	67.62	0.58	14.69	2.17	0.09	0.55	1.60	4.31	4.74	0.08	0.07	96.50
07/08/2023	**Aso-G**	FLF153	67.37	0.59	15.16	2.25	0.12	0.62	1.70	3.31	4.67	0.11	0.09	95.99
07/08/2023	**Aso-G**	FLF153	67.32	0.60	14.93	2.22	0.08	0.58	1.78	3.13	4.42	0.11	0.08	95.24
07/08/2023	**Aso-G**	FLF153	67.25	0.60	14.91	2.13	0.10	0.57	1.56	4.10	4.52	0.10	0.09	95.93
07/08/2023	**Aso-G**	FLF153	66.58	0.57	14.83	2.21	0.11	0.58	1.50	4.15	4.72	0.11	0.10	95.46
03/11/2023	**Aso-H**	FLF219	66.00	0.61	14.48	2.46	0.11	0.63	1.79	4.37	4.64	0.15	0.08	95.33
03/11/2023	**Aso-H**	FLF219	66.29	0.65	14.79	2.34	0.11	0.67	1.71	4.08	4.64	0.13	0.08	95.50
03/11/2023	**Aso-H**	FLF219	65.92	0.59	14.67	2.52	0.10	0.69	1.87	4.02	4.51	0.14	0.09	95.14
03/11/2023	**Aso-H**	FLF219	66.16	0.63	14.59	2.46	0.12	0.59	1.74	3.87	4.57	0.15	0.09	94.97
03/11/2023	**Aso-H**	FLF219	65.58	0.67	14.33	2.50	0.10	0.74	1.81	4.24	4.59	0.13	0.08	94.76
03/11/2023	**Aso-H**	FLF219	66.21	0.64	14.67	2.42	0.09	0.71	1.76	4.18	4.64	0.19	0.10	95.60
03/11/2023	**Aso-H**	FLF219	64.68	0.65	14.38	2.43	0.12	0.62	1.76	4.14	4.66	0.16	0.08	93.68
03/11/2023	**Aso-H**	FLF219	65.89	0.64	14.42	2.56	0.11	0.65	1.76	4.05	4.72	0.14	0.09	95.03
03/11/2023	**Aso-H**	FLF219	66.16	0.64	14.92	2.50	0.09	0.68	1.86	4.05	4.56	0.09	0.09	95.64
03/11/2023	**Aso-H**	FLF219	66.06	0.66	14.45	2.51	0.13	0.65	1.70	4.10	4.68	0.22	0.08	95.24
03/11/2023	**Aso-H**	FLF219	66.15	0.60	14.68	2.45	0.10	0.60	1.71	4.10	4.62	0.14	0.09	95.24
03/11/2023	**Aso-H**	FLF219	66.76	0.67	14.63	2.54	0.08	0.64	1.68	4.02	5.02	0.18	0.10	96.31
03/11/2023	**Aso-H**	FLF219	65.91	0.62	14.41	2.51	0.14	0.73	1.83	3.77	4.81	0.16	0.08	94.97
03/11/2023	**Aso-H**	FLF219	66.37	0.68	14.61	2.50	0.10	0.68	1.75	4.00	4.86	0.17	0.09	95.82
03/11/2023	**Aso-H**	FLF219	65.94	0.66	14.59	2.47	0.13	0.71	1.74	4.08	4.67	0.17	0.08	95.24
03/11/2023	**Aso-H**	FLF219	66.43	0.64	14.76	2.48	0.08	0.63	1.75	3.94	4.68	0.11	0.09	95.59
03/11/2023	**Aso-H**	FLF219	65.90	0.66	14.83	2.67	0.10	0.74	1.89	3.96	4.64	0.16	0.08	95.64
03/11/2023	**Aso-H**	FLF219	67.60	0.61	14.68	2.46	0.12	0.66	1.79	4.09	4.62	0.10	0.09	96.82
03/11/2023	**Aso-H**	FLF219	66.23	0.64	14.56	2.55	0.09	0.65	1.83	4.07	4.82	0.10	0.09	95.63
03/11/2023	**Aso-H**	FLF217	65.17	0.68	14.61	2.59	0.11	0.66	1.83	3.95	4.63	0.15	0.07	94.47
03/11/2023	**Aso-H**	FLF217	65.29	0.59	14.57	2.45	0.09	0.64	1.77	4.18	4.79	0.08	0.07	94.51
03/11/2023	**Aso-H**	FLF217	66.01	0.63	14.51	2.45	0.07	0.71	1.81	4.16	4.65	0.15	0.10	95.23
03/11/2023	**Aso-H**	FLF217	65.25	0.65	14.44	2.50	0.13	0.66	1.85	3.89	4.63	0.15	0.08	94.23

Date of Analysis	Sample	Label	SiO_2	TiO_2	Al_2O_3	FeO_t	MnO	MgO	CaO	Na_2O	K_2O	P_2O_5	Cl	Analytical Total
03/11/2023	**Aso-H**	FLF217	65.80	0.61	14.57	2.45	0.08	0.65	1.88	4.15	4.62	0.26	0.10	95.18
03/11/2023	**Aso-H**	FLF217	66.32	0.66	14.64	2.45	0.09	0.68	1.82	4.05	4.64	0.11	0.08	95.55
03/11/2023	**Aso-H**	FLF217	65.82	0.65	14.56	2.47	0.12	0.70	1.87	4.20	4.61	0.17	0.08	95.26
03/11/2023	**Aso-H**	FLF217	65.46	0.63	14.52	2.42	0.07	0.69	1.85	3.90	4.60	0.17	0.08	94.40
03/11/2023	**Aso-H**	FLF217	65.86	0.65	14.30	2.59	0.14	0.74	1.89	4.06	4.55	0.21	0.06	95.06
03/11/2023	**Aso-H**	FLF217	65.98	0.65	14.78	2.46	0.09	0.71	1.84	3.95	4.84	0.15	0.07	95.53
03/11/2023	**Aso-H**	FLF217	65.51	0.64	14.59	2.59	0.09	0.69	1.89	4.15	4.61	0.19	0.10	95.05
03/11/2023	**Aso-H**	FLF217	65.39	0.65	14.59	2.53	0.10	0.67	1.86	3.88	4.69	0.16	0.08	94.61
03/11/2023	**Aso-H**	FLF217	65.52	0.67	14.81	2.61	0.12	0.66	1.98	4.09	4.44	0.13	0.08	95.11
03/11/2023	**Aso-H**	FLF217	67.12	0.57	14.76	2.64	0.10	0.61	1.73	4.29	4.61	0.16	0.09	96.68
03/11/2023	**Aso-H**	FLF217	65.18	0.67	14.61	2.54	0.09	0.71	1.97	4.06	4.53	0.16	0.09	94.59
03/11/2023	**Aso-H**	FLF217	65.75	0.61	14.61	2.50	0.12	0.64	1.78	4.11	4.64	0.27	0.09	95.11
03/11/2023	**Aso-H**	FLF217	65.82	0.68	14.74	2.60	0.11	0.71	1.93	4.08	4.56	0.15	0.08	95.45
03/11/2023	**Aso-H**	FLF217	65.83	0.65	14.66	2.48	0.09	0.68	1.80	3.99	4.70	0.15	0.09	95.14
03/11/2023	**Aso-H**	FLF213	65.01	0.60	14.60	2.51	0.12	0.65	1.81	3.87	4.54	0.12	0.08	93.91
03/11/2023	**Aso-H**	FLF213	65.04	0.66	14.50	2.46	0.13	0.66	1.86	4.19	4.60	0.17	0.08	94.35
03/11/2023	**Aso-H**	FLF213	65.31	0.62	14.69	2.56	0.11	0.68	1.90	4.17	4.56	0.13	0.10	94.82
03/11/2023	**Aso-H**	FLF213	64.79	0.64	14.43	2.32	0.07	0.64	1.86	3.82	4.60	0.26	0.09	93.52
03/11/2023	**Aso-H**	FLF213	65.68	0.61	14.54	2.54	0.07	0.62	1.85	4.05	4.52	0.11	0.09	94.68
03/11/2023	**Aso-H**	FLF213	66.03	0.64	14.73	2.64	0.07	0.67	1.81	4.26	4.53	0.14	0.09	95.60
03/11/2023	**Aso-H**	FLF213	67.54	0.62	15.16	2.82	0.15	0.78	1.94	4.41	4.74	0.21	0.10	98.46
03/11/2023	**Aso-H**	FLF213	66.09	0.69	14.72	2.61	0.11	0.69	1.95	4.21	4.60	0.19	0.09	95.93
03/11/2023	**Aso-H**	FLF213	66.85	0.71	14.98	2.75	0.07	0.71	1.98	4.33	4.42	0.17	0.07	97.04
03/11/2023	**Aso-H**	FLF213	66.85	0.64	14.90	2.51	0.06	0.71	1.87	4.25	4.67	0.09	0.09	96.65
03/11/2023	**Aso-H**	FLF213	66.23	0.63	14.75	2.53	0.10	0.71	1.94	4.27	4.61	0.12	0.09	95.98
03/11/2023	**Aso-H**	FLF213	65.64	0.62	14.61	2.33	0.10	0.67	1.82	4.18	4.63	0.14	0.09	94.83
03/11/2023	**Aso-H**	FLF213	66.53	0.65	14.68	2.39	0.12	0.60	1.77	4.18	4.60	0.17	0.09	95.79
03/11/2023	**Aso-H**	FLF213	66.29	0.62	14.82	2.40	0.10	0.72	1.81	4.09	4.61	0.19	0.10	95.75
03/11/2023	**Aso-H**	FLF213	64.40	0.61	14.55	2.40	0.07	0.66	1.88	4.07	4.51	0.20	0.10	93.44
03/11/2023	**Aso-H**	FLF213	66.35	0.59	14.78	2.31	0.07	0.61	1.78	4.08	4.70	0.14	0.09	95.50
03/11/2023	**Aso-H**	FLF213	66.18	0.63	14.90	2.60	0.11	0.78	2.07	4.19	4.62	0.10	0.09	96.27
03/11/2023	**Aso-H**	FLF213	65.69	0.71	14.73	2.47	0.08	0.60	1.87	4.24	4.58	0.13	0.11	95.23
03/11/2023	**Aso-H**	FLF208	66.40	0.67	14.34	2.77	0.09	0.72	1.76	3.94	4.69	0.19	0.11	95.68

Date of Analysis	Sample	Label	SiO_2	TiO_2	Al_2O_3	FeO_t	MnO	MgO	CaO	Na_2O	K_2O	P_2O_5	Cl	Analytical Total
03/11/2023	**Aso-H**	FLF208	64.58	0.55	14.56	2.31	0.06	0.71	1.88	4.16	4.57	0.16	0.11	93.65
03/11/2023	**Aso-H**	FLF208	64.57	0.66	14.47	2.64	0.12	0.76	2.18	4.30	4.38	0.17	0.08	94.33
03/11/2023	**Aso-H**	FLF208	64.60	0.69	14.56	2.74	0.12	0.80	2.22	4.19	4.34	0.12	0.11	94.51
03/11/2023	**Aso-H**	FLF208	67.95	0.71	15.45	2.91	0.11	0.85	2.21	4.29	4.51	0.20	0.08	99.27
03/11/2023	**Aso-H**	FLF208	64.85	0.69	14.83	2.60	0.11	0.80	2.11	4.24	4.45	0.22	0.09	94.99
03/11/2023	**Aso-H**	FLF208	63.98	0.72	14.27	2.64	0.13	0.73	2.08	4.19	4.36	0.18	0.11	93.38
03/11/2023	**Aso-H**	FLF208	64.49	0.70	14.83	2.63	0.11	0.78	2.26	4.13	4.26	0.18	0.08	94.45
03/11/2023	**Aso-H**	FLF208	64.64	0.63	14.98	2.56	0.11	0.81	2.11	4.18	4.46	0.19	0.10	94.78
03/11/2023	**Aso-H**	FLF208	64.98	0.67	14.79	2.77	0.12	0.85	2.23	4.23	4.42	0.15	0.10	95.31
03/11/2023	**Aso-H**	FLF208	65.05	0.66	14.66	2.75	0.10	0.77	2.14	4.21	4.31	0.13	0.11	94.89
03/11/2023	**Aso-H**	FLF208	64.76	0.65	14.95	2.78	0.11	0.81	2.09	4.11	4.61	0.21	0.06	95.13
03/11/2023	**Aso-H**	FLF208	65.53	0.63	14.95	2.52	0.14	0.75	2.07	4.25	4.35	0.16	0.08	95.43
03/11/2023	**Aso-H**	FLF208	64.46	0.65	15.01	2.75	0.12	0.78	2.12	4.18	4.25	0.15	0.09	94.54
03/11/2023	**Aso-H**	FLF208	66.56	0.68	15.21	2.91	0.08	0.81	2.21	4.39	4.44	0.18	0.09	97.57
03/11/2023	**Aso-H**	FLF208	64.79	0.65	14.78	2.88	0.14	0.77	2.13	4.05	4.39	0.15	0.10	94.83
03/11/2023	**Aso-H**	FLF208	64.95	0.67	14.84	2.81	0.09	0.81	2.20	4.04	4.30	0.23	0.07	94.99
03/11/2023	**Aso-I**	FLF207	68.51	0.75	15.23	3.05	0.11	0.58	1.77	4.14	4.53	0.05	0.10	98.82
03/11/2023	**Aso-I**	FLF207	65.99	0.65	14.64	2.26	0.09	0.63	1.74	4.15	4.64	0.16	0.11	95.04
03/11/2023	**Aso-I**	FLF207	65.82	0.61	14.72	2.45	0.10	0.66	1.84	4.07	4.59	0.14	0.11	95.11
03/11/2023	**Aso-I**	FLF207	65.87	0.69	14.75	2.44	0.08	0.66	1.85	4.01	4.64	0.15	0.09	95.24
03/11/2023	**Aso-I**	FLF207	66.51	0.64	14.75	2.47	0.13	0.68	1.85	4.23	4.57	0.11	0.09	96.03
03/11/2023	**Aso-I**	FLF207	66.17	0.65	14.75	2.30	0.09	0.63	1.72	3.99	4.68	0.13	0.09	95.21
03/11/2023	**Aso-I**	FLF207	67.95	0.48	14.65	1.94	0.09	0.42	1.29	3.98	5.01	0.09	0.11	96.02
03/11/2023	**Aso-I**	FLF207	66.02	0.60	14.67	2.42	0.10	0.65	1.82	4.08	4.54	0.09	0.08	95.07
03/11/2023	**Aso-I**	FLF207	65.53	0.61	14.47	2.31	0.11	0.66	1.79	3.96	4.52	0.12	0.12	94.20
03/11/2023	**Aso-I**	FLF207	66.60	0.58	14.54	2.14	0.09	0.57	1.63	4.06	4.75	0.09	0.12	95.18
03/11/2023	**Aso-I**	FLF207	66.87	0.61	14.94	2.36	0.06	0.61	1.77	4.15	4.41	0.11	0.09	95.97
03/11/2023	**Aso-I**	FLF207	66.07	0.68	14.69	2.32	0.10	0.66	1.83	4.24	4.61	0.22	0.12	95.54
03/11/2023	**Aso-I**	FLF207	65.97	0.60	14.57	2.25	0.10	0.63	1.68	4.11	4.55	0.21	0.09	94.75
03/11/2023	**Aso-I**	FLF207	66.13	0.60	14.66	2.53	0.09	0.64	1.89	4.11	4.56	0.11	0.09	95.41
03/11/2023	**Aso-I**	FLF207	67.04	0.53	14.39	1.85	0.11	0.45	1.33	4.08	4.89	0.09	0.10	94.86
03/11/2023	**Aso-I**	FLF207	66.73	0.50	14.31	2.03	0.09	0.46	1.39	4.00	4.75	0.16	0.11	94.53
03/11/2023	**Aso-I**	FLF207	66.09	0.58	14.74	2.21	0.10	0.62	1.68	4.17	4.60	0.18	0.08	95.04
03/11/2023	**Aso-I**	FLF207	66.75	0.49	14.28	1.96	0.09	0.45	1.35	4.12	4.75	0.07	0.12	94.43

Date of Analysis	Sample	Label	SiO_2	TiO_2	Al_2O_3	FeO_t	MnO	MgO	CaO	Na_2O	K_2O	P_2O_5	Cl	Analytical Total
03/11/2023	**Aso-I**	FLF207	66.29	0.63	14.67	2.37	0.12	0.62	1.77	4.06	4.56	0.17	0.08	95.34
03/11/2023	**Aso-I**	FLF206	66.19	0.56	14.58	2.22	0.07	0.60	1.79	4.20	4.61	0.12	0.11	95.06
03/11/2023	**Aso-I**	FLF206	65.47	0.59	14.42	2.26	0.09	0.57	1.65	3.93	4.54	0.06	0.09	93.67
03/11/2023	**Aso-I**	FLF206	66.58	0.59	14.41	2.26	0.08	0.62	1.68	4.25	4.53	0.12	0.08	95.20
03/11/2023	**Aso-I**	FLF206	65.58	0.59	14.58	2.29	0.14	0.59	1.77	3.98	4.59	0.05	0.09	94.25
03/11/2023	**Aso-I**	FLF206	66.16	0.61	14.51	2.34	0.11	0.63	1.87	4.04	4.77	0.13	0.09	95.25
03/11/2023	**Aso-I**	FLF206	66.26	0.63	14.71	2.28	0.09	0.61	1.74	4.11	4.56	0.11	0.07	95.17
03/11/2023	**Aso-I**	FLF206	65.48	0.63	14.76	2.33	0.10	0.66	1.91	4.34	4.50	0.09	0.09	94.90
03/11/2023	**Aso-I**	FLF206	66.05	0.64	14.68	2.23	0.12	0.60	1.75	4.16	4.61	0.16	0.09	95.09
03/11/2023	**Aso-I**	FLF206	65.96	0.62	14.52	2.32	0.10	0.63	1.78	4.15	4.49	0.06	0.10	94.73
03/11/2023	**Aso-I**	FLF206	65.71	0.68	14.26	2.35	0.08	0.64	1.72	4.09	4.54	0.16	0.11	94.34
03/11/2023	**Aso-I**	FLF206	65.88	0.62	14.78	2.29	0.10	0.67	1.81	4.10	4.56	0.14	0.08	95.03
03/11/2023	**Aso-I**	FLF206	65.25	0.58	14.22	2.23	0.09	0.58	1.74	4.17	4.56	0.08	0.10	93.59
03/11/2023	**Aso-I**	FLF206	65.78	0.65	14.68	2.41	0.11	0.64	1.81	4.08	4.43	0.16	0.07	94.82
03/11/2023	**Aso-I**	FLF206	66.05	0.57	14.50	2.15	0.12	0.56	1.58	4.04	4.69	0.08	0.11	94.44
03/11/2023	**Aso-I**	FLF206	66.01	0.61	14.77	2.42	0.10	0.63	1.81	3.99	4.52	0.16	0.11	95.13
03/11/2023	**Aso-I**	FLF206	65.05	0.62	14.62	2.34	0.09	0.67	1.80	4.15	4.56	0.15	0.09	94.14
03/11/2023	**Aso-I**	FLF206	65.91	0.63	14.60	2.25	0.07	0.66	1.79	4.21	4.53	0.11	0.11	94.87
03/11/2023	**Aso-I**	FLF206	66.26	0.63	15.03	2.38	0.09	0.58	1.76	4.09	4.66	0.10	0.09	95.68
03/11/2023	**Aso-I**	FLF206	65.31	0.66	14.70	2.60	0.09	0.63	1.84	4.12	4.46	0.14	0.13	94.68
03/11/2023	**Aso-I**	FLF206	66.32	0.55	14.58	2.14	0.07	0.56	1.61	4.13	4.73	0.15	0.09	94.94
03/11/2023	**Aso-J**	FLF202	64.63	0.73	14.55	2.76	0.14	0.78	2.14	4.06	4.33	0.19	0.10	94.40
03/11/2023	**Aso-J**	FLF202	65.29	0.74	14.65	2.79	0.11	0.77	2.10	4.17	4.51	0.20	0.11	95.42
03/11/2023	**Aso-J**	FLF202	64.26	0.70	14.61	2.58	0.10	0.77	2.04	4.07	4.40	0.17	0.09	93.79
03/11/2023	**Aso-J**	FLF202	64.86	0.69	14.91	2.71	0.12	0.72	2.18	4.13	4.65	0.18	0.09	95.24
03/11/2023	**Aso-J**	FLF202	65.23	0.69	14.79	2.69	0.12	0.79	2.14	3.95	4.45	0.17	0.09	95.11
03/11/2023	**Aso-J**	FLF202	64.79	0.68	14.84	2.92	0.11	0.81	2.05	4.26	4.53	0.22	0.09	95.29
03/11/2023	**Aso-J**	FLF202	65.21	0.65	14.73	2.71	0.08	0.81	2.10	3.95	4.58	0.19	0.08	95.08
03/11/2023	**Aso-J**	FLF202	65.03	0.65	14.95	2.82	0.08	0.78	2.09	4.13	4.48	0.17	0.09	95.27
03/11/2023	**Aso-J**	FLF202	65.04	0.66	14.78	2.68	0.10	0.79	2.07	4.25	4.53	0.13	0.10	95.12
03/11/2023	**Aso-J**	FLF202	65.71	0.69	14.93	2.72	0.10	0.74	2.14	4.30	4.61	0.12	0.11	96.17
03/11/2023	**Aso-J**	FLF202	65.56	0.68	14.87	2.74	0.12	0.77	2.04	4.32	4.64	0.18	0.09	96.01
03/11/2023	**Aso-J**	FLF202	65.93	0.68	14.70	2.83	0.08	0.78	2.18	3.97	4.61	0.16	0.09	96.01

Date of Analysis	Sample	Label	SiO_2	TiO_2	Al_2O_3	FeO_t	MnO	MgO	CaO	Na_2O	K_2O	P_2O_5	Cl	Analytical Total
03/11/2023	**Aso-J**	FLF202	64.94	0.68	14.94	2.80	0.09	0.77	2.10	4.05	4.41	0.13	0.09	95.00
03/11/2023	**Aso-J**	FLF202	65.25	0.70	14.77	2.77	0.09	0.80	2.14	4.13	4.42	0.13	0.07	95.26
03/11/2023	**Aso-J**	FLF202	65.06	0.66	14.89	2.68	0.07	0.77	2.06	4.16	4.51	0.12	0.09	95.06
03/11/2023	**Aso-J**	FLF202	63.81	0.67	14.51	2.82	0.11	0.72	2.10	4.23	4.42	0.17	0.13	93.70
03/11/2023	**Aso-J**	FLF202	65.20	0.72	14.90	2.76	0.13	0.76	2.11	4.09	4.50	0.14	0.08	95.37
03/11/2023	**Aso-J**	FLF202	64.33	0.69	14.83	2.70	0.11	0.76	2.06	4.08	4.53	0.21	0.10	94.39
03/11/2023	**Aso-J**	FLF202	64.48	0.60	14.62	2.70	0.09	0.74	2.09	4.08	4.50	0.21	0.08	94.18
03/11/2023	**Aso-J**	FLF203	65.38	0.75	14.55	2.65	0.10	0.70	1.96	4.04	4.64	0.22	0.09	95.07
03/11/2023	**Aso-J**	FLF203	65.65	0.70	14.79	2.80	0.15	0.73	2.00	3.95	4.48	0.20	0.07	95.51
03/11/2023	**Aso-J**	FLF203	65.25	0.67	14.74	2.75	0.14	0.70	1.94	3.98	4.54	0.20	0.08	94.98
03/11/2023	**Aso-J**	FLF203	65.22	0.73	14.60	2.71	0.11	0.71	1.91	4.00	4.41	0.20	0.08	94.68
03/11/2023	**Aso-J**	FLF203	66.08	0.67	14.97	2.65	0.10	0.77	2.02	3.91	4.77	0.19	0.09	96.21
03/11/2023	**Aso-J**	FLF203	65.23	0.68	14.79	2.79	0.09	0.69	2.01	4.13	4.45	0.20	0.05	95.11
03/11/2023	**Aso-J**	FLF203	65.69	0.73	14.88	2.84	0.09	0.75	1.90	3.96	4.68	0.15	0.07	95.76
03/11/2023	**Aso-J**	FLF203	65.31	0.70	14.55	2.61	0.13	0.73	1.98	3.97	4.54	0.17	0.09	94.78
03/11/2023	**Aso-J**	FLF203	65.59	0.72	14.85	2.67	0.11	0.74	1.95	4.12	4.64	0.10	0.09	95.58
03/11/2023	**Aso-J**	FLF203	65.13	0.64	14.77	2.82	0.11	0.70	2.02	3.97	4.57	0.12	0.07	94.92
03/11/2023	**Aso-J**	FLF203	65.18	0.74	14.68	2.63	0.08	0.70	1.96	4.13	4.56	0.17	0.09	94.90
03/11/2023	**Aso-J**	FLF203	65.63	0.67	14.89	2.76	0.13	0.75	2.18	3.76	4.58	0.17	0.04	95.55
03/11/2023	**Aso-J**	FLF203	65.22	0.67	14.82	2.59	0.08	0.73	1.96	3.92	4.71	0.13	0.09	94.91
03/11/2023	**Aso-J**	FLF203	65.25	0.58	14.61	2.61	0.09	0.73	2.04	4.07	4.53	0.17	0.10	94.76
03/11/2023	**Aso-J**	FLF203	66.23	0.69	14.90	2.69	0.12	0.77	2.30	3.91	4.64	0.17	0.06	96.48
03/11/2023	**Aso-J**	FLF203	65.01	0.72	14.43	2.71	0.10	0.74	2.08	4.13	4.52	0.22	0.09	94.74
03/11/2023	**Aso-J**	FLF203	65.18	0.64	14.82	2.73	0.11	0.77	1.99	4.18	4.67	0.18	0.10	95.36
03/11/2023	**Aso-K**	FLF201	66.12	0.72	15.10	2.81	0.09	0.78	2.20	4.29	4.44	0.14	0.09	96.77
03/11/2023	**Aso-K**	FLF201	66.27	0.72	15.14	2.72	0.14	0.74	2.04	4.04	4.54	0.17	0.07	96.59
03/11/2023	**Aso-K**	FLF201	64.94	0.68	14.81	2.82	0.14	0.76	2.07	4.06	4.36	0.17	0.07	94.88
03/11/2023	**Aso-K**	FLF201	65.07	0.71	14.84	2.62	0.14	0.75	2.10	4.16	4.54	0.17	0.08	95.16
03/11/2023	**Aso-K**	FLF201	65.63	0.67	14.80	2.80	0.12	0.77	2.05	4.16	4.56	0.17	0.09	95.80
03/11/2023	**Aso-K**	FLF201	65.25	0.72	14.74	2.62	0.11	0.73	2.09	4.01	4.57	0.21	0.08	95.12
03/11/2023	**Aso-K**	FLF201	65.42	0.68	14.80	2.68	0.09	0.75	2.10	4.17	4.50	0.17	0.07	95.44
03/11/2023	**Aso-K**	FLF201	64.83	0.67	14.76	2.73	0.11	0.75	2.09	4.08	4.43	0.25	0.09	94.78
03/11/2023	**Aso-K**	FLF201	64.73	0.67	14.76	2.74	0.11	0.80	2.15	4.08	4.36	0.19	0.10	94.69

Date of Analysis	Sample	Label	SiO_2	TiO_2	Al_2O_3	FeO_t	MnO	MgO	CaO	Na_2O	K_2O	P_2O_5	Cl	Analytical Total
03/11/2023	**Aso-K**	FLF201	65.00	0.64	14.69	2.60	0.10	0.69	2.03	3.86	4.30	0.15	0.08	94.13
03/11/2023	**Aso-K**	FLF201	67.93	0.72	15.27	2.87	0.11	0.75	2.19	4.25	4.64	0.15	0.06	98.93
03/11/2023	**Aso-K**	FLF201	64.37	0.73	14.62	2.71	0.07	0.79	2.11	4.06	4.38	0.17	0.09	94.09
03/11/2023	**Aso-K**	FLF201	64.62	0.67	14.73	2.71	0.14	0.81	2.14	4.21	4.40	0.22	0.10	94.75
03/11/2023	**Aso-K**	FLF201	64.63	0.65	14.65	2.66	0.13	0.79	2.16	4.12	4.36	0.18	0.09	94.41
03/11/2023	**Aso-K**	FLF201	65.74	0.66	14.74	2.71	0.11	0.75	2.14	4.08	4.69	0.15	0.09	95.86
03/11/2023	**Aso-K**	FLF201	65.15	0.72	14.88	2.72	0.10	0.78	2.14	3.97	4.58	0.17	0.09	95.31
03/11/2023	**Aso-K**	FLF201	64.69	0.68	14.58	2.83	0.10	0.73	2.11	3.98	4.38	0.14	0.08	94.31
03/11/2023	**Aso-K**	FLF201	65.37	0.67	15.04	2.85	0.12	0.70	2.06	4.18	4.57	0.17	0.09	95.81
03/11/2023	**Aso-K**	FLF201	65.02	0.71	14.94	2.84	0.11	0.81	2.13	4.08	4.39	0.15	0.09	95.27
03/11/2023	**Aso-K**	FLF200	63.73	0.71	14.48	2.76	0.15	0.78	2.24	3.92	4.29	0.18	0.08	93.32
03/11/2023	**Aso-K**	FLF200	65.33	0.64	14.83	2.84	0.12	0.77	2.08	3.86	4.32	0.11	0.09	94.99
03/11/2023	**Aso-K**	FLF200	64.95	0.71	14.76	2.79	0.13	0.74	2.04	4.12	4.41	0.22	0.08	94.96
03/11/2023	**Aso-K**	FLF200	64.72	0.64	14.58	2.79	0.07	0.72	2.16	4.11	4.44	0.18	0.07	94.48
03/11/2023	**Aso-K**	FLF200	65.36	0.74	14.91	2.77	0.12	0.74	2.03	4.09	4.40	0.16	0.07	95.40
03/11/2023	**Aso-K**	FLF200	67.00	0.71	15.40	2.83	0.10	0.79	2.14	4.31	4.51	0.13	0.09	98.01
03/11/2023	**Aso-K**	FLF200	64.02	0.72	14.67	2.82	0.11	0.74	2.15	4.11	4.40	0.12	0.06	93.93
03/11/2023	**Aso-K**	FLF200	65.36	0.67	14.98	2.57	0.10	0.79	2.30	3.79	4.24	0.18	0.09	95.07
03/11/2023	**Aso-K**	FLF200	64.82	0.64	14.90	2.65	0.10	0.77	2.11	4.18	4.36	0.17	0.07	94.77
03/11/2023	**Aso-K**	FLF200	65.18	0.63	14.75	2.73	0.07	0.75	2.20	4.23	4.73	0.19	0.10	95.58
03/11/2023	**Aso-K**	FLF200	64.92	0.67	14.70	2.76	0.12	0.70	2.14	4.16	4.50	0.16	0.09	94.91
03/11/2023	**Aso-K**	FLF200	65.11	0.68	14.69	2.69	0.14	0.78	2.11	4.02	4.48	0.15	0.08	94.91
03/11/2023	**Aso-K**	FLF200	64.52	0.68	14.82	2.71	0.13	0.76	2.09	4.16	4.48	0.17	0.08	94.60
03/11/2023	**Aso-K**	FLF200	65.66	0.66	14.86	2.78	0.12	0.76	2.09	4.05	4.45	0.11	0.07	95.61
03/11/2023	**Aso-K**	FLF200	65.15	0.69	14.96	2.74	0.11	0.79	2.07	4.23	4.49	0.16	0.08	95.46
03/11/2023	**Aso-K**	FLF200	64.77	0.70	14.85	2.78	0.11	0.76	2.21	4.12	4.42	0.11	0.09	94.91
03/11/2023	**Aso-K**	FLF200	65.17	0.75	14.99	3.21	0.14	0.75	2.19	4.30	4.40	0.12	0.10	96.13
03/11/2023	**Aso-K**	FLF200	64.98	0.66	14.84	2.75	0.11	0.75	2.08	4.17	4.49	0.08	0.08	94.98
03/11/2023	**Aso-K**	FLF200	66.35	0.69	14.97	2.78	0.10	0.70	2.16	4.39	4.56	0.18	0.10	96.98
03/11/2023	**Aso-L**	FLF197	65.87	0.62	14.75	2.43	0.06	0.63	1.72	4.07	4.56	0.13	0.09	94.93
03/11/2023	**Aso-L**	FLF197	65.49	0.63	14.65	2.34	0.12	0.59	1.68	3.98	4.66	0.18	0.08	94.42
03/11/2023	**Aso-L**	FLF197	66.42	0.66	14.70	2.43	0.05	0.62	1.71	3.98	4.74	0.13	0.09	95.54
03/11/2023	**Aso-L**	FLF197	65.47	0.63	14.68	2.49	0.08	0.59	1.75	3.87	4.68	0.13	0.06	94.44

Date of Analysis	Sample	Label	SiO_2	TiO_2	Al_2O_3	FeO_t	MnO	MgO	CaO	Na_2O	K_2O	P_2O_5	Cl	Analytical Total
03/11/2023	**Aso-L**	FLF197	66.41	0.67	14.90	2.37	0.09	0.63	1.72	4.15	4.68	0.14	0.07	95.82
03/11/2023	**Aso-L**	FLF197	65.69	0.62	14.55	2.28	0.06	0.60	1.72	3.87	4.84	0.17	0.09	94.49
03/11/2023	**Aso-L**	FLF197	65.82	0.61	14.52	2.26	0.09	0.57	1.69	4.06	4.55	0.04	0.09	94.30
03/11/2023	**Aso-L**	FLF197	67.05	0.67	14.63	2.31	0.12	0.59	1.79	3.94	4.83	0.11	0.08	96.13
03/11/2023	**Aso-L**	FLF197	66.20	0.61	14.81	2.23	0.05	0.50	1.74	4.16	4.55	0.15	0.08	95.07
03/11/2023	**Aso-L**	FLF197	66.37	0.66	14.66	2.27	0.08	0.61	1.71	3.91	4.72	0.09	0.07	95.15
03/11/2023	**Aso-L**	FLF197	65.68	0.59	14.67	2.23	0.09	0.62	1.71	3.97	4.70	0.18	0.08	94.52
03/11/2023	**Aso-L**	FLF197	66.05	0.66	14.76	2.51	0.10	0.62	1.74	3.84	4.94	0.14	0.09	95.45
03/11/2023	**Aso-L**	FLF197	66.06	0.59	14.64	2.43	0.05	0.63	1.70	3.95	4.79	0.13	0.07	95.04
03/11/2023	**Aso-L**	FLF197	68.05	0.62	15.05	2.44	0.07	0.62	1.77	4.27	4.98	0.13	0.09	98.10
03/11/2023	**Aso-L**	FLF197	66.11	0.61	14.46	2.39	0.05	0.58	1.70	3.95	4.82	0.14	0.05	94.86
03/11/2023	**Aso-L**	FLF197	66.45	0.62	14.97	2.48	0.11	0.60	1.73	3.97	4.84	0.10	0.08	95.94
03/11/2023	**Aso-L**	FLF197	66.43	0.58	14.66	2.41	0.07	0.61	1.75	4.04	4.75	0.14	0.10	95.54
03/11/2023	**Aso-L**	FLF197	66.18	0.60	14.53	2.31	0.11	0.58	1.71	3.79	4.79	0.09	0.09	94.77
03/11/2023	**Aso-L**	FLF197	66.68	0.65	14.49	2.42	0.10	0.56	1.72	4.14	4.71	0.12	0.05	95.64
05/02/2024	**Aso-L**	FLF247	65.53	0.66	14.91	2.21	0.04	0.57	1.70	4.15	4.53	0.11	0.08	94.49
05/02/2024	**Aso-L**	FLF247	64.80	0.77	15.40	3.15	0.11	0.56	2.59	4.15	4.50	0.28	0.09	96.41
05/02/2024	**Aso-L**	FLF247	66.40	0.62	15.03	2.40	0.14	0.59	1.72	3.80	4.77	0.11	0.07	95.64
05/02/2024	**Aso-L**	FLF247	68.72	0.65	15.45	2.47	0.06	0.57	1.73	4.22	4.96	0.14	0.05	99.02
05/02/2024	**Aso-L**	FLF247	68.40	0.63	15.30	2.50	0.07	0.63	1.74	4.42	4.75	0.05	0.10	98.59
05/02/2024	**Aso-L**	FLF247	69.18	0.71	14.48	2.66	0.10	0.69	1.57	5.28	3.09	0.15	0.10	98.02
05/02/2024	**Aso-L**	FLF247	66.61	0.58	15.04	2.28	0.12	0.64	1.69	3.85	4.62	0.08	0.08	95.59
05/02/2024	**Aso-L**	FLF247	67.88	0.61	15.18	2.37	0.09	0.56	1.70	4.39	4.66	0.11	0.09	97.64
05/02/2024	**Aso-L**	FLF247	68.96	0.66	15.45	2.37	0.09	0.65	1.75	4.38	4.80	0.11	0.09	99.31
05/02/2024	**Aso-L**	FLF247	66.20	0.68	14.68	2.25	0.08	0.67	1.75	3.67	4.97	0.09	0.07	95.11
05/02/2024	**Aso-L**	FLF247	65.49	0.60	14.84	2.29	0.10	0.60	1.66	4.11	4.45	0.10	0.06	94.30
05/02/2024	**Aso-L**	FLF247	66.39	0.60	14.85	2.32	0.08	0.71	1.69	3.93	4.56	0.13	0.09	95.33
04/08/2023	**Aso-M**	FLF72	64.55	0.68	14.90	2.84	0.10	0.78	2.22	4.43	4.59	0.24	0.11	95.44
04/08/2023	**Aso-M**	FLF72	63.96	0.70	14.77	2.78	0.09	0.81	2.10	4.17	4.46	0.15	0.11	94.10
04/08/2023	**Aso-M**	FLF72	63.30	0.64	14.75	2.77	0.11	0.74	1.99	4.12	4.34	0.12	0.14	93.02
04/08/2023	**Aso-M**	FLF72	64.51	0.72	15.31	3.07	0.13	0.88	2.31	4.21	4.27	0.19	0.07	95.66
04/08/2023	**Aso-M**	FLF72	64.74	0.67	15.39	3.12	0.10	0.86	2.26	4.28	4.52	0.15	0.08	96.17
04/08/2023	**Aso-M**	FLF72	64.94	0.70	15.03	2.91	0.11	0.78	2.16	4.16	4.47	0.13	0.08	95.48

Date of Analysis	Sample	Label	SiO_2	TiO_2	Al_2O_3	FeO_t	MnO	MgO	CaO	Na_2O	K_2O	P_2O_5	Cl	Analytical Total
04/08/2023	**Aso-M**	FLF72	65.17	0.66	15.16	2.87	0.09	0.80	2.05	4.09	4.42	0.16	0.09	95.56
04/08/2023	**Aso-M**	FLF72	63.91	0.67	14.98	2.92	0.10	0.77	2.04	4.17	4.47	0.17	0.07	94.27
04/08/2023	**Aso-M**	FLF72	63.61	0.67	14.80	2.74	0.11	0.78	2.09	4.24	4.40	0.14	0.10	93.68
04/08/2023	**Aso-M**	FLF72	64.20	0.70	14.84	2.88	0.08	0.78	2.11	4.10	4.44	0.10	0.08	94.31
04/08/2023	**Aso-M**	FLF72	64.93	0.66	15.12	2.85	0.09	0.77	2.04	4.11	4.59	0.16	0.07	95.40
04/08/2023	**Aso-M**	FLF72	64.64	0.69	14.95	2.76	0.12	0.78	2.14	4.18	4.51	0.16	0.07	94.99
04/08/2023	**Aso-M**	FLF72	61.16	0.49	16.83	2.27	0.06	0.50	3.26	4.15	3.57	0.12	0.09	92.50
04/08/2023	**Aso-N/Z-2**	FLF69	69.01	0.26	13.32	1.77	0.01	0.12	0.79	3.20	5.87	0.02	0.10	94.48
04/08/2023	**Aso-N/Z-2**	FLF69	69.21	0.25	13.20	1.83	0.06	0.11	0.80	3.11	5.96	0.02	0.10	94.65
04/08/2023	**Aso-N/Z-2**	FLF69	69.36	0.22	13.35	1.68	0.05	0.14	0.80	3.07	6.00	0.02	0.13	94.81
04/08/2023	**Aso-N/Z-2**	FLF69	68.99	0.28	13.29	1.73	0.07	0.14	0.79	3.26	6.01	0.01	0.11	94.67
04/08/2023	**Aso-N/Z-2**	FLF69	69.11	0.25	13.36	1.71	0.07	0.17	0.79	3.34	5.86	0.01	0.13	94.80
04/08/2023	**Aso-N/Z-2**	FLF69	69.31	0.20	13.39	1.76	0.05	0.14	0.76	3.20	5.93	0.00	0.10	94.83
04/08/2023	**Aso-N/Z-2**	FLF69	69.13	0.25	13.30	1.76	0.06	0.12	0.78	3.45	5.85	0.02	0.10	94.84
04/08/2023	**Aso-N/Z-2**	FLF69	69.40	0.25	13.56	1.61	0.05	0.15	0.76	3.25	5.83	0.04	0.13	95.01
04/08/2023	**Aso-N/Z-2**	FLF69	69.16	0.24	13.23	1.71	0.06	0.10	0.78	3.20	5.84	0.05	0.13	94.50
04/08/2023	**Aso-N/Z-2**	FLF69	69.51	0.22	13.50	1.67	0.06	0.14	0.82	3.17	5.80	0.05	0.11	95.04
04/08/2023	**Aso-N/Z-2**	FLF69	69.24	0.24	13.55	1.71	0.04	0.10	0.80	3.20	5.97	0.03	0.13	94.99
04/08/2023	**Aso-N/Z-2**	FLF69	68.52	0.24	13.20	1.77	0.05	0.18	0.79	3.11	5.81	0.04	0.11	93.82
04/08/2023	**Aso-N/Z-2**	FLF69	68.81	0.23	13.21	1.68	0.06	0.15	0.75	2.83	6.52	0.03	0.13	94.41
04/08/2023	**Aso-N/Z-2**	FLF69	69.52	0.26	13.50	1.76	0.08	0.11	0.79	3.29	5.86	0.03	0.14	95.34
04/08/2023	**Aso-N/Z-2**	FLF67	68.66	0.27	13.72	1.71	0.04	0.17	0.75	3.13	5.84	0.00	0.11	94.40
04/08/2023	**Aso-N/Z-2**	FLF67	67.26	0.27	13.21	1.68	0.04	0.15	0.74	3.06	5.83	0.04	0.13	92.42
04/08/2023	**Aso-N/Z-2**	FLF67	69.18	0.25	13.38	1.69	0.06	0.12	0.77	3.27	5.84	0.01	0.10	94.67
04/08/2023	**Aso-N/Z-2**	FLF67	69.28	0.28	13.55	1.70	0.02	0.16	0.77	3.21	5.95	0.04	0.10	95.06
04/08/2023	**Aso-N/Z-2**	FLF67	69.14	0.27	13.33	1.86	0.05	0.17	0.79	3.36	5.74	0.03	0.13	94.87
04/08/2023	**Aso-N/Z-2**	FLF67	69.58	0.26	13.34	1.72	0.04	0.14	0.78	3.31	6.00	0.00	0.12	95.29
04/08/2023	**Aso-N/Z-2**	FLF67	69.50	0.28	13.54	1.73	0.03	0.12	0.82	3.18	5.99	0.00	0.13	95.31
04/08/2023	**Aso-N/Z-2**	FLF67	68.88	0.26	13.34	1.84	0.08	0.15	0.77	3.28	6.01	0.03	0.12	94.76
04/08/2023	**Aso-N/Z-2**	FLF67	69.16	0.25	13.39	1.76	0.09	0.13	0.79	3.28	5.87	0.02	0.12	94.87
04/08/2023	**Aso-N/Z-2**	FLF67	69.14	0.24	13.41	1.80	0.03	0.15	0.77	3.27	5.89	0.02	0.11	94.83
04/08/2023	**Aso-N/Z-2**	FLF67	65.91	0.53	14.82	2.43	0.09	0.57	1.63	4.23	4.75	0.11	0.09	95.15
04/08/2023	**Aso-N/Z-2**	FLF67	68.84	0.28	13.37	1.71	0.07	0.11	0.79	3.07	5.94	0.01	0.11	94.30

Date of Analysis	Sample	Label	SiO_2	TiO_2	Al_2O_3	FeO_t	MnO	MgO	CaO	Na_2O	K_2O	P_2O_5	Cl	Analytical Total
04/08/2023	**Aso-N/Z-2**	FLF67	69.16	0.26	13.34	1.82	0.04	0.14	0.78	3.17	6.10	0.02	0.14	94.97
04/08/2023	**Aso-N/Z-2**	FLF67	69.28	0.26	13.22	1.58	0.06	0.12	0.79	3.30	6.03	0.00	0.13	94.75
24/04/2024	**Aso-Z-6**	FLF227	65.50	0.60	15.15	3.30	0.10	0.83	2.36	3.61	4.84	0.17	0.09	96.55
24/04/2024	**Aso-Z-6**	FLF227	63.72	0.65	15.07	3.43	0.12	0.83	2.22	3.71	5.12	0.20	0.10	95.17
24/04/2024	**Aso-Z-6**	FLF227	65.00	0.64	15.55	3.58	0.10	0.96	2.58	4.24	4.83	0.20	0.09	97.76
24/04/2024	**Aso-Z-6**	FLF227	64.94	0.64	15.34	3.73	0.11	0.97	2.68	4.01	4.41	0.19	0.11	97.14
24/04/2024	**Aso-Z-6**	FLF227	63.94	0.61	14.89	3.43	0.10	0.92	2.51	3.78	4.73	0.18	0.09	95.18
24/04/2024	**Aso-Z-6**	FLF227	65.08	0.62	15.10	3.27	0.10	0.83	2.36	3.80	4.89	0.20	0.09	96.32
24/04/2024	**Aso-Z-6**	FLF227	64.91	0.62	15.66	3.15	0.11	0.94	2.58	3.77	4.59	0.21	0.08	96.61
24/04/2024	**Aso-Z-6**	FLF227	64.10	0.47	16.65	2.40	0.04	0.25	3.20	3.81	4.41	0.13	0.05	95.50
24/04/2024	**Aso-Z-6**	FLF227	62.95	0.58	14.69	3.33	0.10	0.93	2.48	3.87	4.51	0.17	0.10	93.71
24/04/2024	**Aso-Z-6**	FLF227	64.14	0.60	14.89	3.58	0.11	0.76	2.48	3.79	4.70	0.15	0.09	95.28
24/04/2024	**Aso-Z-6**	FLF227	65.40	0.64	15.79	3.53	0.11	0.95	2.68	3.87	5.11	0.18	0.09	98.35
24/04/2024	**Aso-Z-6**	FLF227	64.80	0.62	15.70	3.34	0.11	0.94	2.52	3.80	4.63	0.18	0.09	96.73
24/04/2024	**Aso-Z-6**	FLF227	64.70	0.60	15.06	3.30	0.10	0.93	2.44	3.84	4.66	0.18	0.09	95.90

Table C2. Major element glass analyses of the MPI-DING reference glass (StHs6/80-G, GOR132-G and ATHO-G) (un-normalised).

Date of Analysis	Label	SiO_2	TiO_2	Al_2O_3	FeO_t	MnO	MgO	CaO	Na_2O	K2O	P_2O_5	Cl	Analytical Total
04/08/2023	**ATHO-G**	75.69	0.28	12.14	3.11	0.10	0.09	1.73	4.09	2.65	0.03	0.06	100.0
04/08/2023	**ATHO-G**	75.67	0.24	12.46	3.10	0.07	0.10	1.68	4.29	2.65	0.01	0.04	100.3
04/08/2023	**ATHO-G**	75.58	0.25	12.30	3.26	0.12	0.08	1.70	4.14	2.58	0.03	0.05	100.1
04/08/2023	**ATHO-G**	75.92	0.27	12.23	3.19	0.10	0.11	1.73	4.15	2.63	0.00	0.05	100.4
04/08/2023	**ATHO-G**	75.94	0.28	12.33	3.20	0.10	0.12	1.67	4.05	2.62	0.03	0.02	100.4
04/08/2023	**ATHO-G**	75.57	0.23	12.29	3.12	0.11	0.10	1.69	4.13	2.69	0.03	0.04	100.0
04/08/2023	**ATHO-G**	75.70	0.23	12.29	3.33	0.14	0.12	1.68	4.15	2.71	0.07	0.03	100.5
04/08/2023	**ATHO-G**	75.43	0.25	12.26	3.18	0.12	0.09	1.65	4.29	2.69	0.00	0.05	100.0
04/08/2023	**ATHO-G**	75.48	0.21	12.24	3.26	0.10	0.09	1.67	4.20	2.65	0.05	0.04	100.0
04/08/2023	**ATHO-G**	75.15	0.25	12.32	3.20	0.11	0.12	1.70	4.16	2.63	0.03	0.05	99.70
05/02/2024	**ATHO-G**	75.59	0.26	12.51	3.16	0.10	0.16	1.74	4.08	2.67	0.00	0.06	100.31
05/02/2024	**ATHO-G**	75.94	0.28	12.26	3.26	0.15	0.11	1.68	4.18	2.70	0.00	0.01	100.58
05/02/2024	**ATHO-G**	75.92	0.23	12.38	3.08	0.11	0.06	1.69	4.06	2.69	0.04	0.05	100.32
05/02/2024	**ATHO-G**	75.59	0.25	12.30	3.24	0.13	0.14	1.72	4.04	2.68	0.00	0.01	100.10
05/02/2024	**ATHO-G**	76.10	0.22	12.38	3.14	0.14	0.10	1.64	4.11	2.61	0.02	0.01	100.48
06/02/2024	**ATHO-G**	75.63	0.23	12.54	3.16	0.12	0.10	1.74	4.09	2.69	0.01	0.05	100.36
06/02/2024	**ATHO-G**	75.83	0.22	12.16	3.12	0.12	0.11	1.72	3.99	2.70	0.01	0.04	100.03
06/02/2024	**ATHO-G**	75.82	0.23	12.29	3.10	0.10	0.07	1.72	3.94	2.66	0.04	0.01	99.99
06/02/2024	**ATHO-G**	75.50	0.23	12.34	3.12	0.14	0.10	1.69	4.09	2.68	0.00	0.02	99.92
06/02/2024	**ATHO-G**	75.59	0.24	12.35	3.17	0.07	0.09	1.76	4.01	2.68	0.04	0.05	100.05
06/02/2024	**ATHO-G**	75.94	0.27	12.27	3.13	0.10	0.08	1.74	4.12	2.72	0.01	0.02	100.39
07/02/2024	**ATHO-G**	76.00	0.25	12.17	3.25	0.10	0.11	1.69	4.00	2.65	0.02	0.02	100.27
07/02/2024	**ATHO-G**	75.72	0.21	12.33	3.25	0.08	0.06	1.66	3.99	2.59	0.00	0.05	99.95
07/02/2024	**ATHO-G**	75.63	0.27	12.11	3.12	0.12	0.10	1.67	4.04	2.66	0.05	0.01	99.78
07/02/2024	**ATHO-G**	75.35	0.25	12.32	3.19	0.10	0.11	1.72	3.80	2.62	0.03	0.04	99.53
07/02/2024	**ATHO-G**	75.63	0.27	12.44	3.13	0.10	0.09	1.67	3.88	2.61	0.00	0.00	99.82
07/02/2024	**ATHO-G**	75.69	0.24	12.42	3.15	0.08	0.12	1.69	3.83	2.59	0.00	0.06	99.85
07/02/2024	**ATHO-G**	75.86	0.22	12.30	3.03	0.08	0.08	1.68	3.94	2.62	0.00	0.03	99.83
07/02/2024	**ATHO-G**	75.57	0.24	12.33	3.17	0.13	0.10	1.72	3.73	2.60	0.04	0.05	99.68

Date of Analysis	Label	SiO_2	TiO_2	Al_2O_3	FeO_t	MnO	MgO	CaO	Na_2O	K2O	P_2O_5	Cl	Analytical Total
04/08/2023	**StHs6/80**	63.78	0.72	17.85	4.21	0.09	1.95	5.27	3.79	1.26	0.13	0.01	99.1
04/08/2023	**StHs6/80**	63.91	0.68	17.75	4.31	0.10	2.00	5.34	4.64	1.24	0.13	0.01	100.1
04/08/2023	**StHs6/80**	63.76	0.71	17.95	4.33	0.09	2.00	5.24	4.74	1.26	0.11	0.01	100.2
04/08/2023	**StHs6/80**	63.46	0.72	17.68	4.28	0.08	1.98	5.23	4.41	1.27	0.14	0.02	99.3
04/08/2023	**StHs6/80**	63.66	0.75	17.61	4.23	0.06	1.90	5.27	4.62	1.27	0.12	0.00	99.5
04/08/2023	**StHs6/80**	63.49	0.71	17.90	4.25	0.10	2.01	5.21	4.67	1.28	0.11	0.00	99.7
04/08/2023	**StHs6/80**	63.85	0.71	17.76	4.32	0.06	1.94	5.26	4.48	1.25	0.17	0.01	99.8
04/08/2023	**StHs6/80**	64.11	0.70	17.72	4.33	0.08	1.94	5.32	4.86	1.29	0.17	0.02	100.5
04/08/2023	**StHs6/80**	63.66	0.72	17.86	4.13	0.07	1.98	5.32	4.53	1.28	0.12	0.01	99.7
04/08/2023	**StHs6/80**	63.59	0.70	17.88	4.30	0.07	1.93	5.27	4.26	1.27	0.18	0.01	99.5
05/02/2024	**StHs6/80**	63.73	0.71	17.46	4.35	0.06	1.98	5.18	4.61	1.31	0.16	0.02	99.57
05/02/2024	**StHs6/80**	63.45	0.70	17.75	4.19	0.08	2.01	5.23	4.67	1.31	0.14	0.02	99.54
05/02/2024	**StHs6/80**	63.83	0.70	17.92	4.35	0.08	1.97	5.23	4.85	1.26	0.09	0.01	100.28
05/02/2024	**StHs6/80**	63.46	0.70	17.54	4.25	0.06	1.95	5.31	4.53	1.26	0.10	0.01	99.17
05/02/2024	**StHs6/80**	63.93	0.64	17.78	4.45	0.08	2.01	5.21	4.45	1.28	0.10	0.01	99.96
06/02/2024	**StHs6/80**	63.68	0.76	17.88	4.34	0.07	1.95	5.31	4.59	1.29	0.13	0.00	99.99
06/02/2024	**StHs6/80**	63.49	0.75	17.73	4.30	0.08	2.01	5.29	4.59	1.28	0.14	0.01	99.67
06/02/2024	**StHs6/80**	63.36	0.67	17.75	4.25	0.07	1.98	5.25	4.66	1.29	0.15	0.01	99.43
06/02/2024	**StHs6/80**	63.49	0.68	17.74	4.37	0.06	1.97	5.28	4.60	1.30	0.13	0.01	99.63
06/02/2024	**StHs6/80**	63.30	0.69	17.44	4.38	0.05	1.98	5.33	4.74	1.34	0.11	0.02	99.36
06/02/2024	**StHs6/80**	63.77	0.66	17.58	4.32	0.06	1.98	5.27	4.71	1.31	0.13	0.00	99.80
07/02/2024	**StHs6/80**	63.98	0.70	17.82	4.34	0.06	1.95	5.07	4.44	1.30	0.14	0.00	99.80
07/02/2024	**StHs6/80**	63.52	0.64	17.52	4.39	0.10	2.05	5.14	4.36	1.28	0.08	0.02	99.10
07/02/2024	**StHs6/80**	63.73	0.68	17.83	4.37	0.03	2.13	5.39	4.55	1.32	0.08	0.01	100.13
07/02/2024	**StHs6/80**	64.15	0.72	17.48	4.31	0.05	1.89	5.18	4.26	1.25	0.08	0.02	99.38
07/02/2024	**StHs6/80**	63.48	0.68	17.63	4.36	0.07	1.92	5.15	4.47	1.28	0.09	0.00	99.13
07/02/2024	**StHs6/80**	63.65	0.70	17.55	4.40	0.09	1.98	5.20	3.69	1.23	0.12	0.00	98.62
07/02/2024	**StHs6/80**	63.57	0.65	17.56	4.27	0.05	1.89	5.10	4.24	1.25	0.11	0.03	98.72
07/02/2024	**StHs6/80**	63.44	0.66	17.71	4.36	0.05	1.91	5.13	4.34	1.25	0.16	0.00	99.00
04/08/2023	**GOR132**	45.76	0.29	10.97	10.01	0.16	22.67	8.46	0.88	0.04	0.01	0.01	99.2
04/08/2023	**GOR132**	45.55	0.35	10.94	9.99	0.16	22.56	8.64	0.86	0.02	0.04	0.01	99.1

Date of Analysis	Label	SiO_2	TiO_2	Al_2O_3	FeO_t	MnO	MgO	CaO	Na_2O	K2O	P_2O_5	Cl	Analytical Total
04/08/2023	**GOR132**	45.54	0.30	11.04	9.86	0.16	22.60	8.53	0.78	0.02	0.02	0.00	98.9
04/08/2023	**GOR132**	45.73	0.29	11.00	9.97	0.16	22.53	8.51	0.75	0.03	0.06	0.02	99.0
04/08/2023	**GOR132**	45.00	0.34	10.97	10.15	0.13	22.62	8.59	0.79	0.03	0.06	0.00	98.7
04/08/2023	**GOR132**	45.43	0.34	10.91	10.25	0.16	22.38	8.53	0.78	0.03	0.04	0.00	98.8
04/08/2023	**GOR132**	45.33	0.31	10.81	9.89	0.14	22.40	8.51	0.83	0.04	0.03	0.00	98.3
04/08/2023	**GOR132**	45.68	0.26	10.68	10.12	0.15	22.49	8.55	0.81	0.03	0.05	0.00	98.8
04/08/2023	**GOR132**	45.26	0.28	11.01	9.93	0.13	22.56	8.49	0.86	0.02	0.00	0.01	98.5
04/08/2023	**GOR132**	45.47	0.31	10.99	10.06	0.15	22.64	8.46	0.87	0.02	0.06	0.01	99.0
05/02/2024	**GOR132**	45.60	0.30	11.08	10.17	0.20	23.52	8.49	0.79	0.04	0.03	0.01	100.23
05/02/2024	**GOR132**	45.44	0.28	10.89	10.28	0.17	23.39	8.59	0.77	0.05	0.02	0.00	99.89
05/02/2024	**GOR132**	45.52	0.33	10.97	10.04	0.17	23.33	8.60	0.83	0.02	0.04	0.00	99.84
05/02/2024	**GOR132**	45.91	0.33	11.06	10.30	0.14	23.23	8.53	0.88	0.03	0.06	0.00	100.47
05/02/2024	**GOR132**	45.09	0.29	11.04	10.24	0.15	23.57	8.63	0.89	0.03	0.02	0.00	99.95
06/02/2024	**GOR132**	45.41	0.30	11.06	10.14	0.09	23.13	8.60	0.84	0.05	0.00	0.00	99.62
06/02/2024	**GOR132**	45.73	0.30	10.90	10.38	0.16	22.91	8.60	0.98	0.04	0.02	0.02	100.04
06/02/2024	**GOR132**	45.49	0.29	10.94	10.04	0.16	22.94	8.63	0.77	0.03	0.07	0.00	99.34
07/02/2024	**GOR132**	45.34	0.31	10.93	10.15	0.14	23.40	8.57	0.86	0.03	0.02	0.01	99.76
07/02/2024	**GOR132**	45.63	0.30	11.05	10.10	0.16	23.25	8.44	0.82	0.03	0.03	0.00	99.80
07/02/2024	**GOR132**	45.44	0.32	10.83	10.10	0.15	23.28	8.53	0.84	0.03	0.06	0.01	99.57
07/02/2024	**GOR132**	45.52	0.30	11.10	10.20	0.15	22.84	8.59	0.85	0.02	0.00	0.02	99.59
07/02/2024	**GOR132**	45.36	0.31	10.85	10.16	0.12	22.72	8.50	0.80	0.04	0.04	0.01	98.91
07/02/2024	**GOR132**	45.42	0.29	10.87	10.26	0.13	22.70	8.42	0.69	0.04	0.02	0.00	98.84
07/02/2024	**GOR132**	45.24	0.33	11.11	10.21	0.12	22.66	8.48	0.82	0.03	0.02	0.00	99.01
07/02/2024	**GOR132**	45.42	0.31	10.83	10.21	0.12	22.52	8.46	0.69	0.02	0.06	0.01	98.65

Table C3. Trace element glass analyses of the proximal Aso tephra units.

Date of Analysis	Sample	Label	Rb	Sr	Y	Zr	Nb	Ba	La	Ce	Pr	Nd	Sm	Eu	Gd	Dy	Er	Yb	Lu	Hf	Ta	Pb	Th	U
13/02/2024	**ACP4**	FLF191	151	194	32.8	291	16.4	827	31.5	68.6	8.13	33.3	6.59	1.37	6.60	5.49	3.62	4.22	0.55	7.36	1.13	23.4	14.2	4.34
13/02/2024	**ACP4**	FLF191	146	181	38.1	288	15.5	734	31.2	70.4	8.80	33.9	8.30	1.64	6.62	6.66	4.22	4.37	0.61	7.91	1.14	22.5	14.0	3.94
13/02/2024	**ACP4**	FLF191	148	170	35.9	317	16.8	709	30.9	68.6	8.53	33.2	6.29	1.39	6.37	6.54	4.05	4.26	0.60	8.67	1.24	20.7	15.3	4.32
13/02/2024	**ACP4**	FLF191	150	167	36.0	300	16.5	801	32.5	72.0	8.60	35.4	7.29	1.47	6.33	6.27	4.17	4.10	0.66	8.10	1.19	21.1	14.3	4.14
13/02/2024	**ACP4**	FLF191	151	158	34.6	298	16.3	796	31.8	70.1	8.12	32.7	7.13	1.46	6.39	5.93	3.63	4.24	0.68	8.14	1.13	21.8	13.7	4.03
13/02/2024	**ACP4**	FLF190	162	126	34.6	309	16.7	816	32.2	70.6	8.07	34.2	6.85	1.30	5.93	6.09	3.55	3.77	0.66	8.19	1.17	24.4	15.0	4.29
13/02/2024	**ACP4**	FLF190	151	119	34.8	323	17.4	755	31.0	67.3	8.12	35.1	7.17	1.32	6.46	5.63	3.72	4.60	0.57	8.47	1.32	23.3	14.0	4.47
13/02/2024	**ACP4**	FLF190	159	132	35.3	309	16.9	824	32.8	71.4	8.37	34.5	7.50	1.29	6.29	6.59	3.89	4.22	0.63	7.90	1.17	23.6	14.7	4.35
13/02/2024	**ACP4**	FLF190	167	124	35.8	309	17.1	816	32.4	72.9	8.51	34.0	7.59	1.28	5.60	6.46	3.77	4.41	0.63	9.27	1.17	24.0	14.9	4.22
13/02/2024	**ACP4**	FLF190	165	113	35.1	302	16.7	784	31.9	70.9	8.42	33.2	6.85	1.11	6.51	6.35	4.11	4.07	0.65	8.46	1.17	26.2	14.0	4.14
13/02/2024	**ACP4**	FLF189	157	119	34.6	314	16.9	822	30.5	68.4	7.77	33.4	6.09	1.30	6.03	6.28	3.52	3.85	0.59	8.25	1.18	22.9	13.6	4.19
13/02/2024	**ACP4**	FLF189	150	158	36.7	302	17.0	826	32.9	74.7	8.80	34.6	7.51	1.39	6.73	5.75	4.19	4.43	0.63	8.20	1.22	24.2	14.4	4.04
13/02/2024	**ACP4**	FLF189	163	131	35.9	316	17.1	851	32.9	71.8	8.52	34.3	8.00	1.42	6.33	5.91	3.92	4.56	0.67	8.10	1.22	24.8	14.5	4.37
13/02/2024	**ACP4**	FLF189	157	120	34.0	305	16.3	807	30.9	69.9	7.75	31.8	6.92	1.24	6.25	5.91	3.49	4.01	0.60	7.91	1.14	25.9	14.2	4.30
13/02/2024	**ACP4**	FLF189	150	167	36.1	303	16.5	843	32.5	71.9	8.25	35.4	7.75	1.43	6.16	6.58	3.86	4.38	0.59	7.99	1.26	24.0	13.9	4.25
13/02/2024	**ACP4**	FLF189	158	120	34.3	304	16.6	822	31.7	71.5	8.10	33.2	6.74	1.30	6.11	6.05	3.66	4.31	0.65	7.93	1.14	23.4	14.2	4.34
13/02/2024	**ACP4**	FLF189	154	123	35.4	315	17.1	823	32.1	75.3	8.35	33.2	6.97	1.34	5.91	6.12	3.88	4.28	0.63	8.37	1.17	23.6	14.4	4.26
13/02/2024	**ACP6**	FLF186	177	68.9	34.0	290	16.2	745	32.3	68.9	8.10	31.8	7.13	1.14	6.77	5.94	3.80	3.83	0.60	7.92	1.20	23.2	16.1	4.83
13/02/2024	**ACP6**	FLF186	179	47.0	35.6	278	15.8	704	33.9	75.6	8.43	35.7	7.44	0.91	6.75	6.17	3.96	4.47	0.67	7.28	1.23	25.4	17.3	4.91
13/02/2024	**ACP6**	FLF186	167	98.4	34.8	321	16.5	830	32.7	71.7	8.03	34.7	7.41	1.18	6.24	6.26	3.97	4.25	0.58	8.55	1.19	24.2	15.6	4.48
13/02/2024	**ACP6**	FLF186	166	67.0	35.2	321	17.0	724	32.1	67.8	8.09	33.8	7.06	1.23	6.51	7.13	3.83	4.02	0.60	8.25	1.36	23.8	16.8	4.48
13/02/2024	**ACP6**	FLF186	173	67.6	36.0	312	16.9	739	33.1	72.3	8.35	33.2	7.35	1.13	6.15	6.32	4.20	4.26	0.66	8.38	1.27	24.2	17.4	4.77
13/02/2024	**ACP6**	FLF186	146	177	35.7	277	16.9	859	32.5	71.2	8.31	35.4	8.02	1.52	6.50	6.28	3.80	4.31	0.65	7.24	1.14	25.6	13.0	3.89
13/02/2024	**ACP6**	FLF186	167	106	34.9	325	16.5	857	32.8	71.9	8.38	33.8	6.96	1.46	5.84	6.51	3.54	4.05	0.67	9.04	1.17	23.8	15.5	4.58
13/02/2024	**ACP6**	FLF186	143	213	34.0	273	16.0	787	31.4	68.0	8.02	34.2	8.05	1.48	6.46	6.24	4.02	3.92	0.58	7.29	1.12	22.8	13.0	3.67
13/02/2024	**ACP6**	FLF186	157	175	36.8	326	17.7	828	34.3	75.5	8.78	36.1	7.75	1.43	6.82	6.81	4.11	4.11	0.59	8.65	1.25	25.5	16.1	4.33
13/02/2024	**ACP6**	FLF186	169	94.9	35.6	319	16.3	813	33.4	72.2	8.29	34.5	7.52	1.17	6.02	6.74	3.75	4.56	0.64	8.72	1.19	24.6	16.0	4.57
13/02/2024	**ACP6**	FLF186	145	191	36.4	284	17.2	805	32.9	72.0	8.49	36.6	7.60	1.55	7.53	6.80	3.80	4.36	0.62	7.44	1.19	22.1	13.6	3.95
13/02/2024	**ACP6**	FLF186	167	105	35.9	315	16.4	804	33.2	71.8	8.84	33.4	6.85	1.24	6.38	6.23	3.97	4.22	0.65	8.16	1.22	24.2	16.0	4.57
13/02/2024	**ACP6**	FLF186	175	72.6	35.9	310	16.6	755	33.3	74.0	8.38	34.4	7.19	1.23	5.99	6.09	4.30	4.53	0.64	8.83	1.28	24.9	16.8	4.99
13/02/2024	**ACP6**	FLF186	172	68.1	32.6	281	15.8	702	29.7	64.9	7.73	29.3	6.46	0.96	5.42	5.86	3.21	4.67	0.59	7.93	1.02	23.5	13.1	3.98
13/02/2024	**ACP6**	FLF186	165	115	35.1	316	16.2	817	33.0	72.5	8.68	33.9	7.12	1.14	6.20	6.09	3.97	4.11	0.63	7.99	1.18	24.1	15.0	4.49
13/02/2024	**ACP6**	FLF186	172	86.0	36.9	351	18.8	786	34.9	78.6	9.11	35.7	7.09	1.27	6.14	6.73	4.60	4.65	0.70	10.43	1.40	29.5	18.5	5.09
13/02/2024	**ACP6**	FLF186	167	65.4	35.4	303	16.5	707	32.4	71.3	8.34	32.8	8.00	1.04	5.80	6.21	3.85	4.22	0.64	8.38	1.19	23.4	16.3	4.74
19/12/2023	**YmP5**	P-B4	143	418	31.1	242	13.0	735	29.1	63.9	7.70	32.5	7.36	1.75	6.14	5.48	3.70	3.56	0.53	6.57	0.92	19.8	13.0	3.82
19/12/2023	**YmP5**	P-B4	140	394	30.7	234	12.6	714	29.1	65.3	7.61	32.9	7.33	1.73	5.52	5.84	3.40	3.68	0.47	6.39	0.94	26.3	13.4	4.01
19/12/2023	**YmP5**	P-B4	141	398	30.5	235	13.1	712	28.5	65.9	7.39	32.6	7.52	1.75	4.93	6.21	3.72	2.77	0.50	6.90	0.90	20.7	12.8	3.75
19/12/2023	**YmP5**	P-B4	131	547	25.6	200	11.1	695	26.6	56.7	6.73	28.3	6.36	1.53	4.72	4.54	2.99	2.83	0.39	5.20	0.80	19.3	10.9	3.29
19/12/2023	**YmP5**	P-B4	132	463	31.1	237	12.8	727	28.9	63.9	7.75	32.7	7.03	1.60	6.16	5.65	3.22	3.74	0.51	6.42	0.90	19.1	13.1	3.69
19/12/2023	**YmP5**	P-B4	137	411	31.1	230	12.4	704	28.0	60.8	7.55	30.6	6.50	1.41	5.71	5.64	2.97	2.71	0.44	5.66	0.85	19.3	12.3	3.42

Date of Analysis	Sample	Label	Rb	Sr	Y	Zr	Nb	Ba	La	Ce	Pr	Nd	Sm	Eu	Gd	Dy	Er	Yb	Lu	Hf	Ta	Pb	Th	U
19/12/2023	**YmP5**	P-B4	145	429	32.0	249	13.1	770	29.9	65.2	7.97	34.1	7.13	1.55	6.06	5.80	3.28	3.52	0.57	5.83	0.95	21.6	13.1	3.81
19/12/2023	**YmP5**	P-B4	145	441	30.1	234	13.3	748	28.9	61.3	7.79	32.2	6.93	1.73	7.46	4.73	3.35	3.42	0.48	6.19	0.85	20.3	12.2	3.61
19/12/2023	**YmP5**	P-B4	146	411	31.6	249	13.4	781	30.5	65.6	8.03	34.2	7.25	1.47	6.38	5.84	3.68	3.58	0.55	6.15	0.96	21.1	12.9	3.84
19/12/2023	**YmP5**	P-B4	128	667	28.0	215	11.3	758	26.9	60.0	6.53	30.0	6.95	1.97	5.84	4.75	2.87	3.32	0.50	6.01	0.88	19.2	11.3	3.65
19/12/2023	**YmP5**	P-B4	147	431	31.5	241	12.9	767	30.7	67.3	9.15	32.0	6.85	1.77	6.68	5.71	3.62	3.67	0.52	6.62	0.95	21.9	13.5	3.80
19/12/2023	**YmP6**	P-B5/4	123	486	31.4	198	10.6	601	26.7	61.1	7.48	32.6	7.68	1.72	6.35	5.84	3.19	3.58	0.45	5.62	0.75	19.8	10.8	3.18
19/12/2023	**YmP6**	P-B5/4	94	585	24.9	152	8.64	508	22.1	45.6	5.90	25.1	5.50	1.63	5.31	4.59	2.65	2.93	0.39	3.89	0.57	14.1	8.2	2.19
19/12/2023	**YmP6**	P-B5/4	114	538	28.3	186	10.0	599	26.3	58.1	7.24	30.8	7.03	1.65	5.83	5.18	3.10	2.75	0.49	5.36	0.71	17.4	10.6	3.17
19/12/2023	**YmP6**	P-B5/4	152	161	15.9	155	9.82	498	19.1	39.9	4.36	16.5	3.23	0.60	2.95	2.79	1.70	1.96	0.30	4.47	0.94	17.8	12.4	4.51
19/12/2023	**YmP6**	P-B5/4	169	195	24.3	240	13.1	656	26.5	57.5	6.50	24.9	5.37	0.94	4.29	4.18	2.73	2.70	0.39	6.54	1.05	20.9	15.4	4.92
19/12/2023	**YmP6**	P-B5/4	121	360	34.3	209	10.6	604	27.8	61.0	7.67	34.5	7.97	1.87	6.41	5.98	3.86	3.55	0.53	5.41	0.77	17.5	11.0	3.24
19/12/2023	**YmP6**	P-B5/4	153	164	16.5	162	10.1	502	19.7	40.9	4.33	17.6	3.77	0.56	3.03	3.01	1.67	1.75	0.26	4.76	1.00	19.2	12.9	4.80
19/12/2023	**YmP6**	P-B5/4	114	537	27.2	190	9.71	613	24.8	55.9	6.70	28.5	6.38	1.64	5.57	4.85	2.98	2.96	0.40	5.11	0.73	15.8	9.9	2.72
19/12/2023	**YmP6**	P-B5/4	113	548	28.8	187	10.0	620	26.3	58.8	6.99	32.0	6.90	1.67	5.81	5.21	3.22	2.97	0.48	5.14	0.73	16.9	10.5	3.21
19/12/2023	**YmP6**	P-B5/4	111	562	28.2	179	9.64	587	25.2	57.7	6.86	31.1	6.79	1.66	5.38	5.35	3.00	2.92	0.44	4.99	0.69	16.2	10.0	2.83
19/12/2023	**YmP6**	P-B5/4	117	536	28.8	191	10.4	619	26.3	60.0	7.21	30.9	7.01	1.68	5.80	5.38	3.24	2.90	0.47	5.51	0.72	17.1	11.5	3.18
19/12/2023	**YmP7**	P-B5	116	535	29.5	205	10.5	622	28.2	62.4	7.39	32.6	7.89	1.73	6.13	5.84	2.99	2.99	0.53	5.52	0.77	16.7	11.4	3.47
19/12/2023	**YmP7**	P-B5	116	478	25.5	173	9.57	581	23.5	54.1	6.56	32.0	6.23	1.57	4.98	4.90	3.16	3.15	0.43	4.13	0.64	15.3	9.0	2.71
19/12/2023	**YmP7**	P-B5	105	498	25.7	162	8.89	555	22.3	51.6	5.26	28.0	7.89	1.69	5.75	3.54	2.55	2.97	0.32	4.02	0.58	12.7	7.0	2.63
19/12/2023	**YmP7**	P-B5	108	506	29.9	195	10.0	622	26.9	60.5	7.00	33.5	8.26	1.97	6.24	6.15	3.42	3.28	0.53	4.85	0.69	16.7	10.7	3.28
19/12/2023	**YmP7**	P-B5	110	564	29.1	191	9.48	596	26.2	72.3	7.17	32.7	7.38	1.80	5.11	5.81	2.61	3.37	0.45	4.93	0.70	16.3	10.3	3.08
19/12/2023	**YmP7**	P-B5	112	547	28.7	194	10.0	604	26.3	57.8	7.40	33.3	7.48	1.77	6.19	5.12	3.14	3.43	0.44	5.40	0.72	15.7	10.9	2.97
19/12/2023	**YmP7**	P-B5	118	514	28.9	206	10.7	650	27.1	59.6	7.42	31.5	6.64	1.71	6.09	5.16	3.15	3.05	0.46	5.36	0.77	16.8	10.7	3.18
19/12/2023	**YmP7**	P-B5	114	488	24.5	169	9.19	546	22.6	52.5	6.12	26.0	6.80	1.83	5.12	4.42	2.50	2.66	0.38	4.08	0.65	17.9	9.2	3.01
19/12/2023	**YmP7**	P-B5	113	544	28.6	198	10.1	624	26.5	60.8	7.45	31.1	7.35	1.77	6.57	5.89	3.02	3.11	0.45	4.84	0.75	16.6	10.3	3.15
19/12/2023	**YmP7**	P-B5	114	551	30.6	206	10.6	665	27.8	64.7	7.95	34.2	7.75	2.17	6.98	5.93	3.09	3.55	0.47	5.44	0.79	17.6	11.6	3.37
19/12/2023	**YmP7**	P-B5	84	925	23.3	155	8.18	547	21.5	48.0	5.93	29.1	5.51	1.83	4.66	4.87	2.57	2.65	0.37	3.86	0.58	12.9	8.2	2.54
19/12/2023	**YmP8**	P-B6	160	373	29.6	299	16.2	941	29.6	60.2	7.68	33.5	8.08	1.75	5.69	5.93	3.43	3.52	0.44	8.19	1.26	23.6	17.5	4.14
19/12/2023	**YmP8**	P-B6	165	349	29.8	270	14.9	869	30.8	64.6	8.35	32.4	6.98	1.56	5.33	4.56	3.32	3.40	0.49	6.20	1.08	22.2	15.1	4.47
19/12/2023	**YmP8**	P-B6	165	350	31.1	287	15.4	844	32.0	63.2	7.90	33.4	7.10	1.68	5.20	5.84	3.32	2.91	0.57	5.69	1.03	22.2	14.1	4.63
19/12/2023	**YmP8**	P-B6	165	354	31.3	281	14.8	824	32.4	71.1	8.15	33.1	7.80	1.59	5.85	5.93	3.54	3.12	0.50	7.19	1.12	23.3	16.0	4.73
19/12/2023	**YmP8**	P-B6	168	335	30.2	265	14.3	762	30.0	64.7	7.97	31.1	6.63	1.28	6.73	5.45	3.24	3.78	0.43	6.67	0.93	22.3	13.6	4.04
19/12/2023	**YmP8**	P-B6	164	355	32.0	285	15.1	840	32.7	69.9	8.04	34.9	7.42	1.43	6.14	5.13	3.58	3.94	0.52	7.36	1.10	23.3	16.2	4.87
19/12/2023	**YmP8**	P-B6	159	370	29.8	298	15.2	919	31.5	84.1	7.76	32.6	8.69	1.43	5.17	5.27	3.52	4.61	0.48	6.01	1.06	23.7	13.6	4.27
19/12/2023	**YmP8**	P-B6	170	363	32.6	299	15.4	856	32.9	71.5	8.17	32.9	6.79	1.54	6.39	5.54	3.61	3.72	0.52	7.20	1.14	23.2	16.9	4.73
19/12/2023	**YmP8**	P-B6	164	351	33.7	283	14.6	829	32.4	70.4	8.02	33.4	8.82	1.69	6.13	5.90	3.87	3.89	0.52	6.87	1.03	21.2	15.0	4.39
19/12/2023	**YmP8**	P-B6	170	364	31.9	295	15.3	836	33.8	71.5	8.22	34.2	7.47	1.67	5.84	5.45	4.43	3.48	0.50	7.96	1.11	24.9	16.6	4.86
13/02/2024	**Aso-4X**	FLF195	170	148	34.1	310	16.1	813	34.8	75.6	8.56	34.6	7.42	1.42	6.74	5.47	3.60	4.18	0.61	7.69	1.20	24.0	16.7	4.80
13/02/2024	**Aso-4X**	FLF195	166	145	34.1	306	16.2	810	34.8	74.8	8.76	35.5	7.76	1.24	6.15	6.03	3.72	3.96	0.59	7.93	1.20	23.8	16.4	4.77
13/02/2024	**Aso-4X**	FLF195	165	152	34.5	309	16.3	822	35.0	74.0	8.85	35.8	6.96	1.37	6.98	6.54	3.36	4.19	0.62	8.06	1.16	22.1	16.7	4.60
13/02/2024	**Aso-4X**	FLF195	162	143	33.2	302	16.0	804	32.7	71.7	8.23	32.2	6.86	1.33	6.18	5.50	3.62	3.83	0.62	7.66	1.15	23.6	15.7	4.87
13/02/2024	**Aso-4X**	FLF195	169	132	34.4	313	16.0	808	35.3	75.4	8.49	36.6	6.61	1.19	6.57	5.94	3.52	4.34	0.58	8.05	1.23	24.5	16.8	4.75
13/02/2024	**Aso-4X**	FLF195	164	162	33.2	289	15.7	825	33.5	71.4	8.22	35.1	6.66	1.33	5.84	5.61	3.62	3.52	0.58	8.04	1.15	22.6	16.0	4.76

Date of Analysis	Sample	Label	Rb	Sr	Y	Zr	Nb	Ba	La	Ce	Pr	Nd	Sm	Eu	Gd	Dy	Er	Yb	Lu	Hf	Ta	Pb	Th	U
13/02/2024	**Aso-4X**	FLF195	168	137	34.7	304	16.1	792	34.1	75.2	8.68	36.5	7.36	1.42	6.58	6.19	3.91	4.05	0.59	7.86	1.22	22.9	16.7	4.87
13/02/2024	**Aso-4X**	FLF195	165	144	31.5	277	15.4	807	32.4	70.5	8.37	33.0	6.65	1.18	5.77	6.09	3.10	4.22	0.61	7.19	1.13	22.4	15.8	4.78
13/02/2024	**Aso-4X**	FLF195	165	158	33.9	302	16.5	815	34.7	70.7	8.62	35.8	6.81	1.22	5.59	5.83	3.79	4.15	0.60	8.31	1.21	24.1	17.3	4.71
13/02/2024	**Aso-4X**	FLF195	172	144	33.8	305	16.7	798	35.2	74.7	8.50	35.8	8.07	1.30	5.82	5.64	3.45	4.18	0.60	7.27	1.21	24.9	16.9	4.93
13/02/2024	**Aso-4X**	FLF195	163	183	32.6	292	15.6	832	34.5	73.0	8.29	34.9	6.70	1.40	5.66	5.64	3.79	4.20	0.61	7.78	1.17	24.3	17.1	5.12
13/02/2024	**Aso-4X**	FLF195	174	108	35.3	318	16.7	769	36.2	78.6	9.12	35.7	7.39	1.35	6.27	6.64	3.81	4.51	0.65	8.69	1.26	25.0	17.5	5.12
13/02/2024	**Aso-4X**	FLF194	164	144	34.0	304	15.8	793	33.4	74.6	8.90	35.7	7.56	1.22	5.39	6.02	3.56	4.03	0.62	7.99	1.18	23.5	16.4	4.68
13/02/2024	**Aso-4X**	FLF194	167	145	34.3	311	16.5	800	34.4	75.9	8.97	35.1	7.42	1.20	5.85	5.74	3.91	3.77	0.61	8.31	1.18	23.8	17.0	4.93
13/02/2024	**Aso-4X**	FLF194	169	138	32.0	297	15.4	773	32.9	71.5	8.39	35.2	6.63	1.34	5.44	5.34	3.31	3.65	0.59	7.83	1.16	25.6	16.1	4.80
13/02/2024	**Aso-4X**	FLF194	178	170	31.4	283	18.3	797	31.1	64.1	8.21	33.1	6.50	1.28	5.76	5.13	3.82	3.88	0.50	6.92	1.12	23.0	14.3	4.62
13/02/2024	**Aso-4X**	FLF194	166	151	32.8	301	16.1	787	33.4	70.6	8.46	35.3	6.78	1.34	5.97	5.88	3.34	3.58	0.51	6.94	1.15	23.9	15.2	4.89
13/02/2024	**Aso-4X**	FLF194	167	146	33.7	302	15.9	800	34.3	74.6	8.86	35.7	7.40	1.31	6.24	5.67	3.54	3.75	0.63	7.45	1.17	24.3	16.4	4.83
13/02/2024	**Aso-4X**	FLF194	165	167	33.6	306	15.9	827	34.1	74.6	8.51	35.3	7.10	1.25	5.78	6.35	3.60	3.92	0.56	7.86	1.19	25.2	16.6	4.82
13/02/2024	**Aso-4X**	FLF194	156	181	34.2	304	16.1	829	34.3	73.9	8.79	36.3	6.87	1.44	6.15	6.02	3.57	4.07	0.61	8.00	1.16	22.6	16.4	5.01
13/02/2024	**Aso-4X**	FLF194	161	195	33.8	302	15.9	850	34.9	73.6	8.78	35.3	6.72	1.46	6.23	6.17	3.44	3.72	0.57	7.76	1.18	23.3	16.1	4.57
14/11/2023	**Aso-4X**	FLF150	172	155	36.2	331	17.0	859	37.0	77.1	9.11	35.7	7.50	1.45	6.17	6.32	3.87	4.14	0.70	8.63	1.30	25.1	17.2	5.37
14/11/2023	**Aso-4X**	FLF150	175	133	34.5	310	16.4	795	35.2	75.8	9.13	35.7	7.50	1.09	5.75	6.55	3.81	4.09	0.58	8.77	1.20	24.2	17.0	5.15
14/11/2023	**Aso-4X**	FLF150	174	138	30.9	279	15.4	741	31.8	71.3	8.15	33.4	6.54	1.21	6.12	5.61	3.30	3.52	0.50	7.74	1.11	24.4	14.8	4.46
14/11/2023	**Aso-4X**	FLF150	173	158	36.8	325	17.4	837	37.0	75.7	9.13	38.9	7.52	1.59	6.61	6.37	4.05	4.56	0.58	8.54	1.25	26.2	17.8	4.76
14/11/2023	**Aso-4X**	FLF150	178	134	31.0	277	15.9	751	31.8	66.5	8.28	30.4	5.82	1.27	5.54	5.45	2.94	3.66	0.49	7.14	1.06	23.3	13.7	4.05
14/11/2023	**Aso-4X**	FLF150	172	139	34.2	317	16.6	787	35.0	76.1	8.92	34.9	7.24	1.24	6.65	5.63	3.89	3.84	0.58	8.76	1.22	24.0	17.3	5.13
14/11/2023	**Aso-4X**	FLF150	170	134	34.7	305	16.0	788	35.8	75.7	8.84	37.0	7.65	1.36	5.96	5.93	3.50	3.88	0.68	8.38	1.24	23.4	17.4	4.97
14/11/2023	**Aso-4X**	FLF150	170	146	33.3	295	16.1	796	33.9	75.2	8.57	35.2	7.32	1.13	6.64	5.53	3.59	4.34	0.61	8.03	1.19	24.1	16.6	4.91
14/11/2023	**Aso-4X**	FLF150	178	137	31.5	273	15.4	775	32.2	70.2	8.17	32.8	6.23	1.17	6.06	5.05	3.51	3.29	0.51	8.18	1.05	24.6	14.2	4.58
14/11/2023	**Aso-4X**	FLF150	168	146	33.6	296	16.2	805	34.0	74.4	8.61	36.2	7.31	1.19	6.51	5.76	3.82	3.99	0.57	8.36	1.19	24.8	16.5	4.97
14/11/2023	**Aso-4X**	FLF150	169	150	34.6	309	16.2	807	35.3	76.0	8.64	37.0	7.21	1.25	5.85	6.10	3.52	4.17	0.64	8.16	1.21	23.4	16.5	4.92
14/11/2023	**Aso-4X**	FLF150	169	137	32.8	280	14.9	772	31.8	70.6	7.92	34.1	6.80	1.51	5.76	6.25	3.36	3.97	0.53	8.52	0.98	21.6	13.2	4.70
14/11/2023	**Aso-4X**	FLF150	175	148	34.5	291	16.1	831	34.4	72.2	9.00	37.3	7.62	1.27	6.25	6.02	3.71	4.76	0.54	6.92	1.13	22.8	15.0	4.89
03/07/2023	**Aso-Y**	FLF66	176	155	34.2	305	16.6	794	36.0	78.8	8.78	35.5	7.39	1.15	6.32	5.91	3.54	4.05	0.67	8.27	1.21	24.0	16.9	4.96
03/07/2023	**Aso-Y**	FLF66	170	138	34.6	302	15.9	785	35.8	76.6	8.71	35.2	7.69	1.26	6.29	5.66	3.52	3.50	0.69	8.39	1.20	24.1	17.1	5.59
03/07/2023	**Aso-Y**	FLF66	170	147	33.8	296	16.0	776	35.0	75.4	8.45	33.9	7.74	1.38	6.01	6.19	3.55	4.03	0.62	7.59	1.22	23.9	16.1	4.96
03/07/2023	**Aso-Y**	FLF66	173	143	34.8	309	16.4	795	35.8	77.9	9.00	35.1	7.83	1.24	5.88	6.00	3.72	4.47	0.62	7.92	1.20	24.8	17.3	4.96
03/07/2023	**Aso-Y**	FLF66	177	119	33.1	298	16.3	753	33.4	72.3	8.59	31.8	7.30	1.19	6.04	5.44	3.79	3.91	0.63	7.89	1.17	24.1	16.8	4.83
03/07/2023	**Aso-Y**	FLF66	164	106	28.5	256	14.0	650	29.1	63.4	7.50	28.3	5.31	0.97	4.66	5.21	3.49	3.31	0.48	6.77	0.90	20.2	13.8	4.36
03/07/2023	**Aso-Y**	FLF66	162	150	32.4	277	14.7	736	31.7	66.6	8.21	30.6	6.96	1.26	5.50	5.08	3.46	3.63	0.53	7.79	1.01	21.7	13.7	4.09
03/07/2023	**Aso-Y**	FLF66	174	128	35.1	302	16.2	785	33.9	73.9	8.52	36.9	6.94	1.10	6.22	6.54	3.81	3.66	0.63	8.21	1.16	22.6	16.8	5.03
03/07/2023	**Aso-Y**	FLF66	172	138	34.4	301	16.2	780	34.4	75.5	8.72	36.2	6.55	1.39	6.21	5.97	3.86	3.72	0.58	7.66	1.13	23.1	16.9	4.90
03/07/2023	**Aso-E**	FLF74	178	190	34.8	285	16.6	847	34.6	74.6	8.73	36.7	7.71	1.24	6.14	6.17	4.27	3.78	0.56	7.93	1.20	22.6	16.5	4.93
03/07/2023	**Aso-E**	FLF74	171	194	35.3	299	16.9	872	35.2	77.9	9.16	37.0	7.93	1.39	6.66	6.33	3.74	4.32	0.61	7.95	1.21	23.4	16.8	4.82
03/07/2023	**Aso-E**	FLF74	169	192	35.6	298	16.4	853	35.2	76.9	8.52	38.2	7.98	1.49	6.32	6.19	3.91	3.96	0.60	7.69	1.18	23.4	17.2	4.88
03/07/2023	**Aso-E**	FLF74	169	181	33.9	288	15.9	840	33.9	70.6	8.49	35.2	7.46	1.34	6.02	5.53	3.45	3.64	0.57	7.93	1.19	23.4	15.6	4.74
03/07/2023	**Aso-E**	FLF74	161	179	34.2	288	17.0	870	33.1	68.0	8.34	34.8	7.76	1.46	5.88	6.33	3.81	3.83	0.55	7.62	1.20	24.3	15.7	4.57
03/07/2023	**Aso-E**	FLF74	171	190	35.6	292	16.5	844	35.5	76.2	8.96	35.8	7.93	1.50	6.17	6.63	4.21	4.19	0.58	8.22	1.21	22.8	15.8	4.77

Date of Analysis	Sample	Label	Rb	Sr	Y	Zr	Nb	Ba	La	Ce	Pr	Nd	Sm	Eu	Gd	Dy	Er	Yb	Lu	Hf	Ta	Pb	Th	U
03/07/2023	**Aso-E**	FLF74	161	183	35.3	308	17.3	882	33.9	73.8	9.17	35.6	8.35	1.28	6.85	6.29	4.12	4.18	0.63	7.70	1.23	23.9	17.8	4.67
03/07/2023	**Aso-E**	FLF74	173	196	35.8	299	16.8	890	35.2	76.8	9.21	37.6	7.82	1.71	6.59	6.31	4.08	3.93	0.61	8.11	1.21	23.9	17.0	4.84
03/07/2023	**Aso-E**	FLF74	166	192	36.0	292	16.4	875	34.1	74.5	8.67	36.7	7.91	1.58	6.24	6.59	3.70	3.89	0.63	7.92	1.18	23.5	16.0	5.08
03/07/2023	**Aso-E**	FLF74	177	202	37.1	313	17.5	938	37.3	81.3	9.67	39.1	9.02	1.64	6.99	6.31	4.35	4.11	0.71	8.39	1.27	26.2	18.0	4.88
03/07/2023	**Aso-E**	FLF74	172	195	35.5	303	16.6	878	36.0	77.5	9.00	38.2	8.05	1.50	6.32	6.55	3.96	4.12	0.57	8.36	1.19	23.9	16.2	4.87
03/07/2023	**Aso-E**	FLF74	172	196	37.2	307	17.3	904	36.8	77.6	9.38	37.1	8.32	1.54	6.22	6.59	4.36	4.27	0.63	7.82	1.26	23.4	18.3	5.11
03/07/2023	**Aso-F**	FLF73	181	199	33.0	319	16.9	895	36.6	77.0	8.77	35.6	7.38	1.39	5.91	5.93	3.34	3.35	0.61	8.46	1.26	24.8	18.0	5.00
03/07/2023	**Aso-F**	FLF73	185	225	33.3	313	17.1	913	37.3	80.1	9.16	37.7	7.57	1.45	5.62	6.03	3.60	3.62	0.59	8.49	1.27	24.2	18.4	5.20
03/07/2023	**Aso-F**	FLF73	238	166	35.2	380	21.3	929	41.5	87.7	10.01	38.6	8.05	1.10	6.39	6.34	3.90	4.06	0.63	10.33	1.61	29.5	24.0	7.07
03/07/2023	**Aso-F**	FLF73	240	179	34.8	384	21.4	911	41.0	86.7	9.83	38.7	8.82	1.28	6.60	6.52	4.01	4.00	0.62	10.45	1.63	29.3	23.9	6.62
03/07/2023	**Aso-F**	FLF73	186	184	33.2	329	17.2	847	37.0	80.6	9.18	36.7	7.70	1.32	6.23	5.72	3.82	3.80	0.60	8.99	1.33	25.4	18.5	5.33
03/07/2023	**Aso-F**	FLF73	190	247	33.6	308	18.3	867	36.9	79.6	9.01	35.7	7.51	1.58	6.88	5.78	3.88	3.62	0.57	7.90	1.27	25.2	17.5	4.94
03/07/2023	**Aso-F**	FLF73	184	178	30.9	311	16.8	803	35.2	75.5	8.50	33.6	6.43	1.21	5.42	5.41	3.29	4.31	0.57	8.01	1.22	26.0	17.7	5.52
03/07/2023	**Aso-F**	FLF73	182	219	31.8	309	16.8	863	35.6	76.7	8.83	33.3	7.70	1.38	5.85	5.67	3.68	3.66	0.56	8.28	1.18	24.2	16.9	4.84
03/07/2023	**Aso-F**	FLF73	183	204	31.3	308	16.4	835	34.3	73.3	8.17	33.9	6.63	1.37	5.55	5.46	3.54	4.03	0.55	8.30	1.22	23.1	16.3	4.95
03/07/2023	**Aso-F**	FLF73	245	152	34.1	389	20.5	877	40.2	86.1	9.62	36.6	7.42	1.16	6.86	5.95	4.11	3.87	0.60	10.59	1.56	29.4	24.2	7.07
03/07/2023	**Aso-F**	FLF73	164	214	29.3	262	15.2	744	31.0	66.1	7.74	32.1	6.82	1.28	5.88	5.77	3.00	3.39	0.49	6.75	1.04	20.9	13.8	4.07
03/07/2023	**Aso-F**	FLF73	186	197	32.3	324	16.9	850	36.1	78.2	8.88	33.9	7.30	1.44	5.79	5.78	3.51	3.65	0.53	8.23	1.23	24.6	17.6	5.24
03/07/2023	**Aso-F**	FLF73	179	199	32.2	317	16.6	841	36.0	76.2	8.78	35.0	6.89	1.31	5.76	5.57	3.39	3.82	0.58	8.61	1.23	25.2	17.2	4.89
23/11/2023	**Aso-G**	FLF229	171	216	33.2	297	16.7	815	34.7	76.7	8.63	35.5	8.07	1.33	6.22	5.97	3.70	3.70	0.58	7.73	1.20	23.5	16.2	4.77
23/11/2023	**Aso-G**	FLF229	172	206	30.3	272	16.1	791	31.6	69.8	8.09	34.7	7.03	1.26	5.19	5.71	3.53	3.59	0.51	6.50	1.08	23.6	13.9	4.47
23/11/2023	**Aso-G**	FLF229	177	218	33.0	289	16.6	817	34.1	74.5	8.41	36.6	7.23	1.39	6.16	5.98	3.37	3.38	0.50	7.47	1.19	22.4	16.1	4.69
23/11/2023	**Aso-G**	FLF229	146	420	26.6	232	13.5	763	29.9	64.3	7.14	29.7	6.22	1.42	4.66	4.80	2.78	3.04	0.44	5.85	0.95	18.5	12.1	3.56
23/11/2023	**Aso-G**	FLF229	167	217	33.5	304	16.6	821	34.7	76.8	8.44	35.0	8.17	1.33	6.38	5.64	3.28	4.05	0.59	8.06	1.20	23.7	16.6	4.93
23/11/2023	**Aso-H**	FLF219	171	252	33.5	301	17.2	827	35.6	78.6	8.71	37.4	7.64	1.54	6.51	6.56	3.83	3.77	0.55	8.01	1.22	23.8	16.5	4.75
23/11/2023	**Aso-H**	FLF219	173	242	33.3	304	17.1	817	35.1	76.7	8.78	36.4	7.41	1.55	6.49	6.14	3.41	3.82	0.58	8.04	1.25	23.8	16.4	4.93
23/11/2023	**Aso-H**	FLF219	165	253	33.7	296	17.3	793	36.2	78.0	9.28	37.3	7.22	1.53	7.10	6.36	3.47	3.95	0.59	7.90	1.22	22.3	16.4	4.78
23/11/2023	**Aso-H**	FLF219	178	241	33.2	297	16.8	811	35.6	76.7	8.68	37.7	7.70	1.54	6.73	6.05	3.76	4.24	0.53	8.05	1.21	23.1	15.9	4.74
23/11/2023	**Aso-H**	FLF219	162	247	33.7	301	16.9	841	35.1	75.2	8.76	35.8	7.78	1.37	6.71	6.05	3.96	3.88	0.58	8.30	1.24	22.5	15.7	4.66
23/11/2023	**Aso-H**	FLF219	171	238	32.6	300	17.0	813	35.3	76.1	8.88	36.4	7.69	1.44	5.97	6.25	3.67	4.01	0.57	8.09	1.25	24.0	16.6	4.66
23/11/2023	**Aso-H**	FLF219	131	589	25.6	233	13.3	771	28.9	59.0	7.06	28.8	5.72	1.70	4.96	4.25	2.67	2.47	0.44	6.41	0.94	19.0	12.2	3.66
23/11/2023	**Aso-H**	FLF219	172	236	33.1	304	17.3	830	35.1	78.2	8.81	38.0	7.62	1.48	6.51	5.89	3.60	3.83	0.58	7.42	1.25	24.5	16.7	4.95
23/11/2023	**Aso-H**	FLF217	166	248	32.5	286	16.6	795	34.0	73.9	8.57	36.8	6.93	1.39	5.80	5.41	3.35	3.57	0.52	7.15	1.14	22.5	15.2	4.71
23/11/2023	**Aso-H**	FLF217	168	247	32.4	293	16.6	818	34.7	75.3	8.46	35.8	7.89	1.43	6.06	6.10	3.51	3.79	0.56	7.51	1.21	23.4	16.3	4.88
23/11/2023	**Aso-H**	FLF217	170	241	32.9	294	16.6	810	34.6	74.9	8.88	36.5	7.91	1.30	6.58	6.01	3.59	3.85	0.56	7.98	1.21	22.6	16.0	4.75
23/11/2023	**Aso-H**	FLF217	171	230	31.6	288	16.7	778	33.6	72.8	8.40	35.2	6.89	1.31	5.88	5.24	3.52	3.48	0.55	7.92	1.20	23.4	15.4	4.70
23/11/2023	**Aso-H**	FLF217	168	246	32.6	293	16.7	815	34.6	74.4	8.66	36.3	7.51	1.38	6.06	5.54	3.50	3.51	0.55	7.99	1.21	22.8	16.1	4.61
23/11/2023	**Aso-H**	FLF217	168	250	33.2	296	16.6	827	34.8	76.0	8.76	36.6	8.09	1.57	6.08	5.71	3.43	3.97	0.59	7.98	1.21	22.7	16.0	4.72
23/11/2023	**Aso-H**	FLF217	167	252	32.8	294	16.5	809	34.0	74.1	8.52	35.9	7.29	1.32	6.04	6.23	3.65	3.79	0.51	8.09	1.23	24.4	15.7	4.72
23/11/2023	**Aso-H**	FLF217	167	233	32.3	293	16.5	803	34.2	74.2	8.66	35.9	8.10	1.39	6.72	6.01	3.95	3.85	0.54	8.06	1.21	22.7	15.9	4.66
23/11/2023	**Aso-H**	FLF213	169	222	30.1	272	15.9	761	31.7	70.0	7.87	32.1	6.61	1.25	5.43	5.25	3.11	3.37	0.52	7.13	1.11	24.7	14.9	4.71
23/11/2023	**Aso-H**	FLF213	160	286	31.3	274	15.7	785	32.8	73.1	8.32	34.0	7.29	1.35	5.82	5.55	3.81	3.57	0.53	7.44	1.11	24.4	14.8	4.48

Date of Analysis	Sample	Label	Rb	Sr	Y	Zr	Nb	Ba	La	Ce	Pr	Nd	Sm	Eu	Gd	Dy	Er	Yb	Lu	Hf	Ta	Pb	Th	U
23/11/2023	**Aso-H**	FLF213	172	245	31.2	277	16.4	810	33.0	71.5	8.47	33.5	7.15	1.33	5.94	5.35	3.19	3.77	0.50	7.33	1.15	22.9	15.4	6.79
23/11/2023	**Aso-H**	FLF213	165	264	32.2	278	16.4	804	34.0	74.8	8.36	34.9	7.54	1.54	5.95	5.68	3.56	3.79	0.52	7.68	1.15	22.3	15.2	4.57
23/11/2023	**Aso-H**	FLF213	172	215	31.9	287	16.9	825	34.4	74.3	8.39	34.8	6.62	1.36	5.33	4.85	3.36	3.80	0.49	7.46	1.15	23.8	15.2	4.44
23/11/2023	**Aso-H**	FLF213	164	241	31.5	278	16.5	789	33.6	71.6	8.27	34.8	7.47	1.28	5.89	5.73	3.21	3.41	0.50	7.78	1.17	22.7	15.5	4.70
23/11/2023	**Aso-H**	FLF213	151	365	25.4	251	13.3	832	31.6	64.8	7.13	28.6	6.65	1.45	4.39	4.63	2.64	2.59	0.48	6.51	0.97	20.5	13.9	4.46
23/11/2023	**Aso-H**	FLF213	169	225	31.0	279	16.3	768	32.5	72.0	8.08	34.1	7.04	1.43	5.33	5.42	3.29	3.57	0.57	7.52	1.18	22.3	15.3	4.87
23/11/2023	**Aso-H**	FLF213	159	268	31.3	270	15.7	771	32.3	71.9	8.28	33.7	7.25	1.51	6.33	5.71	3.78	3.35	0.51	7.75	1.12	22.9	14.9	4.53
23/11/2023	**Aso-H**	FLF213	167	236	31.5	282	16.4	786	33.6	71.8	8.49	35.4	7.62	1.41	5.75	5.87	3.39	3.71	0.60	7.40	1.17	22.6	15.4	4.69
23/11/2023	**Aso-H**	FLF213	169	224	29.2	255	15.2	761	30.0	68.0	8.07	33.3	7.09	1.37	5.41	5.28	3.09	3.17	0.43	6.51	0.96	20.7	13.3	4.17
23/11/2023	**Aso-H**	FLF213	167	228	31.1	279	16.3	784	33.1	72.0	8.33	34.0	6.87	1.23	5.77	5.34	3.42	3.23	0.51	7.20	1.16	23.2	15.0	4.63
23/11/2023	**Aso-H**	FLF208	161	282	31.5	266	15.8	777	33.0	70.6	8.33	35.1	7.59	1.41	5.79	5.42	3.56	3.44	0.50	6.97	1.10	21.0	13.7	4.53
23/11/2023	**Aso-H**	FLF208	159	284	31.6	271	16.0	786	32.9	72.4	8.29	34.5	7.12	1.37	5.58	5.61	3.47	3.40	0.56	7.21	1.10	21.9	14.7	4.39
23/11/2023	**Aso-H**	FLF208	175	259	26.4	230	14.8	784	29.5	63.7	7.62	32.5	6.93	1.51	4.73	4.33	2.98	3.99	0.55	5.96	0.92	19.2	11.7	4.04
23/11/2023	**Aso-H**	FLF208	168	290	31.3	266	15.9	802	32.3	71.4	8.29	31.6	7.08	1.57	5.40	5.99	3.48	3.23	0.55	7.24	1.07	21.8	13.4	4.29
23/11/2023	**Aso-H**	FLF208	165	293	32.6	281	16.3	839	34.3	74.1	8.59	35.6	8.02	1.51	6.00	5.47	3.45	3.22	0.51	7.90	1.16	22.2	15.1	4.62
23/11/2023	**Aso-H**	FLF208	165	288	31.6	276	16.4	810	33.5	72.3	8.33	34.5	6.77	1.53	6.00	5.55	3.57	3.66	0.57	7.26	1.14	21.9	14.4	4.47
23/11/2023	**Aso-H**	FLF208	162	292	31.3	271	15.7	795	33.3	71.9	8.30	34.5	7.51	1.46	5.69	5.32	3.66	3.30	0.54	7.17	1.07	21.6	14.3	4.17
23/11/2023	**Aso-H**	FLF208	158	285	30.7	266	15.8	770	32.6	71.4	8.17	34.3	7.27	1.52	6.26	5.41	3.33	3.47	0.53	7.42	1.13	22.2	14.9	4.61
23/11/2023	**Aso-H**	FLF208	171	208	31.2	293	16.3	803	33.1	73.7	8.22	33.1	6.94	1.47	5.62	5.52	3.37	3.30	0.54	7.64	1.24	23.3	16.5	4.74
23/11/2023	**Aso-I**	FLF207	185	223	31.9	281	16.8	795	33.4	72.9	8.05	35.8	6.44	1.62	5.62	5.63	3.33	3.57	0.53	7.64	1.17	26.2	15.4	4.56
23/11/2023	**Aso-I**	FLF208	184	217	33.1	307	17.6	842	35.2	76.3	8.72	35.8	7.30	1.59	6.51	6.22	3.68	3.83	0.59	7.81	1.24	24.5	16.9	4.82
23/11/2023	**Aso-I**	FLF209	182	254	32.6	295	16.5	817	35.5	70.1	8.88	33.3	7.56	1.72	5.98	5.40	3.39	3.76	0.55	7.98	1.06	22.2	14.5	3.87
23/11/2023	**Aso-I**	FLF210	177	259	33.1	295	17.5	853	35.6	76.4	8.90	35.3	7.72	1.40	6.32	5.92	3.46	3.85	0.58	7.11	1.18	22.9	15.6	4.75
23/11/2023	**Aso-I**	FLF211	182	261	39.0	341	19.8	888	41.9	90.0	11.3	44.6	10.16	1.85	8.15	6.86	4.72	4.61	0.70	8.03	1.28	25.4	17.9	5.16
23/11/2023	**Aso-I**	FLF212	186	250	33.3	297	17.6	843	35.3	74.7	8.77	33.8	6.65	1.42	6.20	5.40	3.72	3.79	0.51	8.14	1.19	23.0	14.9	4.42
23/11/2023	**Aso-I**	FLF213	178	243	33.7	301	17.2	852	35.2	73.9	8.72	36.3	7.45	1.64	6.61	5.82	3.76	3.94	0.55	8.09	1.19	23.2	15.9	4.69
23/11/2023	**Aso-I**	FLF214	177	264	34.2	303	17.2	858	36.3	78.5	8.95	37.9	7.27	1.70	6.58	6.08	3.35	3.72	0.59	7.86	1.24	23.8	16.5	4.74
23/11/2023	**Aso-I**	FLF215	175	260	34.4	292	17.3	821	36.0	75.0	9.12	40.8	7.33	1.54	5.80	6.04	3.51	3.75	0.59	7.80	1.18	24.5	15.4	4.76
23/11/2023	**Aso-I**	FLF206	177	273	36.1	300	17.4	834	37.3	81.9	9.54	39.6	8.41	1.73	6.92	6.19	3.80	4.05	0.61	7.64	1.21	24.1	16.5	4.96
23/11/2023	**Aso-I**	FLF206	183	227	33.6	303	17.3	868	35.7	76.9	8.57	35.6	7.54	1.45	6.33	6.01	3.59	3.94	0.59	8.40	1.28	25.0	17.0	5.08
23/11/2023	**Aso-I**	FLF206	182	232	31.9	275	16.6	786	33.6	68.9	8.30	33.9	7.05	1.60	6.39	5.00	3.60	3.90	0.48	6.91	1.05	23.5	13.6	4.26
23/11/2023	**Aso-I**	FLF206	178	246	33.8	302	17.4	841	35.5	77.0	8.80	35.5	7.76	1.51	5.92	5.74	3.58	3.98	0.58	8.10	1.28	24.4	17.0	4.97
23/11/2023	**Aso-I**	FLF206	181	250	32.8	290	17.2	840	34.7	74.2	8.50	35.6	7.91	1.40	6.20	5.53	3.51	3.61	0.59	7.74	1.24	23.6	15.8	4.62
23/11/2023	**Aso-I**	FLF206	179	266	34.2	298	17.7	851	35.9	77.8	8.96	36.8	7.37	1.54	7.25	6.45	3.96	3.85	0.56	7.96	1.26	24.1	16.8	4.91
23/11/2023	**Aso-I**	FLF206	186	247	32.2	287	17.1	840	33.9	74.0	8.32	32.5	8.00	1.33	6.17	5.52	3.32	3.94	0.50	7.22	1.13	22.5	14.4	4.21
23/11/2023	**Aso-I**	FLF206	188	254	33.7	309	16.8	852	36.5	77.9	8.22	36.7	8.08	1.46	6.70	6.05	3.42	3.88	0.54	7.35	1.21	23.2	16.3	4.34
23/11/2023	**Aso-I**	FLF206	183	242	32.8	290	17.3	819	34.4	75.7	8.59	35.2	7.68	1.54	6.20	5.55	3.48	4.03	0.57	7.85	1.21	26.0	15.6	4.69
23/11/2023	**Aso-I**	FLF206	185	242	31.2	273	16.9	817	33.5	74.3	8.15	36.3	6.68	1.27	6.32	5.53	3.20	3.71	0.50	7.03	1.11	23.2	14.0	4.49
23/11/2023	**Aso-I**	FLF206	181	231	31.8	277	17.2	777	32.9	72.9	7.66	34.1	6.32	1.59	5.62	5.14	3.33	3.78	0.60	7.28	1.23	25.7	15.1	4.39
23/11/2023	**Aso-I**	FLF206	178	251	32.7	285	16.5	806	34.6	71.9	8.65	34.9	7.35	1.51	6.95	5.91	3.69	4.04	0.53	7.75	1.17	23.3	16.0	4.62
23/11/2023	**Aso-I**	FLF206	181	244	33.1	294	17.1	822	34.7	72.7	8.58	35.6	7.70	1.59	5.52	5.89	3.59	4.10	0.59	7.72	1.19	24.1	16.7	4.24
23/11/2023	**Aso-I**	FLF206	187	218	32.6	304	17.9	831	34.6	75.9	8.35	34.3	7.18	1.27	6.80	5.31	3.58	3.66	0.55	7.95	1.22	25.5	16.2	4.80
23/11/2023	**Aso-I**	FLF206	182	240	33.0	288	17.0	814	34.2	74.2	8.36	33.8	6.98	1.46	5.85	5.46	3.50	3.98	0.53	7.33	1.22	22.3	14.9	4.41

Date of Analysis	Sample	Label	Rb	Sr	Y	Zr	Nb	Ba	La	Ce	Pr	Nd	Sm	Eu	Gd	Dy	Er	Yb	Lu	Hf	Ta	Pb	Th	U
14/11/2023	**Aso-I**	FLF151	176	244	32.9	293	16.7	833	34.7	75.2	8.43	36.8	7.72	1.48	6.79	6.26	3.31	3.75	0.59	7.95	1.23	23.6	15.9	4.84
14/11/2023	**Aso-I**	FLF151	168	196	28.5	603	89.0	731	29.8	66.3	7.81	33.7	5.84	1.14	5.34	4.88	3.45	4.38	0.48	19.57	5.56	21.1	11.9	3.52
14/11/2023	**Aso-I**	FLF151	178	248	33.6	302	17.1	829	34.9	75.5	8.74	36.3	7.79	1.59	6.18	6.28	3.21	3.65	0.58	8.17	1.24	22.8	16.3	4.67
14/11/2023	**Aso-I**	FLF151	176	247	31.8	281	16.2	818	34.0	72.4	8.46	33.8	6.92	1.37	6.00	5.45	3.44	3.57	0.54	7.53	1.13	22.9	15.7	4.56
14/11/2023	**Aso-I**	FLF151	184	208	31.5	278	16.7	810	33.5	73.2	7.82	34.8	6.49	1.44	5.36	5.09	3.01	3.53	0.57	6.88	1.14	22.5	14.5	4.90
14/11/2023	**Aso-I**	FLF151	181	210	32.3	293	16.6	846	34.8	74.3	8.54	37.2	6.91	1.45	6.22	6.04	3.49	3.69	0.56	8.48	1.21	24.5	15.7	4.54
23/11/2023	**Aso-J**	FLF202	169	285	32.9	284	16.4	800	34.0	74.4	8.65	35.9	7.74	1.70	5.87	6.11	3.44	3.62	0.54	7.57	1.20	22.2	15.2	4.54
23/11/2023	**Aso-J**	FLF202	175	284	33.0	288	16.9	810	35.0	76.6	8.72	35.9	7.89	1.62	6.30	5.51	3.71	4.05	0.55	7.39	1.21	24.4	15.7	4.76
23/11/2023	**Aso-J**	FLF202	171	280	32.1	278	16.7	792	33.9	75.1	8.65	36.0	7.45	1.59	6.07	5.76	3.70	3.55	0.54	7.31	1.21	24.6	15.4	4.58
23/11/2023	**Aso-J**	FLF202	178	276	30.9	266	16.1	781	32.5	71.7	8.34	35.0	6.99	1.50	5.82	5.32	3.18	2.93	0.47	6.64	1.04	22.0	13.6	4.10
23/11/2023	**Aso-J**	FLF202	193	269	31.6	263	16.1	754	31.4	69.1	7.54	30.1	7.90	1.60	6.86	5.49	3.21	3.07	0.37	6.98	1.07	24.1	12.3	3.63
23/11/2023	**Aso-J**	FLF202	186	297	32.9	279	16.4	841	34.2	75.8	8.62	37.0	7.56	1.52	6.03	5.71	3.56	3.59	0.57	7.37	1.20	24.3	15.4	4.55
23/11/2023	**Aso-J**	FLF202	176	274	31.7	271	16.1	789	32.6	72.9	8.70	35.1	7.62	1.55	6.34	5.38	3.36	3.39	0.49	7.22	1.15	21.5	14.3	4.41
23/11/2023	**Aso-J**	FLF202	174	314	32.5	283	16.7	818	34.6	76.0	8.64	36.3	7.85	1.51	6.63	5.68	3.76	3.68	0.57	7.95	1.21	23.5	15.8	4.58
23/11/2023	**Aso-J**	FLF202	172	293	33.7	286	17.0	831	35.0	78.2	9.15	37.5	7.89	1.50	6.43	6.15	3.75	3.67	0.56	7.67	1.20	23.0	16.2	4.60
23/11/2023	**Aso-J**	FLF202	182	293	32.4	277	16.6	830	34.4	75.2	8.97	35.8	8.71	1.56	6.26	5.73	3.32	3.82	0.54	7.16	1.17	23.3	15.3	4.44
23/11/2023	**Aso-K**	FLF201	171	290	32.8	291	16.7	824	34.3	75.2	9.25	35.9	8.01	1.56	6.10	5.71	3.37	3.81	0.53	7.52	1.20	24.3	15.7	4.41
23/11/2023	**Aso-K**	FLF201	167	293	33.1	287	16.7	813	35.0	76.3	9.02	37.6	7.85	1.73	6.07	6.17	3.85	3.76	0.55	7.78	1.20	23.7	16.4	4.77
23/11/2023	**Aso-K**	FLF201	172	283	32.6	276	17.7	808	34.2	73.3	8.86	36.0	7.55	1.57	6.22	5.52	3.70	3.75	0.57	7.27	1.15	23.7	15.4	4.59
23/11/2023	**Aso-K**	FLF201	172	294	33.3	285	16.6	826	35.0	75.8	8.84	37.1	7.59	1.71	6.25	6.22	3.34	4.05	0.53	7.72	1.16	25.0	15.8	4.61
23/11/2023	**Aso-K**	FLF201	165	298	34.3	293	16.9	813	35.1	77.1	8.50	37.1	6.94	1.72	6.24	6.72	3.35	3.24	0.52	7.93	1.21	23.4	16.0	4.38
23/11/2023	**Aso-K**	FLF201	171	290	33.7	288	16.7	824	35.6	77.0	8.92	37.9	8.22	1.55	6.44	5.80	3.73	3.59	0.53	7.59	1.23	23.1	16.3	4.66
23/11/2023	**Aso-K**	FLF201	171	302	34.1	294	17.2	844	36.5	78.7	9.02	38.6	7.77	1.50	6.24	5.97	3.74	3.92	0.59	8.19	1.23	24.2	16.4	4.77
23/11/2023	**Aso-K**	FLF201	170	293	32.9	284	16.5	826	35.0	74.8	8.61	36.5	7.55	1.64	6.25	5.79	3.66	3.23	0.59	6.93	1.19	24.1	15.3	4.43
23/11/2023	**Aso-K**	FLF201	165	298	32.9	285	16.7	809	34.4	77.2	8.81	37.2	7.87	1.62	6.51	5.87	3.48	3.42	0.57	7.55	1.21	23.6	15.7	4.66
23/11/2023	**Aso-K**	FLF201	171	302	33.3	284	16.8	819	34.7	77.4	8.58	37.0	7.58	1.51	6.68	5.89	3.49	3.72	0.56	7.59	1.19	24.7	15.6	4.56

Table C4. Trace element glass analyses of the MPI-DING reference glass (StHs6/80-G and ATHO-G)

Date of Analysis	Sample	Rb	Sr	Y	Zr	Nb	Ba	La	Ce	Pr	Nd	Sm	Eu	Gd	Dy	Er	Yb	Lu	Hf	Ta	Pb	Th	U
14/11/2023	**StHs6_80**	30.4	480	11.0	115	6.50	301	11.6	25.4	3.1	13.4	2.72	0.93	2.56	2.18	1.08	1.09	0.16	2.96	0.41	9.18	2.28	0.99
14/11/2023	**StHs6_80**	30.7	480	11.1	116	6.51	299	11.6	24.4	3.0	12.6	3.03	0.84	2.41	2.25	1.12	1.03	0.17	3.15	0.39	8.61	2.21	1.05
14/11/2023	**StHs6_80**	30.3	470	10.9	115	6.56	297	11.5	25.1	2.9	12.7	2.95	0.81	2.23	2.22	1.20	1.23	0.16	2.95	0.40	9.30	2.25	0.98
14/11/2023	**StHs6_80**	30.0	478	11.0	113	6.47	304	11.8	24.6	2.9	13.1	2.79	0.84	2.61	1.97	1.20	1.25	0.14	2.68	0.41	9.12	2.16	0.97
23/11/2023	**StHs6_80**	31.4	483	11.2	115	6.57	306	11.7	25.3	3.0	12.9	2.98	0.88	2.45	2.06	1.03	1.21	0.17	2.88	0.40	9.29	2.20	1.05
23/11/2023	**StHs6_80**	30.5	471	10.8	114	6.57	297	11.4	24.9	3.0	12.0	2.74	0.89	2.47	2.22	1.18	1.14	0.16	3.10	0.40	9.48	2.30	1.04
23/11/2023	**StHs6_80**	31.8	487	11.2	117	6.82	308	12.0	25.6	3.0	12.9	2.76	0.88	2.36	2.15	1.10	1.24	0.16	3.11	0.41	9.35	2.21	1.09
23/11/2023	**StHs6_80**	31.0	483	10.9	114	6.67	297	11.6	25.0	3.0	12.1	3.02	0.95	2.64	2.07	1.19	1.26	0.17	3.12	0.41	9.52	2.33	1.03
23/11/2023	**StHs6_80**	30.4	490	11.6	118	6.85	310	12.1	25.5	3.1	12.6	2.70	0.96	2.33	2.23	1.07	1.26	0.18	2.95	0.40	9.43	2.19	1.10
23/11/2023	**StHs6_80**	30.4	481	10.9	115	6.59	311	11.5	25.2	3.0	12.5	2.51	0.92	2.46	2.00	1.33	1.29	0.17	3.03	0.39	9.13	2.25	1.13
23/11/2023	**StHs6_80**	29.9	473	10.8	115	6.46	299	11.2	24.9	2.9	12.7	2.72	0.84	2.38	2.10	1.04	1.18	0.19	3.02	0.39	9.41	2.09	0.88
23/11/2023	**StHs6_80**	29.5	474	11.2	115	6.63	301	11.4	24.9	3.0	12.7	2.97	0.92	2.39	2.09	1.22	1.09	0.15	3.12	0.39	9.37	2.33	1.08
23/11/2023	**StHs6_80**	29.5	477	10.9	116	6.65	297	11.6	25.3	2.9	12.8	2.61	0.95	2.08	2.10	1.16	1.22	0.17	2.82	0.40	8.83	2.06	0.99
23/11/2023	**StHs6_80**	29.4	476	11.0	117	6.58	298	11.5	24.8	3.0	13.0	2.97	0.90	2.50	2.49	1.21	1.19	0.16	3.22	0.40	9.16	2.27	0.93
23/11/2023	**StHs6_80**	28.8	477	11.1	116	6.60	300	11.6	24.9	3.0	13.1	2.92	0.86	2.43	2.23	1.30	1.23	0.17	3.07	0.40	8.70	2.25	0.92
19/12/2023	**StHs6_80**	30.4	474	10.9	113	6.51	302	11.4	25.2	2.9	12.7	2.96	0.99	2.64	2.19	1.17	1.29	0.16	2.89	0.39	9.07	2.29	1.00
19/12/2023	**StHs6_80**	29.8	474	11.1	113	6.56	304	11.5	25.0	2.9	12.0	2.78	0.91	2.50	2.17	1.15	1.14	0.16	3.01	0.39	9.48	2.18	1.05
19/12/2023	**StHs6_80**	29.9	475	11.0	115	6.44	307	11.4	25.1	2.9	12.4	2.82	0.88	2.40	2.06	1.13	1.10	0.17	3.03	0.39	9.10	2.30	0.95
19/12/2023	**StHs6_80**	30.9	481	10.9	119	6.82	308	11.9	25.1	2.9	13.1	3.05	0.84	2.67	2.28	1.33	1.45	0.19	3.32	0.41	9.28	2.41	1.17
19/12/2023	**StHs6_80**	30.9	478	10.9	120	6.68	310	11.5	25.5	3.0	13.4	3.23	0.89	2.56	2.25	1.10	1.33	0.18	2.60	0.40	8.94	2.28	1.11
19/12/2023	**StHs6_80**	32.6	488	11.0	117	6.90	312	11.6	25.5	3.0	14.0	3.30	1.03	2.79	2.38	1.26	1.42	0.20	2.99	0.41	9.76	2.11	1.02
13/02/2024	**StHs6_80**	30.5	466	11.1	115	6.49	302	11.4	24.8	3.0	12.7	3.35	0.93	2.84	2.22	1.17	1.12	0.17	3.03	0.39	9.33	2.08	0.96
13/02/2024	**StHs6_80**	28.8	473	10.9	115	6.47	304	11.7	25.1	2.8	13.0	2.87	0.88	2.41	2.13	1.07	1.11	0.16	2.99	0.38	8.83	2.34	0.94
13/02/2024	**StHs6_80**	29.4	474	10.8	113	6.58	298	11.5	24.8	2.8	12.5	2.84	0.89	2.39	1.97	1.20	1.30	0.18	2.95	0.39	9.03	2.22	0.97
14/11/2023	**ATHO_G**	65.8	91.7	90.1	482	60.0	557	54.5	122	14.2	61.7	14.4	2.27	14.6	16.5	9.9	9.9	1.52	13.8	3.69	4.59	7.34	2.25
14/11/2023	**ATHO_G**	66.3	93.3	92.3	504	60.6	563	55.8	122	14.5	63.9	14.6	2.31	14.0	15.9	10.3	10.2	1.52	14.4	3.78	4.24	7.57	2.35
14/11/2023	**ATHO_G**	67.0	93.8	91.7	502	60.4	561	55.2	121	14.4	62.3	14.4	2.60	14.4	17.1	10.2	10.4	1.51	14.4	3.80	4.24	7.43	2.29
23/11/2023	**ATHO_G**	67.0	94.6	91.7	490	59.8	557	55.6	124	14.5	61.6	14.9	2.47	13.8	16.6	10.7	10.4	1.53	13.9	3.77	4.61	7.50	2.33
23/11/2023	**ATHO_G**	67.3	94.9	92.8	500	60.7	566	56.3	126	14.7	62.6	15.5	2.55	15.3	16.5	10.6	10.7	1.58	13.6	3.78	4.56	7.33	2.34
23/11/2023	**ATHO_G**	67.1	96.6	93.2	505	61.6	574	56.0	125	14.7	62.4	15.2	2.56	14.5	16.4	10.1	10.8	1.52	14.4	3.84	5.23	7.41	2.29
23/11/2023	**ATHO_G**	63.8	92.6	90.3	494	59.7	556	54.3	120	14.5	60.6	14.5	2.52	14.5	17.1	10.0	10.2	1.55	14.2	3.72	4.88	7.25	2.29
23/11/2023	**ATHO_G**	63.8	93.2	90.4	499	58.7	547	54.8	121	14.2	63.0	14.8	2.46	14.0	16.9	10.3	11.2	1.57	13.6	3.70	4.74	7.34	2.26
19/12/2023	**ATHO_G**	65.7	92.4	90.5	496	60.3	562	55.5	123	14.5	63.7	14.9	2.43	14.9	16.3	10.5	10.5	1.53	13.9	3.70	4.60	7.46	2.27
19/12/2023	**ATHO_G**	68.4	93.8	92.4	502	62.4	571	56.5	124	14.8	61.0	15.6	2.53	15.8	17.4	10.4	10.6	1.61	13.9	3.84	4.68	7.58	2.32
13/02/2024	**ATHO_G**	63.5	93.6	92.4	499	60.0	550	55.2	120	14.1	61.5	14.8	2.51	14.8	17.2	10.0	10.6	1.54	13.6	3.69	4.93	7.50	2.30
13/02/2024	**ATHO_G**	63.6	93.9	92.1	498	60.3	565	55.6	122	14.5	64.3	14.1	2.45	14.3	16.3	10.3	10.6	1.57	13.4	3.73	4.68	7.59	2.39